
Sequence-Control in Styrene/Isoprene Tapered Multiblock Copolymers: From Fundamental Kinetics to Morphologies and Mechanics of Thermoplastic Elastomers

Dissertation
zur Erlangung des Grades
„Doktor der Naturwissenschaften“
im Promotionsfach Chemie

am Fachbereich
Chemie, Pharmazie, Geographie und Geowissenschaften
der Johannes Gutenberg-Universität
in Mainz

Marvin Steube
geb. in Heppenheim

Mainz, Mai 2020

This thesis was carried out from March 2017 to May 2020 in the group of Professor Holger Frey at the Department of Chemistry, Johannes Gutenberg University, Mainz.

Reviewer 1: Prof. Dr. Holger Frey

Reviewer 2: XXXXXXXXXX

Date of oral examination: 02.07.2020

Referring to §10 section 3d of the Doctoral Degree Regulations (24.07.2007), I hereby declare that I wrote the dissertation submitted without any unauthorized external assistance and used only sources acknowledged in the work. All textual passages which are appropriated verbatim or paraphrased from published and unpublished texts as well as all information obtained from oral sources are duly indicated and listed in accordance with bibliographical rules. I have not or had not submitted the work now submitted as dissertation to other state or academic examinations. I had not submitted the dissertation now submitted or parts of it to any other faculty or department.

Für 

“Nicht der Einzelne, sondern die Mannschaft wird für zähes Rudern gelobt.”

Ralph Waldo Emerson

DANKSAGUNGEN

Zum erfolgreichen Abschluss dieser Arbeit haben während meines Studiums und der Zeit meiner Bachelor-, Master- und Doktorarbeit zahlreiche Menschen beigetragen. Hiermit möchte ich mich bei allen recht herzlich bedanken.

An erster Stelle gilt der Dank meinem Doktorvater, **Prof. Dr. Holger Frey**, für die Möglichkeit meine Bachelor-, Master- und Doktorarbeit unter seiner Betreuung absolvieren zu dürfen. Insbesondere bedanke ich mich bei Ihnen für das entgegengebrachte Vertrauen und das vielseitige Interesse an neuen Ideen und Gedanken. Ebenso bedanke ich mich für Ihre exzellente Betreuung und Unterstützung in zahlreichen Kooperationsprojekten. Ich war stets froh mich auf Sie verlassen zu können.

Gleichermaßen möchte ich mich bei meinem "zweiten Doktorvater" und Cobetreuer **Prof. Dr. Axel H.E. Müller** für die enge Zusammenarbeit, die zahlreichen Diskussionen und die inspirierenden Gespräche bedanken. Diese trugen einen beträchtlichen Anteil zur Fertigstellung mehrerer Projekte bei. Ihr konstruktiv-kritischer Blick hat diese Arbeit maßgeblich in vielen Aspekten vorangetrieben und bereichert. Vielen Dank dafür!

Alle Kapitel dieser Arbeit hätten ohne Kooperationen nicht entstehen können. Ich möchte mich herzlich bei allen für die angenehme Zusammenarbeit bedanken. Die Zusammenarbeit mit Euch hat es mir ermöglicht mein Sichtfeld zu erweitern und Einblicke in viele weitere Themengebiete zu bekommen.

Prof. Dr. George Floudas danke ich für die Untersuchung zum Phasenverhalten und der Rheologie der Copolymere. Ohne euer Interesse und eure Kompetenz hätte ein wesentlicher Teil dieser Arbeit gefehlt.

möchte ich für die enge Zusammenarbeit in morphologischen Fragestellungen danken. Die zahlreichen TEM Bilder in dieser Arbeit zeugen von eurer tatkräftigen Unterstützung.

und danke ich für die Tomografie und Mikroskopie der tetragonalen Morphologie. Durch Euren Einsatz, konnten letztendlich auch diese Rätsel gelüftet werden.

und bedanke ich mich für die Zusammenarbeit und den dadurch gewonnenen Einblick in das Gebiet der Modellierung und der Simulation des Phasenverhaltens von Polymeren.

██████████ und ██████████ danke ich für die Unterstützung in experimentellen und instrumentellen Bereichen. Ohne euch wäre diese Arbeit nicht möglich gewesen.

██████████ danke ich für die wichtige Unterstützung durch exzellente Charakterisierungsmethoden.

██████████ danke ich für die anregenden Diskussionen anlässlich seines Besuchs in Mainz.

Ebenso danke ich ██████████ für die netten und hilfreichen Diskussionen.

Ein besonderer Dank gilt ██████████
██████████ und ██████████ für die angenehme Zusammenarbeit im Gebiet der carbanionischen Polymerisation. Jeder von euch hat diese Arbeit auf seine eigene Art und Weise bereichert.

Insbesondere möchte ich mich bei meinem langjährigen Freund und Mitstreiter ██████████ für die zahlreichen netten und zielführenden Diskussionen, seine offene Meinung und seine große Hilfsbereitschaft bedanken. Die enge Zusammenarbeit mit dir hat mir stets Freude bereitet und diese Arbeit unübersehbar aufgewertet. Vielen Dank!

Bei ██████████ danke ich für die zahlreichen Gespräche, seine langjährige Erfahrung und seine geschickten Hände, welche letztendlich jedes Glas meinen Wünschen entsprechend formten.

Auch möchte ich mich bei ██████████ und ██████████ für die Hilfe im Labor bedanken. Ich habe mich sehr über eure Motivation und euer Interesse an meiner Forschung gefreut.

██████████ danke ich für die vielen GPC Messungen und die tatkräftige Unterstützung bei alltäglichen Laboraufgaben. Ebenso danke ich ██████████ und ██████████. Bei Problemen jeglicher Art seid ihr immer zur Stelle gewesen. Ebenso möchte ich mich bei ██████████ für die Hilfe bei organisatorischen Aufgaben bedanken. ██████████
██████████ danke ich für Viskositäts-Messungen.

Für die großartige Arbeitsatmosphäre möchte ich mich vor allem bei ██████████
██████████
██████████ und
██████████ bedanken.

Ganz besonders bedanke ich mich beim ganzen Arbeitskreis für die angenehme Arbeitsatmosphäre, die Feierabendgespräche sowie alles Weitere bis hin zu Bildern beim „blutigen Engel“. Unsere Hüttenseminare, Seewochenenden, Grillabende, Chemiker-Partys, AK-Ausflüge sowie Fastnachts- und Weihnachtsfeiern werden mir immer in Erinnerung bleiben. Ohne diese Traditionen hätten wir nur halb so viel zusammen gelacht.

Ein besonderer Dank gilt [REDACTED] und [REDACTED] für die super Atmosphäre im Arbeitsalltag, sowie während der Vielzahl an Freizeitaktivitäten. Mit euch war die Promotion einfach klasse!

Auch möchte ich mich bei meinen Freunden außerhalb des Arbeitskreises bedanken, die mich während des Studiums begleitet haben. Vielen Dank [REDACTED] sowie [REDACTED]

Ich bedanke mich bei meinen engen Freunden aus der Schulzeit. Insbesondere möchte ich hier bei [REDACTED] und [REDACTED] bedanken. Ich bin froh euch regelmäßig zu sehen!

Ein großer Dank geht an [REDACTED] und [REDACTED], für die allgegenwärtige Unterstützung! Ohne eure Hilfe wäre diese Arbeit nicht möglich gewesen.

Abschließend möchte ich mich mit ganzem Herzen bei [REDACTED] bedanken. Danke, für die tägliche Unterstützung, deine Geduld und die regelmäßige Erinnerung auch mal einen Blick zurück zu werfen. Weiterhin vielen Dank für Rat und Tat zur Überwindung aller Schwierigkeiten, die eine Promotion eben so mit sich bringt. Vielen Dank für die vielen kleinen und großen Dinge, die du ohne mein Wissen erledigt hast. Kurz gesagt: Einfach Danke für Alles!

CONTENTS

Motivation and Objectives	10
Abstract	15
Zusammenfassung	19
Graphical Abstract	23
Chapters	25
1 Rational Design of Thermoplastic Elastomers	25
2 Tapered Multiblock Copolymers	75
3 Tapered Multiblock Copolymer Blends	141
4 Near-Infrared Probing and Temperature Effects on Copolymerization Kinetics . . .	177
5 THF - A "Randomizing" Additive?	273
Appendix	381
Chain Relaxations in Tapered Multiblock Copolymers	381
Curriculum Vitae	408
List of Publications	410

MOTIVATION AND OBJECTIVES

Polymers are advanced materials with highly diverse properties. Nowadays, they facilitate our everyday life as a part of a vast variety of products. Their properties can be adjusted by the combination of several monomers in a tailored “macromolecular architectures”.¹ Already the simple combination of two monomers offers sheer endless possibilities to fulfill the engineering goals as set by a specific application.² For example, the chemical linkage of flexible (i.e. low glass transition temperature) polymers with short, glassy endblocks can lead to phase segregated ABA type architectures, where the rubbery midblock is pinned by the vitrified, spherical domains.^{3,4} As a consequence, the otherwise sticky homopolymer is transformed into a form-stable elastic material. If instead the rubbery midblock is linked to much larger glassy endblocks, hard materials are obtained. In case of crack initiation, the rubbery domains are able to dissipate energy, stop crack propagation and prevent ultimate failure of the material. Hence increased impact resistance is observed in these thermoplastic materials. In both cases, superior properties are observed for ABA triblock copolymers in comparison to the homopolymers leading to their use in shoes or medical devices as well as a broad range of other applications as for example sealings or insulations.⁵

Thermoplastic materials capitalizing on phase separated glassy and rubbery domains, have been investigated intensely.⁶ They are widely established on the commercial scale as so called “thermoplastic elastomers” (TPEs) or “impact resistant thermoplastics”, depending on which component is the majority part. In contrast to permanently (i.e. chemically) crosslinked vulcanizates, physical crosslinking via glassy domains is reversible and allows to recycle or process the material also by thermal or solvent annealing. This is especially important in industry, where high-speed extrusion at elevated temperature is the method of choice for polymer processing.⁷

Since the first description of „Living Polymers“ in 1956, the living anionic polymerization has evolved to an excellent tool to design block copolymer architectures in academia and industry.^{8,9} Following this strategy, the absence of side-reactions allows for the anionic chain end to remain active or “living” even after full monomer consumption. This allows the polymerization to proceed by consecutive (co)monomer addition steps. As a consequence, the controlled polymerization of 1,3-dienes and styrene enables the synthesis of well-defined block copolymer architectures and their correlation with morphological and mechanical properties.¹⁰ High molecular weight block copolymers are highly entangled, mechanically stable, phase separated bulk materials. Outstanding mechanical properties were observed for the polystyrene/polyisoprene based SIS triblock copolymer architecture, and attributed to the fraction of endblocks anchored at different domain interfaces (i.e. bridging conformation).¹¹ A further increase of the block number

leads to so-called multiblock copolymers, which have shown mechanical properties superior to triblocks, attributed to the bridging of multiple domains by single polymer chains.¹¹ However, multiblock synthesis necessitated an increasing number of monomer addition steps, increasing the risk of irreversible termination of the highly sensitive carbanionic ends. Furthermore, the typically strong tendency of block copolymers to phase segregate was also found to impede the processing at elevated temperatures.¹²

In contrast, the so-called „tapered“ block copolymers formed in a statistical copolymerization are an attractive alternative to block copolymers prepared by sequential addition of both monomers.¹³ These block-like architectures with a rather steep gradient are also capable of phase separation. However, the rather smooth block transition enhances miscibility of the blocks. This enables to access high molecular weights, which are able to undergo an order-disorder transition at elevated temperatures typically used for processing by extrusion.¹⁴ The alkyllithium initiated living anionic copolymerization in hydrocarbons is known to result in tapered diblock copolymers. Although the synthetic principle has been known since 1958, its use as a building block in TPE materials has been rarely investigated.^{4,15,16} Hence, implementing tapered architectures in multiblock copolymers (Figure 1) leads to an uncertain correlation of thermal, morphological and mechanical properties, which led us to the question:

„Can one utilize the consecutive statistical copolymerization in one-pot to obtain tapered multiblock copolymers as phase-separated, tough materials with tailored order-disorder transitions?“

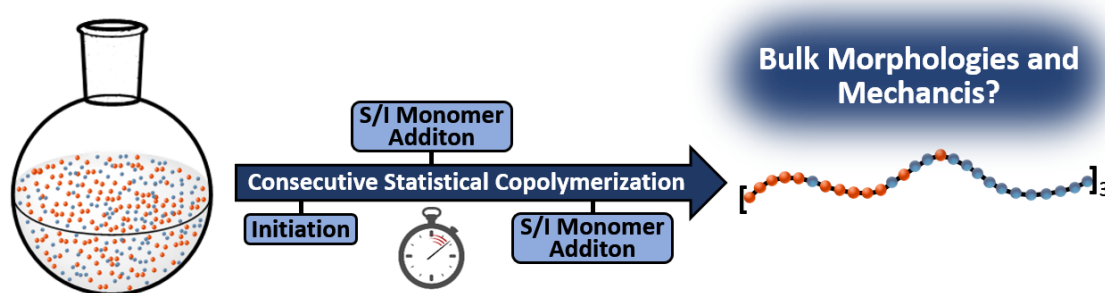


FIGURE 1 Visualization of the alkyllithium initiated consecutive statistical copolymerization of styrene and isoprene in hydrocarbon solvents, leading to a tapered multiblock copolymer architecture. The representative structure visualizes a tapered hexablock copolymer obtained by a three step procedure in one-pot, respectively.

The statistical copolymerization is of great interest because rather complex comonomer sequences can be obtained in a single step, which otherwise require exhausting multi-step polymerization procedures.

Even though this principle is rather old, the interest in sequence-controlled polymers has strongly increased in recent years.¹⁷ Although the resulting comonomer sequence is known to be affected by the monomer pair, the solvent and the temperature, systematic studies are rare.¹⁸ In addition, these copolymerization data usually lack precise quantification of kinetic rate constants.¹⁹ To systematically track the formation of various monomer sequences (Figure 2) and their resulting material properties, we asked the question:

„How can we adjust and track the copolymerization kinetics and how does the gradient profile in tapered block copolymers affect thermal, morphological and mechanical properties?“

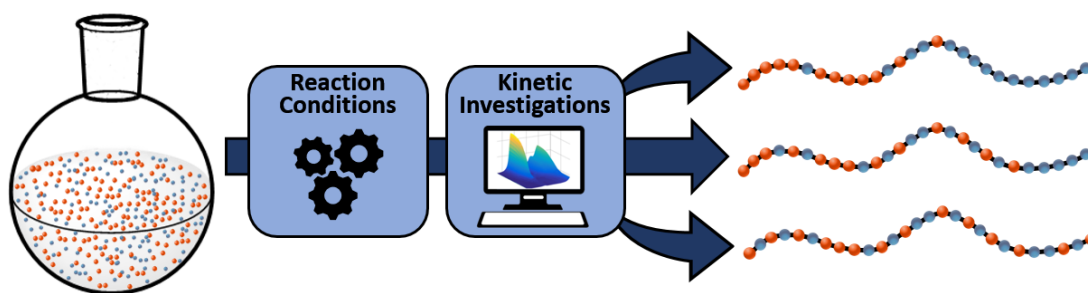


FIGURE 2 Visualization of the applied strategy used to systematically vary and track the statistical copolymerization kinetics. In dependence of the reaction conditions, the polymerization leads to different monomer sequences in the backbone which allows the correlation with material properties.

References

- (1) Hadjichristidis, N.; Iatrou, H.; Pitsikalis, M.; Mays, J. *Prog. Polym. Sci.* **2006**, *31* (12), 1068–1132. DOI: 10.1016/j.progpolymsci.2006.07.002.
- (2) Bates, F. S.; Hillmyer, M. A.; Lodge, T. P.; Bates, C. M.; Delaney, K. T.; Fredrickson, G. H. *Science* **2012**, *336* (6080), 434–440. DOI: 10.1126/science.1215368.
- (3) Morton, M. In *Multicomponent polymer systems: A symposium co-sponsored by the Division of Industrial and Engineering Chemistry, the Division of Polymer Chemistry at the 159th meeting of the American Chemical Society, Houston, Tex., Feb. 23 - 26, 1970*; Platzer, N. A. J., Ed.; Advances in chemistry series 99; American Chemical Society: Washington, DC, 1971; pp 490–509.
- (4) Geoffrey, H.; Milkovich, R. Block polymers of monovinyl aromatic hydrocarbons and conjugated dienes. 3,265,765, Jan 29, 1962.
- (5) Hadjichristidis, N.; Pispas, S.; Floudas, G. *Block Copolymers*; John Wiley & Sons, Inc: Hoboken, USA, 2002.
- (6) Noshay, A.; McGrath, J. E. *Block copolymers: Overview and critical survey*, 2nd print; Acad. Pr: Orlando u.a., 1987.
- (7) Knoll, K.; Nießner, N. *Macromol. Symp.* **1998**, *132* (1), 231–243. DOI: 10.1002/masy.19981320122.
- (8) Szwarc, M. *Nature* **1956**, *178* (4543), 1168–1169. DOI: 10.1038/1781168a0.
- (9) Szwarc, M.; Levy, M.; Milkovich, R. *J. Am. Chem. Soc.* **1956**, *78* (11), 2656–2657. DOI: 10.1021/ja01592a101.
- (10) Qiao, L.; Leibig, C.; Hahn, S. F.; Winey, K. I. *Ind. Eng. Chem. Res.* **2006**, *45* (16), 5598–5602. DOI: 10.1021/ie0511940.
- (11) Spontak, R. J.; Smith, S. D. *J. Polym. Sci. B* **2001**, *39* (9), 947–955. DOI: 10.1002/polb.1070.
- (12) Sinturel, C.; Bates, F. S.; Hillmyer, M. A. *ACS Macro Lett.* **2015**, *4* (9), 1044–1050. DOI: 10.1021/acsmacrolett.5b00472.
- (13) Singh, N.; Tureau, M. S.; Epps, I. T. H.I.I. *Soft Matter* **2009**, *5* (23), 4757. DOI: 10.1039/b908739g.
- (14) Hodrokoukes, P.; Floudas, G.; Pispas, S.; Hadjichristidis, N. *Macromolecules* **2001**, *34* (3), 650–657. DOI: 10.1021/ma001479i.
- (15) Cunningham, R. E.; Treiber, M. R. *J. Appl. Polym. Sci.* **1968**, *12* (1), 23–34. DOI: 10.1002/app.1968.070120104.
- (16) Phillips Petroleum Company. 888,624, 1958.
- (17) Badi, N.; Lutz, J.-F. *Chem. Soc. Rev.* **2009**, *38* (12), 3383–3390. DOI: 10.1039/B806413J.
- (18) Spirin, Y. L.; Arest-Yakubovich, A. A.; Polyakov, D. K.; Gantmakher, A. R.; Medvedev, S. S. *J. Polym. Sci.* **1962**, *58* (166), 1181–1189. DOI: 10.1002/pol.1962.1205816674.
- (19) Tsukahara, Y.; Nakamura, N.; Hashimoto, T.; Kawai, H.; Nagaya, T.; Sugimura, Y.; Tsuge, S. *Polym. J.* **1980**, *12* (7), 455–466. DOI: 10.1295/polymj.12.455.

ABSTRACT

Since around 1600 BC, naturally occurring elastomers have been known to produce materials, capable of recovering after macroscopic deformation. With the seminal discovery of the vulcanization process by Charles Goodyear and Thomas Hancock around 1840, a broad range of elastomers with stable properties became available. The field saw immense growth in the 20th century with synthetic elastomers based on butadiene and isoprene as well as the introduction of thermoplastic elastomers (TPEs) in the 1960s. Nowadays, an in-depth understanding of the chemical structure and the viscoelastic deformation behaviour enables the design of macromolecular architectures with tailored physical properties. The living anionic polymerization is the method of choice to synthesize complex, welldefined polymer architectures and is highly established on the industrial scale for the production of thermoplastic elastomers. A particular emphasis of this thesis is placed on tapered di- and multiblock structures of the (IS)_n.

This thesis focuses on (i) methods for the precise manipulation and determination of the copolymerization kinetics of styrene (S) and isoprene (I) and the (ii) applicability of these principles for the synthesis of TPE materials with precisely controlled phase behavior and mechanical properties.

Chapter 1 gives an introduction and highlights the rational design of tapered block copolymers for application as TPEs. A brief historical overview reveals the progress in elastomers facilitated by the natural availability of gum chicle and stimulated by the excellent properties of the vulcanizates. As a guideline for the synthetic chemist, individual molecular parameters (e.g. block sequence, comonomer sequence, molecular weight) are discussed in respect to their impact on morphological and mechanical properties. In particular the lithium initiated, living anionic (co)polymerization in hydrocarbons is highlighted as the method of choice to adjust molecular architectures aiming a high *cis* 1,4 polyisoprene content (i.e. structure of natural rubber). *In situ* monitoring techniques are presented as a valuable tool to track the formation of the desired copolymer structure in real-time and to determine kinetic parameters. The latter can be used to simulate the copolymerization via kinetic Monte Carlo simulation. This technique is a valuable practical tool for the chemist to facilitate polymer synthesis (e.g. calculation of reaction times) or to understand rather complex comonomer sequences by enabling access to each individual chain *in silico*.

Chapter 2. The alkyllithium initiated copolymerization of styrene and isoprene in hydrocarbons has been known to result in tapered block copolymers for decades. These block-like structures are favored in terms of their accessible order-disorder transition even at high molecular weights. Although multiblock copolymers are known as tough materials, and the copolymerization ap-

proach facilitates their synthesis, tapered multiblock copolymers were not considered as TPE materials before. In collaboration with [REDACTED], kinetic Monte Carlo simulation was used to optimize reaction times for the repeated statistical copolymerization of styrene and isoprene. Additional simulation results were in accordance with experimental data obtained by the selective degradation of the polyisoprene repeating units, confirming the successful formation of tapered multiblock structures. Transmission electron microscopy (TEM, collaboration with [REDACTED]) was used to image the phase separated morphology in real-space. In-depth morphological studies revealed a strong dependence of the phase state as a function of the molecular weight and the number of blocks. A desired strong reduction of the order-disorder transition temperature in these types of block-like copolymer structures was proven by temperature dependent small angle X-ray scattering (SAXS) experiments and rheology (collaboration with Prof. George Floudas). This is explained by the repetitive block sequence, which allows to connect multiple glassy domains in the phase separated bulk morphology. Tensile tests revealed superior mechanical properties for tapered multiblock copolymers with increasing number of blocks. The concurrent decrease of the block size is accompanied by increasing miscibility, thus limiting the capability for microphase separation. Comparing different multiblock structures, tapered hexablock copolymers were found to best combine structural integrity and mechanical toughness. The potential of these unique molecular architectures is further highlighted in chapter 2 and the appendix.

Chapter 3. The living anionic copolymerization of styrene and isoprene can be utilized to synthesize tapered diblock copolymers in a single step. Although highly ordered materials are obtained, the poor mechanical properties of tapered diblock copolymers are evident in the low elongation at break, observed in tensile tests. In the previous chapter, repeated statistical copolymerization of styrene and isoprene in a one-pot approach was used to prepare tapered multiblock copolymers as tough materials. In this chapter, binary blends of tapered diblock/multiblock copolymers were investigated. The increase of the multiblock copolymer content in the blend resulted in a loss of a certain order. However, already a low amount of added multiblock copolymer transformed the diblock copolymers to tough and elastic materials, illustrating the effect of bridged domains in the bulk morphology. Depending on the microdomain spacing of the individual block copolymers, miscible, partially miscible and immiscible blends were observed via SAXS (collaboration with Prof. George Floudas). Consequences of miscibility were systematically investigated by tensile tests. Surprisingly, even highly diverging domain sizes of diblock- and multiblock component did not lead to a significant loss of mechanical properties.

Chapter 4. To obtain defined block copolymer structures in multi-step reactions, it is crucial to carry out the monomer addition when the majority of the monomer of the previous addition

step has reacted. Thus, the reaction time becomes a crucial parameter in optimizing the polymer synthesis. However, in the statistical copolymerization a simple increase of the reaction temperature can influence the gradient profile caused by the different activation energies of the individual propagation rates. In close collaboration with [REDACTED], for the first time *in situ* real-time near-infrared (NIR) measurements were used to derive the individual time-dependent monomer conversion of styrene and isoprene during the statistical copolymerization. Activation energies were determined by precise evaluation of rate constants in the range of 10 to 60 °C. This allows to predict the gradient profiles via kinetic Monte Carlo simulations resulting in a fundamental understanding of the experimentally observed change of the bulk morphology (collaborations with [REDACTED]) for a copolymer synthesized at elevated temperature. Real-time monitoring was used to follow the comonomer consumption. To demonstrate the power of the NIR method, the successful synthesis of a tapered decablock copolymer (described in chapter 2) was followed. In addition, the high temporal resolution of NIR spectroscopy enabled to successfully monitor a copolymerization experiment accelerated and modified by tetrahydrofuran (THF) as an additive. This concept was further established in the ensuing chapter.

Chapter 5. The alkyllithium initiated copolymerization of styrene and isoprene in rather polar solvents is known to proceed with remarkably different kinetics compared to hydrocarbon solvents. In this chapter, the high temporal resolution of the real-time NIR probing, established in chapter 4, is utilized to track the individual monomer consumptions of styrene and isoprene during the copolymerization in the presence of THF as polar additive. In collaboration with [REDACTED], a systematic increase of the THF content was found to invert the reactivity ratios. Tapered, gradient and random copolymers as well as the inverted analogue comonomer sequences were obtained. Their systematic investigation led to a fundamental understanding of the consequences of the monomer sequence statistic on thermal, morphological and mechanical properties via differential scanning calorimetry (DSC), SAXS (by Prof. George Floudas), TEM (by [REDACTED]) and tensile testing. Finally, a synthetic strategy was presented to incorporate these comonomer sequences as phase compatibilizing gradient block into the well-established SIS block copolymers.

With the developments presented in Chapter 4 and 5 the NIR monitoring technique has been established in our group as the method of choice to follow the living anionic copolymerization of 1,3-dienes with styrene and styrene derivatives in polar and hydrocarbon solvents. Currently, this concept is used in several ongoing projects and will help to understand the synthesis and effects of complex polymer architectures in the future.

Appendix. This work represents a continuation of the studies on tapered di- and multiblock copolymers based on polystyrene and polyisoprene (chapters 2 and 3) carried out in collaboration with Prof. George Floudas. In a tapered comonomer sequence, polyisoprene repeating units carrying a dipole moment along the copolymer chains are interrupted by dielectrically inactive PS repeating units. Dielectric spectroscopy was utilized to investigate the local and (sub-)chain dynamics of polyisoprene in isoprene/styrene based copolymers. A remarkable influence of the tapered interface on the PI chain relaxation was found. The observed longer scale motion of PI repeating units resulted mainly from the PI sub-chain with one free end. The results were also compared to isoprene/4-methyl styrene copolymers. In qualitative accordance to the results of kinetic Monte Carlo simulations, longer polyisoprene sub-chains were found to participate in the dynamics of the 4-methyl styrene based copolymers. This led to a fundamental understanding of the segment length distribution in tapered di- and multiblock copolymer architectures.

ZUSAMMENFASSUNG

Seit 1600 v.Chr sind Produkte natürlich vorkommender Elastomere als Materialien bekannt, welche nach makroskopischer Verformung ihre ursprüngliche Form zurückerlangen. Mit der bahnbrechenden Entdeckung des Vulkanisationsprozesses durch Charles Goodyear und Thomas Hancock um 1840, wurde eine breite Palette an Elastomeren mit verschiedenen Eigenschaften zugänglich. Im 20. Jahrhundert verzeichnete das Gebiet einen immensen Aufschwung durch synthetische Elastomere auf Basis von Butadien und Isopren sowie der Einführung von Thermoplastischen Elastomeren (TPEs) um 1960. Heutzutage trägt das tiefgreifende Verständnis der chemischen Zusammensetzung und des viskoelastischen Verformungsverhaltens dazu bei, makromolekulare Architekturen mit maßgeschneiderten physikalischen Eigenschaften herzustellen. Die lebende Anionische Polymerisation ist die Methode der Wahl für die Synthese von komplexen, wohl definierten Polymerarchitekturen und ebenso bei der Produktion von Thermoplastischen Elastomeren im industriellen Maßstab hoch etabliert.

Diese Arbeit zielt auf (i) Methoden zur präzisen Manipulation und der Bestimmung von Copolymerisationskinetiken von Styrol (S) und Isopren (I) ab sowie (ii) deren Anwendbarkeit für die Synthese von TPEs mit hoch definiertem Phasenverhalten und mechanischen Eigenschaften.

Kapitel 1 leitet die Thematik ein und hebt das rationelle Design von verjüngten Blockcopolymeren sowie deren Anwendung für TPEs hervor. Ein kurzer historischer Abriss zeigt den technischen Fortschritt dieser Materialien begünstigt durch die natürliche Verfügbarkeit von Gummissaft und angetrieben durch die exzellenten Eigenschaften der Vulkanisate. Als Leitfaden für den synthetischen Chemiker, werden individuelle Parameter (z.B. die Blocksequenz, die Comonomersequenz oder das Molekulargewicht) im Hinblick auf morphologische und mechanische Eigenschaften diskutiert. Vor allem die Lithium-initiierte, lebende Anionische Copolymerisation in Kohlenwasserstoffen wird als Methode der Wahl hervorgehoben, um angepasste Architekturen mit einem hohen *cis* 1,4 Polyisoprenanteil (also der chemischen Struktur von natürlichem Gummissaft) zu erhalten. *In situ* Methoden zur Verfolgung von Messungen werden als wertvolles Hilfsmittel vorgestellt, um die Synthese des gewünschten Polymers in Echtzeit zu anzuzeigen und kinetische Parameter zu bestimmen. Letztere können für die Simulation der Copolymerisation über kinetische Monte Carlo Simulationen genutzt werden. Diese Methode ist wertvolles Hilfsmittel für Chemiker, um Copolymerisationsreaktionen zu optimieren (z.B. Berechnung von Reaktionszeiten) oder um das Verständnis komplexer Comonomersequenzen über den Zugang zu einzelnen Ketten durch *in silico* Methoden zu ermöglichen.

Kapitel 2. Wie seit Jahrzehnten bekannt, führt die Alkyllithium-initiierte Copolymerisation von Styrol und Isopren in Kohlenwasserstoffen zu verjüngten Blockcopolymeren. Solche blockartigen

Strukturen sind aufgrund der erreichbaren der Ordnungs-Unordnungs-Übergangstemperatur bevorzugt, welche sogar bei hohen Molekulargewichten noch gegeben ist. Obwohl Multiblockcopolymerer als zähe Materialien bekannt sind und das Copolymerisationsprinzip deren Synthese erleichtert, wurden verjüngte Multiblockcopolymerer bisher nicht als Thermoplastische Elastomere in Betracht gezogen. In Zusammenarbeit mit [REDACTED] wurde eine kinetische Monte-Carlo Simulation verwendet, um Reaktionszeiten für aufeinanderfolgende Copolymerisationen von Styrol und Isopren zu optimieren. Zusätzliche Ergebnisse der Simulation zeigten darüber hinaus eine gute Übereinstimmung mit experimentellen Daten, welche durch selektiven Abbau der Polyisopreneinheiten erhalten wurden. Die erfolgreiche Synthese der angestrebten verjüngten Multiblockcopolymer-Struktur konnte so bestätigt werden. Transmissionselektronenmikroskopie (TEM, Kooperation mit [REDACTED]) wurde genutzt um phasenseparierte Morphologien im Realraum abzubilden. In tiefgreifenden morphologische Studien wurde eine starke Abhängigkeit des Phasenverhaltens als Funktion des Molekulargewichts und der Blockanzahl offenbart. Die gewünschte starke Reduktion der Ordnung-Unordnung Übergangstemperatur wurde über temperaturabhängige Kleinwinkelröntgenstreuung (SAXS) und Rheologiemessungen nachgewiesen (Kooperation mit Prof. George Floudas). Zugfestigkeitstests bestätigten überlegene mechanische Eigenschaften von verjüngte Blockcopolymerer für steigende Blockanzahlen. Die damit einhergehende Reduktion der Blockgröße ist von einer erhöhten Mischbarkeit der Strukturen begleitet, welche gleichzeitig die Befähigung zur Phasenseparation limitiert. Es wurde festgestellt, dass verjüngte Hexablockcopolymerer am besten strukturelle Integrität und mechanische Zähigkeit kombinieren. Das Potenzial dieser einzigartigen molekularen Architekturen ist weiter in Kapitel 2 und dem Appendix hervorgehoben.

Kapitel 3. Die lebende Anionische Copolymerisation von Styrol und Isopren kann verwendet werden, um verjüngte Diblockcopolymerer in einem einzelnen Schritt herzustellen. Obwohl hoch geordnete Materialien erhalten werden, lassen sich die schlechten mechanischen Eigenschaften der verjüngten Diblockcopolymerer durch niedrige Bruchdehnungen über Zugfestigkeitstests nachweisen. Im vorherigen Kapitel wurde die aufeinanderfolgende statistische Copolymerisation von Styrol und Isopren in einer Ein-Topf Reaktion genutzt, um verjüngte Multiblockcopolymerer als zähe Materialien zu erhalten. In diesem Kapitel wurden binäre Mischungen von verjüngten Diblock- und Multiblockcopolymeren untersucht. Der Erhöhung des Multiblock-Gehalts in der Mischung führte zu einem gewissen Ordnungsverlust. Bereits eine geringe Menge der zugesetzten Multiblockcopolymerer wandelte die Diblockcopolymerer jedoch in zähe und elastische Materialien um, was den Effekt verbrückter Domänen in der Festkörper Morphologie veranschaulicht. In Abhängigkeit des Mikrodomänenabstands der einzelnen Blockcopolymerer wurden mischbare, teilweise mischbare und unmischbare Zusammensetzungen über SAXS beobachtet (Kooperation mit Prof. George Floudas). Anschließend wurden die Folgen der Mischbarkeit systematisch

über Zugfestigkeitsversuche untersucht. Überraschenderweise führten selbst stark voneinander abweichende Domänengrößen der Diblock- und Multiblock-Komponente nicht zu einem signifikanten Verlust der mechanischen Eigenschaften.

Kapitel 4. Um definierte Blockstrukturen über Multistufensynthesen zu erhalten, ist es notwendig die darauffolgende Monomerzugabe durchzuführen, wenn das Monomer vom vorherigen Zugabeschritt nahezu vollständig umgesetzt wurde. Die Reaktionszeit wird daher zu einem entscheidenden Parameter bei der Optimierung der Polymersynthese. In der statistischen Copolymerisation kann jedoch eine einfache Erhöhung der Temperatur das Profil des Gradientens beeinflussen. Dies ist den verschiedenen Aktivierungsenergien individueller Polymerisationsraten geschuldet. In enger Zusammenarbeit mit [REDACTED] wurde erstmals *in situ* Nah-Infrarot (NIR) Spektroskopie genutzt, um die einzelnen zeitabhängigen Monomerumsätze von Styrol und Isopren während der Copolymerisation abzuleiten. Durch die präzise Auswertung von Polymerisationsraten im Bereich von 10 bis 60 °C, wurden die jeweiligen Aktivierungsenergien bestimmt. Dies erlaubte die Vorhersage von Gradientenprofilen über kinetische Monte Carlo Simulation, wodurch ein fundamentales Verständnis der experimentellen Beobachtungen resultierte: Beispielsweise die Änderung einer Festkörper-Morphologie eines Copolymers (Kooperationen mit [REDACTED]), welches bei höherer Temperatur synthetisiert wurde. Mittels Echtzeitüberwachung wurden Änderungen in der Monomerkonzentration verfolgt. Um die Stärke der NIR Methode zu demonstrieren wurde die erfolgreiche Synthese eines Decablockcopolymers, wie in Kapitel 2 beschrieben, verifiziert. Zusätzlich erlaubte die hohe zeitliche Auflösung der Nah-Infrarot Spektroskopie die erfolgreiche Überwachung einer Copolymerisation beschleunigt und modifiziert durch Tetrahydrofuran (THF) als Additiv. Dieses Konzept wurde im anschließenden Kapitel weiter vertieft.

Kapitel 5. Die Alkylithium-initiierte Copolymerisation von Styrol und Isopren in polaren Lösungsmitteln verläuft mit merklich unterschiedlicher Kinetik verglichen zur Polymerisation in Kohlenwasserstoffen. In diesem Kapitel wird die hohe zeitliche Auflösung der Echtzeit NIR Spektroskopie genutzt (etabliert in Kapitel 4), um die individuellen Monomerkonzentrationen von Styrol und Isopren während der Copolymerisation in Anwesenheit des polaren Additivs THF zu verfolgen. In Zusammenarbeit mit Tobias Johann wurde festgestellt, dass eine Erhöhung des THF-Anteils zu einer Invertierung der Reaktivitätsparameter führt. Es wurden Copolymere mit verjüngten, gradientenartigen und zufälligen Verteilungen sowie die entsprechenden invertierten Monomersequenzen erhalten. Deren systematische Untersuchung führte zu einem grundlegenden Verständnis der Folgen von Monomersequenzstatistiken auf thermische, morphologische und mechanische Eigenschaften über Dynamische Differenzkalorimetrie (DSC), TEM (durch [REDACTED]), SAXS (durch Prof. George Floudas) und Zugfestigkeitsmessungen. Letztendlich wurde eine

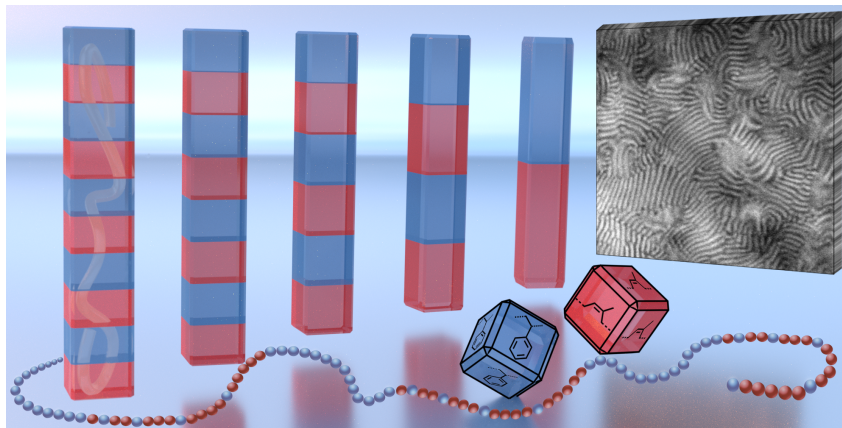
Synthesestrategie vorgestellt, um die untersuchten Comonomersequenzen als Gradientenblock zur Phasenkompatibilisierung in weit-verbreitete SIS Blockcopolymeren einzubauen.

Mit den in Kapitel 4 und 5 vorgestellten Erschließung der Nah-Infrarot Echtzeitüberwachung, ist dieses Messprinzip in unserer Forschungsgruppe als Mittel der Wahl zur Verfolgung der lebenden Anionischen Copolymerisation von 1,3-Dienen mit Styrolderivaten in sowohl polaren, als auch Kohlenwasserstoff basierten Lösungsmitteln etabliert. Aktuell wird dieses Konzept in mehreren weiterführenden Projekten genutzt, um auch in Zukunft zum Verständnis von Synthese und Eigenschaften komplexer Polymerarchitekturen beizutragen.

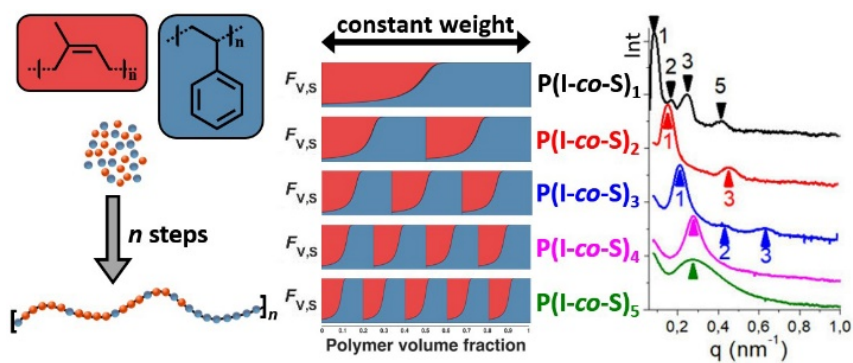
Appendix 1. Diese Arbeit stellt eine Weiterführung der Studien zu den verjüngten Di- und Multiblockcopolymeren auf Basis von Styrol und Isopren dar (Kapitel 2 und 3) und wurde in Zusammenarbeit mit Prof. George Floudas durchgeführt. In einer verjüngenden Comonomersequenz werden die Dipolmomente von Polyisopren-Wiederholungseinheiten entlang der Kette durch dielektrisch inaktive Polystyrol-Wiederholungseinheiten unterbrochen. Dielektrische Spektroskopie wurde benutzt, um lokale und (Unter)Kettendynamiken von Polyisopren in Polyisopren/Polystyrol basierten Copolymeren zu untersuchen. Es wurde ein bemerkenswerter Einfluss der verjüngten Schnittstelle auf die Kettenrelaxation des Polyisoprens gefunden. Die beobachtete Bewegung von Polyisopren-Wiederholungseinheiten längerer Maßstäbe resultierte hauptsächlich von den Polyisopren-Unterketteneinheiten mit einem freien Kettenende. Die Ergebnisse wurden ebenfalls mit Copolymeren auf Basis von Isopren und 4-Methylstyrol verglichen. In qualitativer Übereinstimmung mit Ergebnissen der kinetischen Monte Carlo Simulation wurde die Beteiligung längerer Polyisopren Unterketten in den Dynamiken der 4-Methylstyrol basierenden Copolymeren gefunden. Dies führte zu einem fundamentalen Verständnis der Segmentlängenverteilung in verjüngten Di- und Multiblockcopolymer Architekturen.

GRAPHICAL ABSTRACT

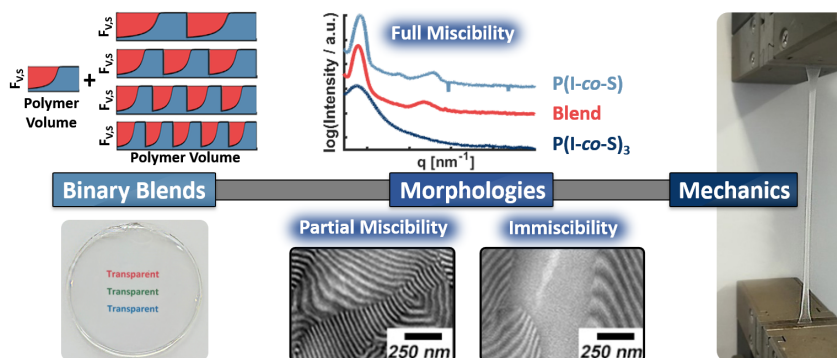
CHAPTER 1 | Rational Design of Thermoplastic Elastomers



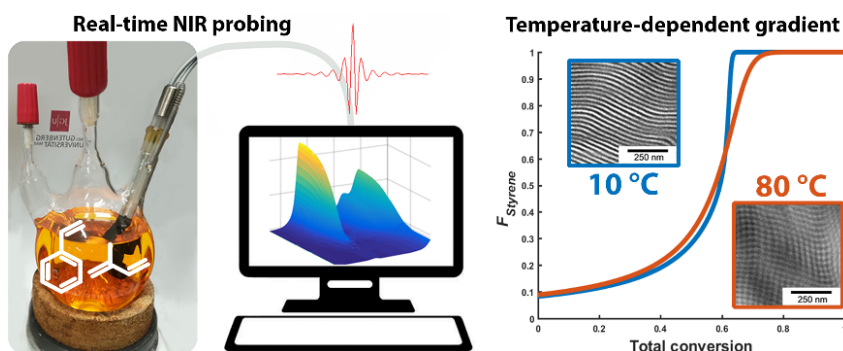
CHAPTER 2 | Tapered Multiblock Copolymers



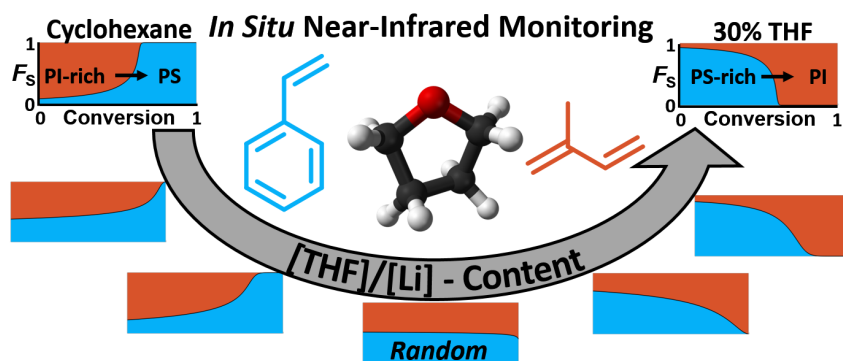
CHAPTER 3 | Tapered Multiblock Copolymer Blends



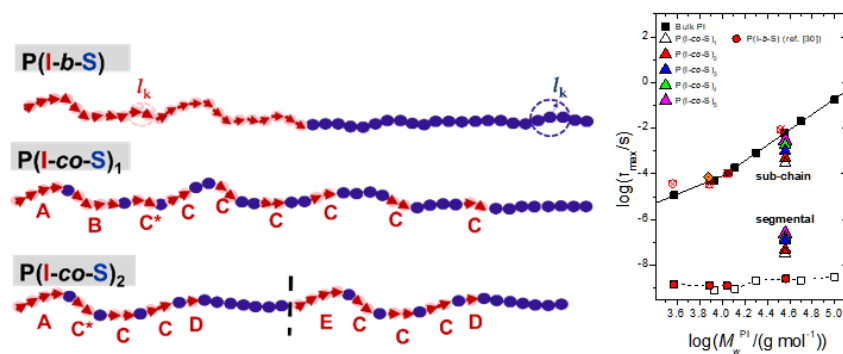
CHAPTER 4 | Near-Infrared Probing and Temperature Effects on Copolymerization Kinetics



CHAPTER 5 | THF - A "Randomizing" Additive?



APPENDIX | Chain Relaxations in Tapered Multiblock Copolymers



CHAPTER 1

RATIONAL DESIGN OF THERMOPLASTIC ELASTOMERS

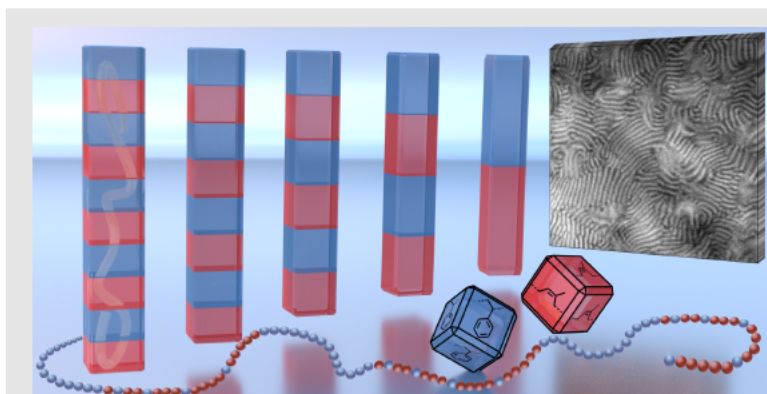
CHAPTER 1

To be Submitted

Rational Design of Thermoplastic Elastomers: Comonomer- and Block Sequence Control in Tapered Multiblock Copolymer Architectures

Marvin Steube¹, Tobias Johann¹, Axel H.E. Müller¹ and Holger Frey^{1*}

¹Department of Chemistry, Johannes Gutenberg-University, Duesbergweg 10-14, 55128 Mainz, Germany



Thermoplastic Elastomers (TPEs) combine features of both vulcanized thermoset rubbers and thermoplastic materials in their phase separated microdomain structure. As a consequence soft, flexible and resilient materials are obtained, which can be high-speed processed in the melt state. In the last decades, a broad variety of polymerization techniques

evolved and were proven successful for the synthesis of block copolymers for TPE materials on industrial scale. Motivated by the outstanding properties of natural rubber (*cis* 1,4-polyisoprene), the alkyllithium initiated anionic polymerization of isoprene and butadiene was investigated and found to proceed in the absence of termination reactions. This enabled the synthesis of formstable, elastic block copolymers based on styrene and 1,3-dienes, which do not require chemical crosslinking. Since then, the "living" character of the carbanionic chain end was utilized in numerous studies to synthesize rather complex, defined comonomer sequences by multi-step synthesis. The systematic variation of numerous parameters, as for example the block size and sequence allowed to correlate the resulting mechanical and morphological properties. This review addresses individual parameters of the molecular architecture to enable a general understanding for the design of TPE materials with tailor-made properties. Additionally the statistical copolymerization kinetics is highlighted as the method of choice to synthesize rather complex monomer sequences in a single step. For this purpose, on-line spectroscopic methods are presented which enable to track the monomer consumption during the polymerization. To enable a precise insight into the comonomer composition of the formed chains, an overview of the theory of copolymerization and the determination of reactivity ratios is given. To further extend the understanding of the comonomer sequence, the kinetic Monte Carlo simulation (kMC) is presented as a versatile tool. Utilizing the experimentally determined kinetic rate constants the polymerization can be performed in silico. This enables access to numerous parameters, as for example the conversion as a function of the time as

well as the the composition and monomer-by-monomer sequence in individual chains, which allow a rational design and evaluation of synthetic experiments.

Introduction

Elastomers are based on covalently crosslinked macromolecules, named after their outstanding elastic recovery in response to macroscopic deformation.¹ The first elastomers were based on natural rubber and used as early as 1600 BC by ancient mesoamericans.² The crosslinking process is essential to transform the sticky chicle into a soft and form-stable material. At this time, this was achieved by mixing the latex of a the rubber tree (*Castilla elastica*), consisting of *cis* 1,4 polyisoprene (PI), with plant juice (*Ipomoea alba*) to form solid rubber balls.^{2,3} In 1839 Charles Goodyear patented the hardening of rubbers, later called "vulcanization",^{4,5} which describes the covalent crosslinking of natural rubber by thermal processing with sulphur and white lead ($2\text{PbCO}_3 \cdot \text{Pb(OH)}_2$).^{6,7} Nowadays, the reaction is known to crosslink linear polyisoprene chains by the intermolecular replacement of C-H bonds by sulfur chains and is still used for certain materials, e.g. hockey pucks or mouthpieces for instruments.⁸

1 From Buna to Tapered Triblocks – The History of Elastic Compounds

Only one year after the development of the vulcanization process Robert William Thomson presented the first air-filled rubber tire, consequently leading to an increasing demand for natural rubber. In 1860 G. Williams was able to isolate a substance, he named isoprene, from caoutchouc (\approx *cis* 1,4-PI) as well as guttapercha (\approx *trans* 1,4-PI). 50 years later, Matthews made the essential observation of a viscous solid with rubber-like properties, by storing isoprene in the presence of sodium metal⁹ and patented the fabrication of synthetic rubber in Great Britain.¹⁰ Only two months later, the German company Bayer registered the same innovation independently. In 1911 Matthews also acquired a German patent, forcing Bayer to withdraw their registration.¹¹ Not until 15 years later, the alkali metal initiated anionic polymerization became patent-free and was in the focus of the company IG Farben.¹² Within the next 2 years the heterogenous sodium initiated polymerization of butadiene was driven to synthetic rubbers of different molecular weights (Buna 32, Buna 85 and Buna 115) and mainly used for tire production.¹³ In 1937 also potassium metal was used in the technical scale.¹⁴ At the same time (1929), Walter Bock invented the radical emulsion polymerization for styrene-butadiene rubbers (DIN/ISO 1629 SBR), with superior properties for the use as tire materials. However no sodium was involved in the synthetic process, the product was later commercialized as Buna S by IG Farben and highly used for the production of tires during the second world war.^{13,15}

1.1 The Development of Thermoplastic Elastomers (TPEs)

The possible drawback of the vulcanization process is the covalent, irreversible crosslinking of chains, which does not allow for recycling (*i.e.* reshaping of the material) or thermal processing.^{16,17} Starting from fundamental blending experiments on elastic compounds in the late 1930s, within the next 30 years immense progress in the synthetic chemistry finally enabled to install elastic properties in block copolymer architectures. Physically crosslinked elastomers have since then been revealed as an attractive alternative for the chemically crosslinked rubber materials. A fundamental understanding of polymer miscibility and block compatibility finally resulted in the nowadays well-known class of thermoplastic elastomers (TPEs). In these materials, the issue related to irreversible crosslinking is solved by the modification of the elastomers with glassy blocks. As a consequence of chemical incompatibility, the adjacent blocks microphase separate in the bulk state and thereby pin the rubbery mid-block. These vitrified domains act as crosslinks and allow for thermoreversible melting.

The first fundamental observations were made in the late 1930s by blending liquid plasticized PVC (polyvinylchloride) with NBR (acrylonitrile-butadiene rubber).¹⁸⁻²² As a consequence, elastic materials with rubber-like properties were obtained which did not require vulcanization. The major breakthrough was achieved with the discovery of the diisocyanate polyaddition reaction in 1937, followed by the invention of elastic linear copolyesters 15 years later.^{23,24} Combining these principles allowed the synthesis of polyesterurethane based elastomers, composed of soft (*i.e.* flexible polyester chains) and hard polyurethane segments (*i.e.* physical crosslinks). The latter is usually formed by the addition of so-called "chain extenders" (*e.g.* water or low molecular weight diols), which react with the diisocyanate to form polar, crystalline urethane based structures.²⁵ The processability allowed to make fibers by melt extrusion or spinning from solution that retained excellent elastic properties of elastomers.^{26,27} Hence these polyester-urethane based structures can be considered as the first thermoplastic elastomers (TPEs). Commercial polyurethane-based TPEs (also known as TPUs) were introduced in the 1960s by B.F. Goodrich, Mobay, Upjohn, Bayer A.G. and Elastogran and nowadays still in the focus of interest.¹⁸

1.2 The Living Anionic Polymerization

Another milestone was set by Michael Szwarc, who discovered the living anionic polymerization in 1956. This reaction proceeds without chain termination or transfer reactions.^{28,29} The living nature of the anionic chain end was confirmed, based on the observed increase in viscosity upon the consecutive addition of a styrene solution after completion of the previous polymerization step. Although triblock copolymers were synthesized, the sequence of monomer addition steps resulted in an unfavoured ISI block sequence (section 2.4). In addition, the bifunctional

sodium naphthalenide initiator required THF as a solvent, resulting in a high content of the 3,4-PI regioisomer and consequently a glass transition temperature (T_g) raised to ambient temperature (undesired).³⁰ Since the research on polyisoprene elastomers via anionic polymerization targeted high *cis* 1,4-PI content (*i.e.* the natural rubber structure), the elastomer research groups were not interested in the polar solvent systems used by Szwarc.^{30,31} Only one year later Hsieh and Tobolsky reported a method for the homogenous initiation of isoprene by replacing the lithium metal by *n*-butyllithium.³² They also observed the desired, nearly exclusive formation of the *cis*-1,4 structure when the reaction was performed in *n*-heptane, as well as the increased content of 3,4-PI in diethyl ether and THF.³²⁻³⁴ Later in that year, Porter combined the principle of alkyllithium initiation and the living nature of the monofunctional carbanions to produce SBS block copolymers with the desired high *cis*-1,4 PI content.³⁵ In 1958 Phillips Petroleum Company patented the polymerization of styrene, butadiene and the respective copolymerization.^{30,31,36} Already at that time, the amount of styrene incorporation was estimated to increase with conversion, leading to a gradient structure, the so-called "tapered" blocks (shown for P(I-co-S) in Figure 1).³⁷ Similar to PI-*b*-PS block copolymers obtained by consecutive polymerization steps, this structure possesses a block-like character, which enables phase separation. However, instead of a pure polydiene block, a polydiene-rich copolymer block is formed, increasing in its styrene content until a pure PS block is present ($F_{V,S} \approx 10\%_{\text{mol}} 100\%_{\text{mol}}$). Such types of block-like architectures were later found to be attractive to design the phase behaviour of block copolymers in TPEs (section 2.5).³⁸⁻⁴¹ In 1960, shortly after Ziegler's discovery that suspensions obtained by treating TiCl_4 with Et_3Al can polymerize ethylene, Horne and colleagues patented the synthesis of polyisoprene based on a similar process.⁴² A larger 1,4-*cis*-PI content was achieved by this process ($\approx 96\%$) compared to the lithium metal and alkyllithium initiated polymerizations ($\approx 85\text{-}92\%$).^{32,43,44} Two years later, Holden and Milkovich of Shell Co. produced ABA triblock copolymers relying on both polyisoprene and polybutadiene as flexible component.³⁷ They also utilized the statistical copolymerization to produce tapered triblocks (Figure 1) and showed that both the non-tapered and tapered block architectures are thermoplastic elastomers.³⁷ In 1965 a series of triblock copolymers was introduced as a commercially available product with the trademark "Thermolastic", which was later changed to Kraton and can be considered as the first commercialized TPEs produced by living anionic (co)polymerization.³⁷

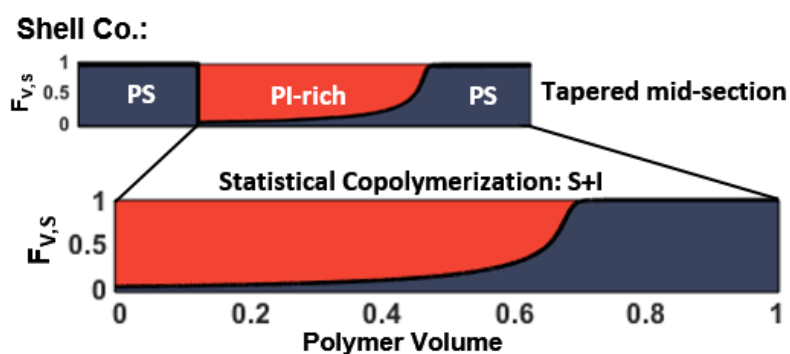


FIGURE 1 Top: Visualization of a tapered SIS block copolymer. Bottom: Highlighted gradient profile (*i.e.* $F_{V,S}$ as a function of the polymer volume; $F_{V,S}$: Instantaneous styrene volume incorporation) of a tapered block copolymer, obtained by statistical copolymerization (alkyllithium initiation; hydrocarbon solvent).

In the last decades, the living anionic polymerization has shown to be an effective tool to correlate comonomer sequences with properties of the resulting materials.⁴⁵ The “living” nature of the anionic chain ends allows to adjust block sequences by consecutive addition of monomers or monomer mixtures with defined molecular weights and narrow distributions (usually $\mathcal{D} > 1.1$).

2 Rational Design of Sequence-Controlled TPEs

Over the last decades, the control of the comonomer sequences has turned out to be crucial for the development of macromolecules with defined properties.^{46–48} For example biomacromolecules (*e.g.* nucleic acids, proteins or silk) with controlled chirality and sequences act as key components in our everyday life.⁴⁶ Usually rather demanding and timeconsuming strategies, are applied for the synthesis of uniform, monodisperse ($\mathcal{D} = 1$) *sequence-defined* macromolecules.^{49,50}

In contrast, the synthesis of TPE materials usually relies on rather simple, albeit straightforward processes, leading to non-uniform, multidisperse ($\mathcal{D} > 1$; usually $1 < \mathcal{D} \leq 1.4$ for chain-growth polymerization techniques), *sequence-controlled* materials. For example, in the living anionic polymerization, consecutive monomer addition steps, or copolymerization reactions are employed to control the copolymer gradient to determine the resulting properties on an industrial scale. The variety of parameters (*e.g.* monomer composition, comonomer sequence, topology) lead to a rather broad range of accessible properties, which need to be tailored to the final application. An overview of their consequences on morphologies and mechanical properties is given in the following sections.

2.1 Choice of the Monomers

Although the living anionic polymerization can be utilized to produce acrylate-based TPE materials (e.g. Kurarity from Kuraray),^{51,52} the polymerization of 1,3-dienes (low T_g component) with styrene derivatives (high T_g component) is usually the method of choice.^{47,53} While the latter typically shows full monomer conversion in the absence of side-reactions ($T_{\text{polym.}} \approx 20\text{-}80\text{ }^\circ\text{C}$; alkyllithium initiation, hydrocarbon solvents),⁵⁴⁻⁵⁸ the polymerization of (meth)acrylic monomers requires tailored reaction conditions (low temperatures, less nucleophilic and sterically hindered initiators, Lewis Base or Lewis acid ligands), depending on the monomer in order to avoid reaction of the active anions with the carbonyl group.⁵⁹⁻⁶² As the high stability of the acrylate-based anionic species impedes the controlled crossover reaction (Scheme 1) to styrene or (non-functional) 1,3-dienes, the polymerization of the acrylate has to be initiated by the more reactive polystyryllithium or polydienyllithium species.⁶³ In addition, bifunctional initiators, coupling strategies or macromonomer approaches can be used to widen the scope of accessible block sequences (section 2.4) and chain topologies (section 2.6). However, in terms of the resulting material properties limitations are not only set by the controlled (co)polymerization.

In the polymerization of 1,3-dienes the *cis* 1,4 repeating unit (Figure 2a) is preferred due to its low T_g , high thermal stability and low entanglement molecular weight. Consequently, functionalized heteronuclear 1,3-dienes are usually avoided, as they tend to coordinate the lithium atom, increase the side-chain vinyl content and consequently the T_g (i.e. "randomizer-effect" (section 3.1). Nevertheless it has to be noted that a high vinyl content is sometimes desired for post-polymerization modification reactions⁶⁴⁻⁶⁷ or to suppress crystallization, which is especially pronounced in the hydrogenated 1,4-polybutadiene.⁶⁸ Cyclic 1,3-dienes (e.g. 1,3-cyclohexadiene⁶⁹⁻⁷¹ or benzofulvene⁷²⁻⁷⁴) are less attractive as rubbery component TPE materials, as the polymerization leads to covalently bridged backbone atoms and a rather high T_g .⁷⁵⁻⁷⁹ However, depending on the microstructure composition (i.e. use of hydrocarbon or polar solvent during the polymerization; section 3.1), they can serve as high T_g component.⁷⁹

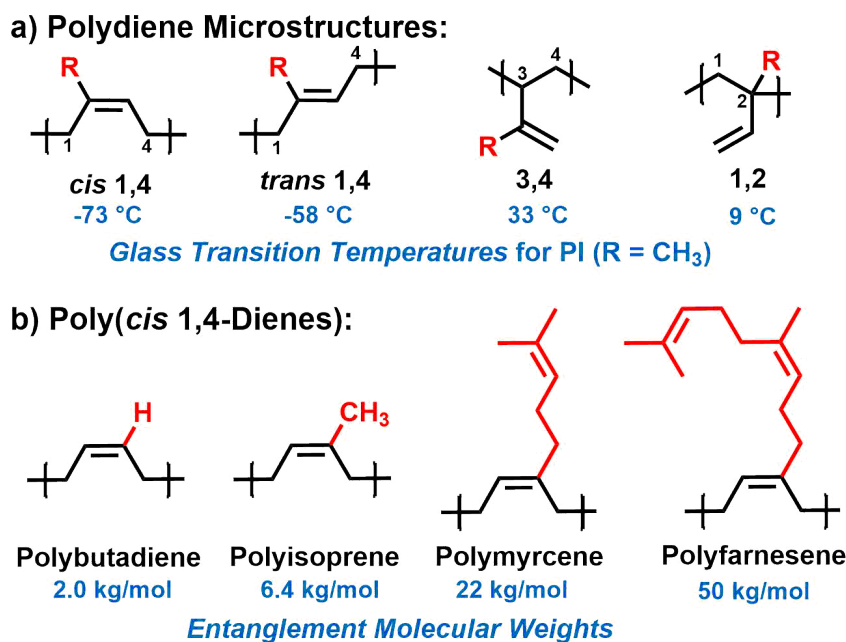


FIGURE 2 a) Stereo- and regioisomers of polydienes. b) Selection of polydienes obtained by living anionic copolymerization and their entanglement molecular weights.^{80–83}

Considering these limitations, the choice of 1,3-dienes comprises the structures shown in Figure 2. By increasing the length of the side-chain from polybutadiene to polyfarnesene, an increase of the entanglement molecular weight from $M_e = 2.0$ to 50 kg/mol is observed.^{80,81} This shifts the topology stepwise from a linear chain to a graft copolymer architecture, also resulting in remarkably different properties (section 2.6). Due to their good accessibility in large quantities and low entanglement molecular weight, polyisoprene and polybutadiene are currently by far the most prominent examples of synthetic rubbers. Compared to polyisoprene, the lack of solely one methyl group in butadiene leads to a strong lowering of the entanglement molecular weight by a factor exceeding 3.⁸⁰ However, this also contributes to its difficult handling ($T_{\text{boiling}} \approx 4$ °C) as well as the undesired crystallization in the hydrogenated state.⁶⁸

Also, the choice of the styrenic, high- T_g component has to be carefully considered. Also in this case, heteroatoms are able to coordinate the lithium atom leading to a comparably large vinyl content of the polydiene in the copolymerization or subsequent polymerization steps. Alkyl-substituted styrene derivatives contain acidic benzylic protons that can participate in chain transfer reactions. However, poly(4-alkyl styrene) homo- and copolymers with controlled, predictable molecular weight and narrow molecular weight distribution can be prepared when the temperature is maintained at room temperature or below.^{84–90} As shown for the poly(4-methyl styrene)/PI and the poly(4-*tert*-butyl styrene)/PI systems, the use of alkyl-

substituted styrene derivatives implies an increased miscibility for the corresponding block copolymers in general (*i.e.* lower the effective Flory-Huggins parameter; χ_{eff}).^{91,92} Although this can be desired to lower the T_{ODT} (section 2.2) of high molecular weight block copolymers, styrene is still the monomer of choice for polymerizations on the technical scale (*e.g.* low price and good availability). In this context, the manipulation of the monomer sequence (*i.e.* gradient structures) has been established as a powerful alternative to reduce χ_{eff} (section 2.5).⁵³

2.2 Effect of Molecular Weight and Physical Limitations

The strong segregation of block copolymers with flexible, low- T_g blocks and high- T_g blocks results in elastomers that are thermoreversibly crosslinked by vitrified domains. Hence, phase separation is a basic requirement for TPEs. Based on the selfconsistent mean-field theory (SCFT) by Leibler and the randomphase approximation by de Gennes, it is possible to predict the expected phase state for block copolymers (*e.g.* PI-*b*-PS).^{93,94} The molecular weight directly affects the segregation strength, which is quantified by the product $\chi_{\text{AB}} \cdot N$, where χ_{AB} is the Flory-Huggins parameter (*i.e.* enthalpic interaction for the given repeating units of type A and B) and N the degree of polymerization (entropic contributions; $N \sim M_n$). For the phase behaviour of symmetric diblock copolymers, the order-disorder transition (ODT) is predicted for $(\chi_{\text{AB}} \cdot N)_{\text{ODT}} = 10.5$ (Figure 3).⁹³ In general, large molecular weights ($M_n \sim N$) are desired for phase separation, depending on the magnitude of χ_{AB} (typically $M_n \approx 10$ kg/mol for S/I diblock copolymers).⁹⁵ In addition, high block molecular weights exceeding the entanglement values by far are necessary to provide mechanically stable materials via entanglements (Figure 2).⁹⁶

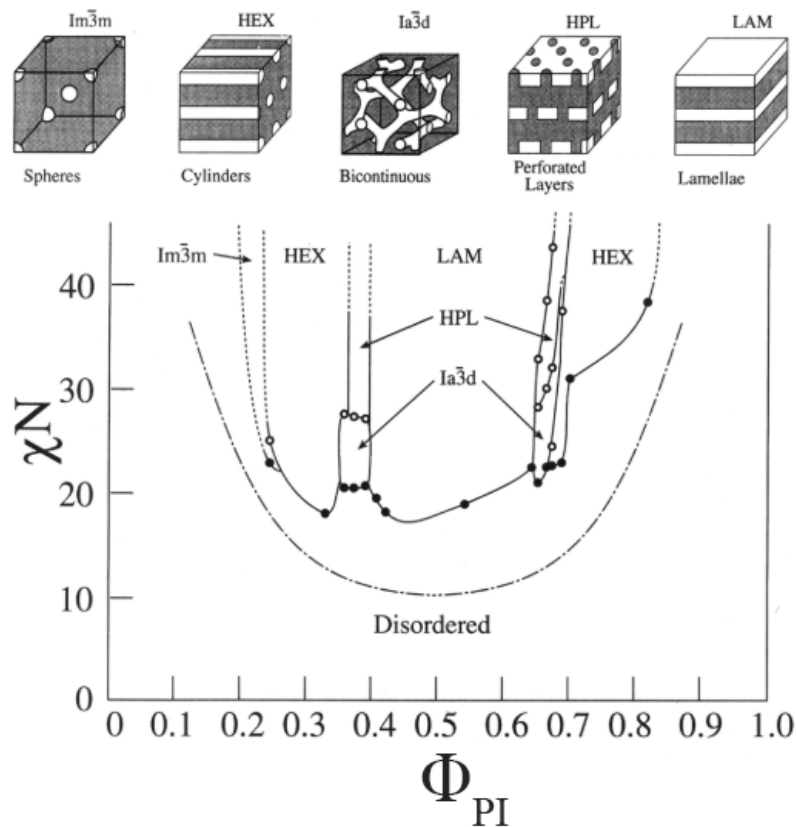


FIGURE 3 Phase diagram experimentally determined for PI-*b*-PS diblock copolymers. Respective morphologies found are illustrated above. The dashed-dotted line is the mean field prediction for the ODT.⁹³ Reprinted (adapted) with permission from A. K. Khandpur, S. Förster, F. S. Bates, I. W. Hamley, A. J. Ryan, W. Bras, K. Almdal and K. Mortensen, *Macromolecules*, 1995, **28**, 8796–8806. Copyright 1995 American Chemical Society.

However, the handling of thermoplastic elastomers typically relies on high-speed processing by melt extrusion. For this purpose disordered melts are preferred in terms of their lower melt viscosities compared to their phase separated analogues.^{53,97,98} The vast majority of hydrocarbon polymers exhibits a pronounced miscibility at higher temperatures due to the temperature dependence of $\chi_{AB}(T)$. The order-disorder transition temperature must be located above the highest glass transition (or melting) temperature of the copolymer. Otherwise, cooling the sample from the disordered state (*i.e.* $T > T_{ODT}$ and $T > T_g$) vitrifies the domains (*i.e.* $T \approx T_g$), which impedes the consecutive self-assembly to macrophase-separated domains at lower temperatures (*i.e.* $T < T_{ODT}$ but $T < T_g$). Hence, carefully adjusting N leads to a T_{ODT} located in between the T_g of high T_g compound but below the degradation temperature of the polymer.⁹⁵ For the most block copolymers this fits in the range of $T_{ODT} \approx 100$ -250 °C.⁸⁰ Taking a volume symmetric PS-*b*-PI diblock copolymer as an example ($\chi_{IS}(T_{ODT}) \cdot N = 10.5$), the T_{ODT} can be calculated in dependence of the molecular weight (Equation Set S1). As visualized in Figure 4, the T_{ODT} (dotted

vertical lines) increase from $T_{\text{ODT}} \approx 130$ °C to ≈ 250 °C by increasing $M_n = 10$ to 18 kg/mol.

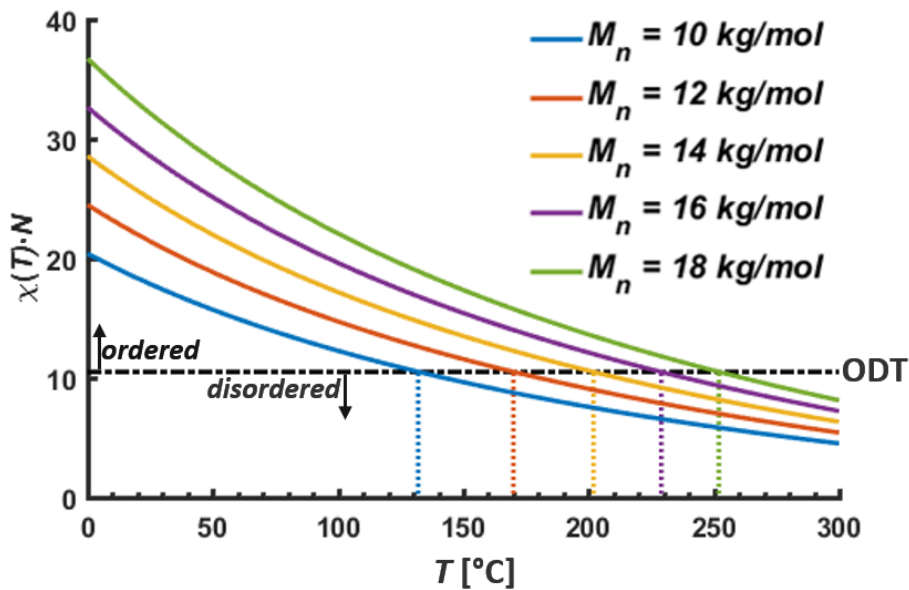


FIGURE 4 Visualization of the phase segregation strength $\chi_{IS}(T) \cdot N$ as a function of the temperature for PI-*b*-PS of different molecular weights ($M_n \sim N$). The dashed-dotted horizontal line is the mean field prediction for the ODT at $\Phi_{PI} = 0.5$.⁹³ Order-disorder transition temperatures for $\chi_{IS}(T) \cdot N = 10.5$ are indicated as a dotted vertical line.

As a consequence, the targeted molecular weight has to be adjusted carefully to the location of the ODT of the respective morphology and $\chi_{AB}(T)$ of the monomer combination. Of course, the latter is a function of several parameters, as for example the chosen monomer combination, the comonomer sequence (section 2.5) and the polymer topology (e.g. linear- or star-type, section 2.6).

2.3 Microdomain Morphologies

The *block volume fraction* ($\Phi_A = 1 - \Phi_B$ for diblock copolymers), directly determines the formed microdomain morphology in the melt. A quantitative interpretation is done by the phase diagram (Figure 3), which assigns Φ_A to the respective morphology for a given value of $\chi_{AB} \cdot N$. In general, the ODT shifts to larger values for asymmetric block volume fractions ($\Phi_{PI} > 0.5$ or $\Phi_{PI} < 0.5$) beyond the classical lamellar phase.⁵⁷ Hence, a change of the block volume fraction can also lead to an ODT for similar molecular weights. Usually phases are distributed asymmetrically around $\Phi_A = 0.5$ explained by differences in the space-filling characteristics (i.e. the conformational asymmetry), which tends to shift the phases aside the value anticipated for symmetric diblocks ($\Phi_{\text{LAM}} = 0.5$).^{57,99}

The microdomain morphology found in the bulk state dictates the resulting mechanical proper-

ties. For example, Cohen *et al.* oriented lamellar morphologies of SBS triblock copolymers and investigated the mechanical properties in dependence of the lamellar orientation.¹⁰⁰ Stretching the lamellae along their axis (parallel orientation), caused the PS layers to break up and release the rubbery layers. In contrast, the perpendicular orientation folded into a "chevron"-like morphology with diagonal orientations. As a consequence, a comparably larger elastic modulus was observed in the case of the parallel orientation. Increasing the asymmetry in the block volumes pronounces curvature of the domains in the melt, which finally leads to order-order transitions (OOTs) from lamellar layers over cylinders to spheres (classical morphologies). Although, in a mathematical sense, an (infinitely thin) lamella is a two dimensional (2-dim) object, it is anisotropic in one dimension only. Following this principle, the cylindrical phase is a 2-dim and the spherical morphology a 3-dim morphology, consequently only leading to fully isotropic properties in the latter case. However, solvent or thermal annealing usually results in random oriented grains leading to anisotropic properties in all cases. In the nonlamellar morphologies, the mechanical properties are usually governed by the matrix (*i.e.* continuous phase). For example, the elastic deformation in a continuous low T_g phase ($\Phi_{\text{elastic}} > 0.5$) can occur without deformation of the high- T_g phase, which leads to a highly reversible elastic deformation. Depending on monomer combination and comonomer sequence, also bicontinuous (non-classical) morphologies are observed (*e.g.* the gyroid structure, space group $Ia\bar{3}d$).⁵⁷ For these structures, an increase of the molecular weight can also lead to an OOT. For these structures a comparably large elastic modulus is observed. This is explained by a bicontinuous morphology, also leading to a 3-dim interconnected continuous high- T_g phase, which must deform as the low- T_g matrix is deformed.¹⁰¹

2.4 Effect of Block Sequences

Either *ABA* or *BAB* triblock copolymers are obtained by further increasing the block number of an *AB* diblock copolymer. It is well-known that this change of the block sequence influences the microphase separation and the affiliated mechanical response. For example, the need to locate two block junctions at the domain interface reduces the conformational entropy. This leads to an increased miscibility of an $A_{n/2}B_mA_{n/2}$ triblock compared to an A_nB_m diblock copolymer (*i.e.* similar chain length).¹⁰²⁻¹⁰⁷ However, compared to a $A_{n/2}B_m$ diblock obtained by hypothetically snipping the triblock into half, phase separation is facilitated for the triblock copolymer as revealed in experimental and theoretical studies. This trend follows by further increasing the block numbers to multiblock copolymers (see later in this section).

In triblock copolymers, the presence of a midblock enables different chain conformations.¹⁰⁸ Whereas in the *bridged conformation* both block junctions are tethered to different inter-

faces, both end blocks reside in the similar microdomain in the *looped conformation* (Figure 2). The bridging and looping fraction can have a significant influence on the equilibrium morphologies.^{55,109,110} As shown by Spontak *et al.*, the bridging conformation leads to a comparably larger reduction in the equilibrium domain sizes than the looping conformation.¹¹⁰

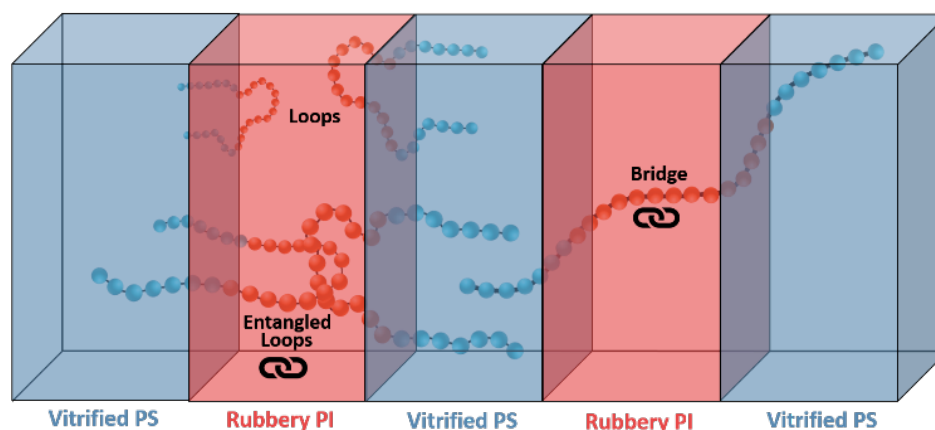


FIGURE 5 Top: Visualization of a tapered SIS block copolymer. Bottom: Highlighted gradient profile (*i.e.* $F_{V,S}$ as a function of the polymer volume; $F_{V,S}$: Instantaneous styrene volume incorporation) of a tapered block copolymer, obtained by statistical copolymerization (alkylolithium initiation; hydrocarbon solvent)

Although changes in the phase behavior are evident, they are less significant in comparison to those observed in the mechanical properties of SIS triblock copolymers.^{96,111-113} Here, the bridged midblocks connect the vitrified domains beyond entanglements and thus enhance the mechanical properties of the copolymer.^{102,109,112,114-116} As a consequence the fraction of bridged midblocks ($\approx 45\%$) is of particular interest and focus of several studies.^{56,109,117-120} For example Bates *et al.* were able to favour the bridged (or looped) conformation, in dependence of the applied shear rate and amplitude. This resulted in an orientation of the lamellar domains in the perpendicular or parallel orientation.^{116,121}

By comparing the SIS with the inverted ISI block sequence, significant differences are found in their elastic and rheological behaviour.^{96,113} The mechanical properties of the SIS architectures show comparable results to PI vulcanizates (SBR rubber), and can be considered as a recyclable, melt-processable alternative.¹²² In contrast, "crosslinking" in ISI triblock copolymers occurs via flexible, low- T_g endblocks, which undergo chain-pullout in the respective domains.^{108,123}

Theoretical results of Matsen *et al.* indicate that even the symmetry of the triblock copolymer (*i.e.* the relative size of the two end blocks) and the total composition play a crucial role on the morphology.^{111,112} Comparable experimental results were obtained by Spontak *et al.*, who demonstrated that the T_{ODT} s of SIS triblock copolymers are also sensitive to the individual vol-

ume fractions of the endblocks for a similar total composition.¹²⁴

A reasonable attempt to increase the number of bridges by the design of the molecular architecture is manifested in the so-called *multiblock copolymers* $(AB)_n$. Until the 90s almost all multiblock copolymers were synthesized by condensation reaction of one type or another.¹⁷ Unfortunately the fundamental concept of the step-growth polymerization leads to a high dispersity ($\mathcal{D} \leq 2$) as well as a non-defined product (mixture of different block-numbers), which hampered the systematic investigation of the molecular architecture. Although defined multiblock copolymer architectures produced by the consecutive multi-step chain-growth polymerization method was already described in 1960, the found examples are rather rare.¹²⁵⁻¹²⁸ Since the 1990s Spontak, Bates and others have demonstrated how to overcome the issue of preliminary termination of the highly sensitive carbanionic chain end and investigated the phase behavior and the dynamic-mechanical properties of defined $(AB)_n$ multiblock copolymers based on styrene and isoprene.^{56,110,129,130} Bates *et al.* found an increased immiscibility for multiblock copolymers with increasing block number and constant block size (*i.e.* increasing chain length; Figure 6b).¹³¹ Spontak *et al.* investigated a series of multiblock copolymers, with a similar chain length and a series with constant block length (Figure 6). Although a contraction of domain sizes is expected for the series with decreasing block sizes (Figure 6a), even the domain sizes of multiblock copolymers with a constant block size were found to decrease with increasing block number (Figure 6b).^{56,110} This was explained by the increased number of bridged PI blocks caused by the multiblock architecture, which also lead to superior mechanical properties (*e.g.* increase of the Young's modulus and the strain at break). In the following years, the unique morphological and mechanical behavior of styrene/isoprene based multiblock copolymers was in focus of numerous studies.^{53,116,129,131-138} In 2018 and 2019 our group published the synthesis of tapered multiblock copolymers based on styrene (or 4-methyl styrene) and isoprene by consecutive copolymerization steps (a tapered diblock is visualized in Figure 1).^{85,91,139} In this case, the multiblock architecture resulted in increased toughness, whereas the "multigradient" comonomer sequence lowered χ_{IS} and allowed to reduce the T_{ODT} in the accessible range for block molecular weights far beyond the entanglement molecular weight (*e.g.* $T_{ODT} \approx 185$ °C for $P(I-co-S)_3$ with $M_{n,total} \approx 240$ kg/mol).¹³⁹

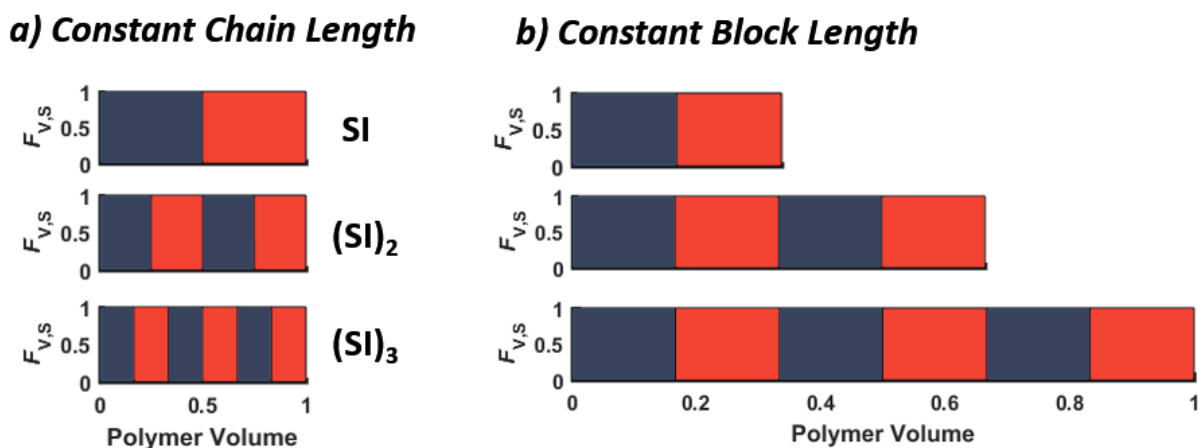


FIGURE 6 Visualization of $(AB)_n$ multiblock copolymers with $n = 1-3$. a) Increasing the number of blocks leads to a decrease of the block length. b) Increasing the number of blocks leads to an increase of the chain molecular weight.

2.5 Copolymer Blocks – Adjusting the Phase Behaviour

In theory, the consecutive polymerization of two monomers allows to realize every comonomer sequence by multi-step reactions. In practice, the experimental effort increases with the monomer addition steps, the targeted molecular weight and the reaction time.¹³⁹ This sets limitations based on the effort and skill of the synthetic chemist.¹⁴⁰ The statistical copolymerization has been proven as an excellent tool to design otherwise rather exhausting comonomer sequences in a single step. These are usually classified as block, gradient or alternating copolymers.

Since 1958 up to now the alkyllithium initiated copolymerization of 1,3-dienes with styrene has been of industrial and academic interest.^{36,37,141,142} The resulting "tapered" block structure is considered as an polybutadiene block copolymer containing a small amount of styrene followed by a polystyrene block.¹⁴³ The term "tapered block copolymer" was introduced by Geoffrey and Milkovich of Shell Co. to account for both the gradient as well as the block-like sequence (Figure 1).³⁷ In the following years, the copolymerization kinetics and the resulting comonomer sequence were focus of several studies.^{141,142,144-146} In extensive work, Kraus compared the influence of the comonomer sequence on thermal and dynamic-mechanic properties of block, tapered block and random copolymers and found an increased miscibility (e.g. single T_g s) for random and tapered copolymers.^{144,147,148} Cirilin reported the substantial interfacial mixing to play a key role during mechanical failure of TPEs.¹⁴⁹ To estimate the degree of segregation and account for the reduction in the enthalpic incompatibility by the polymer composition, the effective Flory-Huggins parameter ($\chi_{AB,eff}$) was introduced according to the binary interaction theory.^{115,150-152} This reduction of χ_{AB} to $\chi_{AB,eff}$ was utilized in 1983 by Gronski *et al.* who synthesized IS block

copolymers with varying length of random P(*IranS*) copolymer midblocks (Figure 7a). This allowed to investigate the dynamic-mechanic properties by systematically increasing the volume fractions of the interphase.¹⁵³⁻¹⁵⁵ In contrast, Hadjichristidis *et al.* used tapered copolymer midblocks with the gradient profile visualized in Figure 1. In accordance to the results of Gronski, the size of the copolymer midblock enhanced the compatibility in the system. Furthermore, the stronger reduction of χ_{eff} for the inverse tapered systems in comparison to the tapered systems (Figure 7b) was explained by the opposite block sequencing (*i.e.* the discontinuity in the gradient profile $F_{V,S}$ vs. polymer volume; Figure 1). Hence, beyond the size, also the gradient profile (*i.e.* the comonomer sequence) of the copolymer block dictates the phase behavior¹⁵⁶ and allows to adjust the resulting thermal and mechanical properties by another independent parameter.

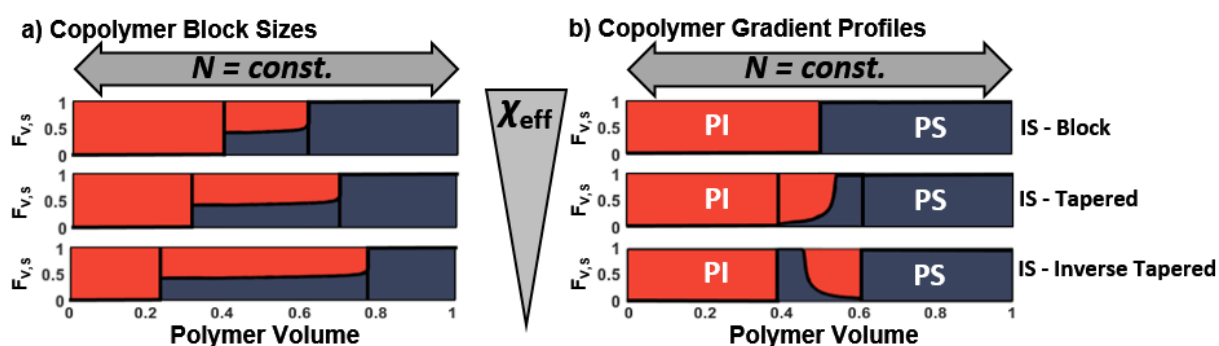


FIGURE 7 Parameters, which influence the effective Flory-Huggins Parameter (χ_{eff}) for a given monomer pair. χ_{eff} was found to decrease with a) the copolymer block size and b) the copolymer gradient profile.

2.6 Non-Linear Chain Topologies

Beyond the classical linear chain topology, also star and brush block copolymers are successfully established TPE materials. These topologies can be obtained by coupling strategies, multifunctional initiators or synthetic approaches relying on macromonomers and can show remarkably different properties.^{59,79,157,158}

By comparing a *block copolymer* of a star $(AB)_n$ type with the AB linear-type arms (compare structure SI linear and $(SI)_4$ star in Figure 8), an increased immiscibility is observed for the star-type architecture in theoretical and experimental studies.^{59,159-161} Phase diagrams obtained by SCFT calculations show similar microdomain morphologies as found for the diblock analogues.^{57,162} However, the found asymmetry in the phase diagram shows a preference for the inner block of the arms to locate inside of the cylindrical or spherical structure.^{59,162}

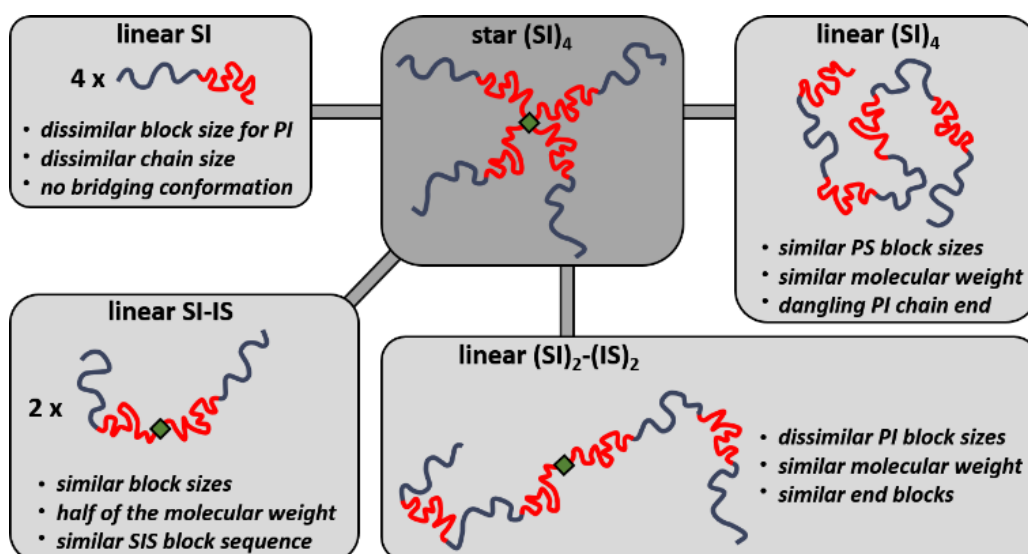


FIGURE 8 Comparison of a (SI)₄ star topology with linear di-, tri- and multiblock analogueous structures (grey: PS-chain; red: PI-chain). Symmetries, which allow the use of a coupling agent are indicated by a green diamond.

An increase of mechanical properties is observed for this kind of coupling experiments. However, in this case the coupling reaction (*i.e.* formation of (SI)₄ star) increases the molecular weight and enables bridging of the PI midblock. Hence the observed toughening cannot be solely attributed to the star architecture and is also a function of the SIS block sequence and the increased molecular weight (entanglements), obtained with a bifunctional coupling reagent (structure SI-IS linear in Figure 8). for the linear coupling of polymer chains. Hence, this affect cannot be solely ascribed to the star topology. It is also a consequence of the SIS block sequence (section 2.4) and the increasing molecular weight (*i.e.* entanglements; section 2.2).

Consequently, the linear coupled analogue ((SI-IS)₂ linear in Figure 8) serves for a better comparison with the (SI)₄ star. In contrast to theoretical expectations,¹⁶³ the confined star architecture leads to an increased miscibility compared to the linear analogues.^{164,165} Fetters *et al.* compared the mechanical characteristics of (IS)_n star block copolymers with their linear SIS type analogues.¹⁶⁶ They found that these star block copolymers had superior tensile properties compared to their linear SIS analogues, saturating when the number of arms is larger than six. The higher tensile strength was attributed to the star topology, leading to an equitable distribution of stress throughout the network formed by the multiplicity of arms crosslinked at one center (*i.e.* multiple bridging by a single chain). Similar observations are known and intensively studied for linear multiblock copolymer architectures (section 2.4).^{55,56,91,139}

These studies emphasize the conclusion that the core junction in multi-arm star topologies acts

as a permanent crosslink. An increasing number of arms leads to tough and mechanically stable materials. Similar results are obtained for linear block junctions as obtained for an increasing number of blocks in linear multiblock copolymer architectures. To the best of our knowledge, a direct comparison with the linear multiblock analogues has not been made. However, this is not straightforward, as the mechanical properties are function of several, usually not-independent parameters (phase state, entanglement behaviour, molecular conformations), which are difficult to investigate individually (compare $(SI)_4$ star with $(SI)_4$ linear and $(SI)_2$ - $(IS)_2$ linear in Figure 8).

Beyond star-copolymers, *brush-like block copolymers* are an attractive method to control the physical properties by the conformation of the macromolecular chain.¹⁶⁷ Usually parameters, as the length, the density and the entropic and enthalpic repulsion of the side-chain as well as the length and flexibility of the backbone define the resulting morphological¹⁶⁸ and mechanical properties.^{167,169-173}

Compared to their linear analogues, the repulsive interactions of the side-chains causes the backbone to stretch.¹⁷⁴ Hence, with increasing side-chain length and density the entanglement molecular weight (M_e) increases. Interestingly, Hillmyer *et al.* found lower graft densities to improve mechanical performances. However, this appeared to have less impact on polymers with rigid backbones.¹⁶⁷ Relying on this concept, Mays *et al.* combined sufficiently large molecular weights with comparably low grafting densities and observed an increase of mechanical properties in acrylate-based graft block copolymers. These elastic materials showed an excellently high elongation at break ($\approx 1500\%$) and recovery ($\approx 5\%$ residual strain). In accordance to the results of multi-arm star block copolymers, and linear multiblock copolymers, this was explained by the high T_g PMMA side-chains, which allow to pin the structure in multiple vitrified domains (i.e. multiple bridging by single chains).¹⁷⁵

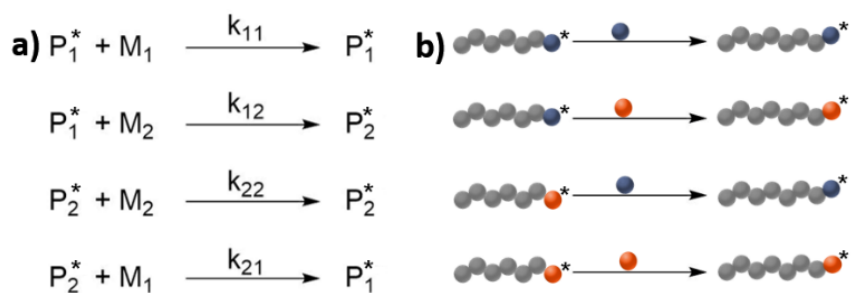
For both star and graft block copolymer architectures a large recovery as well a comparably low melt viscosity is described, underlining the similarities in these highly branched structures.^{167,171,173,175,176}

3 Statistical Copolymerization - "in situ" Measurements for "in silico" Simulations

In 1944 Mayo and Lewis solved "The Problem of Copolymerization" as they called it.¹⁷⁷ Alfrey and Goldfinger independently developed a similar equation in the same year.¹⁷⁸ Four fundamental reactions for the formation of copolymers (Scheme 1, Equation 1 and S2) are proposed for the "terminal copolymerization model" : The homopropagation of either monomer 1 (rate constant k_{11}) or monomer 2 (k_{22}) and the crossover reaction from a chain end bearing monomer 1 to monomer 2 (k_{12}) and vice versa (k_{21}). The reactivity ratios are defined by the ratio of homo-

propagation to crossover rate constant ($r_1 = k_{11}/k_{12}$, $r_2 = k_{22}/k_{21}$).

SCHEME 1 Fundamental reactions for the formation of a copolymer via living anionic copolymerization.^{177,178}
 a) Reaction equations b) Visualization of the terminal model. The reactivity of the last repeating unit (coloured) is representative for the polymer chain.



Interestingly, three years before the introduction of the terminal copolymerization model a simplified approach only considering the monomer reactivities was reported by Wall ("non-terminal copolymerization model"; $k_{11}=k_{21}$, $k_{22}=k_{12}$, $r_1 r_2=1$).¹⁷⁹ In subsequent works the copolymerization models were further advanced to also account for the repeating unit adjacent to the chain end ("penultimate copolymerization model").¹⁸⁰

$$\frac{d[M_1]}{d[M_2]} = \frac{[M_1](r_1[M_1] + [M_2])}{[M_2]([M_1] + r_2[M_2])}$$

Equation 1. The copolymerization equation as described by Mayo and Lewis.¹⁷⁷

For the industrial synthesis and final application, the Mayo-Lewis copolymerization equation has been proven to be of great importance. To run radical batch polymerizations up to high conversions the polymerization must be performed at the azeotropic point. At this point, the compositional drift shows no significant dependence from the conversion and hence the polymer composition resembles the monomer feed. For polymerizations performed in the absence of chain-transfer or irreversible termination reactions (e.g. the living anionic copolymerization of styrene and 1,3-dienes^{28,29,43} or the controlled radical copolymerization of methyl methacrylate and *n*-butyl acrylate^{181,182}), the reactivity ratios directly resemble the resulting comonomer sequence in the polymer backbone (e.g. flat or steep gradient). For this method, the large compositional heterogeneity found in radical copolymerization is avoided. Though the principle has long been known, the interest in sequencecontrolled TPEs is still focus of present studies.^{53,139,183,184}

3.1 Kinetics of the Anionic Copolymerization

The (co)polymerization of styrene with dienes in *non-polar, non-coordinating hydrocarbons* is usually performed by alkyllithium initiation, as the lithium counterion leads to a comparably large content of the *cis*-1,4-polydiene microstructure.^{32,185,186} A comparably fast initiation of 1,3-dienes and styrene is known for *sec*-butyllithium,^{58,187-190} which enables to kinetically separate chain initiation and prevent broadening of the molecular weight distribution.¹⁹¹

Although the propagation rates generally show a first order dependence with respect to the monomer concentration (butadiene,¹⁸⁵ isoprene,¹⁸⁵ styrene¹⁹²⁻¹⁹⁶), different dependences are found in respect to the initiator concentration. This is explained by the peculiar reaction mechanism, where lithium-aggregated anionic polymer chain ends are in equilibrium with the respective non-aggregated species. Only the non-aggregated species is assumed to add monomer via lithium coordination.^{38,141,143,197-200} Related to the aggregation number (N_{agg}) of the respective anionic species, the kinetic order dependence is given by $1/N_{\text{agg}}$, which enables a facile treatment of the complex aggregation-deaggregation equilibria. For polystyryllithium the formation of dimers ($N_{\text{agg}} = 2$) is generally accepted.^{58,194,196,201-205} For polybutadienyllithium^{198,204,206-209} and polyisoprenyllithium,^{62,205-207,209,210} controversial results are discussed. Worsfold and Bywater observed a gradual change from the tetrameric to the dimeric PILi species as a result of a decreasing chain-end concentration.^{206,211}

The copolymerization of 1,3-dienes with styrene derivatives usually results in steep gradients, so-called tapered structures (see also section 1.2 and 2.5).^{54,84,145,211-213} Although the homopropagation of styrene proceeds faster than that of the polydiene, *e.g.* isoprene ($k_{\text{SS}} > k_{\text{II}}$), the latter is preferentially incorporated.^{54,142,211,212} This is explained by the magnitude of the cross-propagation constants, which highly favor polyisoprenyllithium (PI-Li) chain ends ($k_{\text{SI}} \gg k_{\text{IS}}$; $r_{\text{I}} = 10.2$; $r_{\text{S}} = 0.01$ at 20 °C).⁵⁴

Whereas rather similar reactivity ratios (*i.e.* gradient profiles, *e.g.* for isoprene and styrene, $r_{\text{I}} \gg r_{\text{S}}$) are observed for the alkyllithium initiated copolymerization in various hydrocarbon solvents (Figure 1),^{211,212} rather polar, coordinative solvents (Lewis bases) remarkably affect the reactivity ratios. Taking the copolymerization of isoprene and styrene in THF as an example, the reactivity ratios are inverted ($r_{\text{I}} \ll r_{\text{S}}$).²¹⁴ These observations are explained by the solvation of lithium by THF. As a consequence, the polymerization-active center (*i.e.* carbanionic chain end) is further polarized. Hence, less associated chain ends are assumed, which is further supported by the observed first-order dependence of the polymerization rate on the active chain-end concentration.^{185,215} A comparable trend is observed by the exchange of the counterion (*i.e.* Lewis acid) with its higher homologues (*e.g.* sodium) or ionic additives (*e.g.* potassium *tert*-butanolate).^{53,216-219} To achieve a randomization ($r_{\text{Diene}} \approx 1$; $r_{\text{S}} \approx 1$), in some cases the copolymerization is performed

in hydrocarbons with added Lewis base.^{137,141,155,220-230} Care should be taken as the gradient profile (*i.e.* reactivity ratios) does not solely depend on the Lewis base. Parameters as the [randomizer]/[Li] ratio^{141,231} and the temperature^{54,214} need to be adjusted in respect to the polar modifier to obtain a (strictly) random comonomer incorporation.

The ionization of the carbon-metal bond also remarkably affects the microstructure of the formed polydiene.^{32,34,232-235} An increase of the side-chain vinyl regio-isomers (3,4- and 1,2-units; Figure 2) is accompanied by an increase of the T_g .^{33,43,235-238} This increase of the side-chain vinyl content is generally not desired for TPE materials utilizing the polydiene as rubbery component.⁵³ However, there are also examples utilizing a high side-chain vinyl content in post-polymerization reactions (section 2.1).

3.2 *In Situ* Monitoring Techniques

The determination of the polymer composition at different stages of the reaction is a straightforward method to estimate the comonomer sequence.^{141,220,221,236,239} As several batches of a similar copolymerization experiment need to be quenched and analyzed at different conversions, this leads to a comparably high experimental effort and nowadays belongs to the more traditional approaches.

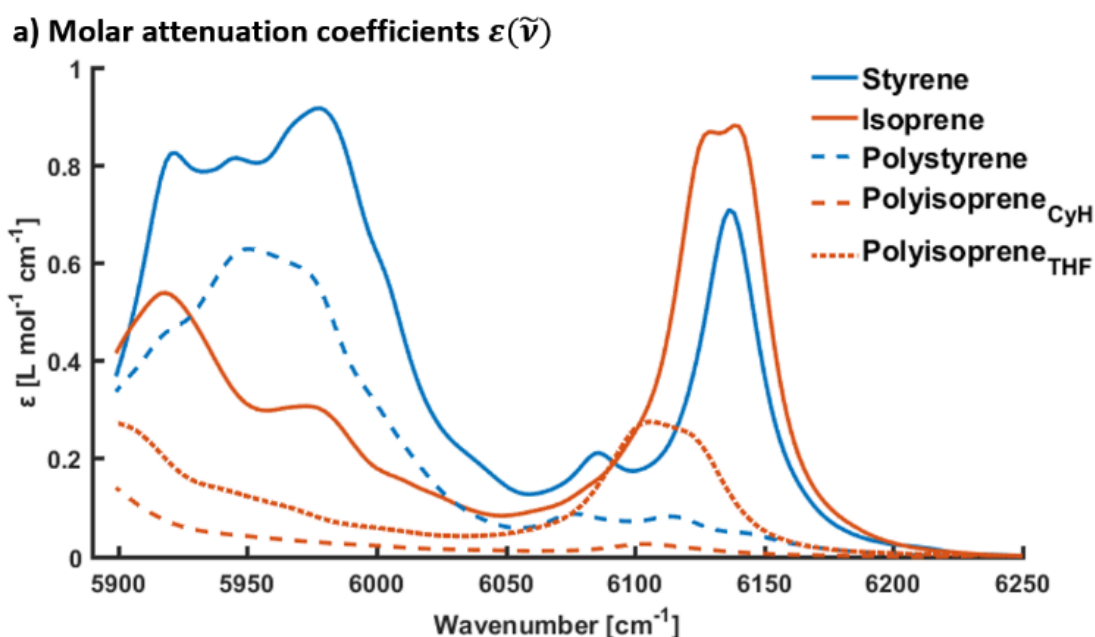
Nowadays, on-line methods allow the real-time monitoring of the monomer conversion via NMR,^{84,86,240,241} near-infrared (NIR),^{54,242,243} mid-infrared (mid-IR),^{212,244} or ultraviolet (UV) spectroscopy.^{194,196,245} These methods feature high temporal resolution and are able to monitor the complete polymerization within one experiment. Thus, high data resolution (depending on the measurement method up to 20,000 data points or more) within only one experiment is achievable. Hence, these on-line studies are currently the method of choice to monitor and analyse copolymerization experiments.

In recent years, on-line NMR spectroscopy has been proven as an efficient tool to track the depletion of individual monomer over time. However, the time resolution is limited (≈ 1 min) and typically the polymerization conditions must be tailored to be performed within an NMR tube (use of deuterated solvent, adjusted initiator and monomer concentrations, preparation in a glove box). Both issues can be solved by *in situ* probing the reaction via UV, NIR or mid-IR spectroscopy. The temporal resolution is much faster and since the probe is directly attached to the reaction vessel, the progress of a reaction can be tracked on the very same batch used to investigate material properties.⁵⁴ This is especially useful in multi-step reactions (section 2.4), where a defined polymer structure can only be obtained by postponing the monomer addition until the majority of the previous addition step has reacted.⁵⁴ As shown by Fontanille *et al.* mid-

IR spectroscopy is an efficient method to *in situ* monitor the copolymerization, by tracking the depletion of the well resolved monomer absorption peaks ($\tilde{\nu}_S = 1597\text{cm}^{-1}$; $\tilde{\nu}_I = 1630\text{cm}^{-1}$). Unfortunately, the implementation of mid-IR spectroscopy is technically challenging because the optical fibres require crystalline media, *e.g.* AgCl, or hollow waveguides resulting in mechanically less robust and expensive conduits, which require permanent installation in a polymerization setup.²⁴⁶

This issue is solved by using *in situ* UV spectroscopy to monitor the absorption of the monomer and the anionic chain ends. Already in 1960 Worsfold *et al.* started to quantify homo- and cross propagation rates of styrene, isoprene and butadiene via *in situ* measurements.^{58,145,194,245,247} As shown by Fontanille *et al.*, this setup can also be used to probe the homo- and copolymerization of styrene and isoprene.²¹² As stated by Worsfold,¹⁴⁵ it is unfortunate that the absorption band of polybutadienyllithium ($\lambda_{\text{PBLi}} \approx 275 \text{ nm}$) is largely masked by that of styrene ($\lambda_S \approx 290 \text{ nm}$) and of polystyrene ($\lambda_{\text{PS}} \approx 260 \text{ nm}$). However, the absorption band of polystyryllithium ($\lambda_{\text{PSLi}} \approx 330 \text{ nm}$) appeared at a measurable rate. Hence, in on-line UV studies, the determination of cross-propagation rate constants is not derived by the tracking the individual monomer consumption rates during the copolymerization reaction. Instead they were determined by the respective cross-addition step (*i.e.* adding isoprene to polystyryllithium (kSI) or vice versa (kIS); Scheme 1). Also for this "model reaction", Fontanille *et al.* stated that the formation of mixed aggregates only allowed an evaluation for the first moments of the crossover reaction.²¹²

In accordance with UV-spectroscopy, also NIR spectroscopy utilizes comparably small wavelengths, enabling a facile setup by using affordable, flexible, mineral glass or polymer based optical fibers.^{54,248} Long *et al.* found the kinetic data evaluation hampered by the overlapping absorption bands of styrene, isoprene and the respective repeating units formed during the (co)polymerization.²⁴² In 2019 our group started to utilize differences in the individual molar attenuation coefficients, $\varepsilon(\tilde{\nu})$, in a part of the NIR spectrum to access the individual monomer and polymer concentrations at any time.^{54,231} For this purpose, the spectra in the range $\tilde{\nu} = 5900 - 6250 \text{ cm}^{-1}$ at a 1.9 cm^{-1} data interval were recorded and used to solve a linear equation system (184 equations) for every spectrum (typically 4 s resolution in up to 12,000 spectra; Figure 9).⁵⁴ This allowed to determine the reactivity ratios of isoprene and styrene in cyclohexane as a function of the temperature ($T = 10\text{-}60 \text{ }^\circ\text{C}$). In addition, the effect of THF (so-called "randomizer") was visualized.



b) Deconvolution via linear equation system:

$$A(\tilde{\nu}) = \underbrace{c_S \cdot \varepsilon_S(\tilde{\nu}) + c_I \cdot \varepsilon_I(\tilde{\nu})}_{\text{monomer absorptions}} + \underbrace{c_{PS} \cdot \varepsilon_{PS}(\tilde{\nu}) + c_{PI_{CyH}} \cdot \varepsilon_{PI_{CyH}}(\tilde{\nu}) + c_{PI_{THF}} \cdot \varepsilon_{PI_{THF}}(\tilde{\nu})}_{\text{polymer absorptions}}$$

FIGURE 9 Deconvolution of the combined monomer and polymer absorption band of the species present during the living anionic copolymerization of styrene and isoprene. The individual concentrations were calculated by solving the linear equation system (b) with the determined molar attenuation coefficients (a).^{54,231}

3.3 Determination of Reactivity Ratios

Reactivity ratios are the foundation to understand the copolymerization behavior and determine the comonomer sequence formed during the copolymerization reaction. Based on the fundamental importance of these parameters, several methods for the evaluation of reactivity ratios were introduced. At their time of introduction, typically graphical methods (*i.e.* evaluation with pen and paper) were employed. The first prominent method was reported by Fineman and Ross in 1950 by linearizing the Mayo-Lewis equation (Equation Set S3).²⁵⁰ The Fineman-Ross formalism enables direct determination of reactivity ratios from the slope and intercept of the linear graph. Kelen and Tüdös further optimized the Fineman-Ross method by eliminating biases introduced by the linearization using a symmetrisation factor (Equation Set S4).²⁵¹ While these methods can be performed by hand without any computer (although speed may be somewhat dependent on the mathematical skills of the scientist) they rely on the differential copolymerization equation and require both the monomer feed ($f_1 = M_1 / (M_1 + M_2)$) and the instantaneous mole fraction of each monomer incorporated into the polymer ($F_1 = dM_1 / (dM_1 + dM_2)$) for

evaluation (Equation Set S5).

Although *in situ* monitoring techniques enable a comparably high data resolution, the determination of reactivity ratios is still not straightforward. To obtain the instantaneous monomer incorporation mole fraction F_1 , the derivative of the measurement needs to be calculated. Unfortunately, this calculation is highly influenced by data noise and thus prone to result in erroneous reactivity ratios. However, this issue can partially be solved by using advanced methods for differentiation, such as the total-variation regularization-based numerical differentiation.²⁵² As an alternative to the differential methods, the integrated form of the Mayo-Lewis equation as reported by Meyer and Lowry can be used (Equation S6).²⁵³ Meyer and Lowry analytically integrated the copolymerization equation derived by Skeist.²⁵⁴ In contrast to "old" graphical methods, this equation requires non-linear fitting methods. In the particular case of an ideal copolymerization ($r_1 r_2 = 1$, non-terminal model) the Meyer-Lowry equation can be simplified and linearized, leading to the evaluation method proposed by Jaacks (Equation S7).²⁵⁵ Various rearranged equations based on the simplified Meyer-Lowry or Jaacks formalism have been used for the determination of reactivity ratios with surprisingly high accuracy even at non-ideal conditions.²⁵⁶⁻²⁵⁸ In recent works the use of those simplified non-terminal formalisms is recommended as a superior method for the evaluation of reactivity ratios (Scheme S1, Table S1) to reduce potential errors introduced by overfitting.²⁵⁸

3.4 Copolymerization "In Silico" - Kinetic Monte Carlo Simulation

In the last decades computational power has remarkably increased. Hence calculation times are reduced concurrently faster than the experimental time.^{259,260} Nowadays, computer-aided prediction and rational selection of experiments can significantly increase the overall scientific throughput and thus scientific progress. Exceptional work has been performed by introducing the Polymer Self-Consistent Field theory (PSCFT) which significantly helped to understand the phase-segregation behaviour of block copolymers.⁹³ Molecular dynamics (MD) simulations have been used to predict the behaviour of (co)polymer chains in bulk and solution.^{261,262} While many works for the prediction of material properties have been reported, nearly all methods are focused on polymer physics, and only few methods can be regarded as practical tools for the synthetic polymer chemist. In this context we want to highlight to the kinetic Monte Carlo (kMC) simulation

kMC simulations of copolymerization reactions can be performed, by using experimentally determined reaction rates (section 3.3). If the assumed copolymerization reactions and experimentally determined rate constants are correct the simulation perfectly represents the experimental outcome. Hence every single computed polymer chain and the corresponding monomer-by-

monomer sequence can be obtained and analyzed (e.g. regarding the composition distribution, the segment length distribution as well as their drift within the molecular weight distribution as discussed later in this section). This yields not only valuable information to predict experimental data, but can also provide insight into information that is difficult to obtain via experimental methods (e.g. triad composition, length of uninterrupted repeating units)

For living or controlled radical copolymerization methods the implementation of a kMC model is quite simple, as the polymerization active species usually lacks side reactions (e.g. irreversible termination or chain transfer reactions to monomers), which allows to consider only the fundamental copolymerization equations as shown in Scheme 1.

The reported kMC models for controlled and free radical copolymerizations are extremely comprehensive and even specialized methods for, e.g., electrochemically mediated ATRP²⁶³ or laser-induced free-radical polymerizations²⁶⁴ have been developed. Complicated features (e.g. branching) were considered by Broadbelt, D'Hooge and others.²⁶⁵⁻²⁷⁴ Especially the *chemical composition- chain length distribution* (CC-CLD or CoC-CLD; i.e. the copolymer composition distribution as a function of the chain length) was thoroughly investigated.²⁷⁵⁻²⁷⁷

In contrast to radical copolymerization, comprehensive kMC models for the living anionic copolymerization are rarely reported to date. To the best of our knowledge, only the chain length distribution of multiblock copolymers prepared via continuous flow,²⁷⁸ the slow crossover reaction from an alkynyl-functionalized 1,1-diphenylethylenyllithium derivative to styrene,²⁷⁹ and several works in our group have been reported up to date.^{84,139,280} As shown by the following examples, kMC simulations based on the kinetics of the living anionic polymerization of 1,3-dienes and styrene are able to facilitate synthesis and understanding of TPEs. In contrast to the CC-CLD, the compositional drift resembles the change in the *mean* composition of copolymers chains as a function of the chain length (Figure 10a) and can be experimentally accessed via SEC (e.g. analysing the responses of RI and UV detector) or MALDI-ToF-mass spectrometry.^{87,281-283} As an example, in a recent work, the copolymerization of isoprene and styrene derivatives produced a compositional drift in dependence of the molecular weight resulting in a broadening of the molecular weight distribution. However, a prediction of the molecular weight distribution (and SEC curve) via kMC confirmed that indeed a broadened molecular weight distribution was to be expected (Figure S1).

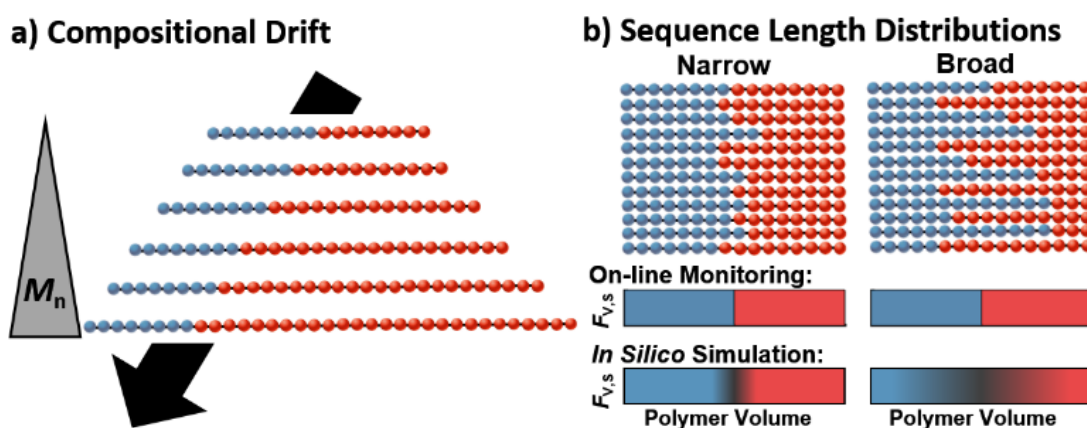


FIGURE 10 Red and blue sphere represent different monomer units. a) Visualization of a compositional drift for increasing molecular weight (M_n). With increasing M_n the content of red spheres increases. b) Visualization of a (i) narrow and (ii) broad sequence length distribution for samples with a similar chain length. The black area in the bars below, visualizes the area in the chains where red and blue spheres are present.

However, copolymers with a narrow molecular weight distribution and similar composition with respect to the molecular weight can still show different compositions on the per-chain level (Figure 10b). For this purpose, the *sequence length distribution* (SLD) affords the per-chain microstructure, enabling a detailed comparison of the monomer sequence of individual polymer chains. These results are not accessible via conventional experimental methods, where always an average value of multiple chains is obtained. As an example, the degradation products of the ozonolysis of a tapered P(I-co-S) multiblock were predicted via kMC. The SLD of the copolymer accurately described the resulting PS segment distribution after cleavage of all isoprene repeating units and verified the desired tapered multiblock architecture.¹³⁹ In addition, the kMC model was also used to reduce reaction times in the multi-step synthesis (Figure S2).

Both parameters, the CoC-CLD and SLD, precisely reflect the microstructure of copolymers and hence are of great interest for the prediction and evaluation of copolymerization experiments in the rational design of TPEs.²⁸⁴

CONCLUSIONS

Nowadays, the progress in synthetic polymer chemistry enables the access of numerous parameters leading to sheer endless combinations. It is the challenge for the synthetic chemist, to rationally design and control the monomer sequence and finally obtain a tailor-made material for the targeted application. Here, we review recent developments in the field of sequence-controlled TPEs to permit an in-depth understanding of the effect of comonomer sequenc-

ing on morphological and mechanical properties. In recent years, the multi-step living anionic (co)polymerization has been proven as an efficient tool to design, synthesize and investigate complex block copolymer architectures in a defined manner. The precise quantification of fundamental kinetic processes in the statistical copolymerization is crucial to secure the formation of the desired comonomer sequence in the polymer backbone. On-line monitoring techniques are established as the method of choice to determine rate constants. To generate an in-depth insight into the (co)polymerization behaviour the kinetic Monte Carlo simulation can be used to simulate the copolymerization *in silico* based on the experimentally determined rate constants. This allows a precise calculation of reaction times and a comparison of individual chains in terms of their composition and sequence. Hence, in situ measurements and in silico simulations has been proven as an effective combination to understand the statistical copolymerization, employed to directly generate complex sequences in a single step.

ACKNOWLEDGEMENTS

The author thanks Christian Wahlen for providing SEC data.

REFERENCES

- (1) In *IUPAC Compendium of Chemical Terminology*; Nič, M., Jirát, J., Košata, B., Jenkins, A., McNaught, A., Eds.; IUPAC: Research Triangle Park, NC, 2009.
- (2) Gumboldt, A. *Chem. unserer Zeit* **1967**, 1 (2), 41–48. DOI: 10.1002/ciuz.19670010203.
- (3) Thomas, S.; Han Chan, C.; Pothen, L.; Joy, J.; Maria, H. *Natural Rubber Materials 2*; Royal Society of Chemistry: Cambridge, 2013.
- (4) T. Hancock. Improvements in the Preparation or Manufacture of Caoutchouc in Combination With Other Substances... 9,952, Apr 21, 1844.
- (5) T. Hancock. *Personal Narrative of the Origin and Progress of the Caoutchouc or India Rubber Manufacture in England*; Longman, Brown, Green, Longmans, & Roberts: London, 1857.
- (6) Goodyear, C. Improvement in the Mode of Preparing Caoutchouc with Sulphur for the Manufacture of Various Articles. 1,090, Feb 24, 1839.
- (7) Goodyear, C. Improvement in India-Rubber Fabrics. 3,633, Jun 15, 1844.
- (8) Hübner, K. *Chem. unserer Zeit* **2016**, 50 (1), 67–71. DOI: 10.1002/ciuz.201500707.
- (9) Race, J. *J. Chem. Technol. Biotechnol.* **1912**, 31 (13), 611–665. DOI: 10.1002/jctb.5000311301.
- (10) Matthews, F. E.; Strange, E. H. GB1910/24790, Oct 25, 1910.
- (11) Matthews, F. E.; Strange, E. H. DE249868, Oct 24, 1911.
- (12) Holt, A. Z. *Angew. Chem.* **1914**, 27 (22), 153–158. DOI: 10.1002/ange.19140272201.
- (13) Requardt, A. *Nachr. Chem.* **2016**, 64 (2), 150–153. DOI: 10.1002/nadc.20164046024.
- (14) Ebert, G.; Orth, P.; Heidebroek, R. DE715825, Oct 2, 1937.
- (15) Requardt, A. *Chem. unserer Zeit* **2020**, 54 (2), 106–115. DOI: 10.1002/ciuz.201900867.
- (16) *Handbook of Thermoplastic Elastomers*; Drobny, J. G., Ed.; Elsevier, 2007.
- (17) Noshay, A.; McGrath, J. E. *Block copolymers: Overview and critical survey*, 2. print; Acad. Pr: Orlando u.a., 1987.
- (18) Drobny, J. G. In *Handbook of Thermoplastic Elastomers*; Drobny, J. G., Ed.; Elsevier, 2007; pp 9–11.
- (19) Christ, A. E.; Hanford, W. E. Formation of Elastic Urethane Products. 2,333,639, 1940.
- (20) 580,524, 1941.
- (21) Hanford, W. E.; Holmes, D. F. 2,284,896, Apr 24, 1939.
- (22) 574,134, 1942.
- (23) Snyder, M. D. 2,632,031, 1952.
- (24) 2,629,873, 1954.
- (25) Drobny, J. G. In *Handbook of Thermoplastic Elastomers*; Drobny, J. G., Ed.; Elsevier, 2007; pp 215–234.
- (26) Schollenberger, C. S. Simulated vulcanizates of polyurethane elastomers. 2,871,218, Dec 1, 1955.
- (27) Schollenberger, C. S.; Scptt, H.; Moore, G. R. *Rubber Chem. Technol.* **1962**, 35 (3), 742–752. DOI: 10.5254/1.3539953.
- (28) Szwarc, M. *Nature* **1956**, 178 (4543), 1168–1169. DOI: 10.1038/1781168a0.
- (29) Szwarc, M.; Levy, M.; Milkovich, R. *J. Am. Chem. Soc.* **1956**, 78 (11), 2656–2657. DOI: 10.1021/ja01592a101.
- (30) Legge, N. R. *Rubber Chem. Technol.* **1987**, 60 (3), 83–117. DOI: 10.5254/1.3536141.

- (31) Legge, N. R. *Rubber Chem. Technol.* **1989**, 62 (3), 529–547. DOI: 10.5254/1.3536257.
- (32) Hsieh, H.; Tobolsky, A. V. *J. Polym. Sci.* **1957**, 25 (109), 245–247. DOI: 10.1002/pol.1957.1202510918.
- (33) Hsieh, H.; Kelley, D. J.; Tobolsky, A. V. *J. Polym. Sci.* **1957**, 26 (113), 240–242. DOI: 10.1002/pol.1957.1202611315.
- (34) Morita, H.; Tobolsky, A. V. *J. Am. Chem. Soc.* **1957**, 79 (22), 5853–5855. DOI: 10.1021/ja01579a004.
- (35) Porter, L. M. Process for Preparing Block Copolymers Utilizing Organolithium Catalysts. 3,149,182, Oct 5, 1957.
- (36) Phillips Petroleum Company. 888,624, 1958.
- (37) Geoffrey, H.; Milkovich, R. Block polymers of monovinyl aromatic hydrocarbons and conjugated dienes. 3,265,765, Jan 29, 1962.
- (38) Cunningham, R. E.; Treiber, M. R. *J. Appl. Polym. Sci.* **1968**, 12 (1), 23–34. DOI: 10.1002/app.1968.070120104.
- (39) Tsukahara, Y.; Nakamura, N.; Hashimoto, T.; Kawai, H.; Nagaya, T.; Sugimura, Y.; Tsuge, S. *Polym. J.* **1980**, 12 (7), 455–466. DOI: 10.1295/polymj.12.455.
- (40) Roy, R.; Park, J. K.; Young, W.-S.; Mastroianni, S. E.; Tureau, M. S.; Epps, T. H. *Macromolecules* **2011**, 44 (10), 3910–3915. DOI: 10.1021/ma1025847.
- (41) Ashraf, A. R.; Ryan, J. J.; Satkowski, M. M.; Lee, B.; Smith, S. D.; Spontak, R. J. *Macromol. Rapid Commun.* **2017**, 38 (17). DOI: 10.1002/marc.201700207.
- (42) Horne, S. E.; Gibbs, F.; Carlson, E. J. 827,365, Feb 3, 1960.
- (43) Quirk, R. P. In *Encyclopedia of Polymer Science and Technology*; Wiley Interscience: Hoboken, NJ, 2004; pp 197–235.
- (44) Stavely, F. W. *Ind. Eng. Chem.* **1956**, 48 (4), 778–783. DOI: 10.1021/ie50556a032.
- (45) Morton, M.; McGrath, J. E.; Juliano, P. C. *J. Polym. Sci. C Polym. Symp.* **1969**, 26 (1), 99–115. DOI: 10.1002/polc.5070260107.
- (46) Badi, N.; Lutz, J.-F. *Chem. Soc. Rev.* **2009**, 38 (12), 3383–3390. DOI: 10.1039/B806413J.
- (47) Hodrokoukes, P.; Floudas, G.; Pispas, S.; Hadjichristidis, N. *Macromolecules* **2001**, 34 (3), 650–657. DOI: 10.1021/ma001479i.
- (48) Qiang, X.; Chakrour, R.; Janoszka, N.; Gröschel, A. H. *Isr. J. Chem.* **2019**, 295, 2418. DOI: 10.1002/ijch.201900044.
- (49) Martens, S.; van den Begin, J.; Madder, A.; Du Prez, Filip E.; Espeel, P. *J. Am. Chem. Soc.* **2016**, 138 (43), 14182–14185. DOI: 10.1021/jacs.6b07120.
- (50) Mori, T.; Masukawa, S.; Kikkawa, T.; Fujimori, A.; Satoh, A.; Matsumoto, K.; Jikei, M.; Oishi, Y.; Shibasaki, Y. *RSC Adv.* **2017**, 7 (54), 33812–33821. DOI: 10.1039/c7ra05161a.
- (51) Varshney, S. K.; Jacobs, C.; Hautekeer, J. P.; Bayard, P.; Jerome, R.; Fayt, R.; Teyssie, P. *Macromolecules* **1991**, 24 (18), 4997–5000. DOI: 10.1021/ma00018a003.
- (52) Kuraray Co. Kurarity™. <https://www.elastomer.kuraray.com/kurarity/what-is-kuraritytm/> (accessed April 7, 2020).
- (53) Knoll, K.; Nießner, N. *Macromol. Symp.* **1998**, 132 (1), 231–243. DOI: 10.1002/masy.19981320122.
- (54) Steube, M.; Johann, T.; Plank, M.; Tjaberings, S.; Gröschel, A. H.; Gallei, M.; Frey, H.; Müller, A. H. E. *Macromolecules* **2019**, 52 (23), 9299–9310. DOI: 10.1021/acs.macromol.9b01790.
- (55) Smith, S. D.; Spontak, R. J.; Satkowski, M. M.; Ashraf, A.; Heape, A. K.; Lin, J. S. *Polymer* **1994**, 35 (21), 4527–4536. DOI: 10.1016/0032-3861(94)90798-6.
- (56) Spontak, R. J.; Smith, S. D. *J. Polym. Sci. B* **2001**, 39 (9), 947–955. DOI: 10.1002/polb.1070.
- (57) Khandpur, A. K.; Förster, S.; Bates, F. S.; Hamley, I. W.; Ryan, A. J.; Bras, W.; Almdal, K.; Mortensen, K. *Macromolecules* **1995**, 28 (26), 8796–8806. DOI: 10.1021/ma00130a012.

- (58) Johnson, A. F.; Worsfold, D. J. *J. Polym. Sci. A: Gen. Pap.* **1965**, *3* (2), 449–455. DOI: 10.1002/pol.1965.100030204.
- (59) Hadjichristidis, N.; Pispas, S.; Floudas, G. *Block Copolymers*; John Wiley & Sons, Inc: Hoboken, USA, 2002.
- (60) Allen, R. D.; Long, T. E.; McGrath, J. E. *Polym. Bull.* **1986**, *15* (2), 127–134. DOI: 10.1007/BF00263389.
- (61) Hadjichristidis, N.; Iatrou, H.; Pispas, S.; Pitsikalis, M. *J. Polym. Sci. A* **2000**, *38* (18), 3211–3234. DOI: 10.1002/1099-0518%2820000915%2938%3A18<3211%3A%3AAID-POLA10>3.0.CO%3B2-L.
- (62) Müller, A. H.E. In *Comprehensive polymer science: The synthesis, characterization, reactions et applications of polymers*; Allen, G., J.C. Bevington, Eds.; Pergamon Press: Oxford, 1989; pp 387–423.
- (63) Odian, G. *Principles of Polymerization*, 4th ed.; Wiley-Interscience: S.I., 2004.
- (64) Pinazzi, C. P.; Soutif, J. C.; Brosse, J. C. *Eur. Polym. J.* **1975**, *11* (7), 523–525. DOI: 10.1016/0014-3057(75)90104-4.
- (65) Gabor, A. H.; Lehner, E. A.; Mao, G.; Schneggenburger, L. A.; Ober, C. K. *Chem. Mater.* **1994**, *6* (7), 927–934. DOI: 10.1021/cm00043a011.
- (66) Ameduri, B.; Boutevin, B.; Nouiri, M. *J. Polym. Sci. A* **1993**, *31* (8), 2069–2080. DOI: 10.1002/pola.1993.080310813.
- (67) Rüttiger, C.; Appold, M.; Didzoleit, H.; Eils, A.; Dietz, C.; Stark, R. W.; Stühn, B.; Gallei, M. *Macromolecules* **2016**, *49* (9), 3415–3426. DOI: 10.1021/acs.macromol.6b00577.
- (68) *Rubber compounding: Chemistry and applications*; Rodgers, B., Ed., Second edition; CRC Press an imprint of Taylor & Francis Group an informa business: Boca Raton, 2016.
- (69) Natori, I.; Inoue, S. *Macromolecules* **1998**, *31* (4), 982–987. DOI: 10.1021/ma9712110.
- (70) Hong, K.; Mays, J. W. *Macromolecules* **2001**, *34* (4), 782–786. DOI: 10.1021/ma0015626.
- (71) Bornani, K.; Wang, X.; Davis, J. L.; Wang, X.; Wang, W.; Hinestrosa, J. P.; Mays, J. W.; Kilbey, S. M. *Soft matter* **2015**, *11* (32), 6509–6519. DOI: 10.1039/C5SM01245G.
- (72) Kosaka, Y.; Kitazawa, K.; Inomata, S.; Ishizone, T. *ACS Macro Lett.* **2013**, *2* (2), 164–167. DOI: 10.1021/mz4000078.
- (73) Kosaka, Y.; Goseki, R.; Kawauchi, S.; Ishizone, T. *Macromol. Symp.* **2015**, *350* (1), 55–66. DOI: 10.1002/masy.201400024.
- (74) Kosaka, Y.; Kawauchi, S.; Goseki, R.; Ishizone, T. *Macromolecules* **2015**, *48* (13), 4421–4430. DOI: 10.1021/acs.macromol.5b00944.
- (75) Cai, Y.; Lu, J.; Zuo, D.; Li, S.; Cui, D.; Han, B.; Yang, W. *Macromolecular rapid communications* **2018**, *39* (20), e1800298. DOI: 10.1002/marc.201800298.
- (76) Nakahara, A.; Satoh, K.; Kamigaito, M. *Macromolecules* **2009**, *42* (3), 620–625. DOI: 10.1021/ma802024t.
- (77) Wang, W.; Schlegel, R.; White, B. T.; Williams, K.; Voyloy, D.; Steren, C. A.; Goodwin, A.; Coughlin, E. B.; Gido, S.; Beiner, M.; Hong, K.; Kang, N.-G.; Mays, J. *Macromolecules* **2016**, *49* (7), 2646–2655. DOI: 10.1021/acs.macromol.5b02642.
- (78) Riyajan, S.-a.; Liaw, D.-J.; Tanaka, Y.; Saktapippanich, J. T. *J. Appl. Polym. Sci.* **2007**, *105* (2), 664–672. DOI: 10.1002/app.25026.
- (79) Wang, W.; Lu, W.; Kang, N.-G.; Mays, J.; Hong, K. In *Elastomers*; Cankaya, N., Ed.; InTech, 2017.
- (80) *Physical Properties of Polymers Handbook*; Mark, J. E., Ed.; Springer New York: New York, NY, 2007.
- (81) Iacob, C.; Yoo, T.; Runt, J. *Macromolecules* **2018**, *51* (13), 4917–4922. DOI: 10.1021/acs.macromol.8b00851.
- (82) Bero, C. A.; Roland, C. M. *Macromolecules* **1996**, *29* (5), 1562–1568. DOI: 10.1021/ma951439s.
- (83) Wu, S. *Polym. Eng. Sci.* **1992**, *32* (12), 823–830. DOI: 10.1002/pen.760321209.
- (84) Grune, E.; Johann, T.; Appold, M.; Wahlen, C.; Blankenburg, J.; Leibig, D.; Müller, A. H. E.; Gallei, M.; Frey, H.

Macromolecules **2018**, 51 (9), 3527–3537. DOI: 10.1021/acs.macromol.8b00404.

(85) Grune, E.; Appold, M.; Müller, A. H. E.; Gallei, M.; Frey, H. *ACS Macro Lett.* **2018**, 807–810. DOI: 10.1021/acs-macrolett.8b00390.

(86) Johann, T.; Leibig, D.; Grune, E.; Müller, A. H. E.; Frey, H. *Macromolecules* **2019**, 52 (12), 4545–4554. DOI: 10.1021/acs.macromol.9b00747.

(87) Tiedemann, P. von; Blankenburg, J.; Maciol, K.; Johann, T.; Müller, A. H. E.; Frey, H. *Macromolecules* **2019**. DOI: 10.1021/acs.macromol.8b02280.

(88) Natalello, A.; Alkan, A.; Tiedemann, P. von; Wurm, F. R.; Frey, H. *ACS Macro Lett.* **2014**, 3 (6), 560–564. DOI: 10.1021/mz500255h.

(89) Quirk, R. P.; Sarkis, M. T.; Meier, D. J. In *Advances in Elastomers and Rubber Elasticity*; Lal, J., Mark, J. E., Eds.; Springer US: Boston, MA, s.l., 1986; pp 143–155.

(90) Chen, J.; Fetters, L. J. *Polym. Bull.* **1981**, 4 (5). DOI: 10.1007/BF00255103.

(91) Galanos, E.; Grune, E.; Wahlen, C.; Müller, A. H. E.; Appold, M.; Gallei, M.; Frey, H.; Floudas, G. *Macromolecules* **2019**, 52 (4), 1577–1588. DOI: 10.1021/acs.macromol.8b02669.

(92) Zhao, J.; Ediger, M. D.; Sun, Y.; Yu, L. *Macromolecules* **2009**, 42 (17), 6777–6783. DOI: 10.1021/ma9008516.

(93) Leibler, L. *Macromolecules* **1980**, 13 (6), 1602–1617. DOI: 10.1021/ma60078a047.

(94) Gennes, P. G. de. *J. Phys. France* **1970**, 31 (2-3), 235–238. DOI: 10.1051/jphys:01970003102-3023500.

(95) Sinturel, C.; Bates, F. S.; Hillmyer, M. A. *ACS Macro Lett.* **2015**, 4 (9), 1044–1050. DOI: 10.1021/acsmacrolett.5b00472.

(96) Georgopoulos, P.; Handge, U. A.; Abetz, C.; Abetz, V. *Polymer* **2016**, 104, 279–295. DOI: 10.1016/j.polymer.2016.02.039.

(97) Hadjichristidis, N.; Xenidou, M.; Iatrou, H.; Pitsikalis, M.; Poulos, Y.; Avgeropoulos, A.; Sioula, S.; Paraskeva, S.; Velis, G.; Lohse, D. J.; Schulz, D. N.; Fetters, L. J.; Wright, P. J.; Mendelson, R. A.; García-Franco, C. A.; Sun, T.; Ruff, C. J. *Macromolecules* **2000**, 33 (7), 2424–2436. DOI: 10.1021/ma991670w.

(98) Gouinlock, E. V.; Porter, R. S. *Polym. Eng. Sci.* **1977**, 17 (8), 535–543. DOI: 10.1002/pen.760170809.

(99) Bates, F. S.; Schulz, M. F.; Khandpur, A. K.; Förster, S.; Rosedale, J. H.; Almdal, K.; Mortensen, K. *Faraday Discuss.* **1994**, 98, 7–18. DOI: 10.1039/FD9949800007.

(100) Cohen, Y.; Albalak, R. J.; Dair, B. J.; Capel, M. S.; Thomas, E. L. *Macromolecules* **2000**, 33 (17), 6502–6516. DOI: 10.1021/ma000513q.

(101) Dair, B. J.; Honeker, C. C.; Alward, D. B.; Avgeropoulos, A.; Hadjichristidis, N.; Fetters, L. J.; Capel, M.; Thomas, E. L. *Macromolecules* **1999**, 32 (24), 8145–8152. DOI: 10.1021/ma990666h.

(102) Mai, S.-M.; Mingvanish, W.; Turner, S. C.; Chaibundit, C.; Fairclough, J. Patrick A.; Heatley, F.; Matsen, M. W.; Ryan, A. J.; Booth, C. *Macromolecules* **2000**, 33 (14), 5124–5130. DOI: 10.1021/ma000154z.

(103) Koberstein, J. T.; Russell, T. P.; Walsh, D. J.; Pottick, L. *Macromolecules* **1990**, 23 (3), 877–881. DOI: 10.1021/ma00205a031.

(104) Gehlsen, M. D.; Almdal, K.; Bates, F. S. *Macromolecules* **1992**, 25 (2), 939–943. DOI: 10.1021/ma00028a066.

(105) Mayes, A. M.; Olvera de la Cruz, Monica. *J. Chem. Phys.* **1991**, 95 (6), 4670–4677. DOI: 10.1063/1.461736.

(106) Mayes, A. M.; Olvera de la Cruz, Monica. *J. Chem. Phys.* **1989**, 91 (11), 7228–7235. DOI: 10.1063/1.457290.

(107) Nakazawa, H.; Ohta, T. *Macromolecules* **1993**, 26 (20), 5503–5511. DOI: 10.1021/ma00072a031.

(108) Legge, N. R.; Holden, G.; Schroeder, H. E. *Thermoplastic elastomers: A comprehensive review*; Hanser Publishers; Distributed in the U.S.A. and in Canada by Oxford University Press: Munich, New York, New York, 1987.

- (109) Karatasos, K.; Anastasiadis, S. H.; Pakula, T.; Watanabe, H. *Macromolecules* **2000**, *33* (2), 523–541. DOI: 10.1021/ma991397y.
- (110) Spontak, R. J.; Zielinski, J. M.; Lipscomb, G. G. *Macromolecules* **1992**, *25* (23), 6270–6276. DOI: 10.1021/ma00049a025.
- (111) Matsen, M. W. *J. Chem. Phys.* **2000**, *113* (13), 5539. DOI: 10.1063/1.1289889.
- (112) Matsen, M. W.; Thompson, R. B. *J. Chem. Phys.* **1999**, *111* (15), 7139–7146. DOI: 10.1063/1.480006.
- (113) Qiao, L.; Leibig, C.; Hahn, S. F.; Winey, K. I. *Ind. Eng. Chem. Res.* **2006**, *45* (16), 5598–5602. DOI: 10.1021/ie0511940.
- (114) Floudas, G.; Paraskeva, S.; Hadjichristidis, N.; Fytas, G.; Chu, B.; Semenov, A. N. *J. Chem. Phys.* **1997**, *107* (14), 5502–5509. DOI: 10.1063/1.474255.
- (115) Watanabe, H.; Matsumiya, Y.; Sawada, T.; Iwamoto, T. *Macromolecules* **2007**, *40* (19), 6885–6897. DOI: 10.1021/ma0712495.
- (116) Wu, L.; Lodge, T. P.; Bates, F. S. *Macromolecules* **2004**, *37* (22), 8184–8187. DOI: 10.1021/ma048635w.
- (117) Drolet, F.; Fredrickson, G. H. *Macromolecules* **2001**, *34* (15), 5317–5324. DOI: 10.1021/ma0100753.
- (118) Matsen, M. W.; Schick, M. *Macromolecules* **1994**, *27* (1), 187–192. DOI: 10.1021/ma00079a027.
- (119) Watanabe, H. *Macromolecules* **1995**, *28* (14), 5006–5011. DOI: 10.1021/ma00118a032.
- (120) Li, B.; Ruckenstein, E. *Macromol. Theory Simul.* **1998**, *7* (3), 333–348. DOI: 10.1002/(SICI)1521-3919(19980501)7:3<333:AID-MATS333>3.0.CO;2-O.
- (121) Hermel, T. J.; Wu, L.; Hahn, S. F.; Lodge, T. P.; Bates, F. S. *Macromolecules* **2002**, *35* (12), 4685–4689. DOI: 10.1021/ma020100k.
- (122) Morton, M. In *Multicomponent polymer systems: A symposium co-sponsored by the Division of Industrial and Engineering Chemistry, the Division of Polymer Chemistry at the 159th meeting of the American Chemical Society, Houston, Tex., Feb. 23 - 26, 1970*; Platzer, N. A. J., Ed.; Advances in chemistry series 99; American Chemical Society: Washington, DC, 1971; pp 490–509.
- (123) Mishra, S.; Badani Prado, R. M.; Lacy, T. E.; Kundu, S. *Soft matter* **2018**, *14* (39), 7958–7969. DOI: 10.1039/c8sm01397g.
- (124) Hamersky, M. W.; Smith, S. D.; Gozen, A. O.; Spontak, R. J. *Phys. Rev. Lett.* **2005**, *95* (16), 168306. DOI: 10.1103/PhysRevLett.95.168306.
- (125) Schlick, S.; Levy, M. *J. Phys. Chem.* **1960**, *64* (7), 883–886. DOI: 10.1021/j100836a015.
- (126) Corbin, N.; Prud'homme, J. J. *J. Polym. Sci. Polym. Chem. Ed.* **1976**, *14* (7), 1645–1659. DOI: 10.1002/pol.1976.170140708.
- (127) Corbin, N.; Prud'homme, J. J. *J. Polym. Sci. Polym. Phys. Ed.* **1977**, *15* (11), 1937–1951. DOI: 10.1002/pol.1977.180151106.
- (128) Cole, M. W.; Futurama, S. Process for Producing Multiblock Copolymer and Products produced thereby. 3,937,760, Apr 29, 1974.
- (129) Spontak, R. J.; Smith, S. D.; Satkowski, M. M.; Ashraf, A.; Zielinski, J. M. In *Polymer Solutions, Blends, and Interfaces*; Noda, I., Ed.; Studies in Polymer Science; Elsevier Science: Burlington, 2012; pp 65–88.
- (130) Smith; Spontak, R. J.; Satkowski; Ashraf; Lin. *Physical review. B, Condensed matter* **1993**, *47* (21), 14555–14558. DOI: 10.1103/physrevb.47.14555.
- (131) Wu, L.; Cochran, E. W.; Lodge, T. P.; Bates, F. S. *Macromolecules* **2004**, *37* (9), 3360–3368. DOI: 10.1021/ma035583m.
- (132) Matsushita, Y.; Mogi, Y.; Mukai, H.; Watanabe, J.; Noda, I. *Polymer* **1994**, *35* (2), 246–249. DOI: 10.1016/0032-3861(94)90686-6.

- (133) Nagata, Y.; Masuda, J.; Noro, A.; Cho, D.; Takano, A.; Matsushita, Y. *Macromolecules* **2005**, *38* (24), 10220–10225. DOI: 10.1021/ma051681r.
- (134) Martin Ganß. *Struktur-Eigenschafts-Beziehungen in Styrol- Butadien basierten Blockcopolymeren mit statistischen Copolymerblöcken*, 2011.
- (135) Matsumiya, Y.; Watanabe, H.; Takano, A.; Takahashi, Y. *Macromolecules* **2013**, *46* (7), 2681–2695. DOI: 10.1021/ma3026404.
- (136) Higaki, Y.; Suzuki, K.; Kiyoshima, Y.; Toda, T.; Nishiura, M.; Ohta, N.; Masunaga, H.; Hou, Z.; Takahara, A. *Macromolecules* **2017**, *50* (16), 6184–6191. DOI: 10.1021/acs.macromol.7b01193.
- (137) Kelsey, J.; Pickering, N.; Clough, A.; Zhou, J.; White, J. L. *Macromolecules* **2017**, *50* (18), 7233–7240. DOI: 10.1021/acs.macromol.7b01476.
- (138) Mastan, E.; He, J. *Macromolecules* **2017**, *50* (23), 9173–9187. DOI: 10.1021/acs.macromol.7b01662.
- (139) Steube, M.; Johann, T.; Galanos, E.; Appold, M.; Rüttiger, C.; Mezger, M.; Gallei, M.; Müller, A. H. E.; Floudas, G.; Frey, H. *Macromolecules* **2018**, *51* (24), 10246–10258. DOI: 10.1021/acs.macromol.8b01961.
- (140) Appold, M.; Grune, E.; Frey, H.; Gallei, M. *ACS Appl. Mater. Interfaces* **2018**, *10* (21), 18202–18212. DOI: 10.1021/acsami.8b02848.
- (141) Kuntz, I. *J. Polym. Sci.* **1961**, *54* (160), 569–586. DOI: 10.1002/pol.1961.1205416020.
- (142) Morton, M.; Eils, F. R. *J. Polym. Sci.* **1962**, *61* (171), 25–29. DOI: 10.1002/pol.1962.1206117105.
- (143) A. A. Korotkov; N. N. Chesnokova. *Polymer Science U.S.S.R.* **1960**, *2*, 284–298.
- (144) Kraus, G.; Childers, C. W.; Gruver, J. T. *J. Appl. Polym. Sci.* **1967**, *11* (8), 1581–1591. DOI: 10.1002/app.1967.070110819.
- (145) Johnson, A. F.; Worsfold, D. J. *Makromol. Chem.* **1965**, *85* (1), 273–279. DOI: 10.1002/macp.1965.020850122.
- (146) O'Driscoll, K. F.; Kuntz, I. *J. Polym. Sci.* **1962**, *61* (171), 19–24. DOI: 10.1002/pol.1962.1206117104.
- (147) Kraus, G.; Rollmann, K. W. *Angew. Makromol. Chemie* **1971**, *16* (1), 271–296. DOI: 10.1002/apmc.1971.050160115.
- (148) Kraus, G.; Railsback, H. E. In *Recent Advances in Polymer Blends, Grafts, and Blocks*; Sperling, L. H., Ed.; Polymer Science and Technology 4; Springer: Boston, MA, 1974; pp 245–267.
- (149) Kaelble, D. H.; Cirlin, E. H. *J. polym. sci., C Polym. symp.* **1973**, *43* (1), 131–148. DOI: 10.1002/polc.5070430114.
- (150) Brinke, G. ten; Karasz, F. E.; MacKnight, W. J. *Macromolecules* **1983**, *16* (12), 1827–1832. DOI: 10.1021/ma00246a006.
- (151) Roe, R.-J.; Zin, W.-C. *Macromolecules* **1980**, *13* (5), 1221–1228. DOI: 10.1021/ma60077a037.
- (152) Paul, D. R.; Barlow, J. W. *Polymer* **1984**, *25* (4), 487–494. DOI: 10.1016/0032-3861(84)90207-6.
- (153) Annighöfer, F.; Gronski, W. *Colloid Polym. Sci.* **1983**, *261* (1), 15–25. DOI: 10.1007/BF01411513.
- (154) Annighöfer, F.; Gronski, W. *Makromol. Chem.* **1984**, *185* (10), 2213–2231. DOI: 10.1002/macp.1984.021851016.
- (155) Gronski, W.; Annighöfer, F.; Stadler, R. *Makromol. Chem.* **1984**, *6* (S19841), 141–161. DOI: 10.1002/macp.1984.020061984111.
- (156) Brown, J. R.; Sides, S. W.; Hall, L. M. *ACS Macro Lett.* **2013**, *2* (12), 1105–1109. DOI: 10.1021/mz400546h.
- (157) Hadjichristidis, N.; Iatrou, H.; Pitsikalis, M.; Mays, J. *Prog. Polym. Sci.* **2006**, *31* (12), 1068–1132. DOI: 10.1016/j.progpolymsci.2006.07.002.
- (158) Hirao, A.; Goseki, R.; Ishizone, T. *Macromolecules* **2014**, *47* (6), 1883–1905. DOI: 10.1021/ma401175m.
- (159) Hashimoto, T.; Ijichi, Y.; Fetters, L. J. *J. Chem. Phys.* **1988**, *89* (4), 2463–2472. DOI: 10.1063/1.455040.

- (160) Ijichi, Y.; Hashimoto, T.; Fetters, L. J. *Macromolecules* **1989**, *22* (6), 2817–2824. DOI: 10.1021/ma00196a048.
- (161) Floudas, G.; Pispas, S.; Hadjichristidis, N.; Pakula, T.; Erukhimovich, I. *Macromolecules* **1996**, *29* (11), 4142–4154. DOI: 10.1021/ma951762v.
- (162) Matsen, M. W.; Schick, M. *Macromolecules* **1994**, *27* (23), 6761–6767. DOI: 10.1021/ma00101a014.
- (163) Olvera de la Cruz, Monica; Sanchez, I. C. *Macromolecules* **1986**, *19* (10), 2501–2508. DOI: 10.1021/ma00164a008.
- (164) Buzza, D. M. A.; Hamley, I. W.; Fzea, A. H.; Moniruzzaman, M.; Allgaier, J. B.; Young, R. N.; Olmsted, P. D.; McLeish, T. C. B. *Macromolecules* **1999**, *32* (22), 7483–7495. DOI: 10.1021/ma9904060.
- (165) Buzza, D. M. A.; Fzea, A. H.; Allgaier, J. B.; Young, R. N.; Hawkins, R. J.; Hamley, I. W.; McLeish, T. C. B.; Lodge, T. P. *Macromolecules* **2000**, *33* (22), 8399–8414. DOI: 10.1021/ma000382t.
- (166) Bi, L.-K.; Fetters, L. J. *Macromolecules* **1976**, *9* (5), 732–742. DOI: 10.1021/ma60053a010.
- (167) Zhang, J.; Schneiderman, D. K.; Li, T.; Hillmyer, M. A.; Bates, F. S. *Macromolecules* **2016**, *49* (23), 9108–9118. DOI: 10.1021/acs.macromol.6b02033.
- (168) Zhulina, E. B.; Sheiko, S. S.; Dobrynin, A. V.; Borisov, O. V. *Macromolecules* **2020**, *53* (7), 2582–2593. DOI: 10.1021/acs.macromol.9b02485.
- (169) Sheiko, S. S.; Sumerlin, B. S.; Matyjaszewski, K. *Prog. Polym. Sci.* **2008**, *33* (7), 759–785. DOI: 10.1016/j.progpolymsci.2008.05.001.
- (170) Sheiko, S. S.; Sun, F. C.; Randall, A.; Shirvanyants, D.; Rubinstein, M.; Lee, H.-i.; Matyjaszewski, K. *Nature* **2006**, *440* (7081), 191–194. DOI: 10.1038/nature04576.
- (171) Zhang, J.; Li, T.; Mannion, A. M.; Schneiderman, D. K.; Hillmyer, M. A.; Bates, F. S. *ACS Macro Lett.* **2016**, *5* (3), 407–412. DOI: 10.1021/acsmacrolett.6b00091.
- (172) Rzayev, J. *Macromolecules* **2009**, *42* (6), 2135–2141. DOI: 10.1021/ma802304y.
- (173) Daniel, W. F. M.; Burdyńska, J.; Vatankhah-Varnoosfaderani, M.; Matyjaszewski, K.; Paturej, J.; Rubinstein, M.; Dobrynin, A. V.; Sheiko, S. S. *Nature materials* **2016**, *15* (2), 183–189. DOI: 10.1038/nmat4508.
- (174) Jiang, L.; Nykypanchuk, D.; Ribbe, A. E.; Rzayev, J. *ACS Macro Lett.* **2018**, *7* (6), 619–623. DOI: 10.1021/acs-macrolett.8b00273.
- (175) Lu, W.; Goodwin, A.; Wang, Y.; Yin, P.; Wang, W.; Zhu, J.; Wu, T.; Lu, X.; Hu, B.; Hong, K.; Kang, N.-G.; Mays, J. *Polym. Chem.* **2017**, *9* (2), 160–168. DOI: 10.1039/C7PY01518F.
- (176) Burns, A. B.; Register, R. A. *Macromolecules* **2016**, *49* (24), 9521–9530. DOI: 10.1021/acs.macromol.6b02175.
- (177) Mayo, F. R.; Lewis, F. M. *J. Am. Chem. Soc.* **1944**, *66* (9), 1594–1601. DOI: 10.1021/ja01237a052.
- (178) Alfrey, T.; Goldfinger, G. *J. Chem. Phys.* **1944**, *12* (6), 205–209. DOI: 10.1063/1.1723934.
- (179) Wall, F. T. *J. Am. Chem. Soc.* **1941**, *63* (7), 1862–1866. DOI: 10.1021/ja01852a016.
- (180) Merz, E.; Alfrey, T.; Goldfinger, G. *J. Polym. Sci.* **1946**, *1* (2), 75–82. DOI: 10.1002/pol.1946.120010202.
- (181) Bevington, J. C.; Harris, D. O. *J. Polym. Sci. B Polym. Lett.* **1967**, *5* (9), 799–802. DOI: 10.1002/pol.1967.110050912.
- (182) Grassie, N.; Torrance, B.J.D.; Fortune, J. D.; Gemmell, J. D. *Polymer* **1965**, *6* (12), 653–658. DOI: 10.1016/0032-3861(65)90048-0.
- (183) Hutchings, L. R.; Brooks, P. P.; Shaw, P.; Ross-Gardner, P. *J. Polym. Sci. A* **2019**, *57* (3), 382–394. DOI: 10.1002/pola.29208.
- (184) Staudinger, U.; Satapathy, B. K.; Thunga, M.; Weidisch, R.; Janke, A.; Knoll, K. *Eur. Polym. J.* **2007**, *43* (6), 2750–2758. DOI: 10.1016/j.eurpolymj.2007.03.022.

- (185) Morton, M.; Bostick, E. E.; Livigni, R. A.; Fetters, L. J. *J. Polym. Sci. A: Gen. Pap.* **1963**, 1 (5), 1735–1747. DOI: 10.1002/pol.1963.100010525.
- (186) Korotkov, A. A.; Chesnokova, N. N.; Trukhmanova, L. B. *Polymer Science U.S.S.R.* **1960**, 1 (1), 10–20. DOI: 10.1016/0032-3950(60)90229-X.
- (187) Hsieh, H. L. *J. Polym. Sci. A: Gen. Pap.* **1965**, 3 (1), 153–161. DOI: 10.1002/pol.1965.100030117.
- (188) Hsieh, H. L. *J. Polym. Sci. A: Gen. Pap.* **1965**, 3 (1), 163–172. DOI: 10.1002/pol.1965.100030118.
- (189) Bywater, S.; Worsfold, D. J. *J. Organomet. Chem.* **1967**, 10 (1), 1–6. DOI: 10.1016/S0022-328X(00)81711-8.
- (190) Roovers, J. E. L.; Bywater, S. *Macromolecules* **1968**, 1 (4), 328–331. DOI: 10.1021/ma60004a010.
- (191) Gold, L. *J. Chem. Phys.* **1958**, 28 (1), 91–99. DOI: 10.1063/1.1744088.
- (192) Welch, F. J. *J. Am. Chem. Soc.* **1960**, 82 (23), 6000–6005. DOI: 10.1021/ja01508a009.
- (193) O'Driscoll, K. F.; Tobolsky, A. V. *J. Polym. Sci.* **1959**, 35 (128), 259–265. DOI: 10.1002/pol.1959.1203512821.
- (194) Worsfold, D. J.; Bywater, S. *Can. J. Chem.* **1960**, 38 (10), 1891–1900. DOI: 10.1139/v60-254.
- (195) Geacintov, C.; Smid, J.; Szwarc, M. *J. Am. Chem. Soc.* **1961**, 83 (5), 1253–1254. DOI: 10.1021/ja01466a057.
- (196) Cubbon, R.C.P.; Margerison, D. *Proc. R. Soc. Lond. A* **1962**, 268 (1333), 260–275. DOI: 10.1098/rspa.1962.0138.
- (197) A. A. Korotkov. *Angew. Chem.* **1958**, 70 (3), 85.
- (198) Margl, P. *Can. J. Chem.* **2009**, 87 (7), 891–903. DOI: 10.1139/V09-032.
- (199) Zelinski, R.; Childers, C. W. *Rubber Chem. Technol.* **1968**, 41 (1), 161–181. DOI: 10.5254/1.3539168.
- (200) Hashimoto, T.; Tsukahara, Y.; Kawai, H. *Polym. J.* **1983**, 15 (10), 699–711. DOI: 10.1295/polymj.15.699.
- (201) Morton, M.; Fetters, L. J.; Bostick, E. E. *J. Polym. Sci. C Polym. Symp.* **1963**, 1 (1), 311–323. DOI: 10.1002/polc.5070010121.
- (202) Cubbon, R.C.P.; Margerison, D. *Polymer* **1965**, 6 (2), 102–106. DOI: 10.1016/0032-3861(65)90022-4.
- (203) Hsieh, H. L. *J. Polym. Sci. A: Gen. Pap.* **1965**, 3 (1), 173–180. DOI: 10.1002/pol.1965.100030119.
- (204) Fetters, L. J.; Balsara, N. P.; Huang, J. S.; Jeon, H. S.; Almdal, K.; Lin, M. Y. *Macromolecules* **1995**, 28 (14), 4996–5005. DOI: 10.1021/ma00118a031.
- (205) Zhao, Y.; Miyamoto, N.; Koizumi, S.; Hashimoto, T. *Macromolecules* **2010**, 43 (6), 2948–2959. DOI: 10.1021/ma902542e.
- (206) Worsfold, D. J.; Bywater, S. *Macromolecules* **1972**, 5 (4), 393–397. DOI: 10.1021/ma60028a012.
- (207) Fetters, L. J.; Morton, M. *Macromolecules* **1974**, 7 (5), 552–559. DOI: 10.1021/ma60041a004.
- (208) Watanabe, H.; Oishi, Y.; Kanaya, T.; Kaji, H.; Horii, F. *Macromolecules* **2003**, 36 (1), 220–228. DOI: 10.1021/ma0213697.
- (209) Niu, A. Z.; Stellbrink, J.; Allgaier, J.; Willner, L.; Radulescu, A.; Richter, D.; Koenig, B. W.; May, R. P.; Fetters, L. J. *J. Chem. Phys.* **2005**, 122 (13), 134906. DOI: 10.1063/1.1866092.
- (210) Bywater, S. *Macromolecules* **1998**, 31 (18), 6010–6013. DOI: 10.1021/ma970963r.
- (211) Worsfold, D. J. *J. Polym. Sci. A* **1967**, 5 (11), 2783–2789. DOI: 10.1002/pol.1967.150051106.
- (212) Quinebèche, S.; Navarro, C.; Gnanou, Y.; Fontanille, M. *Polymer* **2009**, 50 (6), 1351–1357. DOI: 10.1016/j.polymer.2009.01.041.
- (213) Grune, E.; Bareuther, J.; Blankenburg, J.; Appold, M.; Shaw, L.; Müller, A. H. E.; Floudas, G.; Hutchings, L. R.; Gallei, M.; Frey, H. *Polym. Chem.* **2019**, 50 (1), 3. DOI: 10.1039/C8PY01711E.
- (214) Spirin, Y. L.; Arest-Yakubovich, A. A.; Polyakov, D. K.; Gantmakher, A. R.; Medvedev, S. S. *J. Polym. Sci.* **1962**, 58

- (166), 1181–1189. DOI: 10.1002/pol.1962.1205816674.
- (215) Morton, M.; Fetters, L. J. *J. Polym. Sci. A: Gen. Pap.* **1964**, 2 (7), 3311–3326. DOI: 10.1002/pol.1964.100020726.
- (216) *Controlled and living polymerizations: Methods and materials*; Müller, A. H. E., Matyjaszewski, K., Eds.; Wiley-VCH: Weinheim, 2009.
- (217) Roovers, J. E. L.; Bywater, S. *Trans. Faraday Soc.* **1966**, 62, 701. DOI: 10.1039/TF9666200701.
- (218) Garton, A.; Bywater, S. *Macromolecules* **1975**, 8 (6), 694–697. DOI: 10.1021/ma60048a002.
- (219) Sardelis, K.; Michels, H. J.; Allen, G.; S, F. R. *Polymer* **1984**, 25 (7), 1011–1019. DOI: 10.1016/0032-3861(84)90089-2.
- (220) Kelley, D. J.; Tobolsky, A. V. *J. Am. Chem. Soc.* **1959**, 81 (7), 1597–1600. DOI: 10.1021/ja01516a021.
- (221) Antkowiak, T. A.; Oberster, A. E.; Halasa, A. F.; Tate, D. P. *J. Polym. Sci. A* **1972**, 10 (5), 1319–1334. DOI: 10.1002/pol.1972.150100504.
- (222) Wofford, C. F. Production of Random Copolymers in Organolithium Polymerization Systems. 3,498,960, Mar 3, 1970.
- (223) Bywater, S.; Alexander, I. J. *J. Polym. Sci. A* **1968**, 6 (12), 3407–3410. DOI: 10.1002/pol.1968.150061218.
- (224) Lehong, B.; Shengkang, Y. *J. Appl. Polym. Sci.* **1992**, 44 (9), 1507–1511. DOI: 10.1002/app.1992.070440902.
- (225) Liu, F.; Tan, H.-y.; Tang, T. *Chin. J. Polym. Sci.* **2013**, 31 (12), 1647–1659. DOI: 10.1007/s10118-013-1357-x.
- (226) Liao, M.; Wang, Q.; Wang, N.; Xu, L.; Li, C.; Liang, A. *Polym. Sci. Ser. B* **2014**, 56 (6), 753–761. DOI: 10.1134/S1560090415010108.
- (227) Zhao, Z.; Shen, H.; Sui, K.; Wang, G. *Polymer* **2018**, 137, 364–369. DOI: 10.1016/j.polymer.2017.12.070.
- (228) Halasa, A. F.; Gross, B. B.; Hsu, W.-L. *Rubber Chem. Technol.* **2010**, 83 (4), 380–390. DOI: 10.5254/1.3512953.
- (229) Moczygemba, G. A.; Trepka, W. J. Tapered Block Styrene/Butadiene Copolymers. 5,227,419, Dec 20, 1990.
- (230) Moczygemba, G. A.; Knight, N. R.; Trepka, W. J.; Stacy, N. E. Block Copolymers of Monovinylarenes and Conjugated Dienes Containing Two Interior Tapered Blocks. 5,399,628, Dec 2, 1993.
- (231) Steube, M.; Johann, T.; Hübner, H.; Koch, M.; Dinh, T.; Gallei, M.; Floudas, G.; Frey, H.; Müller, A. H.E. *submitted*.
- (232) Bywater, S.; Johnson, A. F.; Worsfold, D. J. *Can. J. Chem.* **1964**, 42 (6), 1255–1260. DOI: 10.1139/v64-197.
- (233) Foster, F. C.; Binder, J. L. In *Homogeneous transition metal catalyzed reactions: Developed from a symposium*; Moser, W. R., Slocum, D. W., Eds.; Advances in chemistry series 230; The Society: Washington, DC, 1992; pp 26–33.
- (234) Szwarc, M. *J. Polym. Sci.* **1959**, 40 (137), 583–586. DOI: 10.1002/pol.1959.1204013734.
- (235) Bywater, S.; Firat, Y.; Black, P. E. *J. Polym. Sci. Polym. Chem. Ed.* **1984**, 22 (3), 669–672. DOI: 10.1002/pol.1984.170220316.
- (236) Tobolsky, A. V.; Rogers, C. E. *J. Polym. Sci.* **1959**, 38 (133), 205–207. DOI: 10.1002/pol.1959.1203813317.
- (237) Tobolsky, A. V.; Rogers, C. E. *J. Polym. Sci.* **1959**, 40 (136), 73–89. DOI: 10.1002/pol.1959.1204013605.
- (238) Widmaier, J. M.; Meyer, G. C. *Macromolecules* **1981**, 14 (2), 450–452. DOI: 10.1021/ma50003a041.
- (239) Lehong, B.; Shengkang, Y. *J. Appl. Polym. Sci.* **1992**, 44 (9), 1499–1505. DOI: 10.1002/app.1992.070440901.
- (240) Obermeier, B.; Wurm, F. R.; Frey, H. *Macromolecules* **2010**, 43 (5), 2244–2251. DOI: 10.1021/ma902245d.
- (241) Herzberger, J.; Leibig, D.; Liermann, J. C.; Frey, H. *ACS Macro Lett.* **2016**, 5 (11), 1206–1211. DOI: 10.1021/acs-macrolett.6b00701.
- (242) Long, T. E.; Liu, H. Y.; Schell, B. A.; Teegarden, D. M.; Uerz, D. S. *Macromolecules* **1993**, 26 (23), 6237–6242. DOI: 10.1021/ma00075a018.

- (243) Lanzendörfer, M. G.; Schmalz, H.; Abetz, V.; Müller, A. H. E. In *In Situ Spectroscopy of Monomer and Polymer Synthesis*; Puskas, J. E., Long, T. E., Storey, R. F., Shaikh, S., Simmons, C. L., Eds.; Springer US: Boston, MA, s.l., 2003; pp 67–81.
- (244) Kim, J. M.; Chakrapani, S. B.; Beckingham, B. S. *Macromolecules* **2020**. DOI: 10.1021/acs.macromol.0c00526.
- (245) Worsfold, D. J.; Bywater, S. *Can. J. Chem.* **1964**, 42 (12), 2884–2892. DOI: 10.1139/v64-426.
- (246) Artyushenko, V. In *Specialty optical fibers, Part of Advanced photonics ; 27 - 31 July 2014, Barcelona, Spain*; OSA The Optical Society: Washington, DC, 2014; 35-39.
- (247) Bywater, S.; Worsfold, D. J. *Can. J. Chem.* **1962**, 40 (8), 1564–1570. DOI: 10.1139/v62-236.
- (248) Takezawa, Y.; Ohara, S. *J. Appl. Polym. Sci.* **1993**, 49 (1), 169–173. DOI: 10.1002/app.1993.070490120.
- (249) Bywater, S.; Worsfold, D. J. *Can. J. Chem.* **1967**, 45 (16), 1821–1824. DOI: 10.1139/v67-293.
- (250) Fineman, M.; Ross, S. D. *J. Polym. Sci.* **1950**, 5 (2), 259–262. DOI: 10.1002/pol.1950.120050210.
- (251) Kelen, T.; Tüdös, F.; Turcsnyi, B. *Polym. Bull.* **1980**, 2 (1), 71–76. DOI: 10.1007/BF00275556.
- (252) Chartrand, R. *ISRN Applied Mathematics* **2011**, 2011 (1–4), 1–11. DOI: 10.5402/2011/164564.
- (253) Meyer, V. E.; Lowry, G. G. *J. Polym. Sci. A: Gen. Pap.* **1965**, 3 (8), 2843–2851. DOI: 10.1002/pol.1965.100030811.
- (254) Skeist, I. *J. Am. Chem. Soc.* **1946**, 68 (9), 1781–1784. DOI: 10.1021/ja01213a031.
- (255) Jaacks, V. *Angew. Chem.* **1967**, 79 (9), 419. DOI: 10.1002/ange.19670790927.
- (256) Beckingham, B. S.; Sanoja, G. E.; Lynd, N. A. *Macromolecules* **2015**, 48 (19), 6922–6930. DOI: 10.1021/acs.macromol.5b01631.
- (257) Lynd, N. A.; Ferrier, R. C.; Beckingham, B. S. *Macromolecules* **2019**. DOI: 10.1021/acs.macromol.8b01752.
- (258) Blankenburg, J.; Kersten, E.; Maciol, K.; Wagner, M.; Zorbakhsh, S.; Frey, H. *Polym. Chem.* **2019**, 116, 2170. DOI: 10.1039/C9PY00500E.
- (259) Smotherman, M.; Spicer, D. *Commun. ACM* **2010**, 53 (12), 28–30. DOI: 10.1145/1859204.1859216.
- (260) Moore, G. E. *IEEE Solid-State Circuits Soc. Newsl.* **2006**, 11 (3), 33–35. DOI: 10.1109/N-SSC.2006.4785860.
- (261) Dünweg, B.; Kremer, K. *J. Chem. Phys.* **1993**, 99 (9), 6983–6997. DOI: 10.1063/1.465445.
- (262) Seo, Y.; Brown, J. R.; Hall, L. M. *Macromolecules* **2015**, 48 (14), 4974–4982. DOI: 10.1021/ma502309h.
- (263) D’hooge, D. R.; Fantin, M.; Magenau, A. J. D.; Konkolewicz, D.; Matyjaszewski, K. *React. Chem. Eng.* **2018**, 3 (6), 866–874. DOI: 10.1039/C8RE00156A.
- (264) Marien, Y. W.; van Steenberge, P. H. M.; Barner-Kowollik, C.; Reyniers, M.-F.; Marin, G. B.; D’hooge, D. R. *Macromolecules* **2017**, 50 (4), 1371–1385. DOI: 10.1021/acs.macromol.6b02627.
- (265) Cho, A. S.; Broadbelt, L. J. *Mol. Simul.* **2010**, 36 (15), 1219–1236. DOI: 10.1080/08927020903513035.
- (266) D’hooge, D. R.; van Steenberge, P. H.M.; Reyniers, M.-F.; Marin, G. B. *Prog. Polym. Sci.* **2016**, 58, 59–89. DOI: 10.1016/j.progpolymsci.2016.04.002.
- (267) D’hooge, D. R. *Macromol. Rapid Commun.* **2018**, 39 (14), e1800057. DOI: 10.1002/marc.201800057.
- (268) Hamzehlou, S.; Reyes, Y.; Leiza, J. R. *Macromol. React. Eng.* **2012**, 6 (8), 319–329. DOI: 10.1002/mren.201200016.
- (269) Lu, J.; Zhang, H.; Yang, Y. *Makromol. Chem., Theory Simul.* **1993**, 2 (5), 747–760. DOI: 10.1002/mats.1993.040020511.
- (270) Regatte, V. R.; Gao, H.; Konstantinov, I. A.; Arturo, S. G.; Broadbelt, L. J. *Macromol. Theory Simul.* **2014**, 23 (9), 564–574. DOI: 10.1002/mats.201400037.
- (271) Smith, A. A. A.; Hall, A.; Wu, V.; Xu, T. *ACS Macro Lett.* **2019**, 8 (1), 36–40. DOI: 10.1021/acsmacrolett.8b00813.

- (272) van Steenberge, P. H. M.; D'hooge, D. R.; Wang, Y.; Zhong, M.; Reyniers, M.-F.; Konkolewicz, D.; Matyjaszewski, K.; Marin, G. B. *Macromolecules* **2012**, 45 (21), 8519–8531. DOI: 10.1021/ma3017597.
- (273) Wang, L.; Broadbelt, L. J. *Macromolecules* **2010**, 43 (5), 2228–2235. DOI: 10.1021/ma9019703.
- (274) Zheng, Z.; Ling, J.; Müller, A. H. E. *Macromolecular rapid communications* **2014**, 35 (2), 234–241. DOI: 10.1002/marc.201300578.
- (275) Anantawaraskul, S.; Soares, J. B. P.; Wood-Adams, P. M. *Macromol. Theory Simul.* **2003**, 12 (4), 229–236. DOI: 10.1002/mats.200390024.
- (276) Fierens, S. K.; van Steenberge, P. H. M.; Reyniers, M.-F.; D'hooge, D. R.; Marin, G. B. *React. Chem. Eng.* **2018**, 3 (2), 128–145. DOI: 10.1039/C7RE00206H.
- (277) Stockmayer, W. H. *J. Chem. Phys.* **1945**, 13 (6), 199–207. DOI: 10.1063/1.1724022.
- (278) Mastan, E.; He, J. *Macromolecules* **2017**, 50 (23), 9173–9187. DOI: 10.1021/acs.macromol.7b01662.
- (279) Yang, L.; Han, L.; Ma, H.; Shen, H.; Li, C.; Zhang, S.; Lei, L.; Hao, X.; Li, Y. *Eur. Polym. J.* **2019**, 120, 109212. DOI: 10.1016/j.eurpolymj.2019.08.039.
- (280) Livitsanou, C.; Steube, M.; Johann, T.; Frey, H.; Floudas, G. *Macromolecules* **2020**, 53 (8), 3042–3051. DOI: 10.1021/acs.macromol.0c00445.
- (281) Willemse, R. X. E.; van Herk, A. M. *J. Am. Chem. Soc.* **2006**, 128 (13), 4471–4480. DOI: 10.1021/ja0579715.
- (282) Willemse, R. X. E.; Staal, B. B. P.; Donkers, E. H. d.; van Herk, A. M. *Macromolecules* **2004**, 37 (15), 5717–5723. DOI: 10.1021/ma049471m.
- (283) Engler, M. S.; Crotty, S.; Barthel, M. J.; Pietsch, C.; Knop, K.; Schubert, U. S.; Böcker, S. *Anal. Chem.* **2015**, 87 (10), 5223–5231. DOI: 10.1021/acs.analchem.5b00146.
- (284) van Steenberge, P.H.M.; D'hooge, D. R.; Reyniers, M.-F.; Marin, G. B. *Chemical Engineering Science* **2014**, 110, 185–199. DOI: 10.1016/j.ces.2014.01.019.

SUPPORTING INFORMATION

1 Calculation of the Order-Disorder Transition Temperature

According to equation S1.1, the Flory-Huggins parameter χ can be calculated for a given temperature.^{1,2} According to Leibler, the order-disorder transition for volume symmetric diblock copolymers is given by equation S1.2. This enables to calculate the Order-Disorder transition temperature (T_{ODT}) as a function of the degree of polymerization (equation S1.3). To calculate the degree of polymerization for a volume-symmetric diblock copolymer (equation S.1.4- S1.9), the densities and the molecular weights of the PI- and PS-repeating units need to be considered.³ The Flory-Huggins parameter for PI-*b*-PS (usually χ_{IS}) is denoted in the following equations as $\chi_{PI,PS}$ as I and S was used for isoprene and styrene monomer.

$$M_I = 68.12 \text{ g/mol}; \rho_{PI}(140 \text{ }^\circ\text{C}) = 0.830 \text{ g/cm}^3;$$

$$M_S = 104.15 \text{ g/mol}; \rho_{PS}(140 \text{ }^\circ\text{C}) = 0.969 \text{ g/cm}^3$$

$$\chi_{PI,PS}(T) = \frac{71.4}{T} - 0.0857 \quad (\text{S1.1})$$

$$\chi_{PI,PS}(T_{ODT}) \cdot N = \left(\frac{71.4}{T_{ODT}} - 0.0857 \right) \cdot N = 10.5 \quad (\text{S1.2})$$

$$T_{ODT} = \frac{71.4}{\frac{10.5}{N} + 0.0857} \quad (\text{S1.3})$$

$$V_{PS} = V_{PI} \quad (\text{S1.4})$$

$$N_{PS} \cdot \frac{M_{PS}}{\rho_{PS}} = N_{PI} \cdot \frac{M_{PI}}{\rho_{PI}} \quad (\text{S1.5})$$

$$\frac{N_{PS}}{N_{PI}} = \frac{\frac{M_{PI}}{\rho_{PI}}}{\frac{M_{PS}}{\rho_{PS}}} = \frac{82.1}{108} \quad (\text{S1.6})$$

$$N = N_{PS} + N_{PI} \quad (S1.7)$$

$$M_{\text{average}} = \frac{N_{PS}}{N} \cdot M_S + \frac{N_{PI}}{N} \cdot M_I = \frac{82.1}{82.1 + 108} \cdot M_S + \frac{108}{82.1 + 108} \cdot M_I = 83.6 \quad (S1.8)$$

$$N = \frac{M_n}{M_{\text{average}}} \quad (S1.9)$$

Equation Set S1. Calculation of the order-disorder transition temperature (T_{ODT}) as a function of the degree of polymerization (N) and Flory-Huggins parameter $\chi_{PI,PS}(T)$ for a volume symmetric diblock copolymer.

2 Methods for the Determination of Reactivity Ratios

$$F_1 = \frac{r_1 f_1^2 + f_1 f_2}{r_1 f_1^2 + 2f_1 f_2 + r_2 f_2^2} \quad (2)$$

Equation S2. Rearranged form of the Mayo-Lewis equation to describe the instantaneous monomer incorporation F in dependence of the monomer feed f . The reactivity ratios r_1 and r_2 can be determined by least square fitting of a corresponding data set.⁴

$$G = \frac{f_1 (2F_1 - 1)}{(1 - f_1) F_1} \quad (3.1)$$

$$H = \frac{f_1^2 (1 - F_1)}{(1 - f_1)^2 F_1} \quad (3.2)$$

$$G = H \cdot r_1 - r_2 \quad (3.3)$$

Equation Set S3. Equations for the Fineman-Ross formalism to determine reactivity ratios via linearization of the Mayo-Lewis equation. The reactivity ratios can be determined from the intercept (r_2) and slope (r_1) when H is plotted versus G .⁵

$$\alpha = (H_{\min} \cdot H_{\max})^{0.5} \quad (4.1)$$

$$\eta = \frac{G}{\alpha + H} \quad (4.2)$$

$$\mu = \frac{H}{\alpha + H} \quad (4.3)$$

$$\eta = \left(r_1 + \frac{r_2}{\alpha} \right) \cdot \mu - \frac{r_2}{\alpha} \quad (4.4)$$

Equation Set S4. Equations for the Kelen-Tüdős formalism. The correction factor α is determined based on the smallest and highest value H of the Fineman-Ross formalism and used to account for biases introduced by the linearization. The reactivity ratios can be determined from the slope and the intercept when μ is plotted versus η .⁶

$$f_1 = \frac{M_1}{M_1 + M_2} \quad (5.1)$$

$$f_2 = 1 - f_1 \quad (5.2)$$

$$F_1 = \frac{dM_1}{d(M_1 + M_2)} \quad (5.3)$$

$$x = 1 - \frac{M_1 + M_2}{M_{1,0} + M_{2,0}} = 1 - \frac{M}{M_0} \quad (5.4)$$

Equation Set S5. Equations to transform the monomer conversion to the variables that are required in the Mayo-Lewis, Meyer-Lowry, Fineman-Ross and Kelen-Tüdős formalism. f describes the monomer feed, F the instantaneous monomer incorporation, X the total monomer conversion.

$$\frac{M}{M_0} = \left(\frac{f_1}{f_{1,0}} \right)^{\left(\frac{r_2}{1-r_2} \right)} \cdot \left(\frac{f_2}{f_{2,0}} \right)^{\left(\frac{r_1}{1-r_1} \right)} \cdot \left(\frac{f_{1,0} - \frac{1-r_2}{2-r_1-r_2}}{f_1 - \frac{1-r_2}{2-r_1-r_2}} \right)^{\left(\frac{1-r_1 \cdot r_2}{(1-r_1) \cdot (1-r_2)} \right)} \quad (6)$$

Equation S6. Meyer-Lowry equation. The reactivity ratios r_1 and r_2 can be obtained via least square fitting of this equation to a corresponding data set based on f_1 and $f_2 = 1 - f_1$ versus $1 - \text{total monomer conversion } (M/M_0 = 1 - X)$.⁷

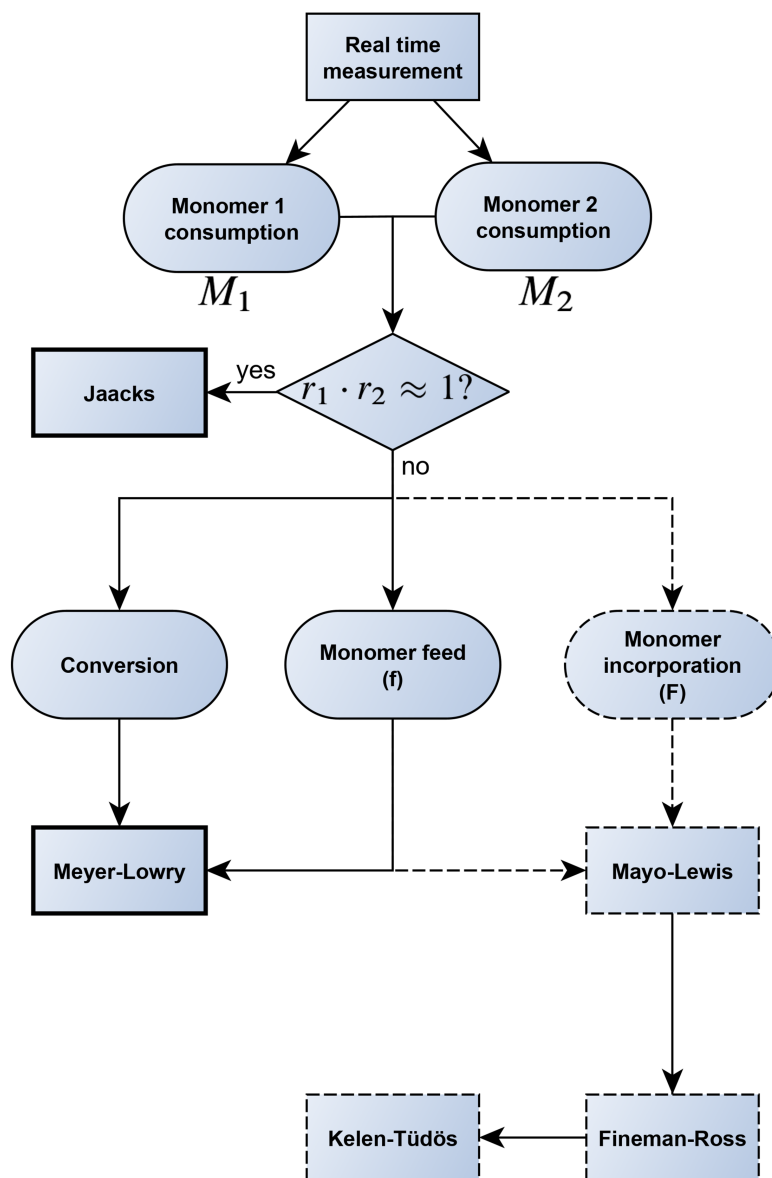
$$\ln \left(\frac{M_{1,0}}{M_1} \right) = r_1 \cdot \ln \left(\frac{M_{2,0}}{M_2} \right) \quad (7)$$

Equation S7. Jaacks equation for the evaluation of an ideal copolymerization ($r_1 \cdot r_2 = 1$). The reactivity ratio can be obtained from the slope of the linear fit by plotting the logarithmic inversed monomer conversion.⁸

TABLE 1 Comparison of the selected methods for evaluation of the reactivity ratios.

Formalism	Model	Data foundation	Prerequisites	Fitting method	Recommended
Mayo-Lewis ⁴	terminal	differential	F_1, f_1	non-linear	no
Fineman-Ross ⁵	terminal	differential	F_1, f_1	linear	no
Kelen-Tüdös ⁶	terminal	differential	Fineman-Ross	linear	no
Mayer-Lowry ⁷	terminal	integrated	$X, f_1, f_{1,0}$	non-linear	yes
Jaacks ⁸	non-terminal	integrated	$M_1, M_2, M_{1,0}, M_{2,0}$	linear	yes
Integrated Ideal ⁹	non-terminal	integrated	$X, f_1, f_{1,0}$	non-linear	yes
BSL ¹⁰	non-terminal	integrated	$M_1, M_2, M_{1,0}, M_{2,0}$	non-linear	yes

SCHEME S1 Overview of the common methods for determination of reactivity ratios. Methods based on the differential copolymer equation are marked by dashed lines and are not recommended for evaluation of copolymerization kinetics. Recommend methods are highlighted in bold.



3 Kinetic Monte Carlo Simulations

The basic principle of every MC simulation relies on stochastics. While each individual calculation is very simple, and only the available brute-force computational power renders this method suitable to accurately predict copolymerization experiments. The foundation to perform kMC simulations was built up by Gillespie.^{11,12} A typical kMC process is based on the reported equations by Gillespie and the conversion of the continuum-based reaction rates to number-based probabilities. These number-based probabilities are then used to determine which reaction is performed next. After selection of the reaction step by a random number, the reaction is applied, and the number of residual molecules is adjusted. Then the process is repeated. (Equation Set S7, Scheme 2). Specifically, for the prediction of chain growth polymerizations like a living anionic copolymerization, a virtual flask is created (10^{-19} L to 10^{-16} L volume), in which chain ends (typically 100,000 or more) are placed and reacted with monomers. The reaction is chosen and simulated based on their reaction probability, which scales with the kinetic rate constants. Like in a real reaction flask, each addition of a monomer to a chain end alters the overall concentration of the monomers.

$$kMC_{11} = \frac{k_{11}}{(NV)^{1/A_1}} \quad (\text{S8.1})$$

$$kMC_{22} = \frac{k_{22}}{(NV)^{1/A_2}} \quad (\text{S8.2})$$

$$kMC_{12} = \frac{k_{12}}{(NV)^{1/A_1}} \quad (\text{S8.3})$$

$$kMC_{21} = \frac{k_{21}}{(NV)^{1/A_2}} \quad (\text{S8.4})$$

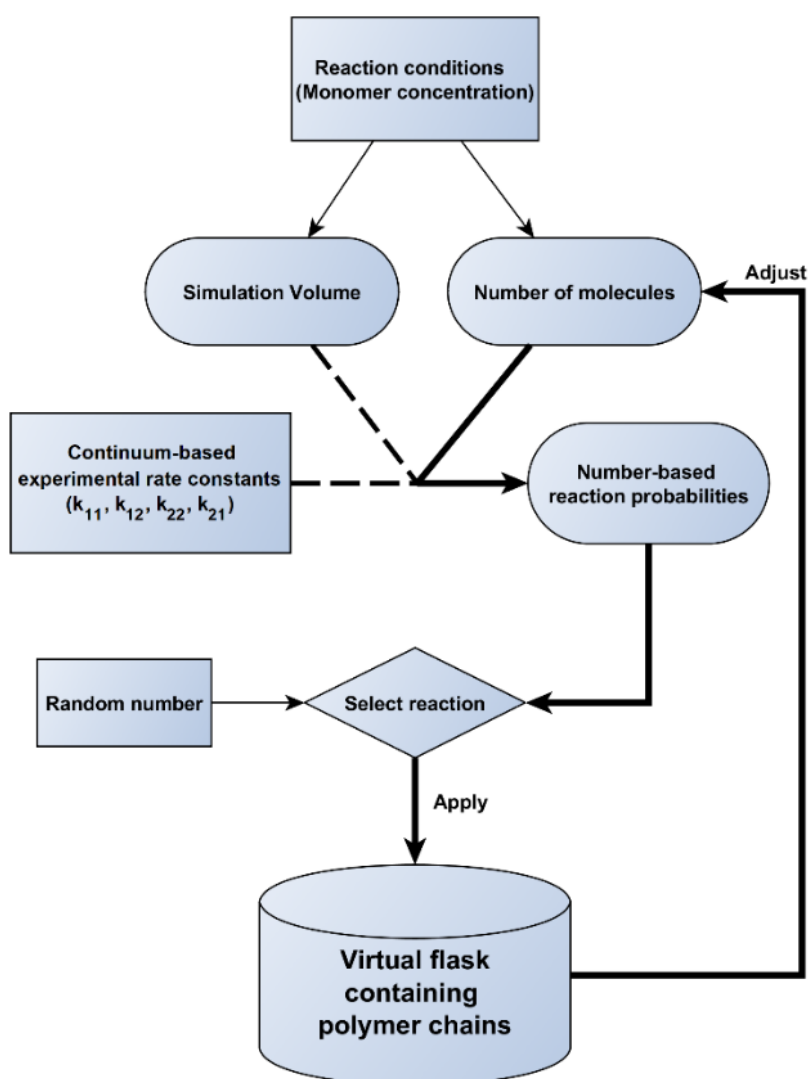
$$P_v = \frac{R_v}{\sum_{M=1}^{\mu-1} R_v} \quad (\text{S8.5})$$

$$\sum_{v=1}^{\mu-1} P_v < rn_1 < \sum_v^{\mu} P_v \quad (\text{S8.6})$$

$$\tau = \frac{1}{\sum_{M=1}^V R_V} \ln \left(\frac{1}{r n_2} \right) \quad (\text{S8.7})$$

Equation Set S8. Equations to perform a kinetic Monte Carlo (kMC) simulation of a living anionic copolymerization. The homopropagation (k_{11} , k_{22}) and crosspropagation (k_{12} , k_{21}) rate constants are transformed to number-based probabilities (k_{MC11} , k_{MC12} , k_{MC22} , k_{MC21}) by the equations 8.1 - 8.4 and the corresponding aggregation number A_1/A_2 (e.g. 2 in case of dimers and 4 in case of tetramers). The corresponding reaction is then determined based on the cumulative probabilities P_V (Eq. 8.5) and a by a uniformly distributed random number $r n_1 = [0 \dots 1]$ (Eq. 8.6). The corresponding time step is calculated by a second random number $r n_2 = [0 \dots 1]$ (Eq. 8.7).

SCHEME S2 Simplified scheme of the process of performing a kMC simulation.



kMC Example: SEC Distributions – Failed polymerization or not?

When performing a living anionic polymerization, a monomodal narrow molecular weight distribution is typically expected. Hence, to determine if a copolymerization was successful, typically the molecular weight distribution (e.g. the dispersity) via SEC is used as the first proxy for evaluation. Prediction of the dispersity of homopolymers prepared via living anionic copolymerization is straightforward based on the Poisson distribution ($\bar{D} = 1 + 1/DP_n - 1/DP_n^2$). In contrast, the dispersity of a copolymerization cannot be predicted in a trivial manner.^{13,14}

In two of our previous works, we synthesized statistical copolymers of styrene derivatives and isoprene.^{13,14} All low molecular weight polymers ($< 5 \text{ kg}\cdot\text{mol}^{-1}$) showed broadening of the molecular weight distribution and thus were first regarded as failed polymerizations due to experimental problems. The low molecular weight fraction of the molecular weight distribution was found to exhibit an increased isoprene content. This was ascribed to the rather slow crossover from a P_{Li} chain end to 4-methyl styrene (4MS) compared to the homopropagation of 4MS.¹³ However, a prediction of the molecular weight distribution (and SEC curve) via kMC showed that indeed a broadened molecular weight distribution was to be expected (Figure S1).

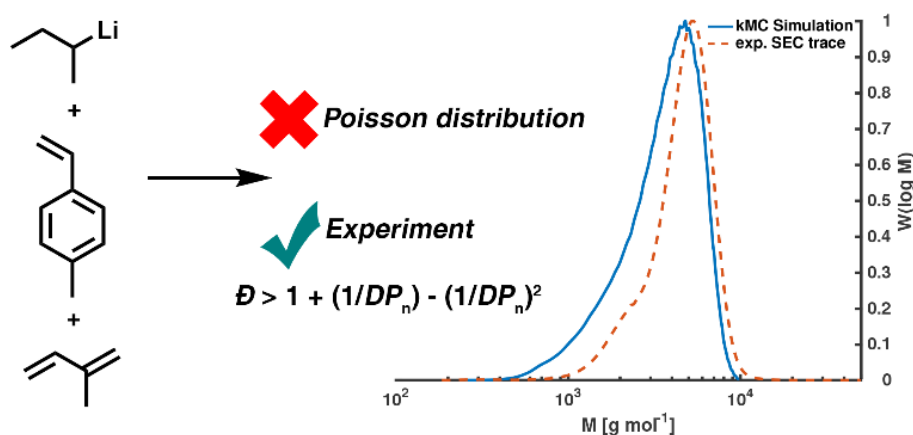


FIGURE S1 The copolymerization of 4-methyl styrene (4MS) and isoprene to obtain statistical P(I-co-4MS) copolymers leads to a broad molecular weight distribution (red dashed line), exceeding the dispersity of an ideal Poisson distribution. kMC simulation (blue solid line) confirmed that this molecular weight distribution is based on kinetic peculiarities.

kMC example: Optimization of the reaction time¹⁵

Due to the high sensitivity of the chain ends towards termination by impurities, the polymerization must be contained in a closed system.¹⁵ Hence, sampling of the polymerization is exceptionally difficult and comprises the risk of irreversible termination by introducing impurities.

In previous works, we employed the living anionic copolymerization to synthesize tapered multi-block copolymers by multiple additions of a monomer mixture to the living polymer solution.^{15,16} To obtain defined polymer structures it is crucial to postpone the monomer addition until the majority of the monomer of the previous addition step has reacted. Thus, a single value parameter such as the reaction time to the desired threshold conversion (e.g. 99.5%) becomes a crucial parameter in optimizing the polymer synthesis.

By feeding all reaction parameters to the kMC model the time-dependent monomer conversion and reaction time can be predicted within less than one minute of calculation effort. The simulation via kMC also accounts for aggregation effects of the chain ends that are present in the living anionic copolymerization of styrene and isoprene in hydrocarbons. This consideration typically leads to errors, when this calculation is performed via solving the ordinary differential equation set based on the Mayo-Lewis equations. Hence, the overall synthesis throughput is optimized by utilizing kMC simulations by knowing the exact waiting time that is required until the polymerization of added monomers is completed (Figure S2).

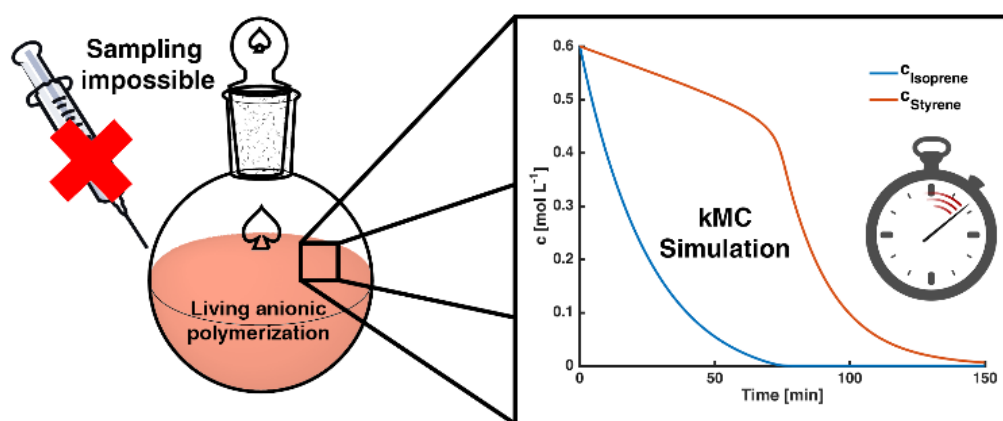


FIGURE S2 Illustration of the use of kMC simulations to predict the time-dependent monomer conversion of a living anionic copolymerization of styrene and isoprene. Based on the actual reaction rates, the kMC simulation enables a prediction of the monomer concentration in the flask at any given time.

REFERENCES

- (1) Bates, F. S.; Schulz, M. F.; Khandpur, A. K.; Förster, S.; Rosedale, J. H.; Almdal, K.; Mortensen, K. *Faraday Discuss.* **1994**, *98*, 7–18. DOI: 10.1039/FD9949800007.
- (2) Khandpur, A. K.; Förster, S.; Bates, F. S.; Hamley, I. W.; Ryan, A. J.; Bras, W.; Almdal, K.; Mortensen, K. *Macromolecules* **1995**, *28* (26), 8796–8806. DOI: 10.1021/ma00130a012.
- (3) Fetters, L. J.; Lohse, D. J.; Richter, D.; Witten, T. A.; Zirkel, A. *Macromolecules* **1994**, *27* (17), 4639–4647. DOI: 10.1021/ma00095a001.
- (4) Mayo, F. R.; Lewis, F. M. *J. Am. Chem. Soc.* **1944**, *66* (9), 1594–1601. DOI: 10.1021/ja01237a052.
- (5) Fineman, M.; Ross, S. D. *J. Polym. Sci.* **1950**, *5* (2), 259–262. DOI: 10.1002/pol.1950.120050210.
- (6) Kelen, T.; Tüdös, F.; Turcsnyi, B. *Polym. Bull.* **1980**, *2* (1), 71–76. DOI: 10.1007/BF00275556.
- (7) Meyer, V. E.; Lowry, G. G. *J. Polym. Sci. A: Gen. Pap.* **1965**, *3* (8), 2843–2851. DOI: 10.1002/pol.1965.100030811.
- (8) Jaacks, V. *Angew. Chem.* **1967**, *79* (9), 419. DOI: 10.1002/ange.19670790927.
- (9) Blankenburg, J.; Kersten, E.; Maciol, K.; Wagner, M.; Zorbakhsh, S.; Frey, H. *Polym. Chem.* **2019**, *116*, 2170. DOI: 10.1039/C9PY00500E.
- (10) Beckingham, B. S.; Sanoja, G. E.; Lynd, N. A. *Macromolecules* **2015**, *48* (19), 6922–6930. DOI: 10.1021/acs.macromol.5b01631.
- (11) Gillespie, D. T. *J. Phys. Chem.* **1977**, *81* (25), 2340–2361. DOI: 10.1021/j100540a008.
- (12) Gillespie, D. T. *J. Comput. Phys.* **1976**, *22* (4), 403–434. DOI: 10.1016/0021-9991(76)90041-3.
- (13) Grune, E.; Johann, T.; Appold, M.; Wahlen, C.; Blankenburg, J.; Leibig, D.; Müller, A. H. E.; Gallei, M.; Frey, H. *Macromolecules* **2018**, *51* (9), 3527–3537. DOI: 10.1021/acs.macromol.8b00404.
- (14) Tiedemann, P. von; Blankenburg, J.; Maciol, K.; Johann, T.; Müller, A. H. E.; Frey, H. *Macromolecules* **2019**. DOI: 10.1021/acs.macromol.8b02280.
- (15) Steube, M.; Johann, T.; Galanos, E.; Appold, M.; Rüttiger, C.; Mezger, M.; Gallei, M.; Müller, A. H. E.; Floudas, G.; Frey, H. *Macromolecules* **2018**, *51*(24), 10246–10258. DOI: 10.1021/acs.macromol.8b01961.
- (16) Galanos, E.; Grune, E.; Wahlen, C.; Müller, A. H. E.; Appold, M.; Gallei, M.; Frey, H.; Floudas, G. *Macromolecules* **2019**, *52*(4), 1577–1588. DOI: 10.1021/acs.macromol.8b02669.

CHAPTER 2

TAPERED MULTIBLOCK COPOLYMERS

CHAPTER 2

Published in *Macromolecules*, 2018. DOI: 10.1021/acs.macromol.8b01961

Isoprene/Styrene Tapered Multiblock Copolymers with up to Ten Blocks: Synthesis, Phase Behavior, Order and Mechanical Properties

Marvin Steube¹, Tobias Johann^{1,2}, Eftyxis Galanos³, Michael Appold⁴,
Christian Rüttiger⁴, Markus Mezger^{5,6}, Markus Gallei⁴, Axel H.E. Müller¹,
George Floudas^{3,5} and Holger Frey^{1*}

¹Institute of Organic Chemistry, Johannes Gutenberg-University, Duesbergweg 10-14, 55128 Mainz, Germany

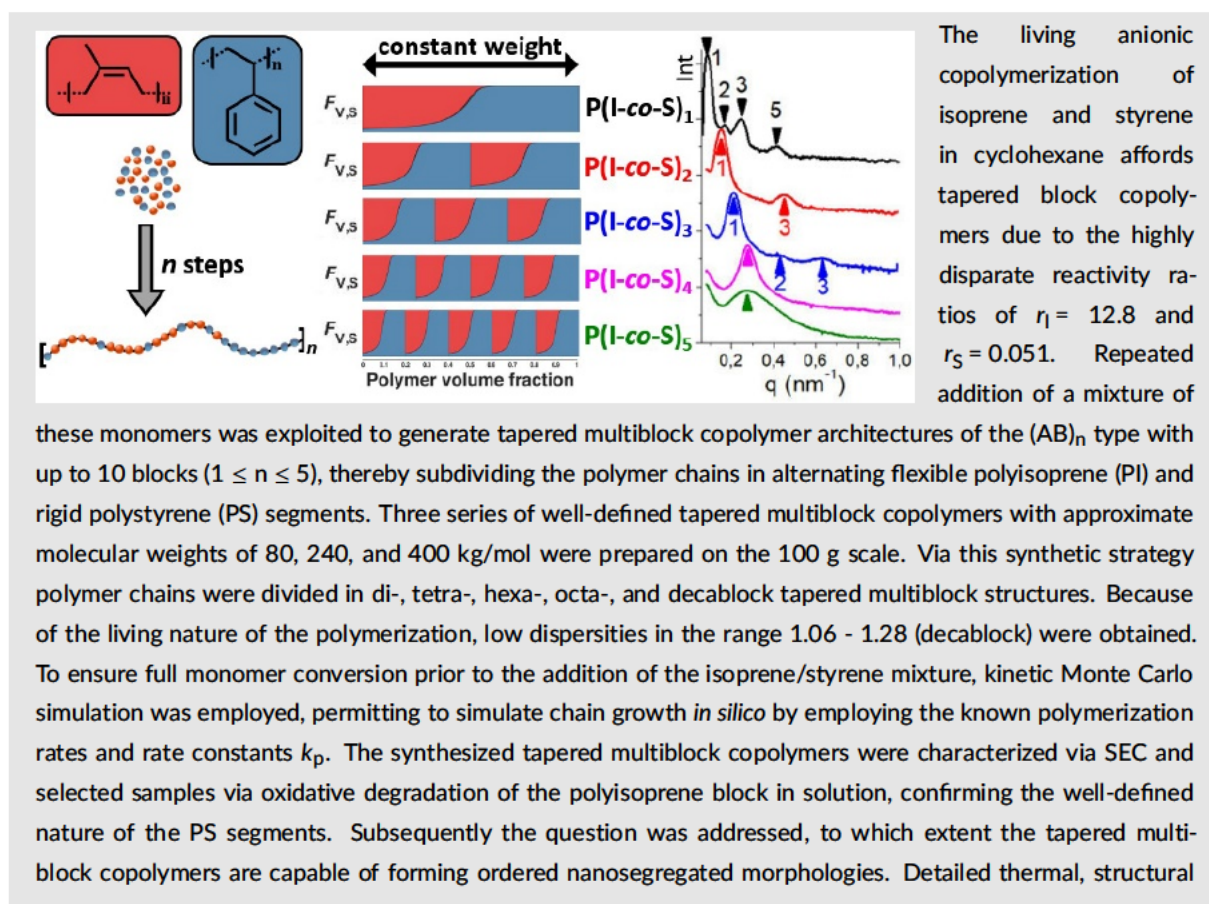
²Max Planck Graduate Center, Staudingerweg 9, 55128, Mainz, Germany

³Department of Physics, University of Ioannina, P.O. Box 1186, 45110 Ioannina, Greece

⁴Macromolecular Chemistry Department, Technische Universität Darmstadt, Alarich-Weiss Str. 4, 64287 Darmstadt, Germany

⁵Max Planck Institute for Polymer Research, Ackermannweg 10, 55128 Mainz, Germany

⁶Institute of Physics, Johannes Gutenberg University, Staudingerweg 7, 55128 Mainz, Germany



and rheological investigations showed that the tapered multiblock copolymers with a molecular weight of 240 kg/mol formed ordered phases with the expected lamellar morphology. However, X-ray scattering data and transmission electron microscopy (TEM) images of the octablock and decablock copolymers reflect weakly ordered structures at ambient temperature. The domain spacing, d , was found to scale as $d \sim N^{0.62}$, where N is the total degree of polymerization, suggesting stretching of chains and nonideal configurations. Following the structure factor, $S(q)$, as a function of temperature revealed that the tapered multiblock copolymers undergo a fluctuation-induced first-order transition at the respective order-to-disorder transition temperature, T_{ODT} . The viscoelastic response of the tapered copolymers was controlled by the nanodomain structure, the degree of segregation, nanodomain-bridging configurations of blocks, and also the proximity to the glass temperature of the vitrified PS domains. Tapered hexablock copolymers were found to best combine structural integrity and mechanical toughness, while maintaining a large strain at break (> 900%).

INTRODUCTION

Block copolymers can self-assemble into a variety of nanosegregated morphologies combining the inherent properties of each block in one material.¹⁻⁶ Strong segregation is a consequence of the immiscibility of the polymer segments.⁷ This unique behavior has inspired a broad range of applications ranging from nanolithographic processes, photonics and nanomedicine to nanoreactors.⁸⁻¹⁴ The combination of flexible, low-glass-temperature (T_g) blocks with high T_g blocks enabled application on a large commercial scale for the "thermoplastic elastomers".¹⁵ In these materials, the simple AB diblock architecture is replaced with an ABA triblock structure, where a rubbery central block (B) such as polybutadiene or polyisoprene is between two hard blocks (A) like polystyrene.¹⁶⁻²⁰ Based on this principle, tough materials with high mechanical stability were developed. Commercial examples are known as Kraton or Styroflex.²¹⁻²⁴ These highly established materials are commonly prepared by living anionic polymerization. The living carbanionic chains remain active even after full monomer conversion and allow to prepare block copolymers by subsequent addition of monomer. Despite the enhanced reaction times, as compared to more polar solvents like THF, the polymerization is usually performed in nonpolar solvents favoring the desired 1,4-polydiene isomeric structure that ensures better mechanical performance and improved thermal stability.²²

Since the extensive work of Kraus *et al.* and Worsfold *et al.* in 1967 it is well-known that the direct (*i.e.*, statistical) copolymerization of butadiene or isoprene with styrene in nonpolar hydrocarbons leads to blocklike structures that were later called "tapered" to describe the strong monomer gradient in these systems.^{21,25,26} This distinguishes these structures from block copolymers prepared by sequential addition of the respective monomers. Further studies on the statistical copolymerization of 1,3-dienes with styrene derivatives revealed highly disparate reactivity ratios for these systems in general, with the diene polymerizing first and the styrene derivative, predominantly, when almost all the diene is converted. Depending on the reactivity ratios of a chosen monomer pair, the steepness of the gradient can be varied.^{24,27-31} Hadjichristidis and coauthors used this copolymerization principle in combination with sequential methods.³² In this manner a tapered region was incorporated between two blocks consisting of the respective homopolymers. By systematically increasing the tapered proportion, increased phase compatibilization was observed. The interruption of pure monomer sequences by the respective comonomer leads to a decrease in the effective Flory-Huggins interaction parameter χ_{eff} and consequently also the order-disorder transition (ODT) temperature T_{ODT} , resulting in the opportunity to anneal away defects of high molecular weight polymers, while avoiding degradation. The possibility of lowering T_{ODT} of high molecular weight block copolymers by tapering is also important for industrial applications, when melt extrusion is the method of choice for high speed

processing.²²

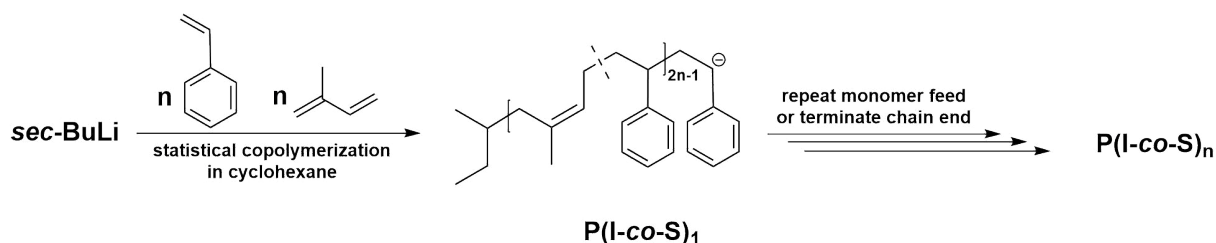
Also, several strategies have been developed to manipulate the composition of the gradient determined by the reactivity ratios of the monomer combination. So called "randomizers"^{33,34} or polar modifiers^{35,36} influence both the copolymerization behavior and the resulting microstructure of the polyisoprene units. A different approach was reported by Epps and coworkers who changed the monomer feed during the reaction via automated syringe pumps to enable manipulation of the gradient to obtain a linear gradient at the interface between the blocks. Improved miscibility was obtained by increasing the length of the tapered region.³⁷⁻⁴⁰ Additionally, the formation of copolymers with the double gyroid structure ($Ia\bar{3}d$ space group) was investigated by Epps and highlighted in a theoretical study by Hall, who found a widening of the double gyroid region as a consequence of tapering.^{38,41} Knoll and co-workers investigated different architectures of tapered and random triblock copolymers in a series of works. The copolymerization behavior was used to adjust structural, morphological, rheological and mechanical properties over a broader range than in common triblock copolymers.⁴²⁻⁴⁴

As already known from ABA triblock copolymers, the formation of bridges and entangled loops results in a strong improvement of mechanical properties.⁴⁵ This effect is even more pronounced upon increasing the number of blocks to obtain $(AB)_n$ multiblock copolymers. While AB and ABA triblock structures are primarily obtained by living anionic polymerization, synthetic pathways for $(AB)_n$ type multiblock structures mostly rely on polycondensation strategies that cannot produce low dispersity multiblock structures.⁴⁶⁻⁴⁹ The limited number of works on well-defined multiblock copolymers to date can be attributed to the demanding implementation by avoiding irreversible termination of living chain ends by using the anionic polymerization as a synthetic pathway. This is especially pronounced in the synthesis of high molecular weights and several monomer addition steps, as it is required for these kinds of structures. However, a living chain growth polymerization allows to adjust key parameters like the effective interaction parameter χ_{eff} , the degree of polymerization N and the number of repeating AB blocks n , keeping dispersity low. Contrary to established step-growth procedures, homogeneous products with defined molecular weights and number of blocks can be obtained, allowing for a systematic investigation of structure-property relationship while changing only one parameter.

In recent years several reports described the synthesis of multiblock copolymers via chain growth polymerization.^{46,48,50-61} While the full potential of these materials is not limited to thermoplastic elastomers, the following considerations need to be made.^{51,52,56,62} First, phase separation represents a basic requirement for applications. Based on the self-consistent mean field theory (SCFT) by Leibler and the random-phase approximation by de Gennes, symmetrical AB diblock copolymers with equal volume fractions for each block ($f_A = f_B$) exhibit phase segregation when

$\chi N \geq 10.5$, where χ is the Flory-Huggins parameter and $N = N_A + N_B$, is the overall degree of polymerization.^{63,64} While in usual block copolymers the interaction parameter depends on the choice of monomers, N can be simply adjusted by variation of the molecular weight.^{40,65} Theoretical and experimental studies reveal a reduction in the order-disorder transition temperature for single AB diblock subunits in symmetrical, linear $(AB)_n$ diblock copolymers when increasing the number of blocks.⁶⁶⁻⁶⁸ However, the overall molecular weight required for phase-separated structures increases due to the larger number of blocks. These findings are in agreement with recent results of Perrier *et. al.* who synthesized multiblock copolymers near the order-disorder regime by radical techniques and observed a transition from the ordered to the disordered state for the tetrablock copolymer, keeping the overall molecular weight constant and increasing the number of blocks.⁶⁹ These results emphasize a second important criterion in the polymer design: high molecular weights must be accessible depending on the number of block and the nature of χ . Third, molecular weights beyond the entanglement molecular weights are desirable to provide mechanical stability of the resulting materials.

Considering these requirements, we can employ the living carbanionic copolymerization of dienes with styrene derivatives to prepare high molecular weight multiblock copolymers in quantitative yields. Unfortunately, the living chain end is highly sensitive to air, moisture, and other impurities. As shown in several works, coupling reactions of the carbanionic chain ends are often the method of choice to reduce the number of monomer addition steps to obtain polymer architectures with several blocks. However, in most cases the coupling does not proceed quantitatively, which results in difficult and time-consuming work-up.^{55,56,67,70,71} In 1977, Corbin and Prud'homme presented the multiple addition of isoprene to a living solution of styrene to produce linear tapered hexablock copolymers.^{29,30} The peculiar kinetics of the polymerization allowed for the addition of isoprene at specific times to switch from polystyryl chain ends to polyisoprenyl chain ends as the predominant active centers until all isoprene was consumed. However, the authors only described two hexablock copolymers of rather high dispersity. In a recent communication we established the principle of repeated statistical copolymerization of isoprene and 4-methylstyrene. There, multiple additions of a monomer mixture resulted in multiblock copolymers with two glass temperatures.⁷²

SCHEME 1 Synthetic Strategy Used for Tapered Multiblock Copolymers.^a

^a The copolymerization of a mixture consisting of styrene and isoprene in cyclohexane leads to tapered diblock copolymers. Due to the living nature of the carbanionic chain end, this procedure can be repeated several times, adding a tapered diblock by every copolymerization step.

In this work we present the synthesis of tapered $(AB)_n$ multiblock copolymers by the repeated addition of mixtures of styrene and isoprene in cyclohexane (Scheme 1). Because the disparate reactivity ratios of this system ($r_1 = 12.8$, $r_5 = 0.051$) lead to tapered diblocks, repeated addition can be used to prepare tapered multiblock copolymers.⁷³ The kinetic preconditions for the synthesis of the multiblock copolymers are studied by detailed kinetic Monte Carlo simulation, relying on the experimentally determined reaction rates. In the second part of this work, a detailed account of the phase state (SAXS and TEM) of the multiblock polymers is provided. The systematic variation of the effective interface at a fixed total molecular weight allows for a direct comparison between the obtained morphologies and the associated mechanical properties.

EXPERIMENTAL SECTION

A detailed version of all synthetic procedures and characterization techniques (DSC, SAXS, TEM) as well as mechanical characterization is given in the Supporting Information.

General polymerization procedure for the synthesis of multiblock copolymers: A mixture of isoprene and styrene was predried over finely ground CaH_2 , degassed by three freeze-thaw cycles, and distilled into a flask containing trioctylaluminum. Subsequently, a second distillation into a graduated ampule was performed. Cyclohexane was dried over sodium with benzophenone as an indicator under reflux. The dried cyclohexane was distilled into the reaction flask, followed by flushing with argon and the addition of $sec\text{-BuLi}$ solution. The polymerization was started via addition of the monomer mixture by using a graduated ampule. The respective reaction times per diblock unit were calculated using kinetic Monte-Carlo simulation. Addition of the monomer mixture was repeated several times until the desired number of blocks was achieved. The living

chain ends were terminated by addition of isopropyl alcohol. To precipitate the polymer, the polymer solution was poured into 8-fold volume excess of 50%_{vol} mixture of isopropyl alcohol and methanol, dried at reduced pressure, and stored under the absence of light at -20 °C.

RESULTS AND DISCUSSION

As shown in previous works, the polymerization of isoprene and styrene in nonpolar solvents, e.g., cyclohexane, leads to block or tapered "blocklike" structures depending on the polymerization strategy.²⁶ In the case of repeated addition of monomer mixtures, fundamental kinetic understanding is indispensable to ensure full monomer conversion and to avoid premature addition of the respective next monomer mixture, which would result in a loss of monomer sequence control.

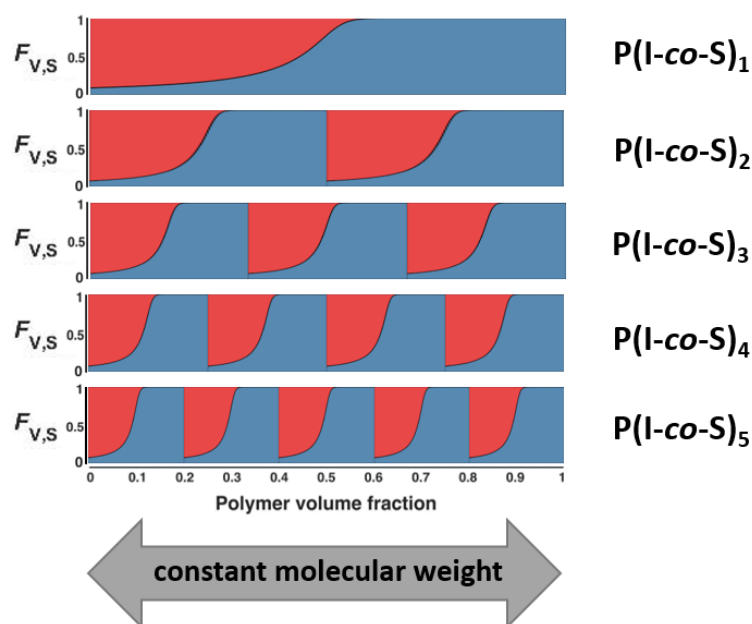


FIGURE 1 Visualization of the polymer microstructure of tapered multiblock copolymers by plotting the mean incorporation volume of styrene, $F_{V,S}$ (blue), as a function of the polymer volume fraction. A constant chain molecular weight was chosen to decouple mechanical properties from the chain length. The tapered monomer sequence is simulated based on the reactivity ratios of isoprene and styrene ($r_1=12.8$ and $r_5=0.051$) determined at 40 °C in cyclohexane.⁷³

The necessary reaction time, t_{total} , can be calculated by eq 1 in the case of the sequential synthesis of block copolymers based on styrene and isoprene. Here x_s and x_i are the desired conversions (e.g. 99%), $[I]_0$ is the initiator concentration, and k_{iI} and k_{sS} are the (apparent) rate constants for homopolymerization. For this simple case sequential homopolymerization of the respective

monomers can be assumed. Contrary to the simple idea of a growing chain, the overall reaction time of an AB diblock copolymer is independent of the degree of polymerization at an invariant target conversion. However, a different correlation with the initiator concentration $[Ini]$ is observed (Eq. 1). This different behavior can be explained by the formation of stable lithium aggregates at the chain end. Dimeric aggregates are formed in the case of polystyryllithium and tetrameric assemblies in the case of polyisoprenyllithium, when considering concentrated solutions as is the case in this work.²⁶

$$t_{\text{total}} = - \underbrace{\frac{\ln(1-x_I)}{k_{II}}}_{\text{const}} \cdot \frac{1}{[Ini]_0^{1/4}} - \underbrace{\frac{\ln(1-x_S)}{k_{SS}}}_{\text{const}} \cdot \frac{1}{[Ini]_0^{1/2}} \quad (1)$$

When the synthesis of multiblock copolymers is performed, the total reaction time multiplies with the number of additions of the mixture of both monomers (Table 1). By use of the kinetic Monte Carlo simulation, the monomer conversion for sequential PI-*b*-PS and *in situ* P(I-co-S) tapered block copolymers can be calculated for any time of the reaction. When comparing the synthetic strategies, we observed a significant acceleration of the kinetics for the *in situ* copolymerization with respect to the sequential homopolymerization of both monomers (Figure 2). The overall reaction time for (AB)_{*n*} multiblock copolymers scales linearly with the number *n* of AB diblock units. This time saving is becoming increasingly important in the synthesis of multiblock copolymers with high block numbers (Table 1; Figures S2 and S3, Table S2).

Independent of the synthetic strategy, it is generally desirable to perform the synthesis in rather concentrated monomer solutions. This leads to minimized reaction times (Table 1) and a decreased risk of irreversible termination reactions due to impurities in the solvent. For this reason, the polymerization was performed at monomer concentrations of 1.2-1.9 mol/L with high concentrations for the lower molecular weight series (Table S3). As another adjustment the polymerization was performed at 40 °C. Heating above room temperature simultaneously lowers viscosity and accelerates kinetics in comparison to the previously reported approach.⁷²

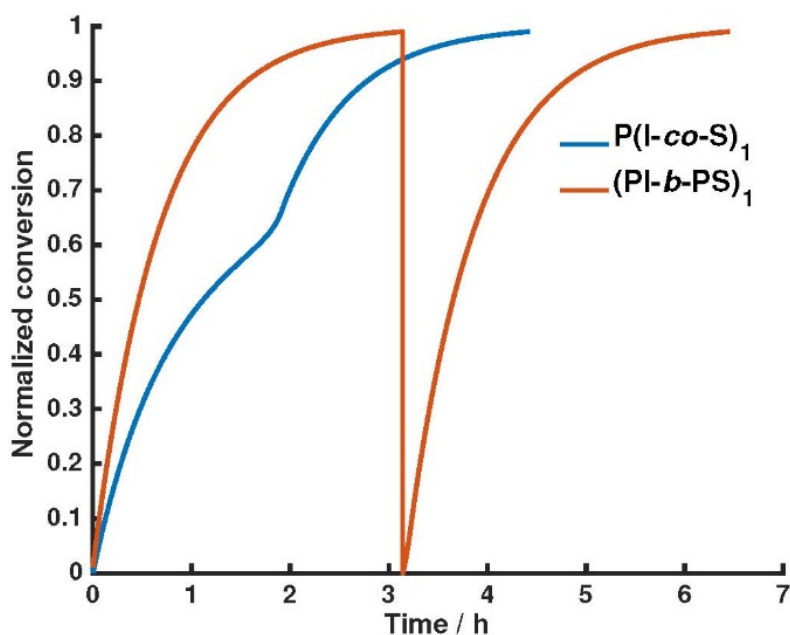


FIGURE 2 Kinetic comparison between copolymers consisting of 50%_{mol} isoprene and styrene obtained by sequential (red) and statistical (blue) copolymerization in cyclohexane at 40 °C. $M_n(\text{theoretical}) = 400$ kg/mol, $[I]_0 = 0.26$ mmol/L, and $[M]_0 = 1.22$ mol/L.

The repeated statistical copolymerization principle employed in this work greatly facilitates the demanding synthesis of $(AB)_n$ multiblock copolymers via living anionic polymerization. The combination of fewer, *i.e.*, merely n monomer additions for $2n$ blocks and the accelerated kinetics lead to a promising synergy in the synthetic approach to obtain uniform materials. The simplified approach enabled the use of standard Schlenk techniques, permitting to produce all of the multiblock copolymers in batch sizes exceeding 100 g.

Polymer Synthesis and Molecular Characterization

In this work we focus on the study of constant molecular weight tapered multiblock copolymers consisting of 50%_{mol} of the respective monomers. For a block copolymer (PI-*b*-PS) obtained by stepwise polymerization of the respective monomers, one would expect a volume fraction of 43%_{vol} polyisoprene and 57%_{vol} polystyrene. In contrast, a 50%_{vol} fraction is obtained by performing the *in situ* tapered diblock formation (P(I-co-S)) which was performed for the structures described in this work. The relative volume shift of the blocks by switching the polymerization strategy is attributed to the obtained tapered block structure. Because of the incorporation of styrene units during the formation of the isoprene-rich block, this first block expands in volume while the second pure polystyrene block shrinks. Because the polymer chains are segmented into

different numbers of rigid PS and rubbery PI segments, a systematic decrease in the strength of the phase segregation $\chi_{\text{eff}}N$ is expected with increasing number of blocks (Table S3).

Three constant molecular weight series of tapered I/S multiblock copolymers with approximate molecular weights of 80, 240, and 400 kg/mol were prepared, covering a broad range of segment architectures, ranging from diblock to decablock copolymers for each series (Figure 1). Lower phase segregation strength is expected for structures with tapered block transitions compared to sequentially synthesized multiblock copolymers. An estimation for the magnitude of $\chi_{\text{eff,taper}}$ is possible by considering the work of Spontak, who recently investigated so-called block-random copolymers.⁶⁵ In this case a random incorporation of monomer units of the respective other block was investigated for AB diblock copolymers. A relationship between $\chi_{\text{eff,random-block}}$ and the proportion of the respective "foreign monomer" (in this work so-called block composition contrast, Δ) could be determined. Keeping in mind that the taper structures in this work are more "blocklike" than these random block copolymers, the true value of $\chi_{\text{eff,taper}}$ should be located in between χ and $\chi_{\text{eff,random-block}}$.

We were able to predict reaction times for the statistical copolymerization of isoprene and styrene using the kinetic Monte-Carlo simulation based on the rate constants determined by Fontanille *et al.* for 40 °C in cyclohexane (see Table 1).⁷³ Upon addition of adding a monomer mixture to the living solution, vigorous stirring had to be ensured to secure instantaneous and uniform propagation of the living chains. For this reason, the maximum initiator concentration was related to the viscosity of the living polymer solution by the last monomer feed of the decablock copolymer. Related initiator and monomer concentrations and calculated reaction times are shown together with other data in Table 1. Relying on the detailed kinetic understanding, reaction times were minimized without the risk of premature addition of a new I/S monomer portion that would result in a deviation of the monomer sequence along the polymer backbone. The color change of the living polymer solution from slight yellow (polyisoprenyllithium) to orange (polystyryllithium) enabling the validation of reaction times was possible in a qualitative manner (Figure S4). Full conversion of the first AB-diblock unit of an P(I-co-S)₂ tapered tetrablock copolymer was confirmed by ¹H NMR spectroscopy and SEC measurements by taking a sample from the living solution (Figures S5 and S6). Because of the high sensitivity of the living carbanionic chain ends toward oxygen and moisture and the associated change of the initiator concentration and difficulty due to the high viscosity of the solution, removal of samples after further monomer addition steps was not possible.

Experimental studies of the tapered structures by performing triad analysis via ¹³C *inverse gated* NMR spectroscopy failed due to the lack of significant differences in the obtained NMR spectra. The calculation of the triad abundances performed via Monte Carlo simulation revealed

only minor changes of the triads for different microstructures within a constant chain molecular weight series. Therefore, triad analysis is not suitable for the characterization of these structures (Table S1). SEC measurements of different tapered multiblock copolymers show monomodal, narrow molecular weight distributions with low dispersity (Figure 3). An overestimation of the molecular weights by SEC is observed that can be referred to the 1,4-polyisoprene units in the polymer backbone when using polystyrene standards.

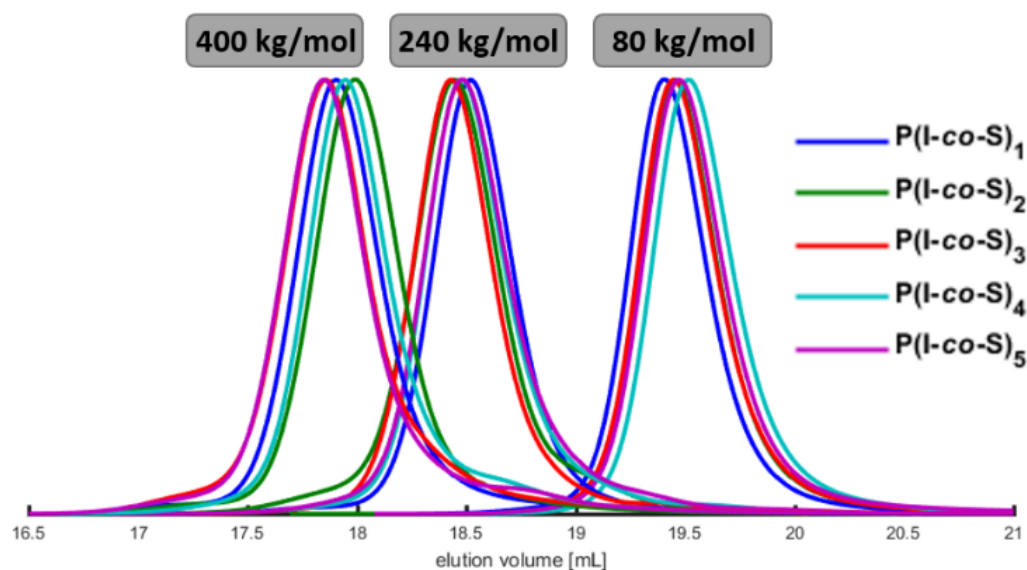


FIGURE 3 SEC traces (THF, PS calibration) of three different $P(I-co-S)_n$ series with constant chain molecular weight. The tapered multiblock copolymers were prepared from a 50%_{mol} mixtures of isoprene and styrene (see Table 1).

Tapered multiblock copolymers with constant molecular weight, but different number of tapered segments, exhibit comparable molecular weights in SEC measurements (Figure 3). This can be expected, considering that these polymers are composed of the same number of isoprene and styrene monomers. Several additions of monomer mixtures did not result in a broadening of the molecular weight distribution, which clearly demonstrates the absence of termination reactions of the living chains. Only the tapered decablock copolymer of the 400 kg/mol molecular weight series exhibited a small shoulder in the SEC eluogram (see also Figure S9).

To study and confirm the monomer sequence in the multiblock structures, the polyisoprene segments were cleaved by oxidative degradation in solution (Figure 4a). Monomodal molecular weight distributions were obtained, showing a uniform size of the polystyrene blocks of the tapered structures (Figure 4b). For large molecular weights of AB units, an increased tailing of the SEC trace indicates the presence of the tapered structure (Figure S14). Absolute molecular weight values of the styrene segments obtained from oxidative degradation were calculated for

both tapered and sequential multiblock copolymers (50%_{mol}) via Monte Carlo simulation and compared to values obtained by the experimental procedure (Figure 4; Figures S12 – S15 and Table S2).

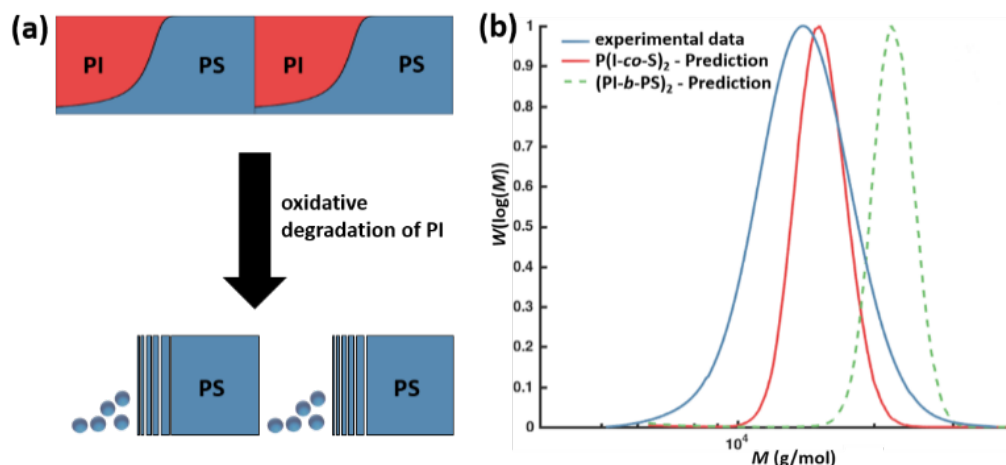


FIGURE 4 (a) Visualization of the oxidative degradation of a tapered tetrablock copolymer. PS fragments in the size of the respective PS block sizes were obtained. (b) PS fragment distribution analyzed by SEC, PS calibration. Theoretical SEC traces for tapered (red straight line) and sequential systems (green dashed line) were predicted by Monte Carlo simulation. Good agreement with experimental data was found for the expected tapered structures (blue straight line). $M_p(\text{exptl data}) = 13 \text{ kg/mol}$, $M_p(\text{P(I-co-S)}_2\text{-prediction}) = 14 \text{ kg/mol}$, and $M_p(\text{(PI-b-PS)}_2\text{-prediction}) = 22 \text{ kg/mol}$.

Good agreement between theoretical and experimental data was found for tapered structures. In contrast, the theoretical data for block copolymers prepared by the sequential method show a strong deviation (Figure 4). These results validate the presence of a tapered microstructure with the detailed perception of the gradient instead of two blocks of the respective homopolymers. In addition, the monomodal distribution of the polystyrene fragments confirms consistent block length within the different multiblock copolymer samples prepared by multiple monomer addition. Also, similar reactivity ratios for each step of addition are represented by the monomodal distribution. This is consistent with the fundamental definition of reactivity ratios by Mayo-Lewis, in which the reactivity ratios only show a dependence on the active chain end. As suggested, increasing viscosity and the associated challenging mixing did not affect reaction times or the resulting microstructures at all. In this way the targeted molecular architectures were confirmed, while demonstrating the kinetic Monte Carlo simulation as a self-consistent tool to understand complex copolymerization kinetics and resulting monomer sequences. The degradation, analysis (SEC, ^1H NMR spectra) and comparison to theoretical data and of different types of tapered multiblock structures can be found in Figures S12-S16 and Table S2.

TABLE 1 Overview of Tapered I/S Multiblock Copolymer Samples and Reaction Parameters Employed.

entry	target M_n [kg/mol]	no. of blocks	target M_n (AB-unit) [kg/mol]	M_n (SEC) [kg/mol]	$\mathcal{D} = M_w / M_n$	$[I]_0$ [mmol/L]	t_{total} [h]
1	80	2	80	92	1.07	1.77	2.16
2	80	4	40	86	1.08	1.94	4.19
3	80	6	27	87	1.06	2.01	6.22
4	80	8	20	82	1.06	2.04	8.27
5	80	10	16	83	1.09	2.06	10.33
6	240	2	240	253	1.09	0.52	3.41
7	240	4	120	265	1.16	0.56	6.61
8	240	6	80	268	1.13	0.58	9.82
9	240	8	60	244	1.15	0.58	13.03
10	240	10	48	248	1.14	0.59	16.25
11	400	2	400	506	1.20	0.26	4.43
12	400	4	200	475	1.18	0.28	8.63
13	400	6	133	512	1.28	0.29	12.83
14	400	8	100	474	1.21	0.29	17.05
15	400	10	80	515	1.28	0.29	21.23

Thermal Characterization

The thermodynamic state of the copolymers studied by DSC reveals two glass temperatures independent of the phase state of the copolymers (ordered or disordered). This is depicted in Figure 5, where the first derivative of the heat flow obtained during the second heating runs is shown. The lower and higher peaks in this representation correspond to the PI and PS glass temperatures, respectively. Although the lower T_g – albeit broad – is always evident, the high T_g is less pronounced especially in the tapered multiblock (tetra-, hexa-, octa- and decablock) copolymers. In the tapered copolymers with the lower molecular weight ($M_w \sim 80$ kg/mol) the two peaks approach each other, especially in the octablock and decablock cases meaning that segmental mobilities are in proximity. In addition to the high and low glass temperatures another very broad peak around 20 ° C is evident for the 240 and 400 kg/mol copolymers. This feature may be associated with an "interphase T_g " of those segments that are intimately mixed within the I/S interface.

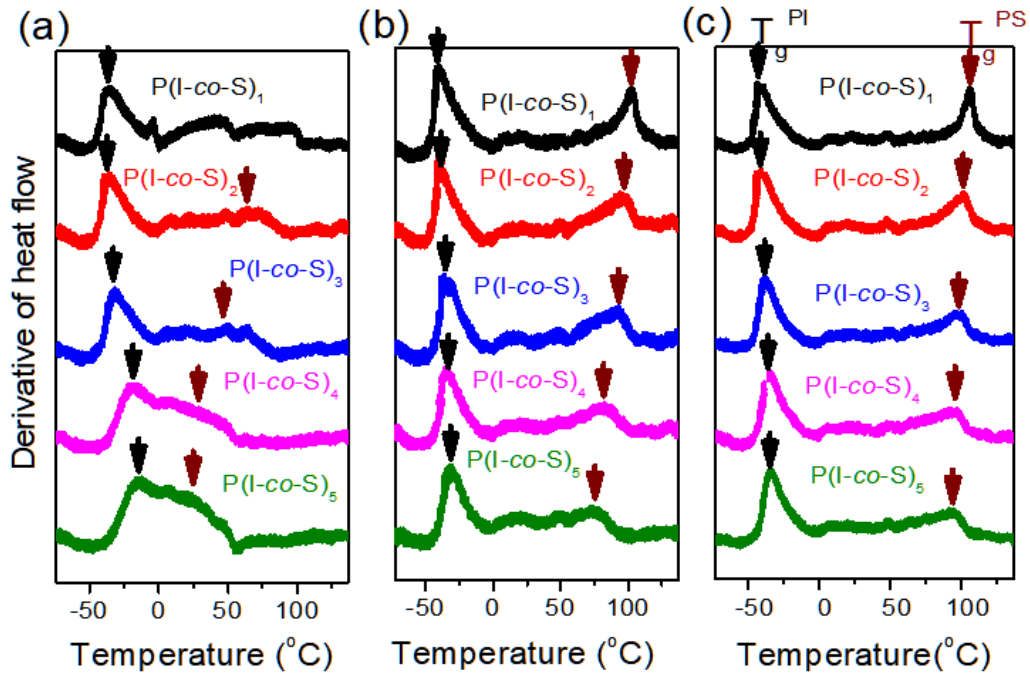


FIGURE 5 Derivative of heat flow obtained during the second heating runs of the tapered multiblock copolymers with approximate molecular weights of 80 (a), 240 (b), and 400 kg/mol (c) at a rate of 10 K/min. Vertical arrows in black and wine colors indicate the PI and PS glass temperatures, respectively.

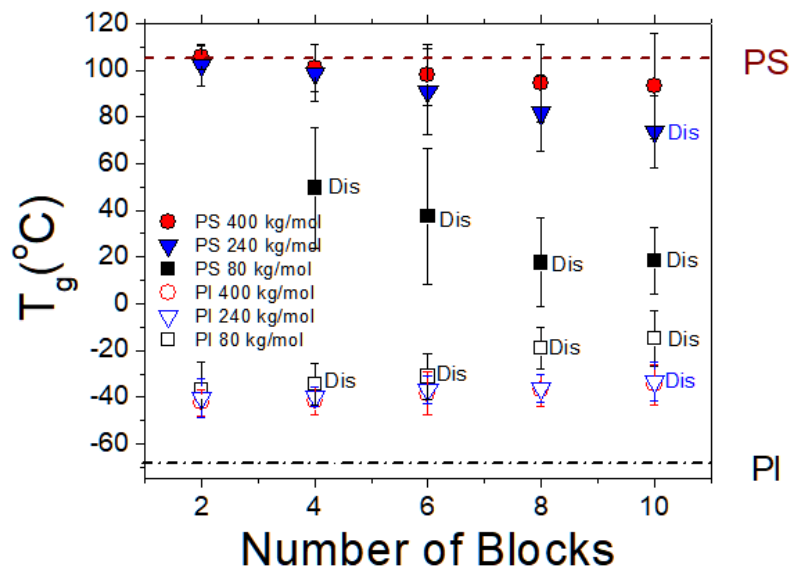


FIGURE 6 Glass temperatures of the tapered multiblock copolymers corresponding to PS (filled symbols) and PI (open symbols). Vertical bars indicate the temperature range of the respective glass temperatures (taken as the full width at half maximum of the derivative of the heat flow shown in Figure 5). Dashed and dash-dotted lines give the glass temperature of PS and PI homopolymers, respectively. Disordered Samples are indicated with the note "Dis".

The results of the DSC investigation with respect to the PI and PS glass temperatures are summarized in Figure 6, which shows the appearance of dual glass temperatures in all cases with a temperature separation that decreases with the number of blocks and with decreasing total molecular weight. In addition, the PI T_g is substantially higher than for a homopolymer PI ($T_g = -65\text{ }^\circ\text{C}$) because of the incorporation of styrene segments within the PI chain.

Morphology

The results of the TEM study on the real-space nanodomain morphology (Figure 7; Figures S17-S20 and Table S4, Supp. Inf.) can be compared with the morphology obtained by SAXS in the inverse space.

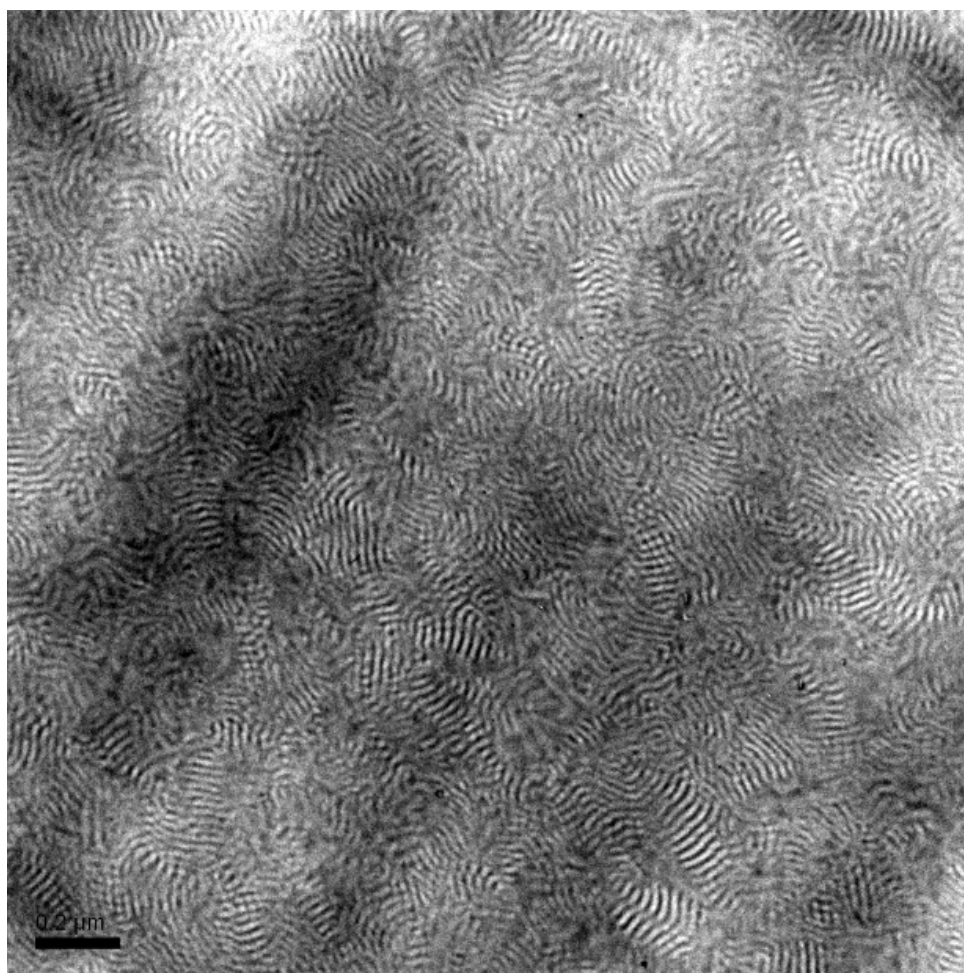


FIGURE 7 TEM image of a 240 kg/mol tapered hexablock copolymer (Table 1, entry 8), stained with OsO_4 ; dark domains PI-rich phase. Domain sizes: $d(\text{PI}) = 10.2 \pm 1.4\text{ nm}$ and $d(\text{PS}) = 12 \pm 1.8\text{ nm}$. The scale bar represents the size of $0.2\text{ }\mu\text{m}$.

The SAXS results for the tapered multiblock copolymers with molecular weights of 80 and 240 kg/mol obtained at ambient temperature are shown in Figure 8. The SAXS scattering curves for the tapered diblock copolymer with $M_w = 80$ kg/mol show Bragg reflections with positions 1:2:3:5 relative to the first peak corresponding to a lamellar morphology. Suppression of the even numbered reflections suggests an equal volume of PI and PS domains within the lamellar morphology. The curves for the tapered hexablock and octablock copolymers reveal a single and broad peak corresponding to scattering from the disordered state (correlation hole scattering). The curve for the tetrablock copolymer exhibits features intermediate to the diblock and multi-block copolymers and corresponds to a weakly ordered state. The final assignment of the exact phase state (ordered versus disordered) as well as the location of the order-to-disorder transition temperature, T_{ODT} , requires temperature-dependent SAXS measurements (see below).^{74,75}

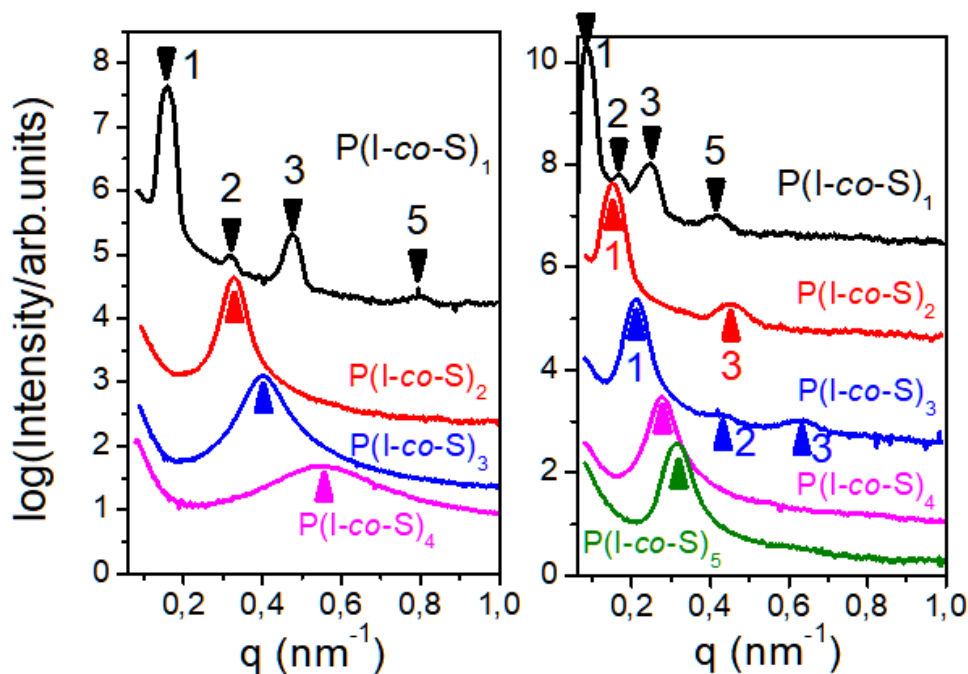


FIGURE 8 SAXS patterns for the tapered multiblock copolymers with molecular weight of 80 kg/mol (left) and 240 kg/mol (right) obtained at ambient temperature. Arrows give the positions of the Bragg reflections corresponding to a lamellar morphology. Curves are shifted vertically for clarity.

The SAXS results for the tapered multiblock copolymers with a molecular weight of 240 kg/mol reveal ordered phases with the expected lamellar morphology. However, the scattering data of the octablock and decablock copolymers reflect weakly ordered structures at ambient temperature with order-to-disorder transition temperatures that are accessible by heating (at 458 and 393 K, respectively, Figure S21). The domain spacing, *i.e.*, the periodicity d of the lamellar structure, obtained from SAXS (as $d = 2\pi/q^*$, q^* is the modulus of the scattering vector cor-

responding to the first maximum) for the tapered multiblock copolymers can be compared to the corresponding spacing in pure PI-*b*-PS copolymers (Figure 9). The figure depicts the domain spacing at ambient temperature as a function of the number of blocks for the different molecular weights as well as a function of the total molecular weight, the latter in a double - logarithmic representation. For pure diblock copolymers the domain spacing varies as $\log(d/\text{nm}) = -1.4165 + 0.62 \log(M_n/(\text{g/mol}))$.⁶⁸⁻⁷³ In the strong segregation limit of diblock copolymers (SSL, *i.e.*, $\chi N \gg 10$) narrow interfaces are formed with an extended block conformation imposed by the combined effects of localization of the block junction points at a narrow interface and an overall uniform density. The effect of the extended chain conformation is evident from the molecular weight dependence of the nanodomain spacing which scales as $d \sim N^\delta$, with $\delta \sim 2/3$ in the SSL, as opposed to $\delta = 1/2$ for the unperturbed (Gaussian) chains. In this limit a self-consistent field theory developed by Helfand⁷⁴ predicted a nanodomain spacing scaling as $d \sim \alpha N^{9/14} \chi^{1/7}$. On the other hand, Semenov argued⁷⁵ that the copolymers are strongly stretched and resemble grafted polymer brushes and surfactant interfaces with $d \sim \alpha N^{2/3} \chi^{1/6}$. Despite these theoretical expressions applicable to strongly segregated diblock copolymers, experiments in several symmetric diblock copolymers have shown a weaker dependence as $d \sim N^{0.61}$, for $\chi N > 29$, as in the present case.

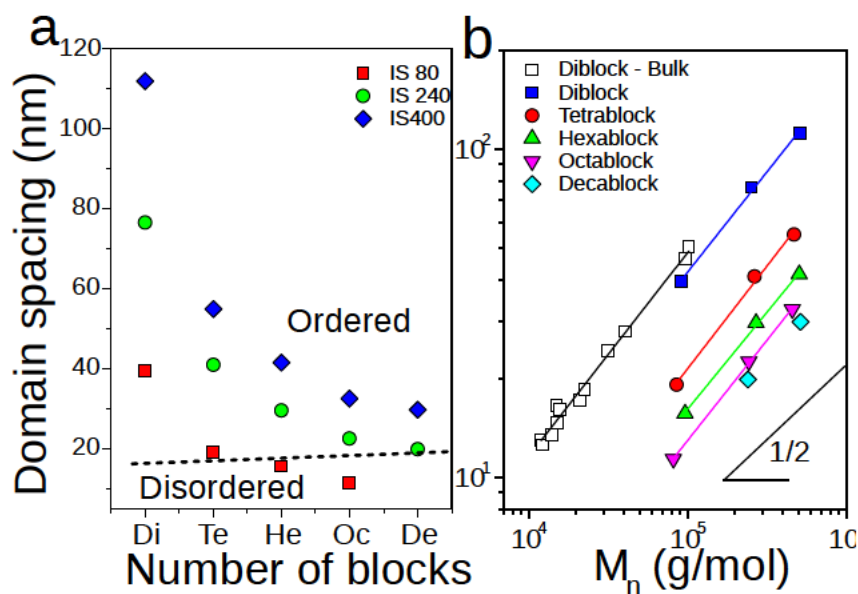


FIGURE 9 (a) Domain spacing obtained from SAXS plotted as a function of the number of blocks for the tapered multiblock copolymers with molecular weights of 80 kg/mol (squares), 240 kg/mol (circles), and 400 kg/mol (rhombi). The dashed line separates the ordered from the disordered states. (b) Domain spacing plotted as a function of molecular weight in a log-log representation for the tapered multiblock copolymers (filled symbols) and for sequential PI-*b*-PS copolymers (open symbols) from the literature. Lines are fits to the experimental data.⁷⁶⁻⁸¹ A line with a slope of 1/2 is shown for comparison.

Even more interesting is a comparison of the domain spacing in the pure diblock copolymers with the tapered multiblock copolymers investigated herein. Figure 9b reveals that a tapered diblock copolymer with $M_n = 91690$ g/mol has a domain spacing ($d = 39.5$ nm) that is only 13% lower than in the corresponding pure PI-*b*-PS copolymer ($d = 45.6$ nm). Given that SEC overestimates the molecular weight in the tapered copolymers, the values are in closer proximity. Evidently, the vastly different reactivity ratios of I and S in cyclohexane led to a tapered diblock with a relatively narrow interface. Multiblock copolymers prepared by the repeated addition of mixtures of styrene and isoprene, however, show very different domain spacings. The tetrablock copolymer shows a domain spacing ($d = 19.2$ nm) that is reduced by 56%, whereas in the octablock ($d = 11.4$ nm) the reduction amounts to 75%. This reveals an increased number of loop formation of unlike segments at the I/S interface. Despite loop formation in the tapered copolymers, the $d \sim N^{0.62}$ scaling is maintained as with diblock copolymers, suggesting stretching of chains and nonideal (Gaussian) configurations. The reinforcement of the interface by entangled loops as well as the existence of bridges is expected to affect the mechanical properties of the multiblock copolymers (see below).^{51,70}

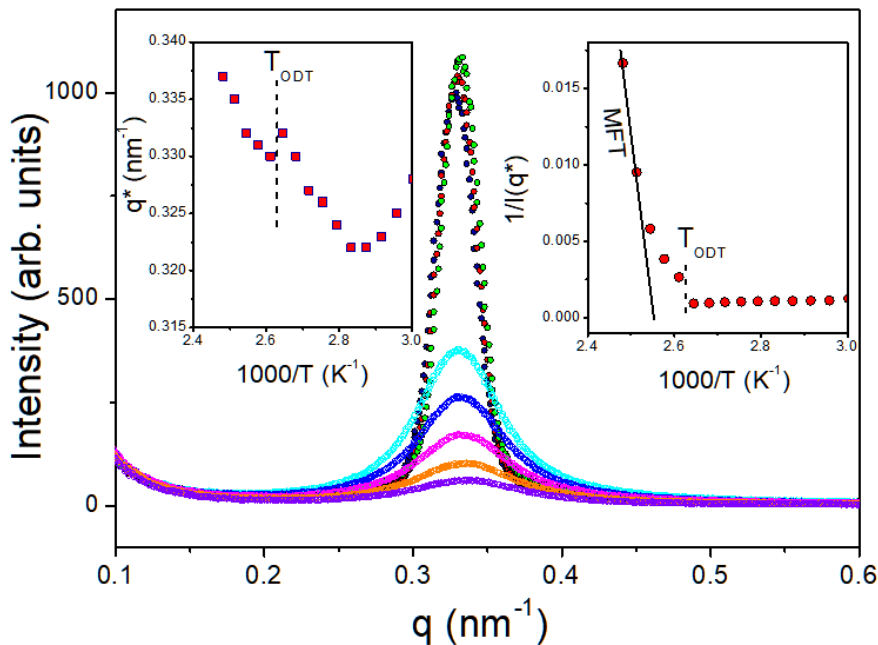


FIGURE 10 SAXS curves of the tapered tetrablock copolymer with a total molecular weight of 80 kg/mol plotted at different temperatures below (filled symbols) and above (open symbols) the order-to-disorder transition; $T = 368$ K (black), 373 K (red), 378 K (green), 383 K (cyan), 388 K (blue), 393 K (magenta), 398 K (orange), and 403 K (violet). The inverse peak intensity is plotted versus inverse temperature as the right inset. The solid line indicates the MFT predictions, whereas the dotted line gives the T_{ODT}^{-1} . Notice the pronounced curvature of $I(q^*)^{-1}$ at temperatures above the transition that contradict the MFT predictions. The left inset gives the peak position as a function of inverse temperature. Notice the discontinuous decrease at the T_{ODT}^{-1} shown by the dashed line.

More information about the phase state can be obtained by following the structure factor, $S(q)$, of the tapered multiblock copolymers as a function of temperature.^{74,75} As an example, the static structure factor for the tapered tetrablock copolymer with a total molecular weight of ~ 80 kg/mol is shown in Figure 10 for temperatures below and above the order-to-disorder transition temperature (T_{ODT}). The transition is evidenced by the sharp change of the structure factor from a narrow solidlike (at $T < T_{\text{ODT}}$) to a broad liquidlike peak at $T > T_{\text{ODT}}$.

According to Leibler's mean-field theory (MFT)⁶³ the equilibrium thermodynamic state of diblock copolymer melts is completely determined by the two variables: volume fraction, f , and χN . For a symmetric diblock copolymer the theory predicts a second-order phase transition from the disordered to the lamellar phase by lowering temperature at the critical point ($\chi N = 10.495$, $f = 1/2$). For asymmetric diblock copolymers the theory predicts a first-order phase transition to a bcc microphase. In addition, Leibler's MFT provided an expression for the disordered phase structure factor, $S(q)$, which was employed in the description of the scattering profiles from disordered copolymers. However, there have been several cases where the predicted phase diagram was inadequate in explaining the rich experimental features, and the suggested structure factor was insufficient to describe the actual experimental data, especially near the ODT. For example, according to Leibler's MFT, $1/S(q)$ should be proportional to $1/T$ in the disordered phase. This prediction is based on the simple approximation that χ is inversely proportional to T . Contrast this with the experimentally obtained $S(q^*)$ shown as the inset to Figure 10. At $T > T_{\text{ODT}}$ there exists a pronounced curvature, which cannot be accounted for by the MFT. Furthermore, the peak intensity at the transition remains finite, and the $S(q^*)$ is discontinuous at the transition. Fredrickson and Helfand⁸² introduced fluctuation corrections to Leibler's MFT for weakly segregated diblock copolymers to demonstrate a fluctuation-induced first-order transition in place of the continuous second-order transition. According to Fredrickson and Helfand, fluctuation corrections apply to both the disordered and ordered phases in the vicinity of the transition. In the disordered phase the structure factor is

$$\frac{N}{S(q)} = F(x, f) - 2\chi N + \frac{c^3 d \lambda}{\bar{N}^{1/2}} \frac{\sqrt{S(q^*)}}{\sqrt{N}} \quad (2)$$

Here, $d = 3x^*/2\pi$ and c, λ are composition-dependent coefficients, where $\bar{N} = N\alpha^6/u^2$, and α, u are the statistical segment length and volume, respectively. Because the last term is independent of q , it is only the peak height that is affected. Thus, approaching the T_{ODT} from high temperatures, the predicted intensities are lower than the ones expected from Leibler's theory.

Furthermore, Eq. 2 predicts a nonlinear dependence of $1/S(q)$ on $1/T$, which is in qualitative agreement with the nonlinear dependence obtained experimentally.

Clearly, the temperature-dependent SAXS investigation (Figures 10 and S23) revealed that tapered multiblock copolymers undergo a fluctuation-induced first order transition and not the second-order transition predicted by MFT, as it is well-known for diblock copolymers. In addition, the tapered octablock copolymer with $M_w = 244.1$ kg/mol shows the same T_{ODT} as a pure diblock copolymer with $M_w = 25.1$ kg/mol (Figure S23). This can be understood from the reduction of the interaction parameter in the tapered copolymers. According to a binary interaction theory,^{57,83-85} the effective interaction parameter, χ_{eff} , is reduced relative to pure diblock copolymers as

$$\chi_{eff} = \chi (f_{SS} - f_{IS})^2 \quad (2)$$

where f_{SS} and f_{IS} are the respective volume fractions of styrene in the styrene-rich and isoprene-rich domains. An estimate of χ_{eff} can be made by assuming the same (χN) value at the T_{ODT} for the pure diblock and the tapered octablock copolymer. For the pure diblock copolymer we employ the known interaction parameter¹ as $\chi = 71.4/T - 0.0857$ ($M_n = 25100$ g/mol, $N = 295$, $T_{ODT} = 457$ K, $\chi_{ODT} = 0.0705$) that results to $(\chi N)_{ODT} = 20.8$ in agreement with the PI-*b*-PS phase diagram that includes fluctuation corrections.¹ Assuming $(\chi_{eff} N)_{ODT} = 20.8$ for the tapered octablock copolymer ($M_n = 244100$ g/mol, $N = 2863$, $T_{ODT} = 458$ K) results to $\chi_{eff} = 0.00726$ at the T_{ODT} , *i.e.*, to a 10-fold reduction relative to the pure diblock case. By employing Eq. 3, we further obtain $f_{SS} - f_{IS} = 0.32$, and this overestimates f_{IS} . This could be associated with the presence of a more blocklike structure in the present copolymers.

Mechanical and Rheological Properties

Rheology is a very sensitive probe of the (i) the order-to-disorder transition, (ii) the different ordered phases, and (iii) the phase transformation kinetics between the disordered and ordered phases as well as of the transformation among the different ordered phases of block copolymers.^{74,75} This sensitivity originates from the large viscoelastic contrast of the disordered and the different ordered phases. Isochronal measurements of the storage modulus performed at low frequencies with low strain amplitudes by slowly heating the specimen provide a way of locating the T_{ODT} . Figure 11 shows the result of isochronal measurements of the storage (G') and loss (G'') moduli at $\omega = 1$ rad/s obtained on heating for the series of the tapered multiblock

copolymers with approximate molecular weights of 80 kg/mol. The figure depicts one tapered copolymer that remains in the ordered phase over the whole temperature range (the $P(I-co-S)_1$), three multiblock copolymers (hexa-, octa-, and decablock) that are in their disordered state and one copolymer (tetrablock) that undergoes a phase transition from an ordered to the disordered state, at 115 °C (some 5 °C higher than in SAXS because of the different heating rates employed). Overall, there is an excellent agreement with the SAXS results with respect to the phase state of the copolymers. In addition to the phase state, the figure depicts the very different viscoelastic responses of the copolymers that are largely controlled by the glass temperature of the hard phase (PS) being a strong function of the number of blocks (Figure 5) and the overall molecular weight. Additional information about the effect of fluctuations in the vicinity of the T_{ODT} can be obtained by following the viscoelastic response under isothermal conditions as a function of frequency. Results of the attempted time-temperature superposition for the tetrablock copolymer are discussed with respect to Figure S22. These results confirm that the order-to-disorder transition is controlled largely by fluctuations.³²

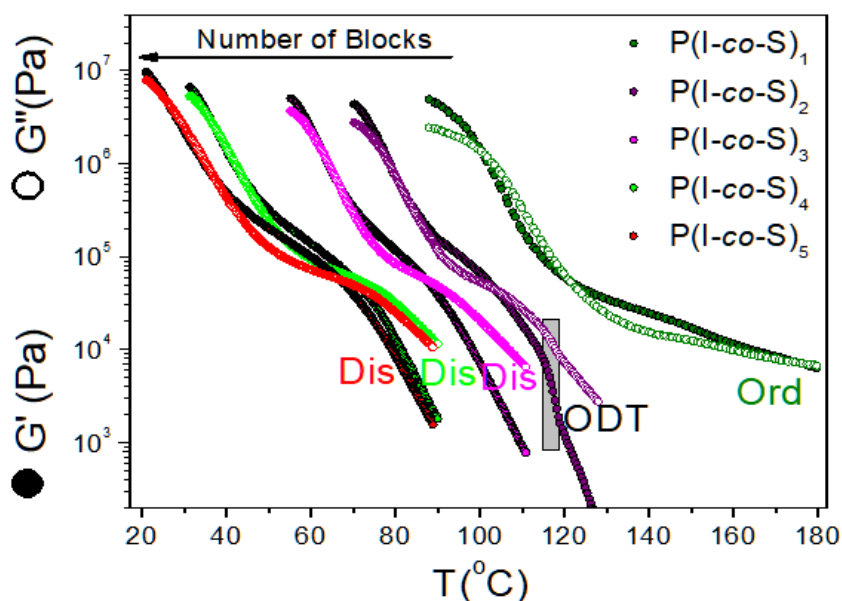


FIGURE 11 Storage (filled symbols) and loss (open symbols) shear moduli during heating with a rate of 5 °C/min at a frequency of 1 rad/s (10 rad/s for the diblock) for the different tapered multiblock copolymers with a total molecular weight of 80 kg/mol. The strain amplitude was typically below 1.4% for all measurements. Ordered and disordered states are indicated as Ord and Dis, respectively. The gray area indicates the order-to-disorder transition temperature for the tetrablock.

Nanodomain structure and block connectivity greatly affect the mechanical properties. A well-known example is SIS triblock copolymers with spherical PS nanodomains that represent excellent thermoplastic elastomers. In this case the equilibrium elasticity is controlled largely by

bridged PI blocks connecting adjacent PS domains. Similarly, in the tapered IS copolymers the equilibrium elasticity is controlled by the nanodomain structure, the degree of segregation, the bridged configurations of blocks, and the proximity to the glass temperature of the PS domains. Figure 12 provides the result of tensile stress-strain (σ - ϵ) curves for the different tapered multiblock copolymers as a function of molecular weight and number of blocks. They show a distinctly different behavior for the P(l-co-S)₁ copolymers with respect to the multiblock tapered copolymers. The former are brittle with elongation at break close to the yield point. This is attributed to the lack of domain bridging as for diblock copolymers prepared sequentially. In pronounced contrast the multiblock copolymers can sustain load to much higher strains up to the break point (typically $\epsilon \sim 900\%$). Elastic moduli and yield stress values are also a function of the multiblock structure (Figures S27-S31 and Table S5). The 80 kg/mol octa- and decablock copolymers do not exhibit separate elastic and viscous regions. This can be attributed to the disordered morphology and the concomitant reduction in the polystyrene T_g . Under these conditions copolymers start to flow even at low strains.

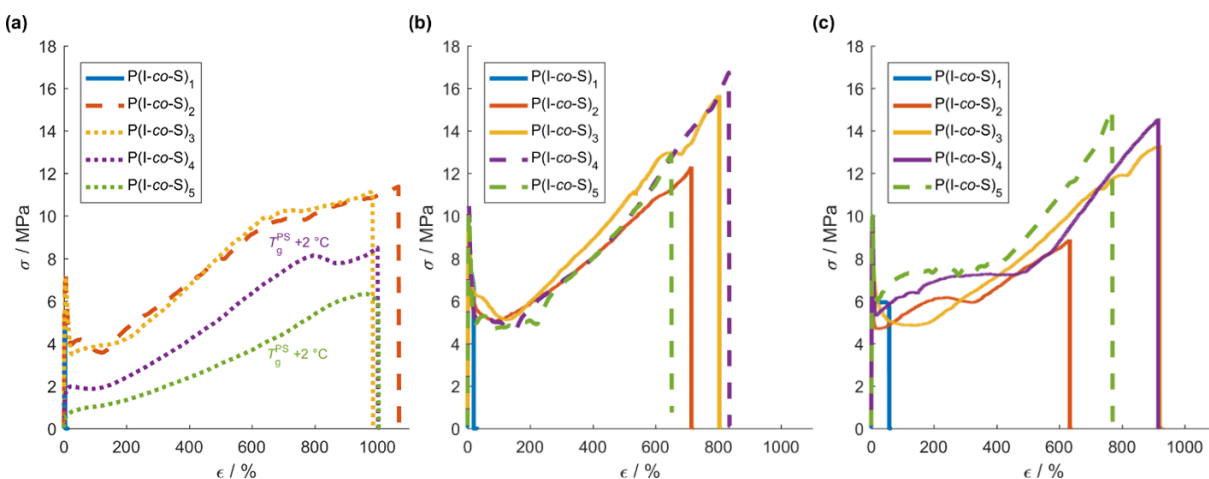


FIGURE 12 Representative stress-strain curves of the three series of multiblock copolymers: (a) 80 (b) 240 and (c) 400 kg/mol. Continuous lines indicate ordered copolymers, whereas dashed and dotted lines represent respectively weakly ordered or disordered samples. Measurements are made at ambient temperature. As noted in (a), the difference to the respective glass transition temperature of the PS block (Figures 5 and 6) is indicated in the diagram.

Toughness is also a peculiar feature of the tapered multiblock structure. Figure 13 provides the obtained toughness as a function of the copolymer molecular weight and number of blocks. The results demonstrate increasing toughness for the tetrablock and hexablock tapered copolymers independent of molecular weight as a result of the bridged configurations and possibly by entangled loops. However, increasing further the block number leads to reduction in toughness,

and this is more pronounced for the 80 kg/mol molecular weight series. This is explained by a collapse of physical cross-linking caused by mixing of unlike domains as evidenced by SAXS and the lowering of the PS glass temperature. From the molecular weights investigated, tapered hexablock copolymers best combine structural order with bridged configurations that enhance the mechanical properties such as the toughness.

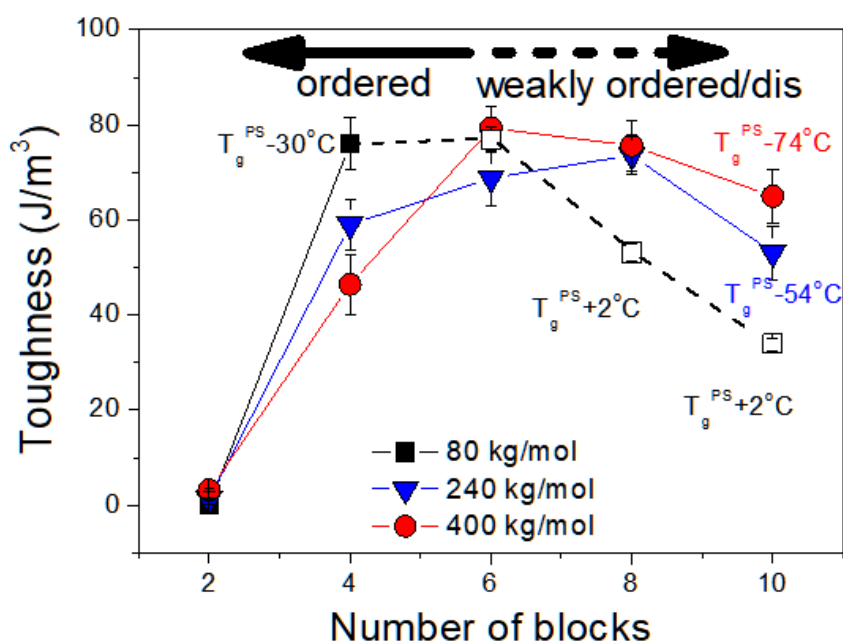


FIGURE 13 Dependence of toughness on the number of blocks in the tapered multiblock copolymers. Solid and dashed arrows indicate ordered and disordered (or weakly ordered) regimes. Open symbols indicate disordered copolymers. Measurements are made at ambient temperature, and the difference to the respective glass transition temperature of the PS block (Figures 5 and 6) is indicated in the diagram.

CONCLUSIONS

Capitalizing on the (direct) living anionic copolymerization of isoprene and styrene in cyclohexane, tapered multiblock copolymers were prepared by repeated addition of an I/S monomer mixture to the living chains in cyclohexane. The tapered block structures formed reflect the highly disparate reactivity ratios $r_I = 12.8$ and $r_S = 0.051$. $(AB)_n$ type polymers with up to 10 blocks were prepared by n addition steps of the monomer mixture, subdividing the polymer chains in alternating, highly flexible polyisoprene (PI) and rigid polystyrene (PS) segments. Three series of well-defined tapered multiblock copolymers with approximate molecular weights of 80, 240, and 400 kg/mol were generated on a scale of 100 g. The polymer chains were divided in di-, tetra-, hexa-, octa-, and decablock tapered multiblock structures. Low overall dispersities in the range

1.06-1.28 (decablock) were obtained. Degradation studies showed that after full degradation of the isoprene-rich blocks well-defined polystyrene blocks were obtained.

These copolymers exhibit some unique thermomechanical and structural features not common to block copolymers prepared by sequential methods. The presence of two glass temperatures corresponding to PS-rich and PI-rich domains was observed for all tapered multiblock copolymers. DSC provided evidence for an additional "interphase" T_g . The structural investigation revealed that tapered multiblock copolymers undergo a fluctuation-induced first order transition from the ordered to the disordered state. The domain spacing scales as $d \sim N^{0.62}$. This behavior is in analogy to sequential diblock copolymers, suggesting stretching of chains and nonideal configurations. Despite the similarity in the scaling exponent the configuration of chains in the former copolymers contains both bridges and loops as evidenced by the large reduction in the domain spacing. The effective interaction parameter was reduced relative to sequential diblock copolymers. The viscoelastic response of the tapered copolymers was controlled by the nanodomain structure, the degree of segregation, the bridged configurations of blocks, and the proximity to the glass temperature of the PS domains. Tapered hexablock copolymers best combine structural integrity and mechanical toughness, while maintaining a large strain at break (over 900%).

To the best of our knowledge, these tapered $(AB)_n$ multiblock copolymers represent a unique polymer architecture permitting to study the effect of segmented macromolecular chain architectures and its effect on a fundamental level, leading to general conclusions regarding order in multiblock structures. Because these multiblock copolymers are obtained from the common monomers isoprene and styrene on a large scale, they possess interesting potential for ordered, yet mechanically stable polymer nanostructures for a variety of applications.

ACKNOWLEDGEMENTS

Eduard Grune and Jan Blankenburg are acknowledged for valuable discussions. We thank Jürgen Ludwig for specialty glassware and Monika Schmelzer for valuable support with SEC measurements. Andreas Hanewald and Kaloian Koynov are acknowledged for help with the mechanical characterization. We also thank Tobias Prenzel for studies regarding the oxidative degradation of the tapered multiblock copolymers. M.G. and M.A. acknowledge the German Research Foundation (DFG GA 2169/1-1) for partial financial support of this work. The authors also thank the RMU Mainz-Darmstadt for funding.

REFERENCES

- (1) Khandpur, A. K.; Förster, S.; Bates, F. S.; Hamley, I. W.; Ryan, A. J.; Bras, W.; Almdal, K.; Mortensen, K. *Macromolecules* **1995**, *28* (26), 8796–8806. DOI: 10.1021/ma00130a012.
- (2) Bates, F. S.; Fredrickson, G. H. *Macromolecules* **1999**, *52* (2), 32–38. DOI: 10.1063/1.882522.
- (3) Bates, C. M.; Bates, F. S. *Macromolecules* **2017**, *50* (1), 3–22. DOI: 10.1021/acs.macromol.6b02355.
- (4) Bates, F. S. *Science* **1991**, *251* (4996), 898–905. DOI: 10.1126/science.251.4996.898.
- (5) Hadjichristidis, N.; Floudas, G.; Pispas, S. *Block copolymers: Synthetic strategies, physical properties, and applications*; Wiley-Interscience: Hoboken, N.J, 2003.
- (6) Lohse, D. J.; Hadjichristidis, N. *Current Opinion in Colloid & Interface Science* **1997**, *2* (2), 171–176. DOI: 10.1016/S1359-0294(97)80023-4.
- (7) Sinturel, C.; Bates, F. S.; Hillmyer, M. A. *ACS Macro Lett.* **2015**, *4* (9), 1044–1050. DOI: 10.1021/acsmacrolett.5b00472.
- (8) Gabor, A. H.; Lehner, E. A.; Mao, G.; Ober, C. K.; Long, T. E.; Schell, B. A.; Tiberio, R. C. *Proc. SPIE* **1925**, 499–506. DOI: 10.1117/12.154785.
- (9) Gabor, A. H.; Lehner, E. A.; Mao, G.; Schneggenburger, L. A.; Ober, C. K. *Chem. Mater.* **1994**, *6* (7), 927–934. DOI: 10.1021/cm00043a011.
- (10) Kim, H.-C.; Park, S.-M.; Hinsberg, W. D. *Chem. Rev.* **2010**, *110* (1), 146–177. DOI: 10.1021/cr900159v.
- (11) Park, C.; Yoon, J.; Thomas, E. L. *Polymer* **2003**, *44* (22), 6725–6760. DOI: 10.1016/j.polymer.2003.08.011.
- (12) Schacher, F. H.; Rupar, P. A.; Manners, I. *Angew. Chem. Int. Ed.* **2012**, *51* (32), 7898–7921. DOI: 10.1002/anie.201200310.
- (13) Feng, H.; Lu, X.; Wang, W.; Kang, N.-G.; Mays, J. *Polymers* **2017**, *9* (12), 494. DOI: 10.3390/polym9100494.
- (14) Appold, M.; Grune, E.; Frey, H.; Gallei, M. *ACS Appl. Mater. Interfaces* **2018**, *10* (21), 18202–18212. DOI: 10.1021/acsmi.8b02848.
- (15) *Modern styrenic polymers: Polystyrenes and styrenic copolymers*; Scheirs, J., Priddy, D., Eds.; Wiley Series in Polymer Science; J. Wiley: Chichester, West Sussex, England, Hoboken, NJ, 2010.
- (16) Holden, G.; Bishop, E. T.; Legge, N. R. *J. Polym. Sci. C Polym. Symp.* **1969**, *26* (1), 37–57. DOI: 10.1002/polc.5070260104.
- (17) Schwier, C. E.; Argon, A. S.; Cohen, R. E. *Polymer* **1985**, *26* (13), 1985–1993. DOI: 10.1016/0032-3861(85)90178-8.
- (18) Georgopoulos, P.; Handge, U. A.; Abetz, C.; Abetz, V. *Polymer* **2016**, *104*, 279–295. DOI: 10.1016/j.polymer.2016.02.039.
- (19) Mai, S.-M.; Mingvanish, W.; Turner, S. C.; Chaibundit, C.; Fairclough, J. Patrick A.; Heatley, F.; Matsen, M. W.; Ryan, A. J.; Booth, C. *Macromolecules* **2000**, *33* (14), 5124–5130. DOI: 10.1021/ma000154z.
- (20) Qiao, L.; Leibig, C.; Hahn, S. F.; Winey, K. I. *Ind. Eng. Chem. Res.* **2006**, *45* (16), 5598–5602. DOI: 10.1021/ie0511940.
- (21) Kraus, G.; Childers, C. W.; Gruver, J. T. *J. Appl. Polym. Sci.* **1967**, *11* (8), 1581–1591. DOI: 10.1002/app.1967.070110819.
- (22) Knoll, K.; Nießner, N. *Macromol. Symp.* **1998**, *132* (1), 231–243. DOI: 10.1002/masy.19981320122.
- (23) Angelo, R. J.; Ikeda, R. M.; Wallach, M. L. *Polymer* **1965**, *6* (3), 141–156. DOI: 10.1016/0032-3861(65)90003-0.
- (24) Cunningham, R. E.; Treiber, M. R. *J. Appl. Polym. Sci.* **1968**, *12* (1), 23–34. DOI: 10.1002/app.1968.070120104.
- (25) Kraus, G.; Rollmann, K. W. *Angew. Makromol. Chemie* **1971**, *16* (1), 271–296.

- DOI: 10.1002/apmc.1971.050160115.
- (26) Worsfold, D. J. *J. Polym. Sci. A* **1967**, 5 (11), 2783–2789. DOI: 10.1002/pol.1967.150051106.
- (27) Zelinski, R.; Childers, C. W. *Rubber Chem. Technol.* **1968**, 41 (1), 161–181. DOI: 10.5254/1.3539168.
- (28) Geoffrey, H.; Milkovich, R. Block polymers of monovinyl aromatic hydrocarbons and conjugated dienes.
- (29) Corbin, N.; Prud'homme, J. J. *Polym. Sci. Polym. Chem. Ed.* **1976**, 14 (7), 1645–1659. DOI: 10.1002/pol.1976.170140708.
- (30) Corbin, N.; Prud'homme, J. J. *Polym. Sci. Polym. Phys. Ed.* **1977**, 15 (11), 1937–1951. DOI: 10.1002/pol.1977.180151106.
- (31) Grune, E.; Johann, T.; Appold, M.; Wahlen, C.; Blankenburg, J.; Leibig, D.; Müller, A. H. E.; Gallei, M.; Frey, H. *Macromolecules* **2018**, 51 (9), 3527–3537. DOI: 10.1021/acs.macromol.8b00404.
- (32) Hodrokoukes, P.; Floudas, G.; Pispas, S.; Hadjichristidis, N. *Macromolecules* **2001**, 34 (3), 650–657. DOI: 10.1021/ma001479i.
- (33) Gronski, W.; Annighöfer, F.; Stadler, R. *Makromol. Chem.* **1984**, 6 (S19841), 141–161. DOI: 10.1002/macp.1984.020061984111.
- (34) Annighöfer, F.; Gronski, W. *Makromol. Chem.* **1984**, 185 (10), 2213–2231. DOI: 10.1002/macp.1984.021851016.
- (35) Velichkova, R.; Toncheva, V.; Getova, C.; Pavlova, S.; Dubrovina, L.; Gladkova, E.; Ponomareva, M. *J. Polym. Sci. A* **1991**, 29 (8), 1107–1112. DOI: 10.1002/pola.1991.080290804.
- (36) Stadler, R.; Auschra, C.; Beckmann, J.; Krappe, U.; Voight-Martin, I.; Leibler, L. *Macromolecules* **1995**, 28 (9), 3080–3097. DOI: 10.1021/ma00113a010.
- (37) Morris, M. A.; Gartner, T. E.; Epps, T. H. *Macromol. Chem. Phys.* **2017**, 218 (5), 1600513. DOI: 10.1002/macp.201600513.
- (38) Roy, R.; Park, J. K.; Young, W.-S.; Mastroianni, S. E.; Tureau, M. S.; Epps, T. H. *Macromolecules* **2011**, 44 (10), 3910–3915. DOI: 10.1021/ma1025847.
- (39) Luo, M.; Brown, J. R.; Remy, R. A.; Scott, D. M.; Mackay, M. E.; Hall, L. M.; Epps, T. H. *Macromolecules* **2016**, 49 (14), 5213–5222. DOI: 10.1021/acs.macromol.6b00946.
- (40) Singh, N.; Tureau, M. S.; Epps, T. H. *Soft Matter* **2009**, 5 (23), 4757. DOI: 10.1039/b908739g.
- (41) Brown, J. R.; Sides, S. W.; Hall, L. M. *ACS Macro Lett.* **2013**, 2 (12), 1105–1109. DOI: 10.1021/mz400546h.
- (42) Adhikari, R.; Godehardt, R.; Lebek, W.; Weidisch, R.; Michler, G. H.; Knoll, K. *J. Macromol. Sci. B.* **2001**, 40 (5), 833–847. DOI: 10.1081/MB-100107564.
- (43) Lach, R.; Weidisch, R.; Knoll, K. *J. Polym. Sci. B* **2005**, 43 (4), 429–438. DOI: 10.1002/polb.20337.
- (44) Thunga, M.; Staudinger, U.; Satapathy, B. K.; Weidisch, R.; Abdel-Goad, M.; Janke, A.; Knoll, K. *J. Polym. Sci. B* **2006**, 44 (19), 2776–2788. DOI: 10.1002/polb.20936.
- (45) Watanabe, H.; Sato, T.; Osaki, K.; Yao, M.-L.; Yamagishi, A. *Macromolecules* **1997**, 30 (19), 5877–5892. DOI: 10.1021/ma9617577.
- (46) Zhu, Y.; Radlauer, M. R.; Schneiderman, D. K.; Shaffer, M. S. P.; Hillmyer, M. A.; Williams, C. K. *Macromolecules* **2018**. DOI: 10.1021/acs.macromol.7b02690.
- (47) Noshay, A.; MacGrath, J. E. *Block copolymers: Overview and critical survey*, 2. print; Acad. Pr: Orlando u.a., 1987.
- (48) Lee, I.; Bates, F. S. *Macromolecules* **2013**, 46 (11), 4529–4539. DOI: 10.1021/ma400479b.
- (49) Valetskii, P. M.; Storozhuk, I. P. *Russ. Chem. Rev.* **1979**, 48 (1), 42–61.
- (50) Higaki, Y.; Suzuki, K.; Kiyoshima, Y.; Toda, T.; Nishiura, M.; Ohta, N.; Masunaga, H.; Hou, Z.; Takahara, A. *Macromolecules* **2017**, 50 (16), 6184–6191. DOI: 10.1021/acs.macromol.7b01193.

- (51) Spontak, R. J.; Smith, S. D. *J. Polym. Sci. B* **2001**, *39* (9), 947–955. DOI: 10.1002/polb.1070.
- (52) Smith, S. D.; Spontak, R. J.; Satkowski, M. M.; Ashraf, A.; Heape, A. K.; Lin, J. S. *Polymer* **1994**, *35* (21), 4527–4536. DOI: 10.1016/0032-3861(94)90798-6.
- (53) Koo, C. M.; Hillmyer, M. A.; Bates, F. S. *Macromolecules* **2006**, *39* (2), 667–677. DOI: 10.1021/ma051098a.
- (54) Aoki, D.; Ajiro, H. *Macromolecules* **2017**, *50* (17), 6529–6538. DOI: 10.1021/acs.macromol.7b00629.
- (55) Phatak, A.; Lim, L. S.; Reaves, C. K.; Bates, F. S. *Macromolecules* **2006**, *39* (18), 6221–6228. DOI: 10.1021/ma0611319.
- (56) Hermel, T. J.; Hahn, S. F.; Chaffin, K. A.; Gerberich, W. W.; Bates, F. S. *Macromolecules* **2003**, *36* (7), 2190–2193. DOI: 10.1021/ma021754w.
- (57) Watanabe, H.; Matsumiya, Y.; Sawada, T.; Iwamoto, T. *Macromolecules* **2007**, *40* (19), 6885–6897. DOI: 10.1021/ma0712495.
- (58) Matsumiya, Y.; Watanabe, H.; Takano, A.; Takahashi, Y. *Macromolecules* **2013**, *46* (7), 2681–2695. DOI: 10.1021/ma3026404.
- (59) Kelsey, J.; Pickering, N.; Clough, A.; Zhou, J.; White, J. L. *Macromolecules* **2017**, *50* (18), 7233–7240. DOI: 10.1021/acs.macromol.7b01476.
- (60) Mastan, E.; He, J. *Macromolecules* **2017**, *50* (23), 9173–9187. DOI: 10.1021/acs.macromol.7b01662.
- (61) Gleede, T.; Rieger, E.; Blankenburg, J.; Klein, K.; Wurm, F. R. *J. Am. Chem. Soc.* **2018**, *140* (41), 13407–13412. DOI: 10.1021/jacs.8b08054.
- (62) Vega, D. A.; Sebastian, J. M.; Loo, Y.-L.; Register, R. A. *J. Polym. Sci. B* **2001**, *39* (18), 2183–2197. DOI: 10.1002/polb.1192.
- (63) Leibler, L. *Macromolecules* **1980**, *13* (6), 1602–1617. DOI: 10.1021/ma60078a047.
- (64) Gennes, P. G. de. *J. Phys. France* **1970**, *31* (2-3), 235–238. DOI: 10.1051/jphys:01970003102-3023500.
- (65) Ashraf, A. R.; Ryan, J. J.; Satkowski, M. M.; Lee, B.; Smith, S. D.; Spontak, R. J. *Macromol. Rapid Commun.* **2017**, *38* (17). DOI: 10.1002/marc.201700207.
- (66) Kavassalis, T. A.; Whitmore, M. D. *Macromolecules* **1991**, *24* (19), 5340–5345. DOI: 10.1021/ma00019a020.
- (67) Wu, L.; Cochran, E. W.; Lodge, T. P.; Bates, F. S. *Macromolecules* **2004**, *37* (9), 3360–3368. DOI: 10.1021/ma035583m.
- (68) Benoit, H.; Hadziioannou, G. *Macromolecules* **1988**, *21* (5), 1449–1464. DOI: 10.1021/ma00183a040.
- (69) Zhang, J.; Deubler, R.; Hartlieb, M.; Martin, L.; Tanaka, J.; Patyukova, E.; Topham, P. D.; Schacher, F. H.; Perrier, S. *Macromolecules* **2017**, *50* (18), 7380–7387. DOI: 10.1021/acs.macromol.7b01831.
- (70) Wu, L.; Lodge, T. P.; Bates, F. S. *Macromolecules* **2004**, *37* (22), 8184–8187. DOI: 10.1021/ma048635w.
- (71) Lee, S.; Lee, H.; Chang, T.; Hirao, A. *Macromolecules* **2017**, *50* (7), 2768–2776. DOI: 10.1021/acs.macromol.6b02811.
- (72) Grune, E.; Appold, M.; Müller, A. H. E.; Gallei, M.; Frey, H. *ACS Macro Lett.* **2018**, 807–810. DOI: 10.1021/acs-macrolett.8b00390.
- (73) Quinebèche, S.; Navarro, C.; Gnanou, Y.; Fontanille, M. *Polymer* **2009**, *50* (6), 1351–1357. DOI: 10.1016/j.polymer.2009.01.041.
- (74) Matsen, M. W.; Bates, F. S. *J. Chem. Phys.* **1997**, *106* (6), 2436–2448. DOI: 10.1063/1.473153.
- (75) Hadjichristidis, N.; Pispas, S.; Floudas, G. *Block Copolymers*; John Wiley & Sons, Inc: Hoboken, USA, 2002.
- (76) Hashimoto, T.; Shibayama, M.; Kawai, H. *Macromolecules* **1980**, *13* (5), 1237–1247. DOI: 10.1021/ma60077a040.
- (77) Floudas, G.; Meramveliotaki, K.; Hadjichristidis, N. *Macromolecules* **1999**, *32* (22), 7496–7503.

DOI: 10.1021/ma990524n.

(78) Floudas, G.; Vlassopoulos, D.; Pitsikalis, M.; Hadjichristidis, N.; Stamm, M. *J. Chem. Phys.* **1996**, *104* (5), 2083–2088. DOI: 10.1063/1.470965.

(79) Han, C. D.; Baek, D. M.; Kim, J. K.; Ogawa, T.; Sakamoto, N.; Hashimoto, T. *Macromolecules* **1995**, *28* (14), 5043–5062. DOI: 10.1021/ma00118a038.

(80) Sakamoto, N.; Hashimoto, T. *Macromolecules* **1995**, *28* (20), 6825–6834. DOI: 10.1021/ma00124a018.

(81) Stühn, B.; Mutter, R.; Albrecht, T. *Europhys. Lett.* **1992**, *18* (5), 427–432. DOI: 10.1209/0295-5075/18/5/009.

(82) Fredrickson, G. H.; Helfand, E. *J. Chem. Phys.* **1987**, *87* (1), 697–705. DOI: 10.1063/1.453566.

(83) Roe, R.-J.; Zin, W.-C. *Macromolecules* **1980**, *13* (5), 1221–1228. DOI: 10.1021/ma60077a037.

(84) Brinke, G. ten; Karasz, F. E.; MacKnight, W. J. *Macromolecules* **1983**, *16* (12), 1827–1832. DOI: 10.1021/ma00246a006.

(85) Paul, D. R.; Barlow, J. W. *Polymer* **1984**, *25* (4), 487–494. DOI: 10.1016/0032-3861(84)90207-6.

SUPPORTING INFORMATION

Derivation of volume fraction of tapered structures

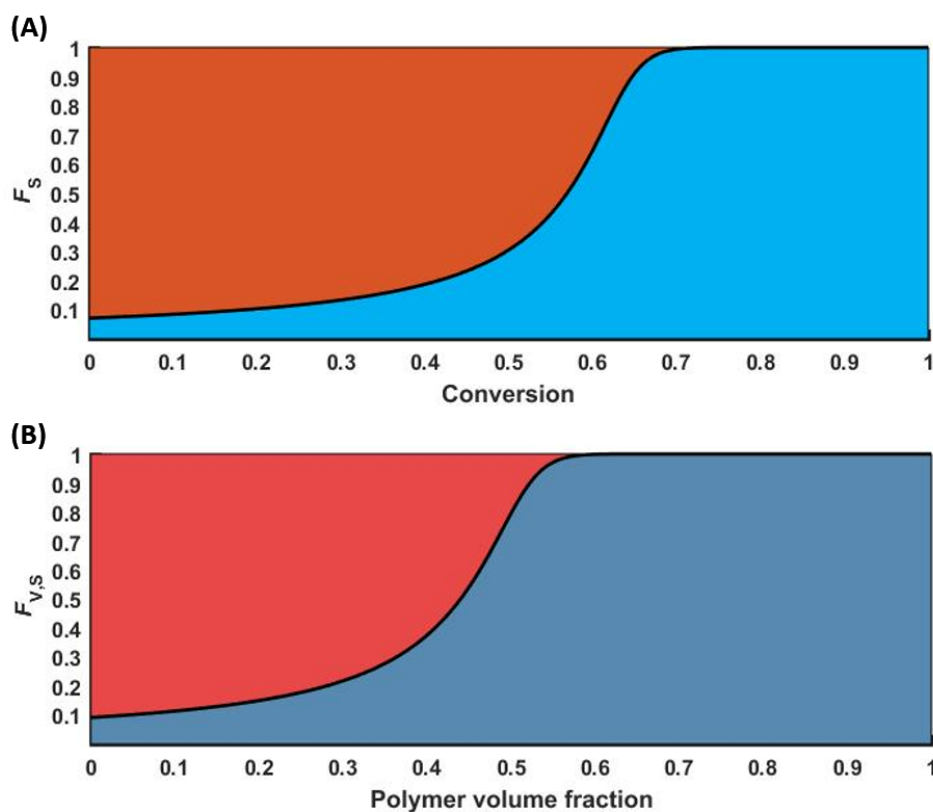


FIGURE S1 Visualization of the tapered structure in the diblock copolymer. (A) The instantaneous styrene incorporation ratio (F_S) in dependence of the monomer conversion. (B) The instantaneous styrene volume incorporation ($F_{V,S}$) in dependence of the Polymer volume fraction.

To visualize the microstructure of the polymer, the established Meyer Lowry equation can be applied to plot the instantaneous monomer incorporation ratio (F) in dependence of the total conversion (X) (Figure S1A). This plot is generated by first calculating the total conversion from the monomer feed (f) and the instantaneous monomer incorporation ratio (F) from the monomer feed (f) as well (Eq. Set S1). By combining both value pairs, F can be described as a function of X , as described by Meyer and Lowry. One downside of this illustration is that the molecular weights of the monomers are not taken into account. It is especially hard to apply this derived information to be used in phase diagrams for the prediction of phase segregation behaviour. To obtain a better perception of the real polymer microstructure, we derived a new equation to describe the volume weighted instantaneous monomer incorporation ratio (F_V) in dependence of the polymer volume fraction. This directly enables to visualize the polymer composition at each

given volume part. For this approach, we first calculated the molar volume from F by scaling F with the molecular weights of the monomers and the polymer volumes. Using substitution, the molar volume (V_m) can then be further expressed in dependence of the total conversion (X). The polymer volume fraction can then be calculated by integration of the molar volume in dependency of the total conversion and normalizing (Eq. Set S2).

As F_V is a function of X and the polymer volume fraction a function of X as well, both can be combined to yield the final description of F_V in dependence of the polymer volume fraction. This illustration enables now a better perception of the resulting polymer in the bulk state (Figure S1B).

For example, in case of an equimolar feed of styrene and isoprene Figure S1A suggest that the polystyrene block is smaller than the isoprene block due to some incorporation of styrene into the isoprene part. Both areas (red and blue) show the same size, as this illustration represents the molar ratio. While this is not false it deceives the real structure in terms of bulk morphologies. Figure S1 shows clearly that the inflection point is at exactly 50% polymer volume. In this graph both areas (red and blue) differ in their size due to the different total volume fraction of styrene (approx. 60 %) and isoprene (approx. 40 %) in case of equimolar feed ratio. For this specific system an equimolar ratio of styrene and isoprene will also lead to equimolar volume fractions due to the incorporation of styrene into the isoprene part, increasing its volume while the size of the styrene part is decreased.

1) Derivation of F_S vs. total conversion, (Equation Set S1):

Meyer-Lowry equation¹

Calculate conversion of styrene X_S in dependence of monomer feed of styrene f_s to obtain $X(f_s)$

$$X = 1 - [M] / [M]_0$$

Mayo-Lewis equation²

Calculation of the molar styrene proportion in the polymer F_S in dependence of the monomer feed of styrene f_s . After these two steps $X(f_s)$ can be combined to yield the function $F_S(X)$ which represents the function of the taper in the F_S vs total conversion diagram visualized in Figure S1.

2) Calculation of the molar polymer volume fraction V_{Polymer} , Volume. (Equation Set S2):

Calculation of total polymer molar volume $V_m(F_S)$

$$V_m(F_S) = F_S (f_S) \cdot \frac{M(\text{Styrene})}{\rho(\text{Polystyrene})} + F_I (f_I) \cdot \frac{M(\text{Isoprene})}{\rho(\text{Polyisoprene})}$$

Calculation of the molar volume weighted volume fraction of styrene $F_{V,S}$

$$F_{V,S} = F_S (f_S) \cdot \frac{M(\text{Styrene})}{\rho(\text{Polystyrene})} \cdot \frac{1}{V_m(F_S)}$$

Eliminate the dependence of f_I

$$V_m(F_S) = F_S (f_S) \cdot \frac{M(\text{Styrene})}{\rho(\text{Polystyrene})} + (1 - F_S (f_S)) \cdot \frac{M(\text{Isoprene})}{\rho(\text{Polyisoprene})}$$

Now V_m is also a function of X .

Calculation of polymer volume fraction:

$$V_{\text{Polymer,Volume}}(X) = \frac{\int_0^{X_S} V_m(X) dx}{\int_0^1 V_m(X) dx}$$

$V_{\text{Polymer,Volume}}(X)$ and $F_{V,S}(X)$ depend on X . Therefore, a combination of the functions to $F_{V,S}(V_{\text{Polymer,Volume}})$ is possible, which represents the function of the taper in the $F_{V,S}$ vs Polymer volume fraction diagram visualized Figure S1b.

The area under the fit represents the volume ratio of styrene in the polymer. The slope represents the change in the volume styrene proportion $F_{V,S}$ in the polymer in dependence of the polymer volume. The following expression can be used to calculate the volume ratio of styrene up to the desired polymer volume $V_{\text{Polymer,+}}$.

$$V_S = \int_0^{V_{\text{Polymer,+}}} F_{V,S}(V_{\text{Polymer}}) dV_{\text{Polymer}}$$

Explanation of Equation (1) (Equation Set S3):

Assumptions: 100 % initiator efficiency, no termination reactions $[P^-] = [\text{BuLi}]_0$

Homopolymerization of styrene:

$$V_{\text{pol,S}} = -\frac{d[S]}{dt} = k_{ss} [P^-]^{1/2} [S] = \underbrace{k_{ss} [\text{BuLi}]_0^{1/2}}_{\text{constant} \rightarrow \text{first order}} [S]$$

$$[S] = [S]_0 \cdot \exp\left(-k_{ss} \cdot [\text{BuLi}]^{1/2} \cdot t_S\right)$$

Homopolymerization of isoprene:

$$V_{\text{pol, I}} = -\frac{d[I]}{dt} = k_{\text{II}}([P^-]^{1/4} [I] = \underbrace{k_{\text{II}} [BuLi]_0^{1/4}}_{\text{constant} \rightarrow \text{first order}} [I])$$

$$[I] = [I]_0 \cdot \exp\left(-k_{\text{II}} \cdot [BuLi]^{1/4} \cdot t_I\right)$$

Conversion of each monomer

$$x_I = 1 - \left(\frac{[I]}{[I]_0}\right) \quad x_S = 1 - \left(\frac{[S]}{[S]_0}\right)$$

Assumption: Crossover reaction from isoprene to styrene is not relevant for the kinetics.

Reaction time for PS-block

$$\frac{[S]}{[S]_0} = 1 - x_S = \exp\left(-k_{\text{SS}} [BuLi]^{1/2} \cdot t_S\right)$$

$$\log(1-x_S) = -k_{\text{SS}} [BuLi]^{1/2} \cdot t_S$$

$$t_S = -\underbrace{\frac{\log(1-x_S)}{k_{\text{SS}}}}_{\text{constant}} \cdot \frac{1}{[BuLi]^{1/2}}$$

Reaction time for PI-block

$$\frac{[I]}{[I]_0} = 1 - x_I = \exp\left(-k_{\text{II}} [BuLi]^{1/4} \cdot t_I\right)$$

$$\log(1-x_I) = -k_{\text{II}} [BuLi]^{1/4} \cdot t_I$$

$$t_I = -\underbrace{\frac{\log(1-x_I)}{k_{\text{II}}}}_{\text{constant}} \cdot \frac{1}{[BuLi]^{1/4}}$$

$$t_{\text{total}} = t_S + t_I \rightarrow \text{Equation 1}$$

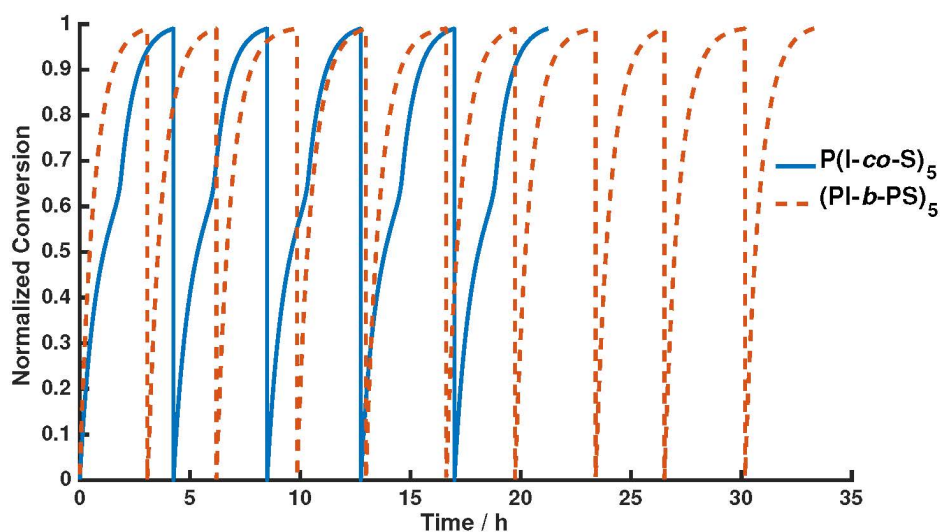


FIGURE S2 Kinetic comparison between a tapered decablock copolymer $P(I-co-S)_5$ and a decablock copolymer $(PI-b-PS)_5$ obtained by alternating addition of the respective monomers. When performing the copolymerization strategy, 10 blocks are already finished whereas the 7th block is just running for the sequential synthetic pathway. $M_n(th.) = 400$ kg/mol, $[I]_0 = 0.29$ mmol/L, $[M]_0 = 1.36$ mol/L, 50%_{mol} isoprene and styrene.

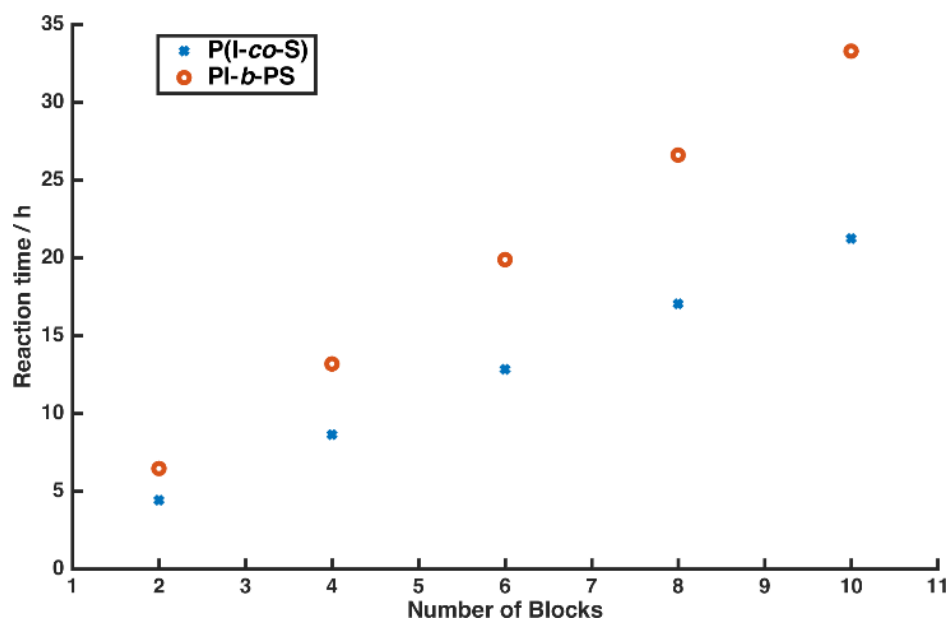


FIGURE S3 Reaction time required for the synthesis of tapered multiblock copolymers of isoprene and styrene with n blocks, based on kinetic Monte Carlo simulation. $[I]$ and $[M]$ for this $M_n = 80$ kg/mol can be found in Table S2.

Materials

All chemicals and solvents were purchased from Acros Organics Co. and Sigma-Aldrich Co. Isopropyl alcohol was used as received without further purification. Cyclohexane was purified via distillation under reflux over sodium wire with benzophenone as indicator. Isoprene and styrene and were purified by distillation over calcium hydride and triethylaluminum. Isoprene, styrene and isopropyl alcohol were degassed by three cycles of freeze-pump-thaw prior to use.

Kinetic Monte Carlo calculations (KMC) (Equation Set S4)

The model was developed based on the stochastic simulation algorithm by Gillespie.^{3,4} Continuum-based reaction rates were converted to number-based probabilities using the following equations:

$$kMC_{II} = \frac{k_{II}}{(NV)^{1/4}} \quad (1.1)$$

$$kMC_{SS} = \frac{k_{SS}}{(NV)^{1/2}} \quad (1.2)$$

$$kMC_{IS} = \frac{k_{IS}}{(NV)^{1/4}} \quad (1.3)$$

$$kMC_{SI} = \frac{k_{SI}}{(NV)^{1/2}} \quad (1.4)$$

Concentrations have been converted by multiplying with Avogadro's number N and simulation volume V . The typical simulation volume was in range of $8E-16$ L to $8E-19$ L. For each simulation 10^6 chains were used. All simulations were performed up to 99% conversion. Each reaction probability was calculated based on the fraction of the total reaction rate:

$$P_v = \frac{R_v}{\sum_{M=1}^{\mu} R_v} \quad (1.5)$$

The corresponding reaction was chosen using a uniform distributed random number $r_1 = [0..1]$ based on the reaction probabilities:

$$\sum_{v=1}^{\mu-1} P_v < r_1 < \sum_v^{\mu} P_v \quad (1.6)$$

The time interval corresponding to the chosen reaction step was calculated using another uniformly distributed random number $r_2 = [0..1]$:

$$\tau = \frac{1}{\sum_{M=1}^{\mu} R_v} \ln \left(\frac{1}{r_2} \right) \quad (1.7)$$

After a reaction was stochastically selected, one randomly corresponding chain was chosen and used to proceed the reaction step. The monomer composition of all chains was tracked.

For performance improvement the main stochastic model was implemented in C code, compiled using MinGW GCC compiler 5.1.0, while evaluation of the computed data was performed using custom written MATLAB scripts.^{3,4}

General Polymerization Procedure For the Synthesis of Multiblock Copolymers

Prior the use of isoprene and styrene, the monomers were filtered through a column containing basic aluminium oxide to remove stabilizers. Afterwards a mixture of isoprene and styrene was dried for 2 days at room temperature over finely ground CaH_2 , degassed by three cycles of freeze-thaw and distilled ($1 \cdot 10^{-3}$ mbar) into a flask containing trioctylaluminum obtained by evaporation of solvent from a trioctylaluminium solution under reduced pressure. After stirring at room temperature for overnight, a second distillation into a graduated ampule was performed.

Cyclohexane was dried over sodium with benzophenone as indicator under reflux. The dried cyclohexane was distilled under normal pressure into a Mortom flask glass reactor equipped

with a rare earth magnetic stirring bar. The reactor was flushed with argon, the required amount of *sec*-BuLi solution was added, and polymerization started via addition of the desired amount of monomer mixture. The respective reaction time was calculated using a kinetic Monte-Carlo simulation. To guarantee full monomer conversion by considering fluctuations in initiator concentration due to difficulties by adding the exact amount of solvent, the calculated reaction times for the conversion of each monomer addition were extended by 10%. Common reaction times are in the range of 2 to 4 h. Exact values can be found in Table 1. The monomer addition was repeated several times, until the desired number of blocks was achieved. The living chain ends were terminated by adding degassed isopropyl alcohol via syringe. To precipitate the polymer, the mixture was poured into an 8-fold volume excess of 50%_{vol} mixture of isopropyl alcohol and methanol, dried at reduced pressure and stored in the absence of light at -20 °C. The pure polymer was obtained as a white solid in quantitative yield.

NMR Spectroscopy

NMR spectra were recorded on a Bruker Avance II 400 spectrometer with 400 MHz (¹H NMR) or 101 MHz (¹³C NMR) and are referenced internally to residual proton signals of the deuterated solvent.

Standard Size Exclusion Chromatography (SEC)

SEC measurement was performed with THF as the mobile phase (flow rate 1 mL min⁻¹) on an SDV column set from PSS (SDV 10³, SDV 10⁵, SDV 10⁶) at 30 °C. Polymer concentrations with a maximum of 1 mg/mL turned out to be suitable to prevent concentration effects. Calibration was carried out using Polystyrene standards (from Polymer Standard Service, Mainz).

Differential Scanning Calorimeter (DSC)

The thermal properties of the tapered multiblock copolymers were studied with a Q2000 (TA Instruments) differential scanning calorimeter (DSC). The instrument was calibrated for best performance on the specific temperature range and heating/cooling rate. The calibration sequence included a baseline calibration for the determination of the time constants and capacitances of the sample and reference sensor using a sapphire standard, an enthalpy and temperature calibration for the correction of thermal resistance using indium as standard ($\Delta H = 28.71$ J/g, $T_m = 428.8$ K), and a heat capacity calibration with sapphire standard. Two cooling and heating cycles were performed at a rate of 10 K/min in a temperature range between 173 K and 433 K and the glass temperatures were extracted from the second cycle.

X-Ray Scattering

Small-angle (SAXS) measurements were made using $\text{CuK}\alpha$ radiation (Rigaku Micro Max 007 X-ray generator, Osmic Confocal Max-Flux curved multilayer optics). 2D diffraction patterns were recorded on an Mar345 image plate detector at a sample-detector distance of 2060 mm. Intensity distributions as function of the modulus of the total scattering vector, $q = (4\pi/\lambda) \sin(2\theta/2)$, where 2θ is the scattering angle, were obtained by radial averaging of the 2D datasets. Samples in the form of thick films (~ 1 mm) were prepared by slow solvent casting. Temperature-dependent measurements of 1 hour long were made by heating the films from 298 K to 503 K in 5 K steps aiming at identifying the corresponding order-to-disorder transition temperatures.

TEM Measurements

For characterization of the tapered block copolymer morphology in the bulk state, the as prepared films were microtomed from surface to surface at -80 °C into thin slices of 50-70 nm thickness. The collected ultrathin sections were subsequently stained with osmium tetroxide (OsO_4) for selective staining of the PI domains, followed by investigation by TEM measurements.

Transmission electron microscopy (TEM) experiments were carried out using a Zeiss EM 10 electron microscope (Oberkochen, Germany) operating at 60 kV with a slow-scan CCD camera obtained from TRS (Tröndle, Morrenweis, Germany) in bright field mode. Camera was computer-aided using the ImageSP software from TRS.

Tensile Tests

Tensile tests were performed using a materials testing machine Z005 (Zwick/Roell, Germany). Tensile tests were carried out by exposing the stamped polymer dogbones to a uniaxial tension. Bone shape samples with thicknesses around 0.2 mm were drawn with rate of 10 mm/min at room temperatures. A Pre-Load of 0.1 N was applied with a Pre-Load speed of 5mm/min. Dependencies of stress vs. draw ratio were recorded. Elastic modulus, elongation at break and stress at break were determined as averages of 2–5 independent drawing experiments performed at the same conditions. All films were prepared with a thickness round 0.2 mm, obtained by slow evaporation from a chloroform solution followed a full removal of the solvent under reduced pressure and used for tensile tests without prior thermal annealing. The measurements were carried out by exposing the stamped polymer dogbones to a uniaxial tension.

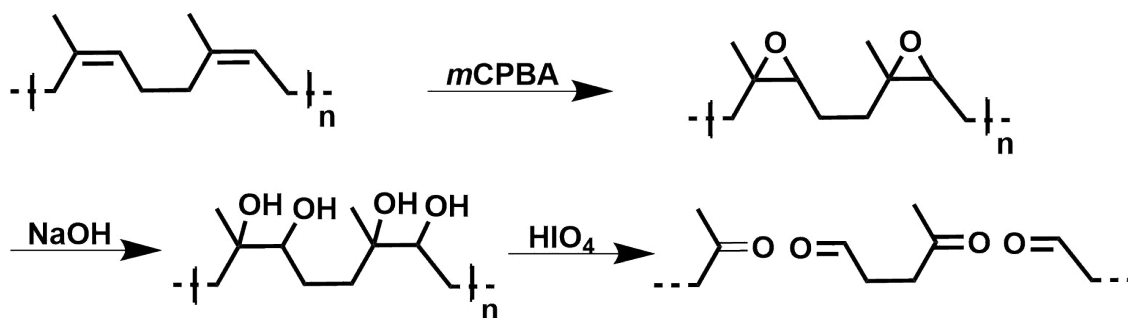
Oxidative Degradation in Solution

This optimized procedure is based on the degradation of a tapered hexablock copolymer described by Corbin.⁵

An excess of *meta*-chloroperbenzoic acid (*m*CPBA) (4 g) was added to a solution of the block copolymer (1.5 g in 200 ml of benzene) and the mixture was gently shaken for 15 hr at room temperature. Afterwards, the benzene was removed by distillation and the dried hydroxylated polymer was dissolved in dioxane (150 ml) and mixed with a solution of HIO₄ (3.5 g in 20 ml of water). The mixture was left for 24 hr at room temperature and then warmed to approximately 60 °C for 30 min. The solvents were removed by distillation at reduced pressure and the dry residue was washed with dilute NaOH and water. The residue was dried, weighed and dissolved in 50 ml of methylethyl ketone. The solution was filtered, and the polymer was isolated by precipitation with methanol.

Dialysis in chloroform was performed using benzoylated tubings from Sigma Aldrich with a cut-off molecular weight of 4 kg/mol.

SCHEME S1 Three step synthesis for the oxidative cleavage of 1,4-polyisoprene units in P(I-co-S)_n tapered multiblock copolymers.



Rheology

A TA Instruments, AR-G2, with a magnetic bearing that allows for nanotorque control was used for recording the viscoelastic properties of the multiblock polymers. Measurements were made with the environmental test chamber (ETC) as a function of temperature. Samples were prepared on the lower rheometer plate (8 mm and 25 mm), the upper plate was brought into contact, and the gap thickness was adjusted. The linear and nonlinear viscoelastic regions were determined by the strain amplitude dependence of the complex shear modulus $|G^*|$ at $\omega = 10$ rad/s. Evidently, tapered multiblock copolymers orient easily by the application of strain. A low strain amplitude (typically below 1.5%) was used to avoid non-linearities. Subsequent measurements involved (i) isothermal frequency scans within the range $10^{-1} < \omega < 10^2$ rad/s at several temperatures and (ii) isochronal temperature ramps with $\omega = 1$ rad/s between 298 K and 493 K.

Removal of samples from living polymer solution



FIGURE S4 Typical change of the color of the reaction solution upon switching of the system from isoprenyllithium chain ends (colorless) to styryllithium chain ends (orange color).

In a first experiment reaction times were validated by taking a sample from the reaction solution. Due to the high sensitivity of the living carbanionic chain ends towards oxygen and moisture and the associated change of the initiator concentration we limited these investigations to a tapered tetrablock copolymer.

After a calculated isoprene conversion of $x_I = 1$ and $x_S = 0.99$ a defined amount of the bright orange living polymer was taken out of the reactor, terminated with isopropanol and analysed. Subsequently, the synthesis was continued in the reactor by adding another monomer mixture. A prolonged reaction time was chosen for the second tapered diblock unit to guarantee full

monomer conversion. The samples were analysed by ^1H NMR spectroscopy (Figure S5) and SEC (Figure S6).

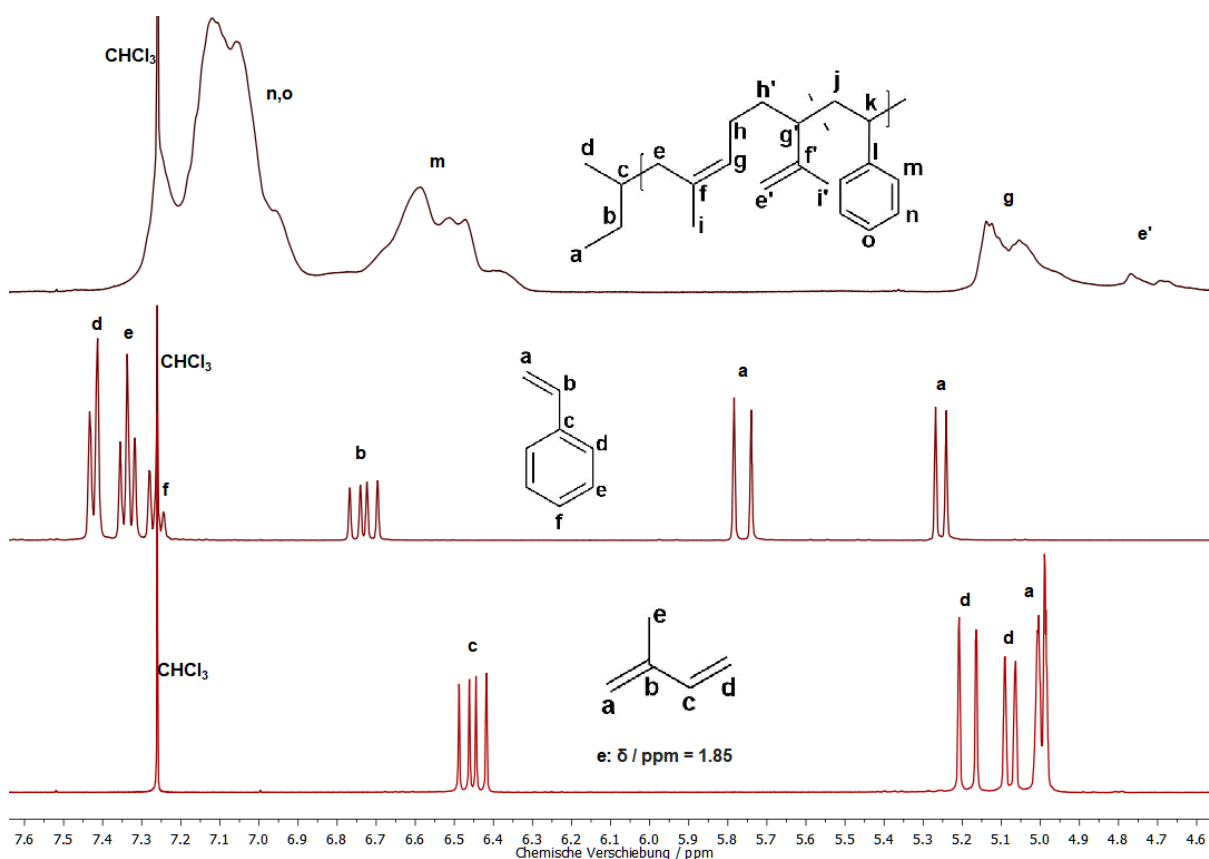


FIGURE S5 Stacked ^1H NMR spectra (400 MHz, CDCl_3) of the crude reaction product (top), styrene (middle) and isoprene (bottom) monomer. Obviously, no signals of unreacted monomer are found in the crude polymer solution. Full conversion to the desired reaction product P(I-co-S)_2 can be assumed.

Due to the high viscosity of the solution, removal of samples by syringe was increasingly difficult, which resulted in a small fraction of coupling products in the syringe caused by oxygen. Due to the molecular weight of the first, which is exactly the half of the second diblock unit, this experiment validates the suggested reaction times obtained by Monte Carlo simulation.

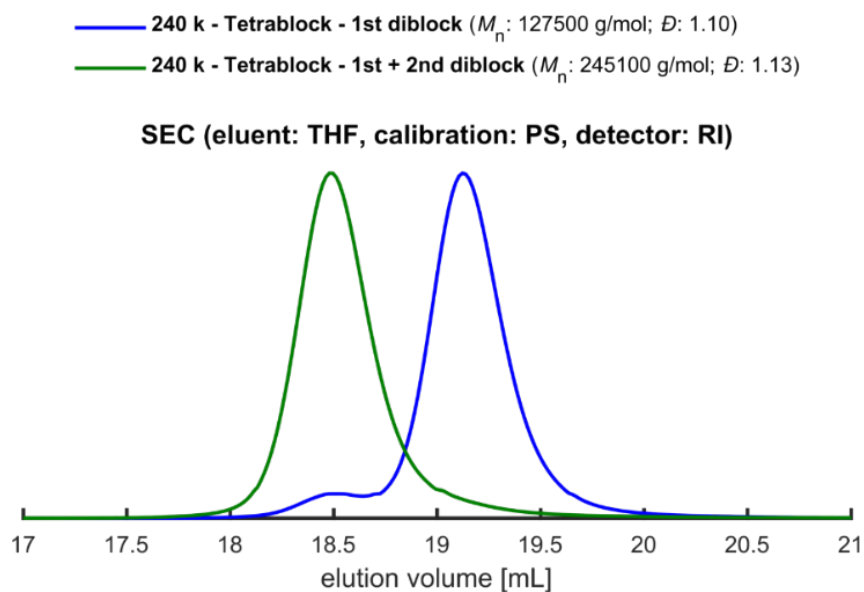


FIGURE S6 A defined amount of living polymer solution was taken from the reaction vessel to verify calculated conversion times. The obtained molecular weights validate full conversion. The small should in the SEC trace of the first block can be attributed to coupling reaction due to exposure of the living polymer solution to oxygen in the syringe.

SEC traces of tapered multiblock copolymers synthesized in this work

The SEC traces of the tapered multiblock copolymers investigated in this work are also shown in Figure 3. In this Figure all molecular weight series are superimposed.

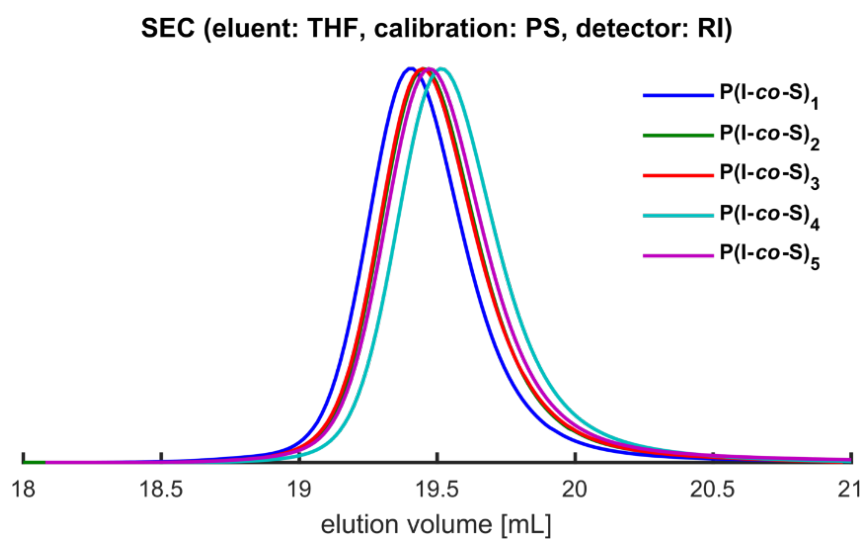


FIGURE S7 SEC traces for 80 kg/mol series.

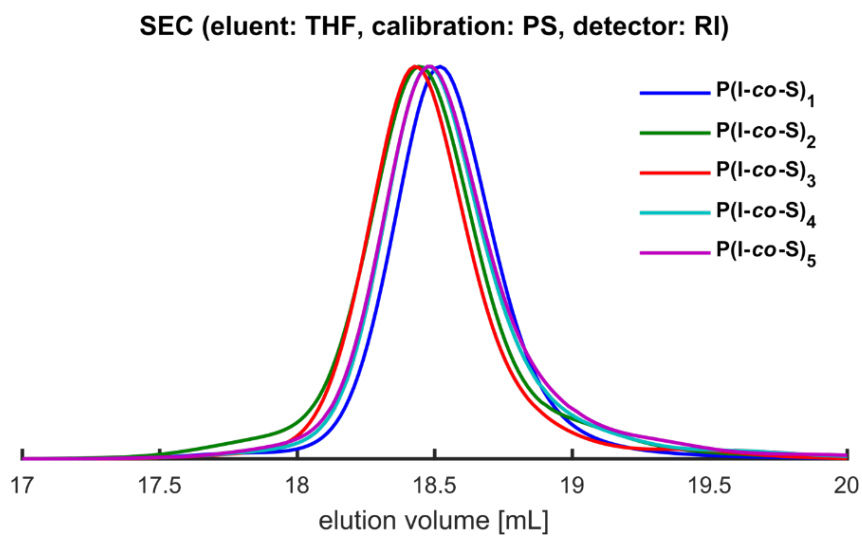


FIGURE S8 SEC traces for 240 kg/mol series.

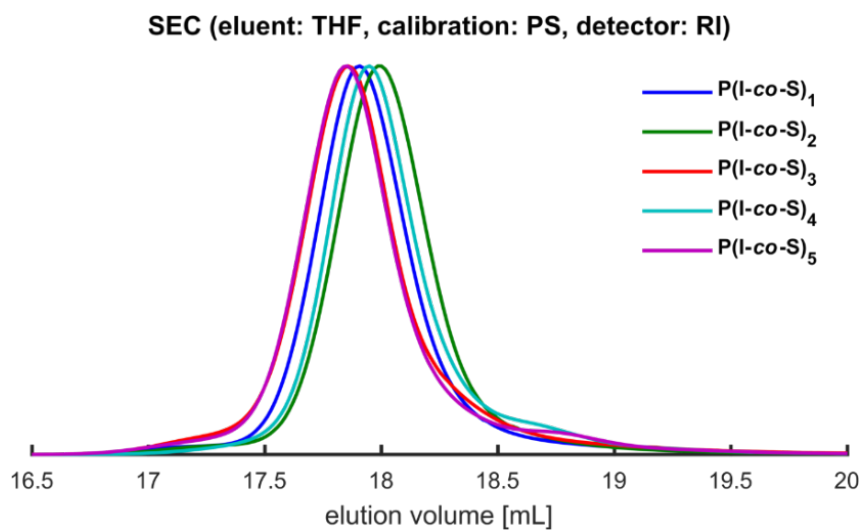


FIGURE S9 SEC traces for 400 kg/mol series.

Experimental and theoretical investigation of the microstructure via triad analysis

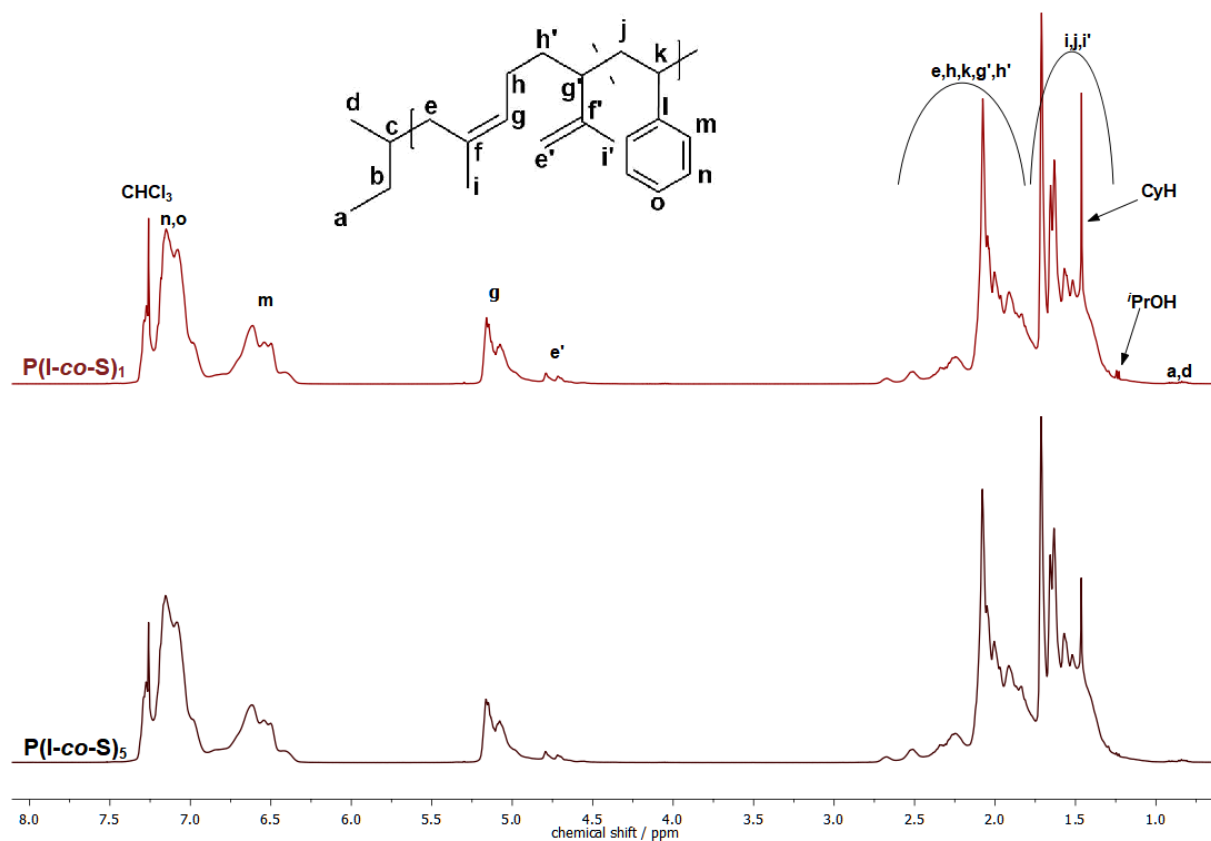


FIGURE S10 Stacked ¹H NMR spectra (400 MHz, CDCl₃) of an 80 kg/mol P(I-co-S)₁ and an 80 kg/mol P(I-co-S)₅ tapered multiblock copolymer. The samples show no difference regarding the spectra despite the strongly diverging monomer sequence along the polymer backbone. Signals which can be attributed to the presence of impurities are present in the spectra and given as follows: ⁱPrOH = 2-Propanol, CyH = Cyclohexane.

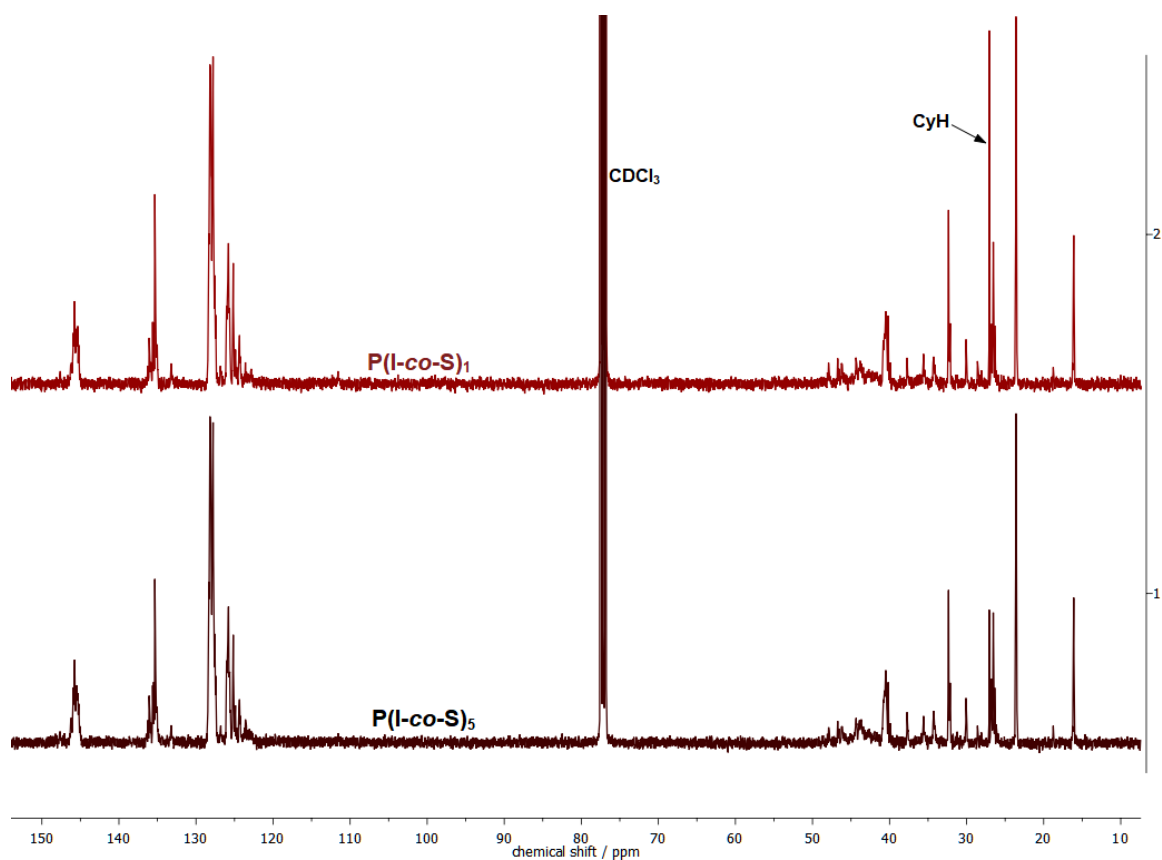


FIGURE S11 Stacked ^{13}C -inverse-gated-NMR spectra (101 MHz, CDCl_3) of an 80 kg/mol P(I-co-S)_1 (top) and an 80 kg/mol P(I-co-S)_5 tapered multiblock copolymer (bottom). The samples show no difference regarding the spectra despite the strongly diverging monomer sequence along the polymer backbone. A signal, which can be attributed to the presence of cyclohexane is shown in the spectra and noted with CyH.

An extensive investigation of ^1H NMR and ^{13}C NMR spectra of polyisoprene and polybutadiene with different compositions of the polydiene microstructures was made by other groups.^{6,7}

TABLE S1 Calculated values for triad analysis performed by kinetic Monte Carlo simulation.

entry	target M_n [kg/mol]	number of blocks	III/ %	IIS/ %	ISI/ %	SII/ %	ISS/ %	SIS/ %	SSI/ %	SSS/ %
1	80	2	34.20	6.58	7.17	2.56	6.58	3.24	2.66	37.00
2	80	4	34.05	6.63	7.16	2.66	6.63	3.30	2.77	36.79
3	80	6	33.90	6.68	7.16	2.77	6.68	3.35	2.87	36.59
4	80	8	33.76	6.73	7.15	2.87	6.73	3.40	2.98	36.38
5	80	10	33.61	6.77	7.15	2.98	6.77	3.45	3.08	36.18
6	240	2	34.22	6.56	7.17	2.56	6.56	3.21	2.60	37.14
7	240	4	34.18	6.57	7.17	2.59	6.57	3.23	2.63	37.07
8	240	6	34.13	6.58	7.17	2.63	6.58	3.24	2.66	37.01
9	240	8	34.08	6.60	7.16	2.66	6.60	3.26	2.70	36.94
10	240	10	34.04	6.61	7.16	2.69	6.61	3.28	2.73	36.88
11	400	2	34.23	6.55	7.17	2.56	6.55	3.20	2.58	37.16
12	400	4	34.21	6.55	7.16	2.58	6.55	3.21	2.60	37.13
13	400	6	34.18	6.56	7.16	2.60	6.56	3.22	2.62	37.09
14	400	8	34.15	6.57	7.16	2.62	6.57	3.23	2.64	37.05
15	400	10	34.12	6.58	7.17	2.64	6.58	3.24	2.66	37.01

Triad analysis was performed by analysing each individual chain calculated by the KMC model and normalizing the values.

Only a subtle decrease (< 1%) of III and SSS segments with increasing number of blocks due to the higher number of tapered zones was observed. Essentially this is no large difference, concluding the size of the tapered zone is more or less just divided by the number of blocks. The relative size of the tapered sections referred to the whole chain does not change with increasing number of blocks.

Also, no influence of the molecular weight on the triad abundance can be detected. This emphasizes that the size and structure of single tapered segments of the tapered multiblock copolymers is merely a function of the block size and the monomer system (e.g. reactivity ratios). The gradient size scales linearly with the molecular weight and can be distributed by increasing the number of blocks without significantly altering the overall size of the gradient.

Oxidative degradation in solution and segment length analysis

Segment analysis was performed by counting the consecutive numbers of monomers without any interruption. This was performed for every polymer chain simulated via the KMC model. After normalization and weighting by the molecular weight of the segments the SEC of the resulting distribution can be plotted. The following figures compare the simulated SEC traces with

experimental data (PS calibration) of tapered multiblock copolymer structures ranging from the 80 kg/mol tetrablock up to the 400 kg/mol decablock copolymer.

Due to the oxidative degradation, the obtained polystyrene fragments are telechelic polymers with hydrophilic end groups. Rinsing out the highly polar low molecular weight fragments of the cleaved isoprene block could also lead to the separation of telechelic polystyrene oligomers. For this reason, the peak maximum of the molecular weight distributions M_p was used for further comparison between experimental and theoretical data.

A good agreement between theoretical and experimental data is found for tapered structures, especially for the 80 kg/mol tapered tetrablock copolymer. While increasing the number of blocks and the molecular weight, a relative increase of the values of the experimental compared to the theoretical data is observed. This effect can be attributed to incomplete cleavage of single isoprene units located in the styrene block. During the polymerization, when isoprene is nearly fully consumed, long segment length were observed for polystyrene rarely interrupted by single isoprene units. When these single units are not fully cleaved the molecular weight of the PS fragments is shifted strongly to higher molecular weights.

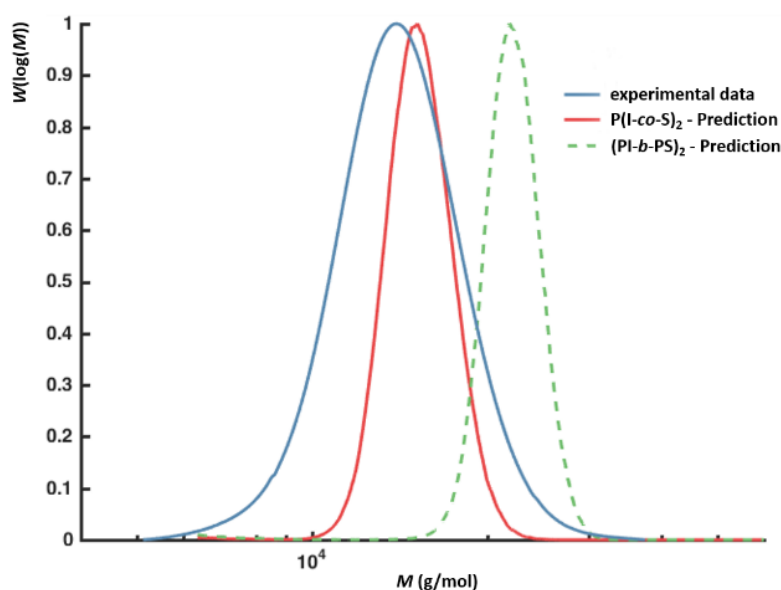


FIGURE S12 SEC trace of polystyrene fragments obtained by oxidative degradation of an 80 kg/mol tapered tetrablock copolymer.

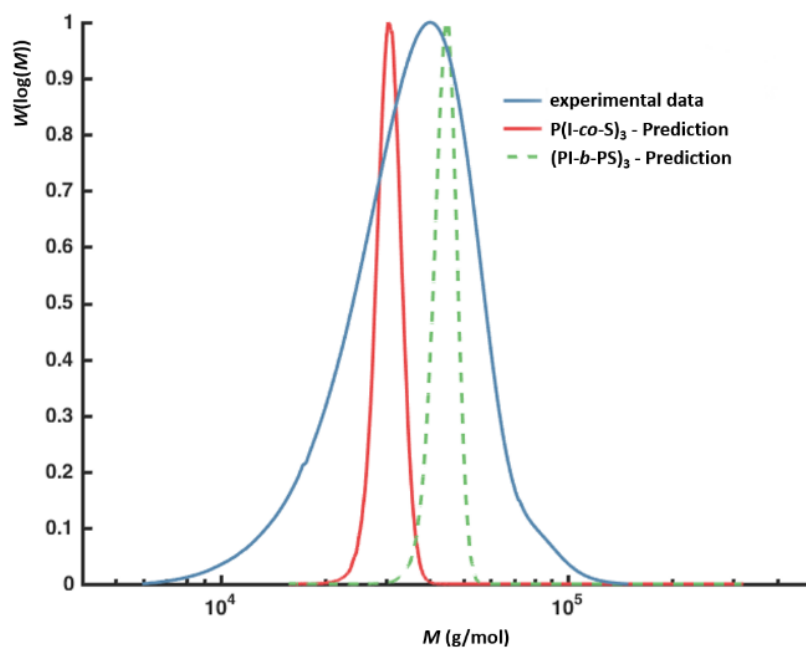


FIGURE S13 SEC trace of polystyrene fragments obtained by oxidative degradation of a 240 kg/mol tapered hexablock copolymer.

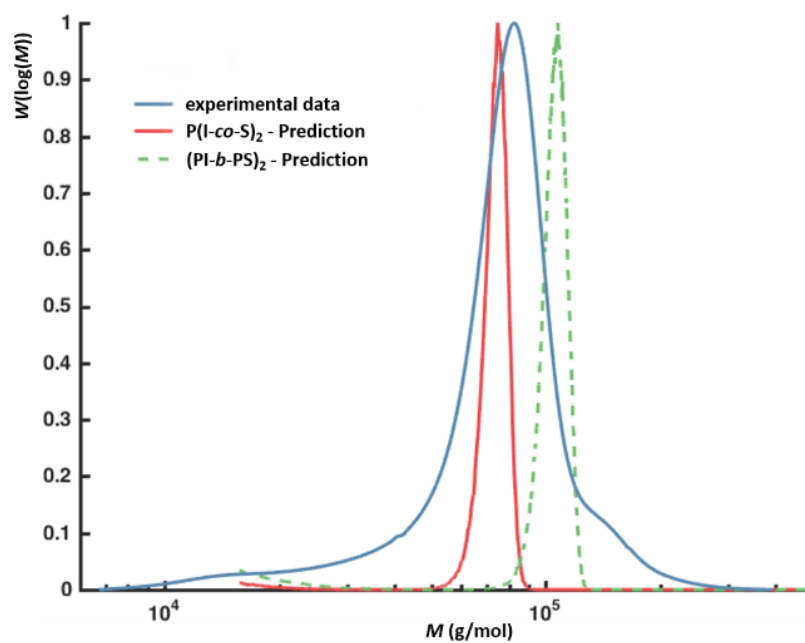


FIGURE S14 SEC trace of polystyrene fragments obtained by oxidative degradation of a 400 kg/mol tapered tetrablock copolymer.

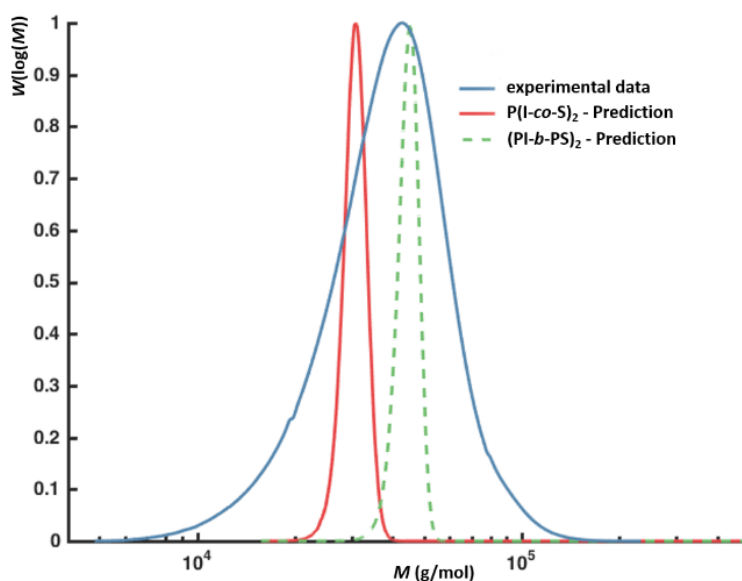


FIGURE S15 SEC trace of polystyrene fragments obtained by oxidative degradation of a 400 kg/mol tapered decablock copolymer.

Additionally, a tailing of the SEC trace is observed in some cases. This tailing is especially pronounced for tapered multiblock copolymers with large blocks e.g. the 400 kg/mol tetrablock copolymer (Figure S14) (high molecular weight and low number of blocks). The observed tailing reflects the tapered region of the multiblock copolymer, shifted to higher molecular weights caused by incomplete glycol cleavage as shown by ^1H NMR spectroscopy (Figure S16, spectra 3c).

Experimental data show a broadening of the molecular weight distribution by increasing the molecular weights from 80 to 400 kg/mol. This can be attributed due to the demanding synthesis due to the relative decrease of the active chain ends, which are highly sensible to a broad range of impurities even in very low concentrations. This increase in the polydispersity complicates the comparison to the theoretical data, which are unaffected by broadening effects due to technical and synthetic difficulties. One should keep in mind, the polystyrene fragments are obtained by performing a multistep polymer synthesis targeting high molecular weight copolymers, followed by a 3 step procedure resulting in the oxidative cleavage of the 1,4-PI units (Scheme S1).

Especially for the cleavage of the 1,4-PI units side reactions as the nucleophilic ring opening of epoxides by glycolate anions can be considered. In addition, 5%_{mol} of the isoprene units consists of 3,4-units, where oxidative cleavage of the double bond does not occur in the backbone. Due to the unknown distribution of 3,4-PI units in respect to the different triads (Table S1) a full cleavage of the PI units was also assumed for the 3,4-PI.

Also underlining the fact, that the obtained telechelic polystyrene fragments are calibrated to non-telechelic polystyrene standards in SEC measurements a good agreement is found between experimental and theoretical values.

TABLE S2 Overview of I/S tapered multiblock copolymer samples and reaction parameters employed.

sample	target $M_n(\text{total})$ [kg/mol]	calculated sequential $M_p(\text{PS-blocks})$ [kg/mol]	calculated tapered $M_p(\text{PS-blocks})$ [kg/mol]	observed $M_p(\text{PS-blocks})$ [kg/mol]	$\bar{D}(\text{PS-blocks})$
P(I-co-S) ₂	80	22	14	13	1.06
P(I-co-S) ₃	240	45	28	41	1.19
P(I-co-S) ₂	400	75	73	84	1.18
P(I-co-S) ₅	400	30	29	43	1.22

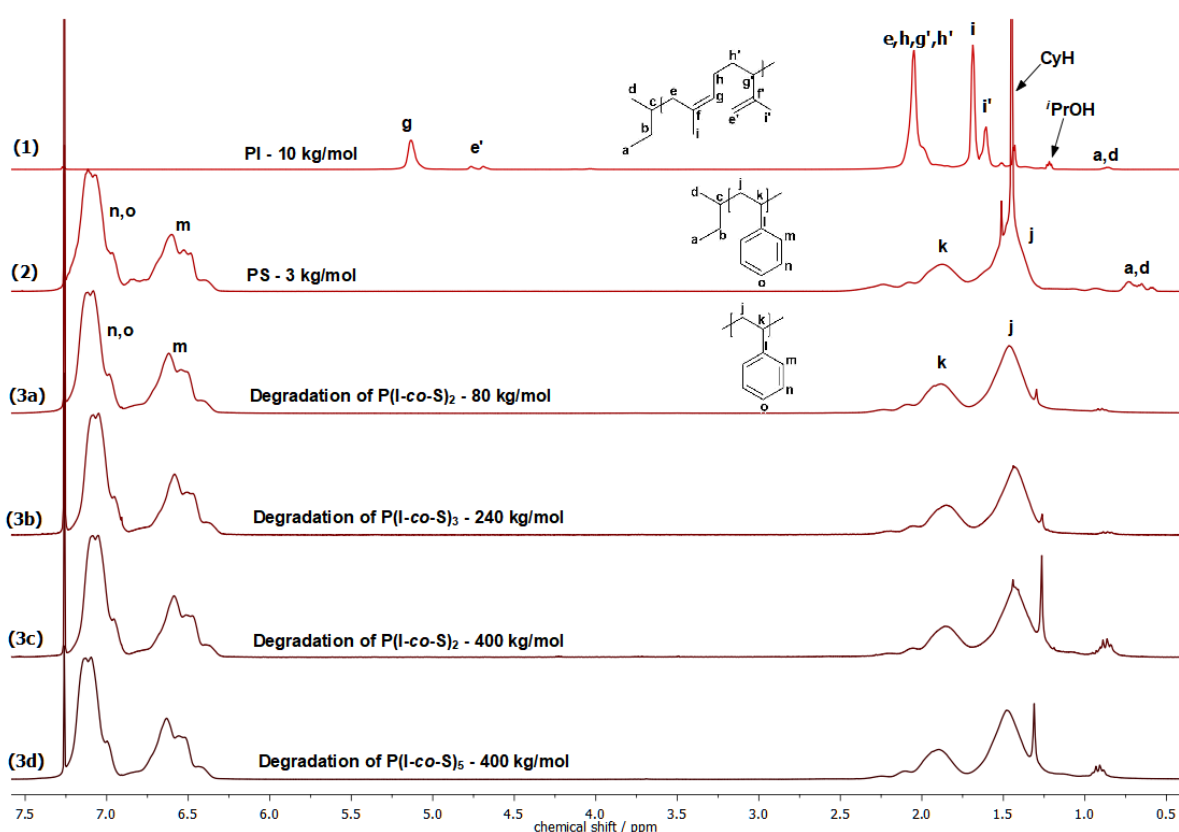


FIGURE S16 Stacked ¹H NMR spectra (400 MHz, CDCl₃) of a polyisoprene (spectrum 1) and polystyrene homopolymer (spectrum 2) obtained by initiating the respective monomers with *sec*-BuLi in cyclohexane. In these NMR spectra the polyisoprene segment shows a comparable microstructure as in the tapered multiblock copolymers investigated in this work (95%_{mol} 1,4-PI, 5%_{mol} 3,4-PI). The spectra 3a to 3d refer to products obtained by deliberate oxidative degradation. Good agreement with the spectra of pure polystyrene is obtained. The chemical shift of the peak at 1.3 ppm fits well with typical shifts also obtained by aliphatic alcohols⁸ and can most likely be assigned to oxidized polyisoprene units which did not undergo glycol cleavage (Scheme S1). This observation supports the results from SEC measurements with the suspicion of incomplete degradation especially observed for the 400 kg/mol series (spectra 3c and 3d).

Calculation of block composition contrast Δ (Equation Set S5)

An effective Flory-Huggins Parameter for random block copolymers $\chi_{\text{eff,random-block}}$ based on isoprene and styrene was derived by Spontak.⁹ In Figure S1 (B) $F_{V,S}$ is visualized in dependence of the polymer volume fraction.

The inflection point of the taper was used to define the size of the blocks leading to polymer volume fraction of 50% for each block:

1st block (0-50%_{polymer volume}) 2nd block (50-100%_{polymer volume})

In this way the volume fraction of each block can be obtained by numerical integration of the different areas in S1(B):

$$f_1(\text{PI}) = 0.802 = \frac{V_1(\text{PI})}{V_1(\text{PI}) + V_1(\text{PS})}$$

$$f_2(\text{PI}) = 0.063 = \frac{V_2(\text{PI})}{V_2(\text{PI}) + V_2(\text{PS})}$$

$$f_1(\text{PS}) = 0.198 = \frac{V_1(\text{PS})}{V_1(\text{PI}) + V_1(\text{PS})}$$

$$f_2(\text{PS}) = 0.937 = \frac{V_2(\text{PS})}{V_2(\text{PI}) + V_2(\text{PS})}$$

The block composition contrast Δ is obtained by using the isoprene volume fractions:

$$\Delta = f_1(\text{PI}) - f_2(\text{PI}) = 0.739$$

Or the styrene volume fractions:

$$\Delta = f_2(\text{PS}) - f_1(\text{PS}) = 0.739$$

Leading to the effective Flory-Huggins Parameter χ_{eff} by using the temperature $T = 298.15$ K:

$$\chi_{\text{eff}} = \chi_{\text{AB}}(T) \cdot \Delta^2$$

TABLE S3 Overview of I/S tapered multiblock copolymer samples and reaction parameters employed.

entry	target M_n [kg/mol]	# of blocks	target M_n (AB-unit) [kg/mol]	$N_{AB}^{[a]}$	$\chi_{AB}N_{AB}^{[b]}$	$\chi_{eff,random}$	block $N_{AB}^{[c]}$	$[I]_0^{[d]}$ [mmol/L]	$[M]_0^{[d]}$ (total) [mol/L]	$[M]_0^{[d]}$ [%w]
1	80	2	80	928	143	78		1.77	1.65	18.1
2	80	4	40	464	71	39		1.94	1.80	19.9
3	80	6	27	309	48	26		2.01	1.86	20.5
4	80	8	20	232	36	19		2.04	1.90	20.9
5	80	10	16	186	29	16		2.06	1.92	21.1
6	240	2	240	2786	428	234		0.52	1.44	15.9
7	240	4	120	1393	214	117		0.56	1.56	17.2
8	240	6	80	929	143	78		0.58	1.60	17.7
9	240	8	60	697	107	59		0.58	1.63	17.9
10	240	10	48	557	86	47		0.59	1.64	18.1
11	400	2	400	4643	714	390		0.26	1.22	13.4
12	400	4	200	2322	357	195		0.28	1.30	14.4
13	400	6	133	1548	238	130		0.29	1.33	14.7
14	400	8	100	1161	178	197		0.29	m1.35	14.9
15	400	10	80	929	143	78		0.29	1.36	15.0

[a] Targeted values for N_{AB} are given in column 5 and were used for calculations. [b] $\chi_{AB}(T) = 71.4/T - 0.0857$ was used to determine the χ_{AB} Parameter at $T = 298.15$ K.¹⁰ [c] $\chi_{eff} = \chi_{AB}(T) \cdot \Delta^2$ with the block composition contrast $\Delta = f_2(PS) - f_1(PS) = 0.739$ with the volume fractions f of PS in block 1 and 2. [d] The volume of cyclohexane and the monomer volume of a single addition of the respective tapered multiblock copolymer was considered as solvent. Polymer which formed during the polymerization was not considered as diluting species.

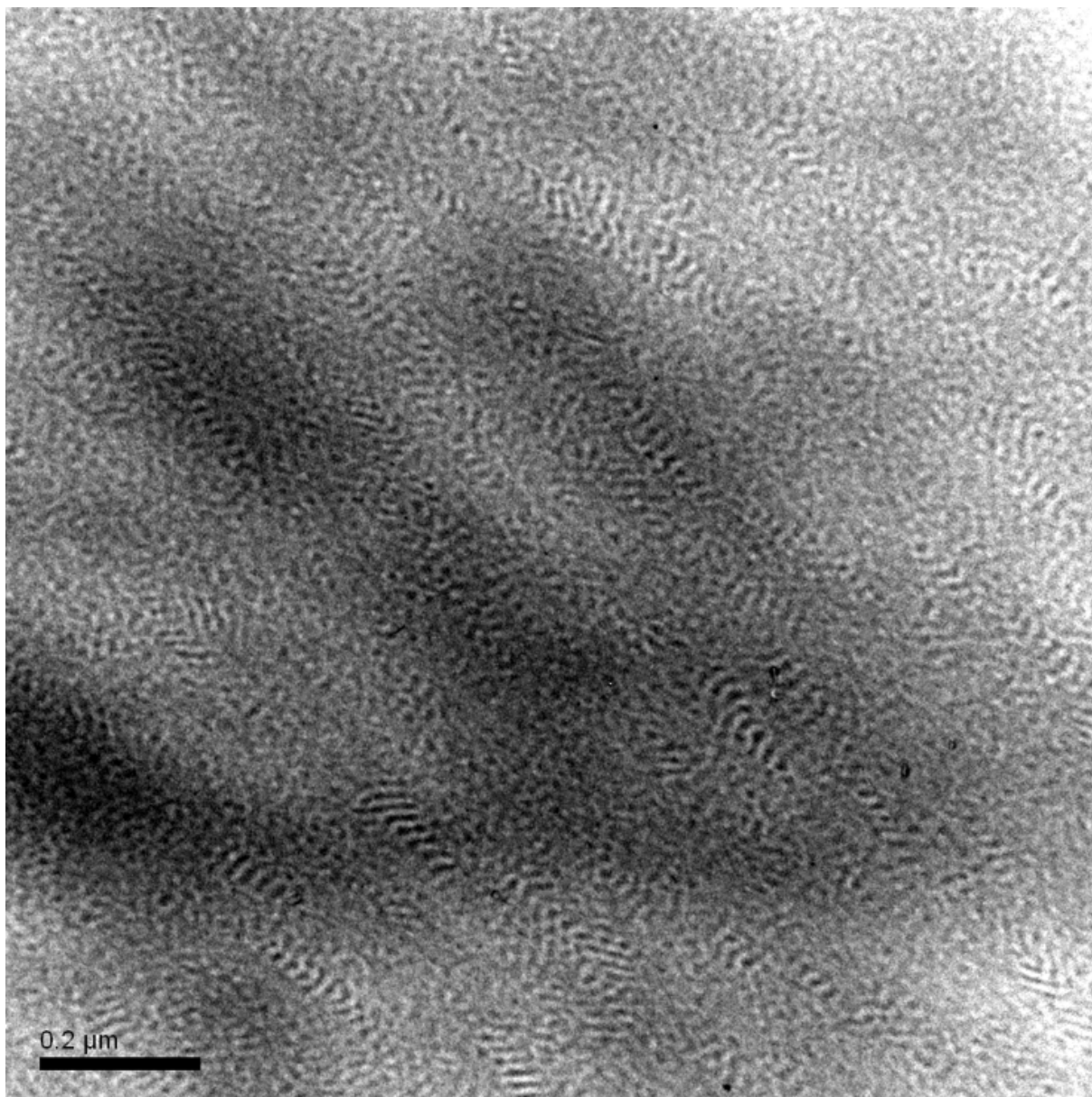
TEM Images

FIGURE S17 TEM image of 80 kg/mol P(I-co-S)₂ tapered tetrablock copolymer.

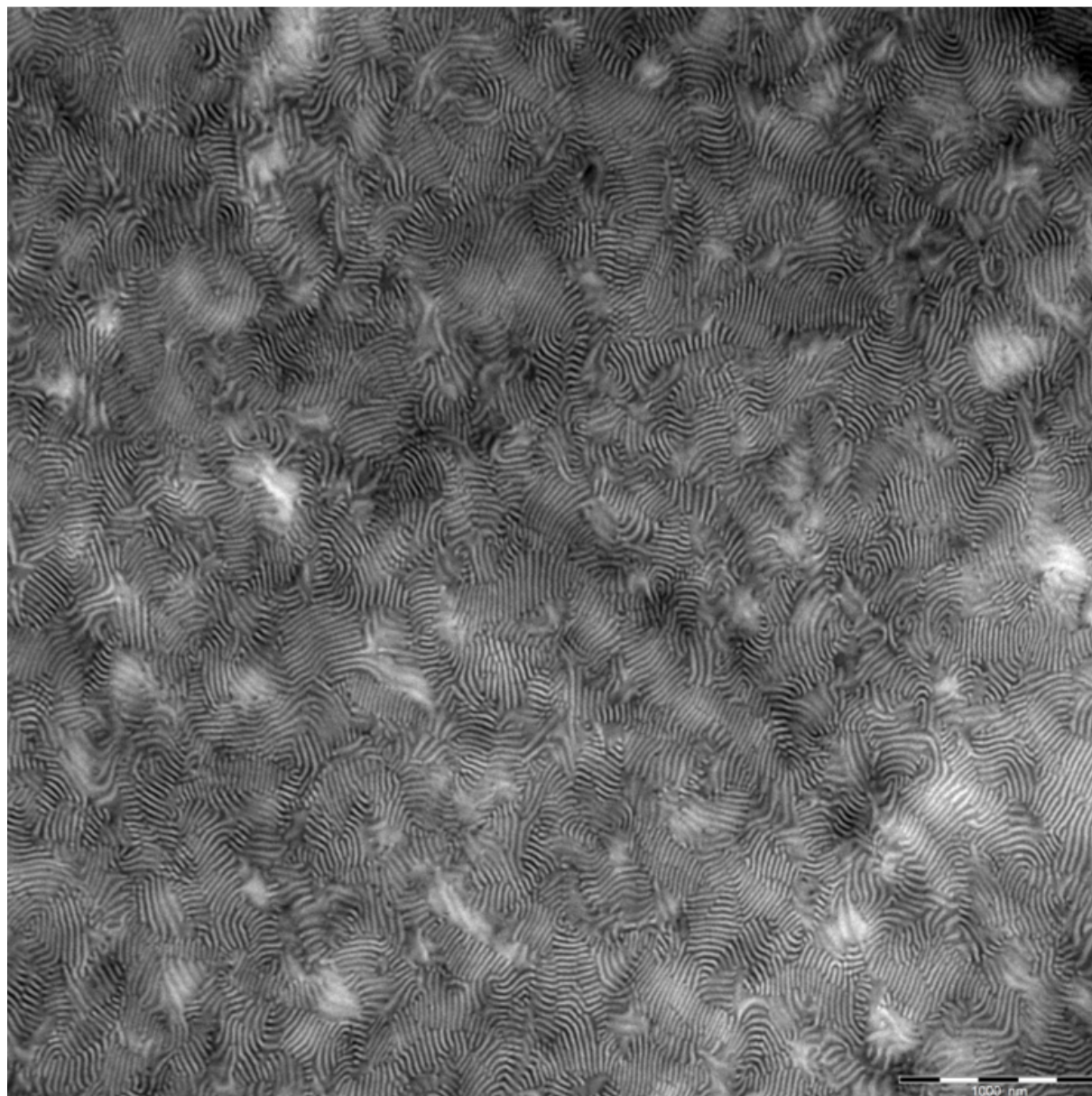


FIGURE S18 TEM image of 400 kg/mol P(I-co-S)₂ tapered tetrablock copolymer.

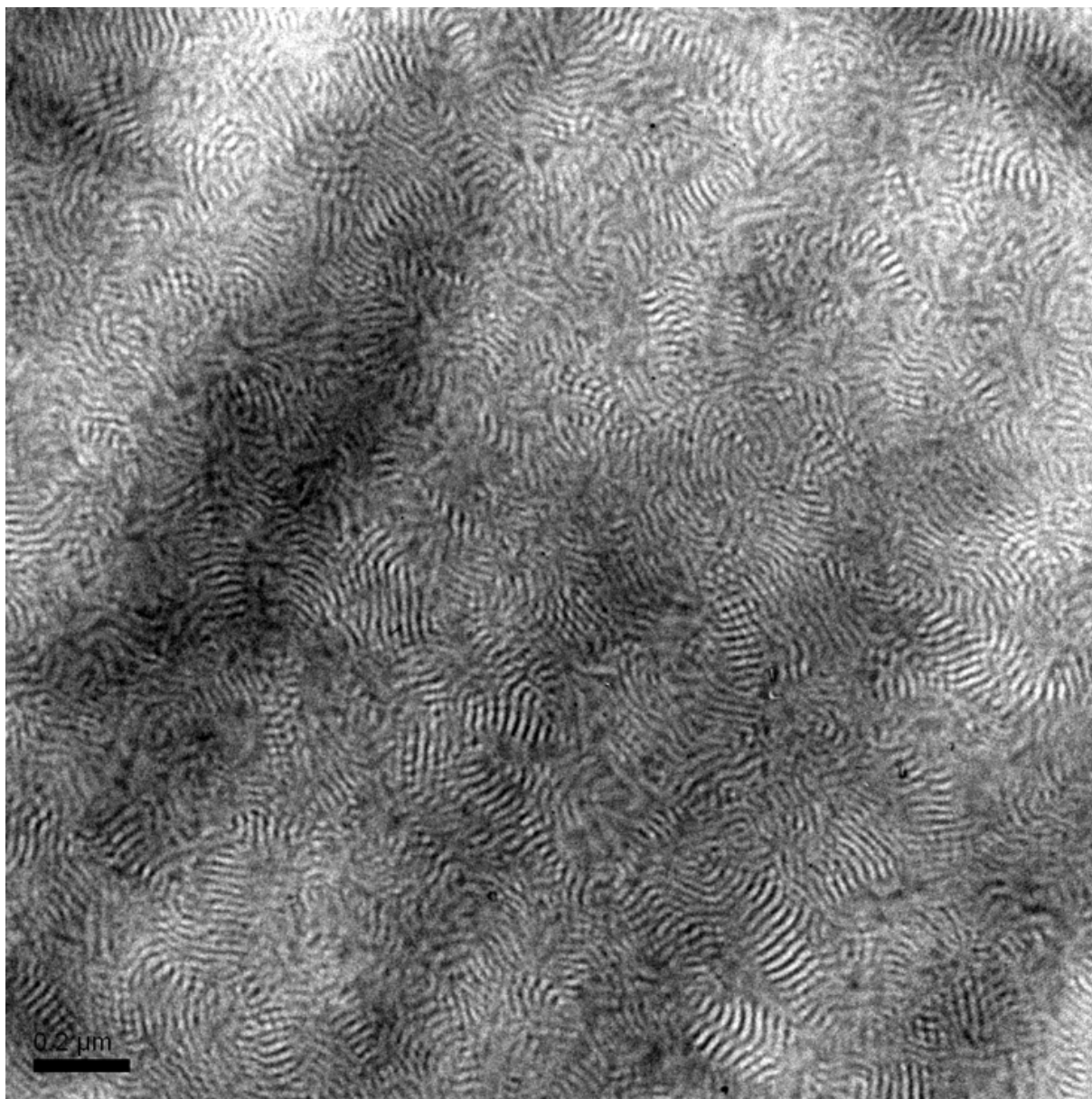


FIGURE S19 TEM image of 240 kg/mol P(I-co-S)₃ tapered hexablock copolymer.

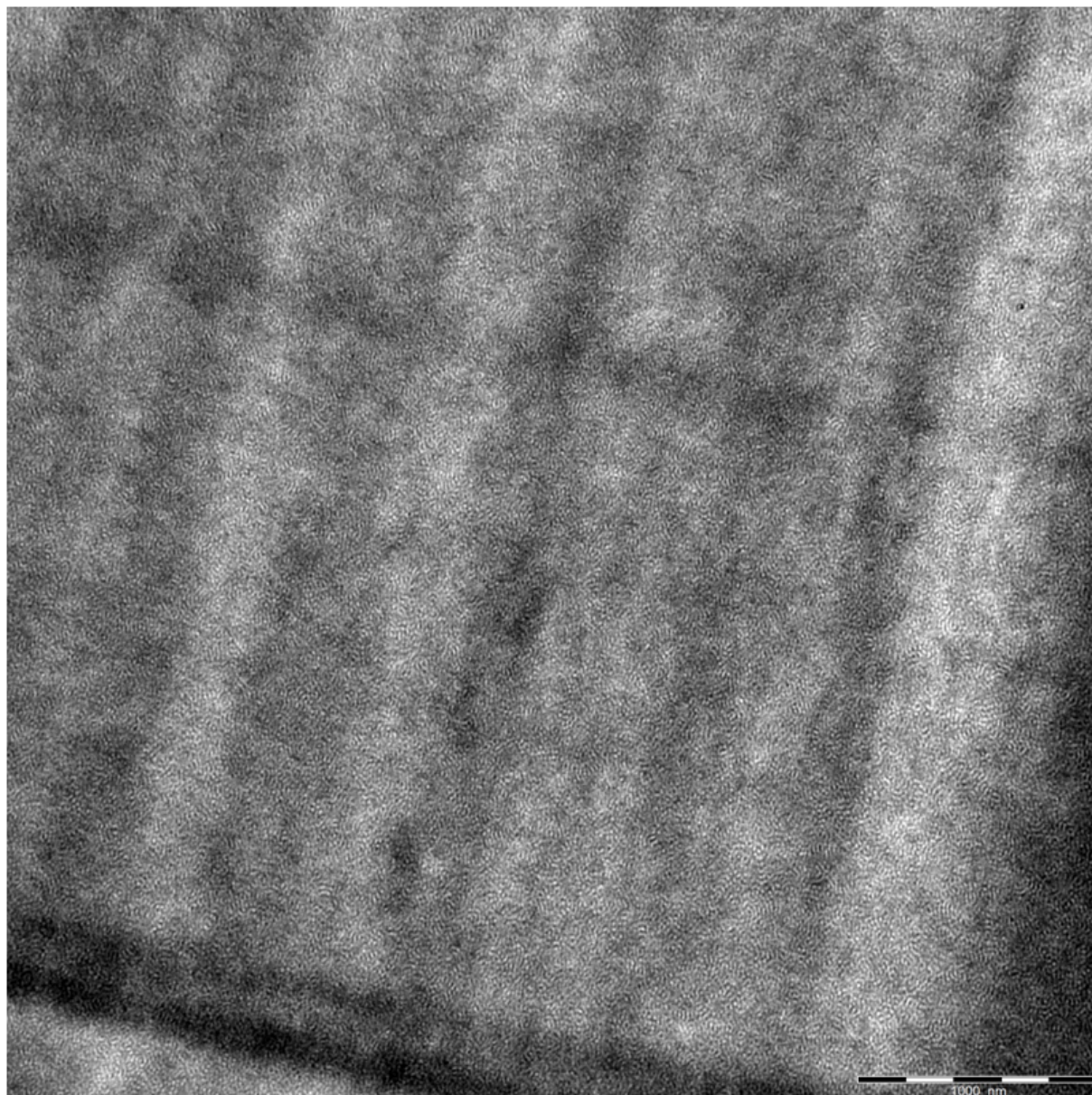


FIGURE S20 TEM image of 400 kg/mol P(I-co-S)₄ tapered octablock copolymer.

TABLE S4 Overview of domain width obtained by TEM and SAXS measurements.

Structure	$M_n(\text{total})/\text{ kg/mol}$	$d_{PI}(\text{TEM})/\text{ nm}$	$d_{PS}(\text{TEM})/\text{ nm}$	$d_{PS+PI}(\text{TEM})/\text{ nm}$
P(I-co-S) ₂	80	7.8 ± 1.3	8.0 ± 1.2	15.8
P(I-co-S) ₃	240	10.2 ± 1.4	12.0 ± 1.8	22.2
P(I-co-S) ₄	400	7.6 ± 1.4	9.3 ± 1.1	16.9
P(I-co-S) ₂	400	16.6 ± 2.5	18.8 ± 2.2	35.4

Temperature-dependent SAXS measurements

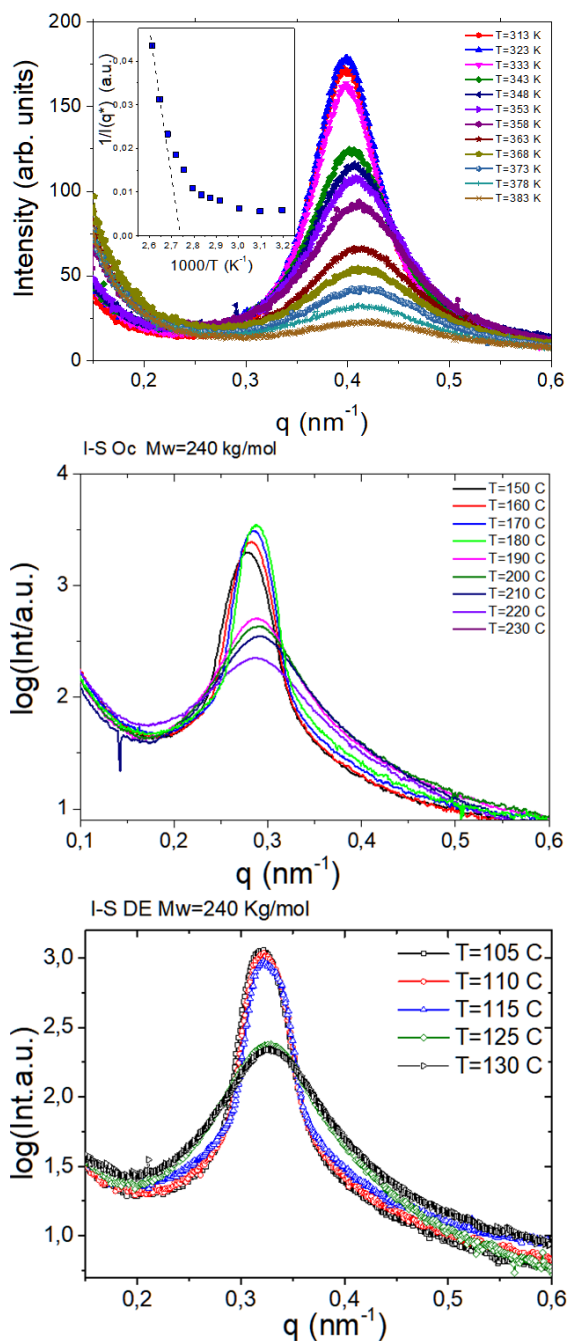


FIGURE S21 SAXS curves of different tapered multiblock copolymers: (top) tapered hexablock multiblock copolymer with a total molecular weight of 80 kg/mol plotted at different temperatures as indicated corresponding to the disordered state. (middle) tapered octablock copolymer with a total molecular weight of 240 kg/mol undergoing an order-to-disorder transition at 448 K. (bottom) tapered decablock copolymer with a total molecular weight of 240 kg/mol undergoing an order-to-disorder transition at 393 K.

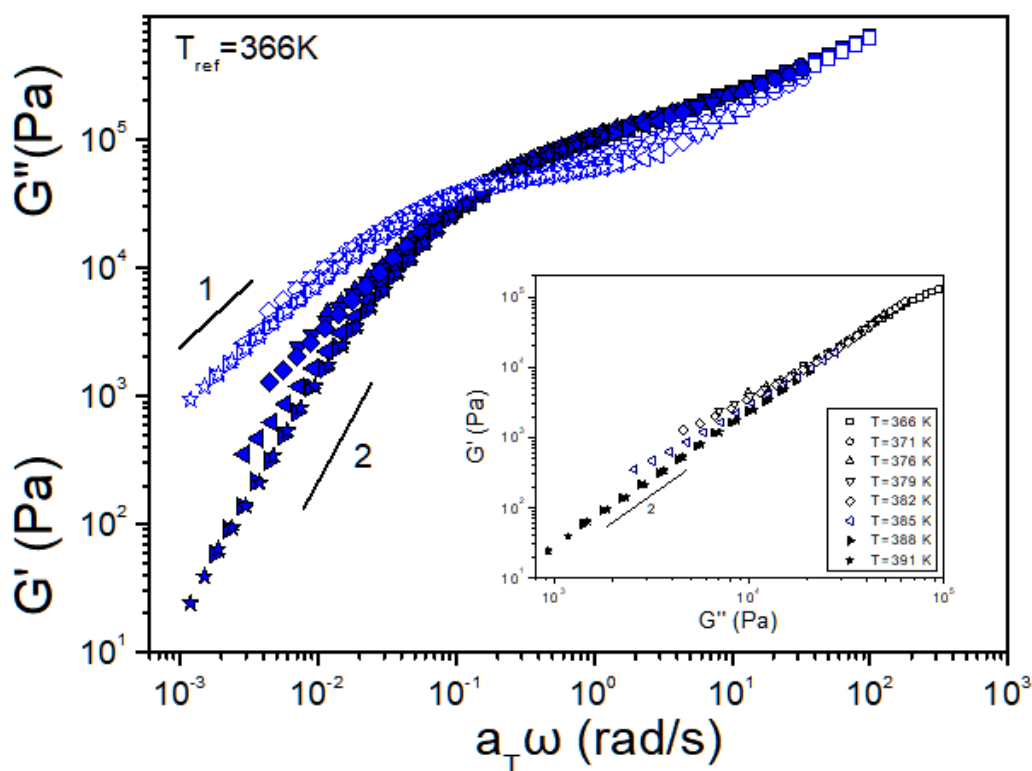


FIGURE S22 Reduced frequency plots for the storage (open symbols) and loss (filled symbols) moduli of a tapered tetrablock copolymer with $M_n = 80$ kg/mol. The strain amplitude in all cases was below 1.3%. Two lines with limiting slopes at low frequencies are shown (2 and 1 for the loss and storage moduli, respectively). The T_{ODT} is at 388 K. In the inset the same data are plotted in the G' vs G'' representation and result in an identical transition temperature.

An example of the influence of the order-to-disorder transition on the frequency dependencies of G' and G'' is shown in Figure S21. The "master curve" show the breakdown of time-temperature superposition (tT s) at low frequencies where the Newtonian behaviour of the disordered state is replaced by a "rubbery" state related to un-relaxed morphology. Strictly speaking, the use of tT s is not permitted in systems with a T -dependent internal structure such as in block copolymers. Another way of determining the ODT, which does not require the use of tT s, is by plotting the logarithm of the storage moduli as a function of the logarithm of the loss moduli for the different temperatures. In this representation, for symmetric copolymers the ODT corresponds to a temperature where the slope attains a value of 2. The application of this representation is also shown in Figure S21 for the same multiblock copolymer. This type of representation is certainly advantageous to the use of tT s in the vicinity of the order-to-disorder transition. It is interesting to note that the two representations (shifted vs unshifted data) provide identical results for the transition temperature.

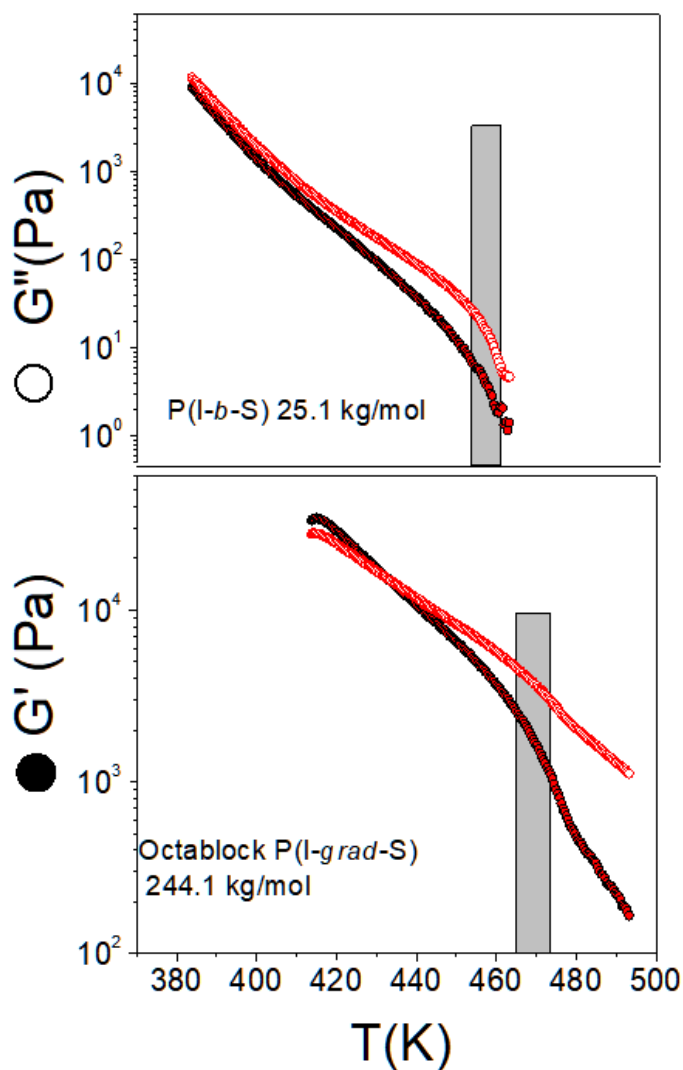


FIGURE S23 Storage (filled symbols) and loss (open symbols) shear moduli during heating with a rate of 2 K/min at a frequency of 1 rad/s for a pure diblock copolymer with a molecular weight of 25.2 kg/mol (top) and a tapered octablock copolymer with a total molecular weight of 244.1 kg/mol (bottom). The shaded areas indicate the order-to-disorder transition temperatures from rheology that are slightly different from SAXS. Notice the proximity of the T_{ODT} for the two copolymers.

Tensile Testing

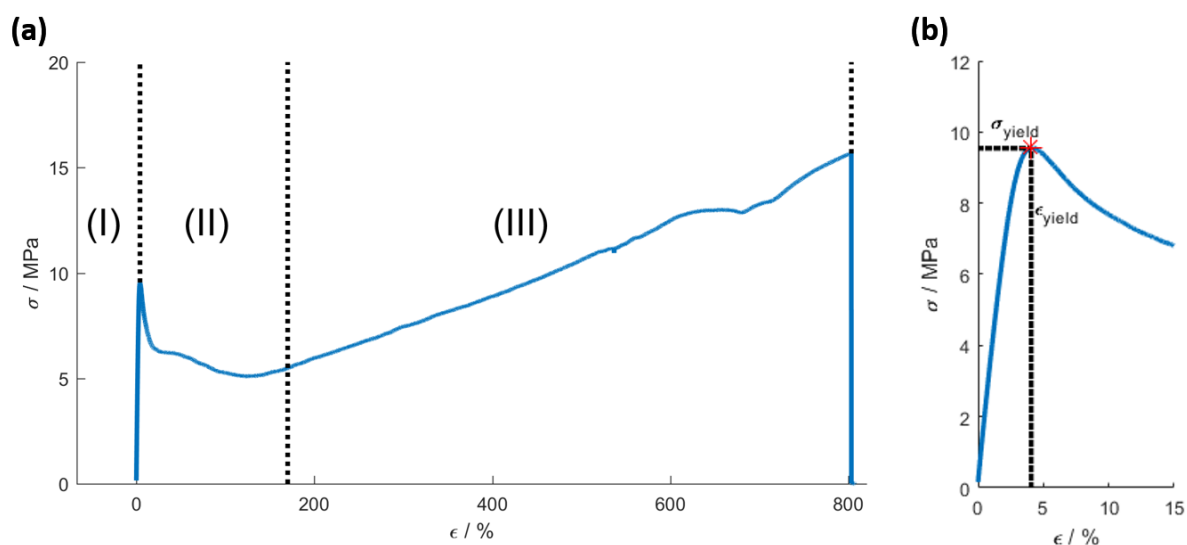


FIGURE S24 (a) Typical Stress-Strain diagram for a well separated P(I-co-S)_n tapered multiblock copolymer. Different regions can be distinguished: (I) elastic area, (II) yield point and necking area, (III) strain hardening area. (b) Enlarged area for $\varepsilon = 0$ -15%. The elastic area is represented by a linear increase of $\sigma(\varepsilon)$ followed by a significant drop usually located in the area around $\varepsilon \approx 5\%$. The yield point is defined as the maximum of $\sigma(\varepsilon)$.

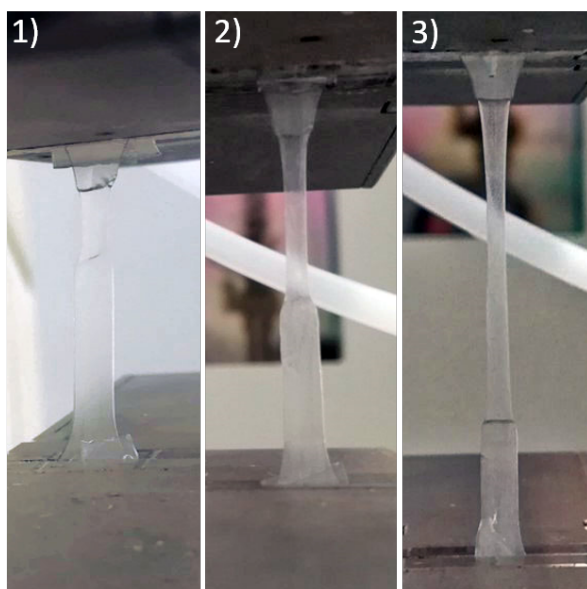


FIGURE S25 Uniaxial stretching of the polymer sample in the necking region (Figure S24, area II). The numbers 1), 2) and 3) indicate the growing of the neck by increasing strain.

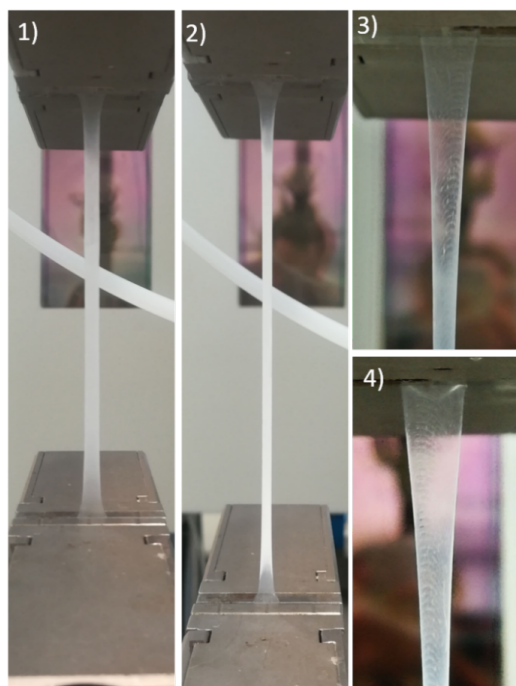


FIGURE S26 Uniaxial stretching of the polymer sample in the strain-hardening region (Figure S24, area III). The pictures 1) and 2) indicate whitening of the sample by increasing Strain. Cavitation is suspected as a familiar mode of failure in solid block copolymers.¹¹ The images 3) and 4) visualize a pattern which was observed by stretching the materials in the strain-hardening region.

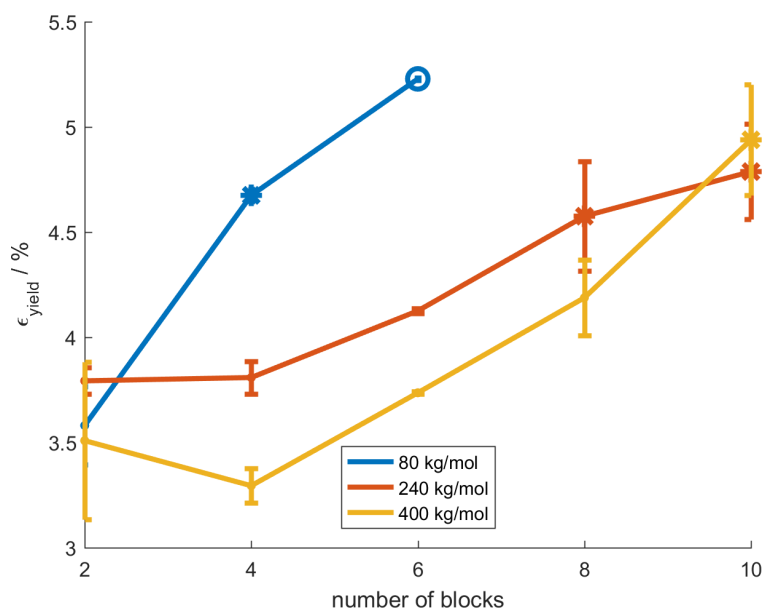


FIGURE S27 Yield Strain of the synthesized tapered multiblock copolymers samples in dependence of the number of blocks.

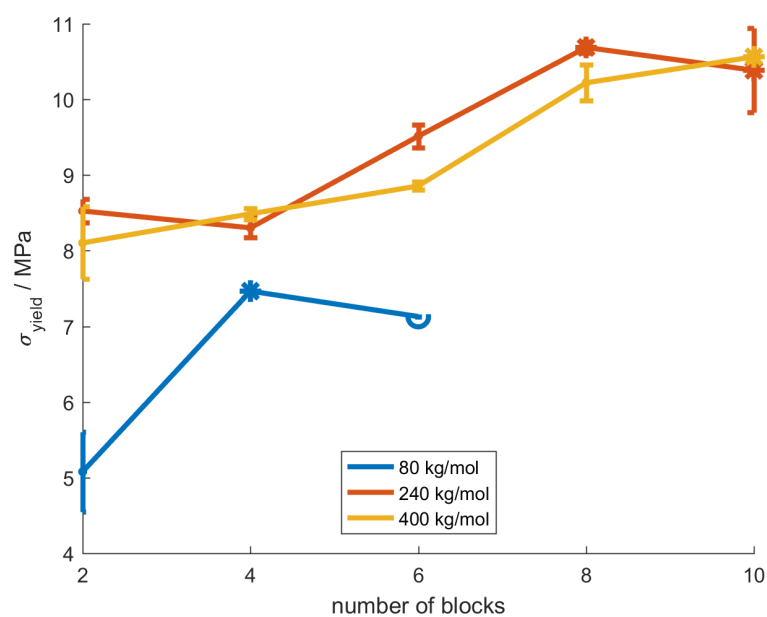


FIGURE S28 Yield Stress of the synthesized tapered multiblock copolymers samples in dependence of the number of blocks.

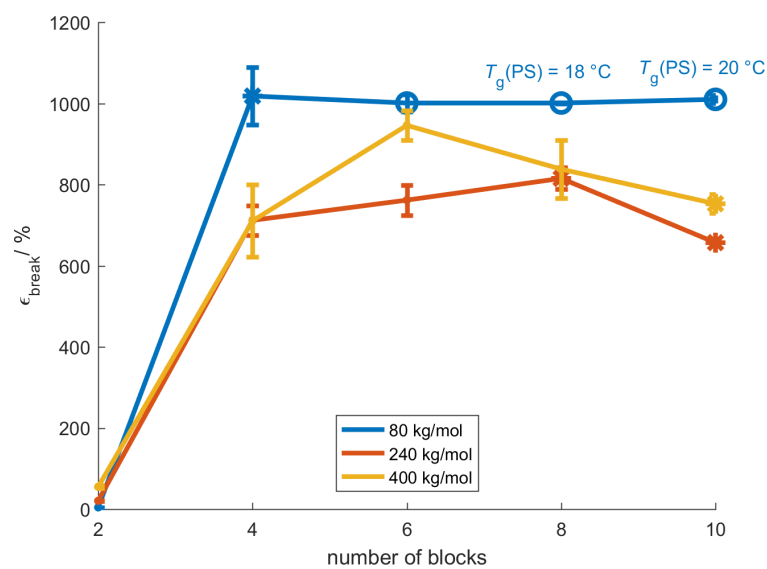


FIGURE S29 Strain at break of the synthesized tapered multiblock copolymers samples in dependence of the number of blocks.

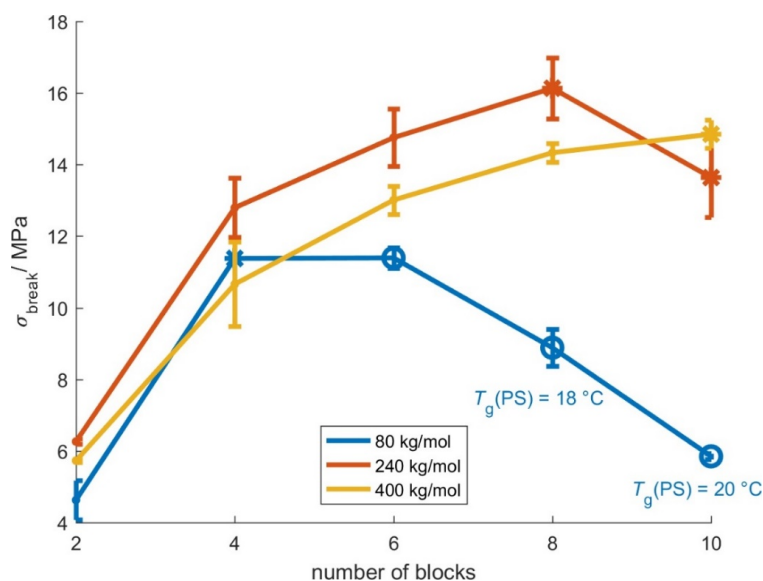


FIGURE S30 Stress at break of the synthesized tapered multiblock copolymers samples in dependence of the number of blocks.

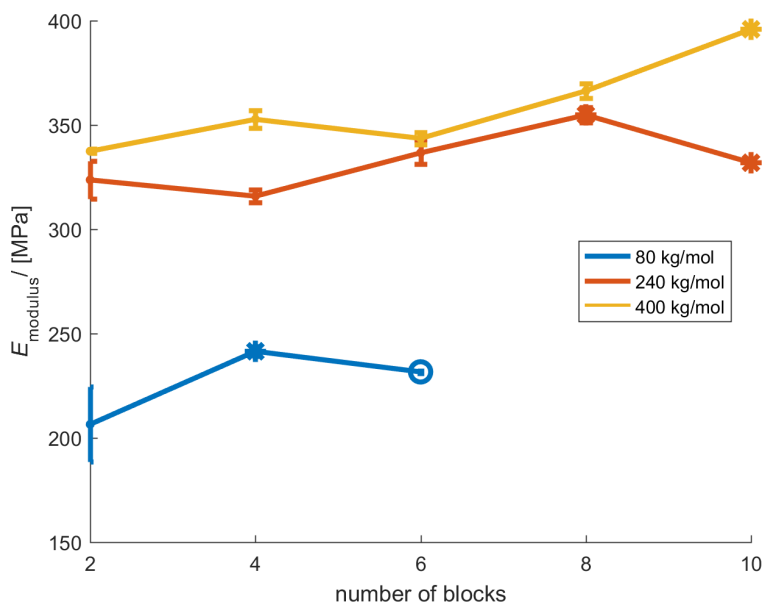


FIGURE S31 Elastic moduli of the synthesized tapered multiblock copolymers samples in dependence of the number of blocks. The 80 kg/mol octa- and decablock copolymers do not exhibit separate elastic and viscous regions. This can be attributed to the disordered morphology and the concomitant reduction in the polystyrene T_g . Elastic moduli are generally higher than reported for linear multiblock copolymers prepared by the sequential method.¹² Presumably this can be explained by the higher content of styrene in the low T_g nanodomains attributed to the incorporation of styrene in the polyisoprene of the tapered P(I-co-S) tapered block structure (Figure S1).

TABLE S5 Overview of yield and break points obtained by tensile tests. Additionally, elastic moduli are included.

entry	target M_n [kg/mol]	# of blocks	ϵ_{yield} [%]	σ_{yield} [MPa]	ϵ_{break} [%]	σ_{break} [MPa]	E_{modulus} [MPa]
1	80	2	3.58	5.08	4.5	4.62	207
2	80	4	4.68	7.47	1018	11.4	242
3	80	6	5.23	7.13	1001	11.4	232
4	80	8	n.d.	n.d.	1001	8.88	n.d.
5	80	10	n.d.	n.d.	1010	5.85	n.d.
6	240	2	3.79	8.53	20.7	6.26	324
7	240	4	3.80	8.30	712	12.8	316
8	240	6	4.12	9.51	762	14.8	337
9	240	8	4.57	10.69	815	16.1	355
10	240	10	4.79	10.39	656	13.6	332
11	400	2	3.79	8.10	20.6	6.26	337
12	400	4	3.81	8.49	712	12.8	353
13	400	6	4.13	8.86	762	14.8	344
14	400	8	4.58	10.2	815	16.1	366
15	400	10	4.79	10.6	657	13.6	396

References

- (1) Meyer, V. E.; Lowry, G. G. *J. Polym. Sci. A: Gen. Pap.* **1965**, 3 (8), 2843–2851. DOI: 10.1002/pol.1965.100030811.
- (2) Mayo, F. R.; Lewis, F. M. *J. Am. Chem. Soc.* **1944**, 66 (9), 1594–1601. DOI: 10.1021/ja01237a052.
- (3) Gillespie, D. T. *J. Comput. Phys.* **1976**, 22 (4), 403–434. DOI: 10.1016/0021-9991(76)90041-3.
- (4) Gillespie, D. T. *J. Phys. Chem.* **1977**, 81 (25), 2340–2361. DOI: 10.1021/j100540a008.
- (5) Corbin, N.; Prud'homme, J. J. *J. Polym. Sci. Polym. Chem. Ed.* **1976**, 14 (7), 1645–1659. DOI: 10.1002/pol.1976.170140708.
- (6) Rozentsvet, V. A.; Khachaturov, A. S.; Ivanova, V. P. *Polym. Sci. Ser. A* **2009**, 51 (8), 870–876. DOI: 10.1134/S0965545X09080045.
- (7) Tanaka, Y.; Takeuchi, Y.; Kobayashi, M.; Tadokoro, H. *J. Polym. Sci. B* **1971**, 9 (1), 43–57. DOI: 10.1002/pol.1971.160090104.
- (8) Fulmer, G. R.; Miller, A. J. M.; Sherden, N. H.; Gottlieb, H. E.; Nudelman, A.; Stoltz, B. M.; Bercaw, J. E.; Goldberg, K. I. *Organometallics* **2010**, 29 (9), 2176–2179. DOI: 10.1021/om100106e.
- (9) Ashraf, A. R.; Ryan, J. J.; Satkowski, M. M.; Lee, B.; Smith, S. D.; Spontak, R. J. *Macromol. Rapid Commun.* **2017**, 38 (17). DOI: 10.1002/marc.201700207.
- (10) Khandpur, A. K.; Förster, S.; Bates, F. S.; Hamley, I. W.; Ryan, A. J.; Bras, W.; Almdal, K.; Mortensen, K. *Macromolecules* **1995**, 28 (26), 8796–8806. DOI: 10.1021/ma00130a012.
- (11) Hermel, T. J.; Hahn, S. F.; Chaffin, K. A.; Gerberich, W. W.; Bates, F. S. *Macromolecules* **2003**, 36 (7), 2190–2193. DOI: 10.1021/ma021754w.
- (12) Smith, S. D.; Spontak, R. J.; Satkowski, M. M.; Ashraf, A.; Heape, A. K.; Lin, J. S. *Polymer* **1994**, 35 (21), 4527–4536. DOI: 10.1016/0032-3861(94)90798-6.

CHAPTER 3

TAPERED MULTIBLOCK COPOLYMER BLENDS

CHAPTER 3

To be Submitted

Building Bridges by Blending: The Mechanical Properties of Binary Tapered Diblock/Multiblock Copolymer Blends

Marvin Steube^a, Martina Plank^b, Markus Gallei^c, Holger Frey^{a,*} and George Floudas^{d,e*}

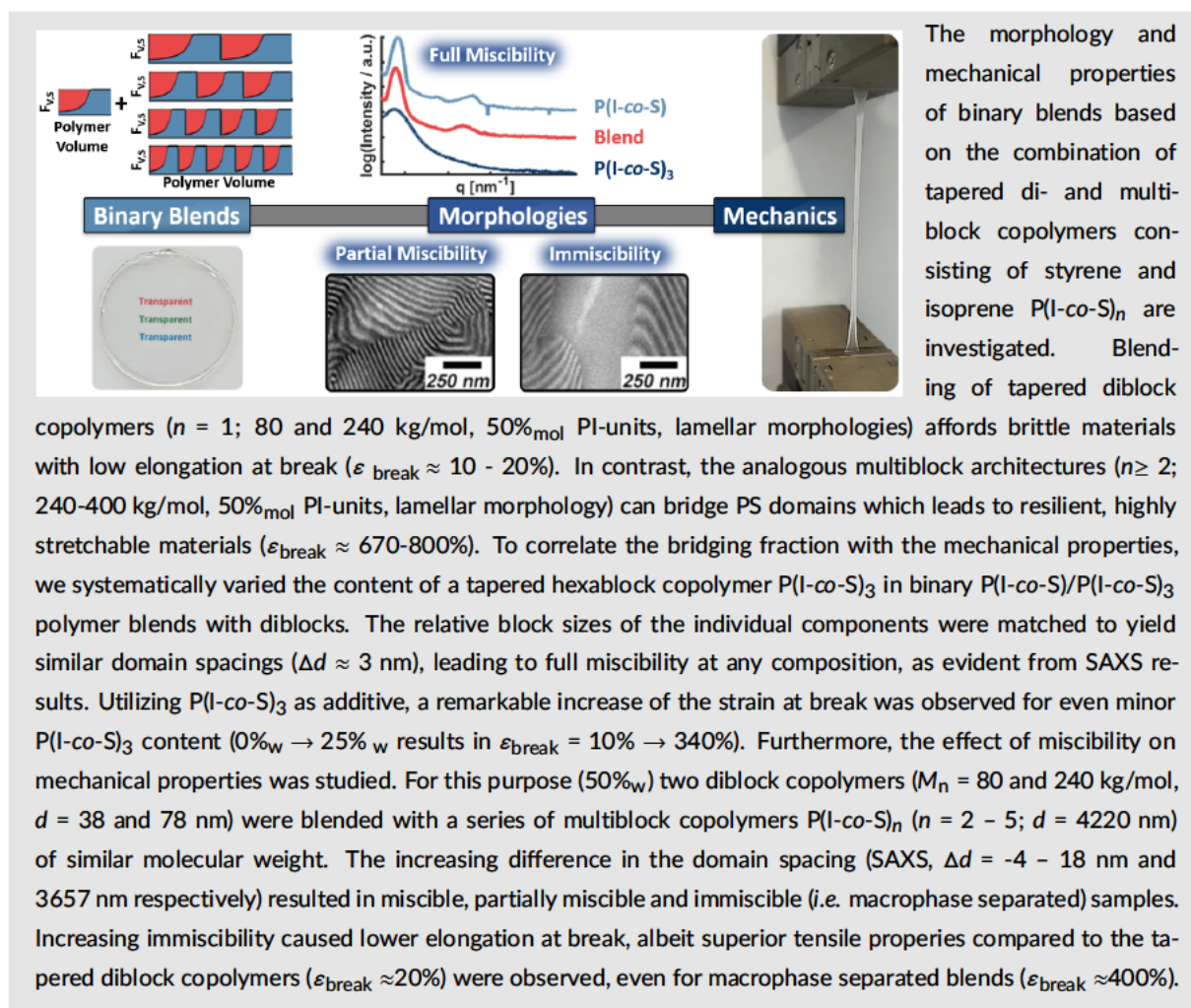
^aDepartment of Chemistry, Johannes Gutenberg Universität Mainz, 55099 Mainz, Germany

^bMacromolecular Chemistry Department, Technische Universität Darmstadt, Alarich-Weiss Str. 4, 64287 Darmstadt, Germany

^cChair in Polymer Chemistry, Saarland University, 66123 Saarbrücken, Germany

^dDepartment of Physics, University of Ioannina, P.O. Box 1186, 451 10 Ioannina, Greece

^eMax Planck Institute for Polymer Research, 55128 Mainz, Germany



The study shows that the addition of a minor fraction of multiblock copolymers to diblock structures can be employed to improve mechanical properties due to domain bridging.

INTRODUCTION

Block copolymers can self-assemble into a variety of micro- or nanophase separated morphologies.^{1,2} Based on this phase behavior, a vast variety of applications ranging from nanolithographic processes to photonics, nanomedicine and nanoreactors were explored over the last decades.³⁻⁹ A concept which has been in the focus of industrial¹⁰⁻¹² as well as academic interest^{1,13,14} for more than 50 years,^{12,14,15} is the use of thermoplastic elastomers (TPEs) as melt processable, elastic materials.^{10,16} The most commonly used TPE architectures combine glassy, *i.e.* high glass-transition temperature (T_g) blocks with rubbery, low T_g blocks. In this case, the phase-separated, vitrified domains act as thermoreversible crosslinks as well as a reinforcing filler material in the rubbery matrix.¹⁷ This thermoreversible crosslinking via high T_g blocks permits melt processing and also possesses potential for future recycling concepts.

Both step-growth¹⁸⁻²⁰ and chain-growth polymerization²¹⁻²⁵ techniques as well as their combinations²⁶⁻²⁸ are used to generate TPEs with a broad range of different monomer combinations and polymer architectures.^{20,29} The living carbanionic polymerization of styrene with 1,3-dienes is known to be a versatile tool for the synthesis of controlled monomer sequences, high molecular weights and narrow dispersity.^{30,31} For example, ABA triblock copolymers based on either polybutadiene (PB) or polyisoprene (PI) with polystyrene (PS) are probably the best investigated ABA-type block copolymer systems (A = PS; B = PB or PI).³²⁻³⁴ A variety of different parameters as the (i) the chosen monomer combination,²⁹ (ii) block sizes,^{34,35} (iii) block ratios,^{36,37} (iv) the tapering,³⁶⁻³⁹ and (v) block sequences^{33,34,40-44} were systematically explored, leading to a fundamental understanding of morphological state and the affiliated thermal and mechanical properties.^{45,46} For the statistical copolymerization of dienes and styrene *in situ* spectroscopy is the method of choice to track monomer conversion and to determine underlying rate constants, which directly reflect the monomer gradient in the chains formed.⁴⁷⁻⁵¹ These kinetic rate constants were also used in kinetic Monte Carlo simulations (*i.e. in silico* polymerization), which provides a further understanding by the access of the monomer-by-monomer sequence of individual chains.^{38,42,50,52,53} To further adjust or expand morphological and mechanical characteristics of well-understood polymer architectures, block copolymer blending represents an efficient and straightforward approach.⁵⁴

The miscibility of polymers can be described by the Flory Huggins theory, derived in 1942 and originally developed to describe polymers in solution.⁵⁵⁻⁶¹ Considering the solvent as another polymer instead of a low-molecular weight compound, leads to a slightly modified form, which is used to describe the miscibility of two polymers, *e.g.* homopolymer blends (Equation 1).⁶²

$$\frac{\Delta G_m}{k_B T} = \underbrace{\frac{f_1 \ln(f_1)}{v_2 N_1} + \frac{f_2 \ln(f_2)}{v_2 N_2}}_{\text{Entropic Contribution}} + \underbrace{\chi_{1,2} \cdot \frac{f_1 f_2}{v_{1,2}}}_{\text{Enthalpic Contribution}} \quad (1)$$

The importance of the degree of polymerization (N) and the Flory-Huggins interaction parameter (χ) are obvious, as they determine the molar free energy of mixing ΔG_m for a constant volume fraction (f) and temperature (T) (k_B = Boltzmann constant; v = arbitrary reference volume of the respective repeating unit). The product of both parameters $\chi_{1,2} \cdot N$ ($N = N_1 + N_2$) is used to quantify the interplay of enthalpy ($\chi_{1,2}$) and entropy (N) and commonly used to predict the demixing in AB homopolymer blends ($\chi \cdot N > 4$ for $f = 0.5$) and block copolymers ($\chi \cdot N > 10.5$ for $f = 0.5$).^{63,64} In the latter, the covalently linked AB diblock architecture leads to a constraint proximity, resulting in microphase separated morphologies with the block transition anchored to the domain boundary.⁴⁵

Binary diblock copolymer blends (AB+A'B') show miscibility depending on their molecular weight ratio. Both components are physically anchored to the domain boundary.^{65,66} Hence, macrophase separation leads to the coexistence of microphase separated areas with different microdomain morphologies, spacings or phase states. In fundamental experimental studies, the miscibility of binary PI-*b*-PS block copolymer blends with different lamellar spacings was shown by Hashimoto *et al.*^{67,68} Complete miscibility was found for block molecular weight ratios up to 1:5.⁶⁷ These results were later confirmed by experimental results of Spontak⁶⁹ and predictions of Matsen using the selfconsistent field theory (SCFT) for block copolymers.⁷⁰

To obtain tough and stretchable elastic materials, triblock copolymer architectures (Figure 1) consisting of a SIS or SBS block sequence, where I, B and S denote a PI, PB and PS block, respectively are highly established.¹ The vitrified high- T_g end blocks pin the rubbery midblock at different domain boundaries (bridging conformation), which leads to mechanical stabilization beyond entanglements. The rheology of triblock copolymer containing blends (A+ABA; B+ABA; AB+ABA) has been investigated in numerous works. In 1971 Morton *et al.* investigated the effect of synthetic imperfections (preliminary termination during anionic polymerization) onto resulting mechanical properties.¹⁷ For this purpose, low contents of PS and PS-*b*-PI were blended with an SIS triblock copolymer. This pioneering work revealed profound effects on the tensile strength for even minor amounts of the diblock copolymer. One year later, Cohen and Tschoegel established SI/SIS blends as a suitable model system to control the amount and length distribution of termi-

nal, dangling PI chains a in rubbery network.^{71,72} Until today, the combination of morphological investigation⁷³⁻⁷⁷ with theoretical predictions^{77,78} has proven to be a powerful tool to explain the rheological features,^{17,71,72,75-77,79,80} also in terms of looping and bridging fractions.^{76,77}

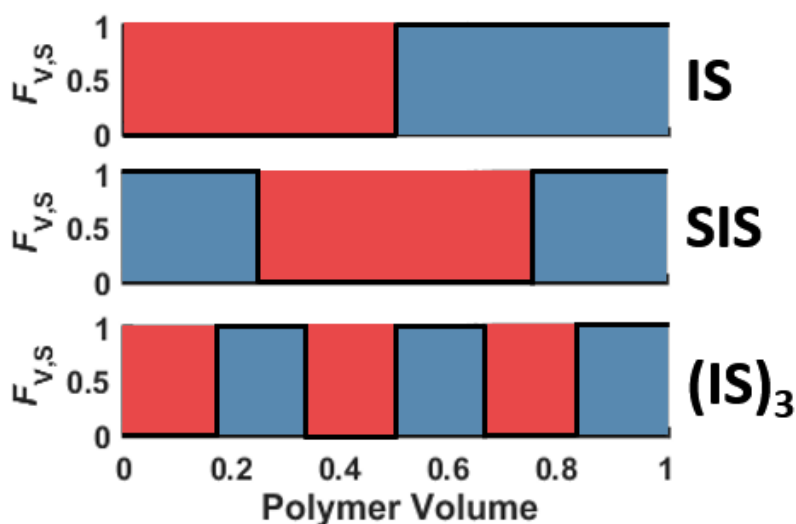


FIGURE 1 Tapered monomer sequences are illustrated as chain model (red sphere: PI- repeating unit; blue sphere: PS- repeating. $F_{V,S}$: instantaneous styrene volume incorporation.

Multiblock copolymers received considerable attention in the last 30 years.^{29,40,81,82} Their repetitive block sequences enables bridging of two or more domains by a single polymer chain. Since the glassy domains serve as physical crosslinks, superior elastic moduli and increased stretchability were observed for such TPEs in several works.^{40,83-85} Morphologies were investigated by Spontak by mixing $(SI)_n$ tetra, hexa- and octablock copolymers (*i.e.* $(PS-b-PI)_n$ with $n = 2 - 4$) with PS⁸⁶ and a tetrablock copolymer $(SI)_2$ with PI.⁸⁷ Different stability for bicontinuous morphologies was found, governed by the number of blocks (*i.e.* $2n$). Blending experiments of an IS diblock copolymer with an $(IS)_4$ octablock copolymer revealed macrophase separation already for a AB block molecular weight ratio of 4:1.⁸⁸ In contrast, binary mixtures of AB diblock copolymers were found to be miscible at even higher ratios (5:1).^{67,69,70} Spontak ascribed the increased immiscibility of the $AB/(AB)_n$ blends to midblock conformations caused by the multiblock architecture. Bates *et al.* effectively presented the toughening of a fully hydrogenated SIS triblock copolymer by addition of $\approx 15\%_w$ of an fully hydrogenated SIS pentablock copolymer.⁸⁵

In contrast to block copolymers, gradient copolymers show a comparably smooth block transition leading to an increased miscibility ($\chi_{eff} < \chi_{1,2}$).⁸⁹ The control of χ_{eff} by the comonomer sequence is an interesting option to decouple the phase segregation strength ($\chi_{eff} \cdot N$) from the molecular weight ($M_n \sim N$).³⁶ Although the alkylolithium initiated copolymerization of styrene

and isoprene in hydrocarbon solvents is known to lead to tapered block copolymers in a single step, their use for TPEs has been hardly investigated.^{12,90} As shown in our previous work, the consecutive multi-step copolymerization affords phase-separated tapered multiblock copolymers $P(I-co-S)_n$ with less synthetic effort, compared to their sequential block analogues $((IS)_n = (PI-b-PS)_n)$.⁴² Their comparably smooth block transition (*i.e.* $\chi_{\text{eff}} < \chi_{SI}$) lowers the order-disorder transitions (T_{ODT}) in comparison to "non-tapered" block copolymers of the same composition. Consequently, the T_{ODT} is located in a range typically used for high-speed processing of the polymer melt (e.g. $T_{\text{ODT}} \approx 185$ °C for $P(I-co-S)_3$ with $M_{n,\text{total}} \approx 240$ kg/mol). The industrial relevance of these structures and their miscible blends was shown by Knoll *et. al.* who investigated binary homo- and triblock copolymer blends with tapered multiblock star copolymer architectures (e.g. trademark Styrolux).^{10,91,92}

In contrast to tapered diblock copolymers, the corresponding multiblock architectures are known as tough and stretchable materials. In this work, we correlate the morphology and mechanical properties with the composition of binary tapered diblock/multiblock copolymer blends based on polystyrene and polyisoprene (*i.e.* $P(I-co-S) / P(I-co-S)_n$ blends with $n = 2-5$). The mechanical properties of these $P(I-co-S) / P(I-co-S)_n$ blends are expected to be highly dependent on the $P(I-co-S)_n$ content, as the latter governs bridging by glassy PS domains. Morphologies and mechanical properties were investigated for a similar tapered diblock/multiblock copolymer blend (Scheme 1 left part) by systematically increasing the content of $P(I-co-S)_n$ in a series of blends. In the second part of the work, the miscibility of tapered diblock/multiblock copolymer blends was systematically varied using differences in the block sizes of both components (Scheme 1 right part). The consequences of (im)miscibility were determined by following the change in morphology (SAXS, TEM) and mechanical characteristics. The key question of this work is, how the mechanical properties of tapered diblock copolymers can be improved by introducing a controlled amount of domain bridges by blending.

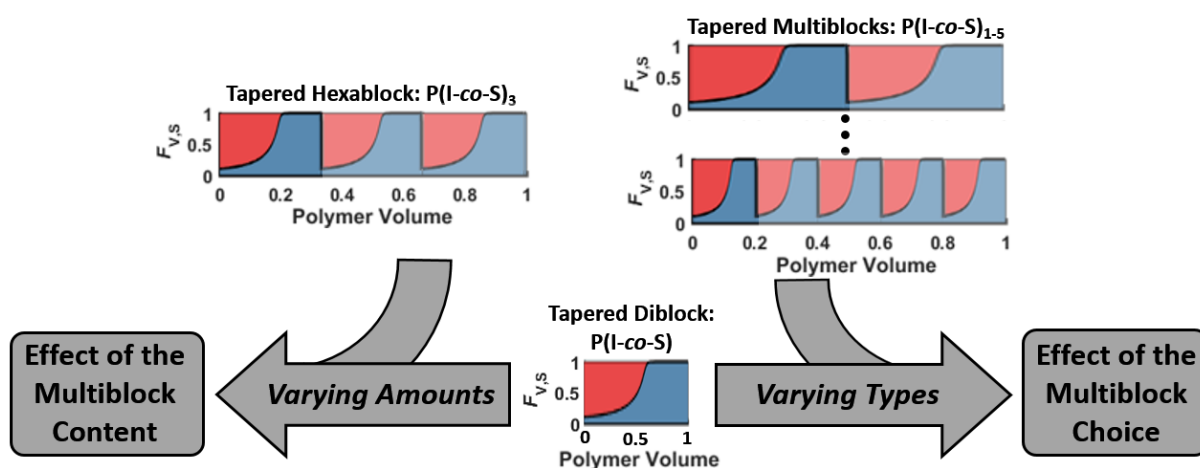
RESULTS AND DISCUSSION

TPEs based on (tapered) multiblock copolymers architectures effectively bridge glassy polystyrene domains in the phase separated bulk state. This enables mechanical properties exceeding those of the corresponding diblocks by far. The combination of both block copolymers in a polymer blend, is a straightforward approach to produce a TPE material, where the mechanical properties are suspected to be controlled by the multiblock content as well as the diblock/multiblock miscibility.

In the first part of this work, we quantify this "multiblock toughening effect", aiming at full misci-

bility of a tapered diblock block copolymer P(I-co-S) with a tapered hexablock copolymer P(I-co-S)₃. For this purpose, a series of polymer blends was prepared by solution blending, only differing in the P(I-co-S)₃ (Scheme 1) content. In the second part of this work we investigate the feasibility of P(I-co-S) / P(I-co-S)_n ($n = 2-5$) blends to form miscible microphase separated bulk structures for increasing differences in their domain spacings ($\Delta d \approx -4$ to 57 nm). The consequences for the mechanical properties were studied via tensile testing.

SCHEME 1 Overview of the blending concepts applied in this work. Left side: The P(I-co-S)₃ fraction was varied in a series of P(I-co-S)/P(I-co-S)₃ blends with similar d ($\Delta d \approx 3$ nm). Right side: The multiblock P(I-co-S)_n was varied ($n = 2-5$) in two series of P(I-co-S)/P(I-co-S)_n blends. Following this principle, differences in domain sizes from $\Delta d = -4$ to 57 nm are covered for a constant P(I-co-S)_n fraction (50%_w).



A. Effect of the Tapered Multiblock Copolymer Content: AB/(AB)₃ Blends

In this part of the work we systematically investigate the effect of the P(I-co-S)_n content in P(I-co-S) / P(I-co-S)_n blends. For this purpose, a series of blends was prepared consisting of the similar segregated tapered block copolymers P(I-co-S)_n ($n = 1$ and 3), differing in their P(I-co-S)₃ content (Table 1, Entry 1). To avoid macrophase separation (i.e. immiscibility), tapered block copolymers with similar domain sizes ($\Delta d = 3$ nm) were selected according to the domain sizes determined by SAXS in a previous work.⁴² The consequences of varying the multiblock copolymer content were studied in terms of morphology (SAXS, TEM) and mechanical characteristics (tensile tests).

TABLE 1 Molecular characteristics of the tapered block copolymers P(I-co-S)_n (n = 1-5) used for blending experiments. Each of the entries (1, 2 and 3) represents a series of blends.

Entry	M_n , target ^{a)} [kg/mol]	M_n (SEC) ^{a,c)} [kg/mol]	Blend Composition	M_n (th.) ^{b)} [kg/mol]	M_n (SEC) ^{b,c)} [kg/mol]	Changed Parameter
1	80	92	P(I-co-S) / P(I-co-S) ₃	400	512	P(I-co-S) _n Content: 0 - 100% _w in 11 steps
2.1	80	92	P(I-co-S) / P(I-co-S) ₂	240	265	Miscibility: $\Delta d = -4 - 18$ nm
2.2	80	92	P(I-co-S) / P(I-co-S) ₃	240	268	
2.3	80	92	P(I-co-S) / P(I-co-S) ₄	240	244	
2.4	80	92	P(I-co-S) / P(I-co-S) ₅	240	248	
3.1	240	253	P(I-co-S) / P(I-co-S) ₂	240	265	Miscibility: $\Delta d = 36 - 57$ nm
3.2	240	253	P(I-co-S) / P(I-co-S) ₃	240	268	
3.3	240	253	P(I-co-S) / P(I-co-S) ₄	240	244	
3.4	240	253	P(I-co-S) / P(I-co-S) ₅	240	248	

Molecular characteristics of a) P(I-co-S) and b) P(I-co-S)_n with $n = 2-5$. c) Values are based on PS standards. Eluograms are given in a previous work.⁴²

Morphologies

To investigate the nanodomain morphology in real-space, samples were OsO₄ stained and studied via transmission electron microscopy (TEM). The images (Figures 2 and S1) show the expected⁴² lamellar morphologies with a longrange order decreasing with the P(I-co-S)₃ content. The latter is evident from decreasing grain sizes (*i.e.* area of lamellae aligned in a similar direction with long range order). However, binary blends (30 and 60%_w P(I-co-S)₃ content) show a uniform LAM domain spacing, representing the excellent miscibility of P(I-co-S) and P(I-co-S)₃ for similar domain spacings.

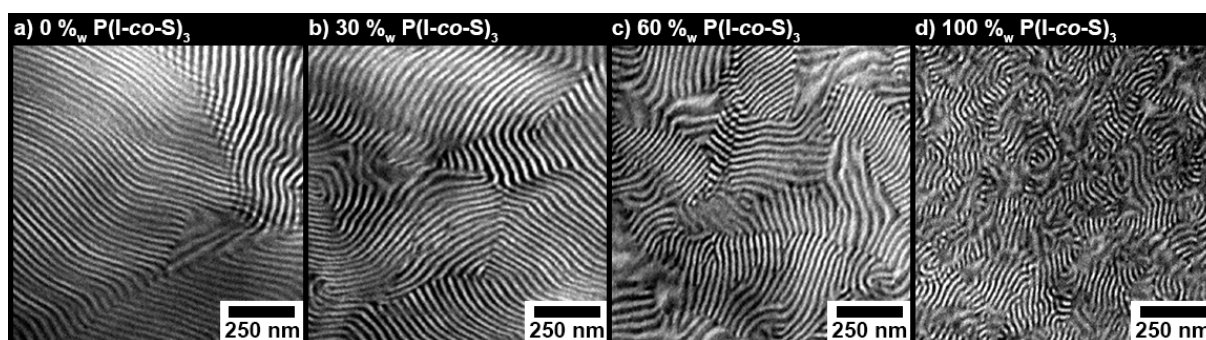


FIGURE 2 TEM measurements for P(I-co-S)/P(I-co-S)₃ blends with increasing content of P(I-co-S)₃. PI-rich phases are OsO₄ stained and appear electron opaque (dark).

These results can be compared with the morphology obtained by small angle X-Ray scattering (SAXS) in the inverse space. SAXS results for the P(I-co-S) and P(I-co-S)₃ copolymers as well

as the respective 50%_w blend are visualized in Figure 3 (other P(I-co-S)₃ contents in Figure S1). As discussed in a previous work,⁴² the scattering pattern of the tapered diblock copolymer displays Bragg reflections with the relative q values of 1:2:3, corresponding to a long-range ordered LAM morphology at ambient temperature. In contrast, the scattering pattern of the hexablock morphology is broadened and lacks higher order reflections giving evidence for a less ordered LAM morphology. SAXS results confirm full miscibility of all blends of this type independent of the composition (Figure S1), proven by a scattering pattern that corresponds to a single-spaced LAM morphology. Taking the 50%_w blend as an example, the lack of the second order reflection clearly indicates the loss of order, as already discussed for the TEM images.

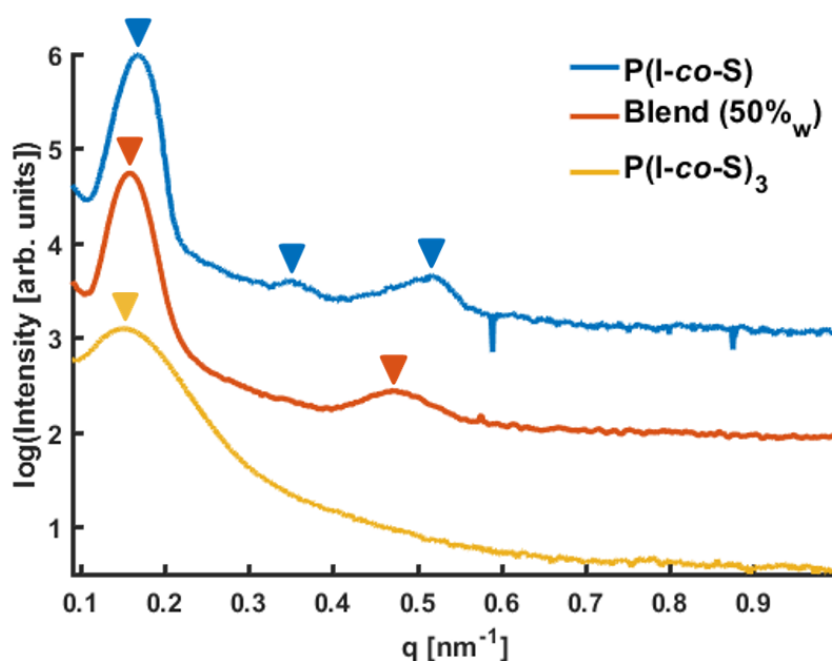


FIGURE 3 SAXS patterns of the P(I-co-S) (blue) and the P(I-co-S)₃ (yellow) copolymer as well as the respective 50%_w blend (red). Arrows indicate the positions of the Bragg reflections. Curves are shifted vertically for clarity.

As visualized in Figure 4, the P(I-co-S)₃ content also affects the domain spacing (*i.e.* the periodicity $d = 2\pi/q^*$; q^* is the modulus of the scattering vector corresponding to the first maximum). Increasing the P(I-co-S)₃ content leads to a rather linear increase of the domain spacing up to the value of the non-blended P(I-co-S)₃ copolymer, which underlines copolymer miscibility over the full composition range. However, differences in the domain spacing are comparably small (≈ 3 nm).

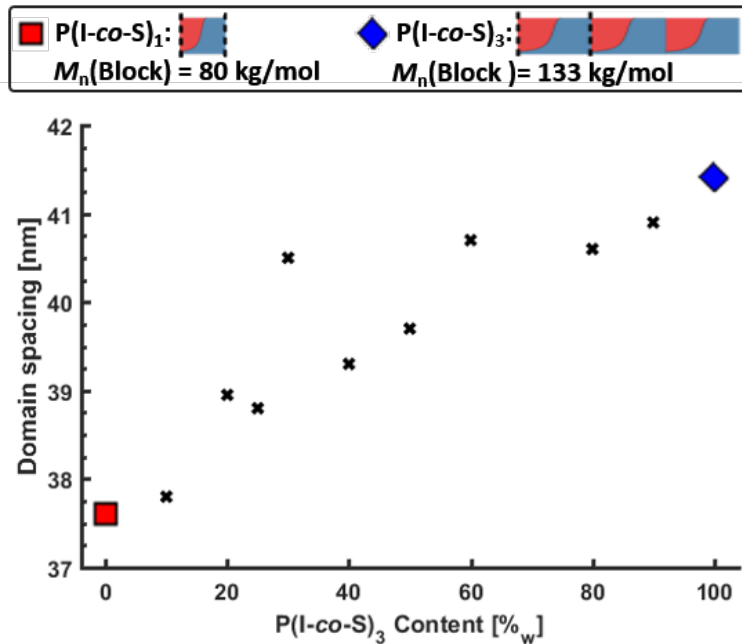


FIGURE 4 Domain sizes of P(I-co-S)/ P(I-co-S)₃ blends as a function of the P(I-co-S)₃ content. The polymer architectures are visualized in accordance to Figure 1 (plot of $F_{V,S}$ vs. polymer volume).

Tensile Properties

Since P(I-co-S)₃ is able to bridge multiple glassy PS domains, an increase of mechanical properties is expected. To correlate mechanical properties with the P(I-co-S)₃ content, polymer films were produced by solution-blending with chloroform as a solvent, subsequently stamped and exposed to uniaxial stress until rupture. Figure 6a visualizes the measured stress as a function of the strain $\sigma(\varepsilon)$ for a selection of representative blend samples (see Figure S3 for other P(I-co-S)₃ contents). All blends show a separate regime of elastic response ($\varepsilon \approx 0\text{-}4\% < \varepsilon_{\text{yield}}$) and plastic flow ($\varepsilon_{\text{yield}} \approx 4\% < \varepsilon < \varepsilon_{\text{break}}$; $\varepsilon_{\text{break}}$ up to 800%), which confirms the phase separated domain structure, as also observed in scattering and TEM experiments discussed before.

An increase of the P(I-co-S)₃ content in the blends resulted in a continuous increase of the strain at break from $\approx 10\%$ to $\approx 800\%$ (Figure 5a and S3d; Table 2). In contrast, no significant changes are observed for the engineered stress $\sigma(\varepsilon)$. This is validated by toughness (*i.e.* integral of the tensile curve, Figure S4), which shows a similar trend compared to the $\varepsilon_{\text{break}}$. Rather slight differences are observed for P(I-co-S)₃ contents $> 60\%$ and mainly caused by the discontinuity of $\sigma(\varepsilon)$, which leads to a comparably large variation of the toughness for small changes in ε for increasing values of ε . Both the increase of $\varepsilon_{\text{break}}$ and the toughness are explained by the molecular architecture of the tapered hexablock copolymer. The covalent linkage of multiple blocks connects the vitrified high T_g microdomains in addition to entanglements.^{17,93,94} Therefore a high P(I-co-S)₃

content leads to a large number of the bridges and consequently to superior mechanical properties. Comparable observations were made by Lach *et al.* who studied toughening by blending a tapered SIS triblock copolymer with a tapered multiblock copolymer with a star topology.⁹¹ However the block copolymers compared in these studies possess different PS content, chain topologies and microdomain morphologies, which does not allow for a direct comparison with the results as targeted in the current work (constant PS content, linear chain topology, lamellar phase state).

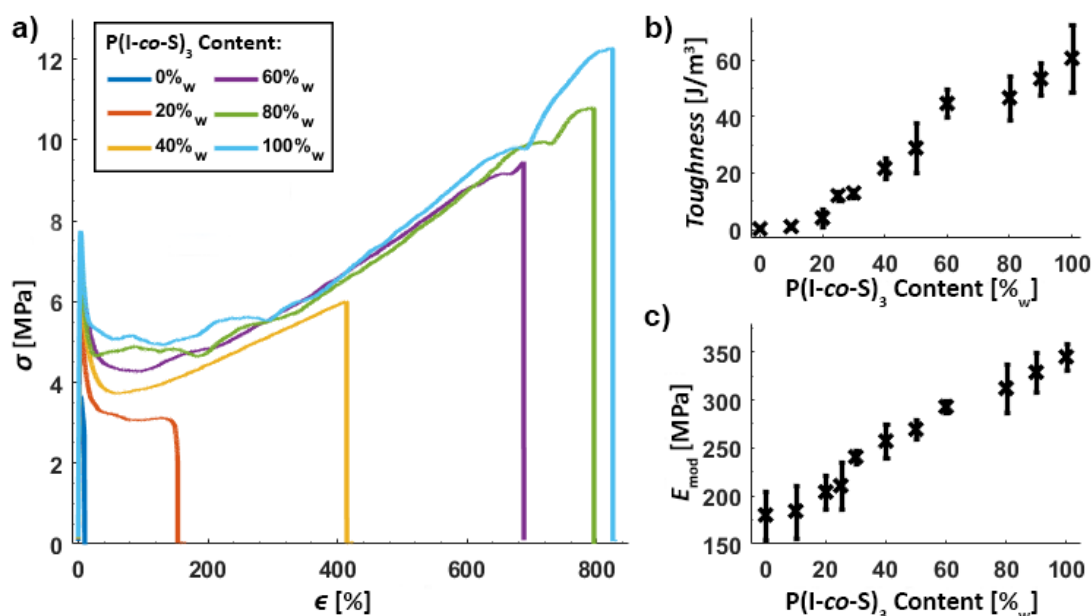


FIGURE 5 a) Representative stress-strain (σ - ϵ) diagrams, b) toughness and c) elastic moduli of miscible P(I-co-S)/P(I-co-S)₃ blends as a function of the P(I-co-S)₃ content.

At comparable low strains ($\epsilon < \epsilon_{\text{yield}} \approx 4\%$; Figure S3b,c and e), sample deformation is fully reversible for all blends of this series and typically results in a linear increase of the stress σ (ϵ) (Figure S3b). The slope of $\sigma(\epsilon)$ (*i.e.* elastic or Young's modulus: $E_{\text{mod}} = \Delta\sigma/\Delta\epsilon$; Figure S4) is visualized in Figure 5c as a function of the P(I-co-S)₃ content. Increasing the latter, leads to an increase of E_{mod} up to the value of the P(I-co-S)₃ copolymer (*i.e.* non-blended = 100%_w). The large value of P(I-co-S)₃ compared to P(I-co-S) is typical for multiblock copolymers and was described in seminal work by Spontak *et al.* for series of (IS)_n block copolymers with increasing block number.^{40,41} A similar trend is also observed for the yield point ($\epsilon_{\text{yield}} \approx \text{const.}$; σ_{yield} increasing; for detailed discussion see Figure S3).⁴⁰ Both effects can be explained by an architecture-enhanced microstructural interconnectivity (*i.e.* number of bridging conformations),⁴⁰ which enables the formation of midblocks pinned at both chain ends.⁹⁵

TABLE 2 Mechanical data of the P(I-co-S) / P(I-co-S)₃ blending series (Table 1, Sample 1) determined via tensile testing. Errors are given as the standard deviation (σ interval) from 8-15 independent drawing experiments.

Sample	P(I-co-S) ₃ Content [% _w]	d[nm]	$\varepsilon_{\text{yield}}$ [%]	σ_{yield} [MPa]	E_{mod} [MPa]	$\varepsilon_{\text{break}}$ [%]	Toughness [J/m ³]
1.1	0	37.6	3.7 ± 0.2	4.2 ± 0.7	180 ± 25	10 ± 5.0	0.33 ± 0.15
1.2	10	37.8	3.9 ± 0.2	4.4 ± 0.9	180 ± 27	41 ± 19	1.1 ± 0.33
1.3	20	39.0	3.9 ± 0.1	5.2 ± 0.5	200 ± 17	120 ± 89	4.2 ± 3.1
1.4	25	38.8	3.9 ± 0.1	5.3 ± 1.0	210 ± 24	340 ± 56	12 ± 1.6
1.5	30	40.5	3.9 ± 0.1	6.2 ± 0.2	240 ± 6.2	320 ± 26	13 ± 1.3
1.6	40	39.3	3.8 ± 0.2	6.6 ± 0.8	260 ± 18	450 ± 86	22 ± 3.5
1.7	50	39.7	3.7 ± 0.1	6.8 ± 0.3	270 ± 9.7	540 ± 153	29 ± 8.7
1.8	60	40.7	3.7 ± 0.1	7.4 ± 0.2	290 ± 5.6	700 ± 55	45 ± 4.9
1.9	80	40.6	3.7 ± 0.1	7.5 ± 0.6	300 ± 22	720 ± 92	47 ± 7.9
1.10	90	40.9	3.6 ± 0.2	8.0 ± 0.7	330 ± 20	750 ± 63	53 ± 5.8
1.11	100	41.4	3.7 ± 0.1	8.5 ± 0.4	340 ± 14	800 ± 96	61 ± 12

The results of this part emphasize that binary blends of P(I-co-S) and P(I-co-S)_n ($n > 1$) copolymers with similar domain spacing form full miscible microphase separated blends, albeit with a longrange order reduced due to to the P(I-co-S)_n content.

Nevertheless, the latter leads to increased elastic moduli and toughness which allows to adjust mechanical properties by adding a minor fractions of a tapered multiblock copolymer.

B. Effect of the Tapered Multiblock Copolymer Miscibility: AB/(AB)_n Blends

Spontak *et al.* investigated the miscibility of (PI-*b*-PS)_n sequential multiblock copolymer blends intensely, albeit their mechanical properties were not reported.^{40,86,88} In this part of the current work, we study the importance of miscibility for mechanical properties of P(I-co-S) / P(I-co-S)_n copolymer blends. For this purpose, we continuously increase the difference in the domain sizes (i.e. immiscibility) of the compounds and track the changes in morphology and mechanics. Two series of P(I-co-S) / P(I-co-S)_n blends were prepared (Table 1, Entries 2 and 3), only differing in the molecular weight of the tapered diblock copolymers P(I-co-S) (Figure 6, $d = 38$ and 77 nm, respectively). Tapered multiblock copolymers P(I-co-S)_n with $n = 2-5$ and a constant molecular weight of 240 kg/mol were used to systematically vary the domain sizes difference Δd within a series (Figure 6; $\Delta d = 418$ nm and $36-57$ nm, respectively).

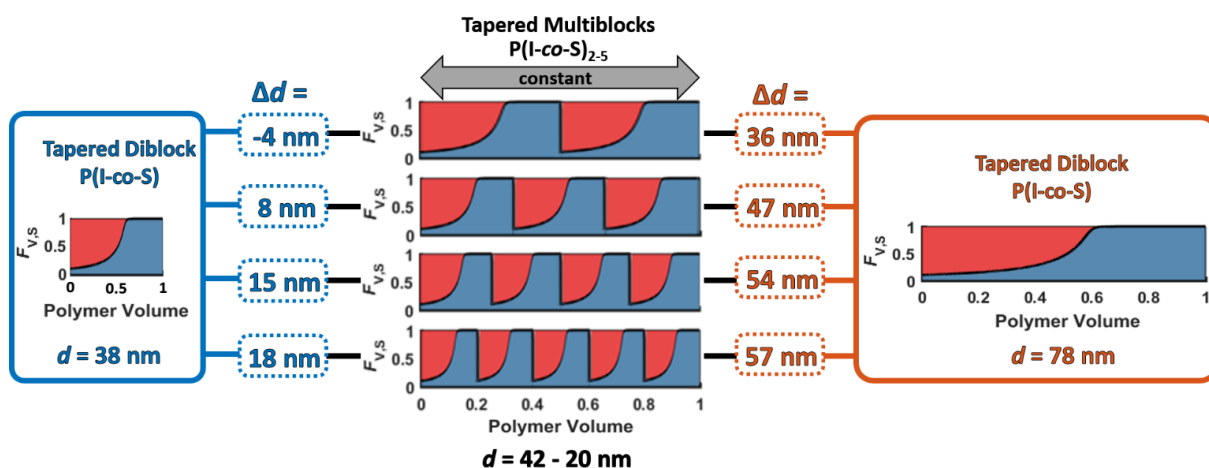


FIGURE 6 Overview of the prepared P(I-co-S)/P(I-co-S)_n blends to study the effect of miscibility. Two series were prepared with systematic variation of Δd by blending distinct tapered diblock copolymers with similar series of tapered multiblock copolymers P(I-co-S)_n.

Morphologies

SAXS was used to study the miscibility of copolymer samples in the bulk state. Scattering patterns of the P(I-co-S)/ P(I-co-S)_n ($n = 2-5$) series with $\Delta d = -4 - 18 \text{ nm}$ are visualized in Figure 7a. As discussed in detail in a previous work,⁴² domain sizes and (LAM; see previous discussions) order decrease ($d \sim 1/q^*$) with increasing number of blocks (*i.e.* $2n$) in P(I-co-S)_n copolymers. For binary blends up to $\Delta d = 15 \text{ nm}$ (*i.e.* $n = 4$) a single Bragg reflection with a value of $q_{\text{P(I-co-S)}}^* < q_{\text{Blend}}^* < q_{\text{P(I-co-S)}_n}^*$ is obtained, indicating miscibility of the copolymer architectures. Increasing the domain size to $\Delta d = 18 \text{ nm}$ (*i.e.* $n = 5$), leads to broadening and the occurrence of a second peak maximum caused by the overlay of two Bragg reflections. This is explained by the onset of macrophase separation, leading to P(I-co-S)-rich ($d = 32 \text{ nm}$) and P(I-co-S)_n-rich ($d = 23 \text{ nm}$) areas (Table 3), with d -spacings approached to the values of the respective copolymers ($d = 38$ and 20 nm ; Table 3 and Figure S5).

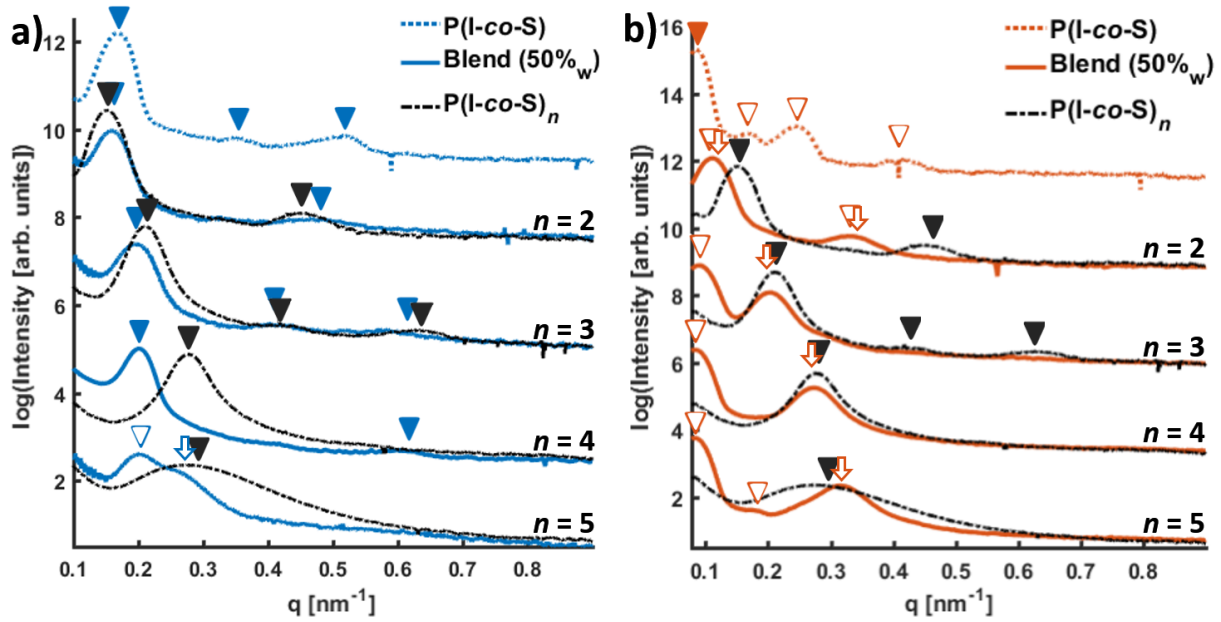


FIGURE 7 SAXS patterns of a P(l-co-S) (colored, dotted line) and P(l-co-S)_n copolymers ($n = 2 - 5$; black, dashed-dotted lines) as well as the respective binary 50%_w blends (colored, straight lines). Blend series with a) $d_{P(l-co-S)} = 38$ nm leading to $\Delta d = -4 - 18$ nm (Table 3 Entry 2) and b) $d_{P(l-co-S)} = 77$ nm leading to $\Delta d = 35 - 57$ nm (Table 3 Entry 3) are given. Arrows indicate Bragg reflections. Open Symbols indicate macrophase separated samples; different arrowtypes indicate Bragg reflections corresponding to (LAM) macrophases with dissimilar d -spacing, respectively. Curves referring to different P(l-co-S)_n samples are shifted vertically for clarity.

TABLE 3 Morphological and mechanical data of the P(l-co-S) / P(l-co-S)_n blend series (50%_w composition) determined via tensile testing. Errors are given as the standard deviation (σ intervall) from 8-15 independent drawing experiments. Molecular and mechanical characteristics of the (non-blended) copolymers are given in Table 1 and S1.

Entry	n of P(l-co-S) _n	$d_{P(l-co-S)}$ [nm]	$d_{P(l-co-S)_n}$ [nm]	Δd [nm]	α ratio ^{a)}	d_{Blend} [nm]	Macrophase Separation	ϵ_{break} [%]	Toughness [J/m ³]
1				see	Table 2				
2.1	2	38	42	-4	0.67:1	40	no	300 ± 72	16 ± 4.5
2.2	3	38	30	8	1.0:1	32	no	500 ± 85	28 ± 7.1
2.3	4	38	23	15	1.3:1	31	no	640 ± 56	42 ± 4.7
2.4	5	38	20	18	1.7:1	32, 23	partial	610 ± 54	41 ± 5.4
3.1	2	77	42	35	2.0:1	57, 55	partial	450 ± 37	31 ± 3.3
3.2	3	77	30	47	3.0:1	71, 31	partial	440 ± 29	23 ± 1.2
3.3	4	77	23	54	4.0:1	75, 23	almost full	390 ± 24	21 ± 2.7
3.4	5	77	20	57	5.0:1	77, 20	full	370 ± 22	20 ± 1.6

a) Values correspond to the block molecular weight ratio $\alpha = M_{n, P(l-co-S)_n} / (n \cdot M_{n, P(l-co-S)})$. M_n : number averaged, targeted molecular weight (Table 1); n : number of repetitive tapered diblock segments in P(l-co-S)_n. $d_{P(l-co-S)_n}$

To further increase the degree of demixing, another blending series was prepared (Table 3 Entry 3) utilizing a tapered diblock copolymer with a larger domain spacing ($d = 77$ nm; $M_{n,target} = 240$ kg/mol). The SAXS patterns are visualized in Figure 7b and can be discussed in analogy to the series before ($\Delta d = 4 - 18$ nm; Figure 7a and Table 3 Entry 2). In contrast, the increased differences in the domain spacings already lead to partial immiscibility for $n = 2$ ($\Delta d = 35$ nm). Increasing the latter ($n = 2 \rightarrow 5$) shifts the Bragg reflections in proximity to the values observed for the corresponding copolymers, explained by the increasing degree of segregation finally leading to pure macrophases for $n = 5$ ($\Delta d = 57$ nm; Table 3 and Figure S5).

These results are confirmed by TEM experiments, which visualize the partial and full macrophase separated blends in real-space. Figure 8a shows the partial macrophase separated blend (SAXS: $\Delta d = 35$ nm; $n = 2$ in Figure 7b), exhibiting lamellar grains with distinct spacings, highlighted at the interfaces by the zoomed insets. Increasing the difference in the domain sizes to $\Delta d = 57$ nm (SAXS: $n = 2$ in Figure 7b), obviously leads to macrophase separation of the $P(I-co-S)_5$ containing blend (Figure 8b). While the long-range ordered lamellae with large domain spacing ($d = 78$ nm) can be assigned to the tapered diblock copolymer, the $P(I-co-S)_5$ macrophase is poorly resolved, which is explained by the comparably small domain sizes (SAXS: $d = 20$ nm).

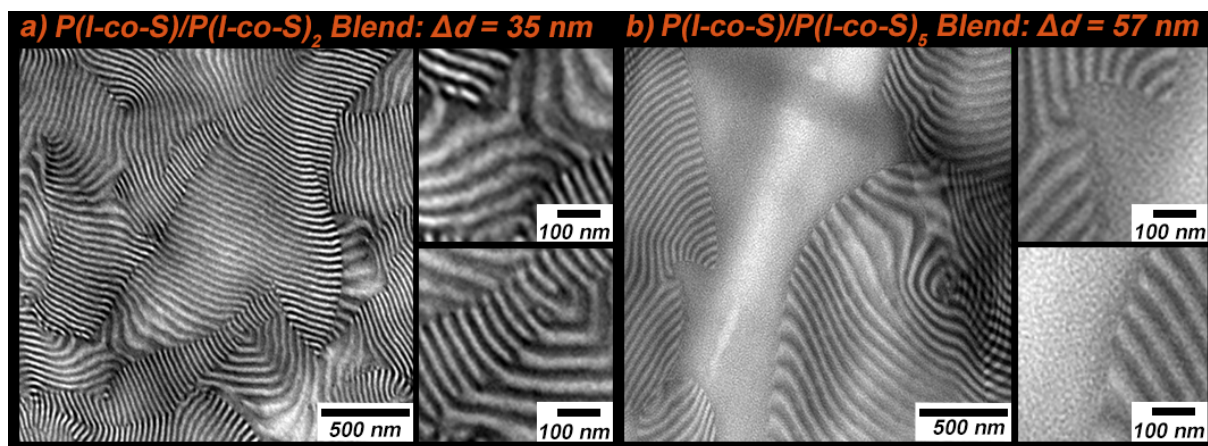


FIGURE 8 TEM measurements of a) $P(I-co-S)/P(I-co-S)_2$ blend (Table 1, entry 3.1) and b) $P(I-co-S) / P(I-co-S)_5$ blend (Table 1, entry 3.4). Insets visualize the interfaces of distinct grains. PI-rich phases are OsO_4 stained and appear electron opaque (dark).

Spontak *et al.* found demixing for a single $(PI-b-PS) / (PI-b-PS)_n$ blend (*cf.* Figure 1) with a block molecular weight ratio (α) of 4 : 1,⁸⁸ which is lower than the 5.2 : 1 limit described for binary $PI-b-PS / (PI-b-PS)'$ blends.⁶⁷⁻⁷⁰ The increased immiscibility of the former binary blend was ascribed to the multiblock copolymer architecture, leading to bridged and looped midblocks, which reduce the lateral extension of chains. In accordance with the results of Spontak *et al.*

for $(PI-b-PS)_n$ multiblock copolymers we find macrophase separation below α -ratios of 5.2 : 1 for the $P(I-co-S)$ tapered multiblock analogue architectures (see Table 3). Furthermore, the series of blends investigated allow to track and to quantify this effect precisely, leading to partial macrophase separation already for $\alpha = 1.7 : 1$ (Table 3, entry 2.4) and full macrophase separation for $\alpha = 5.0 : 1$ (Table 3, entry 3.4) as observed for the $P(I-co-S)_5$ containing blends. However, differences to $(PS-b-PI)_n$ (multi)block copolymers cannot be ruled out. This underlines the unique behavior of the (tapered) multiblock copolymers investigated in this work.

Tensile Properties

Immiscible $P(I-co-S)/P(I-co-S)_n$ blends separate into $P(I-co-S)_n$ rich and $P(I-co-S)$ rich macrophases. The latter exhibit low $P(I-co-S)_n$ content (i.e. number of bridges) and are therefore suspected to be prone to mechanical failure. To quantify the consequences of immiscibility on mechanical properties, tensile properties of miscible, partially miscible and immiscible $P(I-co-S)/P(I-co-S)_n$ blends were evaluated by tensile testing.

In work by Spontak *et al.* the mechanical properties of $(PI-b-PS)_n$ multiblock copolymers are found to be improved when increasing block numbers.^{40,41} This phenomenon is generally attributed to their capability of forming multiple bridged glassy styrene domains, resulting in "stitched" domain boundaries.^{40-42,83,96,97} However, for $P(I-co-S)_n$ architectures with a constant chain molecular weight, the observed increase in mechanics (e.g. higher strain at break and elastic modulus) is limited by the block size (i.e. block number; see Figure 7).⁴² Consequently a further increase of n leads to a decrease of mechanical properties (*cf.* Figure 9 dashed lines and Table S1), explained by the collapse of the physical crosslinks due to increasing miscibility.^{42,43}

Figure 9 visualizes the toughness of $P(I-co-S)$, $P(I-co-S)_n$ and the respective blends (50%_w) as a function of Δd ($\Delta d = d_{P(I-co-S)} - d_{P(I-co-S)_n}$). In Figure 9a the domain size of $P(I-co-S)$ (Table 1 Entry 2, Figure 7 left) exhibits a comparably small difference to the domain spacings of the $P(I-co-S)_n$ ($\Delta d = -5$ to 20 nm), only leading to partial macrophase separation for $\Delta d = 20$ nm (i.e. the $P(I-co-S)_5$ containing blend). Both, the strain at break (Figures S7a and S8a; Table 3) and the toughness (Figures S7a and 9a; Table 3) of the blends, follow the trend of the non-blended $P(I-co-S)_n$ multiblock samples (Figures 9a, S7 and S8a; Table S1). This means that no significant influence of the diverging domain sizes ($\Delta d = -4$ - 18 nm) is observed for the mechanical properties.

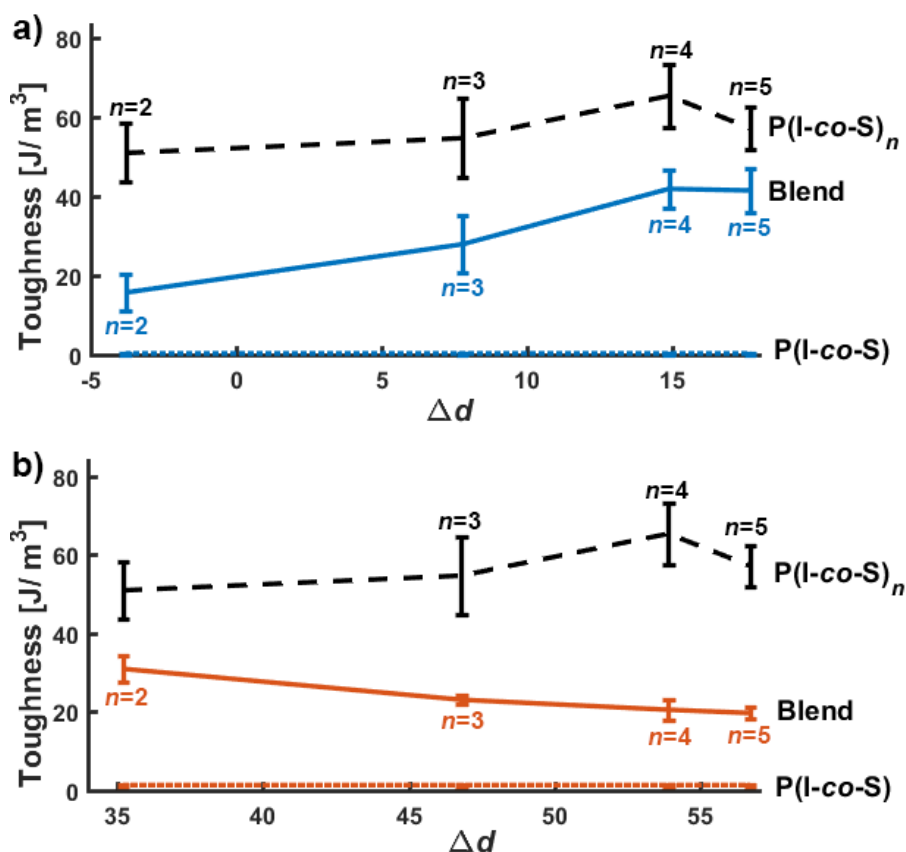


FIGURE 9 Toughness of P(l-co-S) (dashed line), P(l-co-S)_n (dotted line) and the respective blends (straight line) as a function of Δd . a) blending series with $\Delta d = -4 - 18$ nm (blue; Table 1 Entry 2 and Figure 6 left), b) $\Delta d = 35-57$ nm (red; Table 1 Entry 3 and Figure 6 right). The values are interpolated as a guide for the eye.

In Figure 9b the domain size of P(l-co-S) (Table 1 Entry 3, Figure 6 right) exhibits a comparably large difference to the domain spacings of the P(l-co-S)_n ($\Delta d = 36 - 57$ nm), leading to full macrophase separation for $\Delta d = 57$ nm (i.e. the P(l-co-S)₅ containing blend). Although this blend series contains the same P(l-co-S)_n as a mechanically tough components compared to the blends in Figure 9a, the trend in the mechanical behavior is remarkably different. Failure of these materials occurs already at rather low strain values (Figure S7b, Table S1), leading to a continuous decrease in toughness with increasing Δd (Figure 9b). This trend can be explained by the formation of macrophases with low P(l-co-S)_n content (Figures 7 and 8). These are prone to mechanical failure (Figure 5a and b) and can possibly serve as local defects, facilitating crack initialization, growth and ultimate failure of the materials.^{91,98,99}

Although the mechanical properties of these macrophase separated blends are generally worse than for the previously discussed series, it has to be emphasized that even a fully macrophase separated blend (Table 3, Entry 3.4) still exhibits a toughness of 20 J/m³, exceeding the value of

the corresponding diblock by far (1.4 J/m^3 ; Table S1, Entry 2). An interesting and at first sight surprising exception is obtained by comparing the toughness of the P(I-co-S)/P(I-co-S)₂ blends (compare $n = 2$ blends in Figure 9a and b). In this case, the partially macrophase-separated blend (Table 3 Entry 3.1) even exhibits a larger toughness than the fully miscible analogue (Table 3 Entry 2.1; $31 \text{ vs. } 16 \text{ J/m}^3$). A direct comparison of the $\sigma(\varepsilon)$ curves (Figure S9) reveals significant differences in the engineered stress in the partial macrophase separated blend. Although the P(I-co-S) is not capable of bridging vitrified PS domains, it affects the tensile strength in the P(I-co-S)/P(I-co-S)_n blend at elongations far beyond $\varepsilon_{\text{break}}$ of the brittle P(I-co-S) material. This increase in $\sigma(\varepsilon)$ is tentatively explained by the increased $T_{g,\text{PS-rich}}$ ($100 \text{ }^\circ\text{C}$ vs. $80 \text{ }^\circ\text{C}$)⁴² and M_n (240 kg/mol vs. 80 kg/mol) of P(I-co-S) in the partially macrophase separated blend (*cf.* Tables S1 and S2), which increases entanglements and further mechanical stability of PS-rich domains in the bulk state.

CONCLUSIONS

In this work we aimed at understanding the effect of gradually increased extent of domain bridging, introduced in lamellar phase-segregated AB-diblock copolymers. On the one hand, this is important to furnish diblock copolymers with mechanical properties, i.e. toughness, on the other hand we were aiming at an understanding of the mechanics of multiblock copolymers when "diluting" these materials with diblock copolymers. For P(I-co-S)/P(I-co-S)_n copolymer blends, i.e. blends of tapered diblock and structurally analogous multiblock copolymers, the blend composition was systematically correlated with morphological and mechanical properties in the lamellar phase. For this purpose, several blend series were prepared and the effect of the P(I-co-S)_n ($n = 2-5$) weight fraction and miscibility has been investigated. Copolymers with similar domain sizes (SAXS: $\Delta d = 3 \text{ nm}$) resulted in fully miscible blends, however the longrange order decreased with the P(I-co-S)_n content. Elongation at break, toughness and Young's modulus were found to be substantially increased (e.g. $\varepsilon_{\text{break}} \approx 540\%$ for a $50\%_w$ blend) compared to the tapered diblock copolymer with its known poor mechanical properties ($\varepsilon_{\text{break}} \approx 10\%$). The increase of mechanical properties in dependence of the P(I-co-S)₃ content is explained by the bridging multiblock architecture, which is able to connect vitrified PS-rich domains beyond entanglements (*i.e.* bridging conformation).

In the second part of the work the difference in domain spacings (Δd by SAXS) of tapered di- and multiblock copolymers was systematically increased, leading to a decreased miscibility of the added multiblock, indicated by partial macrophase separation at $\Delta d \approx 18 \text{ nm}$ and full macrophase separation at $\Delta d \approx 57 \text{ nm}$. In contrast to miscible P(I-co-S)/P(I-co-S)_n blends, such macrophase

separated blends show a decrease of both strain at break and toughness with increased demixing of the phases. However, the dependence of mechanical properties on Δd is less significant, if compared to the increase by the $P(I-co-S)_n$ content. To our surprise, macrophase separation still leads to mechanical properties exceeding the strain at break and the toughness of the corresponding tapered diblock copolymers by far.

The key objective of this work was to retain the high order of diblock copolymers, which is relevant for many applications, however installing mechanical properties by adding a minor fraction of multiblock copolymers. In essence, our studies show that for fully miscible blends, an enormous increase of mechanical properties, particularly elastic response and toughness is observed due to addition of a limited amount of multiblock copolymers, but we also observe a certain reduction of long-range order. Surprisingly, even highly diverging domain sizes of diblock- and multiblock component did not lead to a significant loss of mechanical properties.

ACKNOWLEDGEMENTS

Philip Dreier and Tobias Johann are acknowledged for helpful discussions. We thank Jürgen Ludwig for specialty glassware and Monika Schmelzer for valuable support with SEC measurements. Andreas Hanewald and Kaloian Koynov are acknowledged for help with the mechanical characterization. M.G. and M.P. acknowledge the German Research Foundation (DFG GA 2169/1-1) for partial financial support of this work. The authors also thank the RMU Mainz-Darmstadt for funding.

REFERENCES

- (1) Hadjichristidis, N.; Floudas, G.; Pispas, S. *Block copolymers: Synthetic strategies, physical properties, and applications*; Wiley-Interscience: Hoboken, N.J. 2003.
- (2) Bates, C. M.; Bates, F. S. *Macromolecules* **2017**, 50 (1), 3–22. DOI: 10.1021/acs.macromol.6b02355.
- (3) Gabor, A. H.; Lehner, E. A.; Mao, G.; Ober, C. K.; Long, T. E.; Schell, B. A.; Tiberio, R. C. *Proc. SPIE* **1925**, 499–506. DOI: 10.1117/12.154785.
- (4) Gabor, A. H.; Lehner, E. A.; Mao, G.; Schneggenburger, L. A.; Ober, C. K. *Chem. Mater.* **1994**, 6 (7), 927–934. DOI: 10.1021/cm00043a011.
- (5) Kim, H.-C.; Park, S.-M.; Hinsberg, W. D. *Chem. Rev.* **2010**, 110 (1), 146–177. DOI: 10.1021/cr900159v.
- (6) Park, C.; Yoon, J.; Thomas, E. L. *Polymer* **2003**, 44 (22), 6725–6760. DOI: 10.1016/j.polymer.2003.08.011.
- (7) Schacher, F. H.; Rugar, P. A.; Manners, I. *Angew. Chem. Int. Ed.* **2012**, 51 (32), 7898–7921. DOI: 10.1002/anie.201200310.
- (8) Feng, H.; Lu, X.; Wang, W.; Kang, N.-G.; Mays, J. *Polymers* **2017**, 9 (12), 494. DOI: 10.3390/polym9100494.
- (9) Appold, M.; Grune, E.; Frey, H.; Gallei, M. *ACS Appl. Mater. Interfaces* **2018**, 10 (21), 18202–18212. DOI: 10.1021/acsami.8b02848.
- (10) Knoll, K.; Nießner, N. *Macromol. Symp.* **1998**, 132 (1), 231–243. DOI: 10.1002/masy.19981320122.
- (11) Wagner, D.; Knoll, K. *Kunststoffe International* **2010**, 09, 186–189.
- (12) Geoffrey, H.; Milkovich, R. Block polymers of monovinyl aromatic hydrocarbons and conjugated dienes. 3,265,765, Jan 29, **1962**.
- (13) Legge, N. R. *Rubber Chem. Technol.* **1987**, 60 (3), 83–117. DOI: 10.5254/1.3536141.
- (14) Drobny, J. G. In *Handbook of Thermoplastic Elastomers*; Drobny, J. G., Ed.; Elsevier, 2007; pp 9–11.
- (15) Morton, M.; McGrath, J. E.; Juliano, P. C. *J. Polym. Sci. C Polym. Symp.* **1969**, 26 (1), 99–115. DOI: 10.1002/polc.5070260107.
- (16) Holden, G.; Bishop, E. T.; Legge, N. R. *J. Polym. Sci. C Polym. Symp.* **1969**, 26 (1), 37–57. DOI: 10.1002/polc.5070260104.
- (17) Morton, M. In *Multicomponent polymer systems: A symposium co-sponsored by the Division of Industrial and Engineering Chemistry, the Division of Polymer Chemistry at the 159th meeting of the American Chemical Society*, Houston, Tex., Feb. 23 - 26, 1970; Platzer, N. A. J., Ed.; Advances in chemistry series 99; American Chemical Society: Washington, DC, 1971; pp 490–509.
- (18) Schimpf, V.; Max, J. B.; Stolz, B.; Heck, B.; Mülhaupt, R. *Macromolecules* **2019**, 52 (1), 320–331. DOI: 10.1021/acs.macromol.8b01908.
- (19) Shibasaki, Y.; Mori, T.; Fujimori, A.; Jikei, M.; Sawada, H.; Oishi, Y. *Macromolecules* **2018**, 51 (23), 9430–9441. DOI: 10.1021/acs.macromol.8b01817.
- (20) Noshay, A.; McGrath, J. E. *Block copolymers: Overview and critical survey, 2. print*; Acad. Pr: Orlando u.a., 1987.
- (21) Watts, A.; Kurokawa, N.; Hillmyer, M. A. *Biomacromolecules* **2017**, 18 (6), 1845–1854. DOI: 10.1021/acs.biomac.7b00283.
- (22) Ntaras, C.; Polymeropoulos, G.; Zapsas, G.; Ntetsikas, K.; Liontos, G.; Karanastasis, A.; Moschovas, D.; Rangou, S.; Stewart-Sloan, C.; Hadjichristidis, N.; Thomas, E. L.; Avgeropoulos, A. *J. Polym. Sci. B* **2016**, 54 (15), 1443–1449. DOI: 10.1002/polb.24058.
- (23) Yang, G.-W.; Wu, G.-P. *ACS Sustainable Chem. Eng.* **2019**, 7 (1), 1372–1380. DOI: 10.1021/acssuschemeng.8b05084.

- (24) Bishop, J. P.; Register, R. A. *Macromolecules* **2010**, 43 (11), 4954–4960. DOI: 10.1021/ma100314z.
- (25) Zhang, Z.; Grijpma, D. W.; Feijen, J. *Macromol. Chem. Phys.* **2004**, 205 (7), 867–875. DOI: 10.1002/macp.200300184.
- (26) Zhu, Y.; Radlauer, M. R.; Schneiderman, D. K.; Shaffer, M. S. P.; Hillmyer, M. A.; Williams, C. K. *Macromolecules* **2018**. DOI: 10.1021/acs.macromol.7b02690.
- (27) Touris, A.; Hadjichristidis, N. *Macromolecules* **2011**, 44 (7), 1969–1976. DOI: 10.1021/ma102900d.
- (28) Martello, M. T.; Schneiderman, D. K.; Hillmyer, M. A. *ACS Sustainable Chem. Eng.* **2014**, 2 (11), 2519–2526. DOI: 10.1021/sc500412a.
- (29) Bates, F. S.; Hillmyer, M. A.; Lodge, T. P.; Bates, C. M.; Delaney, K. T.; Fredrickson, G. H. *Science* **2012**, 336 (6080), 434–440. DOI: 10.1126/science.1215368.
- (30) Hsieh, H. L.; Quirk, R. P. *Anionic Polymerization: Principles and Practical Applications*; *Plastics Engineering* 34; Dekker: New York, 1996.
- (31) Grune, E.; Bareuther, J.; Blankenburg, J.; Appold, M.; Shaw, L.; Müller, A. H. E.; Floudas, G.; Hutchings, L. R.; Gallei, M.; Frey, H. *Polym. Chem.* **2019**, 50 (1), 3. DOI: 10.1039/C8PY01711E.
- (32) Legge, N. R.; Holden, G.; Schroeder, H. E. *Thermoplastic elastomers: A comprehensive review*; Hanser Publishers; Distributed in the U.S.A. and in Canada by Oxford University Press: Munich, New York, New York, 1987.
- (33) Qiao, L.; Leibig, C.; Hahn, S. F.; Winey, K. I. *Ind. Eng. Chem. Res.* **2006**, 45 (16), 5598–5602. DOI: 10.1021/ie0511940.
- (34) Georgopoulos, P.; Handge, U. A.; Abetz, C.; Abetz, V. *Polymer* **2016**, 104, 279–295. DOI: 10.1016/j.polymer.2016.02.039.
- (35) Förster, S.; Khandpur, A. K.; Zhao, J.; Bates, F. S.; Hamley, I. W.; Ryan, A. J.; Bras, W. *Macromolecules* **1994**, 27 (23), 6922–6935. DOI: 10.1021/ma00101a033.
- (36) Singh, N.; Tureau, M. S.; Epps, I. T. H. *Soft Matter* **2009**, 5 (23), 4757. DOI: 10.1039/b908739g.
- (37) Hodrokoukes, P.; Floudas, G.; Pispas, S.; Hadjichristidis, N. *Macromolecules* **2001**, 34 (3), 650–657. DOI: 10.1021/ma001479i.
- (38) Grune, E.; Johann, T.; Appold, M.; Wahlen, C.; Blankenburg, J.; Leibig, D.; Müller, A. H. E.; Gallei, M.; Frey, H. *Macromolecules* **2018**, 51 (9), 3527–3537. DOI: 10.1021/acs.macromol.8b00404.
- (39) Thunga, M.; Staudinger, U.; Satapathy, B. K.; Weidisch, R.; Abdel-Goad, M.; Janke, A.; Knoll, K. *J. Polym. Sci. B* **2006**, 44 (19), 2776–2788. DOI: 10.1002/polb.20936.
- (40) Smith, S. D.; Spontak, R. J.; Satkowski, M. M.; Ashraf, A.; Heape, A. K.; Lin, J. S. *Polymer* **1994**, 35 (21), 4527–4536. DOI: 10.1016/0032-3861(94)90798-6.
- (41) Spontak, R. J.; Smith, S. D. *J. Polym. Sci. B* **2001**, 39 (9), 947–955. DOI: 10.1002/polb.1070.
- (42) Steube, M.; Johann, T.; Galanos, E.; Appold, M.; Rüttiger, C.; Mezger, M.; Gallei, M.; Müller, A. H. E.; Floudas, G.; Frey, H. *Macromolecules* **2018**, 51 (24), 10246–10258. DOI: 10.1021/acs.macromol.8b01961.
- (43) Galanos, E.; Grune, E.; Wahlen, C.; Müller, A. H. E.; Appold, M.; Gallei, M.; Frey, H.; Floudas, G. *Macromolecules* **2019**, 52 (4), 1577–1588. DOI: 10.1021/acs.macromol.8b02669.
- (44) Mai, S.-M.; Mingvanish, W.; Turner, S. C.; Chaibundit, C.; Fairclough, J. Patrick A.; Heatley, F.; Matsen, M. W.; Ryan, A. J.; Booth, C. *Macromolecules* **2000**, 33 (14), 5124–5130. DOI: 10.1021/ma000154z.
- (45) Hamley, I. W. *The physics of block copolymers*; Oxford science publications; Oxford Univ. Press: Oxford, 1998.
- (46) Spontak, R. J.; Patel, N. P. In *Developments in Block Copolymer Science and Technology*, 1st ed.; Hamley, I. W., Ed.; John Wiley Sons Ltd: Chichester, 2004; pp 159–212.
- (47) Worsfold, D. J. *J. Polym. Sci. A* **1967**, 5 (11), 2783–2789. DOI: 10.1002/pol.1967.150051106.

- (48) Quinebèche, S.; Navarro, C.; Gnanou, Y.; Fontanille, M. *Polymer* **2009**, 50 (6), 1351–1357. DOI: 10.1016/j.polymer.2009.01.041.
- (49) Zhao, Y.; Miyamoto, N.; Koizumi, S.; Hashimoto, T. *Macromolecules* **2010**, 43 (6), 2948–2959. DOI: 10.1021/ma902542e.
- (50) Steube, M.; Johann, T.; Plank, M.; Tjaberings, S.; Gröschel, A. H.; Gallei, M.; Frey, H.; Müller, A. H. E. *Macromolecules* **2019**, 52 (23), 9299–9310. DOI: 10.1021/acs.macromol.9b01790.
- (51) Lanzendörfer, M. G.; Schmalz, H.; Abetz, V.; Müller, A. H. E. In *In Situ Spectroscopy of Monomer and Polymer Synthesis*; Puskas, J. E., Long, T. E., Storey, R. F., Shaikh, S., Simmons, C. L., Eds.; Springer US: Boston, MA, s.l., 2003; pp 67–81.
- (52) Mastan, E.; He, J. *Macromolecules* **2017**, 50 (23), 9173–9187. DOI: 10.1021/acs.macromol.7b01662.
- (53) Yang, L.; Han, L.; Ma, H.; Shen, H.; Li, C.; Zhang, S.; Lei, L.; Hao, X.; Li, Y. *Eur. Polym. J.* **2019**, 120, 109212. DOI: 10.1016/j.eurpolymj.2019.08.039.
- (54) Spontak, R. J.; Ryan, J. J. In *Compatibilization of polymer blends: Micro and nano scale phase morphologies, interphase characterization, and properties*; Thomas, S., Ajitha, A. R., Eds.; Elsevier: Amsterdam, 2019; pp 57–102.
- (55) Eichinger, B. E.; Flory, P. J. *Trans. Faraday Soc.* **1968**, 64 (0), 2035–2052. DOI: 10.1039/TF9686402035.
- (56) Eichinger, B. E.; Flory, P. J. *Trans. Faraday Soc.* **1968**, 64 (0), 2053–2060. DOI: 10.1039/TF9686402053.
- (57) Eichinger, B. E.; Flory, P. J. *Trans. Faraday Soc.* **1968**, 64 (0), 2061–2065. DOI: 10.1039/TF9686402061.
- (58) Eichinger, B. E.; Flory, P. J. *Trans. Faraday Soc.* **1968**, 64 (0), 2066–2072. DOI: 10.1039/TF9686402066.
- (59) Flory, P. J.; Ellenson, J. L.; Eichinger, B. E. *Macromolecules* **1968**, 1 (3), 279–284. DOI: 10.1021/ma60003a015.
- (60) Flory, P. J. *J. Chem. Phys.* **1942**, 10 (1), 51–61. DOI: 10.1063/1.1723621.
- (61) Huggins, M. L. *J. Phys. Chem.* **1942**, 46 (1), 151–158. DOI: 10.1021/j150415a018.
- (62) Mark, J. E. *Physical Properties of Polymer Handbook*, 2nd ed; Springer: New York, 2006.
- (63) Hadjichristidis, N.; Pispas, S.; Floudas, G. *Block Copolymers*; John Wiley & Sons, Inc: Hoboken, USA, 2002.
- (64) Leibler, L. *Macromolecules* **1980**, 13 (6), 1602–1617. DOI: 10.1021/ma60078a047.
- (65) Birshtein, T.M.; Liatskaya, Y.V.; Zhulina, E.B. *Polymer* **1990**, 31 (11), 2185–2196. DOI: 10.1016/0032-3861(90)90094-F.
- (66) Zhulina, E. B.; Birshtein, T. M. *Polymer* **1991**, 32 (7), 1299–1308. DOI: 10.1016/0032-3861(91)90235-B.
- (67) Hashimoto, T.; Yamasaki, K.; Koizumi, S.; Hasegawa, H. *Macromolecules* **1993**, 26 (11), 2895–2904. DOI: 10.1021/ma00063a039.
- (68) Hashimoto, T.; Koizumi, S.; Hasegawa, H. *Macromolecules* **1994**, 27 (6), 1562–1570. DOI: 10.1021/ma00084a043.
- (69) Kane, L.; Satkowski, M. M.; Smith, S. D.; Spontak, R. J. *Macromolecules* **1996**, 29 (27), 8862–8870. DOI: 10.1021/ma9613291.
- (70) Matsen, M. W. *J. Chem. Phys.* **1995**, 103 (8), 3268–3271. DOI: 10.1063/1.470260.
- (71) Cohen, R. E.; Tschoegl, N. W. *International Journal of Polymeric Materials and Polymeric Biomaterials* **1972**, 2 (1), 49–69. DOI: 10.1080/00914037208075299.
- (72) Cohen, R. E.; Tschoegl, N. W. *International Journal of Polymeric Materials and Polymeric Biomaterials* **1973**, 2 (3), 205–223. DOI: 10.1080/00914037308075310.
- (73) Hadziioannou, G.; Skoulios, A. *Macromolecules* **1982**, 15 (2), 267–271. DOI: 10.1021/ma00230a013.
- (74) Hashimoto, T. *Macromolecules* **1982**, 15 (6), 1548–1553. DOI: 10.1021/ma00234a017.
- (75) Berglund, C. A.; McKay, K. W. *Polym. Eng. Sci.* **1993**, 33 (18), 1195–1203. DOI: 10.1002/pen.760331807.

- (76) Kane, L.; White, S. A.; Spontak, R. J. *MRS Proc.* **1996**, 461, 149. DOI: 10.1557/PROC-461-75.
- (77) Kane, L.; Norman, D. A.; White, S. A.; Matsen, M. W.; Satkowski, M. M.; Smith, S. D.; Spontak, R. J. *Macromol. Rapid Commun.* **2001**, 22 (5), 281–296. DOI: 10.1002/1521-3927(20010301)22:5<281:AID-MARC281>3.0.CO;2-G.
- (78) Song, J.; Li, Y.; Huang, Q.; Shi, T.; An, L. *J. Chem. Phys.* **2007**, 127 (9), 94903. DOI: 10.1063/1.2764071.
- (79) Diamant, J.; Soong, D.; Williams, M. C. *Polym. Eng. Sci.* **1982**, 22 (11), 673–683. DOI: 10.1002/pen.760221104.
- (80) McKay, K. W.; Gros, W. A.; Diehl, C. F. *J. Appl. Polym. Sci.* **1995**, 56 (8), 947–958. DOI: 10.1002/app.1995.070560808.
- (81) Spontak, R. J.; Zielinski, J. M.; Lipscomb, G. G. *Macromolecules* **1992**, 25 (23), 6270–6276. DOI: 10.1021/ma00049a025.
- (82) Smith; Spontak, R. J.; Satkowski; Ashraf; Lin. *Physical review. B, Condensed matter* **1993**, 47 (21), 14555–14558. DOI: 10.1103/physrevb.47.14555.
- (83) Hermel, T. J.; Hahn, S. F.; Chaffin, K. A.; Gerberich, W. W.; Bates, F. S. *Macromolecules* **2003**, 36 (7), 2190–2193. DOI: 10.1021/ma021754w.
- (84) Fleury, G.; Bates, F. S. *Macromolecules* **2009**, 42 (10), 3598–3610. DOI: 10.1021/ma900183p.
- (85) Mori, Y.; Lim, L. S.; Bates, F. S. *Macromolecules* **2003**, 36 (26), 9879–9888. DOI: 10.1021/ma035300q.
- (86) Spontak, R. J.; Smith, S. D.; Ashraf, A. *Macromolecules* **1993**, 26 (19), 5118–5124. DOI: 10.1021/ma00071a021.
- (87) Laurer, J. H.; Hajduk, D. A.; Dreckötter, S.; Smith, S. D.; Spontak, R. J. *Macromolecules* **1998**, 31 (21), 7546–7549. DOI: 10.1021/ma9807872.
- (88) Spontak, R. J.; Fung, J. C.; Braunfeld, M. B.; Sedat, J. W.; Agard, D. A.; Ashraf, A.; Smith, S. D. *Macromolecules* **1996**, 29 (8), 2850–2856. DOI: 10.1021/ma9515691.
- (89) Hashimoto, T.; Tsukahara, Y.; Tachi, K.; Kawai, H. *Macromolecules* **1983**, 16 (4), 648–657. DOI: 10.1021/ma00238a031.
- (90) Cunningham, R. E.; Treiber, M. R. *J. Appl. Polym. Sci.* **1968**, 12 (1), 23–34. DOI: 10.1002/app.1968.070120104.
- (91) Lach, R.; Adhikari, R.; Weidisch, R.; Huy, T. A.; Michler, G. H.; Grellmann, W.; Knoll, K. *J Mater Sci* **2004**, 39 (4), 1283–1295. DOI: 10.1023/B:JMSE.0000013887.79570.33.
- (92) Adhikari, R.; Buschnakowski, M.; Lebek, W.; Godehardt, R.; Michler, G. H.; Calleja, F. J. B.; Knoll, K. *Polym. Adv. Technol.* **2005**, 16 (2-3), 175–182. DOI: 10.1002/pat.577.
- (93) Karatasos, K.; Anastasiadis, S. H.; Pakula, T.; Watanabe, H. *Macromolecules* **2000**, 33 (2), 523–541. DOI: 10.1021/ma991397y.
- (94) Watanabe, H.; Matsumiya, Y.; Sawada, T.; Iwamoto, T. *Macromolecules* **2007**, 40 (19), 6885–6897. DOI: 10.1021/ma0712495.
- (95) Livitsanou, C.; Steube, M.; Johann, T.; Frey, H.; Floudas, G. *Macromolecules* **2020**, 53 (8), 3042–3051. DOI: 10.1021/acs.macromol.0c00445.
- (96) Hermel, T. J.; Wu, L.; Hahn, S. F.; Lodge, T. P.; Bates, F. S. *Macromolecules* **2002**, 35 (12), 4685–4689. DOI: 10.1021/ma020100k.
- (97) Vigild, M. E.; Chu, C.; Sugiyama, M.; Chaffin, K. A.; Bates, F. S. *Macromolecules* **2001**, 34 (4), 951–964. DOI: 10.1021/ma000709q.
- (98) Adhikari, R.; Lach, R.; Michler, G.H.; Weidisch, R.; Grellmann, W.; Knoll, K. *Polymer* **2002**, 43 (6), 1943–1947. DOI: 10.1016/S0032-3861(01)00755-8.
- (99) *Micro- and nanostructured multiphase polymer blend systems: phase morphology and interfaces*; Harrats, C., Thomas, S., Groeninckx, G., Eds.; Materials science; Taylor & Francis: Boca Raton, Fla., 2006.

SUPPORTING INFORMATION

Materials, Experimental Procedures and Instrumentations

All chemicals and solvents were purchased from Acros Organics Co. and Sigma-Aldrich Co. Chloroform was used as received without further purification.

The synthesis and the characterization of the tapered di- and multiblock copolymers is described in a previous work.¹

X-Ray Scattering

Small-angle (SAXS) measurements were made using $\text{CuK}\alpha$ radiation (Rigaku Micro Max 007 x-ray generator, Osmic Confocal Max-Flux curved multilayer optics). 2D diffraction patterns were recorded on an Mar345 image plate detector at a sample-detector distance of 2060 mm. Intensity distributions as function of the modulus of the total scattering vector, $q = (4\pi/\lambda)\sin(2\theta/2)$, where 2θ is the scattering angle, were obtained by radial averaging of the 2D datasets. Samples in the form of thick films (~ 1 mm) were prepared by slow solvent casting. Temperature-dependent measurements of 1 hour long were made by heating the films from 298 K to 503 K.

TEM Measurements

For characterization of the tapered block copolymer morphology in the bulk state, the as prepared films were microtomed from surface to surface at -80 °C into thin slices of 50-70 nm thickness. The collected ultrathin sections were subsequently stained with osmium tetroxide (OsO_4) for selective staining of the PI domains, followed by investigation by TEM measurements.

Tensile Tests

Tensile tests were performed using a materials testing machine Z005 (Zwick/Roell, Germany). Tensile tests were carried out by exposing the stamped polymer dogbones to a uniaxial tension. Bone shape samples with thicknesses around 0.2 mm were drawn with rate of 10 mm/min at room temperatures. A Pre-Load of 0.1 N was applied with a Pre-Load speed of 5 mm/min. Dependencies of stress vs. draw ratio were recorded. Elastic modulus, elongation at break and stress at break were determined as averages of 8–15 independent drawing experiments performed at the same conditions. Transparent films were prepared with a thickness round 0.2 mm, obtained by slow evaporation from a chloroform solution followed a full removal of the solvent under reduced pressure and used for tensile tests without prior thermal annealing.

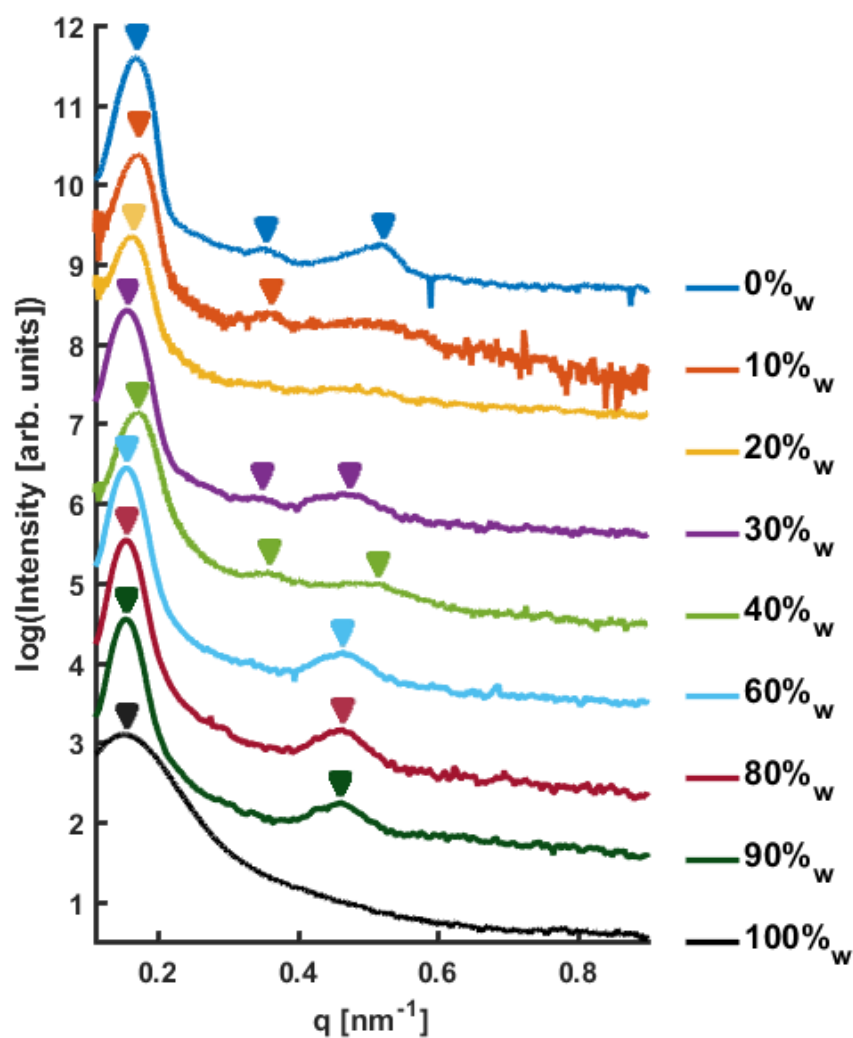
A. Effect of the Tapered Multiblock Copolymer Content: AB/(AB)₃ Blends

FIGURE S1 SAXS patterns of P(I-co-S)/P(I-co-S)₃ copolymer blends (Table 1, Entry 1). Various P(I-co-S)₃ contents are visualized by different colors in an increasing order as visualized next to the image. Hence, the 0%_w sample refers to the non-blended P(I-co-S) copolymer and 100%_w to the P(I-co-S)₃ copolymer, respectively. Arrows indicate the positions of the Bragg reflections. Curves are shifted vertically for clarity.

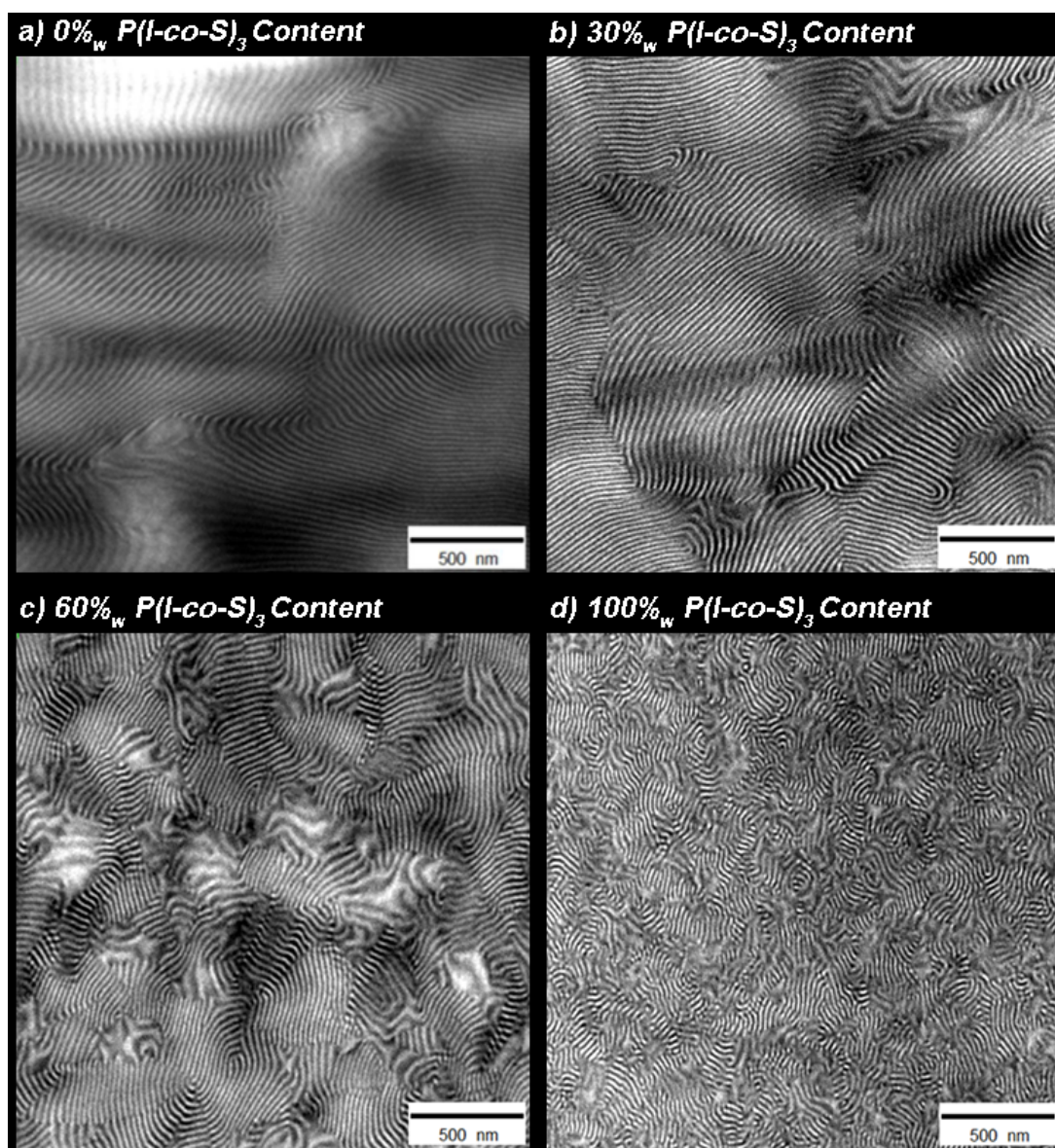


FIGURE S2 TEM images of P(I-co-S), P(I-co-S)/P(I-co-S)₃ blends and P(I-co-S)₃ (Table 1, Entry 1). The P(I-co-S)₃ content is a) 0%, a) 30%, a) 60%, a) 100% (Table 2, Entries 1, 5, 8 and 11), respectively. PI-rich phases are OsO₄ stained and appear electron opaque (dark).

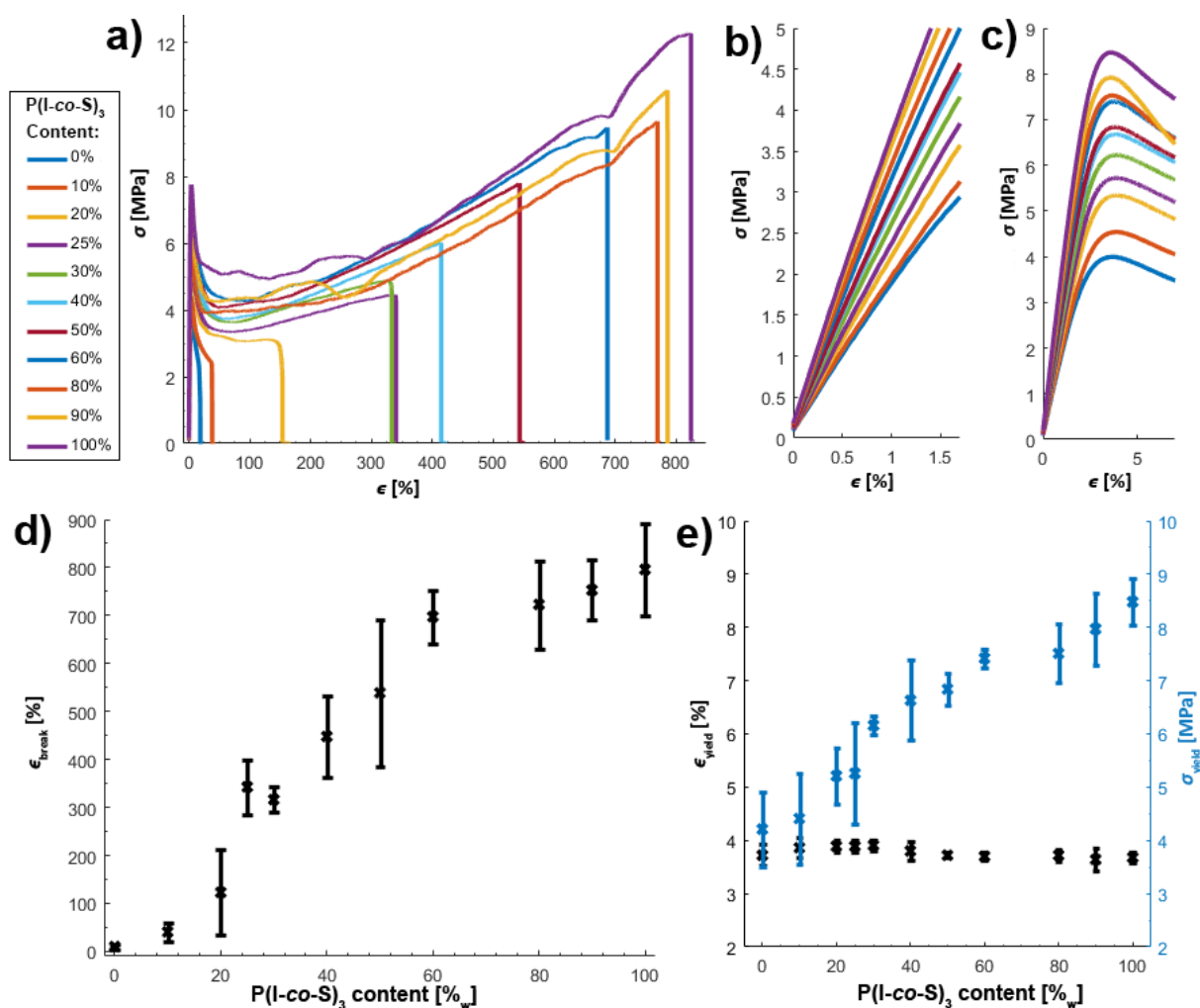


FIGURE S3 A) Representative stress-strain (σ - ϵ) diagrams for P(I-co-S), P(I-co-S)/P(I-co-S)₃ blends and P(I-co-S)₃ (Table 2). b) Linear elastic region ($\epsilon \approx 0 - 1.5\%$), used to determine the Young's modulus. The elastic moduli (E_{mod}) were determined as the slope of first order fits. c) Visualization of the yield points, which were determined as the local maximum $\sigma_{\text{yield}} = \sigma_{\text{max}}(\epsilon \approx 0 - 8\%)$ (see Figure S4b). d) Strain at break (ϵ_{break}) as a function of the P(I-co-S)₃ content. e) Yield Strain (ϵ_{yield}) and yield stress (σ_{yield}) as a function of the P(I-co-S)₃ content.

In contrast to the ϵ_{break} (Figure S3d), the toughness shows a comparably large increase for P(I-co-S)₃ contents > 60%. explained by large values of $\sigma(\epsilon)$ near ϵ_{break} .

Yield Points are also a function of the P(I-co-S)₃ content (Figure S3e). While the yield stress (σ_{yield}) correlates with the P(I-co-S)₃ content, the yield strain does not show significant changes ($\epsilon_{\text{yield}} = 3.8\% \pm 0.1$). The increase in σ_{yield} can be explained by an increasing force required to break the glassy PS domains.² Similar effects are observed by Spontak *et al.* and ascribed to an increased architecture-enhanced microstructural interconnectivity (i.e. number of bridges).³ In this work, this effect is probably also a function of the glass transition temperature of the

PS-rich phase, showing comparably larger values for $P(I-co-S)_3$ ($T_{g,PS-rich} \approx 90$ °C) compared to $P(I-co-S)_1$ ($T_{g,PS-rich} \approx 80$ °C).¹

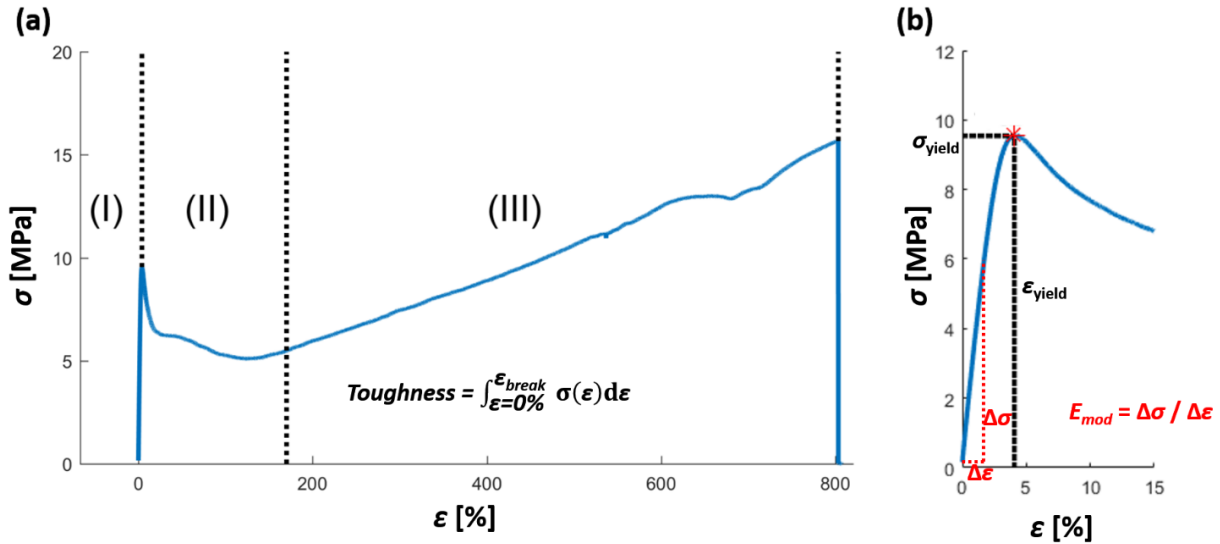


FIGURE S4 a) A typical stress-strain diagram, which is obtained for the multiblock copolymers investigated in this work. (I) Elastic regime, (II) Necking regime, (III). Strain-hardening regime. Stretching the sample in regime (I), leads to a reversible recovery of the material. Further stretching of the sample (regime II and III) also leads to irreversible viscous flow and only partial recovery of the material. The toughness is obtained by numeric integration of $\sigma(\epsilon)$. b) The yield point is obtained as the local maximum at low strains. The elastic modulus is determined as the slope of the first order fit in the linear region of $\sigma(\epsilon)$.

B. Effect of the Tapered Multiblock Copolymer Miscibility: AB/(AB)_n Blends

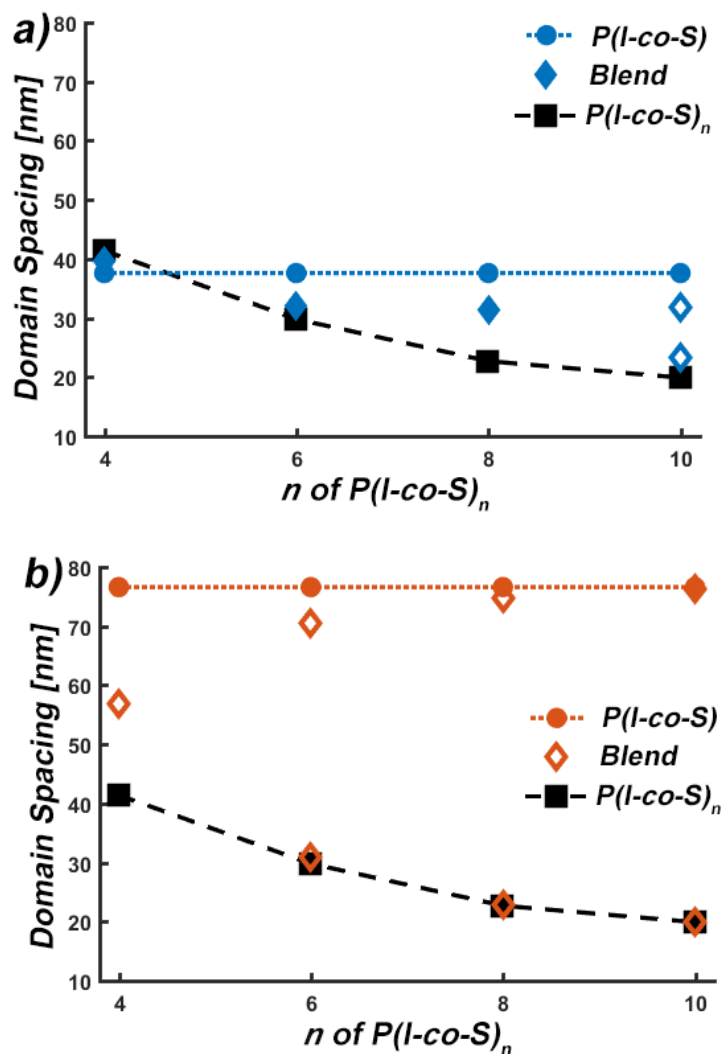


FIGURE S5 Overview of domain sizes observed in scattering results. Blend series with a) $d_{P(l-co-S)} = 38$ nm leading to $\Delta d = -4 - 18$ nm (Table 3 Entry 2) and b) $d_{P(l-co-S)} = 77$ nm leading to $\Delta d = 35 - 57$ nm (Table 3 Entry 3) are given. The domain sizes of the respective $P(l-co-S)$ copolymer are visualized as a colored, dotted line in both plots. The domain sizes of the $P(l-co-S)_n$ copolymers are visualized as black squares as a function of n . Points of the $P(l-co-S)$ and $P(l-co-S)_n$ copolymer are interconnected by lines to guide the eye. Blend samples are visualized as diamonds; open symbols indicate macrophase separation.

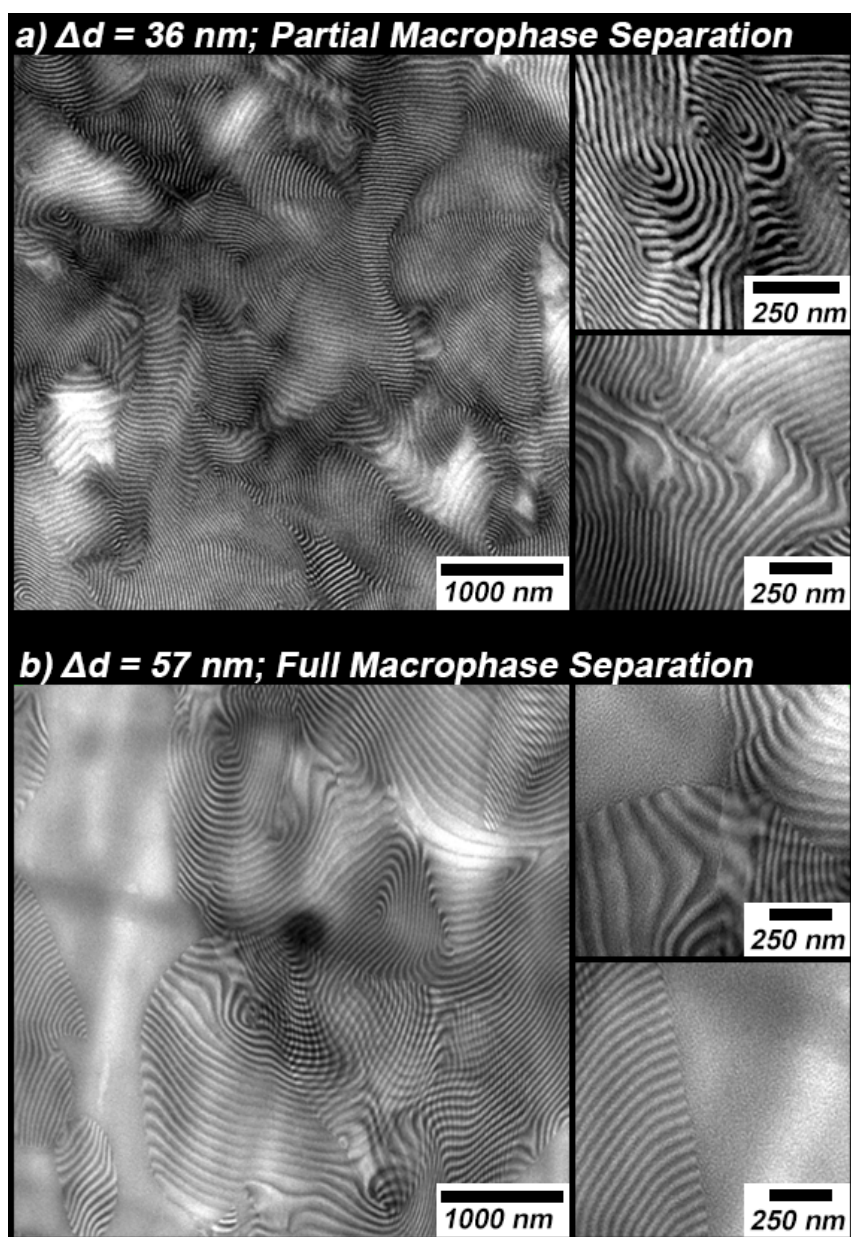


FIGURE S6 TEM measurements of a) P(I-co-S)/P(I-co-S)₂ blend (Table 1 Entry 3.1) and b) P(I-co-S) / P(I-co-S)₅ blend (Table 1 Entry 3.4). PI-rich phases are OsO_4 stained and appear electron opaque (dark).

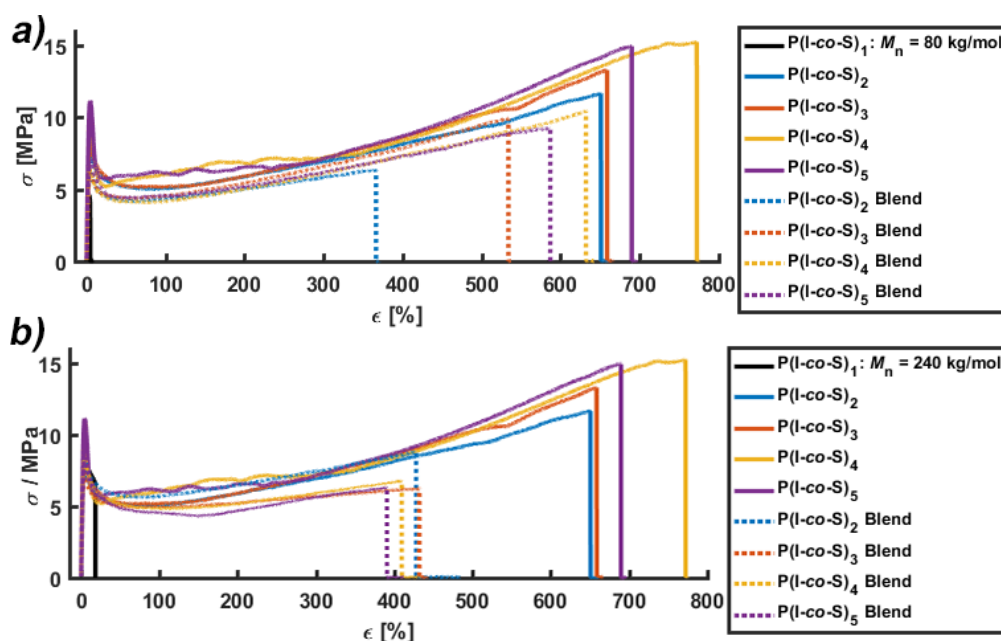


FIGURE S7 Representative stress-strain (σ - ε) diagrams for two P(I-co-S)/P(I-co-S) $_n$ blending series with diverging domain sizes for $n = 2$ -5. a) $\Delta d = -4$ to 18 nm (Table 1; Entry 2); b) $\Delta d = 36$ to 57 nm (Table 1; Entry 3).

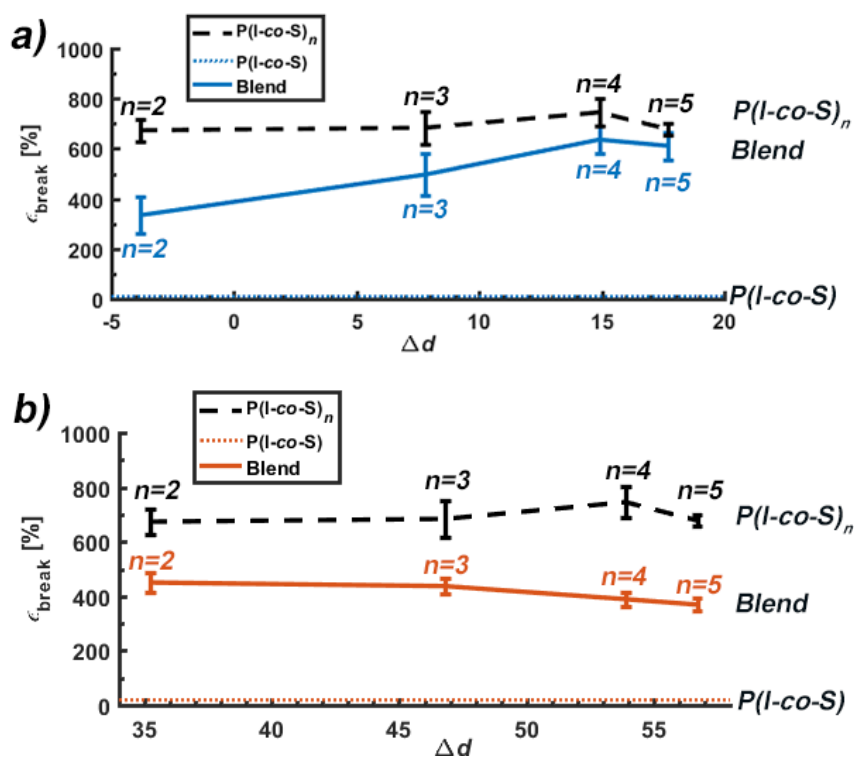


FIGURE S8 The strain at break of P(I-co-S) (dashed line), P(I-co-S) $_n$ (dotted line) and the respective blendblends (straight line) as a function of Δd . a) blending series with $\Delta d = -4$ - 18 nm (blue; Table 1 Entry 2 and Figure 6 left), b) $\Delta d = 35$ - 57 nm (red; Table 1 Entry 3 and Figure 6 right). The values are interpolated as a guideline for the eye.

TABLE S1 Mechanical data of P(l-co-S) and P(l-co-S)_n copolymers (cf. Table 1) determined via tensile testing. Errors are given as the standard deviation (σ intervall) from 8-15 independent drawing experiments.

Entry	Tapered Copolymer	$M_{n,target}$ [kg/mol]	ϵ_{break} [%]	Toughness [J/m ³]	$T_{g,PI-rich}$ ^{a)}	$T_{g,PS-rich}$ ^{a)}
1	P(l-co-S)	80	10 ± 5.0	0.33 ± 0.15	-37 ± 12	80 ± 11
2	P(l-co-S)	240	19 ± 1.8	1.4 ± 0.12	-40 ± 8	102 ± 8
3.1	P(l-co-S) ₂	240	670 ± 45	51 ± 7.4	-40 ± 4	99 ± 12
3.2	P(l-co-S) ₃	240	680 ± 65	55 ± 9.9	-37 ± 6	91 ± 18
3.3	P(l-co-S) ₄	240	750 ± 56	65 ± 7.8	-36 ± 6	82 ± 16
3.4	P(l-co-S) ₅	240	680 ± 22	57 ± 5.2	-33 ± 8	74 ± 15

a) The first derivative of the heat flow is given in a previous work.¹

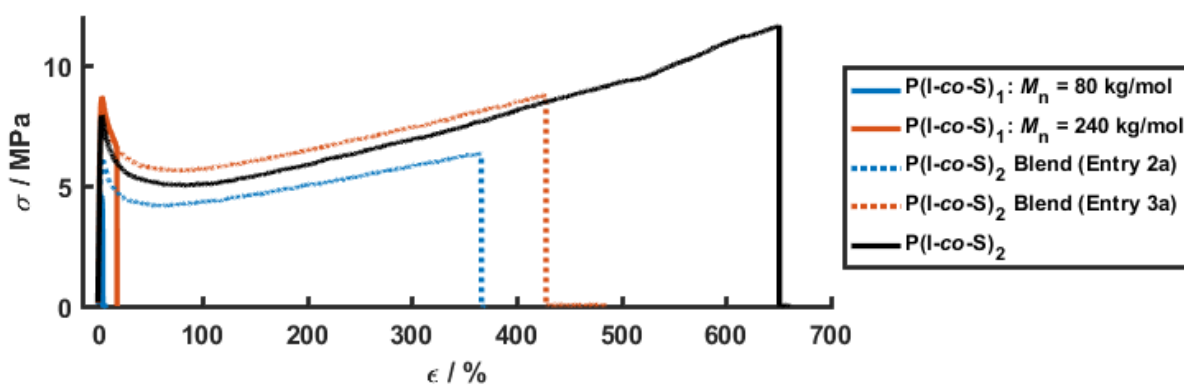


FIGURE S9 Representative stress-strain (σ - ϵ) diagrams for two P(l-co-S)/P(l-co-S)₂ blends (Table 1 Entry 2.1 and 3.1) as well as the respective P(l-co-S) and P(l-co-S)₂ copolymers.

REFERENCES

References

- (1) Steube, M.; Johann, T.; Galanos, E.; Appold, M.; Rüttiger, C.; Mezger, M.; Gallei, M.; Müller, A. H. E.; Floudas, G.; Frey, H. *Macromolecules* **2018**, 51 (24), 10246–10258. DOI: 10.1021/acs.macromol.8b01961.
- (2) Long, D.; Sotta, P. *Rheol Acta* **2007**, 46 (8), 1029–1044. DOI: 10.1007/s00397-007-0187-6.
- (3) Smith, S. D.; Spontak, R. J.; Satkowski, M. M.; Ashraf, A.; Heape, A. K.; Lin, J. S. *Polymer* **1994**, 35 (21), 4527–4536. DOI: 10.1016/0032-3861(94)90798-6.

CHAPTER 4

NEAR-INFRARED PROBING AND TEMPERATURE
EFFECTS ON COPOLYMERIZATION KINETICS

CHAPTER 4

Published in *Macromolecules*, 2019. DOI: 10.1021/acs.macromol.9b01790

Kinetics of Anionic Living Copolymerization of Isoprene and Styrene using *in situ* NIR Spectroscopy: Temperature Effects on Monomer Sequence and Morphology

Marvin Steube^{‡1}, Tobias Johann^{‡1}, Martina Plank², Stefanie Tjaberings³,
André H. Gröschel³, Markus Gallei⁴, Holger Frey¹ and Axel H.E. Müller^{1*}

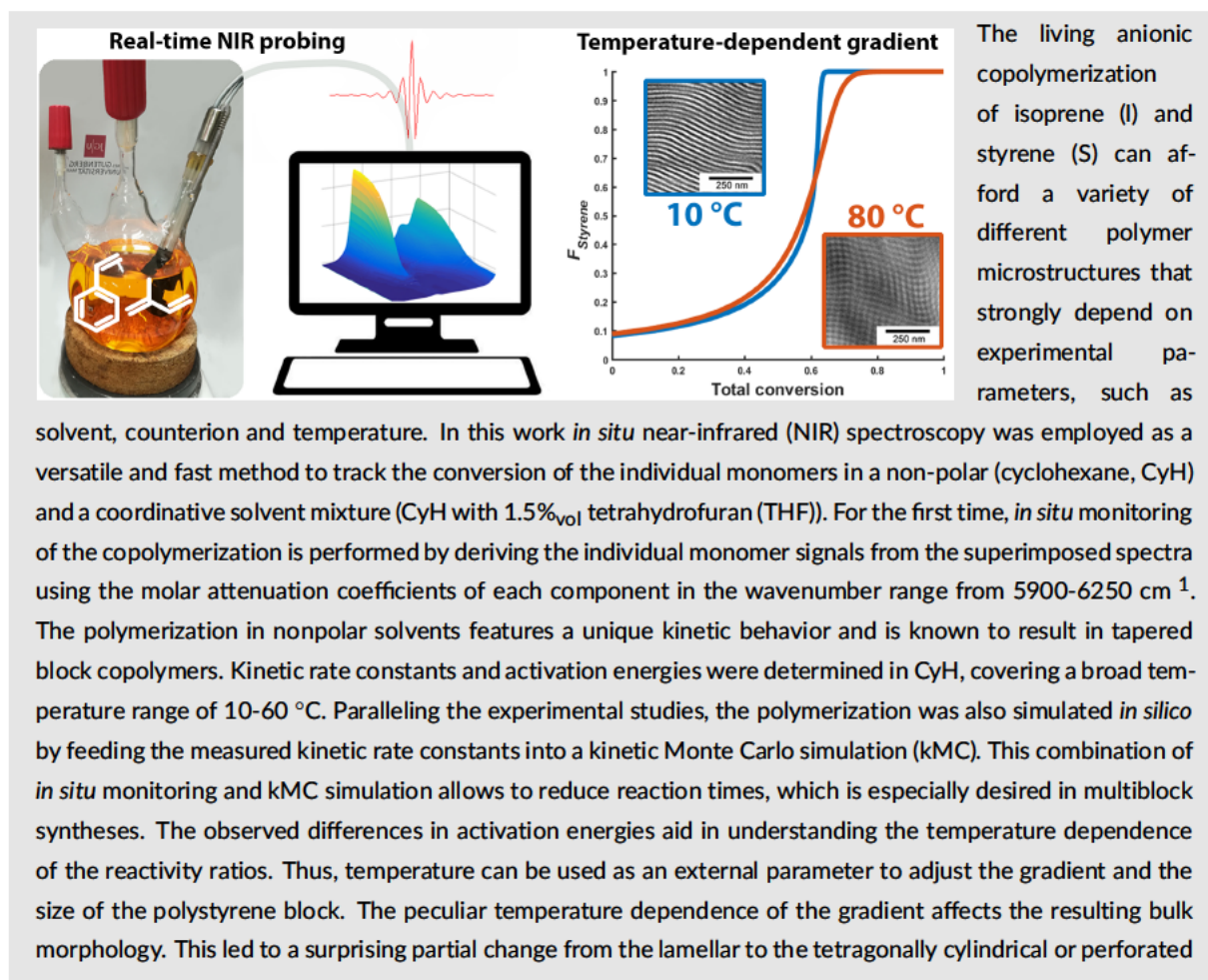
¹Institute of Organic Chemistry, Johannes Gutenberg-University, Duesbergweg 10-14, 55128 Mainz, Germany

²Macromolecular Chemistry Department, Technische Universität Darmstadt, Alarich-Weiss Str. 4, 64287 Darmstadt, Germany.

³Physical Chemistry, University of Duisburg-Essen, Carl-Benz-Str. 199, 47057 Duisburg, Germany

⁴Chair in Polymer Chemistry, Saarland University, 66123 Saarbrücken, Germany

[‡]Equally contributing authors.



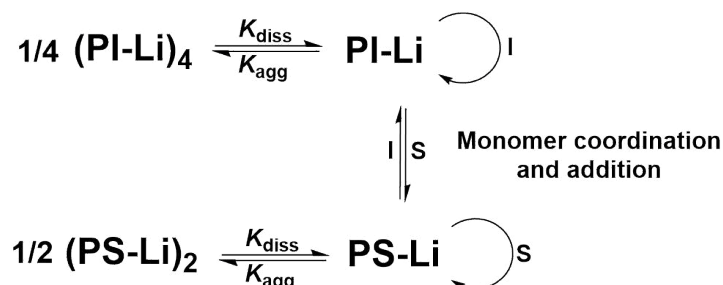
lamellar structure at the identical isoprene/styrene composition, only caused by a change of the polymerization temperature. *In situ* NIR probing is established as a fast and accurate method for real-time copolymerization monitoring that enables tracking complex copolymerization procedures, such as multiblock formation with a temporal resolution exceeding current standards set by ^1H NMR kinetics.

INTRODUCTION

The self-assembly of block copolymers represents a well-known key strategy to combine the inherent properties of different polymers in one material and may be considered to be the most relevant supramolecular concept in polymer science.¹ The direct, *i.e.* statistical living anionic copolymerization of 1,3-dienes with styrene can be utilized to generate different monomer sequences, combined with high molecular weights and low dispersity, exceeding the entanglement molecular weight² by far. This is a precondition to obtain mechanically tough materials. The synthesis of high-molecular-weight ABA triblock copolymers possessing A-blocks with a high glass-transition temperature, T_g , is highly established on the industrial scale to obtain phase-segregated thermoplastic elastomers.^{3,4}

When initiating the statistical copolymerization of 1,3-butadiene (B) and styrene (S) with *sec*-butyllithium in nonpolar solvents, tapered blocklike structures can be obtained in a one-step reaction. This is due to the highly disparate reactivity ratios ($r_B \approx 20$, $r_S \approx 0.05$) leading to preferential incorporation of butadiene early in the polymerization.⁵ In this polymerization, the anionic polymer chain ends form lithium aggregates, which are in equilibrium with the deaggregated polymer species (scheme 1). It is generally believed that the nonaggregated lithium species add monomer via lithium coordination,⁶ resulting in the exceptional kinetic feature of the preferential 1,3-diene incorporation in apolar media. First descriptions of this phenomenon were given by Korotkov,^{5,7} followed by several in-depth studies from Kuntz,⁸ Childers,⁹ and others.^{6,10,11} A very similar behavior is known for the isoprene/styrene system.¹²⁻¹⁶ A quantitative interpretation can be given by the comparison of homo- and cross-propagation rate constants. Although isoprene exhibits a lower homopropagation rate constant, k_{II} , than styrene, k_{SS} , isoprene is preferentially incorporated in the polymer chain at first, and polyisoprene segments are only rarely interrupted by single styrene units. While the polymerization proceeds, the decreasing concentration of isoprene favors the incorporation of styrene units into the polymer chain, finally resulting in a pure polystyrene block.¹⁴ This observation can be explained by a closer look at the cross-propagation rate constants, which strongly favor isoprene as the living chain end ($k_{SI} \gg k_{IS}$).

SCHEME 1 Reaction Mechanism for the Living Carbanionic Copolymerization of Styrene and Isoprene.
 $K_{\text{diss/agg}}$: Equilibrium constant of dissociation/aggregation.



While first-order kinetics are found for both monomers, the kinetic order of initiation and propagation differs due to the aggregation number, N_{agg} , of the respective lithiated monomer unit at the chain end (Eq. 1.1 and 1.2).

$$-\frac{d[\text{Ini}]}{dt} = k_{\text{ini}} [\text{M}] [\text{Ini}]_0^{\frac{1}{N_{\text{agg, initiator}}}} \quad (1.1)$$

$$-\frac{d[\text{M}]}{dt} = k_{\text{p}} [\text{M}] [\text{Ini}]_0^{\frac{1}{N_{\text{agg, chain end}}}} \quad (1.2)$$

The rate constants include the corresponding aggregation equilibrium constants (see also Supporting Information Section 7.1). This simplification enables a facile treatment of the complex aggregation-deaggregation equilibria. A fast initiation reaction is required to kinetically separate chain initiation and propagation,¹⁷ which would otherwise lead to undesired broadening of the molecular-weight distribution approaching a value of 1.33, as predicted by Gold.¹⁸ An aggregation number of $N_{\text{agg}} = 4$ has been determined for *sec*-butyllithium (*sec*-BuLi) in cyclohexane and benzene,¹⁹⁻²¹ which is the initiator of choice for fast initiation of styrene and 1,3-dienes.²² The formation of dimers ($N_{\text{agg}} = 2$) is generally accepted for polystyryllithium in aliphatic and aromatic hydrocarbon solvents.^{20,23-27} For polyisoprenyllithium controversial results led to discussions, whether dimeric or tetrameric species are involved.^{28,29} In-depth reviews of the results were provided by Fetters, Bywater, and Müller.²⁹⁻³² Worsfold and Bywater reported a gradual change in the aggregation number from tetramers to dimers in dependence of the chain end concentration, leading to dimers with decreasing initiator concentration on the order of

$$[Ini] \approx 10^{-3} - 10^{-6} \text{ mol L}^{-1}.^{12,31}$$

A first estimation of reactivity ratios was given as early as 1962 by Korotkov *et al.* ($r_1 \approx 7$, $r_5 \approx 0.14$) by determining the styrene content of the copolymers at different stages of the copolymerization.¹⁵ A few years later, Onsager¹⁶ and Worsfold¹² discussed the relevance of aggregation phenomena for the kinetic order. Additionally, reactivity ratios were reexamined by Worsfold ($r_1 = 14.4$, $r_5 = 0.045$) via *in situ* measurements, taking advantage of the UV signal of polystyryllithium. In 1990, Miller *et al.* investigated the microstructure and composition of polymers based on styrene and butadiene via near-infrared (NIR) spectroscopy.³³ Overtone and combination vibrations were assigned to polystyrene and polybutadiene in a broad spectral range. In a fundamental work, Long *et al.* established the principle of *in situ* near-infrared probing, allowing to monitor the time-dependent combined monomer conversion of isoprene and styrene in cyclohexane and THF.³⁴ For this purpose, the absorbance at 6158 cm^{-1} was interpreted as the excitation of the vinyl C-H bonds of isoprene and styrene as well as of polyisoprene and polystyrene. Unfortunately, an overlap of these individual absorption bands did not allow for determination of the respective concentrations and therefore prohibited the simultaneous determination of rate constants for this statistical copolymerization. Since *in situ* mid-IR spectroscopy is also known as a reliable method for real-time monitoring of copolymerizations,^{35,36} Fontanille and co-workers investigated the copolymerization of styrene and isoprene by taking advantage of the different spectral range, leading to nonoverlapping monomer signals.¹³ The setup was supplemented by a UV-visible probe allowing to monitor changes in the concentrations of polyisoprenyllithium and polystyryllithium chain ends. The homo- and cross-propagation constants reported by Fontanille are in agreement with the results of Worsfold, both taking into account tetrameric aggregates for isoprene and dimeric aggregates for styrene based on the kinetic order dependences of the active chain ends as well as light scattering experiments reported by Worsfold.^{12,20} In addition, temperature dependences were examined by Fontanille *et al.*. Various aromatic solvents showed a higher activation energy for the homopolymerization rate constant of isoprene, k_{II} , compared to the other rate constants k_{SS} , k_{SI} , and k_{IS} . However, consequences for the temperature dependence of reactivity ratios were not discussed.

A detailed understanding of the gradient structure is indispensable to tailor the thermal and mechanical properties.^{14,37-44} From the disparate activation energies in benzene, the question arose, how a simple change of the polymerization temperature changes the gradient structure. Additionally, short reaction times are desired from an industrial point of view. In this case, *in situ* NIR spectroscopy is often the method of choice, due to the experimental simplicity combined with low cost and high time resolution of about 4 ms. Additionally, reactions can be monitored directly on a large scale to ensure the formation of the desired polymer structure and thus prod-

uct quality. For a detailed discussion on selecting the most suitable method for following the kinetics of carbanionic copolymerizations, see Supporting Information Section 3.

In this work, we present the *in situ* monitoring of individual concentrations of isoprene and styrene in cyclohexane and the determination of reactivity ratios for styrene and isoprene by applying real-time near-infrared spectroscopy. Following this approach, the temperature dependence (providing activation energies) of the homo- and cross-propagation steps was determined and found to affect the gradient structure of the statistical copolymers in a systematic way. Furthermore, the reaction time up to 99.5% conversion was evaluated, which is crucial to minimize the reaction times of each reaction step in the preparation of tapered multiblock structures.^{4,41} Based on these measurements, the differences in monomer sequences were investigated by kinetic Monte Carlo (kMC) simulation striving for a fundamental understanding of the temperature-dependent copolymerization kinetics of styrene and isoprene. Finally, the tapered block copolymers obtained at various temperatures were compared with regard to the monomer sequence, the regioisomeric structure of the polyisoprene units, the length of the polystyrene block, thermal behavior, and the resulting microphase-separated bulk morphology.

EXPERIMENTAL SECTION

A detailed description is found in Supporting Information Sections 1 and 2.

RESULTS AND DISCUSSION

The main difficulty of monitoring a living anionic copolymerization via NIR real-time probing is the overlap of the absorption bands of both monomers, styrene (S) and isoprene (I), which formed repeating units of the polymers, polystyrene (PS) and polyisoprene (PI), respectively. In this work, we focused on the data evaluation of NIR spectroscopy to establish this real-time method as a fast and versatile choice (see Supporting Information Section 4 and Table S1 for detailed discussion). Applying this method, we investigated the statistical copolymerization of isoprene and styrene at different temperatures.

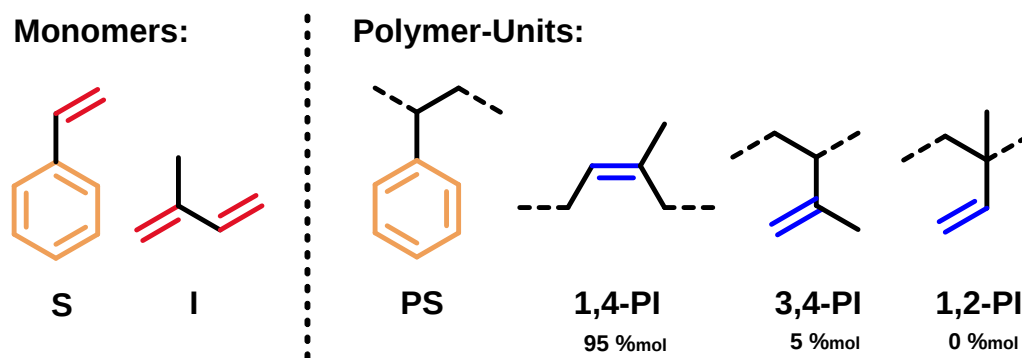
As experimental setup, an NIR probe was attached to a 1 L glass reactor via an additional joint (Figure S1, Supporting Information). The same type of glass reactor was used for earlier experiments, allowing multiple additions of different monomers or monomer mixtures to generate

copolymers of up to 400 kg mol^{-1} on a $>100 \text{ g}$ scale.⁴¹ We emphasize that using NIR monitoring, the evaluation of *in situ* kinetic experiments and materials properties is performed on the very same batch. Therefore, uncertainties in initiator concentration become evident from non-correlation of kinetic parameters as well as characterization studies like NMR and size exclusion chromatography (SEC) (see polymer discussion below).

Conversion of Raw NIR Data to Time-Concentration Data.

The foundation for all kinetic evaluations are time-concentration correlations. Due to the excitation of overtone and combination vibrations, the evaluation of NIR data is not straightforward. As reported by Long *et al.* in 1993, styrene and isoprene show overlapping NIR spectra in the range from $5800\text{-}6300 \text{ cm}^{-1}$ with a maximum of the molar attenuation coefficient at 6158 cm^{-1} .³⁴ In this work, the evaluation of the results was stated to be impeded by the additional overlap of the absorption bands of polyisoprene and polystyrene, which arise during the polymerization (Scheme 1). Thus, in this fundamental work only the course of absorption at 6158 cm^{-1} was used for evaluation, and therefore, only the combined total monomer conversion was obtained. To determine the individual monomer concentrations at any reaction time, we considered the molar attenuation coefficients of all reagents and reaction products over the full range from 5900 cm^{-1} to 6250 cm^{-1} (Scheme 2 and Figure 1). The percentage values in Scheme 1 denote the typical isomer distribution of PI obtained via living anionic polymerization in cyclohexane at $40 \text{ }^\circ\text{C}$. The double bonds highlighted in red correspond to absorption bands, which decrease during the course of the polymerization, while the bonds highlighted in blue are formed and thus overlap with the monomer absorption bands.³⁴ The aromatic system of S and PS (orange bonds) is unaltered during polymerization, and thus, the corresponding absorption bands are altered less significantly.

SCHEME 2 Reagents (S, I) and Reaction Products (PS, PI) during Polymerization.



Considering the determined molar attenuation coefficients, a significant difference within all spectra can be seen (Figure 1). Surprisingly, the overall contribution of polyisoprene is rather negligible compared to polystyrene, which was not quantified in the work of Long and co-workers.³⁴ To account for both PI and PS and to derive the individual monomer concentrations, two prerequisites are necessary:

- (i) The assumption that the complex absorption spectra obtained during measurement can be generated via a linear combination of the individual components for all wavenumbers (eq. S1.1).
- (ii) All reaction components need to exhibit significant differences within the molar attenuation coefficient over the desired spectral range (Figure 1.)

Based on these conditions and the known molar attenuation coefficients, the individual concentrations can be determined by simultaneously solving the linear equation system (eq. S1, see Supporting Information Section 4 for a detailed description).

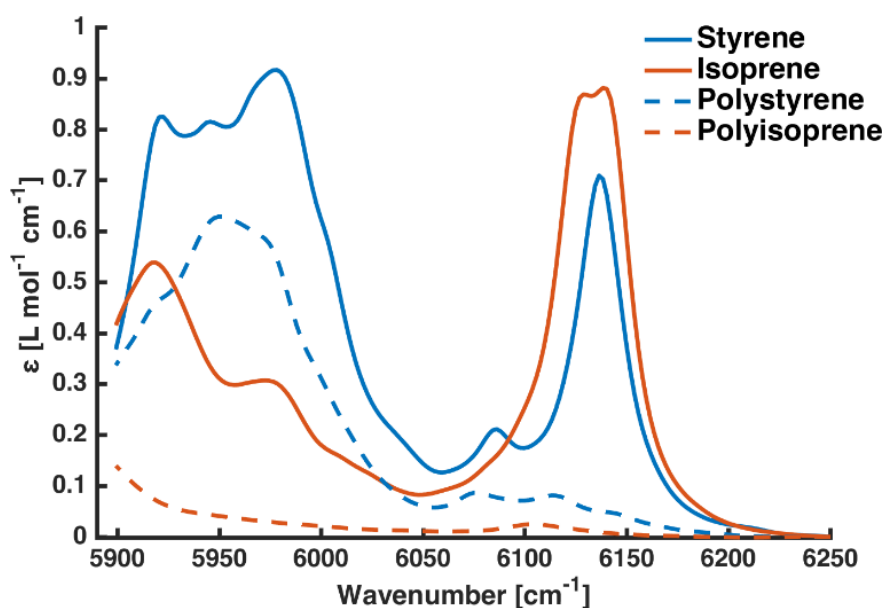


FIGURE 1 Molar attenuation coefficients of all reagents (S, I) and reaction products (PS, PI) during polymerization. The molar attenuation coefficient of polyisoprene represents the typical isomer mixture obtained in cyclohexane (95% 1,4, 5% 3,4). For full list of all ϵ values see Table S10.

This linear equation system (184 equations, 1.9 cm^{-1} data interval) was solved for each recorded NIR spectrum (between 600 and 12000 spectra, typically 4 s per spectrum), and finally the individual absolute monomer concentrations were determined, which are the foundation for further kinetic evaluation.

Determination of k_{SS} and k_{II} from Homopolymerization Kinetics.

Homopolymerization rate constants, k_{SS} and k_{II} , were determined by following the time-dependent monomer conversion of styrene and isoprene polymerization, respectively, via the described approach. Monomer conversion in the homopolymerization of both monomers follows first-order kinetics; thus, linearization can be achieved by plotting the logarithmic concentration versus time in which the slope yields the apparent polymerization rate constant, k_{app} (Eq. 2, Table S2, Figures S2-3).

$$\ln\left(\frac{[M]}{[M]_0}\right) = -k_{SS/II}^{app} \cdot t \quad (2)$$

This apparent value must be divided by the initiator concentration weighted by the aggregation number (e.g., $[\text{BuLi}]_0^{1/4}$ for isoprene, $[\text{BuLi}]_0^{1/2}$ for styrene) to obtain the effective rate constants, $k_{SS/II}$ (Table S2). These effective rate constants contain the corresponding aggregation-deaggregation equilibria constants (see Supporting Information Section 7, eqs S2.23, S2.26). This enables a facile calculation of the reaction rates by combining the aggregation equilibrium constant, K_{agg} (which is not known) and the absolute rate constant to obtain the effective rate constant. Hence, complex individual treatment of the aggregation phenomena can be omitted by this approach. To investigate the temperature dependence of k_{SS} and k_{II} , (see Supporting Information Section 5), each homopolymerization was started at 10 °C, and then subsequently the temperature was increased by 5 °C steps up to 45 °C (Figure 2).

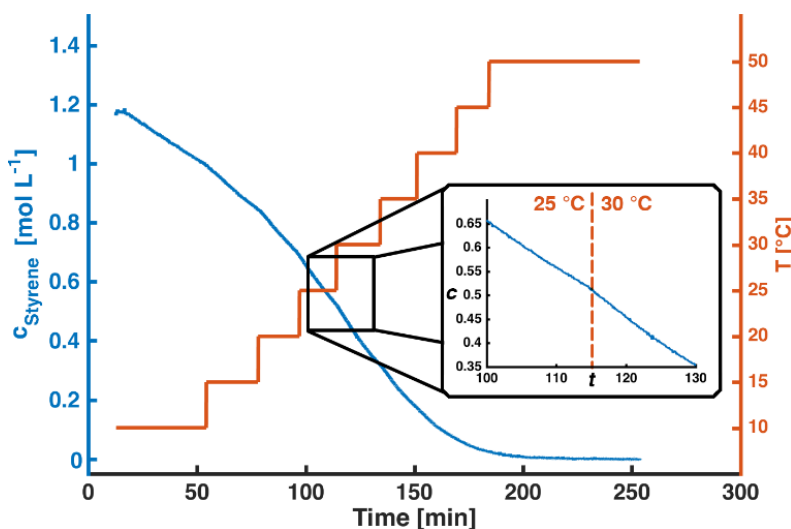


FIGURE 2 Plot of styrene concentration (blue; for isoprene, see Figure S4b) during polymerization with stepwise increased temperature (red).

Each temperature plateau was kept for at least 15 min to ensure temperature equilibrium in the reaction flask. This equilibrium time was previously tested to be achieved in less than 5 min. The determination of several homopropagation rate constants within one experiment eliminates statistical inaccuracies otherwise caused by initiator dosing. Volume changes due to the temperature-dependent densities of cyclohexane were corrected in all calculations. Size exclusion chromatography (SEC, Figure S5) reveals a monomodal distribution for both polymerizations. Using a 1,4-PI or PS calibration for the respective homopolymer, a low dispersity ($\bar{D} \approx 1.05$) and a molecular weight within 5% of the theoretical value were observed. Since it is indispensable for subsequent NMR studies, the homopolymers were also investigated via ^1H , ^{13}C , and two-dimensional (2D) NMR spectroscopy (Figures S6-S7). All signals of the atactic polystyrene could be assigned. The evaluation of the signals in the NMR spectra of polyisoprene is rather complex, due to the presence of different isomers (*cis*-1,4, *trans*-1,4, 3,4), as discussed in detail in the Supporting Information (Section 6.1). Due to the high rate of monomer consumption at elevated temperatures, homopolymerization rate constants at 50 and 60 °C were determined within an additional experiment by employing four sequential monomer additions in the synthesis of a tetrablock copolymer (Figure S8). As discussed before, the SEC analysis (Figure S9) shows a monomodal, narrow molecular weight distribution ($\bar{D} \approx 1.06$) and a molecular weight error within 5% of the average M_n value.

Determination of k_{IS} and k_{SI} from Copolymerization Kinetics.

As an example, Figure 3 shows the time-conversion plots of the statistical copolymerization of styrene and isoprene at 50 °C. As expected, isoprene is incorporated preferentially in the first stage of the copolymerization. When isoprene is fully consumed, the homopolymerization of styrene proceeds with a simultaneous acceleration of the polymerization. As already shown by Worsfold¹² and Fontanille,¹³ this is based on the preferential addition of isoprene to polyisoprenyllithium chain ends. Crossover reaction to styrene under these conditions is less likely until no isoprene is left. Only then the styrene homopolymerization proceeds, which is faster than the actual isoprene homopolymerization ($k_{SS} > k_{II}$ but $k_{IS} \ll k_{SI}$), thus copolymerization behavior is controlled by crossover rate constants and barely influenced by the homopolymerization rate constants. This proves the utmost importance of considering the individual rate constants instead of merely the reactivity ratios for a detailed understanding of this crossover-controlled copolymerization, as explored in previous studies.¹⁴

Multiple copolymerizations of isoprene and styrene were monitored via NIR spectroscopy varying the temperature from 10 °C up to 60 °C in 10 °C steps to obtain P(I-co-S) tapered diblock copolymers. All polymerizations showed quantitative conversion (Figures S10 and S11) with

narrow molecular weight distributions ($\bar{D} \approx 1.08 \pm 0.01$, Table 1). The nearly perfect overlap of the SEC eluograms (Figure 4) evidences precise control of the molecular weight with values ($M_n = 79.2 \pm 0.8 \text{ kg mol}^{-1}$, Table 1) close to the targeted molecular weight of 80 kg mol^{-1} . The commonly used PS standards are found to overestimate the M_n by $\approx 10\%$ with an nonsignificant narrowing of the polydispersity ($\Delta\bar{D} \approx 0.01$). This is also observed for 50%_{mol} PI/PS tapered multiblock copolymers (vide infra).⁴¹ Hence, the targeted molecular weights were achieved and possible errors caused by dosing or irreversible termination of the initiator can be ruled out.

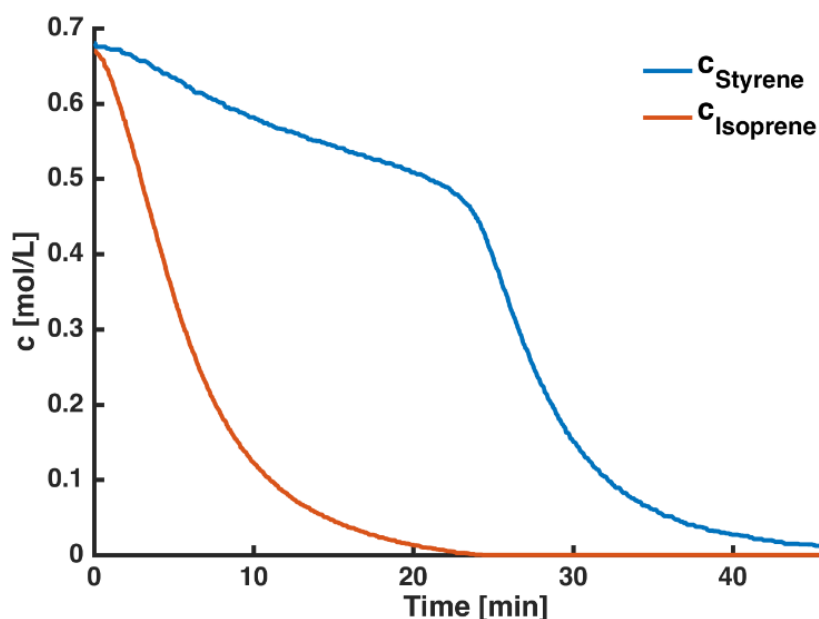


FIGURE 3 Individual monomer concentrations determined via the linear equation system (eq S1.4) in the styrene/isoprene copolymerization at 50°C . The upper time limit of the time axis correlates with 99.5% total styrene conversion. $[\text{BuLi}]_0 = 1.43 \text{ mmol L}^{-1}$.

In contrast to the direct determination of k_{SS} and k_{II} from simple homopolymerization experiments, the evaluation of the cross-propagation rate constants, k_{IS} and k_{SI} , by fitting them to the time-conversion plots is not straightforward, which is due to numerical problems. Consequently, we chose to determine the reactivity ratios, $r_S = k_{SS}/k_{SI}$, $r_I = k_{II}/k_{IS}$, for each temperature separately (Table 1), from which the cross-propagation rate constants were then calculated.

Reactivity ratios were calculated using the Meyer-Lowry formalism (eq. S2.42, Figure S12 and S13, Table S3).⁴⁵ This integrated form of the Mayo-Lewis equation omits the calculation of the monomer incorporation, F , necessary for evaluation via Mayo-Lewis, Fineman-Ross or Kelen-Tüdös formalism (see Supporting Information Section 7.1).

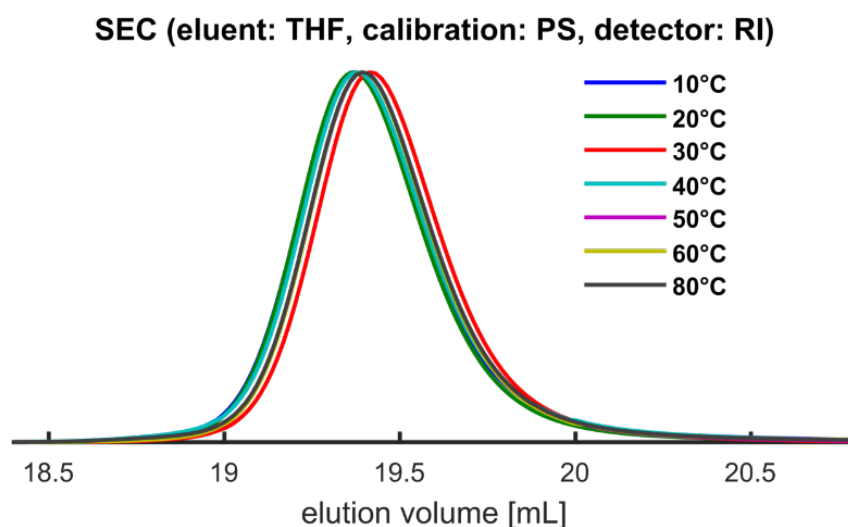


FIGURE 4 SEC traces (THF, RI detector) of the P(I-co-S) tapered diblock copolymers, prepared at different reaction temperatures. The nearly perfect overlap of the traces confirms control of the molecular weight and the initiator concentration, which is essential for kinetic data evaluation. For molecular weights and dispersities, see Table 1.

TABLE 1 SEC Data, Initiator Concentrations, Reaction Times and Kinetic Data Obtained for the Prepared P(I-co-S) copolymers at Different Temperatures.^e

<i>T</i> [° C]	<i>M_n</i> ^a [kg/mol]	<i>D</i> ^a	[<i>Ini</i>] ₀ [mmol/L] ^b	<i>t</i> _{99.5%} [h] ^c	10 ⁻³ <i>k</i> _{II} [(L/mol) ^{0.25} ·s ⁻¹]	10 ⁻³ <i>k</i> _{SS} [(L/mol) ^{0.5} ·s ⁻¹]	10 ⁻³ <i>k</i> _{IS} [(L/mol) ^{0.25} ·s ⁻¹]	10 ⁻³ <i>k</i> _{SI} [(L/mol) ^{0.5} ·s ⁻¹]	<i>r</i> _I	<i>r</i> _S	<i>r</i> _I · <i>r</i> _S
10	80.0	1.10	1.57	48.3	0.12	1.79	0.0115	179	10.2	0.010	0.10
20	79.2	1.07	1.57	14.2	0.50	4.43	0.0496	341	10.1	0.013	0.13
30	77.9	1.07	1.56	5.38	1.47	10.9	0.132	644	11.2	0.017	0.19
40	78.8	1.09	1.59	2.30	3.81	23.2	0.348	799	10.9	0.029	0.32
50	78.8	1.08	1.52	0.79	10.9	65.2	1.10	1970	9.91	0.033	0.33
60	79.9	1.07	1.56	0.37	24.2	140	2.44	3580	9.93	0.039	0.39
80 ^d	79.7	1.08	1.56	n.d.	n.d.	n.d.	n.d.	n.d.	10.03 ^d	0.072 ^d	0.72 ^d

a) Values are based on an interpolated calibration curve based on PI and PS standards (see SI, Instrumentation Section).

b) [*I*]₀ ≈ 0.725 mol/L = 6.3%_w; [*S*]₀ ≈ 0.725 mol/L = 9.7%_w c) Time to reach 99.5% styrene conversion (Figure 5,

Figure S11). d) Heating the monomer mixture to 80 °C in a closed reaction flask leads to a high pressure due to the comparably low boiling point of isoprene (*T_b* = 34 °C). The used specialized glassware lacks pressure certification.

For that reason, the reaction flask was fully immersed in a water bath surrounded by splinter protection. No attempt was made to monitor the copolymerization at 80 °C. The given reactivity ratios are extrapolated based on the activation energies. e) See Table S2 for homopropagation rate constants at 15, 25, 35 and 45 °C and apparent homopropagation rate constants for all applied temperatures.

The determined homopropagation rate constants at 40 °C (Table 1) differ only slightly from the values reported by Fontanille (*k*_{SS,Ref} = 2.4 · 10⁻² [(L/mol)^{0.5} · s⁻¹], *k*_{II,Ref} = 3.2 · 10⁻³ [(L/mol)^{0.25} · s⁻¹]).¹³ While the rate constants at 40 °C reported by Fontanille are in

good agreement with the values of Worsfold we have found significant differences regarding the cross-propagation rate constants.^{12,13} The cross-propagation rate constant for the reaction of a polystyrenyllithium chain end with isoprene was reported to be significantly lower, $k_{SI,Ref} = 0.47 \text{ [(L/mol)}^{0.50} \cdot \text{s}^{-1}]$, compared to the value reported in this work (Table 1). The differences may be based on the different method of determination of the chain-ends via UV-Vis spectroscopy employed by Fontanille and co-workers. While our approach relies on the tracking of the monomer conversion in a closed system during the copolymerization of styrene and isoprene, the determination by UV-Vis spectroscopy is performed on a model reaction, tracking only the single step crossover by addition of isoprene to a polystyrylithium solution. Due to the high rate of this reaction ($t_{1/2} = 1.47 \text{ s}$ at $40 \text{ }^\circ\text{C}$), the rate constant might be underestimated by the determination via UV-Vis spectroscopy.

The calculated rate constants were used for a kinetic Monte-Carlo (kMC) simulation (Figure S11, see Supporting Information Section 9). In all cases, a good agreement of the results obtained *in silico* with the experimental NIR data was achieved. The relative mean deviation of the calculated reaction time required for 99.5% monomer conversion is 11%. This deviation is mainly based on the homopropagation rate constant of isoprene, k_{II} . Homo-propagation rates were measured in cyclohexane, while during the copolymerization a large fraction of styrene is present ($[S]_0 \approx 0.73 \text{ mol L}^{-1}$, corresponding to 11%_w). The presence of an aromatic monomer might interfere with the anionic coordination polymerization mechanism of isoprene, leading to a change of the homopropagation rate constants. Additionally, all kMC simulations have been performed with invariant aggregation numbers ($N_{agg} = 2$ (PS-Li); $N_{agg} = 4$ (PI-Li), eq. 1.2). However, the formation of mixed aggregates, which additionally may alter reaction kinetics, also occurs during the copolymerization, thereby leading to further deviation of the experimental results and the simulation.

Temperature Dependence of the Reactivity Ratios and Rate Constants.

As shown in Figure 5 the regression based on the Arrhenius equation shows an excellent linear correlation, and the calculated error (σ interval) is rather low. For the copolymerization of isoprene and styrene ($E_{A,II} = 81 \text{ kJ} \cdot \text{mol}^{-1}$; $E_{A,SS} = 67 \text{ kJ} \cdot \text{mol}^{-1}$) the activation energies are in accordance with the behavior in benzene reported by Fontanille ($E_{A,II} = 75 \text{ kJ} \cdot \text{mol}^{-1}$; $E_{A,SS} = 61 \text{ kJ} \cdot \text{mol}^{-1}$). In analogy, polymerization in cyclohexane also shows a higher activation energy for homopolymerization of isoprene compared to styrene ($\Delta E_A = 14 \text{ kJ} \cdot \text{mol}^{-1}$). However, both activation energies determined in cyclohexane in this work exhibit 5-6 $\text{kJ} \cdot \text{mol}^{-1}$ higher energy barriers compared to the values previously reported for benzene.

For the crosspropagation reactions, we determined the activation energies as $E_{A,IS} =$

$83 \pm 3 \text{ kJ} \cdot \text{mol}^{-1}$ and $E_{A,SI} = 46 \pm 5 \text{ kJ} \cdot \text{mol}^{-1}$. While a good correlation of the homo-propagation activation energies in cyclohexane and benzene is achieved, the determined cross-propagation activation energies differ from those in benzene reported by Fontanille *et al.*: $E_{A,IS} = 64 \text{ kJ} \cdot \text{mol}^{-1}$; $E_{A,SI} = 59 \text{ kJ} \cdot \text{mol}^{-1}$.¹³ The differences are ascribed to the different solvents and may also be influenced by the use of UV-Vis spectroscopy for the determination, as discussed above. CyH is a nonpolar solvent that cannot undergo π -interactions in contrast to benzene. Considering the lower dielectric constant of CyH, this might lead to a higher stability of the chain-end aggregates and thus to higher activation energies. A similar behavior was predicted by Morita and Van Beylen via density functional theory (DFT) calculations.⁴⁶ In their work, the energy of $(\text{PS-Li})_2$ dimer formation was correlated to the dielectric strength of the solvent (THF vs CyH; THF was simulated only via its dielectric properties and no direct coordination was modeled). They found significantly less stable dimers when THF was used for the simulation.

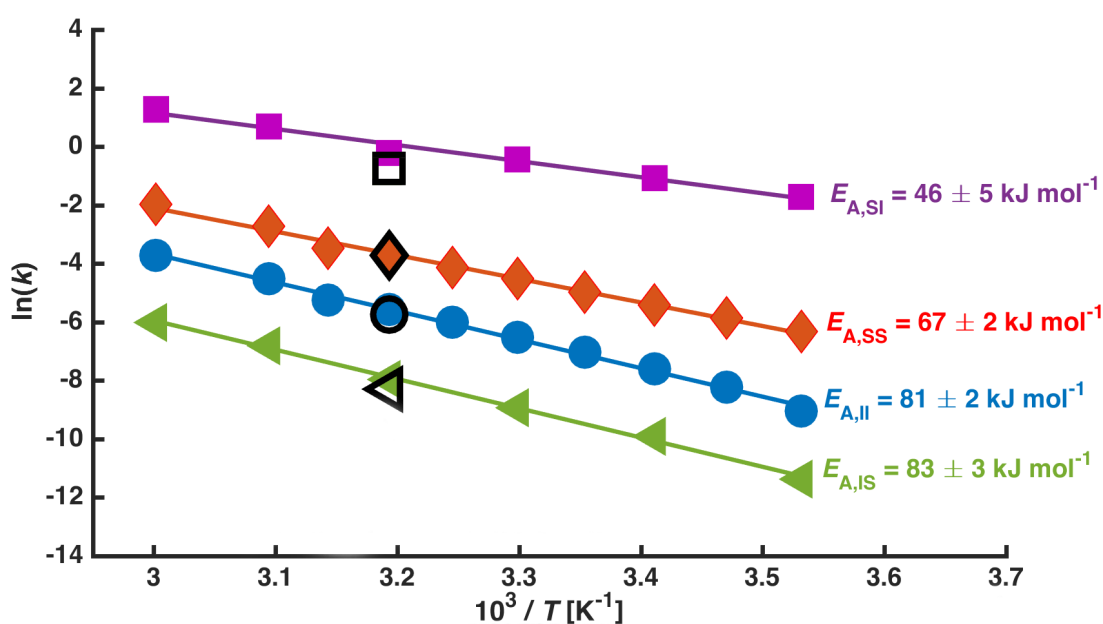


FIGURE 5 Arrhenius plots of all reaction steps involved in the homo- and cross-propagation in the copolymerization of styrene and isoprene in cyclohexane. The open symbols indicate rate constants determined by Fontanille *et al.* at 40 °C.¹³

Considering the polymerization mechanism in detail, the addition of a monomer unit (either styrene or isoprene) to a polyisoprenyllithium chain end exhibits an activation energy of more than $80 \text{ kJ} \cdot \text{mol}^{-1}$ in both cases. In contrast, the addition of either styrene or isoprene to a polystyryllithium chain end shows significantly lower reaction barriers ($\leq 67 \text{ kJ} \cdot \text{mol}^{-1}$). The activation energies are in line with the rate constants of the corresponding reaction.

The temperature dependence of the reactivity ratios and thus the change in polymer microstructure are mainly determined by the rate constant of the cross-propagation from polystyryllithium to isoprene, k_{IS} . Hence, only a subtle influence of the temperature on r_I can be seen (Table 1 and Figure S17a). The reactivity ratio of isoprene, r_I , slightly decreases with increasing temperature, leading to a higher amount of styrene in the isoprene-rich part. These findings are in contrast to the behavior in benzene reported by Fontanille. The activation energies reported for benzene as a solvent¹³ lead to the conclusion that with increasing temperature also $r_{I,Benzene}$ rises, while $r_{S,Benzene}$ is influenced less significantly. These differences can be explained by either the effect of benzene on the aggregation state of polyisoprenyllithium or on the respective transition states or the determination via UV-Vis spectroscopy as described above.

Interestingly, a significant effect of temperature on the reactivity ratio of styrene can be observed, when the copolymerization is performed in cyclohexane instead: here, r_S increases 4-fold from $r_S = 0.01$ at 10 °C to $r_S = 0.04$ at 60 °C (Figure S17b). As a direct result, the copolymerization becomes more ideal, *i.e.* less alternating ($r_I \cdot r_S \rightarrow 1$) (Figure S17c). Additionally, the steepness of the gradient decreases at higher reaction temperatures (Figures 6 and S17d). Thus, the polymer chain can be seen as consisting of an isoprene-rich gradient copolymer block ("gradient block") and a pure polystyrene block.

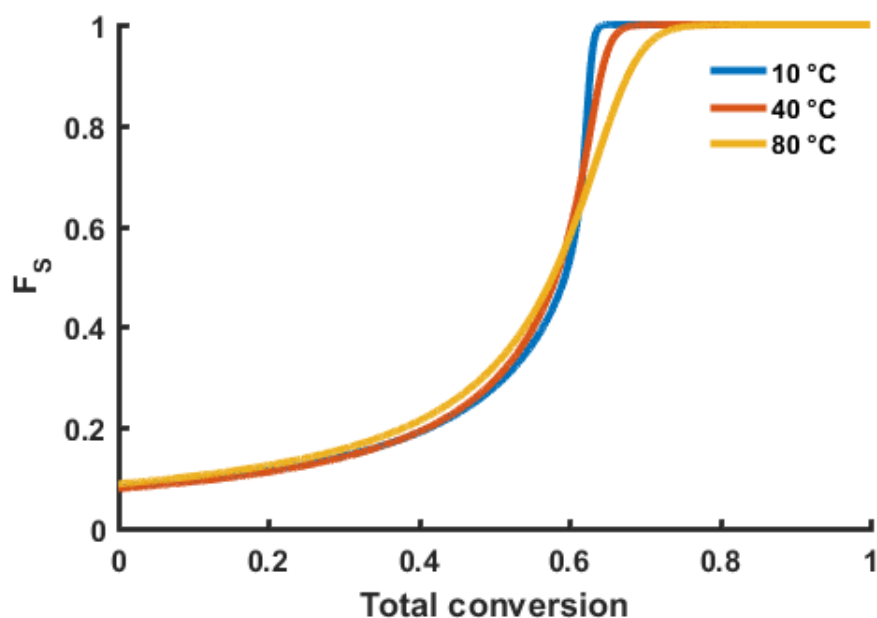


FIGURE 6 Representation of the gradient shape (conversion diagram) calculated for the copolymerizations at 10, 40 and 80 °C. The change in the mole fraction of styrene, F_S , in dependence of the total conversion directly corresponds to the mean composition at a given chain position and therefore is an accurate description of the gradient.

Comonomer Sequence of Tapered Diblock Copolymers.

In terms of microstructural changes within the polymer the probability for styrene segments with more than one styrene unit increases with increasing temperature (Figures S18-S20), as shown by the kMC simulation. At $T = 10\text{ }^{\circ}\text{C}$, styrene shows a highly alternating copolymerization behavior ($r_S = 0.01$), leading to nearly exclusive single styrene units disrupting the isoprene-rich segment. At $T = 60\text{ }^{\circ}\text{C}$ the incorporation of styrene approaches an ideal behavior (increasing ISS/SSI triads content) (Table S4). As expected, the molecular weight fraction of styrene segments with more than one unit in the PI block increases at higher temperatures (Figure S20b). Due to mass conservation, the styrene block length simultaneously decreases from $M_n = 35\text{ kg} \cdot \text{mol}^{-1}$ at $10\text{ }^{\circ}\text{C}$ to $28.2\text{ kg} \cdot \text{mol}^{-1}$ at $80\text{ }^{\circ}\text{C}$ (Figures 7 and S20a). In other words, with increasing temperature, the copolymerization becomes closer to ideal and the gradient less sharp (Figure 6).

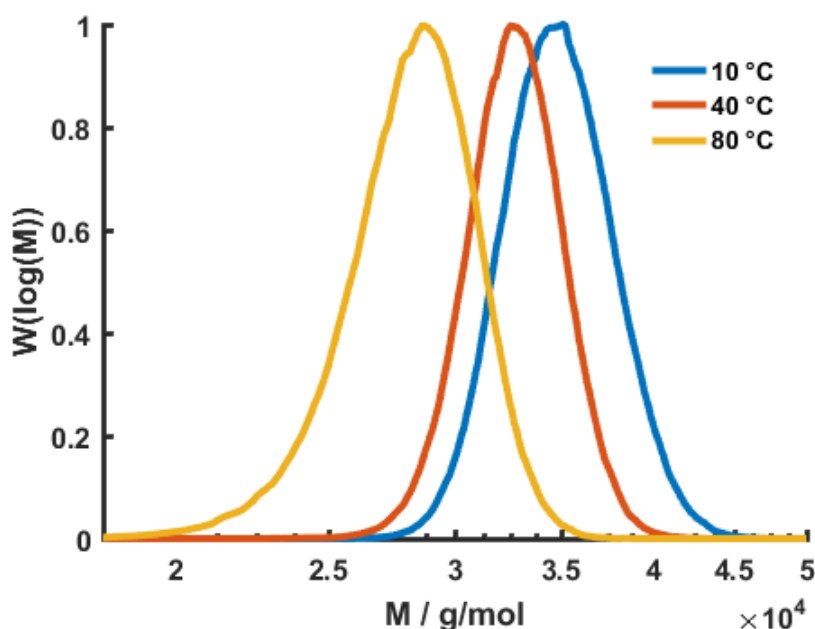


FIGURE 7 Simulated molecular weight distribution of the pure PS block formed in the course of the P(I-co-S) formation by statistical copolymerization. With increasing temperature, the length of the pure PS block decreases due to lower steepness of the gradient and higher incorporation of styrene during the gradient.

Use of NIR Kinetics for monitoring the Synthesis of Multiblock Copolymers.

To demonstrate the advantages and scope of the NIR method as a tool for real-time polymerization monitoring, the multistep synthesis of a tapered decablock copolymer by the repeated addition of a monomer mixture was monitored throughout all steps. As reported earlier, us-

ing a copolymerization temperature of 40 °C, phase-separated tapered multiblock structures $P(I-co-S)_n$ with up to ten blocks ($n = 5$) and molecular weights of 400 kg/mol can be prepared by 4 further monomer addition steps to the living tapered structure formed in the first copolymerization. The linkage of several tapered diblock sequences in one polymer chain is beneficial in terms of materials properties. For this purpose, the synthesis of a tapered decablock structure was monitored in real time, following five subsequent additions of an equimolar S/I monomer mixture *in situ* (Figures 8 and S21).

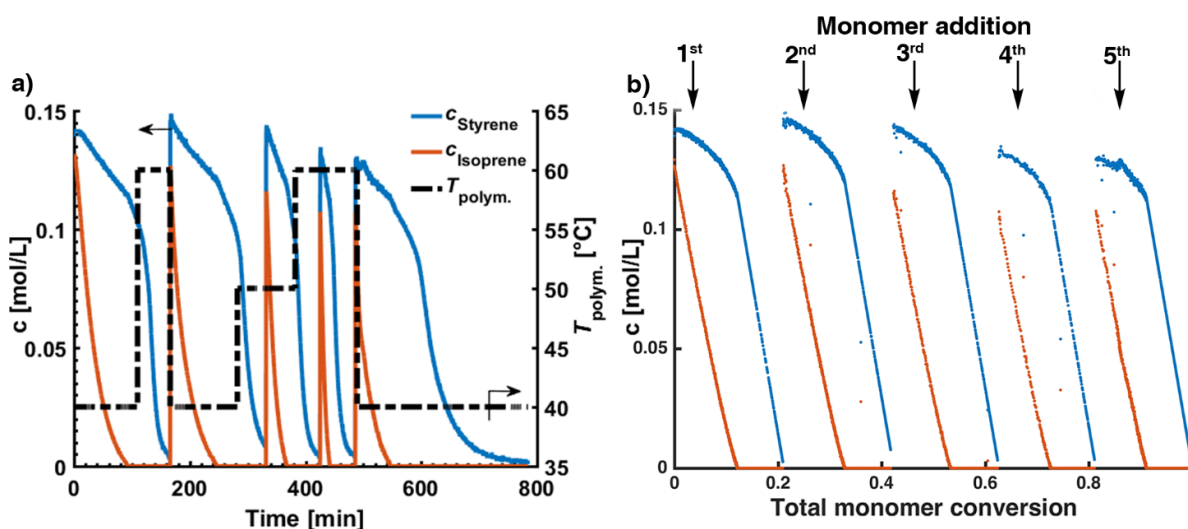


FIGURE 8 Kinetics of $P(I-co-S)_5$ multiblock synthesis ($c_{sec\ BuLi,0} = 0.5\text{ mmol}$, $c_{final,polymer} = 1.44\text{ mol L}^{-1} = 15.7\%_w$). The structure was prepared by five subsequent additions of an equimolar mixture of the pure monomers and variation of the reaction temperature. (a) Individual monomer conversion versus time; (b) individual monomer conversion versus total monomer conversion.

The exact time of each addition was adjusted to the reaction rate and monomer conversion that was extracted from real time NIR measurements. To demonstrate the influence of temperature within one experiment, several temperature profiles were applied and compared (Figure 8a). During the first three additions the temperature was increased to 50 or 60 °C as soon as the pure PS block was formed during the polymerization to accelerate the reaction without altering the gradient. Additionally, the starting temperature was also raised to 50 and 60 °C for the third and fourth additions, respectively. NIR monitoring shows that the reaction time required for the first block (40 °C; increased to 60 °C) is reduced by 30% by this approach, compared to the last block that was performed without temperature increase at 40 °C. The change in temperature can be directly detected in the time-conversion data. Additionally, no alteration of the copolymerization behavior was found compared to the preparation of single tapered diblocks (Figure 8b). Thus, the already present (multi)block structure shows no influence on the copolymerization behavior.

Each addition during the multiblock synthesis essentially behaves like a tapered diblock. Only the expected subtle changes in microstructure due to the different temperatures employed for the third and fourth additions can be detected.

To sum up, real-time NIR monitoring enabled the optimized synthesis and verification of the multiblock microstructure, which can be assumed to be equal to a repetition of the monomer sequence found in P(I-co-S) diblocks.

Effect of THF as Coordinative Co-Solvent.

In a further experiment, the effect of THF as a coordinative modifier was investigated by adding THF (100 equiv relative to butyllithium; 1.5%_{vol} THF in total) to cyclohexane prior to the polymerization at 25 °C (Figures S22 and S23, Supporting Information Section 12). NIR monitoring showed that both monomers add at comparable rates, leading to a copolymer strongly deviating in the monomer sequence, i.e., with different gradient compared to the synthesis in pure cyclohexane. The solvation of the lithium ion with THF suppresses the formation of aggregates, which greatly accelerates the polymerization, typically beyond the time resolution of online NMR techniques.^{32,47} Therefore, probing via NIR is a promising method to follow this much faster kinetics than in cyclohexane. Hence, the polymerization was followed with a time resolution of 0.33 s per spectrum (for details, see Supporting Information Section 12). As expected, NIR monitoring showed that the polymerization proceeds fast with a half-life of less than 10 min at 25 °C (as compared to ≈ 1 h at 25 °C for the PI block in pure cyclohexane). The addition of 1.5%_{vol} THF leads to a nearly ideal random copolymerization, with a slight gradient due to preferential incorporation of styrene in the early stages ($r_1 = 0.61$; $r_5 = 1.84$). These reactivity ratios are in between those obtained in pure cyclohexane at 30 °C (this work; $r_1 = 11.2$, $r_5 = 0.017$) and the values reported by Spirin *et al.*⁴⁸ in THF at 27 °C ($r_1 \approx 0.1$; $r_5 \approx 9$). In summary, the addition of a small amount of THF already leads to a drastic change in the microstructure of the polymer and a highly increased reaction rate. Thus, NIR monitoring enables to correlate the amount of THF added with this well-known "randomizer effect", that is also used in commercial processes. Further studies in this area are in progress.

Microstructural Investigation of the Tapered Diblock Copolymers.

The kinetic measurements revealed a gradual change in the monomer sequence in dependence of the temperature. To study changes in the regio- and stereoisomeric composition of PI and to verify changes in the monomer sequence by an additional method, we investigated the synthesized polymer batches by an in-depth NMR characterization.

A small temperature dependence is known for the regio- and stereoisomeric composition of poly(1,3-dienes).^{49,50} As commonly known from previous works, both effects, (i) the monomer sequence^{37,38,41,42,49,50} and (ii) the isomeric composition of the polydiene block,⁵¹⁻⁵³ are highly relevant in terms of thermal stability,⁴ thermal properties⁴¹ and mechanical properties.⁴ These properties are governed by the capability to form entanglements² and result in changes of block copolymer microphase morphologies.⁵⁴ It requires an in-depth NMR study to elucidate the individual influences on the reaction temperature. To the best of our knowledge, no work has been reported with the full assignment of all signals of PS as well as all signals of the regio- and stereoisomers of PI that are obtained in a copolymerization in nonpolar solvents. Consequently, ¹H and ¹³C NMR spectroscopy signals of polystyrene and polyisoprene were assigned in this work by using 2D NMR techniques (COSY, HSQC, HMBC; Figure S24) under consideration of existing literature, which was indispensable for the assignment of the PI isomers.

(i) Differences in the monomer sequence of S/I copolymers with comparable isomeric composition and different monomer sequences are visualized by stacking the ¹H and ¹³C NMR spectra of a PS-*b*-PI block copolymer with the spectra of a tapered block copolymer and the respective homopolymers (Figure S25). The direct comparison of these spectra shows the presence of additional signals that only occur in the tapered copolymer P(I-*co*-S). These additional signals can be attributed to mixed triads consisting of styrene and isoprene (ISS etc.), which are not present in a perfectly sequential PI-*b*-PS block copolymer. These triad signals were observed in the tapered block copolymer synthesized in the whole temperature range from 10 °C to 80 °C (Figure S26C). Dissimilar intensities of these triad signals validate a difference in the monomer sequence (Figure S26D) as also calculated via kMC simulation (Table S4). Unfortunately, the numerous possible triads attributed to different isomeric structures of PI (*cis*-1,4; *trans*-1,4; 3,4) and different configurations (head-to-head, head-to-tail, etc.) led to a complex spectrum with overlapping ¹³C NMR signals. Thus, quantitative evaluation of the triads in the tapered block copolymers was not possible (see Supporting Information Section 3 for a detailed discussion). Nevertheless, a prediction of the triad abundance in the tapered copolymers was performed *in silico* via kMC simulation, as discussed before (Table S4).

(ii) Comparing the regioisomers of PI in the copolymer at the two temperature extremes of 10 °C and 80 °C, a slight decrease in the 1,4 units (from 95 to 93%) and therefore an increase of the 3,4-units (from 5 to 7%) was observed via ¹H NMR spectroscopy (Table 2 and Figures S26A,B). Simultaneously, the ratio of *trans*- to *cis*-1,4 stereoisomers increases by ca. 22% (Figures S26E,F and Table S5). Further parameters are known to affect the isomeric composition of PI. For this reason, monomer and initiator concentrations were kept constant.⁵⁵⁻⁵⁷ The comparatively low changes in pressure (use of glass reactors) can be neglected.⁵⁸ Therefore, minor

changes of the isomeric composition of PI segments can be attributed to temperature changes. The copolymerization results are consistent with the results obtained for the homopolymerization of isoprene or butadiene.^{59,60} Consequently, the temperature-dependent shift of the isomeric composition seems to be unaltered in the presence of styrene as an aromatic species.

Thermal Properties of Tapered Diblock Copolymers.

The principle of thermoplastic elastomers is based on a rubbery component that is reversibly cross-linked by the vitrified glassy domains.^{61,62} For this purpose, phase separation and consequently the presence of disparate glass-transition temperatures, T_g , is a precondition. It is well known that the T_g of PI strongly depends on the microstructure (Table S6). However, as Figure S27 and Tables 2 and S7 show, the T_g of the PI-rich part of the copolymers fluctuates in the range of -44 to 40 °C. Thus, the small changes in the microstructure at different temperatures do not significantly affect the T_g of the PI-rich part. The T_g of the PS block is difficult to quantify by DSC measurements, but is suspected at a value around 80 °C. Consequently, the shorter reaction times at elevated temperatures can be utilized for fast preparation of copolymers without deteriorating the thermal properties of the final copolymer.

TABLE 2 Change of the Isomeric Structures of Polyisoprene and Glass Transition Temperature resulting from the Copolymerization with Styrene.

T [°C]	1,4 [%] ^a	3,4 [%] ^a	T_g [°C]
10	94.7	5.3	-41
40	93.1	6.9	-39
80	92.9	7.1	-40

^a Signals at $\delta = 5.2 - 4.85$ ppm and $\delta = 4.85 - 4.45$ ppm were used for integration (see Figure S26B).

Bulk Morphologies of Tapered Diblock Copolymers.

Especially for tapered block copolymers, morphologies and consequently T_g 's have to be discussed under the following considerations: (i) Mixing of PI and PS phases is more pronounced for tapered block copolymers in comparison to conventional PS-*b*-PI block structures, as the enthalpic contribution of the phase segregation strength (Flory-Huggins parameter, χ) is reduced ($\chi_{\text{eff}} < \chi$) by a comparably smooth block transition (tapered region).^{37,41,42} (ii) As concluded from our experiments, the temperature dependent lengths of both the gradient block and the pure PS block (Figure 7) lead to a shift in their volume fraction. This can favor or disfavor phase separation, depending on the position in the phase diagram (see Figure S28 and Table S8 for the volume diagram of the prepared polymers). (iii) The slightly different regio/stereoisomeric com-

position resulting from temperature variation can lead to different values for χ_{eff} . (iv) A change in the conformational asymmetry attributed to a change in the monomer sequence and the isomeric structure can lead to different order-order transitions and consequently a different phase diagram, as known for PI-*b*-PS block copolymers.⁶³

Transmission electron microscopy (TEM) was used to image the morphologies of the tapered block copolymers synthesized at low (10 °C), moderate (40 °C) and high temperatures (80 °C) (Figures 9 and S30, Table S9). The expected long-range ordered lamellar morphology is obtained for copolymers prepared at 40 °C, confirming previous investigations by X-ray scattering.⁴¹ The morphology obtained for samples prepared at 10 °C does not show significant differences. In contrast, the morphology for the sample synthesized at 80 °C exhibits particular areas of another structural feature coexisting with areas containing the classic lamellar structure. This particularity was reproduced in multiple films. Also thermal annealing did not affect the morphology significantly (Figure S29).

To obtain a tomographic image of these microdomains, the morphology of a non-lamellar region was imaged at tilt angles of $\pm 60^\circ$ at 3° increments. Figure 9d shows a non-tilted TEM image of this area. The corresponding tomographic reconstructions in Figure 9e,f (see also videos in the Supporting Information) visualize the tetragonal order of the morphology from different locations. Increasing electron densities are displayed from green (low) to yellow and red (high electron density), representing the PI-rich microdomains (OsO_4 -stained). We observe tetragonally arranged PS-rich cylinders (color omitted for clarity, i.e., black voids) in a PI-rich matrix. The reconstruction in Figure 9f contains red areas with highest electron density, which cannot be assigned to lamellae crossing each other (due to homogeneous electron density) but most likely originate from the onset of the formation of tetragonally perforated PI-rich lamellae. A perforated layer morphology was also observed for PI-*b*-PS block copolymers before, albeit as a metastable phase with a hexagonal arrangement of the perforations.^{63,64} So far, the tetragonally perforated lamella (TPL) morphology was only reported for a block copolymer of styrene with perfluorinated butadiene⁶⁵ and ABC triblock terpolymers containing polybutadiene blocks.^{66,67}

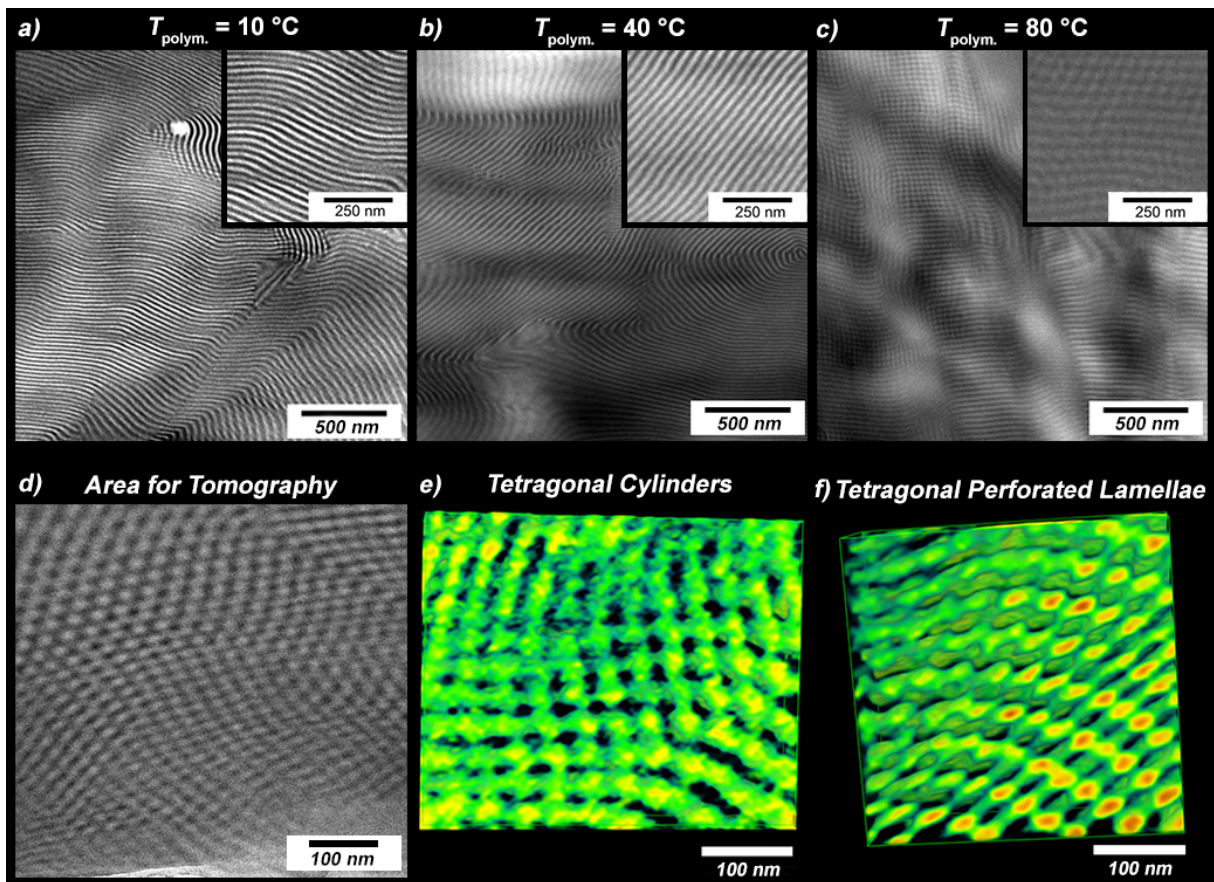


FIGURE 9 (a-c) TEM images of P(I-co-S) synthesized at polymerization temperatures of (a) 10, (b) 40 and (c) 80 °C. PI-rich units are stained with OsO₄ and appear electron-opaque (dark). (d-e) Electron tomography of the sample synthesized at 80 °C. (e) TEM overview of image in (d). (e,f) Reconstructions of selected areas highlighting the tetragonal order of PS-rich cylinders (black voids) in the PI-rich matrix (colored) in (e) and a possible onset of transition to tetragonally perforated lamellae (TPL) morphology (f). Two videos showing 360° rotations in the *x,y* direction are given as Supporting Information.

At first sight, this morphological change with PI as the majority phase is a rather surprising result, taking into account the constant isoprene fraction of $50\%_{\text{mol}} = 43\%_{\text{vol}}$ for all tapered diblock copolymers prepared. As pointed out above, the temperature dependence of the reactivity ratios (Table 1) leads to a change in the comonomer sequence. Consequently, with increasing temperature a flattening of the tapered region and a decrease of the molecular weight of the pure PS block is observed (Figure 7, Table S8). As tapered block copolymers show a smooth transition, the location of the phase boundary between the PI-rich and PS-rich phases is not as obvious and as clearly defined as for PI-*b*-PS block copolymers. Consequently, a direct comparison of volume fractions of the tapered (Φ_{tapered}) and the sequential block copolymers (Φ_{block}) is not straightforward.

A systematic decrease of the volume fraction of the pure PS block (defined as $F_{V,S} \geq 99.9\%$) in the tapered block copolymer ($\Phi_{PS,tapered}$) shows a clear trend from $\Phi_{PS,tapered}(10\text{ }^\circ\text{C}) \approx 38\%_{vol}$ over $\Phi_{PS,tapered}(40\text{ }^\circ\text{C}) \approx 35\%_{vol}$ to $26\%_{vol}$ for $80\text{ }^\circ\text{C}$ (Figure S28 and Table S8). However, a semiquantitative discussion based on the lamellar spacings (Supporting Information, Table S9 and Figure S30) reveals that the phase boundary (as obtained via OsO_4 staining) is located in a region of about 41-44%_{vol} of the PI-rich phase. Thus, the PS-rich phase consists of the pure PS block and a fraction of nonstained short PI segments (presumably IIS, ISS, and SIS triads). The effect of PI-selective staining with OsO_4 for tapered copolymers has not been explored yet. Khandpur *et al.* reported a phase diagram for PS-*b*-PI block copolymers, where a hexagonally perforated layer (HPL) phase is in between the lamellar phase (LAM) and hexagonally arranged cylinders (CYL) ($\Phi_{PI,block}(LAM) > 40\%_{vol}$; $\Phi_{PI,block}(HPL) \approx 36\text{-}40\%_{vol}$; $\Phi_{PI,block}(CYL) < 36\%_{vol}$).⁶⁴ In our case, the comparably smooth block transition in the tapered copolymers does not allow for a quantitative comparison but could possibly affect the interfacial behavior, leading to a tetragonal packing.

Another interesting effect observed is the decreasing contrast of the TEM images at increasing temperatures (Figure 9). While the TEM image at $10\text{ }^\circ\text{C}$ clearly visualizes the PI- (dark) and PS-rich (bright) phases, images at higher temperatures are comparatively poor in contrast. This can be explained by increased mixing of both phases, attributed to a shift to asymmetric volume fractions, which require a higher phase segregation strength (see PI-*b*-PS phase diagram⁶³). Additionally, the higher content of polystyrene in the PI-rich block can lower χ_{eff} .

Consequently, both conclusions drawn from the kinetic data (less steep gradient and thus smaller volume fraction of PS and higher PS content during the taper formation in case of higher polymerization temperatures) are supported by the phase-segregated structures in the TEM images and emphasize the importance of temperature effects on the copolymerization of styrene and isoprene in apolar media.

CONCLUSIONS

We investigated the statistical copolymerization of styrene and isoprene in the temperature range from $10\text{-}80\text{ }^\circ\text{C}$, which is well known to lead to a tapered block copolymer P(I-*co*-S). Real-time NIR probing was successfully employed as a versatile method to monitor the kinetics of both homo- and the statistical copolymerization of the two monomers in the temperature range from $10\text{-}60\text{ }^\circ\text{C}$. Despite the complex superposition of the individual absorption spectra of the components, tracking of the individual comonomer conversions was achieved in the reaction mixture by simultaneously solving a system of 184 linear equations for a large range of the spectra. The high resolution of the NIR measurement ($> 10^4$ data points) enabled the highly ac-

curate determination of the reactivity ratios and homo- and cross-propagation rate constants as well as their activation energies. The observed differences in activation energies mainly affect the reactivity ratio of styrene. The results, in conjunction with kinetic Monte Carlo simulations, indicate distinct temperature-dependent changes in the microstructure for the tapered copolymers, P(I-co-S). With increasing temperature, both the steepness of the gradient and the length of the pure PS block decrease. Additionally, real-time NIR probing enabled validation of the complex structure of a P(I-co-S)₅ multiblock polymer at all stages of multiblock formation. Supplementing the NIR results, the effects of temperature on the polymer microstructure in the copolymer (regio- and stereoisomers of polyisoprene), as investigated by NMR spectroscopy, are minor. DSC measurements reveal no significant effect of temperature on the thermal properties of the tapered block copolymers. Surprisingly, despite unchanged monomer composition and molecular weight, elevated polymerization temperature altered the microphase-separated bulk morphologies of the tapered copolymers. At 80 °C, the bulk morphology partially changed from the lamellar to the tetragonally cylindrical or perforated lamellae morphology, which is explained by shortening of the pure PS segment of the tapered block copolymers. Thus, the polymerization temperature is an important parameter that significantly affects the comonomer distribution in tapered copolymers and enables the manipulation of the bulk morphologies. To sum up, NIR *in situ* monitoring over a large range of the spectra represents a powerful method to follow statistical living copolymerizations, offering a high temporal resolution even for rather high reaction rates, e.g., in case of polar additives. The NIR method permits to follow the formation of tapered polymer architectures with high precision and enables the elucidation of subtle details of the copolymerization kinetics.

ACKNOWLEDGEMENTS

The authors thank Jürgen Ludwig for specialty glassware and Monika Schmelzer for valuable support with SEC measurements. Ramona Barent, Philip Dreier, and Christian Wahlen is thanked for valuable discussions. M.G. and M.P. acknowledge the German Research Foundation (DFG GA 2169/7-1) for partial financial support of this work. The authors also thank the RMU Mainz-Darmstadt for funding. The authors made use of the Imaging Center for Analytics on the Nanoscale (ICAN) at the Nano Energy technic Centre (NETZ). A.H.G. thanks Evonik industries for the financial support through an endowed professorship (2016-2022). S.T. and A.H.G. acknowledge the German Research Foundation (DFG) for funding through an Emmy Noether Young Researcher Group (No. 376920678).

REFERENCES

- (1) Hadjichristidis, N.; Floudas, G.; Pispas, S. *Block copolymers: Synthetic strategies, physical properties, and applications*; Wiley-Interscience: Hoboken, N.J., 2003.
- (2) Mark, J. E. *Physical Properties of Polymer Handbook*, 2nd ed; Springer: New York, 2006.
- (3) Bishop, E. T.; Davison, S. J. *Polym. Sci. C Polym. Symp.* **1969**, 26 (1), 59–79. DOI: 10.1002/polc.5070260105.
- (4) Knoll, K.; Nießner, N. *Macromol. Symp.* **1998**, 132 (1), 231–243. DOI: 10.1002/masy.19981320122.
- (5) A. A. Korotkov; N. N. Chesnokova. *Vysokomol. soed.* **1960**, 2, 365.
- (6) Margl, P. *Can. J. Chem.* **2009**, 87 (7), 891–903. DOI: 10.1139/V09-032.
- (7) A. A. Korotkov. *Angew. Chem.* **1958**, 70 (3), 85.
- (8) Kuntz, I. J. *Polym. Sci.* **1961**, 54 (160), 569–586. DOI: 10.1002/pol.1961.1205416020.
- (9) Zelinski, R.; Childers, C. W. *Rubber Chem. Technol.* **1968**, 41 (1), 161–181. DOI: 10.5254/1.3539168.
- (10) Cunningham, R. E.; Treiber, M. R. *J. Appl. Polym. Sci.* **1968**, 12 (1), 23–34. DOI: 10.1002/app.1968.070120104.
- (11) Hashimoto, T.; Tsukahara, Y.; Tachi, K.; Kawai, H. *Macromolecules* **1983**, 16 (4), 648–657. DOI: 10.1021/ma00238a031.
- (12) Worsfold, D. J. *J. Polym. Sci. A* **1967**, 5 (11), 2783–2789. DOI: 10.1002/pol.1967.150051106.
- (13) Quinebèche, S.; Navarro, C.; Gnanou, Y.; Fontanille, M. *Polymer* **2009**, 50 (6), 1351–1357. DOI: 10.1016/j.polymer.2009.01.041.
- (14) Grune, E.; Johann, T.; Appold, M.; Wahlen, C.; Blankenburg, J.; Leibig, D.; Müller, A. H. E.; Gallei, M.; Frey, H. *Macromolecules* **2018**, 51 (9), 3527–3537. DOI: 10.1021/acs.macromol.8b00404.
- (15) Korotkov, A. A.; Rakova, G. V. *Polymer Science U.S.S.R.* **1962**, 3 (6), 990–1000. DOI: 10.1016/0032-3950(62)90002-3.
- (16) Sinn, V. H.; Lundborg, C.; Onsager, O. T. *Makromol. Chem.* **1964**, 70 (1), 222–259. DOI: 10.1002/macp.1964.020700116.
- (17) Hsieh, H. L. *J. Polym. Sci. A: Gen. Pap.* **1965**, 3 (1), 153–161. DOI: 10.1002/pol.1965.100030117.
- (18) Gold, L. *J. Chem. Phys.* **1958**, 28 (1), 91–99. DOI: 10.1063/1.1744088.
- (19) Bywater, S.; Worsfold, D. J. *J. Organomet. Chem.* **1967**, 10 (1), 1–6. DOI: 10.1016/S0022-328X(00)81711-8.
- (20) Johnson, A. F.; Worsfold, D. J. *J. Polym. Sci. A: Gen. Pap.* **1965**, 3 (2), 449–455. DOI: 10.1002/pol.1965.100030204.
- (21) Roovers, J. E. L.; Bywater, S. *Macromolecules* **1968**, 1 (4), 328–331. DOI: 10.1021/ma60004a010.
- (22) Hsieh, H. L. *J. Polym. Sci. A: Gen. Pap.* **1965**, 3 (1), 163–172. DOI: 10.1002/pol.1965.100030118.
- (23) Worsfold, D. J.; Bywater, S. *Can. J. Chem.* **1960**, 38 (10), 1891–1900. DOI: 10.1139/v60-254.
- (24) Morton, M.; Fetters, L. J.; Bostick, E. E. *J. Polym. Sci. C Polym. Symp.* **1963**, 1 (1), 311–323. DOI: 10.1002/polc.5070010121.
- (25) Cubbon, R.C.P.; Margerison, D. *Proc. R. Soc. Lond. A* **1962**, 268 (1333), 260–275. DOI: 10.1098/rspa.1962.0138.
- (26) Cubbon, R.C.P.; Margerison, D. *Polymer* **1965**, 6 (2), 102–106. DOI: 10.1016/0032-3861(65)90022-4.
- (27) Hsieh, H. L. *J. Polym. Sci. A: Gen. Pap.* **1965**, 3 (1), 173–180. DOI: 10.1002/pol.1965.100030119.
- (28) Fetters, L. J.; Morton, M. *Macromolecules* **1974**, 7 (5), 552–559. DOI: 10.1021/ma60041a004.
- (29) Bywater, S. *Macromolecules* **1998**, 31 (18), 6010–6013. DOI: 10.1021/ma970963r.

- (30) Niu, A. Z.; Stellbrink, J.; Allgaier, J.; Willner, L.; Radulescu, A.; Richter, D.; Koenig, B. W.; May, R. P.; Fetters, L. J. *J. Chem. Phys.* **2005**, *122* (13), 134906. DOI: 10.1063/1.1866092.
- (31) Worsfold, D. J.; Bywater, S. *Macromolecules* **1972**, *5* (4), 393–397. DOI: 10.1021/ma60028a012.
- (32) Müller, A. H.E. In *Comprehensive polymer science: The synthesis, characterization, reactions et applications of polymers*; Allen, G., J.C. Bevington, Eds.; Pergamon Press: Oxford, 1989; pp 387–423.
- (33) Miller, C. E.; Eichinger, B. E.; Gurley, T. W.; Hermiller, J. G. *Anal. Chem.* **1990**, *62* (17), 1778–1785. DOI: 10.1021/ac00216a011.
- (34) Long, T. E.; Liu, H. Y.; Schell, B. A.; Teegarden, D. M.; Uerz, D. S. *Macromolecules* **1993**, *26* (23), 6237–6242. DOI: 10.1021/ma00075a018.
- (35) Williamson, D. T.; Buchanan, T. D.; Elkins, C. L.; Long, T. E. *Macromolecules* **2004**, *37* (12), 4505–4511. DOI: 10.1021/ma035040c.
- (36) *In Situ Spectroscopy of Monomer and Polymer Synthesis*; Puskas, J. E., Long, T. E., Storey, R. F., Shaikh, S., Simmons, C. L., Eds.; Springer US: Boston, MA, s.l., 2003.
- (37) Hodrokoukes, P.; Floudas, G.; Pispas, S.; Hadjichristidis, N. *Macromolecules* **2001**, *34* (3), 650–657. DOI: 10.1021/ma001479i.
- (38) Singh, N.; Tureau, M. S.; Epps, I. T. H.I.I. *Soft Matter* **2009**, *5* (23), 4757. DOI: 10.1039/b908739g.
- (39) Lach, R.; Weidisch, R.; Knoll, K. *J. Polym. Sci. B* **2005**, *43* (4), 429–438. DOI: 10.1002/polb.20337.
- (40) Thunga, M.; Staudinger, U.; Satapathy, B. K.; Weidisch, R.; Abdel-Goad, M.; Janke, A.; Knoll, K. *J. Polym. Sci. B* **2006**, *44* (19), 2776–2788. DOI: 10.1002/polb.20936.
- (41) Steube, M.; Johann, T.; Galanos, E.; Appold, M.; Rüttiger, C.; Mezger, M.; Gallei, M.; Müller, A. H. E.; Floudas, G.; Frey, H. *Macromolecules* **2018**, *51* (24), 10246–10258. DOI: 10.1021/acs.macromol.8b01961.
- (42) Galanos, E.; Grune, E.; Wahlen, C.; Müller, A. H. E.; Appold, M.; Gallei, M.; Frey, H.; Floudas, G. *Macromolecules* **2019**, *52* (4), 1577–1588. DOI: 10.1021/acs.macromol.8b02669.
- (43) Grune, E.; Bareuther, J.; Blankenburg, J.; Appold, M.; Shaw, L.; Müller, A. H. E.; Floudas, G.; Hutchings, L. R.; Gallei, M.; Frey, H. *Polym. Chem.* **2019**, *50* (1), 3. DOI: 10.1039/C8PY01711E.
- (44) Hutchings, L. R.; Brooks, P. P.; Shaw, P.; Ross-Gardner, P. *J. Polym. Sci. A* **2019**, *57* (3), 382–394. DOI: 10.1002/pola.29208.
- (45) Meyer, V. E.; Lowry, G. G. *J. Polym. Sci. A: Gen. Pap.* **1965**, *3* (8), 2843–2851. DOI: 10.1002/pol.1965.100030811.
- (46) Morita, H.; van Beylen, M. *Polymers* **2016**, *8* (10). DOI: 10.3390/polym8100371.
- (47) *Controlled and living polymerizations: Methods and materials*; Müller, A. H. E., Matyjaszewski, K., Eds.; Wiley-VCH: Weinheim, 2009.
- (48) Spirin, Y. L.; Arest-Yakubovich, A. A.; Polyakov, D. K.; Gantmakher, A. R.; Medvedev, S. S. *J. Polym. Sci.* **1962**, *58* (166), 1181–1189. DOI: 10.1002/pol.1962.1205816674.
- (49) Brown, J. R.; Sides, S. W.; Hall, L. M. *ACS Macro Lett.* **2013**, *2* (12), 1105–1109. DOI: 10.1021/mz400546h.
- (50) Ashraf, A. R.; Ryan, J. J.; Satkowski, M. M.; Lee, B.; Smith, S. D.; Spontak, R. J. *Macromol. Rapid Commun.* **2017**, *38* (17). DOI: 10.1002/marc.201700207.
- (51) *Polymer handbook*; Brandrup, J., Ed., 4. ed.; Wiley: Hoboken, N. J., 1999.
- (52) Odian, G. *Principles of Polymerization (Fourth Edition)*, 4th ed.; Wiley-Interscience: S.l., 2004.
- (53) Jia, X.; Zhang, X.; Gong, D. *J. Polym. Sci. A* **2018**, *56* (20), 2286–2293. DOI: 10.1002/pola.29201.
- (54) Avgeropoulos, A.; Paraskeva, S.; Hadjichristidis, N.; Thomas, E. L. *Macromolecules* **2002**, *35* (10), 4030–4035. DOI: 10.1021/ma010824g.

- (55) Worsfold, D. J.; Bywater, S. *Macromolecules* **1978**, *11* (3), 582–586. DOI: 10.1021/ma60063a030.
- (56) Gebert, W.; Hinz, J.; Sinn, H. *Makromol. Chem.* **1971**, *144* (1), 97–115. DOI: 10.1002/macp.1971.021440109.
- (57) Morton, M.; Rupert, J. R. In *Initiation of polymerization: ACS Polymer Symposia*; Bailey, F. E., Ed.; ACS Symposium Series 212; American Chemical Society: Washington, DC, 1983; pp 283–289.
- (58) Jenner, G. J. *Macromol. Sci. A* **1975**, *9* (1), 83–93. DOI: 10.1080/00222337508068647.
- (59) Ura-neck, C. A. *J. Polym. Sci. A* **1971**, *9* (8), 2273–2281. DOI: 10.1002/pol.1971.150090814.
- (60) Quirk, R. P. In *Encyclopedia of Polymer Science and Technology*; Wiley Interscience: Hoboken, NJ, 2004; pp 197–235.
- (61) Holden, G. In *Rubber Technology*, Third Edition; Morton, M., Ed.; Springer US: Boston, MA, 1987; pp 465–481.
- (62) Wang, W.; Lu, W.; Goodwin, A.; Wang, H.; Yin, P.; Kang, N.-G.; Hong, K.; Mays, J. W. *Prog. Polym. Sci.* **2019**, *95*, 1–31. DOI: 10.1016/j.progpolymsci.2019.04.002.
- (63) Förster, S.; Khandpur, A. K.; Zhao, J.; Bates, F. S.; Hamley, I. W.; Ryan, A. J.; Bras, W. *Macromolecules* **1994**, *27* (23), 6922–6935. DOI: 10.1021/ma00101a033.
- (64) Khandpur, A. K.; Förster, S.; Bates, F. S.; Hamley, I. W.; Ryan, A. J.; Bras, W.; Almdal, K.; Mortensen, K. *Macromolecules* **1995**, *28* (26), 8796–8806. DOI: 10.1021/ma00130a012.
- (65) Burger, C.; Micha, M. A.; Oestreich, S.; Förster, S.; Antonietti, M. *Europhys. Lett.* **1998**, *42* (4), 425–429.
- (66) Schacher, F. H.; Sugimori, H.; Hong, S.; Jinnai, H.; Müller, A. H. E. *Macromolecules* **2012**, *45* (19), 7956–7963. DOI: 10.1021/ma3012398.
- (67) Betthausen, E.; Dulle, M.; Hanske, C.; Müller, M.; Fery, A.; Förster, S.; Schacher, F. H.; Müller, A. H. E. *Macromolecules* **2014**, *47* (18), 6289–6301. DOI: 10.1021/ma501003z.

SUPPORTING INFORMATION

1. Purification of the Materials

Prior to the use of isoprene and styrene, the monomers were filtered through a column containing basic aluminium oxide to remove stabilizer. Afterwards the targeted monomer volumes of isoprene and styrene were transferred into a flask, dried for 2 days at room temperature over finely ground CaH_2 , degassed by three cycles of freeze-pump-thaw and distilled ($1 \cdot 10^{-3}$ mbar) into a flask containing trioctylaluminum obtained by evaporation of solvent from a trioctylaluminum solution under reduced pressure. After stirring at room temperature overnight, the monomers were degassed by one cycle of freeze-pump-thaw and distilled into a graduated ampoule. The combined monomer volume was determined by the graduation and typically showed a loss $1.5\%_{\text{vol}}$ in respect to the targeted value. This can be explained by the loss of monomer during distillation (autopolymerization of the monomers) as well as volume contraction caused by the miscibility.

Cyclohexane was dried over sodium with benzophenone as an indicator under reflux in an argon atmosphere. The dried cyclohexane was distilled into a Mortom flask glass reactor equipped with a rare earth magnetic stirring bar under normal pressure, as described in a previous work.¹

THF was dried over diphenylethylenyllithium. For this purpose, a molar ratio of *sec*-BuLi to diphenylethylene of 1 : 1.2 was used to prevent the presence of *sec*-BuLi, which is known to undergo side reactions with THF at room temperature. An excess of dry THF was distilled into a graduated ampoule under reduced pressure and the required amount was added by using the graduated flask.

The NIR probe was introduced via an additional glass joint (Figure S1). The reactor was flushed with argon, the required amount of *sec*-BuLi solution was added and the polymerization started via the addition of the desired amount of monomer or monomer mixture.

Synthesis of homopolymers PI, PS and block copolymers (PI-*b*-PS)_n

Removal of the stabilizer and drying of the monomers was carried out in separate flasks (see Purification of the Materials). The graduated ampoules containing the dried monomers were attached to the Mortom flask glass reactor. The homopolymerization of styrene or isoprene was started via the addition of the desired amount of monomer. The temperature of the reaction flask was controlled by an external, stirred water bath containing an electronic temperature sensor. The monomer addition of isoprene or styrene was repeated several times, to obtain the desired polymer architecture.

Synthesis of tapered di- and multiblock copolymers P(I-co-S)_n

Removal of the stabilizers was carried out in separated flasks (see Purification of the Materials). The drying of the monomers was carried out in one flask to reduce the number of distillation steps. The addition of the monomer mixture was repeated several times (*via* a graduated ampoule, see prior section) until the desired number of blocks was achieved.

Synthesis of copolymers with THF addition

Removal of the stabilizer was carried out in separate flasks (see Purification of the Materials). The drying of the monomers was carried out in one flask to reduce the number of distillation steps. A modified procedure was used for this experiment. As the first step, the required amount of dry THF was added to the cyclohexane containing reactor via a graduated ampoule, followed by a measurement of the background spectrum. Subsequently the monomer mixture was added, followed by initiation via *sec*-BuLi solution. 100 equivalents of THF were used with respect to the active chain ends. The temperature of the reaction flask was controlled by an external, stirred water bath containing an electronic temperature sensor

Termination and work-up

Isopropyl alcohol was degassed by three cycles of freeze-pump-thaw prior to use. The living chain ends were terminated by adding degassed isopropyl alcohol via syringe. To precipitate the polymer, the mixture was poured into an 8-fold volume excess of 50% *vol* mixture of isopropyl alcohol and methanol, dried at reduced pressure and stored at -20 °C in the absence of light. The pure, colorless polymer was obtained in a quantitative yield.



FIGURE S1 A solution of living polystyryllithium in the glass reactor that was used for NIR probing. The NIR probe (left) was introduced *via* a glass joint. The small Teflon stopper (right) was used to add initiator while flushing the reaction system with Argon 5.0. The large Teflon stopper (middle) was used for multiple monomer additions and as a connection to the Schlenk line.

2. Instrumentation

Reaction Monitoring via NIR Spectroscopy

Near infrared spectra were recorded on a *Nicolet Magna 560 FT-IR* spectrometer using the *Omnic 7.4 Thermo Scientific* software suite on a PbS detector and a CaF₂ beam splitter. The IR laser source was employed as light source, with an aperture of 88, mirror speed of 0.6329 and internal ADC amplification of 8. Data interval was set to 1.928 cm⁻¹ with an internal resolution of 4. Up to 32 scans per spectrum were recorded, depending on measurement time. The NIR probe was connected via glass fibers. All spectra were recorded in the range of 5900 to 6250 cm⁻¹. A background spectrum was measured at the same conditions with at least 64 scans before every experiment series. After the experiment, each individual spectrum was exported to the corresponding binary file, imported to MATLAB and processed as described in the manuscript.

NMR Spectroscopy

NMR spectra were recorded on a Bruker Avance III 600 spectrometer at 600 MHz (¹H NMR) or 151 MHz (¹³C NMR) using a 5 mm TCI-cryo probe with z-gradient and ATM. Signals are referenced internally to residual proton signals of the deuterated solvent.

Peaks of residual solvents are assigned with the respective chemical sum formula and crossed out with a diagonal line.² Proton Peaks are assigned to the structure pictured in the respective spectrum, and the assignment is given in small letters. Capital Letters are used for the respective carbon atoms. Consequently, the ¹H-¹³C coupling signals are assigned by using a small letter for the proton and a capital letter for the carbon atom. For example, the coupling between the protons a and the carbon B is expressed as a/B.

Standard Size Exclusion Chromatography (SEC)

SEC measurements were performed with THF as the mobile phase (flow rate 1 mL min⁻¹) on an SDV column set from PSS (SDV 10³, SDV 10⁵, SDV 10⁶) at 30 °C. Polymer concentrations with a maximum of 1 mg/mL turned out to be suitable to prevent concentration effects.

As indicated, calibration was carried out using polystyrene and 1,4-polyisoprene standards from PSS Polymer Standard Service, Mainz.

Copolymers were evaluated by using the different response factors of the RI ($f_{PI}(RI) = 0.0287$; $f_{PS}(RI) = 0.0391$) and the UV-detector (275 nm) ($f_{PI}(UV) = 0.0005$; $f_{PS}(UV) = 0.1226$) for 1,4-polyisoprene and polystyrene. Response factors were determined by injecting polystyrene and

1,4-polyisoprene standards at a known concentration onto the column.

The software PSS WinGPC UniChrom (V 8.31, Build 8417) was used to calculate the polyisoprene and polystyrene weight fraction and interpolate the calibration curves of the homopolymer standards to obtain the molecular weight of the copolymer.³

SEC Traces and Polymer Composition

While the evaluation of kinetic and spectroscopic data is usually attributed to the respective repeating units (molar fraction), bulk morphologies depend on the volume fraction of each block.

The conversion diagram (see for example Figure S9) depicts the instantaneous styrene incorporation (F_S) versus the total conversion during the polymerization. To yield the volume related diagram (volume of instantaneous styrene incorporation ($F_{v,S}$) vs. polymer volume fraction) both axes need to be weighted by the molecular weight and the density of the repeating unit, which was described in detail in the Supporting Information of a previous work.¹ The volume fractions of the repeating units are based on the published homopolymer densities at 140 °C ($\rho_{PI} = 0.830 \text{ g/cm}^3$, $\rho_{PS} = 0.969 \text{ g/cm}^3$).⁴ In general a higher molar fraction of polyisoprene units is necessary for a comparable volume of polystyrene repeating units.

Differential Scanning Calorimeter (DSC)

Films were prepared with a thickness of approximately 0.2 mm, obtained by slow evaporation from a chloroform solution, followed by full removal of the solvent under reduced pressure. The thermal properties of the tapered diblock copolymer films were studied with a PerkinElmer DSC 8500 differential scanning calorimeter (DSC) calibrated by *n*-decane and indium standards. Two heating and one cooling cycle were performed at a rate of 20 K/min in a temperature range between -80 and 130 °C and the glass temperatures were extracted from the second heating cycle. The scans were corrected using a multi-point baseline to remove drifting of the heat flow and normalized by the sample mass.

Transmission electron microscopy (TEM)

Films were prepared with a thickness of around 0.2 mm, obtained by slow evaporation from a chloroform solution followed by a full removal of the solvent under reduced pressure. Samples synthesized at 80 °C were thermally annealed for 4 h at 120 °C under nitrogen atmosphere. For characterization of the tapered block copolymer morphology in the bulk state, the films were microtomed from surface to surface at -80 °C into thin slices of 50-70 nm thickness. The col-

lected ultrathin sections were subsequently stained with osmium tetroxide (OsO_4) for selective staining of the PI domains, followed by investigation by TEM measurements.

TEM experiments were carried out using a Zeiss EM 10 CR (60kV)/ Olympus Megaview II/ ITEM Software build 1276 and a EM 10 electron microscope (Oberkochen, Germany) operating at 60 kV with a slow-scan CCD camera obtained from TRS (Tröndle, Morrenweis, Germany) in bright field mode. The camera was computer-aided using the ImageSP software from TRS.

Transmission Electron Tomography (ET). ET measurements were conducted on a JEOL 2200FS instrument, operating at an accelerating voltage of 200 kV. The TEM grid was cut in half with a razor blade to fit into the TEM tomography holder. Images were taken with an 2k x 2k Ultra-Scan 1000XP CCD camera (Gatan). Images and Supporting Video S1 were processed with tomviz.org reconstruction software⁵ using weighted back projection. Volumetric graphics and Supporting Video S2 were compiled with the UCSF Chimera package⁶ and low-pass filtered with Chimera's Gaussian filter with 1.5 voxel radius.

3. Selection of a suitable measurement method for real-time probing of living carbanionic polymerization

Since 2010 our group has been investigating the copolymerization kinetics via online ^1H NMR spectroscopy.^{7,8} This method commonly features excellent distinction of the monomer signals and thus is the method of choice for initial evaluation of reactivity ratios. Typically a good correlation between the polymer microstructure (reactivity ratios) and the resulting physical properties is observed.^{1,9-11} As computing power as well as other *in situ* spectroscopic methods have been technically improved, an evaluation of kinetic data can be pursued without the need for sampling. In contrast, more traditional methods like stop-flow or capillary flow techniques have rarely been used over the last years and can be considered as superseded.¹² In contrast to the many benefits of NMR spectroscopy, time resolution is limited and typically the polymerization conditions must be tailored to be performed within an NMR tube (use of deuterated solvent, adjusted initiator and monomer concentrations, preparation in glove box). Hence, we found NMR spectroscopy to be unsuitable for the investigation of temperature dependent kinetic measurements like in this work which is attributed to the following main reasons:

(i) Typical reaction times for the homo- and copolymerization of styrene and isoprene are in the range of several hours for $[\text{BuLi}]_0 = 1.5 \text{ mmol/L}$ at $40 \text{ }^\circ\text{C}$.¹ By using typical activation energies,¹³ reaction times vary in the order of days for $T = 10 \text{ }^\circ\text{C}$ to a few minutes for $T = 60 \text{ }^\circ\text{C}$, which is not applicable for NMR kinetic investigations. The fast reaction at high temperatures would not yield a sufficient time resolution due to the slow measurement process of NMR spectroscopy (typically not more than one measurement per minute) (Table S1). Additionally, the initial set-up of an NMR measurement can require up to 5 minutes due to the shimming of the magnetic field. To obtain quantitatively reliable results the measurement time must be adjusted to the relaxation time of the protons of interests.

(ii) Also, the NMR tube used as a reaction vessel (typically 1 mL solution with up to 20 weight percent of polymer) prohibits the subsequent investigation of material properties. (iii) In addition, the synthesis of high molecular weight polymers cannot be realized due to difficulties in initiator dosing by targeting an initiator concentration in the range of 10^{-3} mol/L ($\approx 10^{-6} \text{ mol}$ in respect to the total volume of a common NMR tube). Hence, this desired degree of polymerization (DP_n) leads to problems with the dosage of the initiator and no reliable rate constants, which are governed by the initiator concentration. The dilution of the initiator by preparing a stock solution also seems questionable in terms of the high reactivity of butyllithium and irreversible termination, which has been stated as a problem in several works.^{14,15}

TABLE S1 Comparison of *in situ* spectroscopic methods for the real-time reaction monitoring of styrene and isoprene.

Method	physical foundation	setup	costs	<i>in-situ</i>	time resolution	data evaluation ^b
NMR	nuclear induction & relaxation	extremely difficult	extreme	(no) – NMR tube only	~ 1 min	Easy, distinct signals
UV-Vis	electronic interactions	easy	cheap	(yes) via optical-fiber	< 0.1 s ^a	only polymer chain ends
<i>near</i> -IR	overtone & combination molecular vibrations	easy	cheap	(yes) via optical-fiber	< 0.1 s	Difficult – overlap of bands
<i>mid</i> -IR	fundamental molecular vibrations	difficult	high	(yes) via crystalline/hollow waveguides	< 0.1 s	Easy, distinct signals

a) Monochromator-based systems typically require up to 1 minute, however recent technical developments using digital micromirror devices overcome this issue and enable multiple wavelength measurements within extreme short times. b) Data evaluation is highly dependent on the molecular structure of the employed monomers. The ratings are given for the case of isoprene/styrene copolymerization.

Besides NMR spectroscopy UV-Vis,^{13,16,17} *near*-IR,^{18–23} and *mid*-IR^{13,24,25} spectroscopies have been applied for real-time reaction monitoring (Table S1). UV-Vis has been established to monitor the strongly colored polystyryllithium chain end, but it is not suitable for detection of monomer concentrations due to the absence of suitable monomer absorbance bands.¹³ Mid-infrared (*mid*-IR) spectroscopy has been proven to solve the issues in time-resolution and initiator dosing by enabling the monitoring of the individual monomer consumption in the reaction flask rather than an NMR tube. Also, the time resolution is greatly increased by the Fourier transformation method (FT-IR) compared to dispersive measurements. Unfortunately, the implementation of *mid*-IR spectroscopy is technically challenging because the optical fibers require crystalline media, e.g. AgCl, or hollow waveguides resulting in mechanically less robust and expensive fibers, which require permanent installation in a polymerization setup.²⁶ In contrast, *near*-infrared (NIR) spectroscopy utilizes a smaller wavelength for measurement, enabling the use of affordable, flexible silicon-based optical fibers. To summarize, NIR combines the measurement speed of IR spectroscopy by using Fourier transformation with the benefits of optical systems. Comparing all methods, NIR spectroscopy combines a facile setup, low cost and a high time resolution.

4. Linear equation system for the determination of the individual monomer conversion

For each NIR spectrum a linear equation system based on equation S1.4 (184 equations, for each data point corresponding to a data interval of 1.9 cm^{-1}) was formed and solved to obtain the individual monomer concentrations. To prevent overfitting mass conservation was applied (conversion of eq. S1.1 to eq. S1.4 by S1.2 and S1.3), thus the concentration of PI and PS was bound to initial monomer concentrations. Hence the linear equation system is reduced from 4 parameters (c_I , c_S , c_{PI} and c_{PS}) to only 2 (c_I and c_S) (Eq. S2.4).

$$A(\tilde{\nu}) = \underbrace{c_I \cdot \varepsilon_I(\tilde{\nu}) + c_S \cdot \varepsilon_S(\tilde{\nu})}_{\text{monomer absorption}} + \underbrace{c_{PI} \cdot \varepsilon_{PI}(\tilde{\nu}) + c_{PS} \cdot \varepsilon_{PS}(\tilde{\nu})}_{\text{polymer absorption}} \quad (\text{S1.1})$$

$$c_{PI} = c_{I,0} - c_I \quad (\text{S1.2})$$

$$c_{PS} = c_{S,0} - c_S \quad (\text{S1.3})$$

$$A(\tilde{\nu}) - c_{S,0} \cdot \varepsilon_{PS}(\tilde{\nu}) - c_{I,0} \cdot \varepsilon_{PI}(\tilde{\nu}) = c_S \cdot (\varepsilon_S(\tilde{\nu}) - \varepsilon_{PS}(\tilde{\nu})) + c_I \cdot (\varepsilon_I(\tilde{\nu}) - \varepsilon_{IS}(\tilde{\nu})) \quad (\text{S1.4})$$

Equation S1. The total absorption A is described as the sum of the absorption of the four individual components: styrene (S), isoprene (I), polystyrene (PS), and polyisoprene (PI).

5. Theoretical background of the influence of temperature on the preparation of statistical P(I-co-S) copolymers

The polymer microstructure (e.g., regioisomers of polyisoprene, monomer sequence) is highly dependent on the molecular structure of the employed monomers (e.g. ring-substituted styrenes)^{9,27} and monomer feed ratio. As we have shown in one of our previous works, also the overall initial initiator and monomer concentrations do influence the microstructure.⁹ Temperature and the accompanying changes in the pressure can be utilized as a further parameter to manipulate the copolymerization behavior without interfering with the closed polymerization system inside the reaction vessel. The polymerization of isoprene and styrene features two unique properties: (i) The disparate reactivity ratios are mainly dependent on the crossover behavior of both monomers, hence reactivity ratios do not adequately represent the copolymerization behavior.⁹ For sufficient insight, the homo-propagation rate constants, k_{SS} , and k_{II} , and the cross-propagation rate constants, k_{SI} and k_{IS} , must be evaluated. (ii) As shown by Fontanille and coworkers the homopolymerization rate of isoprene, k_{II} , shows a higher activation energy, as compared to the other parameters when performed in aromatic solvents.¹³ Subtle changes between cyclohexane and the more polarizable benzene as a solvent in the anionic polymerization are commonly known.^{13,14,28-30} While precise predictions cannot be made, a comparable behavior can be expected for cyclohexane, meaning different temperature dependencies of the individual propagation rate constants. In this way reactivity ratios and the resulting gradient structure of the tapered block copolymer are postulated to be also dependent on the polymerization temperature when performing the copolymerization in cyclohexane.

6. Determination of k_{SS} and k_{II} from Homopolymerization Kinetics

TABLE S2 Determination of homo-propagation rate constants for isoprene and styrene homopolymerization in the temperature range from 10 to 60 °C. The apparent rate constants k^{app} equal the slope of the logarithmic monomer consumption versus time (Figures S2 and S3) and were converted to the effective rate constants accounting for the chain end concentrations ($c_{BuLi}^{1/2}$ for styrene, $c_{BuLi}^{1/4}$ for isoprene).

T [°C]	$[Ini]_{isoprene}$ [mmol/L]	$10^{-3} k_{II}$ [(L/mol) ^{0.25} · s ⁻¹]	$10^{-3} k_{II}^{app}$ [min ⁻¹]	$[Ini]_{styrene}$ [mmol/L]	$10^{-3} k_{SS}$ [(L/mol) ^{0.5} · s ⁻¹]	$10^{-3} k_{SS}^{app}$ [min ⁻¹]
10	1.17	0.118	1.31	1.57	1.79	4.25
15	1.17	0.276	2.96	1.57	2.87	6.81
20	1.17	0.500	5.53	1.57	4.43	10.5
25	1.17	0.883	9.76	1.57	6.95	16.4
30	1.17	1.47	16.2	1.57	10.9	25.8
35	1.17	2.46	27.1	1.57	16.1	37.9
40	1.17	3.81	41.9	1.57	23.2	54.3
45	1.17	5.25	57.5	1.57	31.0	72.4
50	0.782 ^a	10.1	109	0.753 ^a	65.2	107
60	0.855 ^a	24.2	248	0.816 ^a	140	240

Although these homo-propagation rate constants were determined on the same batch, initiator concentrations differ due to the increasing dilution caused by every monomer addition step.

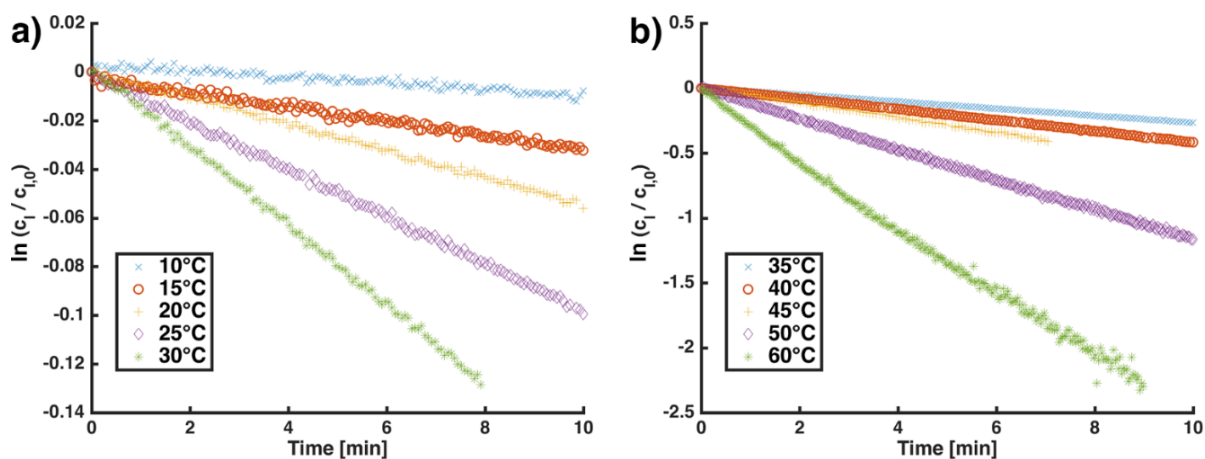


FIGURE S2 Normalized logarithmic monomer consumption versus time for the isoprene homopolymerization. Values for 10 to 45 °C were extracted from the homopolymerization experiments performed within one batch (Figures S4-5), 50 °C and 60 °C were extracted from the (PI-b-PS)₂ tetrablock synthesis (Figures S8-9).

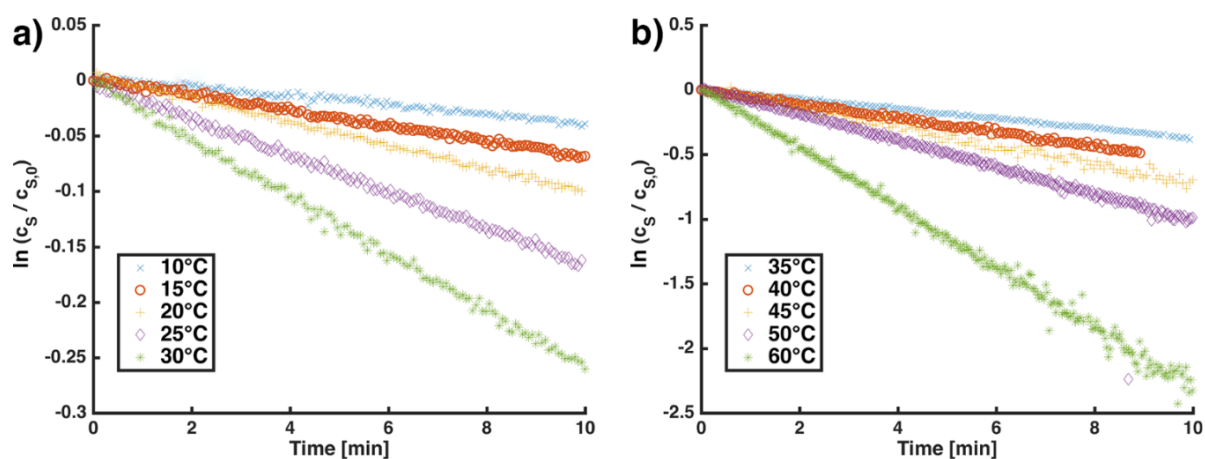


FIGURE S3 a) The reaction flask with the copper-made cooling coil. The radius of the cooling coil was adjusted to the reaction flask. b) A copolymerization of isoprene and styrene in the glass reactor that was used for NIR probing. The yellow color of the solution indicates the presence of living polystyryllithium chain ends. The NIR probe (right) was introduced via a glass joint. The small Teflon stopper (left) was used to add initiator (or THF) via syringe while flushing the reaction system with Argon 5.0. The large Teflon stopper (middle) was used for monomer (or THF) addition via ampoule and serves as a connection to the Schlenk line. Temperature Sensor 1 was attached to the heating plate. Temperature Sensor 2 was attached to the glass surface and served as a temperature data logger (see Figure S3 for temperature profiles).

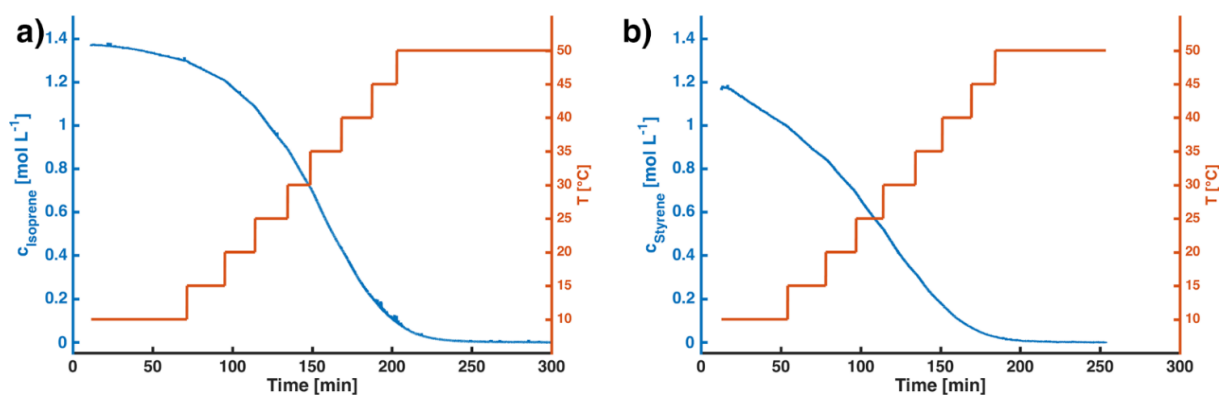


FIGURE S4 Plot of monomer consumption versus time (blue line) for (a) isoprene homopolymerization and (b) styrene homopolymerization experiments. The red line represents the temperature within the reaction flask, which was gradually increased in steps of 5 °C to obtain several temperature dependent rate constants in the range from 10 to 45 °C. Evaluation at 50 °C was not performed due to low monomer content and thus increased measurement noise. Conditions: (a) isoprene homopolymerization: $T = 10$ to 50 °C, $c_{\text{BuLi}} = 1.17$ mmol; (b) styrene homopolymerization: $T = 10$ to 50 °C, $c_{\text{BuLi}} = 1.57$ mmol.

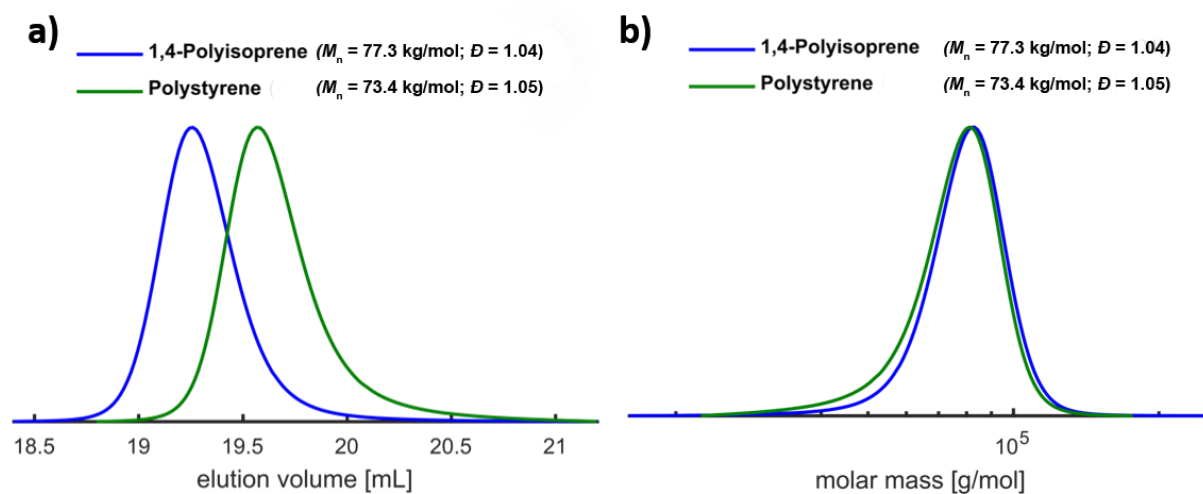
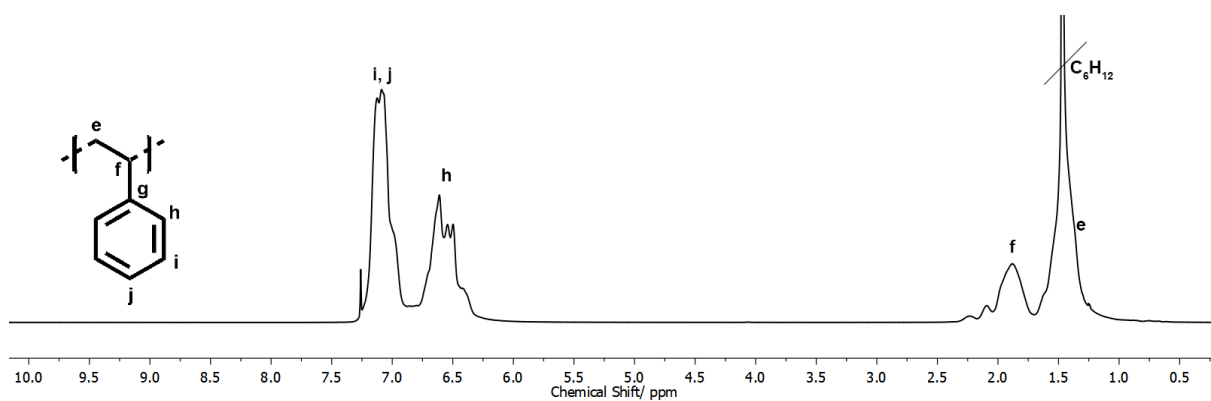
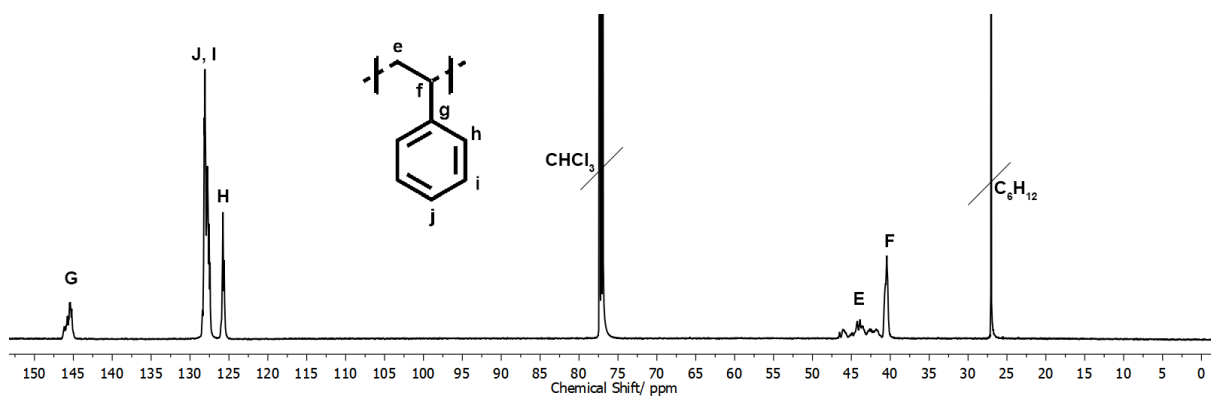


FIGURE S5 A) SEC Eluogram (RI detector) of 1,4-polyisoprene (PI) and polystyrene (PS) homopolymer (Solvent: THF, Detector: RI) used to determine homo-propagation rate constants for PI and PS (Figure S4). B) Molecular weight distributions after calibration. PS standards were used for calibration for measurement of the PS sample, and well-defined PI standards were used for the PI sample. In this manner, absolute molecular weights have been obtained, showing good agreement with the targeted value of $M_n(\text{target}) = 80$ kg/mol. The deviation of the molecular weight can be attributed to autopolymerization of the monomers during the drying period of three days. This is especially pronounced for styrene and clearly visible by a residue in the flask used for purification after distillation of the monomers.

6.1 NMR Spectroscopic Characterization of Polyisoprene and Polystyrene

**FIGURE S6A** ^1H NMR spectrum (600 MHz, CDCl_3) of polystyrene.**FIGURE S6B** ^{13}C NMR spectrum (150 MHz, CDCl_3) of polystyrene.

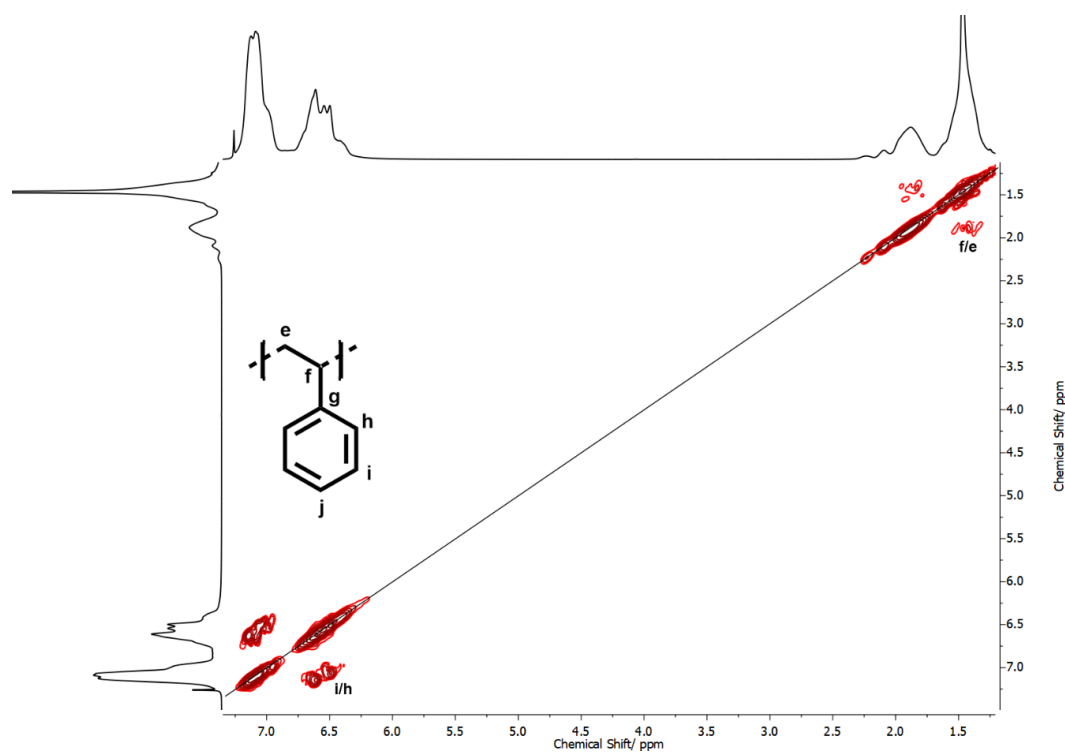


FIGURE S6C ^1H - ^1H COSY NMR spectrum (600 MHz, CDCl_3) of polystyrene.

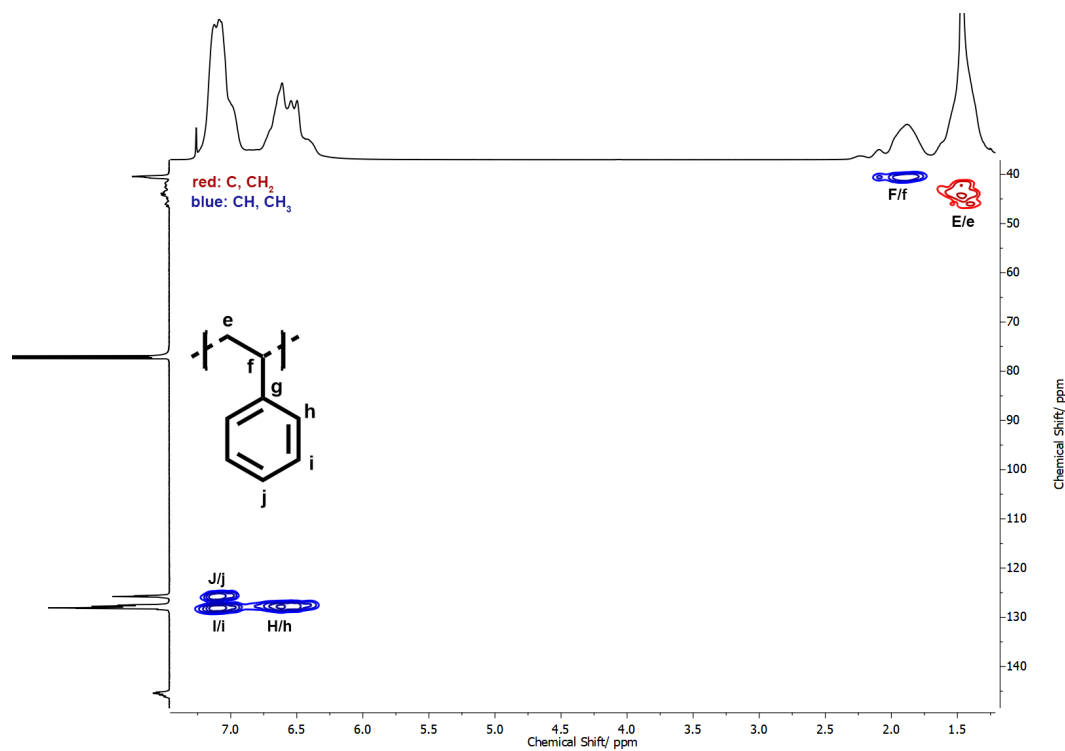


FIGURE S6D ^1H - ^{13}C HSQC NMR spectrum (600 MHz, CDCl_3) of polystyrene.

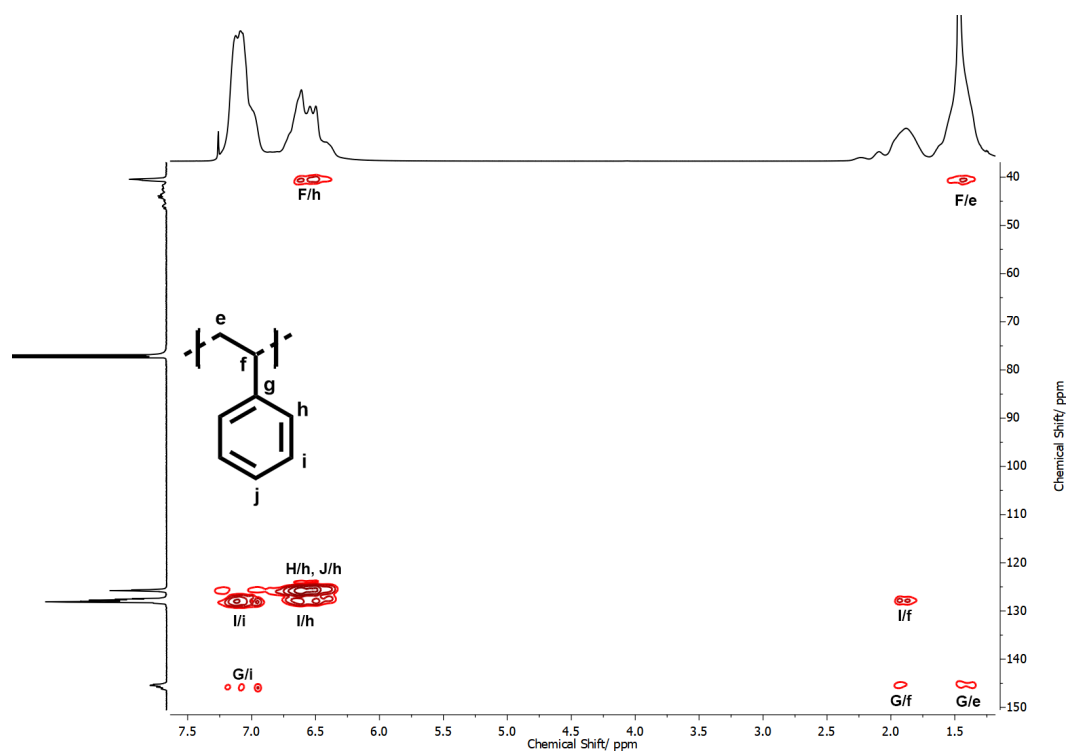


FIGURE S6E ^1H - ^{13}C HMBC NMR spectrum (600 MHz, CDCl_3) of polystyrene.

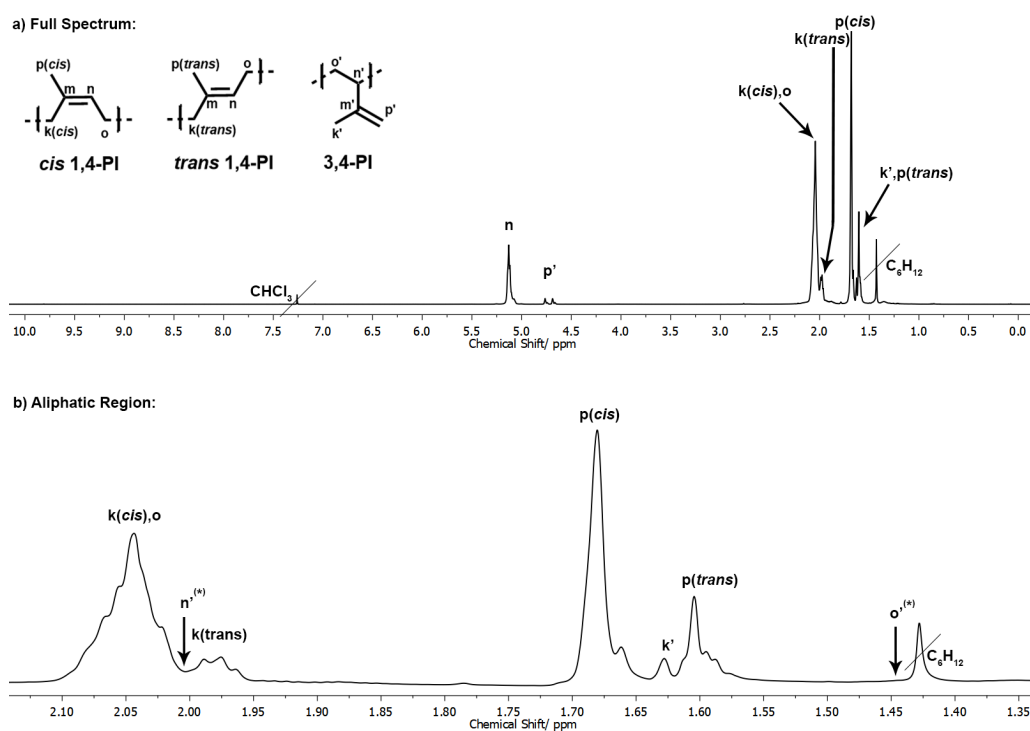


FIGURE S7A ^1H NMR spectrum (600 MHz, CDCl_3) of polyisoprene.

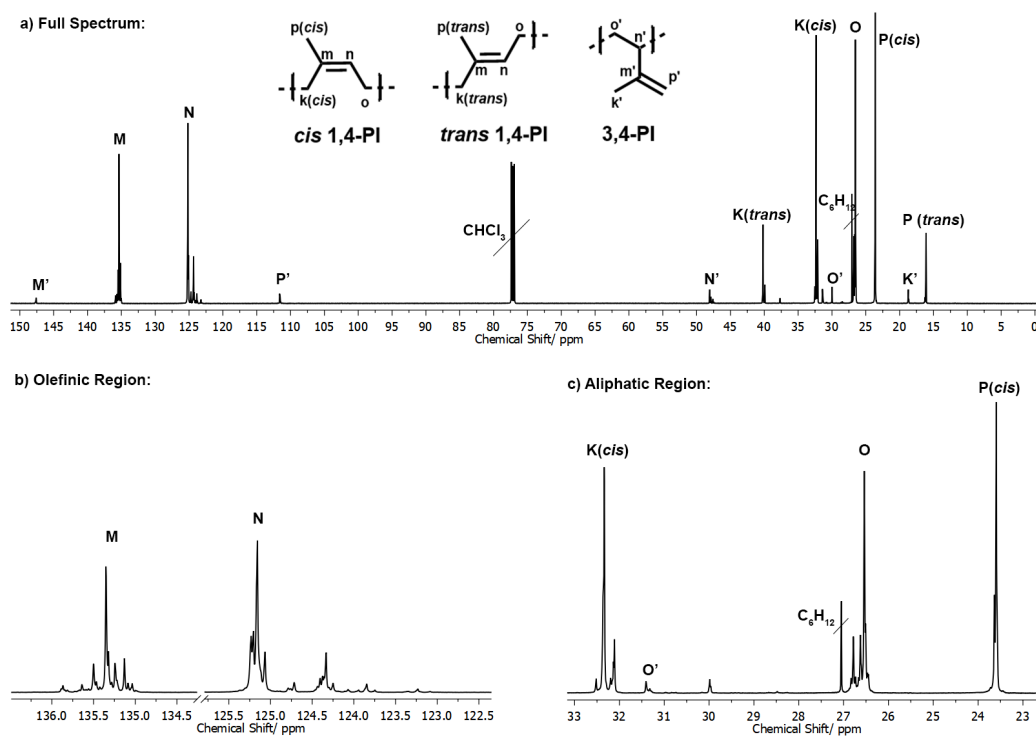


FIGURE S7B ^{13}C NMR spectrum (150 MHz, CDCl_3) of polyisoprene. The shift of the signals marked with (*) are not visible in the ^1H NMR spectrum and have been assigned via 2D NMR spectroscopy.

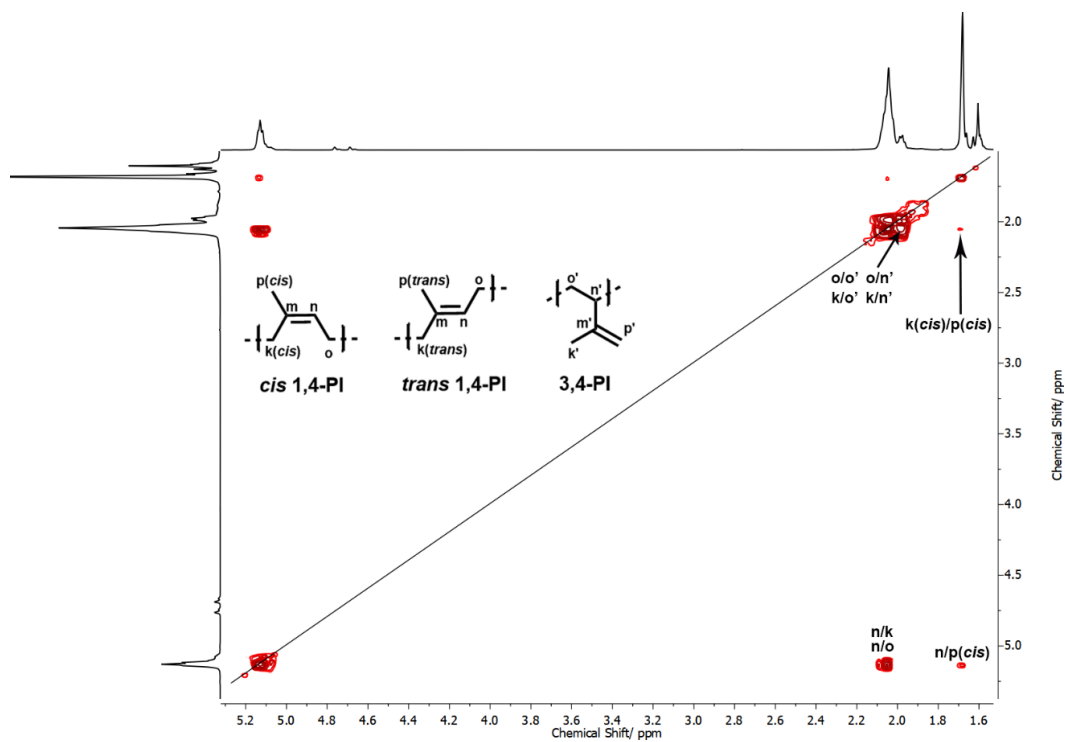


FIGURE S7C ^1H - ^1H COSY NMR spectrum (600 MHz, CDCl_3) of polyisoprene.

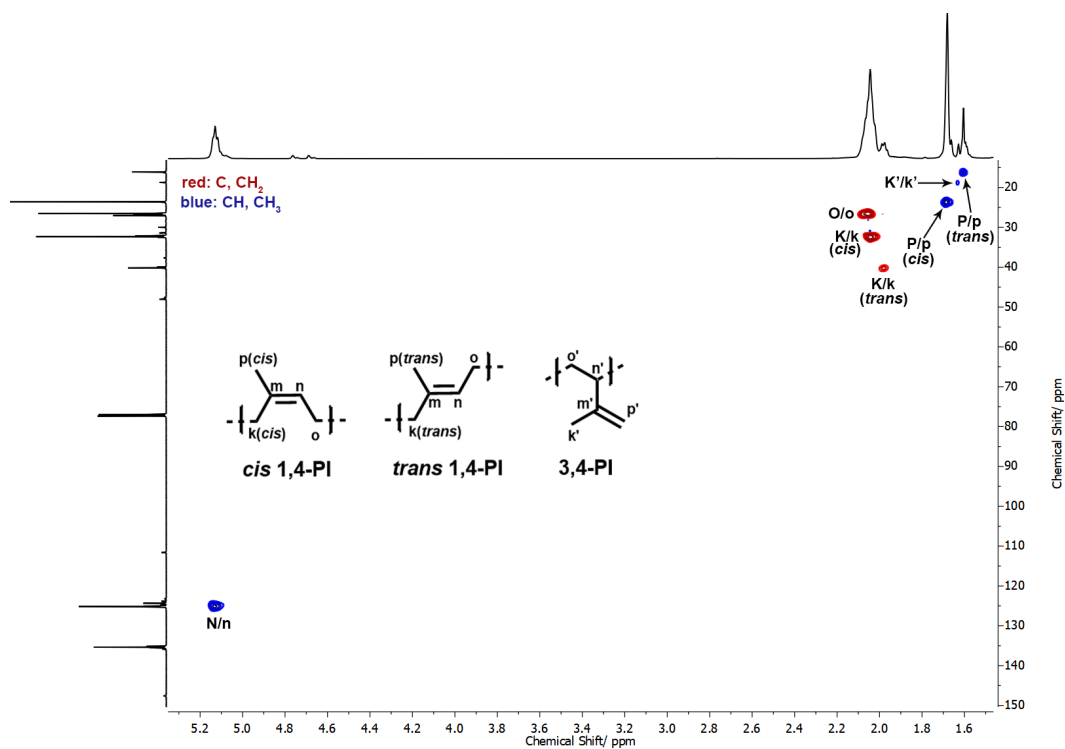


FIGURE S7D ^1H - ^{13}C HSQC NMR spectrum (600 MHz, CDCl_3) of polyisoprene.

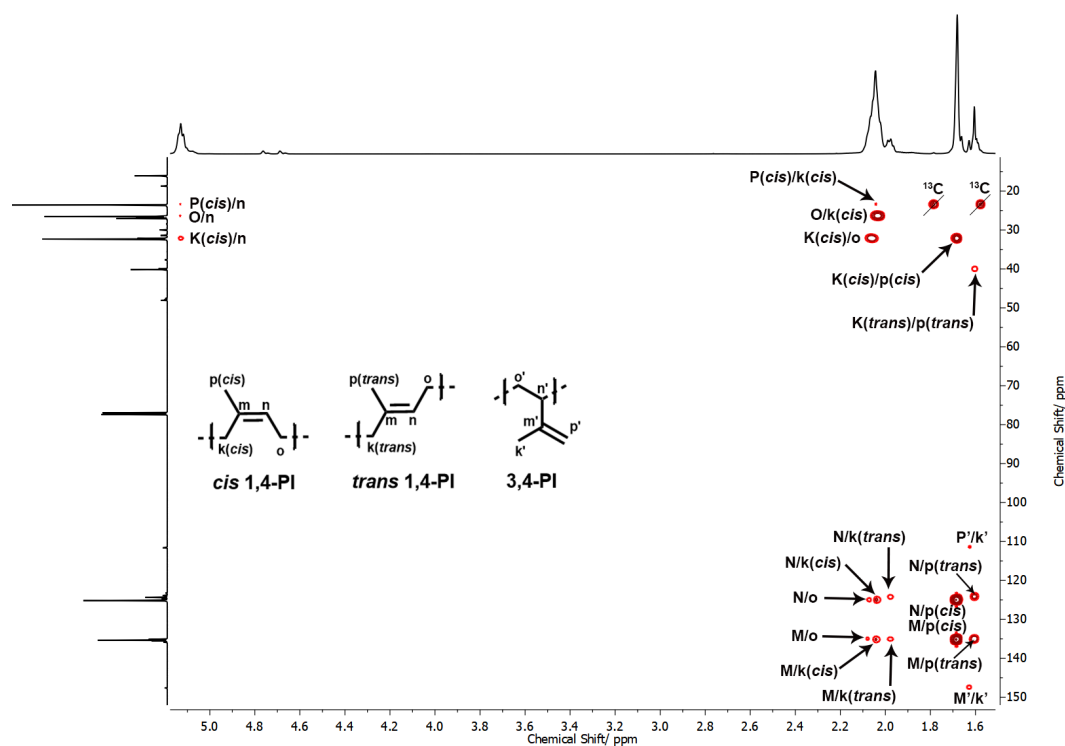


FIGURE S7E ^1H - ^{13}C HMBC NMR spectrum (600 MHz, CDCl_3) of polyisoprene.

The evaluation of the signals in the NMR spectra of polyisoprene is rather complex, due to the presence of different isomers (*cis* 1,4-PI, *trans* 1,4-PI, 3,4-PI). Especially in the ^{13}C NMR spectrum, the formation of different triads consisting of these 3 units, as well as different configurations (head-to-head, tail-to-tail, head-to-tail and the respective inverse configurations) leads to a spectrum rich in signals. Signals that have been assigned in the spectra always belong to the respective repeating unit (*cis* 1,4-PI, *trans* 1,4-PI, 3,4-PI), surrounded by two (*cis* or *trans*) 1,4-PI units, as this is the main unit present in the investigated polymers. No attention has been drawn to other triads due to the negligible amount of these linkages and the significant overlap of the signals in the ^{13}C NMR spectrum ($\Delta\delta \approx 0.5$ ppm). No distinction has been made in the evaluation of the *cis* and *trans* signals of the carbons m, n and o due to the minor difference in the chemical shift in ^1H and ^{13}C NMR spectra.

Chemical shifts of other triads/diads can be found in the work of Tanaka *et. al.* for *trans* and *cis* 1,4-PI³¹ and in the work of Gronski *et. al.*³² and others^{33–36} for 3,4-PI units.

All signals were assigned via 2D NMR spectroscopy (see Figures S7C–S7E) and agree with existing literature on this topic.^{31–36}

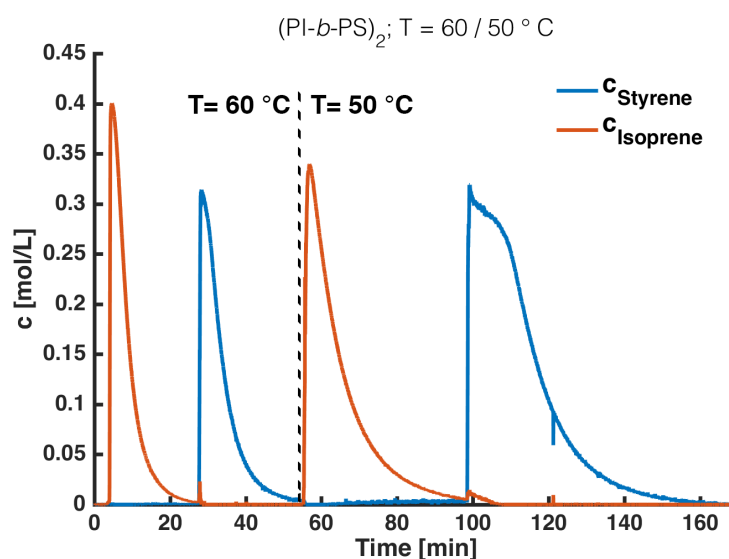
6.2 Kinetics of the Synthesis of a (PI-*b*-PS)₂ Tetrablock monitored via real-time NIR probing

FIGURE S8 Plot of monomer consumption (styrene: blue line, isoprene: red line) versus time of the preparation of a sequential (PI-*b*-PS)₂ tetrablock. The first two blocks were prepared at 60 °C, the subsequent next two blocks at 50 °C. The change in volume at each addition was considered for the calculation of the chain end concentration. Conditions: $T = 50\text{ }^{\circ}\text{C}$, isoprene, $c_{\text{BuLi}} = 0.78\text{ mmol}$; $T = 50\text{ }^{\circ}\text{C}$, styrene, $c_{\text{BuLi}} = 0.75\text{ mmol}$; $T = 60\text{ }^{\circ}\text{C}$, isoprene, $c_{\text{BuLi}} = 0.86\text{ mmol}$; $T = 50\text{ }^{\circ}\text{C}$, styrene, $c_{\text{BuLi}} = 0.82\text{ mmol}$.

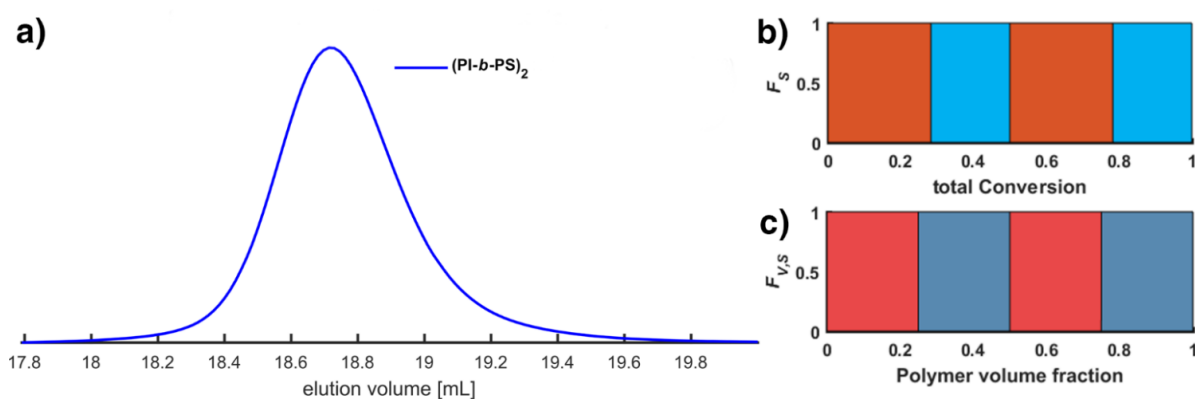


FIGURE S9 a) SEC Eluogram (RI detector) with M_n and \bar{D} based on dual calibration by using PI and a PS standards according to their weight fraction (see Instrumentation Section; $M_n = 154\text{ kg/mol}$; $\bar{D} = 1.10$; $M_n(\text{target}) = 160\text{ kg/mol}$). b) Composition profile according to molar fraction c) Composition profile according to volume fraction of the sequential diblock copolymer (PI-*b*-PS)₂. A 57%_{mol} molar fraction of isoprene was used (see diagram b)) to obtain a 50%_{vol} volume fraction of isoprene (see diagram c)). A lamellar morphology can be expected.

7. Copolymerization Kinetics

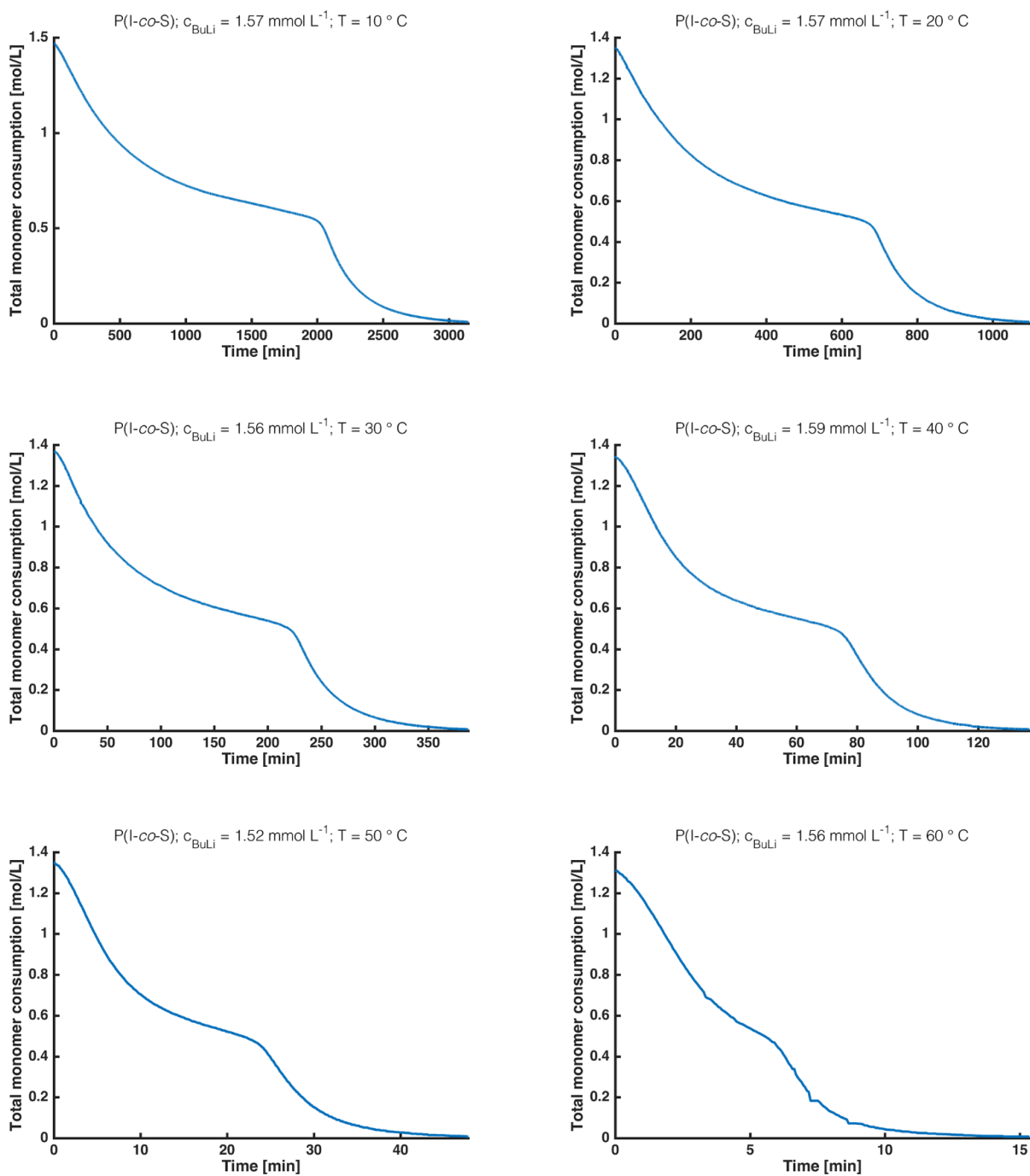


FIGURE S10 Total combined monomer conversion versus reaction time for each performed copolymerization (10 °C to 60 °C) measured in the copolymerization experiments via real-time NIR probing.

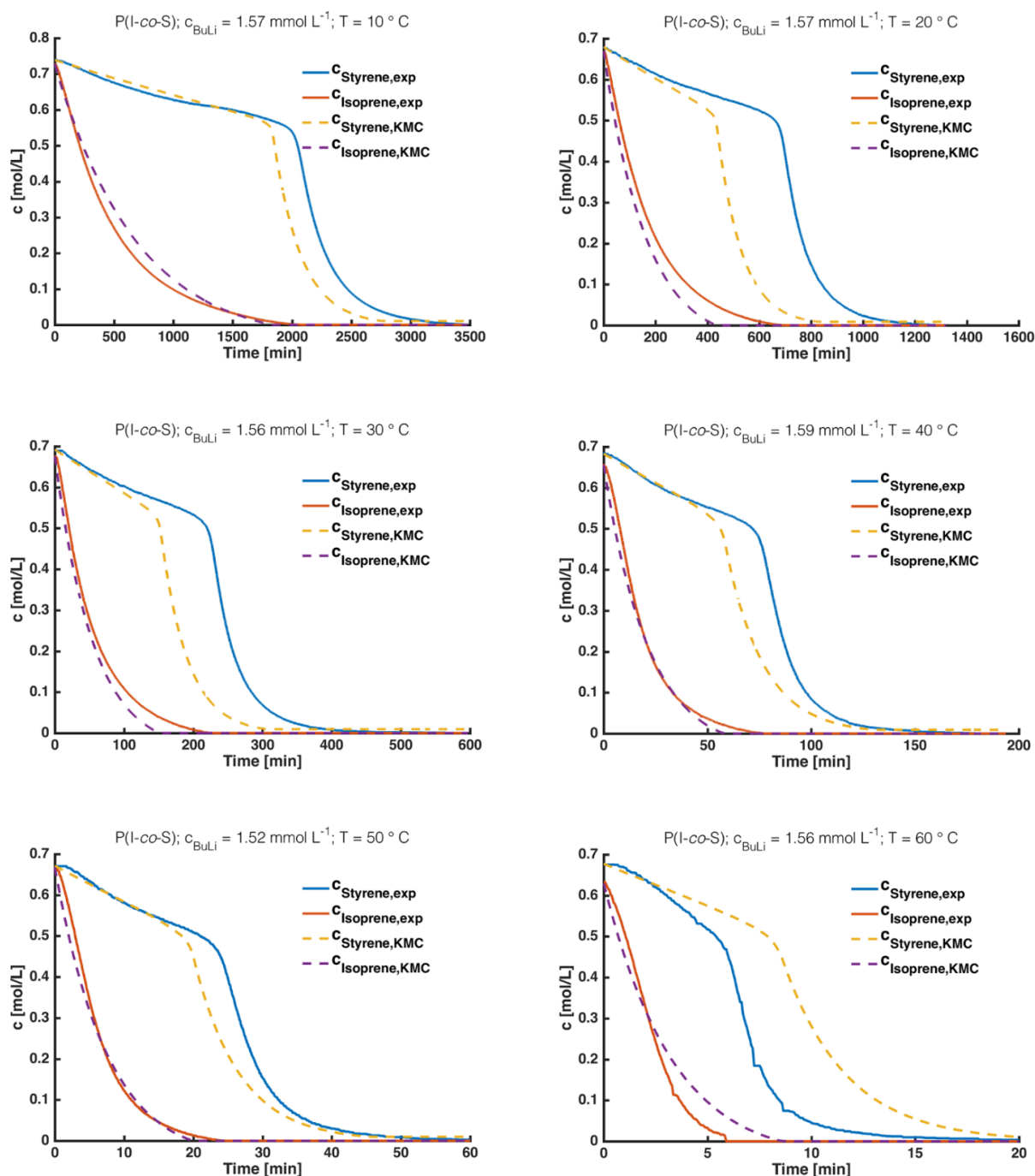


FIGURE S11 Individual monomer conversion (styrene: blue line, isoprene: red line) versus reaction time for each performed copolymerization (10°C to 60°C). The dashed line shows the simulated time-dependent monomer conversion via KMC based on the experimentally determined rate constants. The deviation of the simulated curves from the experimental data is mainly based on the homo-propagation rate of isoprene. Variation in k_{II} influences the period until the polymerization of styrene proceeds, hence the horizontal shift of the styrene conversion is mainly based on k_{II} . During the copolymerization the homo-propagation of isoprene proceeds in the presence of styrene, and thus the rate constant is slightly altered compared to the values obtained in pure homopolymerization experiments.

7.1 Determination of Reactivity Ratios

Theoretical Background

The reactivity ratios are defined as the ratio of homopropagation rate versus crossover rate. In the case of the copolymerization of isoprene and styrene chain end aggregation phenomena need to be considered. Equations S2.1 to S2.26 represents the derivation of the rate equations of copolymerization (S2.27-S2.29) that consider the chain end aggregation phenomena. Based on these equations the Mayo-Lewis equation can be derived (S2.30 to S2.32 to yield S2.33). As shown below, the Mayo-Lewis equation shows no dependence on the aggregation behavior, even though the aggregation-based rate equations were used for the derivation. Hence, the exact knowledge of the aggregation type is not necessary for the evaluation of reactivity ratios. Therefore, in this work the determination of the crosspropagation rate constants was performed by determining the reactivity ratios and calculating the rate constants from those. This approach omits solving of the differential equation system, which is numerically difficult due to the exponents of $1/4$ and $1/2$ in equation S2.27 to S2.29.

The four elemental reactions of copolymerization as proposed by Mayo and Lewis are:



Equations S2.1 to S2.4 can be used to describe the rate of reaction:

$$-\frac{d[S]}{dt} = k'_{SS} [S] [PS^-] + k'_{IS} [S] [PI^-] \quad (S2.5)$$

$$-\frac{d[I]}{dt} = k'_{II} [I] [PI^-] + k'_{SI} [I] [PS^-] \quad (S2.6)$$

$$-\frac{d[PS^-]}{dt} = \frac{d[PI^-]}{dt} = k'_{SI} [I] [PS^-] - k'_{IS} [S] [PI^-] \quad (S2.7)$$

To include the aggregation phenomena the reaction of the chain ends to form aggregates need to be considered:



These reactions S2.8 and S2.9 can be described with the following equilibria:

$$K_{PI,agg} = \frac{[PI_4^-]}{[PI^-]^4} \quad (S2.10)$$

$$K_{PS,agg} = \frac{[PS_2^-]}{[PS^-]^2} \quad (S2.11)$$

Experimentally only the individual concentrations of the aggregated and non-aggregated chain ends are not accessible, hence the total anion concentration per species (PS or PI) is suitable to describe this dependence:

$$[\text{PI}^-]_{\text{total}} = [\text{PI}^-] + 4 [\text{PI}_4^-] \quad (\text{S2.12})$$

$$[\text{PS}^-]_{\text{total}} = [\text{PS}^-] + 2 [\text{PS}_2^-] \quad (\text{S2.13})$$

The combination of equation S2.12 and S2.13 with 2.10 and S2.11 respectively yields the expression of the non-aggregated chain end concentration:

$$[\text{PI}^-] = \left(\frac{[\text{PI}_4^-]}{K_{\text{PI,agg}}} \right)^{1/4} = \left(\frac{\frac{1}{4} ([\text{PI}^-]_{\text{total}} - [\text{PI}^-])}{K_{\text{PI,agg}}} \right)^{1/4} \quad (\text{S2.14})$$

$$[\text{PS}^-] = \left(\frac{[\text{PS}_2^-]}{K_{\text{PS,agg}}} \right)^{1/2} = \left(\frac{\frac{1}{2} ([\text{PS}^-]_{\text{total}} - [\text{PS}^-])}{K_{\text{PS,agg}}} \right)^{1/2} \quad (\text{S2.15})$$

To simplify equation S2.14 and S2.15 the concentration of non-aggregated chain ends are considered negligible compared to the total anion concentration:

$$[\text{PI}^-]_{\text{total}} \gg [\text{PI}^-] \quad (\text{S2.16})$$

$$[\text{PS}^-]_{\text{total}} \gg [\text{PS}^-] \quad (\text{S2.17})$$

Hence, the terms S2.14 and S2.15 are simplified:

$$[\text{PI}^-] = \left(\frac{1/4 ([\text{PI}^-]_{\text{total}})}{K_{\text{PI,agg}}} \right)^{1/4} = \left(\frac{1}{4K_{\text{PI,agg}}} \right)^{1/4} ([\text{PI}^-]_{\text{total}})^{1/4} \quad (\text{S2.18})$$

$$[\text{PS}^-] = \left(\frac{1/2 ([\text{PS}^-]_{\text{total}})}{K_{\text{PS,agg}}} \right)^{1/2} = \left(\frac{1}{2K_{\text{PS,agg}}} \right)^{1/2} ([\text{PS}^-]_{\text{total}})^{1/2} \quad (\text{S2.19})$$

The combination of equation S2.18 and S2.19 with the differential rate equations S2.5-S2.7 yields the rate equations in dependence of the total chain end anion concentration.

$$-\frac{d[\text{S}]}{dt} = k'_{\text{SS}} [\text{S}] \left(\frac{1}{2K_{\text{PS,agg}}} \right)^{1/2} ([\text{PS}^-]_{\text{total}})^{1/2} + k'_{\text{IS}} [\text{S}] \left(\frac{1}{4K_{\text{PI,agg}}} \right)^{1/4} ([\text{PI}^-]_{\text{total}})^{1/4} \quad (\text{S2.20})$$

$$-\frac{d[\text{I}]}{dt} = k'_{\text{II}} [\text{I}] \left(\frac{1}{4K_{\text{PI,agg}}} \right)^{1/4} ([\text{PI}^-]_{\text{total}})^{1/4} + k'_{\text{SI}} [\text{I}] \left(\frac{1}{2K_{\text{PS,agg}}} \right)^{1/2} ([\text{PS}^-]_{\text{total}})^{1/2} \quad (\text{S2.21})$$

$$-\frac{d[\text{PS}^-]}{dt} = \frac{d[\text{PI}^-]}{dt} = k'_{\text{SI}} [\text{I}] \left(\frac{1}{2K_{\text{PS,agg}}} \right)^{1/2} [\text{PS}^-]_{\text{total}}^{1/2} - k'_{\text{IS}} [\text{S}] \left(\frac{1}{4K_{\text{PI,agg}}} \right)^{1/4} [\text{PI}^-]_{\text{total}}^{1/4} \quad (\text{S2.22})$$

To summarize, the chain end aggregation introduces an additional equilibrium of the non-aggregated and aggregated chain ends. Experimentally, this equilibrium is difficult to be considered; therefore, a common approach is to include the equilibrium constant in the rate constants.

$$k_{SS} = k'_{SS} \left(\frac{1}{2K_{PS,agg}} \right)^{1/2} \quad (S2.23)$$

$$k_{SI} = k'_{SI} \left(\frac{1}{2K_{PS,agg}} \right)^{1/2} \quad (S2.24)$$

$$k_{IS} = k'_{IS} \left(\frac{1}{4K_{PI,agg}} \right)^{1/4} \quad (S2.25)$$

$$k_{II} = k'_{II} \left(\frac{1}{4K_{PI,agg}} \right)^{1/4} \quad (S2.26)$$

By combining equations S2.23-S2.26 with the equation S2.20-S2.22 the differential rate equations can be described by experimentally known values such as the total anion concentration, the monomer concentration and the rate constants that can be obtained *via* measurements.

$$-\frac{d[S]}{dt} = k_{SS} [S] ([PS^-]_{total})^{1/2} + k_{IS} [S] ([PI^-]_{total})^{1/4} \quad (S2.27)$$

$$-\frac{d[I]}{dt} = k_{II} [I] ([PI^-]_{total})^{1/4} + k_{SI} [I] ([PS^-]_{total})^{1/2} \quad (S2.28)$$

$$-\frac{d[PS^-]}{dt} = \frac{d[PI^-]}{dt} = k_{SI} [I] ([PS^-]_{total})^{1/2} - k_{IS} [S] ([PI^-]_{total})^{1/4} \quad (S2.29)$$

As described by Mayo and Lewis, the differential rate constants can be used to derive the copolymerization equation. In the first step, equation S2.28 is divided by equation S2.27.

$$\begin{aligned} \frac{d[I]}{d[S]} &= \frac{k_{II}[I]([PI^-]_{total})^{1/4} + k_{SI}[I]([PS^-]_{total})^{1/2}}{k_{SS}[S]([PS^-]_{total})^{1/2} + k_{IS}[S]([PI^-]_{total})^{1/4}} \\ &= \frac{[I]}{[S]} \frac{k_{II}([PI^-]_{total})^{1/4} + k_{SI}([PS^-]_{total})^{1/2}}{k_{SS}([PS^-]_{total})^{1/2} + k_{IS}([PI^-]_{total})^{1/4}} \quad (S2.30) \\ &= \frac{[I]}{[S]} \frac{k_{II} \frac{([PI^-]_{total})^{1/4}}{([PS^-]_{total})^{1/2}} + k_{SI}}{k_{SS} + k_{IS} \frac{([PI^-]_{total})^{1/4}}{([PS^-]_{total})^{1/2}}} \end{aligned}$$

With the steady state assumption that the number of chain ends is constant and hence no termination is present, the following equation can be described:

$$k_{SI}[I]([PS^-]_{total})^{1/2} = k_{IS}[S]([PI^-]_{total})^{1/4} \quad (S2.31)$$

$$\frac{([PI^-]_{total})^{1/4}}{([PS^-]_{total})^{1/2}} = \frac{k_{SI}[I]}{k_{IS}[S]} \quad (S2.32)$$

By combining the steady-state assumption S2.32 with equation S2.30 the Mayo-Lewis equation can be obtained:

$$\frac{d[I]}{d[S]} = \frac{[I]}{[S]} \frac{k_{II} \frac{k_{SI}[I]}{k_{IS}[S]} + k_{SI}}{k_{SS} + k_{IS} \frac{k_{SI}[I]}{k_{IS}[S]}} = \frac{[I]}{[S]} \frac{\frac{k_{II}[I]}{k_{IS}[S]} + 1}{\frac{k_{SS}}{k_{SI}} + \frac{[I]}{[S]}} = \frac{[I]}{[S]} \frac{r_1 \frac{[I]}{[S]} + 1}{r_S + \frac{[I]}{[S]}} = \frac{[I]}{[S]} \frac{r_1 [I] + [S]}{r_S [S] + [I]} \quad (S2.33)$$

As shown in this derivation of the Mayo-Lewis equation S2.33 the chain end aggregation is not present anymore. Hence, the evaluation of reactivity ratios based on methods that rely on the Mayo-Lewis equation such as the Fineman-Ross, Kelen-Tüdös or Meyer-Lowry formalism is independent of chain end aggregation phenomena. Note that in the following equations used for the determination of reactivity ratios the indices can be exchanged, hence the evaluation can be performed on the basis of f_S or f_I .

The equation S2.33 can be described using the monomer feed f and the instantaneous monomer incorporation ratio F :

$$F_I = \frac{r_I f_I^2 + f_I f_S}{r_I f_I^2 + 2f_I f_S + r_S f_S^2} \quad (\text{S2.34})$$

For the Fineman-Ross formalism, equation S2.34 is linearized:

$$G = H r_I - r_S \quad (\text{S2.35})$$

$$G = \frac{f_I (2F_I - 1)}{(1 - f_I) F_I} \quad (\text{S2.36})$$

$$H = \frac{f_I^2 (1 - F_I)}{(1 - f_I)^2 F_I} \quad (\text{S2.37})$$

The Kelen-Tüdős formalism uses a correction factor α to correct for biases in the Fineman-Ross formalism.

$$\eta = \left(r_1 + \frac{r_S}{\alpha} \right) \mu - \frac{r_S}{\alpha} \quad (\text{S2.38})$$

$$\alpha = \sqrt{H_{\min} H_{\max}} \quad (\text{S2.39})$$

$$\eta = \frac{G}{\alpha + H} \quad (\text{S2.40})$$

$$\mu = \frac{H}{\alpha + H} \quad (\text{S2.41})$$

The Meyer-Lowry formalism uses the integrated form of the Mayo-Lewis equation:

$$1 - X = \frac{[I] + [S]}{[I]_0 + [S]_0} = \frac{[M]}{[M]_0} = \left(\frac{f_1}{f_{1,0}} \right)^{\left(\frac{r_S}{1-r_S} \right)} \left(\frac{1-f_1}{1-f_{1,0}} \right)^{\left(\frac{r_1}{1-r_1} \right)} \left(\frac{f_{1,0} - \frac{1-r_S}{2-r_1-r_S}}{f_1 - \frac{1-r_S}{2-r_1-r_S}} \right)^{\left(\frac{1-r_1 r_S}{(1-r_1)(1-r_S)} \right)} \quad (\text{S2.42})$$

In the case of an ideal copolymerization ($r_1 r_S = 1$) the last term of the Meyer-Lowry equation becomes 0 and the equation can be linearized. This essentially leads to the equation proposed by Jaacks:

$$\ln \frac{[I]}{[I]_0} = r_1 \ln \frac{[S]}{[S]_0} \quad (\text{S2.43})$$

Method of determination of reactivity ratios

Reactivity ratios were determined from the time-dependent monomer conversions by using the Mayo-Lewis equation (Eq S2.34) the Fineman-Ross formalism (Eq S2.35-S.37), the Kelen-Tüdős formalism (Eq S2.38-S2.41) and the Meyer-Lowry formalism (Eq S2.42). The calculation of the fraction of S in the copolymer, F_S , is extremely prone to numerical errors, especially in case of only small differences within the data points. Thus, for the determination of highly disparate reactivity ratios via differential approaches (Mayo-Lewis, Fineman-Ross, Kelen-Tüdős) specialized methods for the calculation of the derivative must be applied. Simple calculation of the derivative via finite-difference methods results in noise amplification. We found the differentiation by using total-variation regularization the method of choice.³⁷ Unfortunately, even with optimized methods for the calculation of F the subtle change in gradient cannot be accurately determined via direct fitting of the Mayo-Lewis, Fineman-Ross or Kelen-Tüdős formalism (Figures S14-S16 and Table S3). Hence for the discussion, only the reactivity ratios determined via Meyer-Lowry are considered.³⁸

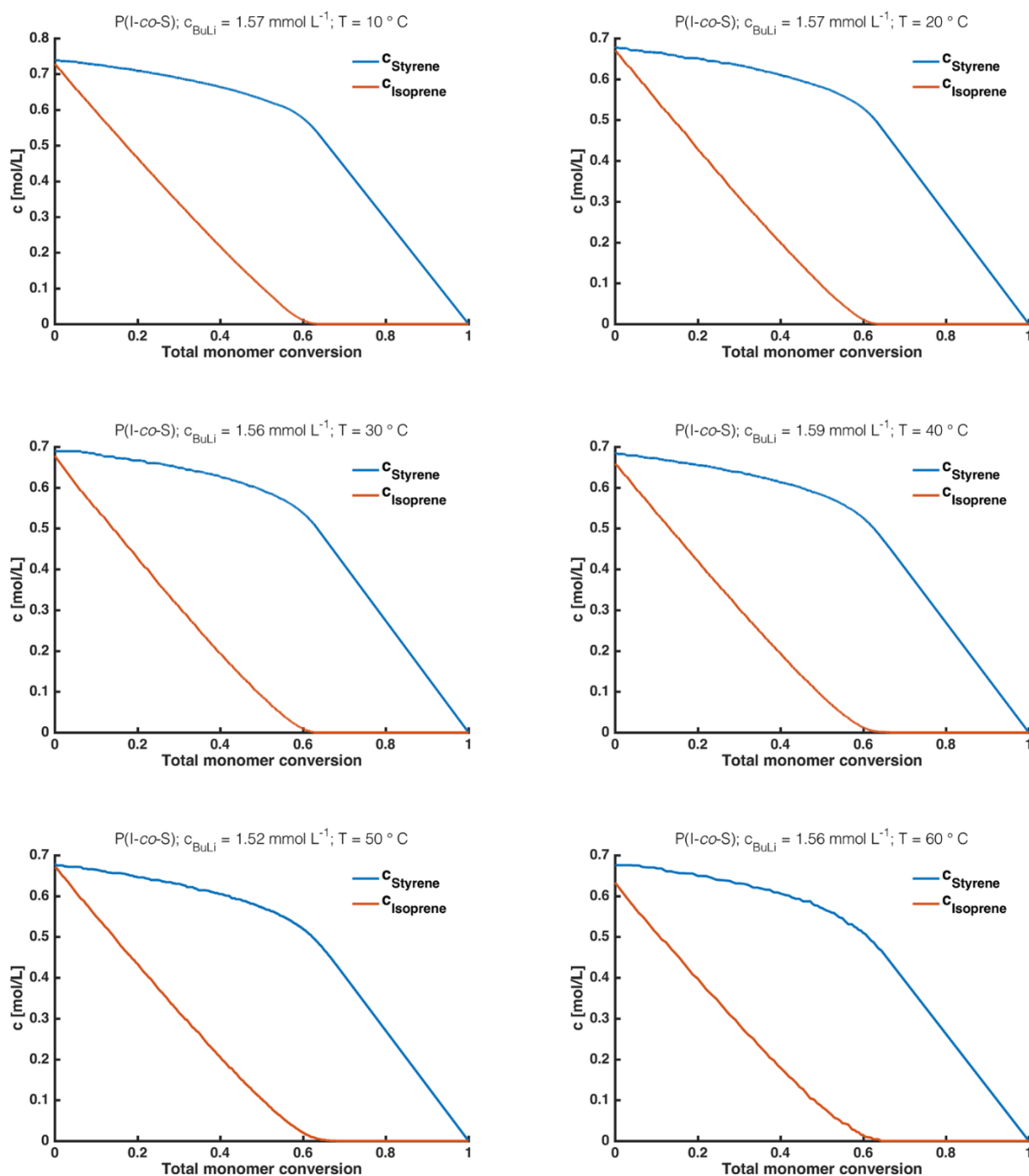


FIGURE S12 Individual monomer conversion (styrene: blue line, isoprene: red line) versus total monomer conversion for each performed copolymerization (10 °C to 60 °C). With increasing temperature, the change in slope becomes less sharp, a first indicator for less pronounced gradient of the resulting copolymer microstructure.

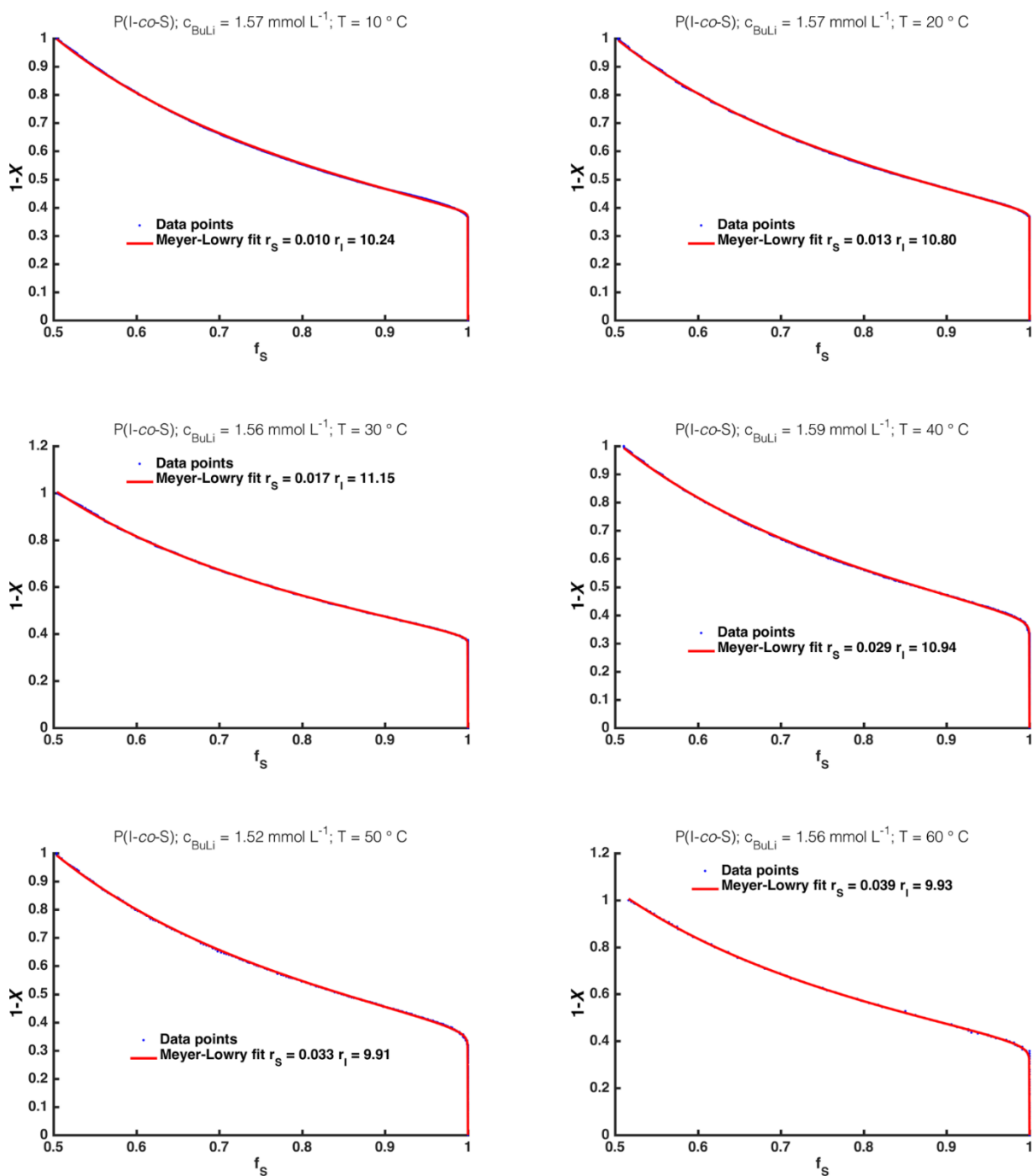


FIGURE S13 Meyer-Lowry fits (red line) ($1-X$ (total conversion)) versus actual fraction of styrene in the feed, f_S used for the evaluation of the reactivity ratios. In all cases excellent correlation was obtained. Due to this excellent correlation the measurement points (blue dots) are overlaid by the Meyer-Lowry fit.

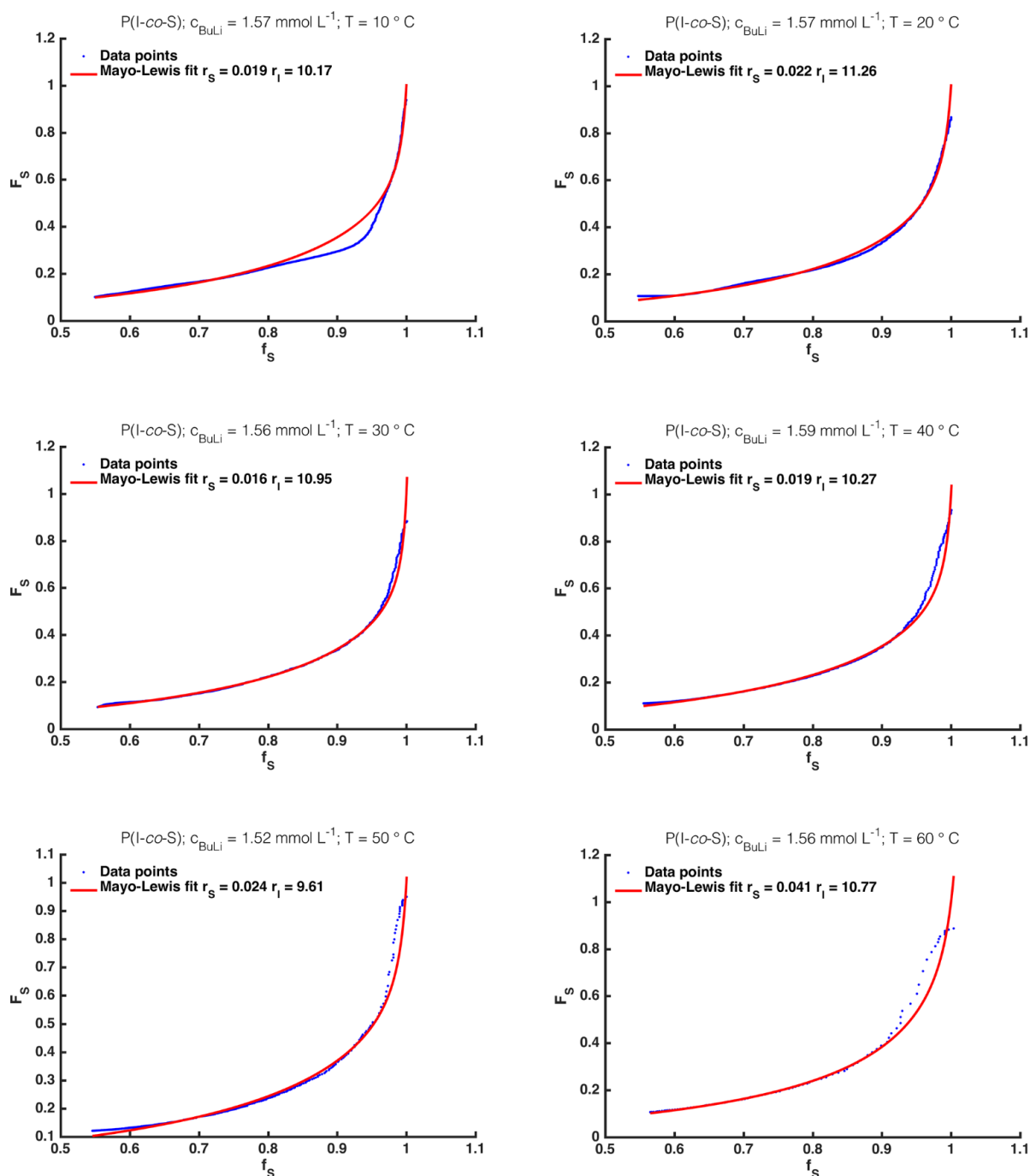


FIGURE S14 Evaluation of reactivity ratios via numerical fitting of the Mayo-Lewis copolymerization equation (red line). The data points (blue dots) were calculated by using total variable regularization method for the calculation of F_S and are prone to numerical noise. Therefore, this method shows increased uncertainty of the determined reactivity ratios and are given for reference only.

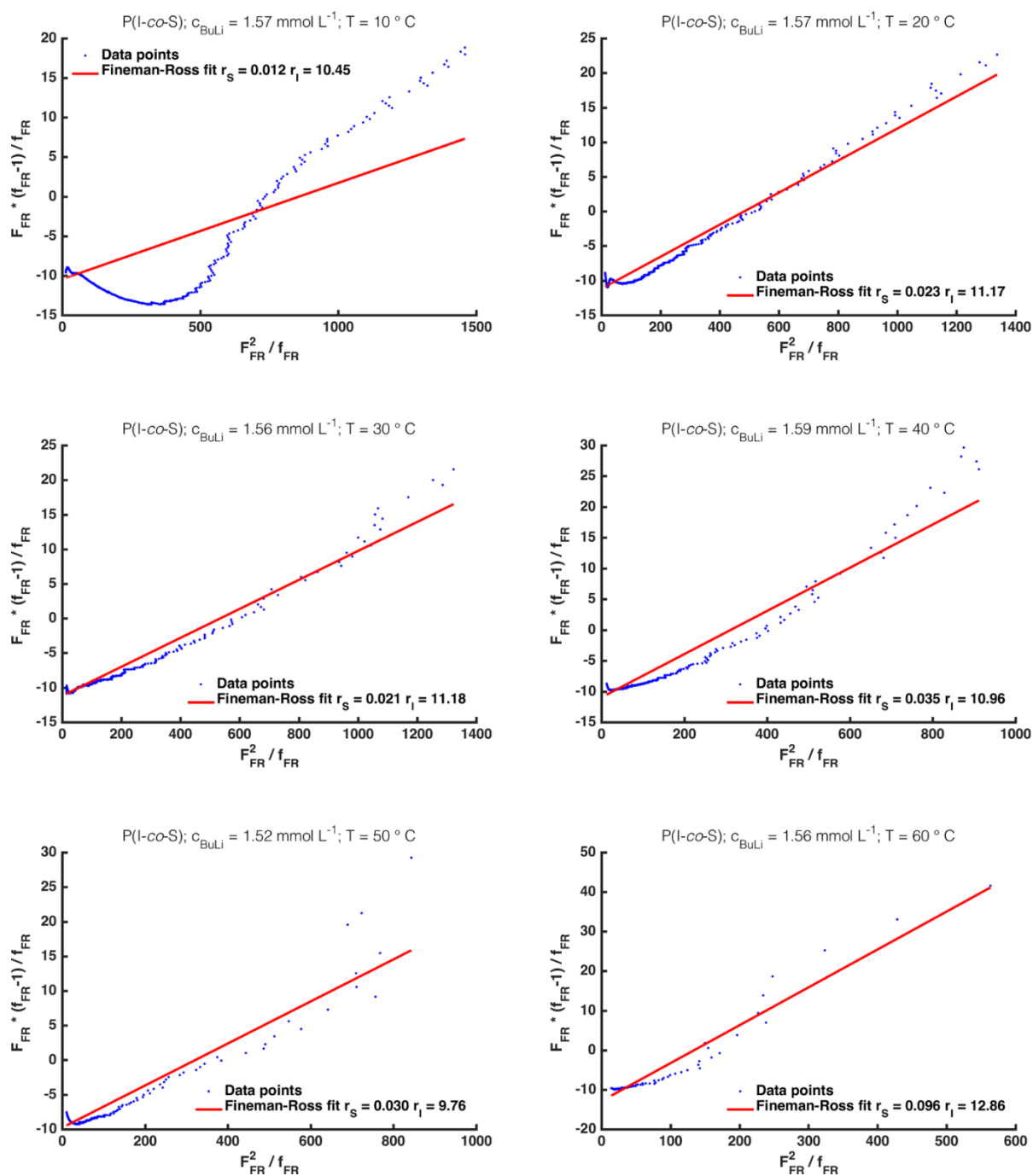


FIGURE S15 Evaluation of reactivity ratios using the Fineman-Ross formalism (red line). The data points (blue dots) were calculated using the total variable regularization method for the calculation of F_S and are prone to numerical noise. Therefore, this method shows increased uncertainty of the determined reactivity ratios and are given for reference only.

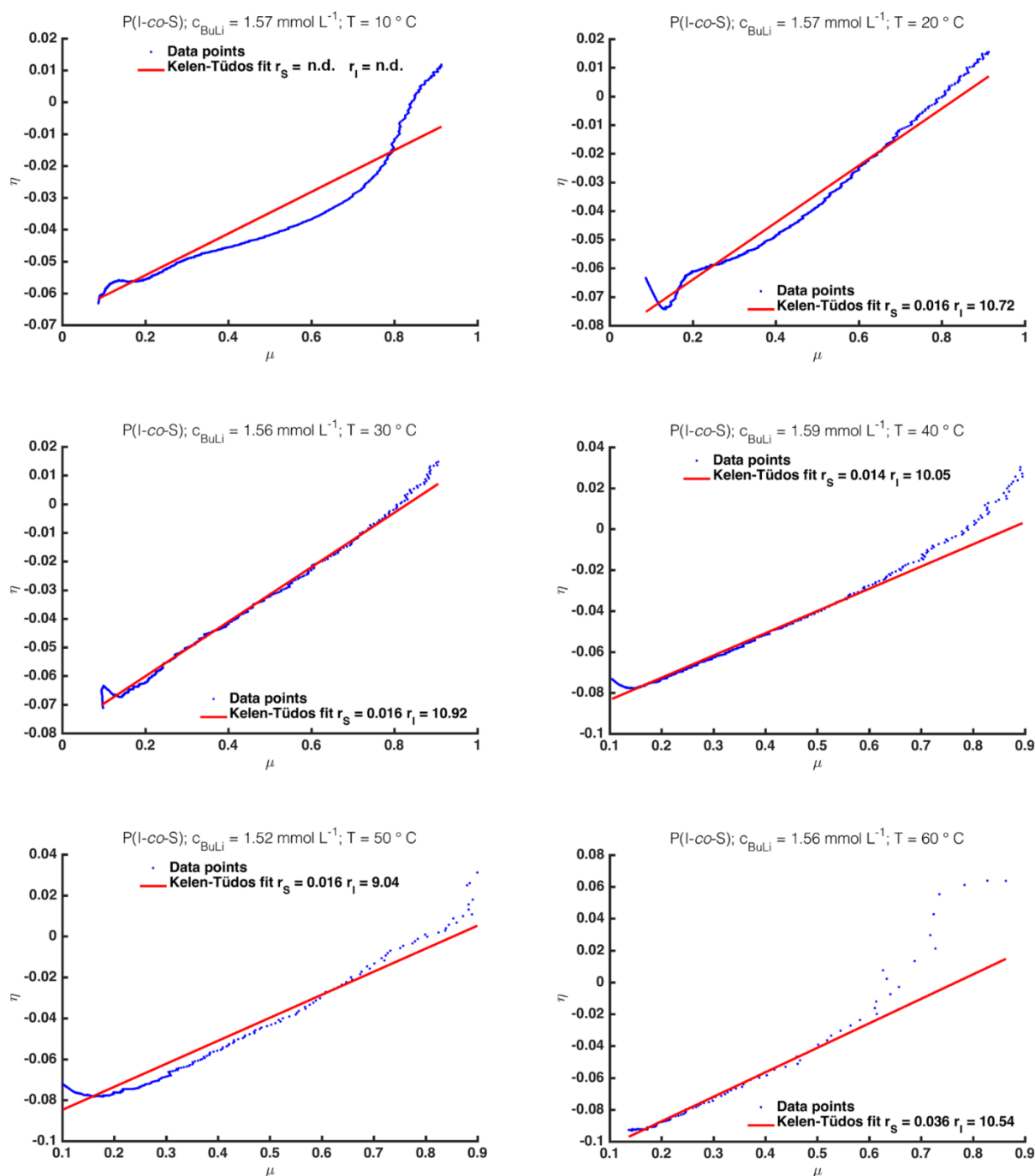


FIGURE S16 Evaluation of reactivity ratios using the Kelen-Tüdös formalism (red line). The data points (blue dots) were calculated using total variable regularization method for the calculation of F_S and are prone to numerical noise. Therefore, this method shows increased uncertainty of the determined reactivity ratios and are given for reference only. The data points are not distributed uniformly in regard of μ . Therefore, discrepancies of the fit to the datapoints are difficult to determine by eye. However, all data points have been used for the linear regression.

8. Temperature Dependence of Reactivity Ratios

TABLE S3 Calculated values for reactivity ratios (see Figure S17 for illustration).

T [°C]	Meyer-Lowry ^a		Mayo-Lewis ^b		Fineman-Ross ^b		Kelen-Tüdös ^b	
	r_1	r_5	r_1	r_5	r_1	r_5	r_1	r_5
10	10.24	0.010	10.17	0.019	10.45	0.012	n.d. ^c	n.d. ^c
20	10.80	0.013	11.26	0.022	11.17	0.023	10.72	0.016
30	11.15	0.017	10.95	0.016	11.18	0.021	10.92	0.016
40	10.94	0.029	10.27	0.019	10.96	0.035	10.05	0.014
50	9.91	0.033	9.61	0.024	9.76	0.030	9.04	0.016
60	9.93	0.039	10.77	0.041	12.86	0.096	10.54	0.036
80 ^d	10.03	0.072	n.d.	n.d.	n.d.	n.d.	n.d.	n.d.
THF (25 °C) ^a	0.61	1.839	n.d. ^c	n.d. ^c	n.d. ^c	n.d. ^c	n.d. ^c	n.d. ^c

a: Only Meyer-Lowry formalism was suitable for accurate evaluation of the reactivity ratios. b: Given only for reference and the comparison of the different methods c: Not determined due to high numerical noise induced by the necessary calculation of F_5 . d: Reactivity ratios are extrapolated by using the activation energies determined by measurements (Figure 3) in the temperature range from 10 to 60 °C.

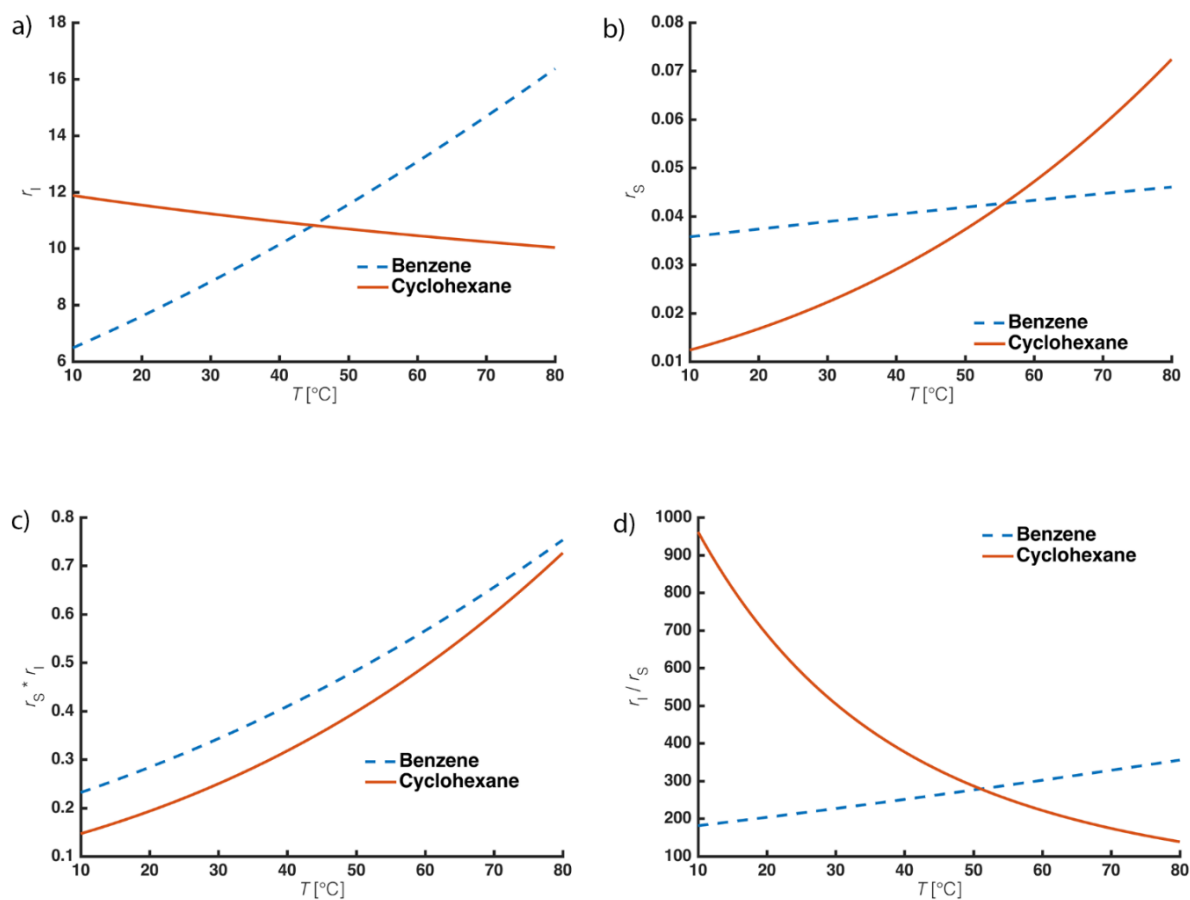


FIGURE S17 Comparison of the reactivity ratios in benzene and cyclohexane in dependency of the reaction temperature. Values in benzene were taken from Fontanille and coworkers.¹³ Prediction of the reactivity ratios were performed by feeding the Arrhenius equation and calculating the reactivity ratios for every temperature in the range of 10 to 80 °C. (a) Reactivity ratio of isoprene versus temperature. In benzene the homopolymerization of isoprene is favored at higher temperatures, leading to high r_1 values. In contrast only a subtle decrease in r_1 can be seen for isoprene in cyclohexane. (b) Reactivity ratio of styrene versus temperature. r_S increases with higher reaction temperature up to 4 fold in the range from 10 to 80 °C. (c) Graph of $r_1 \cdot r_S$ versus temperature to demonstrate the influence of temperature leading to an ideal copolymerization behavior. With increasing temperature, the copolymerization proceeds to show ideal behavior ($r_S \cdot r_1 = 1$) for both cyclohexane and benzene. (d) Graph of the ratio of r_1/r_S versus temperature. A high ratio denotes disparate reactivity values, an indicator for the steepness of the gradient. With increasing temperature, a less steep gradient is observed, when the polymerization is performed in cyclohexane. In contrast to the behavior in benzene an increased gradient is expected.

9. Kinetic Monte Carlo Simulations

The kinetic Monte Carlo simulation model was developed based on the stochastic simulation algorithm by Gillespie.^{39,40} In this approach the continuum-based reaction rates (e.g. rate constants determined via NIR) are converted to number-based probabilities using the following equations:

$$kMC_{II} = \frac{k_{II}}{(NV)^{1/4}}$$

$$kMC_{SS} = \frac{k_{SS}}{(NV)^{1/2}}$$

$$kMC_{IS} = \frac{k_{IS}}{(NV)^{1/4}}$$

$$kMC_{SI} = \frac{k_{SI}}{(NV)^{1/2}}$$

The simulation volume (typically $2 \cdot 10^{-16}$ L) was used to convert the concentration of all reagents to number of molecules (typically 92,800,000 molecules of styrene and 92,800,000 molecules of isoprene) in the kMC simulation. For each simulation, the number of polymer chains were set to 500,000 and the polymerization was performed until a conversion of 99.5% was reached. For better comparison all polymerizations were simulated with the same conditions ($P_n(I) = P_n(S) = 464$, $c_{BuLi} = 1.5$ mmol, target MW = $79933 \text{ g} \cdot \text{mol}^{-1}$).

For each simulation step the reaction probability is calculated based on the fraction of the total reaction rate of all components:

$$P_v = \frac{R_v}{\sum_{M=1}^{\mu} R_v}$$

Then one reaction is chosen using a uniform distributed random number $rn_1 = [0..1]$ based on the reaction probabilities:

$$\sum_{v=1}^{\mu-1} P_v < rn_1 < \sum_{v=1}^{\mu} P_v$$

The necessary reaction step to perform the reaction is calculated using another uniformly distributed number $rn_2 = [0..1]$:

$$\tau = \frac{1}{\sum_{M=1}^{\mu} R_v} \ln \left(\frac{1}{rn_2} \right)$$

After the chosen reaction step has been applied, the calculation is started again, until the number of molecules left in the simulation volume is below the desired threshold, governed by the desired conversion (99.5 %). The resulting data is then used for the prediction of SEC traces, segment length distributions and triads. The segment length is defined as the number of coherent monomers of one type without interruption. Implementation of this model was performed in C code, compiled using MinGW GCC compiler 5.1.

10. Microstructure of Copolymers

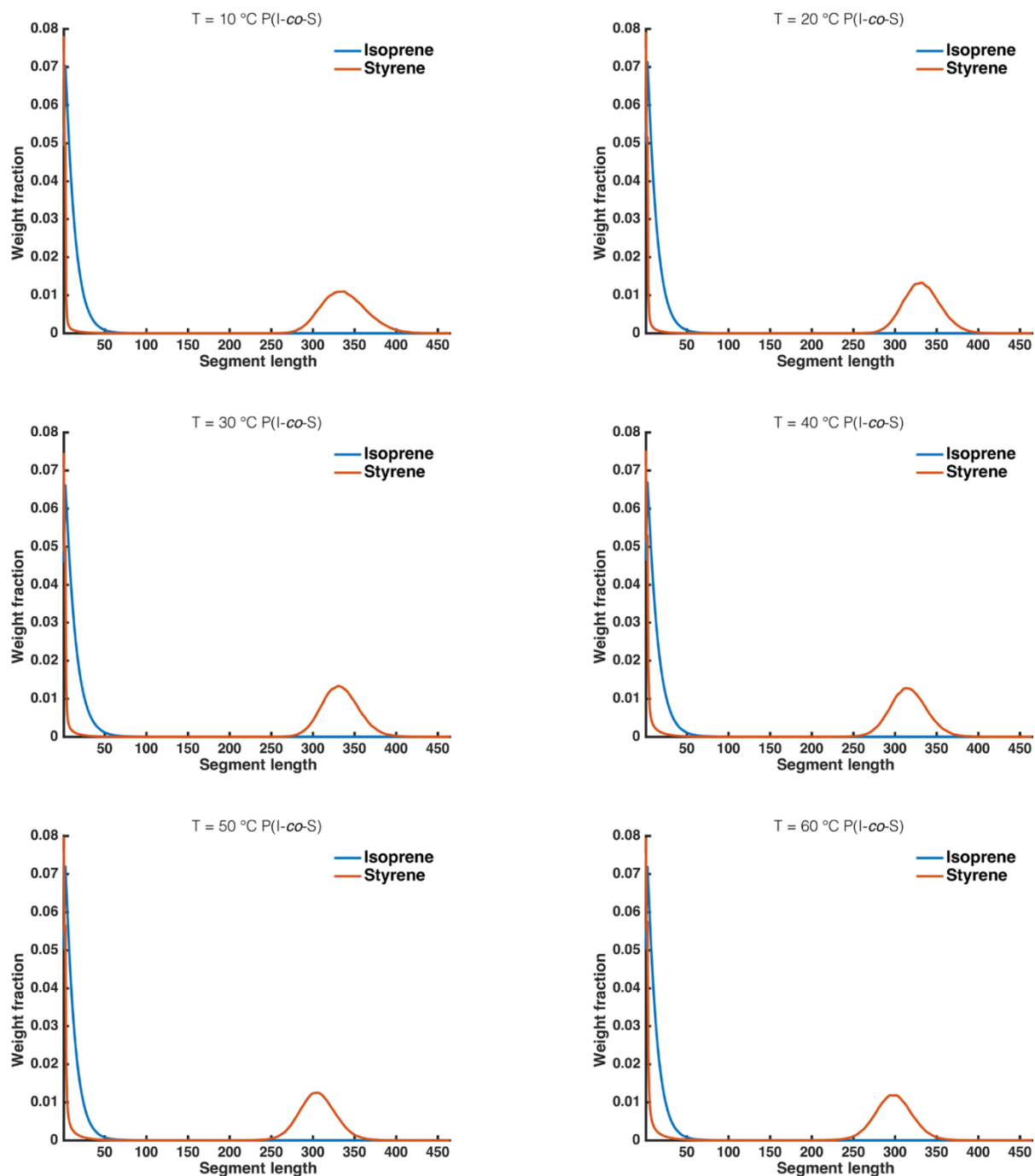


FIGURE S18 Mass weighted segment length distribution for each copolymerization (10 °C to 60 °C) calculated via kMC for isoprene (blue line) and styrene (red line). With increasing temperature, the low molecular weight segments (< 20) for styrene are increased and more styrene is incorporated during the gradient. As a direct result, the size of the styrene block is decreased due to mass conservation.

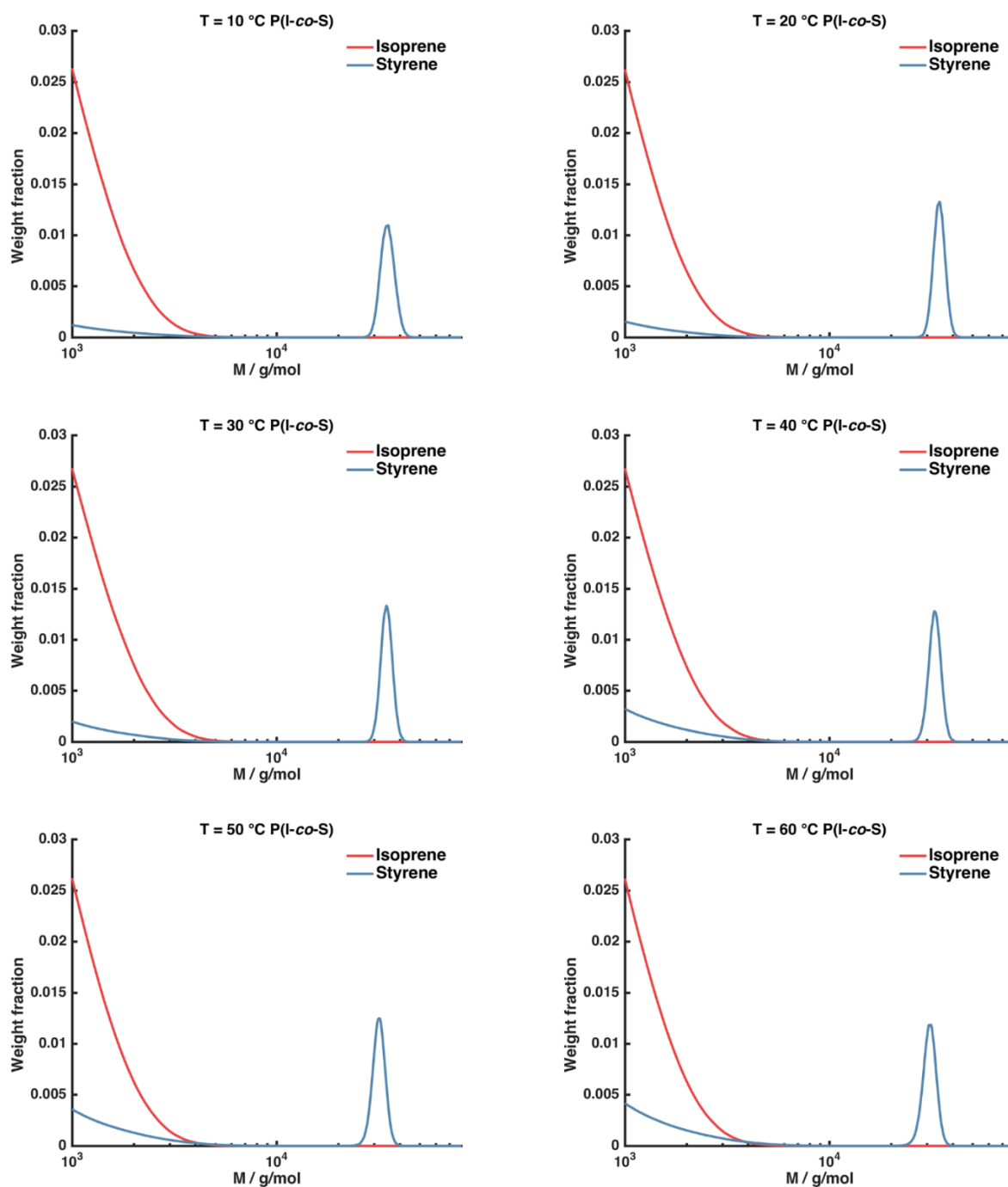


FIGURE S19 Mass weighted molecular weight distribution based on the segment length distribution for each copolymerization (10 °C to 60 °C) calculated via kMC for isoprene (blue line) and styrene (red line). With increasing temperature, the low molecular weight segments ($P_n < 20$) for styrene are increased and more styrene is incorporated during the gradient. As a direct result the size of the styrene block is decreased due to mass conservation.

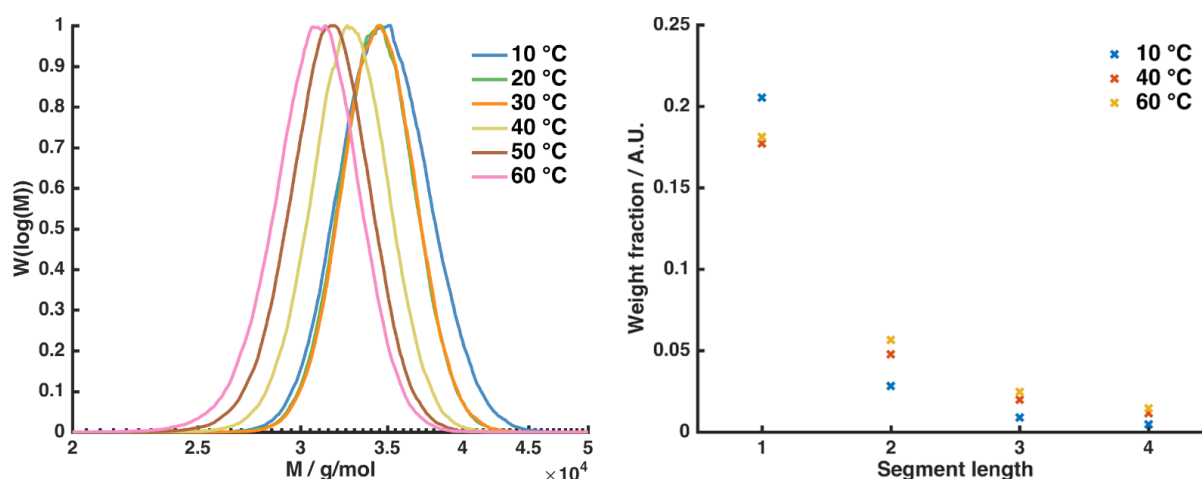


FIGURE S20 a) Simulated molecular weight distribution (left) of the pure PS block formed during the course of P(I-co-S) copolymerization. b) Simulated low molecular weight segment length distribution (weight based) of PS in P(I-co-S) tapered block copolymers.

TABLE S4 Analysis of triad distribution and average degrees of polymerization of segments as calculated by kinetic Monte Carlo simulation.

T [° C]	T _{99.5} ^a [h]	III/ %	IIS + SII/ %	ISI/ %	ISS + SSI/ %	SIS/ %	SSS/ %	DP _n (I) ^b	DP _w (I) ^b	DP _n (S) ^b	DP _w (S) ^b	DP _{Peak} (S) ^b
10	48.3	32	15	10	2.2	4.0	37	4,5	11.5	4.4	247	337
20	14.3	32	15	10	2.5	4.0	37	4,4	11.3	4.3	240	332
30	5.4	33	14	9.2	2.9	3.7	38	4,7	12.3	4.6	241	330
40	2.3	32	14	8.7	4.0	3.7	37	4,7	12.1	4.6	218	311
50	0.8	32	15	9.2	4.5	4.1	36	4,4	11.1	4.3	204	306
60	0.4	32	15	8.9	4.9	4.0	36	4,4	11.2	4.3	194	302

a) Predicted reaction time for total monomer conversion of 99.5 %. b) Number-average and weight-average segment lengths of either isoprene or styrene segments respectively. Based on the less steep gradient, induced by higher reaction temperatures, a significant amount of styrene is incorporated into the isoprene rich part during polymerization, leading to smaller sizes of the PS block formed subsequent to formation of the taper. Therefore, the weight average-based segment length P_w decreases drastically. This microstructural change can also be detected in the increasing number of ISS and SSI triads.

11. Monitoring of decablock copolymer synthesis via NIR real-time probing

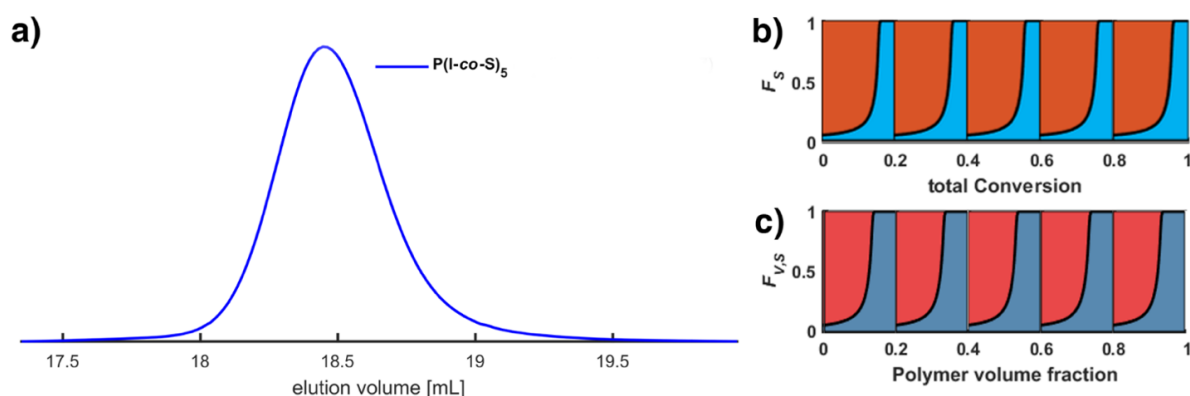


FIGURE S21 a) SEC Eluogram (RI detector) with M_n and \bar{D} based on dual calibration by using PI and a PS standards according to their weight fraction (see Instrumentation Section; $M_n = 215$ kg/mol; $\bar{D} = 1.09$; $M_n(\text{target}) = 240$ kg/mol). b) Composition profile according to molar fraction c) Composition profile according to volume fraction of the sequential diblock copolymer P(I-co-S)₅. In this case a 50%_{mol} molar fraction of isoprene was used (see diagram b)) to obtain a volume fraction, resulting in a lamellar morphology as shown in a previous work.¹ The lower isoprene content as compared to the sequentially made block copolymers is necessary to obtain a 50%_{vol} fraction. This can be attributed to the incorporation of polystyrene into the tapered polyisoprene block. This leads to swelling of the tapered polyisoprene block and a shrinkage of the polystyrene block, shifting the gradient towards lower values of the polymer volume fraction. The inflection point of the gradient in the volume diagram (see c)) was used to determine the polymer volume fraction of the block transition. A more detailed description of these tapered multiblock structures is given in a previous work.¹

12. Kinetics and microstructure in the copolymerization in presence of THF

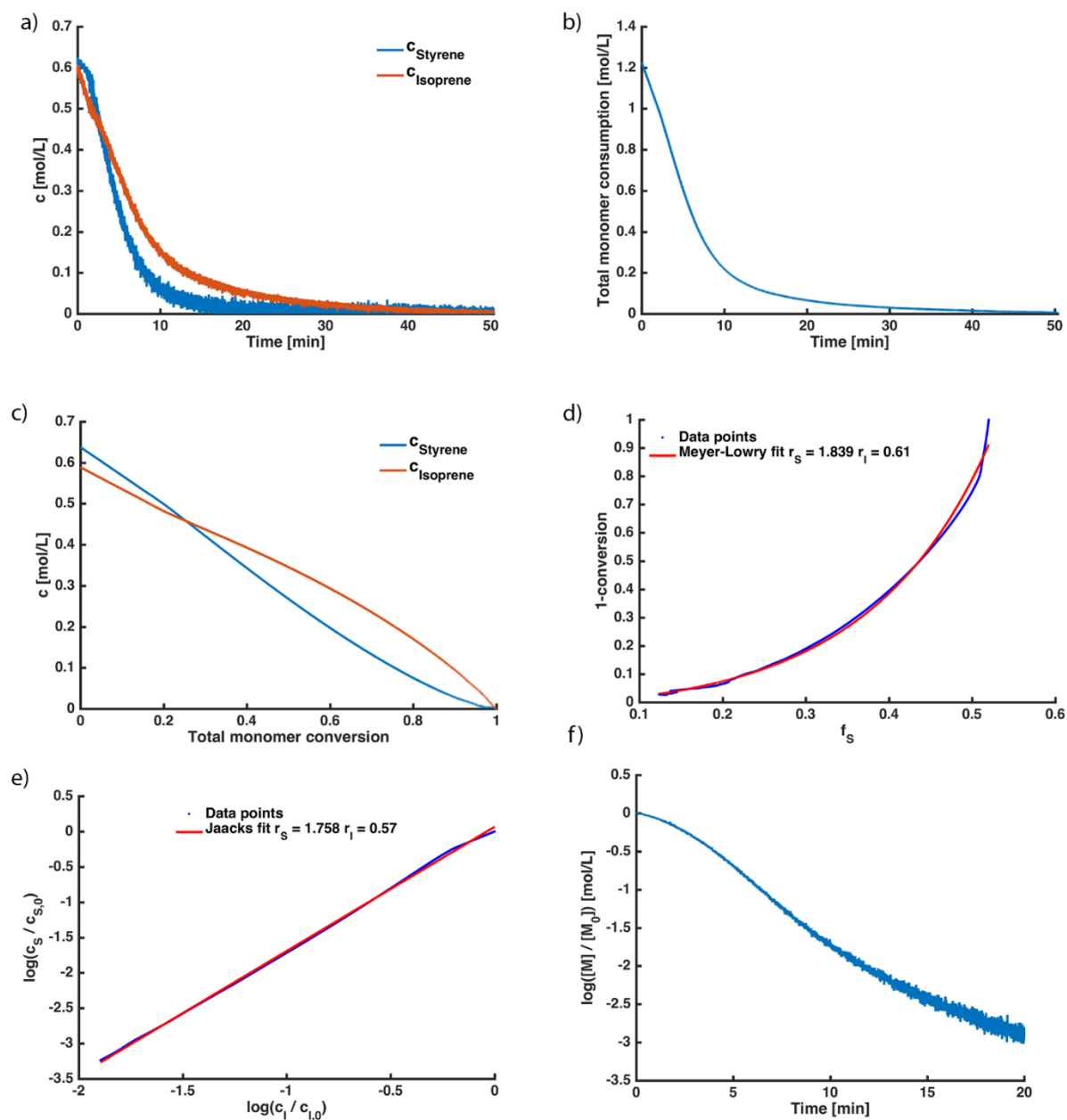


FIGURE S22 Copolymerization of styrene and isoprene in cyclohexane at 25 °C with addition of 100 equivalents of THF relative to butyllithium ($c_{\text{BuLi}} = 1.5 \text{ mmol L}^{-1}$) leading to a copolymer with a strongly deviating monomer sequence as compared to the copolymers prepared in pure cyclohexane. (a) Individual monomer conversions versus time. Due to high temporal resolution (0.33 s per data-point) increased noise is observed. (b) Total monomer conversion versus time after data smoothing. (c) Individual monomer conversion versus total monomer conversion. The slightly favored incorporation of styrene can be seen by the slight curvature of the graph (blue line). (d) Evaluation of the reactivity ratios via Meyer-Lowry formalism. (e) Evaluation of the reactivity ratios via Jaacks method. In this special case an ideal copolymerization ($r_s \cdot r_1 = 1$) is assumed. (f) Logarithmic representation of the normalized total monomer conversion versus time.

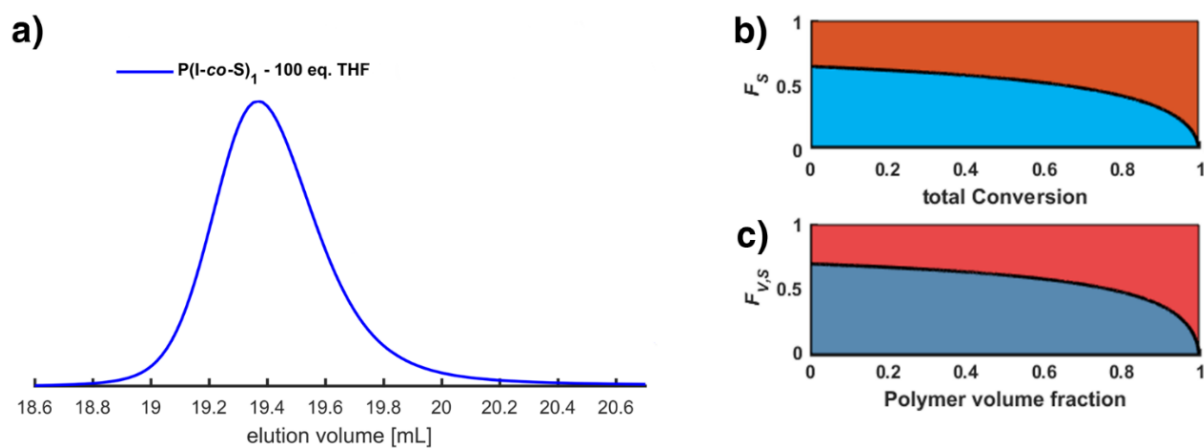
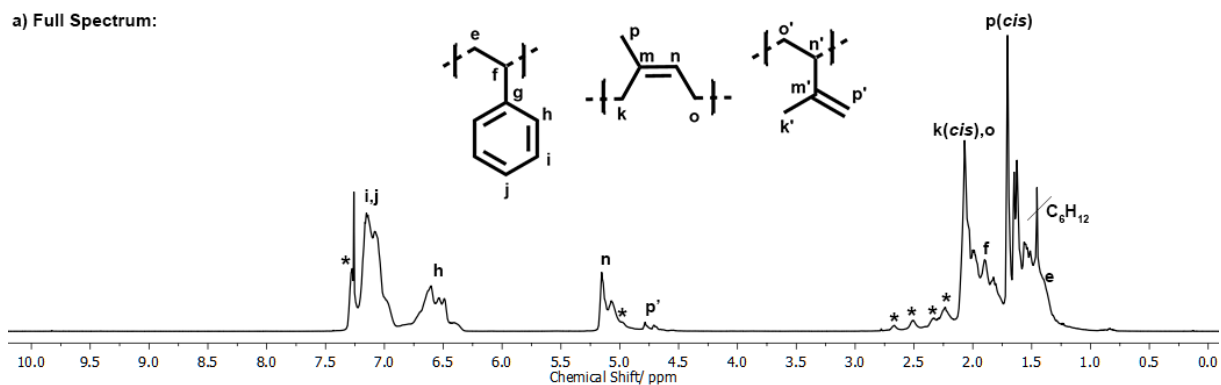


FIGURE S23 a) Eluogram (RI detector) with M_n and \bar{D} based on dual calibration by using PI and a PS standards according to their weight fraction (see Instrumentation Section; $M_n = 79.9$ kg/mol; $\bar{D} = 1.09$; $M_n(\text{target}) = 80$ kg/mol. b) Composition profile according to molar fraction c) Composition profile according to volume fraction of the copolymer P(I-co-S). In this case a 50%_{mol} molar fraction of isoprene was used (see diagram b)) resulting in the volume composition visualized in diagram c).

13. Microstructural Investigations via NMR on the tapered diblock copolymers

1) Poly(isoprene-co-styrene)

a) Full Spectrum:



b) Aliphatic Region:

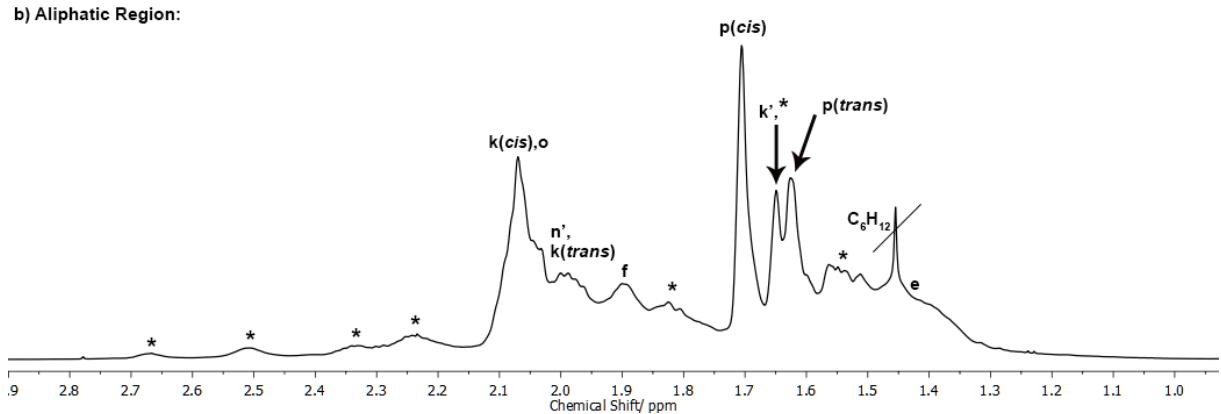


FIGURE S24A ^1H NMR spectrum (600 MHz, CDCl_3) of Poly(isoprene-co-styrene).

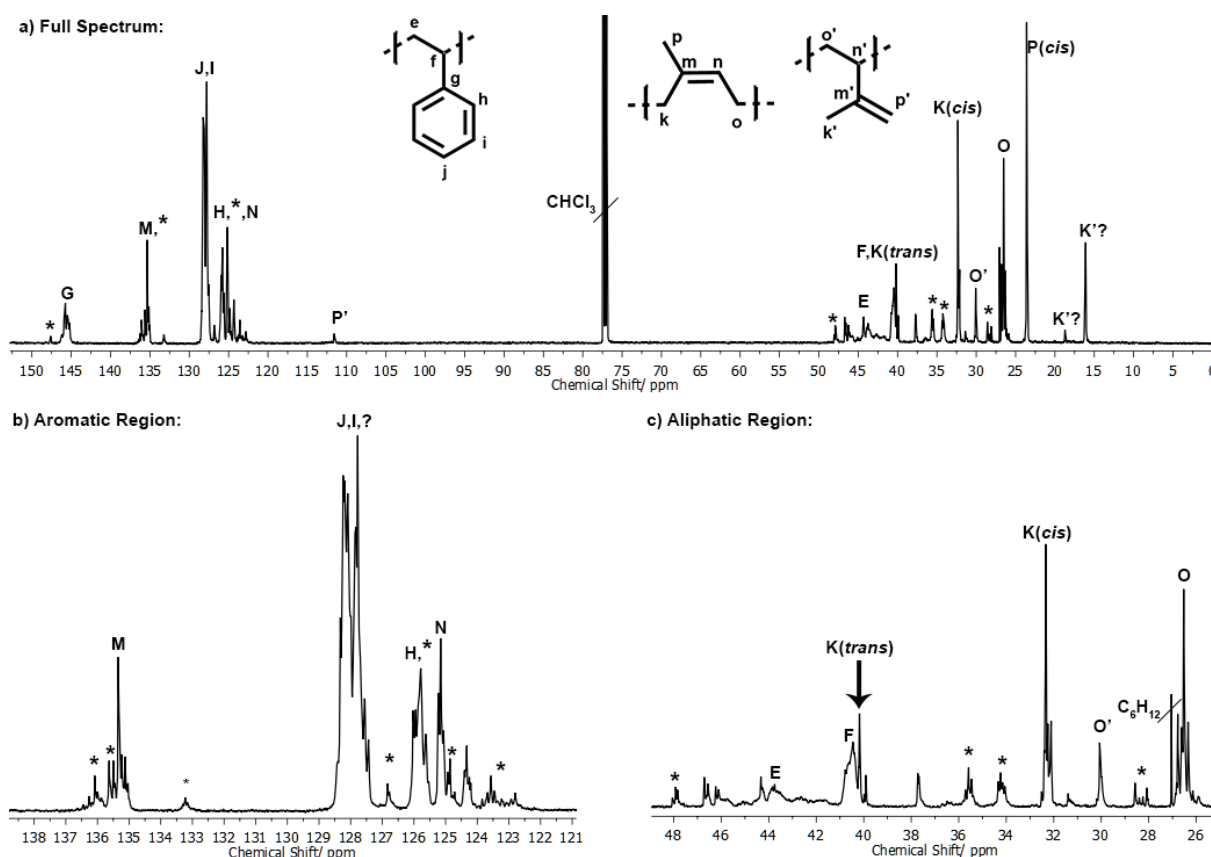


FIGURE S24B ^{13}C NMR spectrum (150 MHz, CDCl_3) of Poly(isoprene-co-styrene). The shift of the signals marked with (*) are not visible in the ^1H NMR spectrum of polyisoprene or polystyrene and attributed to different chemical shift of single monomer units attributed to the presence of different triads (Table S4) than III and SSS which are not present in the homopolymers and the block copolymer (PI-*b*-PS).

The evaluation of the signals in the NMR spectra of polyisoprene homopolymer is known to be rather complex and was discussed in several works. The incorporation of styrene units into the manifold triads of the PI isomers do not allow for an assignment without advanced NMR techniques exceeding the evaluation of ^1H and ^{13}C assignments via the 2 dimensional NMR methods as used for PS (Figure S6) and PI (Figure S7) homopolymers.

2) Comparison of homo-, block- and tapered block copolymers

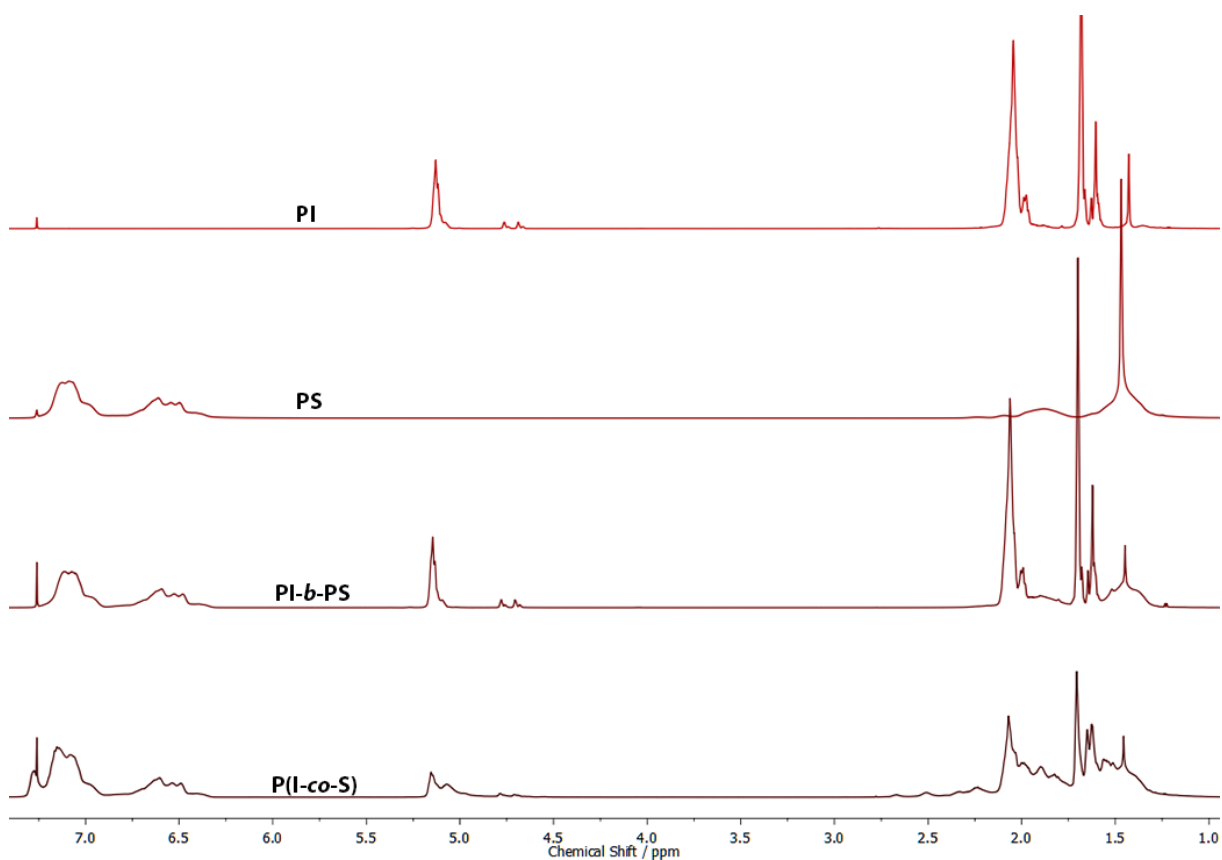


FIGURE S25A Stacked ^1H NMR spectra (600 MHz, CDCl_3) of homopolymers (see also Figure S6 and S7), as well as a block-, and a tapered block copolymer (see also Figure S25), based on styrene and isoprene.

An assignment of the peaks in the ^1H NMR spectrum can be found in Figures S6, S7 and S24. We want to emphasize that the block copolymer PI-*b*-PS is composed of 57%_{mol} polyisoprene units, while the tapered block copolymer exhibits a 50%_{mol} fraction of polyisoprene units P(I-*co*-S).

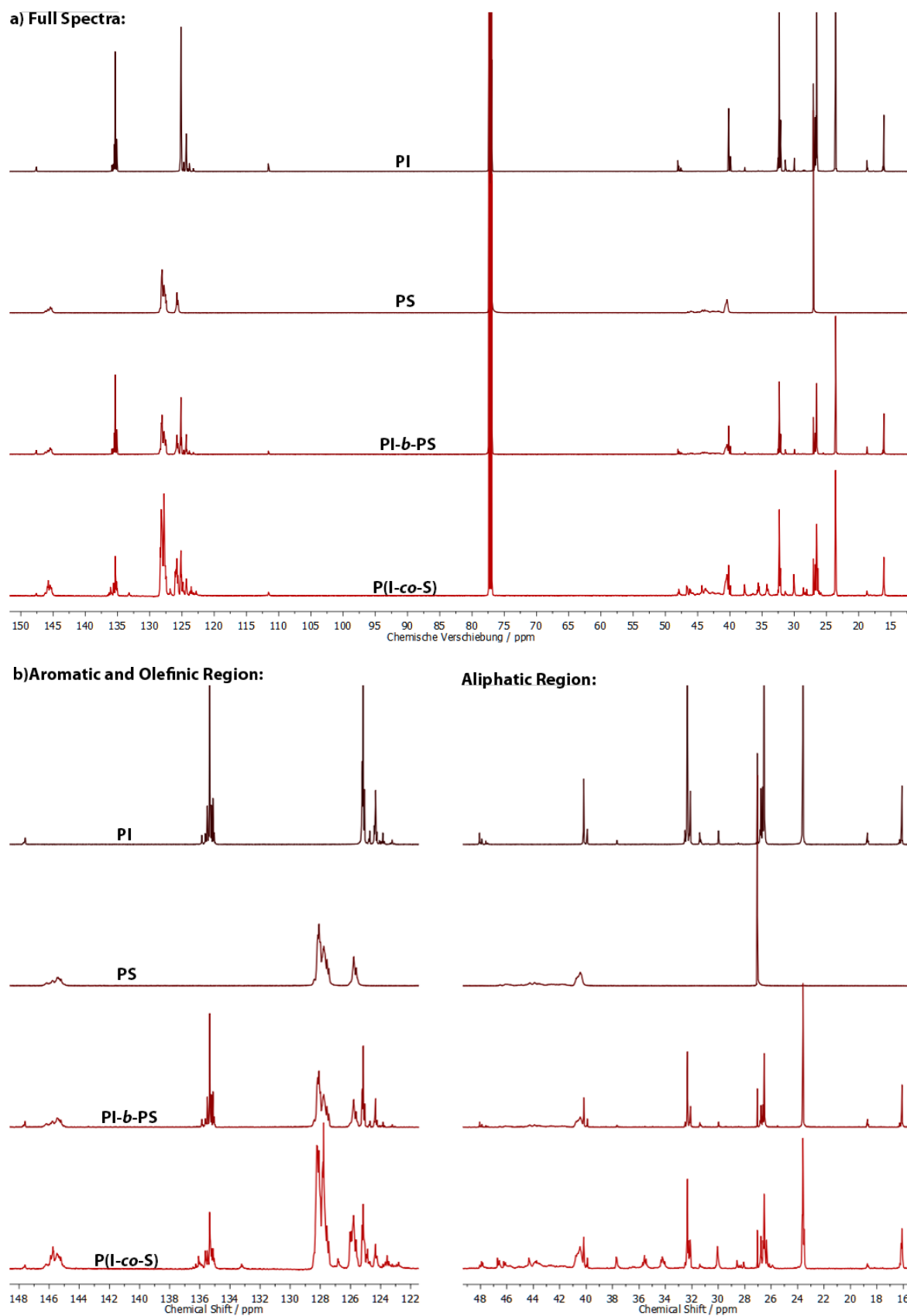


FIGURE S25B Stacked ^{13}C NMR spectra (150 MHz, CDCl_3) of homo-, block-, and tapered block copolymers based on styrene and isoprene.

The selected spectra clearly highlight the differences of block and tapered block copolymers. The simple architecture of an PI-*b*-PS block copolymer can be described as two homopolymers linked together. This is visualized by the stacked ^1H and ^{13}C NMR spectra, as the spectrum of PI-*b*-PS is a simple addition of the signals in the spectra of PI and PS.

In contrast, the spectrum of the tapered block copolymer P(I-*co*-S) exhibit additional signals which cannot be found in the spectrum of PI, PS or PI-*b*-PS (for example: ^1H NMR spectrum: 7.6 ppm, 2.75-2.15 ppm). Additionally, the shape of the signals in the overlapping regions (for example: ^1H NMR spectrum: 5.2 - 4.65 ppm, 2.15 - 1.5 ppm) differs for both copolymers. This can be attributed to different chemical surroundings for the PI and PS repeating units. As only III and SSS triads are present in the homopolymers as well in the block copolymer, the tapered block copolymer also shows ISS / SSI, ISI, SII / IIS and SIS monomer sequences, clearly visible in the spectrum of P(I-*co*-S).

3) Comparison of tapered block copolymers obtained at different polymerization temperatures

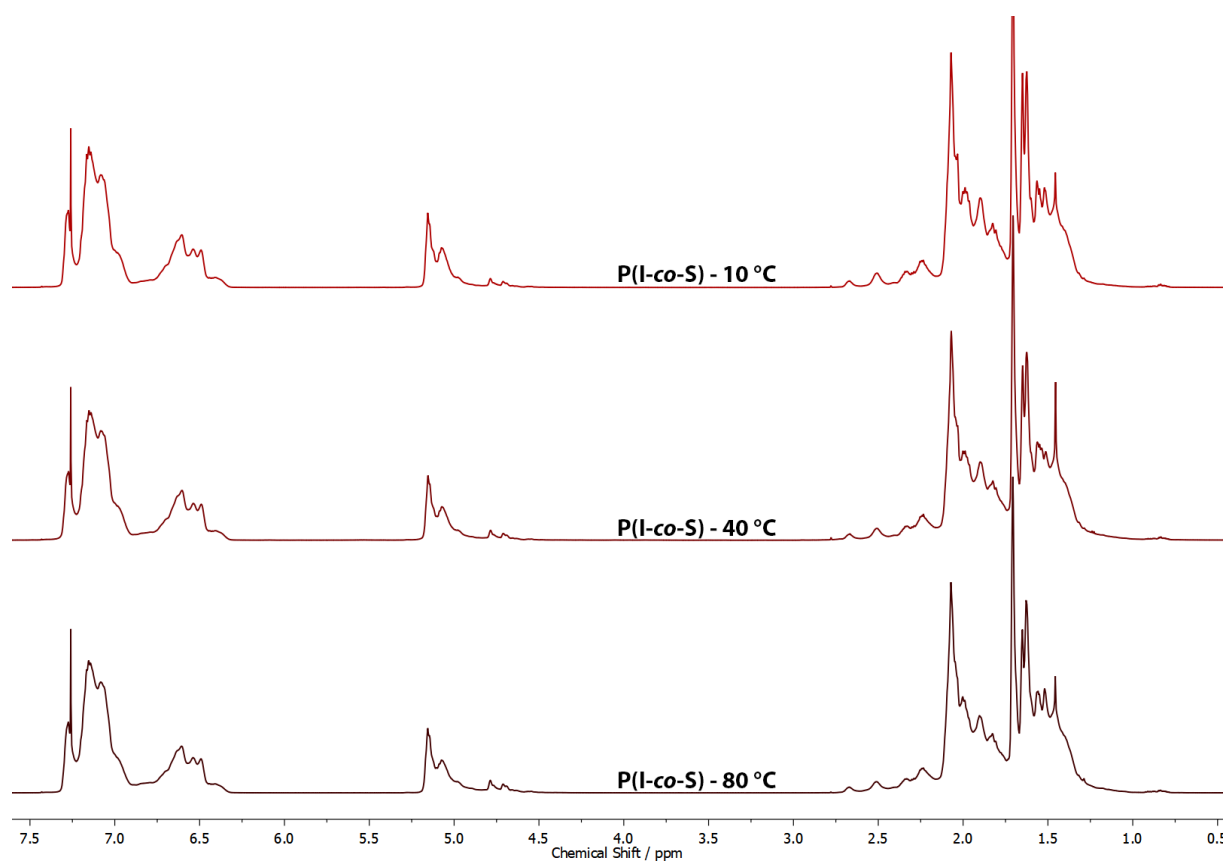


FIGURE S26A Stacked ¹H NMR spectra (600 MHz, CDCl₃) of tapered block copolymers based on styrene and isoprene obtained by the statistical copolymerization at different polymerization temperatures. The different polymerization temperatures have been assigned in the figure next to the respective spectrum. The spectra do not show a significant difference, confirming a comparable monomer sequence for the copolymerization over the temperature range from 10 to 80 °C.

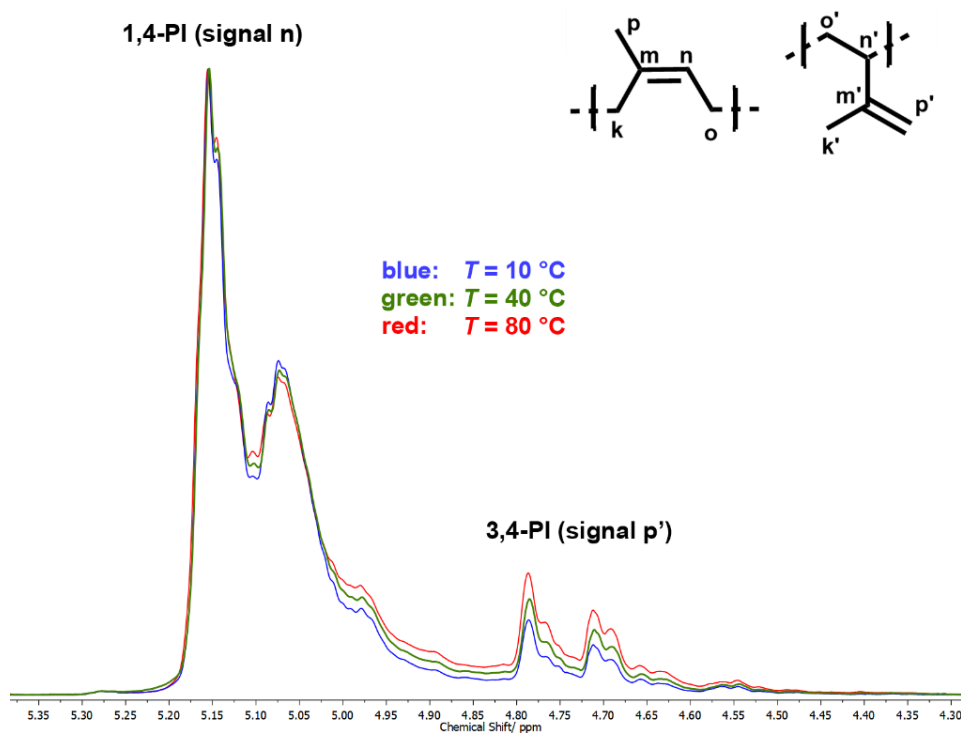


FIGURE S26B Stacked ¹H NMR spectra (600 MHz, CDCl₃) of tapered P(I-co-S) block copolymers based on styrene and isoprene obtained by the statistical copolymerization at different polymerization temperatures. The different polymerization temperatures have been assigned in the figure next to the respective spectrum and show an increase of the proton resonance signal of the 3,4-units in relation to the proton resonance signal of the 1,4-units. This effect is also known for the respective PI homopolymerization.⁴¹

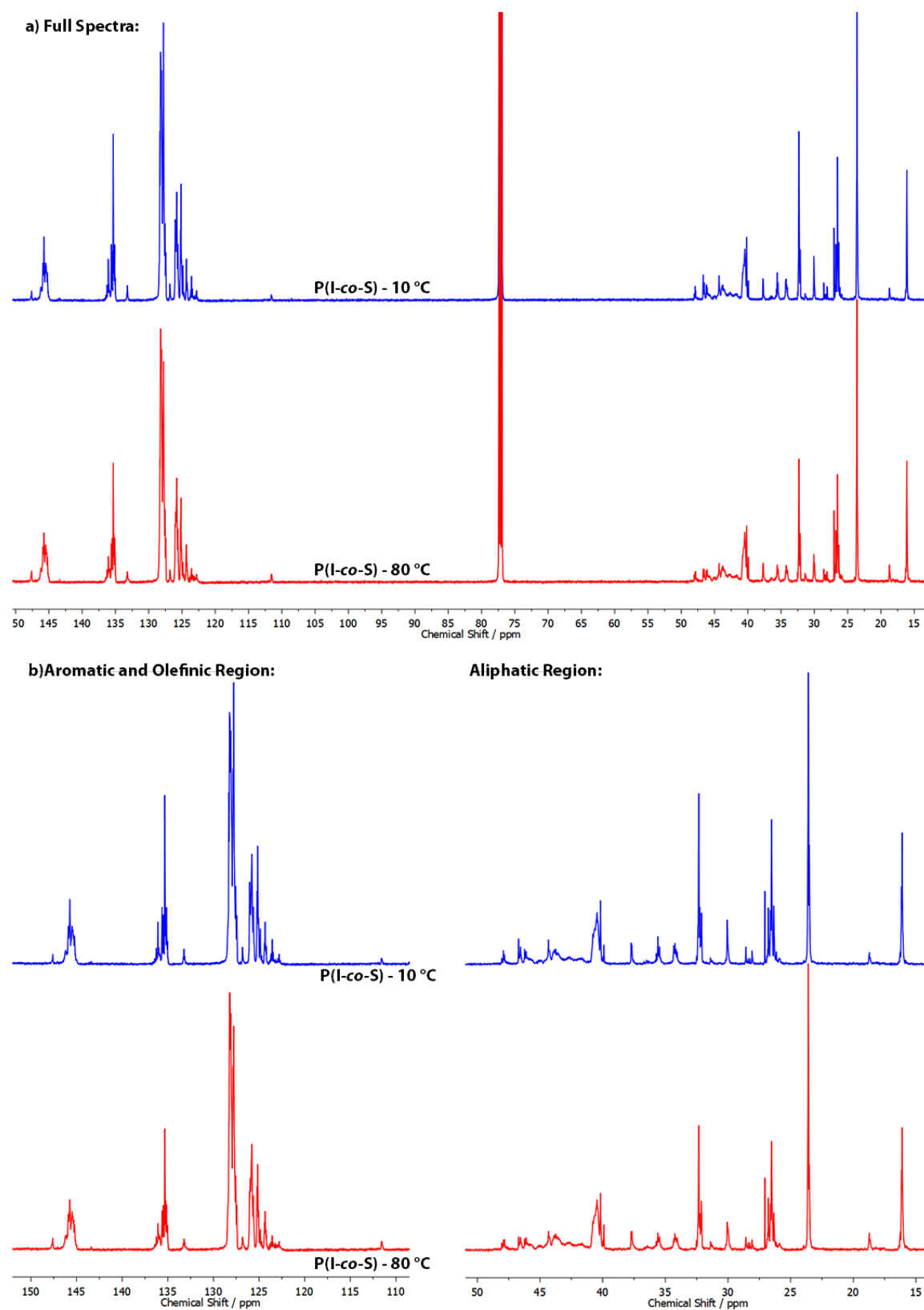


FIGURE S26C Stacked ^{13}C -inverse gated -NMR spectra (600 MHz, CDCl_3) of tapered block copolymers based on styrene and isoprene obtained by the statistical copolymerization at different polymerization temperatures. The different polymerization temperatures have different been assigned in the figure next to the respective spectrum. The spectra do not show a significant difference, confirming the occurrence of similar triades for both tapered block copolymers synthesized at 10 and 80 °C.

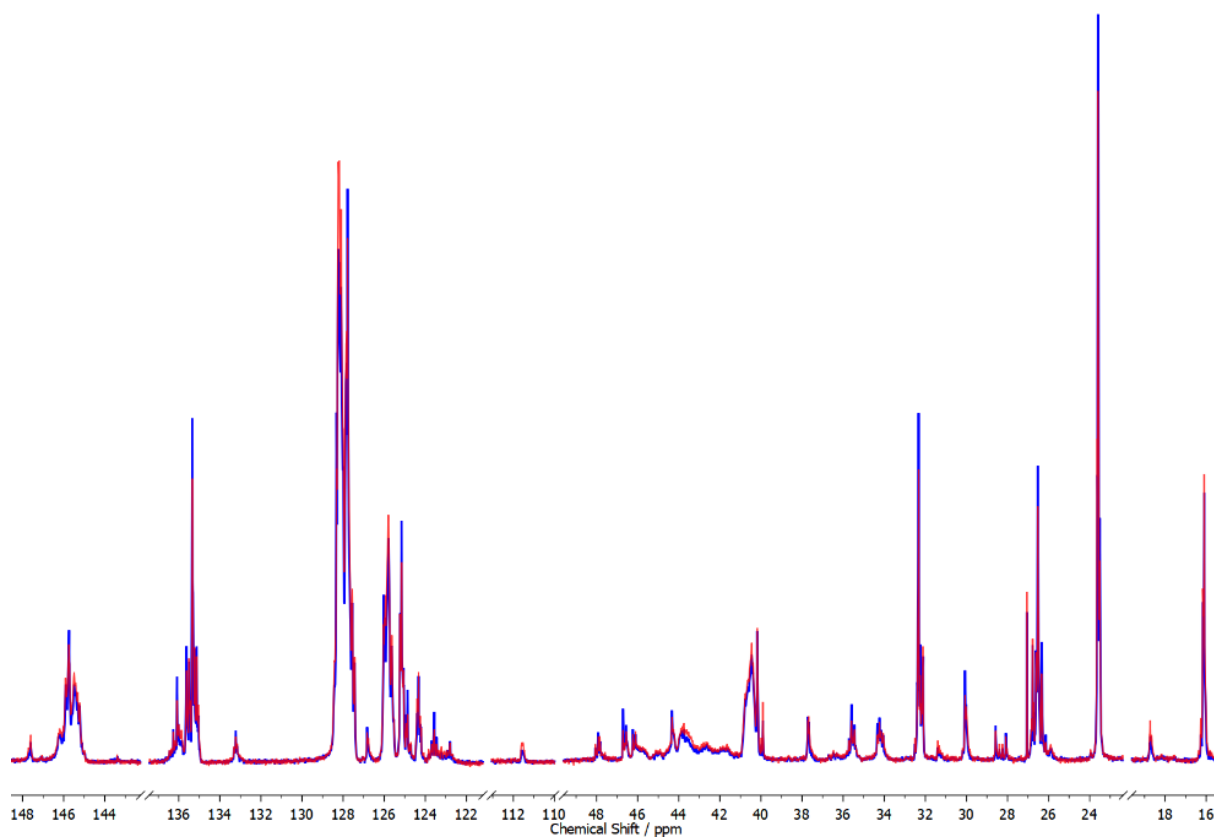


FIGURE S26D Stacked ^{13}C NMR *inverse gated* spectra (600 MHz, CDCl_3) of tapered block copolymers based on styrene and isoprene obtained by the statistical copolymerization at different polymerization temperatures. The different polymerization temperatures have been assigned in the figure next to the respective spectrum. The spectra show a difference in the intensity of various signals. This observation supports the suspected change of the triad composition (Table S4) for the copolymerization over the temperature range from 10 to 80 °C.

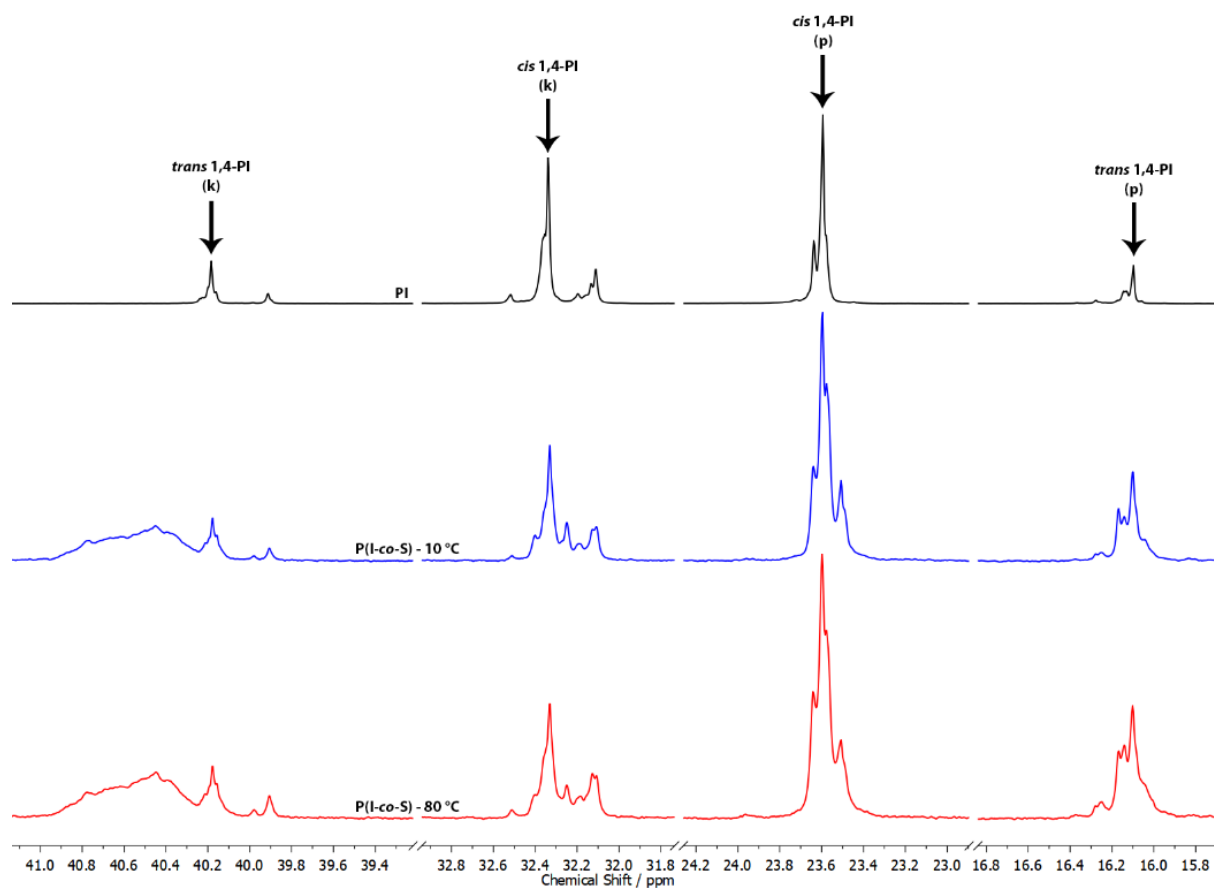


FIGURE S26E Comparison of the zoomed region of the stacked ^{13}C NMR *inverse gated* spectra (600 MHz, CDCl_3) of an PI homopolymer and tapered block copolymers obtained by the statistical copolymerization at different polymerization temperatures. The zoomed area was used to determine the change in the ratio of *cis* to *trans* 1,4-PI units. The different polymerization temperatures have been assigned in the figure next to the respective spectrum. The signals show a significant overlap with signals attributed to pure PS triads (SSS) (Figure S6B) and other triads, which are formed during the copolymerization (Table S4).

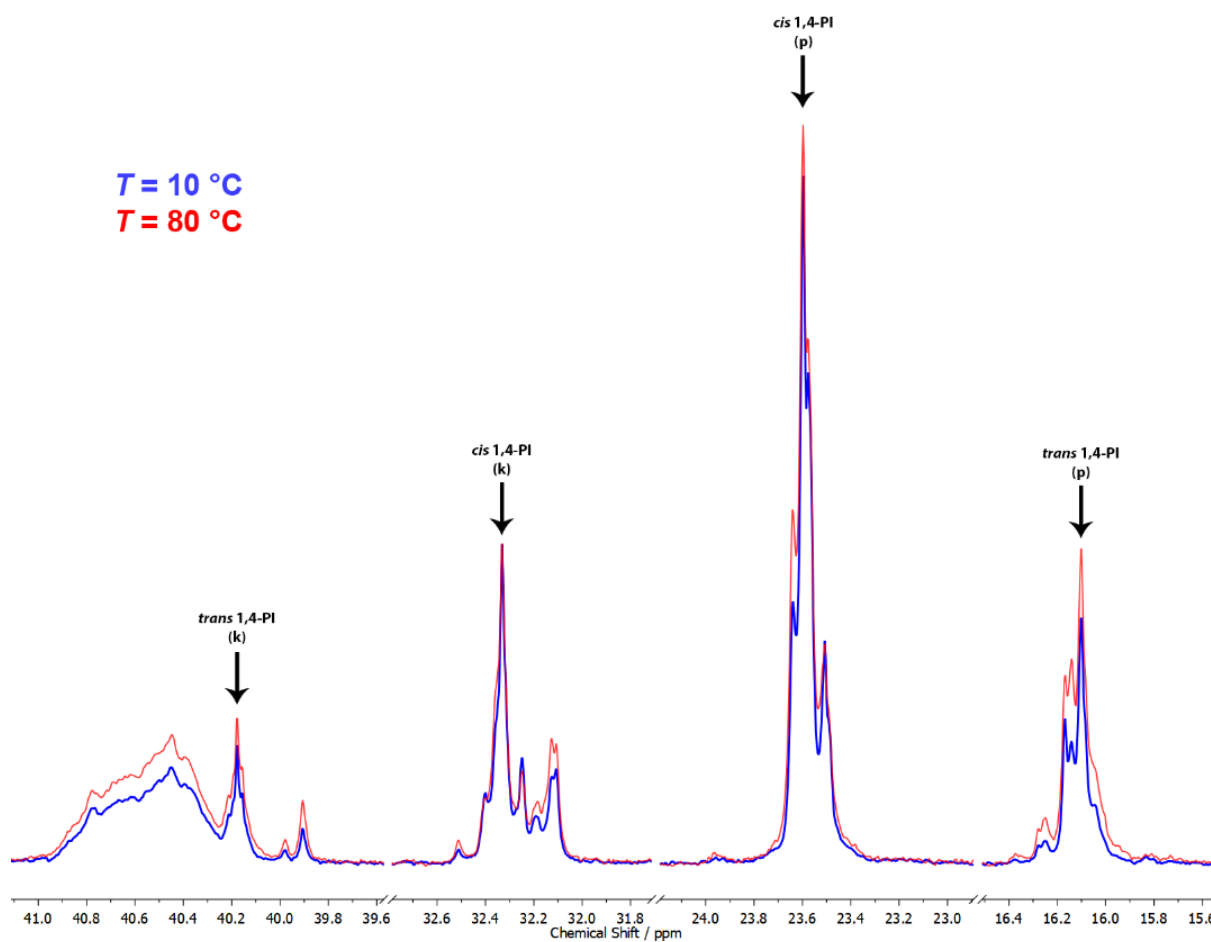


FIGURE S26F Stacked ^{13}C NMR *inverse gated* spectra (600 MHz, CDCl_3) of tapered block copolymers based on styrene and isoprene obtained by the statistical copolymerization at different polymerization temperatures. The zoomed area was used to determine the change in the ratio of *cis* to *trans* 1,4-PI units. The different polymerization temperatures have been assigned in the figure next to the respective spectrum.

TABLE S5 Determined Integrals for the change in the ratio of *cis* to *trans* 1,4-Polyisoprene in the P(I-co-S) tapered block copolymers.

T [°C]	Integral of Carbon Signals k ^a		Integral of Carbon Signals p ^b	
	<i>cis</i> 1,4-PI	<i>trans</i> 1,4-PI	<i>cis</i> 1,4-PI	<i>trans</i> 1,4-PI
10	1	1.63	1.82 (1)	0.75 (0.41)
80	1	1.94	1.90 (1)	0.97 (0.51)

^a The signals at $\delta = 41.0 - 39.8$ ppm and $\delta = 32.6 - 32.0$ ppm were used for integration and referenced to the Signal at $\delta = 41.0 - 39.8$ ppm. ^b The signal at $\delta = 23.8 - 23.2$ ppm and $\delta = 16.4 - 15.8$ ppm were used for integration and referenced to the Signal at $\delta = 41.0 - 39.8$ ppm. Values in the brackets are referenced to the Signal at $\delta = 23.8 - 23.2$ ppm.

¹³C *inverse gated* spectra allow integration of the carbon signals in a quantitative manner by suppressing the nuclear Overhauser effect.

The relative increase of *trans* 1,4-PI units was calculated as follows:

Signal k:

$$\frac{\textit{trans} 1,4 - \text{PI} (T = 80 \text{ }^\circ\text{C})}{\textit{trans} 1,4 - \text{PI} (T = 10 \text{ }^\circ\text{C})} = \frac{1.94}{1.63} = 1.19$$

Signal p:

The normalization on the *cis* 1,4-PI unit of the carbon signal p leads to a correction Factor of 1.82/ 1.90 for the *trans* 1,4-PI units for 80 °C.

$$\frac{\textit{trans} 1,4 - \text{PI} (T = 80 \text{ }^\circ\text{C})}{\textit{trans} 1,4 - \text{PI} (T = 10 \text{ }^\circ\text{C})} = \frac{\frac{1.82}{1.90} \cdot 0.97}{0.75} = 1.24 \rightarrow \frac{0.51}{0.41} = 1.24$$

Evaluating the relative increase of the signals p and k, a relative increase of 22% of the *trans* 1,4-units is observed. Integrals for overlapping Signals (e.g. PS signal (see Figure S24B) for *trans* 1,4-PI for signals k) of the evaluated peak areas are assumed to stay constant for 10 and 80 °C.

14. Thermal properties via DSC measurements

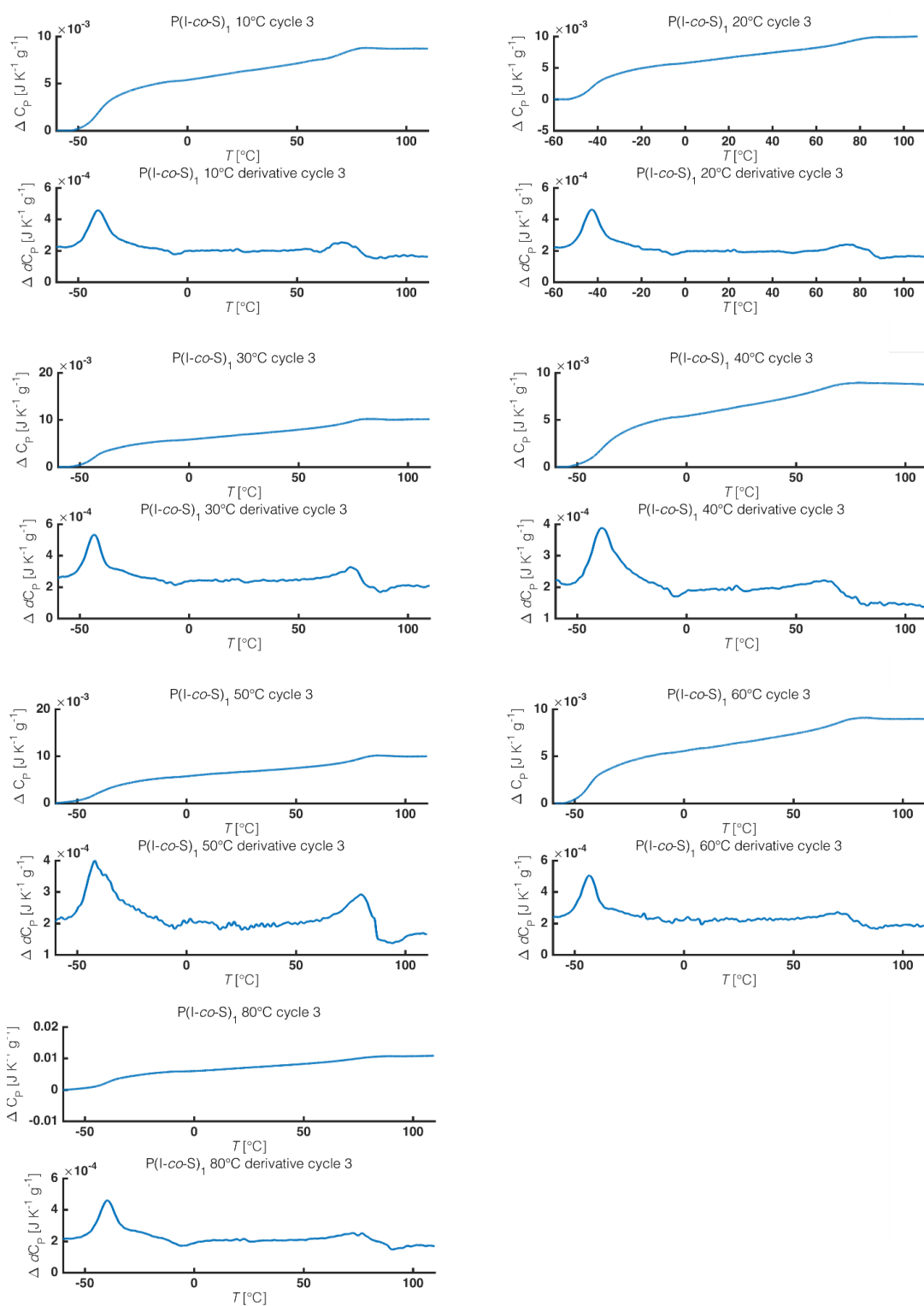


FIGURE S27 DSC data of the tapered block copolymers synthesized at the temperatures indicated in the figure. T_g 's are visualized as inflection points, as well as peak maximum in the derivation of the heat flow.

TABLE S6 Glass transition temperatures for polystyrene (PS) and different isomers of polyisoprene (PI).

	<i>cis</i> 1,4-PI ⁴²	<i>trans</i> 1,4-PI ⁴³	3,4-PI ^a	1,2-PI ^b	PS ⁴²
T_g [°C]	-73	-58	33	9	100

^a Isotactic.⁴⁴ ^b PI composed of 50%_{mol} 1,2- and 3,4-PI units.⁴⁵

TABLE S7 Glass transition temperatures of the PI block determined by DSC measurements. Raw data are plotted in Figure S28.

$T_{\text{synthesis}}$:	10 °C	20 °C	30 °C	40 °C	50 °C	60 °C	80 °C
$T_{g,PI}$ [°C]	-41	-43	-43	-39	-42	-43	-40

No significant differences are observed for the glass transition temperatures. These values can be attributed to the polyisoprene-rich phases.

The glass transition temperature of the polystyrene rich phase can be suspected around 80 °C. Due to the low signal to noise ratio, no values have been assigned for PS.

15. Copolymer Morphologies

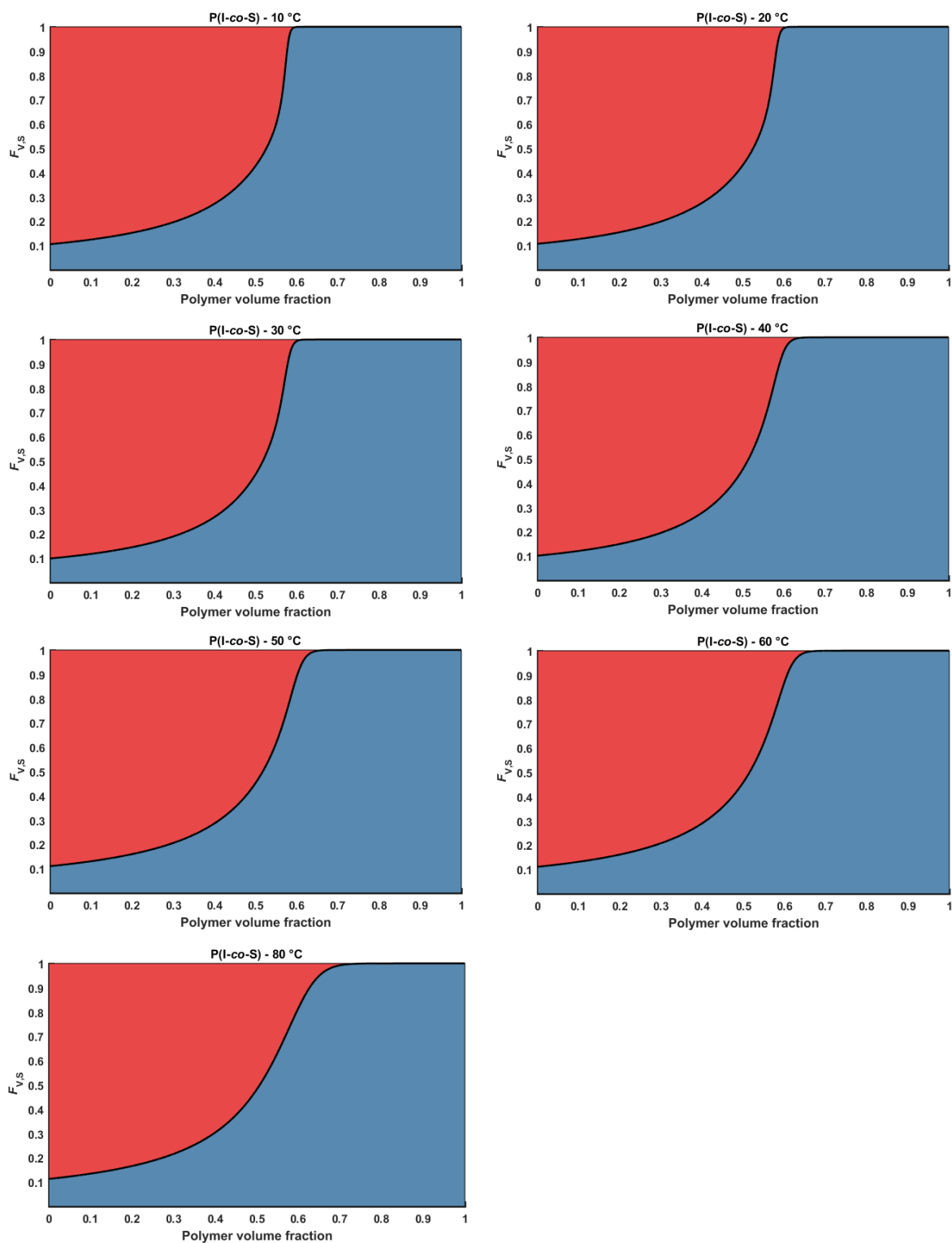


FIGURE S28 Representation of the gradient function (volume diagram) obtained for each polymerization (10 to 80 °C) using the Meyer-Lowry formalism. Note that in Figure 6 the molar composition is shown.

TABLE S8 Volume fractions obtained from the gradient function (F_S vs. total conversion) for each polymerization (10 to 80 °C) using the Meyer-Lowry formalism.

<i>Evaluation of Volume fraction of PI</i>	P(I-co-S) - 10 °C	P(I-co-S) - 20 °C	P(I-co-S) - 30 °C	P(I-co-S) - 40 °C	P(I-co-S) - 50 °C	P(I-co-S) - 60 °C	P(I-co-S) - 80 °C
$F_{V,S} = 0.50$	52.6%	52.4%	52.2%	51.4%	51.7%	51.5%	50.7%
$F_{V,S} = 0.999$	60%	61%	61%	64%	66%	68%	74%
<i>Inflection Point</i>	57%	57%	57%	58%	59%	59%	58%

The values given in Table S8 reflect the change of the gradient structure by increasing temperature. As the increase in temperature mainly affects r_S , styrene incorporation is favored leading to a shift of $\approx 2\%$ of the section with an equal instantaneous incorporation of both monomers ($F_{V,S} = 50$). In contrast a large effect is obtained for the fraction of the pure polystyrene block ($F_{V,S} = 0.999$), shifting from 60% to 74% in the volume fraction. The inflection point, which is located in between both cases, shows a slight shift towards higher values ($\approx 2\%$ change).

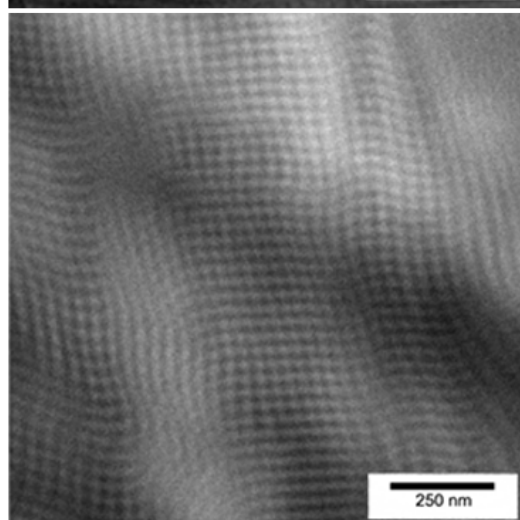
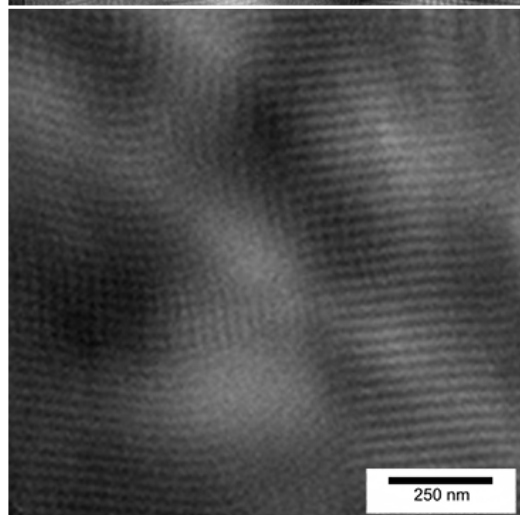
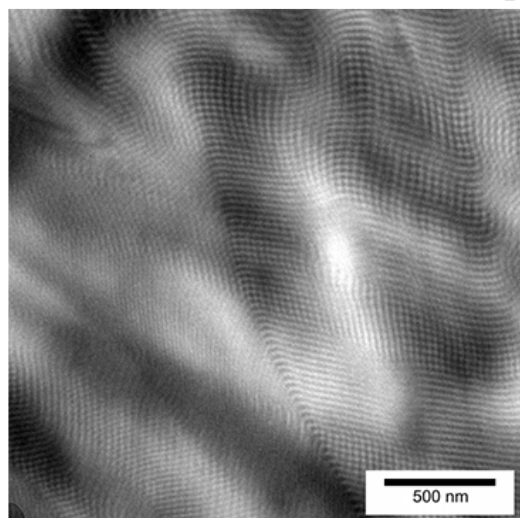
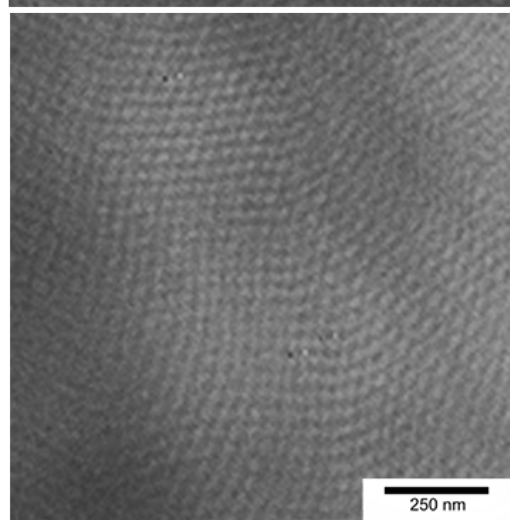
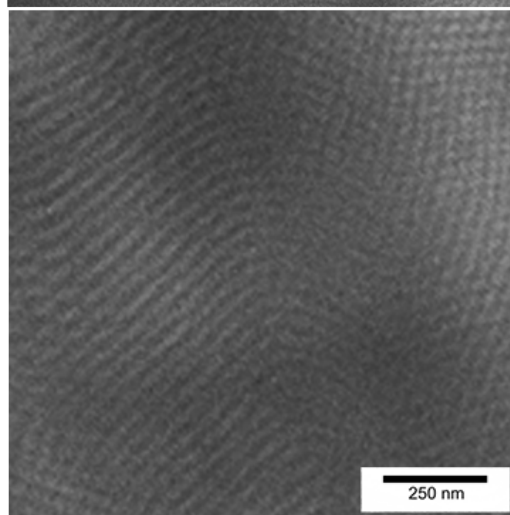
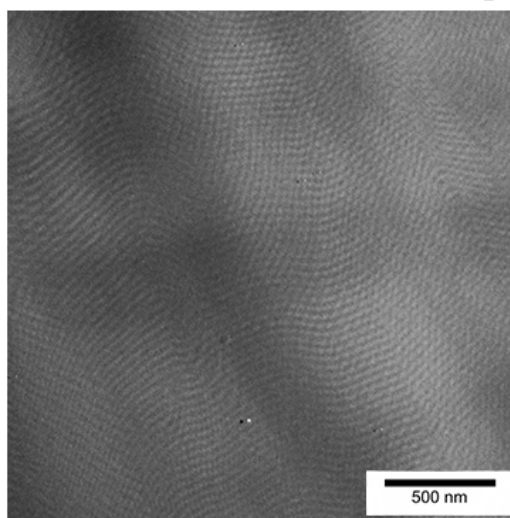
Before Thermal Annealing**After Thermal Annealing**

FIGURE S29 TEM images of tapered diblock copolymers P(I-co-S), synthesized at 80 °C reaction temperature (left: before, right: after thermal annealing). For a better comparison several images are given, showing different parts of the sample with varying resolution as indicated by the scale bar.

TABLE S9 Lamellar domain spacings determined by TEM measurements for different P(I-co-S) tapered block copolymers synthesized at given temperatures. Calculated errors are given in 1σ interval.

$T_{\text{Polymerization}} [^{\circ}\text{C}]$	$d_{\text{PI-rich}} [\text{nm}]$	$d_{\text{PS-rich}} [\text{nm}]$	$d_{\text{PI+PS}} [\text{nm}]$	$d_{\text{PI-rich}} / d_{\text{PI+PS}}$
10	10.0 ± 1.4	14.0 ± 1.2	24.6 ± 1.4	0.41
40	14.6 ± 2.0	20.1 ± 1.5	34.8 ± 1.4	0.42
80	14.4 ± 1.3	17.8 ± 0.9	32.5 ± 2.2	0.44

The PI-rich domains show a smaller domain spacing as compared to the PS-rich domains. The fraction of the PI-rich domains slightly increases with temperature from 0.41 to 0.44. Care must be taken as this effect is not significant and the error in domain sizes is comparably high. In particular at 80 °C the interface becomes very fuzzy. On first sight, these fractions coincide with the stoichiometric volume fraction of the isoprene segments (44%_{vol}). However, a look at Figure S28 shows that at a polymer volume fraction of 44% a part of the isoprene segments is located in the non-stained segment. Thus, the morphology obtained with OsO₄ staining does not separate between a pure PS block and the rest of the copolymer but between a phase consisting of the PS block plus a part of the taper section and the residual PI-rich section. The effect of PI-selective staining with OsO₄ for tapered copolymers has not been explored yet. Further work on this topic including X-ray scattering studies will be published in the future.

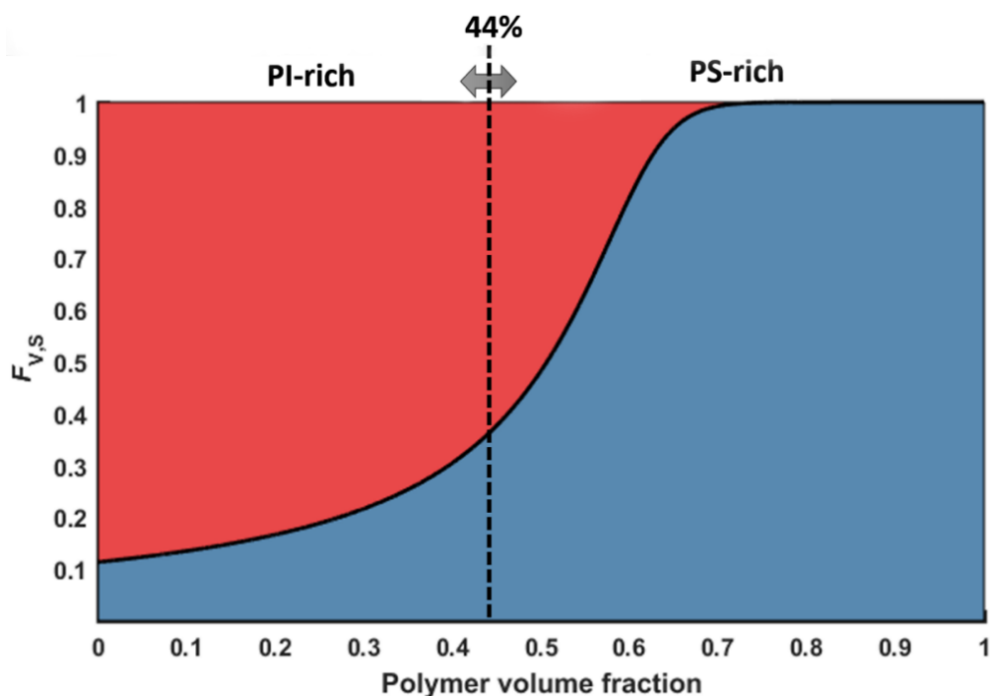


FIGURE S30 Representation of the gradient function (volume diagram) obtained for the polymerization at 80 °C. The dashed line indicates the volume fraction of the PI-rich phase as concluded from TEM measurements using OsO₄ staining (Table S9).

16. References

- (1) Steube, M.; Johann, T.; Galanos, E.; Appold, M.; Rüttiger, C.; Mezger, M.; Gallei, M.; Müller, A. H. E.; Floudas, G.; Frey, H. *Macromolecules* **2018**, *51* (24), 10246–10258. DOI: 10.1021/acs.macromol.8b01961.
- (2) Fulmer, G. R.; Miller, A. J. M.; Sherden, N. H.; Gottlieb, H. E.; Nudelman, A.; Stoltz, B. M.; Bercaw, J. E.; Goldberg, K. I. *Organometallics* **2010**, *29* (9), 2176–2179. DOI: 10.1021/om100106e.
- (3) PSS Polymer Standards Service GmbH. *WinGPC UniChrom User Manual 02/2014*.
- (4) Fetters, L. J.; Lohse, D. J.; Richter, D.; Witten, T. A.; Zirkel, A. *Macromolecules* **1994**, *27* (17), 4639–4647. DOI: 10.1021/ma00095a001.
- (5) Levin, B. D.A.; Jiang, Y.; Padgett, E.; Waldon, S.; Quammen, C.; Harris, C.; Ayachit, U.; Hanwell, M.; Ercius, P.; Muller, D. A.; Hovden, R. *Micros. Today* **2018**, *26* (1), 12–17. DOI: 10.1017/S1551929517001213.
- (6) Pettersen, E. F.; Goddard, T. D.; Huang, C. C.; Couch, G. S.; Greenblatt, D. M.; Meng, E. C.; Ferrin, T. E. *Journal of computational chemistry* **2004**, *25* (13), 1605–1612. DOI: 10.1002/jcc.20084.
- (7) Mangold, C.; Wurm, F. R.; Obermeier, B.; Frey, H. *Macromolecular rapid communications* **2010**, *31* (3), 258–264. DOI: 10.1002/marc.200900472.
- (8) Obermeier, B.; Wurm, F. R.; Frey, H. *Macromolecules* **2010**, *43* (5), 2244–2251. DOI: 10.1021/ma902245d.
- (9) Grune, E.; Johann, T.; Appold, M.; Wahlen, C.; Blankenburg, J.; Leibig, D.; Müller, A. H. E.; Gallei, M.; Frey, H. *Macromolecules* **2018**, *51* (9), 3527–3537. DOI: 10.1021/acs.macromol.8b00404.
- (10) Galanos, E.; Grune, E.; Wahlen, C.; Müller, A. H. E.; Appold, M.; Gallei, M.; Frey, H.; Floudas, G. *Macromolecules* **2019**, *52* (4), 1577–1588. DOI: 10.1021/acs.macromol.8b02669.
- (11) Herzberger, J.; Leibig, D.; Liermann, J. C.; Frey, H. *ACS Macro Lett.* **2016**, *5* (11), 1206–1211. DOI: 10.1021/acs-macrolett.6b00701.
- (12) Ding, J.; Price, C.; Booth, C. *Eur. Polym. J.* **1991**, *27* (9), 891–894. DOI: 10.1016/0014-3057(91)90028-M.
- (13) Quinebèche, S.; Navarro, C.; Gnanou, Y.; Fontanille, M. *Polymer* **2009**, *50* (6), 1351–1357. DOI: 10.1016/j.polymer.2009.01.041.
- (14) Johnson, A. F.; Worsfold, D. J. *J. Polym. Sci. A: Gen. Pap.* **1965**, *3* (2), 449–455. DOI: 10.1002/pol.1965.100030204.
- (15) Bywater, S. *Macromolecules* **1998**, *31* (18), 6010–6013. DOI: 10.1021/ma970963r.
- (16) Viola, G. T.; Bortolotti, M.; Zazzetta, A. *J. Polym. Sci. A* **1996**, *34* (1), 13–24. DOI: 10.1002/(SICI)1099-0518(19960115)34:1<13:AID-POLA1>3.0.CO;2-4.
- (17) Ariura, F.; Carlotti, S.; Deffieux, A. *Macromol. Rapid Commun.* **2004**, *25* (18), 1595–1599. DOI: 10.1002/marc.200400251.
- (18) Long, T. E.; Liu, H. Y.; Schell, B. A.; Teegarden, D. M.; Uerz, D. S. *Macromolecules* **1993**, *26* (23), 6237–6242. DOI: 10.1021/ma00075a018.
- (19) Lanzendörfer, M. G.; Schmalz, H.; Abetz, V.; Müller, A. H. E. In *In Situ Spectroscopy of Monomer and Polymer Synthesis*; Puskas, J. E., Long, T. E., Storey, R. F., Shaikh, S., Simmons, C. L., Eds.; Springer US: Boston, MA, s.l., 2003; pp 67–81.
- (20) Nees, F. W.; Buback, M. *Ber. Bunsenges. Phys. Chem.* **1976**, *80* (10), 1017–1023. DOI: 10.1002/bbpc.19760801017.
- (21) Schilli, C.; Lanzendörfer, M. G.; Müller, A. H. E. *Macromolecules* **2002**, *35* (18), 6819–6827. DOI: 10.1021/ma0121159.
- (22) Schmalz, H.; Lanzendörfer, M. G.; Abetz, V.; Müller, A. H. E. *Macromol. Chem. Phys.* **2003**, *204* (8), 1056–1071. DOI: 10.1002/macp.200390077.
- (23) André, X.; Benmohamed, K.; Yakimansky, A. V.; Litvinenko, G. I.; Müller, A. H. E. *Macromolecules* **2006**, *39* (8), 2773–2787. DOI: 10.1021/ma051506a.

- (24) Idelson, M.; Blout, E. R. *J. Am. Chem. Soc.* **1957**, *79* (15), 3948–3955.
DOI: 10.1021/ja01572a002.
- (25) Williamson, D. T.; Buchanan, T. D.; Elkins, C. L.; Long, T. E. *Macromolecules* **2004**, *37* (12), 4505–4511.
DOI: 10.1021/ma035040c.
- (26) Artyushenko, V. In *Specialty optical fibers*, Part of Advanced photonics ; 27 - 31 July 2014, Barcelona, Spain; OSA The Optical Society: Washington, DC, 2014; 35-39.
- (27) Johann, T.; Leibig, D.; Grune, E.; Müller, A. H.E.; Frey, H. *Macromolecules* **2019**, *52* (12), 4545–4554.
DOI: 10.1021/acs.macromol.9b00747.
- (28) Hsieh, H. L. *J. Polym. Sci. A: Gen. Pap.* **1965**, *3* (1), 153–161.
DOI: 10.1002/pol.1965.100030117.
- (29) Bywater, S.; Worsfold, D. J. *J. Organomet. Chem.* **1967**, *10* (1), 1–6. DOI: 10.1016/S0022-328X(00)81711-8.
- (30) Roovers, J. E. L.; Bywater, S. *Macromolecules* **1968**, *1* (4), 328–331.
DOI: 10.1021/ma60004a010.
- (31) Tanaka, Y. *Polymer* **1976**, *17* (2), 113–116. DOI: 10.1016/0032-3861(76)90078-1.
- (32) Gronski, W.; Murayama, N.; Cantow, H.-J.; Miyamoto, T. *Polymer* **1976**, *17* (4), 358–360. DOI: 10.1016/0032-3861(76)90199-3.
- (33) Beebe, D. H. *Polymer* **1978**, *19* (2), 231–233. DOI: 10.1016/0032-3861(78)90049-6.

CHAPTER 5

THF - A "RANDOMIZING" ADDITIVE?

CHAPTER 5

Submitted to *Macromolecules*, 2020

THF - More than a “Randomizer” in the Living Anionic Copolymerization of Styrene and Isoprene: Kinetics, Microstructures, Morphologies, and Mechanical Properties

Marvin Steube¹, Tobias Johann¹, Hanna Hübner², Marcus Koch³, Thi Dinh¹, Markus Gallei², George Floudas^{4,5}, Holger Frey¹ and Axel H.E. Müller^{1*}

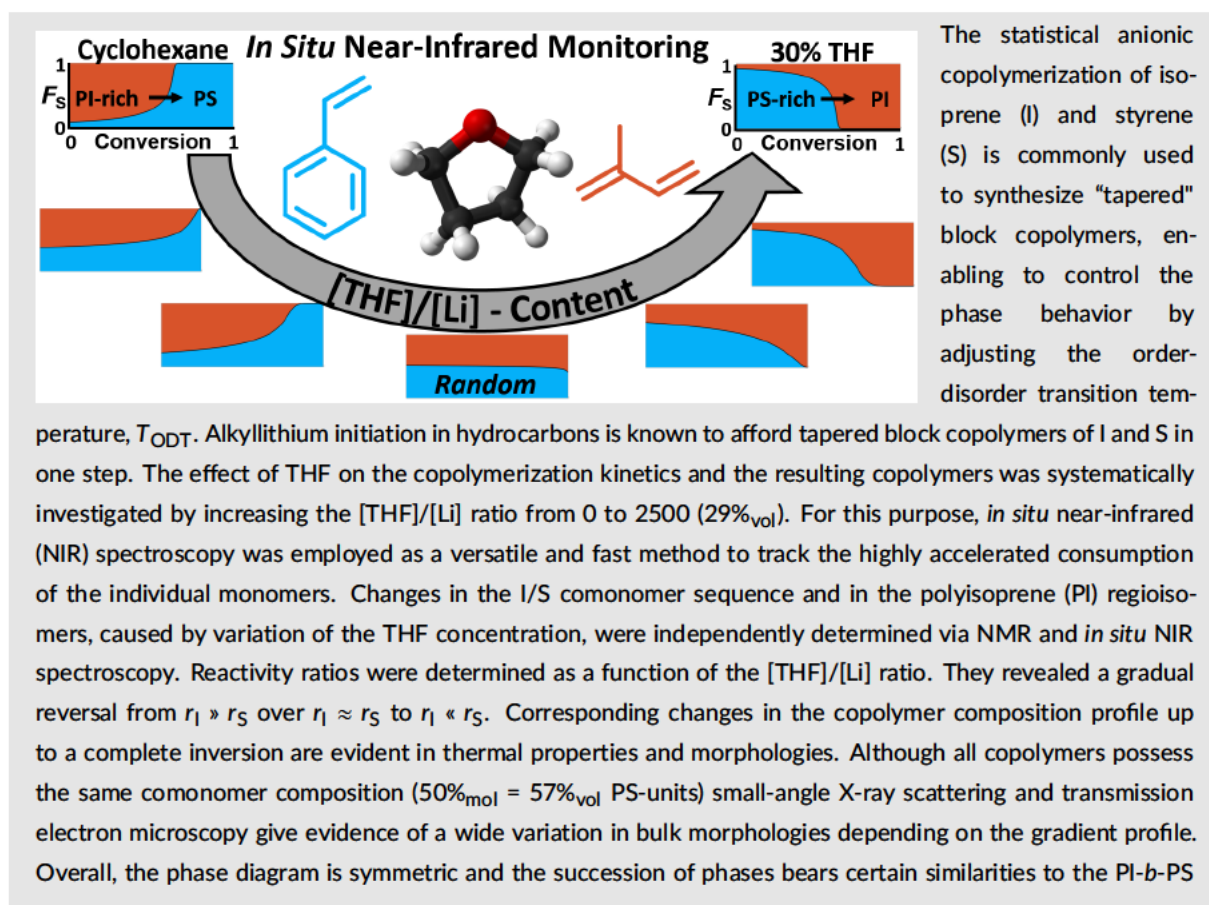
¹Department of Chemistry, Johannes Gutenberg Universität Mainz, 55099 Mainz, Germany

²Chair in Polymer Chemistry, Saarland University, 66123 Saarbrücken, Germany

³INM - Leibnitz Institute for New Materials, Campus D2 2, Saarland University, 66123 Saarbrücken, Germany

⁴Department of Physics, University of Ioannina, P.O. Box 1186, 451 10 Ioannina, Greece

⁵Max Planck Institute for Polymer Research, 55128 Mainz, Germany



case. This is discussed in terms of the increasing incompatibility of PS with 3,4-PI and the more symmetric polymer conformational parameter. The degree of segregation as well as the nanodomain structure was found to control the mechanical properties, showing a remarkably different viscoelastic response either leading to hard/brittle or ductile/soft materials. The accessibility of tailored gradient profiles as well as their in-depth understanding by simply using THF as microstructural modifier opens a variety of possible application. As an example, the synthesis of a PI-selective hydrogenated "tapered triblock" is presented, possessing a THF-modified, phasecompatibilizing tapered block incorporated in the well-established SIS block architecture.

INTRODUCTION

The copolymerization of styrene (S) and 1,3-dienes, in particular butadiene (B) and isoprene (I), can be driven to a variety of different polymer architectures. Moreover, it represents a versatile tool to correlate monomer sequences with material properties.¹⁻³ One of the most important and frequently studied polymer architectures is an ABA triblock copolymer consisting of glassy polystyrene (PS) blocks (A-type) bridged by a rubbery polydiene block, e.g. polyisoprene (PI).⁴⁻⁸ Their comparably large inherent thermodynamic incompatibility ($\chi_{IS,373\text{K}} \approx 5.5 \cdot 10^{-2}$)^{9,10} is utilized for phase separated microdomain structures. In the case of so-called SIS triblock copolymers (PS-*b*-PI-*b*-PS), the PS end blocks serve both as physical crosslinks and filler material inside a rubbery polydiene matrix.⁴

In industry, high-speed melt extrusion favors a disordered structure with comparably low melt viscosities.^{11,12} Nevertheless, the microphase separated bulk morphology and the affiliated material properties need to be restored by cooling the polymer melt to the service temperature (usually in the range $40\text{ °C} \leq T \leq 60\text{ °C}$). Hence, the order-disorder transition (ODT) has to be tailored to a certain temperature range ($T_{g,PS} < T_{ODT} < T_{decomposition}$).¹³ For this purpose, Leibler's fundamental theory can be used to quantify the phase segregation strength $\chi(T) \cdot N$ and related T_{ODT} , where χ is the Flory-Huggins parameter and N the total degree of polymerization.¹⁴

T_{ODT} is directly affected by the product χN .¹³ Hence, the adjustment of N is a straightforward and reasonable approach to avoid a T_{ODT} exceeding the degradation temperature of the polymer. A more challenging strategy focuses on the reduction of the chemical incompatibility for a given block copolymer ($\chi_{eff} < \chi$).¹⁵ As an advantage, this strategy allows to access comparably large molecular weights, exceeding the entanglement molecular weight by far.^{10,16} Consequently, mechanically tough materials with accessible T_{ODT} s can be achieved. Variation of the monomer gradient profile is a promising approach to reduce χ_{eff} for a given monomer pair. For this purpose, the sharp boundary of the blocks is replaced by a gradual transition.^{5,17,18}

The living anionic (co)polymerization of styrene with 1,3-dienes can be utilized to generate polymers with high molecular weight and low dispersity; it is highly established on the industrial scale.^{5,11,19-21} Furthermore, the living chain end allows to adjust monomer sequences, *i.e.* χ_{eff} , via (i) multi-step synthesis and (ii) the choice of solvent (hydrocarbon or Lewis base) and counterion, both affecting the copolymerization kinetics dramatically.²²⁻²⁴ In 1962 Geoffrey and Milkovich of Shell Co. presented an alkyllithium initiated synthesis in hydrocarbons, to obtain so-called "tapered block copolymers".⁵ Upon adding isoprene to an active styrene polymerization (*i.e.* residual styrene monomer was present), the statistical copolymerization formed a polydiene-rich mid-block, where the proportion of styrene units continuously increased in relation to the

polydiene units, finally ending in a pure PS block (Figure 1a). Hence, the term "tapered" relates to this type of PI-rich mid-section. In subsequent works, the properties of those "tapered triblocks"⁶ as well as the statistical copolymerization itself were deepened by others.^{5,16,25-31}

Later, the term "tapered" was extended to modified AB block copolymers, where the statistical copolymer (*i.e.* the PI-rich as well as the PS block) was extended by the respective homopolymer blocks (Figure 1b-d).³²⁻³⁸ These kind of tapered block copolymers were used as phasecompatibilizing mid-block segment in PI-*b*-PS diblock copolymers by Hadjichristidis *et al.*³² For this purpose, various tapered block copolymers (PI-*b*-P(I-co-S)-*b*-PS), and inverse tapered block copolymers (PS-*b*-P(I-co-S)-*b*-PI) were synthesized (Figure 1b). A strong correlation of the T_{ODT} and the volume fraction of the P(I-co-S) tapered PS midblock was found.³² Comparable architectures were also investigated by Epps and co-workers. In these studies,³⁸⁻⁴⁰ the gradient profile was controlled by the monomer feed via automated syringe pumps taking into account the fundamental kinetics. As a result, the typical sinusoidal gradient profile was linearized (Figure 1c).³⁸

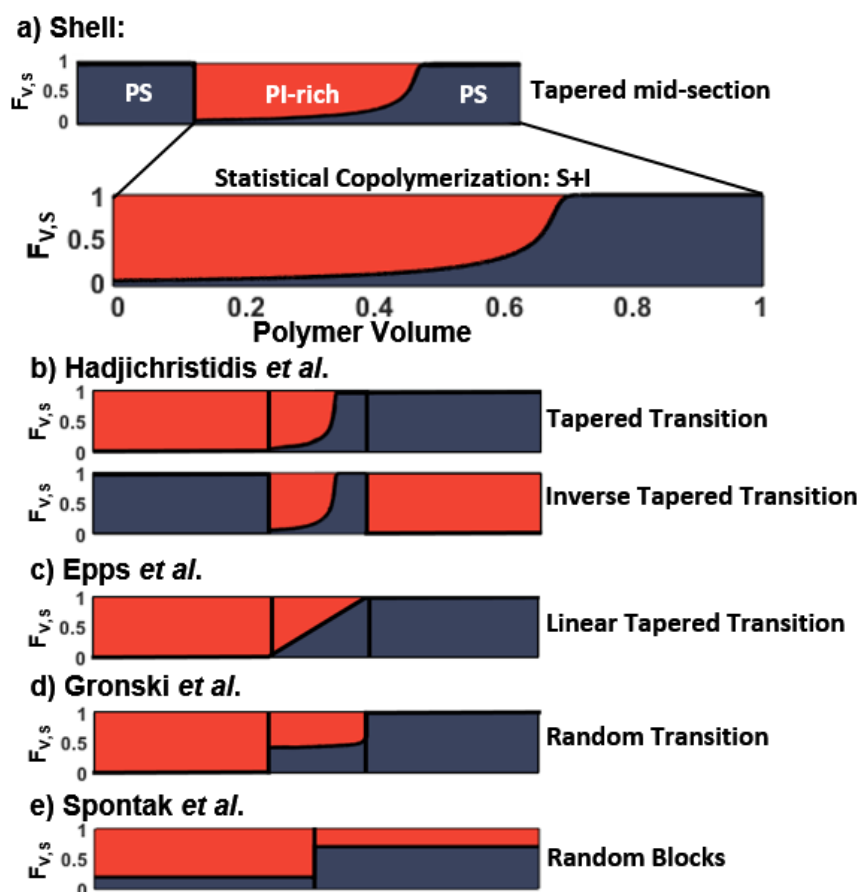


FIGURE 1 Overview of reported polymer architectures based on different PS and PI sequences.^{5,32,38,41,42} $F_{V,S}$ is the instantaneous volume incorporation of styrene.

Since 1958, the coordination of Lewis bases is known to affect the copolymerization kinetics.⁴³⁻⁴⁶ Gronski *et al.* used this principle to "randomize"^{2,47-49} comonomer sequences, and tailor the block transitions for various PI-*b*-PS diblock copolymers (Figure 1d).^{36,41} Here, the copolymerization was performed in the presence of triethylamine to approximate a random incorporation of the monomers (reactivity ratios $r_I = 0.8$; $r_S = 1$ at 25 °C). By varying the content of the random copolymer block from 0 to 33%_w, the fraction of the domain interphase in the bulk state was increased from 8.5 to 65%_{vol}.⁴¹ In an elegant work, Spontak *et al.* manipulated the copolymerization kinetics to obtain random copolymers of styrene and isoprene, which allowed to adjust the phase behavior. Here, the architectures were synthesized by two subsequent random copolymerizations with highly diverging monomer compositions for each "random-block" (Figure 1e). Hence, for these so called "block random copolymers", χ_{eff} could be varied by the inherent composition contrast of both blocks.⁴² This versatile use of *in situ* generated, tailored monomer sequences^{11,34,50-52} emphasizes the importance of (co)polymerization kinetics to engineer monomer sequences and tailor material properties.

The formation of the already mentioned "tapered" gradient copolymers is based on the peculiar kinetics of the butyllithium initiated copolymerization in non-polar, non-coordinative solvents. This, in turn, is due to the aggregation of the anionic chain ends via lithium atoms. These aggregates are at equilibrium with the disaggregated, polymerization-active species.^{22,24} Depending on the chosen monomer, different kinetic orders are found with respect to the concentration of anionic chain ends. This is explained by the aggregation number, N_{agg} , of the corresponding anionic chain end. For polystyryllithium, the formation of dimers ($N_{\text{agg}} = 2$) is generally accepted.^{29,53-59} For polybutadienyllithium⁵⁹⁻⁶⁴ and polyisoprenyllithium,^{29,60,61,63,65,66} controversial results are discussed. Worsfold and Bywater observed a gradual change from the tetrameric to the dimeric PILi species as a result of a decreasing chain-end concentration.^{17,60}

The lithium-initiated copolymerization kinetics of 1,3-dienes with styrene in nonpolar hydrocarbon solvents shows a quite unique behavior. Although the homo-propagation of styrene proceeds faster than that of the polydiene, e.g. isoprene ($k_{SS} > k_{II}$), the latter is preferentially incorporated.^{17,67-69} This is explained by the magnitude of the cross-propagation constants, which highly favor polyisoprenyllithium (PI-Li) chain ends ($k_{SI} \gg k_{IS}$; $r_I = 10.2$; $r_S = 0.01$ at 20 °C).⁶⁸ As described, the copolymerization results in tapered block copolymers. In our previous work,⁶⁸ we determined the homo- and cross-propagation constants in the range from 10 °C to 60 °C in cyclohexane. A remarkable difference from 46 to 83 kJ·mol⁻¹ was found for the activation energies of the individual propagation rate constants, which explains the temperature dependence of the reactivity ratios. This caused a change in the gradient profile leading to a partial order-order transition of the bulk morphology.

In contrast to the tapered copolymers obtained in hydrocarbon solution, the carbanionic copolymerization in rather polar, coordinative solvents like THF results in a completely different succession in the consumption of comonomers. A preferential incorporation of styrene at the beginning of the polymerization was observed in THF for both isoprene and butadiene ($r_1 \approx 0$, $r_5 \approx 40$; $r_B \approx 0.2$, $r_S \approx 8$; $T = -35$ °C)⁷⁰, which leads to an inverted gradient.^{2,43} These observations are explained by a different polymerization mechanism, caused by the peripheral solvation of the lithium atom, leading to a further polarization of the largely covalent carbon-lithium bond (*i.e.* the polymerization active center). In consequence, less associated anionic chain ends are assumed, which is also supported by the first-order dependence of the polymerization rate on the active chain end concentration.^{71,72}

The solvation of the lithium atom by Lewis bases and the ionization of the carbon-lithium bond also remarkably affects the microstructure of the formed polydiene.⁷³⁻⁷⁷ An increase of the side-chain vinyl regio-isomers (3,4- and 1,2-units) at the expense of 1,4-units was observed, which is explained by an altered charge distribution and stabilization of the propagating anionic chain end.^{2,73,78-86} Nevertheless, this increase of the side-chain vinyl content is usually not desired for thermoplastic elastomer (TPE) materials, as it results in an increase of the T_g of the rubbery phase.⁸⁷ However, side-chain vinyl units are desired for post-polymerization modification reactions⁸⁸⁻⁹¹ or to suppress crystallization, especially pronounced in the hydrogenated 1,4-polybutadiene.⁹²

To clarify the reaction mechanism^{24,93,94} of the anionic (co)polymerization, or to alter material properties,^{28,95,96} the polymerization kinetics in the intermediate region between pure hydrocarbon and pure polar solvent are also in focus. For this purpose, the alkyllithium initiated polymerization is usually performed in hydrocarbons, adding small amounts of Lewis bases, called "polar modifiers" or "randomizers".^{47-49,97-99} O'Driscoll, Welch and Bywater investigated the effect of THF on the homo-propagation of styrene in hydrocarbons and found an increase of the reaction rate with a maximum at $[\text{THF}]/[\text{Li}] \approx 20$.¹⁰⁰⁻¹⁰² Morton and Fetters found a similar acceleration in the homo-propagation of isoprene with a maximum at $[\text{THF}]/[\text{Li}] \approx 600$ equivalents.^{71,72} The copolymerization behavior of butadiene with styrene was investigated by Kuntz for increasing $[\text{THF}]/[\text{Li}]$ ratios up to 20.⁴⁴ A raise of the initial styrene incorporation was concluded by sampling experiments.

In this publication, we present an in-depth investigation of the effect of THF as a "randomizer" on the statistical copolymerization of isoprene and styrene at 20 °C in cyclohexane. We follow the individual monomer conversion by using the deconvolution of overlapping absorption bands obtained by *in situ* near-infrared (NIR) spectroscopy, as established for cyclohexane in our previous work.⁶⁸ The dependence of the reactivity ratios on the $[\text{THF}]/[\text{Li}]$ ratio was determined

and found to strongly affect the gradient structure. Based on these statistical copolymers, the effect of the microstructure (*i.e.* comonomer sequence and the regioisomeric PI composition) was further investigated and correlated to thermal, morphological and mechanical properties in the bulk state. Finally, the accessibility of SIS triblock copolymers with a tailored gradient is demonstrated by a multi-step procedure utilizing THF-"randomized" copolymerization kinetics. The high 1,4-PI content and PI-selective hydrogenation are demonstrated, enabling the potential use of the presented comonomer sequences as phasecompatibilizing block in TPE materials.

EXPERIMENTAL SECTION

A detailed description is found in the Supporting Information, Sections 1 and 2.

RESULTS AND DISCUSSION

The living anionic polymerization of styrene and isoprene in the presence of so called "randomizers" leads to a change of kinetics and consequently comonomer sequence (*i.e.* the composition gradient) and polyisoprene microstructure. This is expected to strongly affect bulk morphologies, thermal and mechanical properties. *In situ* NIR monitoring is an attractive method to measure kinetic parameters as it exhibits a sufficient time resolution even at high THF contents. Since the NIR probe is attached to the reaction vessel material properties and copolymerization kinetics are determined on the very same batch.

Synthetic Challenges and Prerequisites for Microstructural Modifiers

The presence of THF in the copolymerization is known to lead to an increased reaction rate.^{71,103} This is accompanied by a comparably fast release of the reaction heat. Nevertheless, a constant reaction temperature is required for an accurate determination of the reactivity ratios. Both show a temperature dependence in cyclohexane (CyH)⁶⁸ and THF.⁷⁰ For this reason, a glass reactor with indented surface was used for improved heat transfer and mixing efficiency. The NIR probe was inserted into the reactor. Temperature was equilibrated by a stirred water bath, equipped with a tailored cooling coil connected to a cryostat (Figure S1). Additionally, the temperature of the reaction was monitored at the glass surface (Figure S3). A series of styrene/isoprene copolymerizations ($c_S = c_I = 0.62\text{-}0.74$ mol/L; $c_S + c_I \approx 15.8\%$) were initiated at $T = 20$ °C with *sec*-butyllithium ($c_{\text{Ini}} = 1.35\text{-}1.57$ mmol/L) in cyclohexane (Table 1). In twelve batch reactions

(≈ 100 g scale), the THF content was systematically increased from 0-2500 equivalents (eq.) relative to the active chain ends, $[\text{THF}]/[\text{Li}]$.¹ The reaction was *in situ* monitored by taking NIR spectra in the range of 5900-6250 cm^{-1} . As expected, the addition of THF results in a strongly altered time-dependence of the individual monomer concentrations, also leading to altered comonomer sequences. In spite of the accelerated monomer consumption at high THF concentrations, a constant temperature plateau with single temperature spikes of $\Delta T_{\text{max}} = 2$ K was observed, which could be later assigned to the comparably fast polymerization of styrene (see Figure S3 for detailed discussion).

Spectra Deconvolution and Determination of the Reactivity Ratios

The determination of reactivity ratios, $r_1 = k_{11}/k_{1S}$, $r_S = k_{SS}/k_{SI}$ via *in situ* near-infrared (NIR) spectroscopy is not straightforward. The overlapping absorption bands^{68,104} of the monomers and the formed polymers hinder the direct determination of the individual monomer concentrations. Hence a deconvolution of the combined absorption spectra (NIR) is indispensable to extract the individual monomer concentrations as a function of time. As shown in our previous work,⁶⁸ differences in the individual molar attenuation coefficients in the range of 5900- 6250 cm^{-1} can be used to solve a linear equation system and determine the individual concentrations at any time.

In the presence of THF we observed another difficulty hampering the deconvolution of the combined absorption spectra: PI synthesized in THF (PI_{THF}) exhibits a stronger absorption than PI synthesized in cyclohexane (PI_{CyH}) (Figure S4). As described in a qualitative manner by Long and co-workers in 1993,¹⁰⁴ this increased absorption is attributed to the larger content of vinylic groups (3,4 and 1,2) in PI_{THF} . To account for these changes, we determined the extinction coefficients of PI_{THF} in the range of 5900-6250 cm^{-1} , which is the range of interest for the deconvolution process (see Supporting Information Section 2.1).⁶⁸

Typically, 12,000 spectra were deconvoluted as described in the Supporting Information, section 2, and the individual monomer concentrations were plotted as a function of time (Figures 2 and S5) and the total conversion (Figure S6). Reactivity ratios (Figure 3, Table 1) were calculated using the Meyer-Lowry formalism (Figure S7).¹⁰⁵ The error range, visualized as the Joint-Confidence region of 95% (Figure S8) is comparably low with respect to the changes of the values caused by the THF addition, underlining the high accuracy of the fitting method.

¹For safety reasons the risk of self-acceleration needs to be avoided in any case. Hence, no attempt was made to monitor the copolymerization for THF contents above 29%_{vol} THF. A potential increase of the styrene fraction should be handled with care, as the conversion of styrene is strongly accelerated at higher amounts of THF.

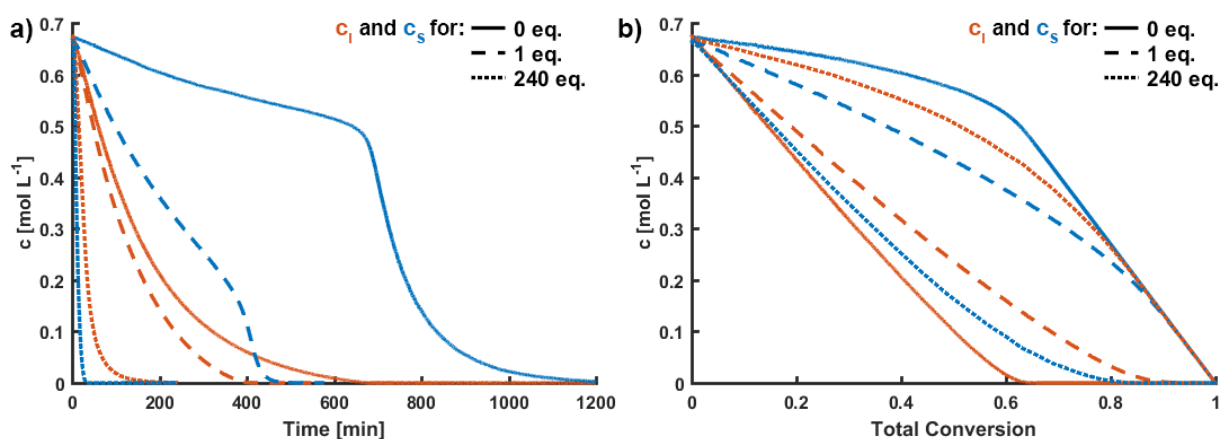


FIGURE 2 Individual conversion plots for styrene (blue) and isoprene (orange) as a function of a) time and b) total conversion. Monomer concentrations were determined via *in situ* NIR spectroscopy at 20 °C with increasing equivalents [THF]/[Li]. For all equivalents, see Figures S5 and S6.

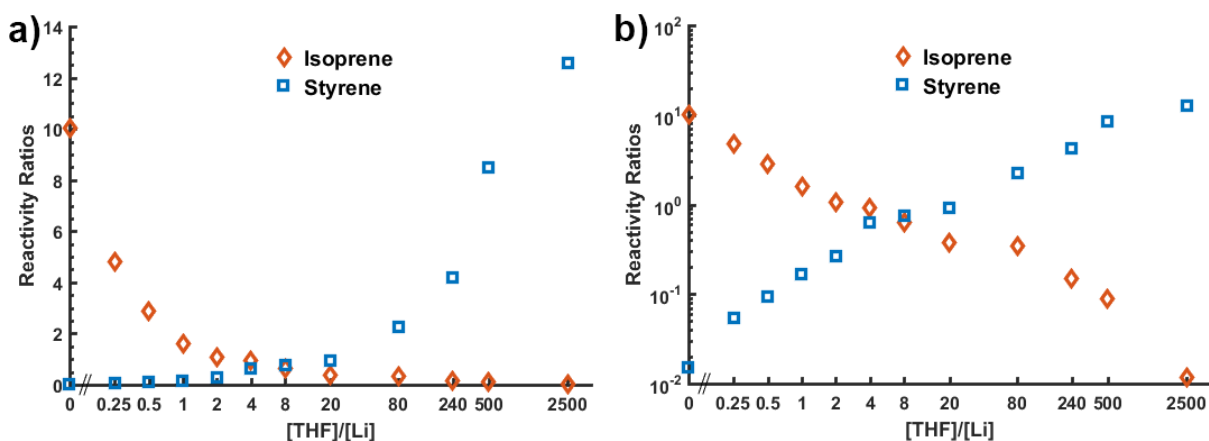
Dramatic changes of the reactivity ratios are evident for even minute amounts of THF (Figure 2), where the dielectric constant of the solvent is nearly unaffected (Table 1, Figure S10). A decrease of r_1 and the simultaneous rise of r_5 are observed for increasing [THF]/[Li] ratios. Consequently, styrene is progressively consumed at earlier stages of the monomer incorporation with increasing [THF]/[Li] ratio and proceeds nearly in parallel to the isoprene consumption for [THF]/[Li]=8. For this sample, the precise determination of the reactivity ratios was hampered by the equimolar monomer feed ($f_1=f_5=50\%$), which impedes a reliable differentiation between random and alternating monomer incorporation. Consequently, the determination of the reactivity ratios was performed in an additional experiment with an isoprene mole fraction of 70% (Figure S9).

At further increase of the [THF]/[Li] ratio the trend continues and again leads to highly disparate, but inverse reactivity ratios ($r_1 = 0.012$ $r_5 = 12.6$ at [THF]/[Li]=2500). To the best of our knowledge, this is the first study which systematically quantifies reactivity ratios as a function of the Lewis base content in the living anionic copolymerization of styrene and isoprene. The observed preferential incorporation of styrene (due to the inversion of the reactivity ratios from $r_1 \gg r_5$ to $r_1 \ll r_5$) was first described by Kelley and Tobolsky in 1959.⁴³ A first estimation of reactivity ratios was given by Spirin *et al.* ($r_1 \approx 0.1$, $r_5 \approx 9$ at 27 °C and $r_1 \approx 0$, $r_5 \approx 40$ at -35 °C) three years later.⁷⁰ However, we observe even more disparate reactivity ratios for [THF]/[Li]=2500, which corresponds to a THF content of only 29%_{vol}. This might be explained by the lower polymerization temperature (20 °C) in our experiments.

TABLE 1 Kinetic results of the copolymerization of styrene (S) and isoprene (I) in THF/cyclohexane mixtures at 20 °C.^{a)}

[THF]/[Li]	[THF] [% _{vol}]	$\epsilon_{\text{Solvent}}$ ^{b)}	[<i>Ini</i>] ₀ [mmol/L]	$t_{1,1/2}$ [min] ^{c)}	$t_{S,1/2}$ [min] ^{c)}	r_I	r_S	$r_I \cdot r_S$	M_n [kg/mol] ^{c)}	\bar{D} ^{d)}
0	0	2.028 ₀	1.57	120	720	10.03	0.015	0.153	88.2	1.06
0.25	0.003	2.028 ₂	1.35	120	520	4.823	0.053	0.257	88.3	1.08
0.50	0.006	2.028 ₄	1.44	120	420	2.856	0.093	0.264	87.8	1.07
1	0.012	2.029 ₀	1.49	100	220	1.607	0.166	0.266	88.6	1.08
2	0.02	2.030 ₀	1.41	75	130	1.060	0.262	0.278	88.1	1.07
4	0.05	2.032	1.52	47	55	0.928	0.624	0.579	87.4	1.08
8	0.10	2.036	1.48	31	32	0.653 ^{e)}	0.740 ^{e)}	0.470 ^{d)}	86.3	1.06
20	0.25	2.049	1.54	18	14	0.374	0.925	0.361	87.9	1.08
80	0.94	2.108	1.44	12	5.5	0.342	2.246	0.796	88.0	1.07
240	3.0	2.293	1.53	23	7.4	0.148	4.196	0.622	87.0	1.08
500	6.4	2.572	1.57	30	5.8	0.089	8.485	0.756	83.2	1.06
2500	29	4.242	1.41	16	0.8	0.012	12.58	0.148	82.5	1.07

a) $[S]_0 = [I]_0 = 0.68 \pm 0.02$ mol/l. b) Dielectric constants interpolated from the reported values for CyH/THF mixtures (Figure S10).¹⁰⁶ c) see Figure S13B d) Values are based on PS standards. e) Reactivity ratios were determined for an isoprene fraction of $f_I = 70\%$ _{mol} (Figure S9).

**FIGURE 3** Reactivity ratios of isoprene and styrene as a function of the THF concentration relative to the active chain ends; please note the double-logarithmic scales in b).

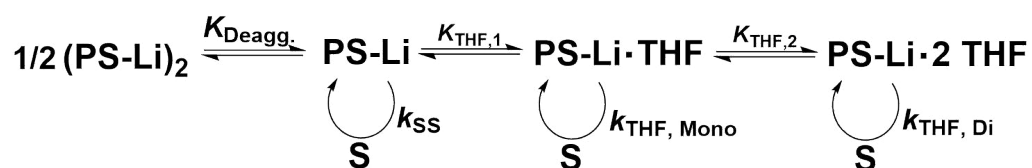
Estimation of Rate Constants.

The kinetics of homo-propagation were investigated by Fetters *et al.*⁷¹ for isoprene (k_{II}^{app}), and Bywater *et al.*¹⁰² for styrene (k_{SS}^{app}). Both systematically varied the amount of THF and found rate maxima at certain $[THF]/[Li]$ ratios.

Based on the results, Bywater expanded the reaction mechanism for the homo-propagation of

styrene in non-polar solvents by the formation of a mono- and a di-etherate adduct. Both species are postulated to be polymerization active, the mono-etherate being more reactive than the di-etherate ($k_{\text{THF, Mono}} > k_{\text{THF, Di}} \approx k_{\text{SS}}$; Scheme 1). Hence, the observed sharp maximum in the polymerization rate for $[\text{THF}]/[\text{Li}] \approx 20$ is explained by the shift of the equilibria towards and beyond the most reactive mono-etherate.

SCHEME 1 Proposed reaction mechanism of styrene homo-propagation in mixtures of hydrocarbon solvent and THF.¹⁰²



For polyisoprene, Fetters *et al.*⁷¹ found a continuous decrease of the aggregation number with increasing THF content. In contrast to styrene, the maximum in ($k_{\text{II}}^{\text{app}}$), was shifted to larger THF equivalents ($[\text{THF}]/[\text{Li}] \approx 600$) and much broader. It is noteworthy that this maximum occurs at the point, where the final disappearance of associated species, is observed. A monoetherate as well as the formation of larger lithium-ether aggregates was considered. Nevertheless, they also stated that there was no direct evidence for those kinds of structures. Furthermore, Fetters *et al.* mentioned that the comparably large amount of THF increases the dielectric constant, ϵ , which could also affect reactivities of the propagating species.⁷¹

However, reactivity ratios ($r_1 = k_{\text{II}}/k_{\text{IS}}$ and $r_2 = k_{\text{SS}}/k_{\text{SI}}$) cannot be used for a direct comparison with the homo-propagation rate constants, k_{II} or k_{SS} . Unfortunately, the direct determination of the homo-propagation rate constants in the copolymerization is not straightforward. Nevertheless, we were able to estimate all individual apparent propagation rate constants by numerically solving the ordinary differential equations of copolymerization and fitting to the time-conversion data (for details, see SI Section 4.1, Figures S11 and S12). The obtained apparent rate constants (Table S1) were compared to the values obtained in hydrocarbon solution in absence of THF (Figure S13).

In accordance to literature,^{71,102} the maximum relative acceleration of the polymerization was also found at $[\text{THF}]/[\text{Li}] \approx 600$ for isoprene and at $[\text{THF}]/[\text{Li}] \approx 20$ for styrene. Additionally, a reasonable agreement was found with respect to the magnitude of the relative acceleration compared to isoprene in hexane (Figure S12A). However, only a qualitative agreement was found for styrene, possibly since Bywater *et al.* used benzene as a solvent. In particular, it is difficult to

take cross-aggregation between PI-Li and PS-Li chain ends into account. Furthermore, as seen from the half-lives, a stronger reduction is observed for the addition of styrene than of isoprene (Figure S12B). This is in line with the accelerated rates for the consumption of styrene (k_{IS} and k_{SS} ; Figure S12B). A detailed discussion is found in the Supporting Information, Section 4.2.

So far, a full quantitative understanding of the observed trends is elusive, since the available data are by far not sufficient to fit all six equilibrium and 12 rate constants when Scheme 1 is extended to copolymerization.

Copolymer Composition

In situ NIR monitoring revealed the reactivity ratios as a function of the [THF]/[Li] content, which can be easily adjusted by the synthetic strategy. The basic criteria for the living carbanionic polymerization are simultaneous initiation of all chains, as well as the absence of termination reactions. Hence, the reactivity ratios can be directly used to describe the monomer sequence in the polymer chains.²⁷ These copolymer compositions are visualized by plotting the instantaneous styrene incorporation, F_S , as a function of the total monomer conversion. The gradient profiles are visualized in Figures 4 and S14. For later discussions (see section: Bulk Morphologies), these mole-based composition profiles are also illustrated in a volume-based composition (Figure S15).

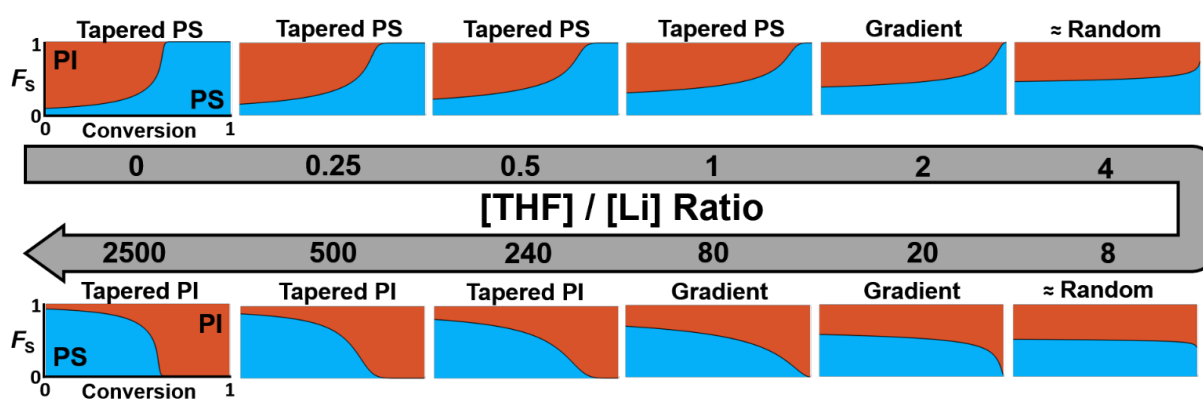


FIGURE 4 Polymer composition profiles. F_S : Instantaneous styrene incorporation. An increase of the [THF]/[Li] ratio, favors styrene incorporation in the early stage of the copolymerization. This finally inverts the gradient from tapered PS block copolymers to tapered PI block copolymers.

Tapered PS block copolymers were obtained in the presence of minor THF contents ($0 \leq [\text{THF}]/[\text{Li}] \leq 1$). For these structures, a PI-rich block ($F_{S,0} < 50\%$) is formed at the early stage of the polymerization (total conversion up to $\approx 40\%$). Hence isoprene is progressively depleted, leading to a sharp increase of F_S as a function of the total conversion (*i.e.* the sinusoidal tapered

profile),⁴⁶ which finally leads to the formation of a pure PS block ($F_S \approx 1$). For larger [THF]/[Li] ratios, the styrene incorporation in the PI-rich block is increased, which consequently leads to a shortened PS block, also quantified in terms of its volume fraction Φ_{Block} (Table 2).

Gradient copolymers are obtained for $2 \leq [\text{THF}]/[\text{Li}] \leq 80$, which lack a pure block and possess a comparably smooth gradient. In the range $4 \leq [\text{THF}]/[\text{Li}] \leq 8$ we approximate *random copolymers* with a nearly flat gradient.

Tapered PI copolymers ($[\text{THF}]/[\text{Li}] \geq 240$) are a result of the progressively favored styrene incorporation. In contrast to the tapered PS copolymers, a PS-rich chain ($F_{S,0} > 50\%$) is tapered to a pure PI block ($F_S \approx 0$).

Molecular Weight Distributions

SEC measurements support the controlled copolymerization, *i.e.* the absence of termination reactions as well as the comparably fast initiation ($k_{\text{ini}}^{\text{app}} \gg k_{\text{p}}^{\text{app}}$) in the presence of THF.^{72,107,108} Narrow molecular weight distributions ($\mathcal{D} \approx 1.07 \pm 0.01$) within a narrow molecular weight range ($M_{\text{n,exp.}} = 87 \pm 2 \text{ kg}\cdot\text{mol}^{-1}$, $M_{\text{target.}} = 80 \text{ kg}\cdot\text{mol}^{-1}$) were obtained (Figures S16, Table 1). The relative deviation (9%) of the targeted molecular weights is caused by the PS calibration, which typically overestimates the molecular weights by 10%, as shown for similar copolymers (P(I-co-S) synthesized in CyH with $f_I = 50\%_{\text{mol}}$ in our previous work.⁶⁸ A rather small deviation of the molecular weight is in the error range caused by dosing of the initiator. A slight systematic decrease (6%) is observed for increasing THF contents, which is in accordance with the shift of the PI isomeric structure from 1,4 towards 3,4 and 1,2 units, as will be discussed in the following section. SEC measurements of other isoprene/styrene based polymers used in this work show similar results (see Figure S17 and S18).

NMR Investigation of the Polyisoprene Microstructure

Real-time NIR monitoring revealed a continuous change of the reactivity ratios for the copolymerization as a consequence of increasing the THF content. Also ^1H NMR spectroscopy can be used for a comparably fast estimation of the so-called "blockiness"¹⁹ (*i.e.* moiety of SSS triads),^{109,110} validating the expected minimum (*i.e.* random sequence) at $[\text{THF}]/[\text{Li}] \approx 4\text{-}8$ (Table S2 and Figure S20B). Beyond the monomer sequence, the regioisomeric composition of polydienes is also sensitive to the THF content^{111,112} and highly relevant in terms of the resulting thermal, morphological and mechanical properties. This change was already seen in the

extinction coefficients measured in the NIR region (Figure S4).

In THF, the variety of PI regioisomers (1,4; 3,4; and 1,2, Figure 5) leads to uncertainties in their quantification due to significant broadening and overlap of the individual signals in the ^1H and ^{13}C NMR spectra (Figures S19 and S20). To obtain reliable and reproducible results, a universal strategy was developed, which relies on the integration of baseline-separated signals for an improved accuracy (Figure S20-S21 and Table S3-S5). To the best of our knowledge, no work has been reported using this principle. An overview of the results is given in Figure 5 and Table 2, showing a significant increase of the 3,4 and 1,2 units for increasing THF contents.

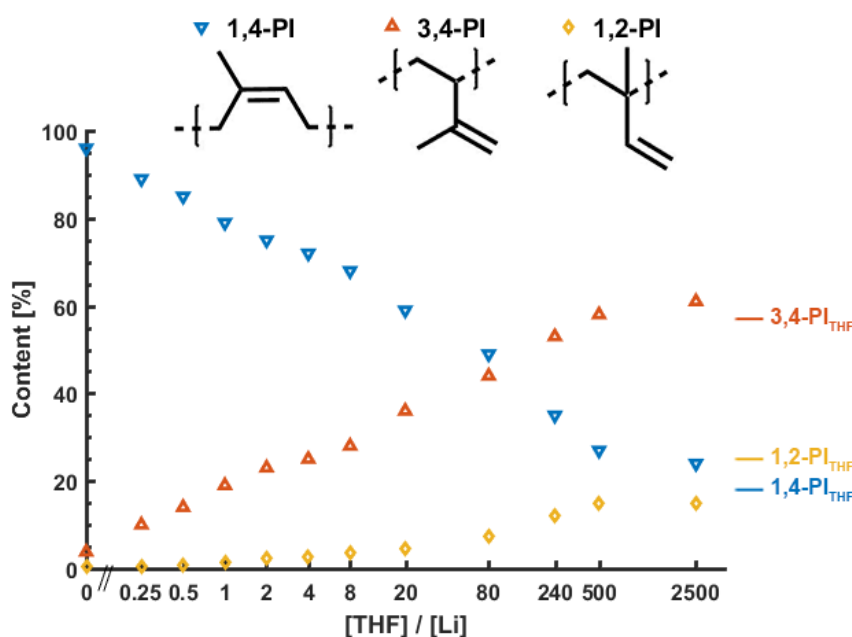


FIGURE 5 PI microstructural composition in P(I-co-S) copolymers as a function of the amount of THF relative to the active chain ends. Values were determined by the combination of ^1H and *Inverse Gated* ^{13}C NMR spectroscopy.

Other parameters,² which affect the stereochemistry, e.g. the counterion,^{2,112,113} the monomer and chain-end concentrations,^{2,82,114,115} and the polymerization temperature,^{46,116,117} were kept constant. Thus, the observed changes can be solely attributed to the presence of THF. The proposed mechanistic step, *i.e.* proposing the Lewis base as lithium coordinating agent,^{71,102,118} is supported by the present results, as even minute amounts of THF ($[\text{THF}]/[\text{Li}] < 1$, $\epsilon \approx \text{const.}$, Figure 5 and Table 2) exert a dramatic effect on the content of 1,4 and 3,4 units.

In contrast, the proportion of 1,2 units is comparatively low and only for larger THF contents ($[\text{THF}]/[\text{Li}] \geq 20$) present in considerable amounts. This is in line with the occurrence of this unit in the PI homopolymerization under similar reaction conditions.^{71,112,118,119}

TABLE 2 PI microstructure, copolymer volume composition, thermal, morphological and mechanical characteristics.

[THF]/[Li]	PI-Microstructure 1,4 / 3,4 / 1,2 [%] ^{a)}	$F_{V,S,0\%}$ [%]	$\Phi_{PI\ rich}$ [%]	Morphology ^{c)}	T_g [°C] ^{d)}	ϵ break [%]	σ_{max} [MPa]
0	96 / 3.8 / 0.6	11	54	LAM (LAM)	-39 / 83	5.7	4.3 ^{e)}
0.25	89 / 10 / 0.4	19	58	n.d. (TPC or TPL)	-24 / 80	18	5.6 ^{e)}
0.50	85 / 14 / 0.9	27	62	HPC (HPC _{PS})	-11 / 60	290	5.3 ^{e)}
1	79 / 19 / 1.4	37	66	n.d. (n.d.)	7	970	2.9
2	75 / 23 / 2.3	45	68	DIS (n.d.)	18	1000	2.7
4	72 / 25 / 2.7	53	-	n.d. (n.d.)	13	1300	1.4
8	68 / 28 / 3.7	59	-	n.d. (n.d.)	22	860	2.9
20	59 / 36 / 4.6	65	31	DIS (n.d.)	25	620	3.2
80	49 / 44 / 7.4	76	35	n.d. (HPC _{PI})	6 / 27	350	11.8 ^{e)}
240	35 / 53 / 12	86	35	HPC (HPC _{PI})	2 / 33	32	16.7 ^{e)}
500	27 / 58 / 15	92	37	BIC (see discussion)	3 / 42	23	22.5 ^{e)}
2500	24 / 61 / 15	95	37	BIC (gyroid)	5 / 55	21	25.5 ^{e)}
pure THF ^{f)}	18 / 57 / 25	-	100	-	2	n.d.	n.d.

a) Determined by combination of ¹H and Inverse Gated ¹³C NMR spectroscopy (Supporting Information, section 7).

b) Volume fraction of the PI-rich part (see Figure S25 for visualization). c) Assigned by SAXS (TEM) measurements (Figures 7, 8 and S24). d) Determined by DSC (Figures 6 and S22). e) For these samples $\sigma_{max} = \sigma_{yield}$ (Figure 10).

f) Values correspond to a polyisoprene homopolymer synthesized in pure THF (Figure S18; $c_{ini} = 1.71$ mmol/L; [THF]/[Li] = 5800).

Good agreement is found with respect to the values determined for homo-PI synthesized in THF. Deviations are in the typical error range (5-10%) of the spectroscopic measurements and provide no evidence for a change of the isomeric composition caused by the presence of styrene. Furthermore, both NIR and NMR spectroscopy independently show considerable agreement in the quantitative determination of the vinyl content (Figure S21).

Thermal Properties as a Function of the Copolymer Microstructure

The principle of TPEs is based on a rubbery phase (low T_g of PI), thermoreversibly crosslinked by a hard phase (high T_g of PS). Hence, microphase separation governs thermal and mechanical properties and is a key requirement to maintain the individual thermal properties of each block. As shown in the previous section, the [THF]/[Li] ratio used in the anionic copolymerizations directly affects (i) the comonomer sequence (Figure 4 and Table 2), and (ii) the PI regiostructure (Figure 5 and Table 2).

Microstructural investigations on the PI units revealed a gradual shift from the comparably low T_g 1,4-PI (≈ -66 °C)^{120,121} to the side-chain vinyl 3,4-, and 1,2-PI units which both possess a remarkably higher T_g ($T_g(3,4) \approx 33$ °C; $T_g(1,2) \approx 9$ °C).^{87,91,122,123}

To quantify the interplay of both effects on the thermal properties of the copolymers, DSC measurements were performed. T_g values were determined as the maximum of the first derivative of the heat flow obtained during the second heating run with a rate of 20 °C/min (Figure S22). The results are summarized in Figure 6 as a function of the [THF]/[Li] ratio.

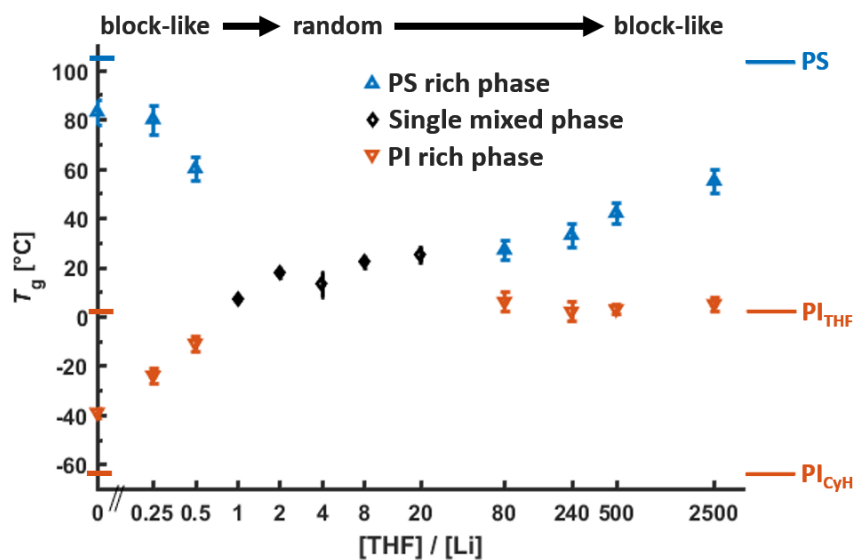


FIGURE 6 Glass transition temperatures (T_g) as a function of the [THF]/[Li] ratio used in the copolymerization of styrene and isoprene. The horizontal lines indicate the homopolymer T_g of PS and polyisoprene synthesized in cyclohexane (PI_{CyH}) and THF (PI_{THF}).

(i) For $[THF]/[Li] \leq 0.5$ two glass transition temperatures are observed. Using very low THF content, still *tapered PS copolymers* are obtained. The most block-like structure is obtained in the absence of THF (*i.e.* 0 eq.) and exhibits two glass transition temperatures at -39 °C (soft PI-rich phase) and 83 °C (glassy PS-rich phase). This result is in accordance with previous works.^{16,68} The observed T_g s do not reach the T_g s of the respective homopolymers ($T_{g,PS} = 103$ °C, $T_{g,PI,CyH} = -64$ °C). This is caused by substantial mixing of both phases, caused by the comparably smooth block transition ($\chi_{eff} < \chi$).¹⁶ A further increase of [THF]/[Li] leads to a flattening of the gradient and a decrease of the size of the pure PS block formed at the end of the polymerization. This leads to an increased proximity of the PS and PI segmental dynamics and, consequently, to a further decreasing $T_{g,PS\ rich}$ and increasing $T_{g,PI\ rich}$. The strong increase of the $T_{g,PI\ rich}$ from ≈ -40 to ≈ -10 °C is additionally supported by the increase of the vinyl content from 4% to 14%.

(ii) In the intermediate region of $1 \leq [THF]/[Li] \leq 20$ a single T_g is observed, indicating the presence of a single mixed phase. As we will see below with respect to the morphology section, in this region *gradient and random copolymers* are formed, which are not capable of phase separa-

tion, due to the smooth gradient ($\chi_{\text{eff}} \ll \chi$). The slight increase of the T_g from $\approx 7^\circ\text{C}$ to $\approx 25^\circ\text{C}$ is explained by the increase of the PI vinyl content from 22% to 43% with increasing amount of THF.

(iii) For $[\text{THF}]/[\text{Li}] \geq 20$ we again observe two T_g s. Here, *tapered PI copolymers* are obtained. This is caused by the comparably steep gradient as well as the formation of a pure PI block at the end of the polymerization. A further increase of the THF content leads to progressively dispartate T_g s, explained by the increasingly steep gradient (Figure 4; increasing χ_{eff}).

An interesting comparison can be drawn for P(I-co-S) synthesized in the presence of 0 eq. THF and the inverted taper obtained for 2500 eq THF. In terms of the similar shape of the gradient, it may be surprising that both architectures possess rather distinct T_g values ($\Delta T_{g,\text{PS-rich}} = 28^\circ\text{C}$; $\Delta T_{g,\text{PI-rich}} = 44^\circ\text{C}$; see Figure 6). Nevertheless, the comparably low $T_{g,\text{PS rich}}$ of the batches with THF as an additive is explained by a "PI contaminated" PS block instead of a pure PS block. The pertinent length scale associated with the dynamic glass temperature is the segmental dynamics within a volume defined by the statistical segment length.¹²⁴ Given the larger statistical segment length of PS with respect to PI we expect that the interruption of longer PS segments by shorter isoprene sequences will lower the PS T_g as more flexible PI segments are located within the PS characteristic volume. In contrast, a pure PI block is formed in the case of the THF modified copolymerization kinetics, leading to tapered PI block copolymer. The comparably high $T_{g,\text{PI rich}}(2500 \text{ eq.}) = 5^\circ\text{C}$ is explained by the high vinyl content (Figure 5). The T_g is in good agreement with the value found for the PI homopolymer synthesized in THF ($T_g(\text{PI}_{\text{THF}}) = 2^\circ\text{C}$; Figure S22B). This suggests a similar PI microstructure composition, which is in excellent agreement with the results of NMR and NIR spectroscopy, both showing no noticeable changes in the PI microstructure for $[\text{THF}]/[\text{Li}] > 2500$.

The above thermal results with respect to the presence of a single vs a dual T_g at specific $[\text{THF}]/[\text{Li}]$ ratios could be used as evidences for the purity of respective phases. We should keep in mind, however, that a mere shift in T_g or even the appearance of a single vs dual T_g in the copolymers can not be taken as a proof of thermodynamic miscibility as even completely miscible systems exhibit dual glass temperatures.¹²⁴ Precise information on the state of miscibility/order requires an additional structural investigation in real (by TEM), and/or in inverse space (by X-ray).

Bulk Morphologies

The exact phase state of the P(l-co-S) copolymers synthesized in the presence of different [THF]/[Li] ratios is discussed with respect to the small-angle X-ray scattering (SAXS) data of Figure 7 and transmission electron microscopy (TEM) images (Figures 8, S25). Additional SAXS curves obtained as a function of temperature are shown in Figure S23. The SAXS patterns of Figure 7 refer to 30 °C with the exception of 2500 eq. (90 °C). The patterns reveal a strong dependence of the phase state on the [THF]/[Li] ratio.

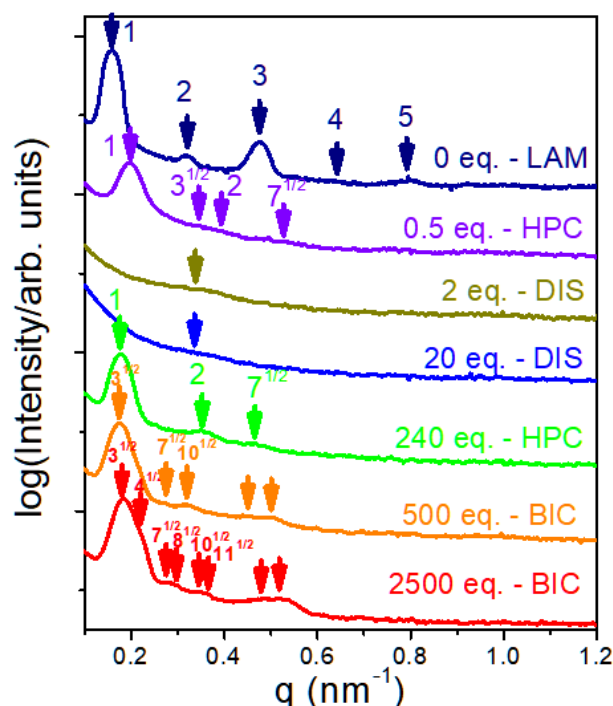


FIGURE 7 SAXS patterns of the P(l-co-S) copolymers synthesized in the presence of different [THF]/[Li] ratios. Curves have been shifted vertically for clarity. All patterns refer to 30 °C with the exception of 2500 equivalents THF (this pattern refers to 90 °C). Arrows indicate the positions of the Bragg reflections corresponding to the different morphologies.

The intensity profile for the previously published [THF]/[Li] = 0 sample,^{16,27} displays Bragg reflections with relative q values of 1:2:3:4:5, corresponding to a lamellar (LAM) structure with a periodicity ($d_0 = 2\pi/q^*$, q^* is the modulus of the scattering vector of the first diffraction maximum) of 39.5 nm. The reduced scattering intensity for the even numbered reflections suggests that the PI-rich and PS-rich domains have similar volume ($d_{\text{PI-rich}} = 21.3$ nm; $d_{\text{PS-rich}} = 18.2$ nm), which is in good agreement with TEM measurements ($d_{\text{PI-rich}} = 17 \pm 3.4$ nm; $d_{\text{PS-rich}} = 16 \pm 2.5$ nm; Figures 8a and S25A).

The intensity profile in the P(I-co-S) copolymer with $[\text{THF}]/[\text{Li}] = 0.5$ exhibits Bragg reflections with relative q values of $1:3^{1/2}:4^{1/2}:7^{1/2}$ suggestive of a hexagonally packed cylindrical (HPC) structure. The periodicity (d_0) is at 32.0 nm, and the inter-cylinder distance, d , is 37.0 nm ($d = d_0(4/3)^{1/2}$). Furthermore, the structure remains weakly ordered after heating to 150 °C (no order-to-order transition within the investigated temperature range). TEM measurements (Figure 8b and S25B) verify the presence of PS-rich cylinders with a diameter of $d_{\text{PS-rich}} = 14 \pm 2.8$ nm embedded in a PI-rich matrix. The rather poor contrast is explained by the fact that the PS-rich cylinders contain PI segments and *vice versa*, which hampers staining by OsO_4 .⁶⁸ An estimate of the PS-rich/PI-rich volume fractions based on the gradient profiles is discussed further below.

The morphologies of the gradient copolymers with $[\text{THF}]/[\text{Li}] = 2$ and 20 are very different. Now both patterns indicate a broad feature characteristic of the correlation hole scattering¹²⁵ (correlation hole distance of ~ 19 nm) within the disordered phase (DIS). Increasing further the $[\text{THF}]/[\text{Li}]$ ratio results in phase inversion (*cf.* Figure 4).

The tapered copolymer with $[\text{THF}]/[\text{Li}] = 240$ displays Bragg reflections with relative q values of $1:4^{1/2}:7^{1/2}$ suggestive of an HPC structure. The periodicity is at 34.6 nm and the inter-cylinder distance at 39.9 nm. On heating there is no order-to-disorder transition up to 150 °C (Figure S23B). TEM measurements verify the assumption of PI-rich cylinders ($d_{\text{PI-rich}} = 14 \pm 1.6$ nm) in a PS-rich matrix (Figures 8c and S25B). In contrast to prior discussed samples, staining with RuO_4 was crucial to obtain a sufficient contrast by TEM imaging (Figure S24). As RuO_4 is also able to stain aromatic PS units, this leads the electron opaque (dark) appearance of PS-rich domains in Figures 8c-d (*i.e.* inverted contrast compared to OsO_4 stained samples).

Further increase of the $[\text{THF}]/[\text{Li}]$ ratio to 500 and 2500 results in specific structural changes. The primary peak broadens asymmetrically and the higher ordered Bragg peaks do not correspond to the earlier HPC morphology. Bragg reflections have relative q values of $3^{1/2}:4^{1/2}:7^{1/2}:8^{1/2}:10^{1/2}:11^{1/2}$ suggestive of a bicontinuous morphology (BIC).¹ TEM measurements revealed the bicontinuous morphology of the $[\text{THF}]/[\text{Li}] = 2500$ sample, as the gyroid morphology (space group $la\bar{3}d$) shown in Figures 8d and S25C. Based on the phase diagram for PI-*b*-PS block copolymers, this morphology is only found in a rather limited range of Φ_{PI} and χN .^{126,127} In addition, Epps *et al.* observed the gyroid morphology for tapered block copolymers with a linear gradient profile (Figure 1c), achieved by controlling the monomer feed via syringe pumps.^{38,39} However, in this work the kinetics are only affected by a rather simple switch of the solvent, enabling the access to this morphology by a one-step initiation of a monomer mixture. SCFT calculations by Hall *et al.* also indicate that tapered copolymer compositions

widen the gyroid region in the phase diagram, which possibly also facilitates the formation of this morphology.³³

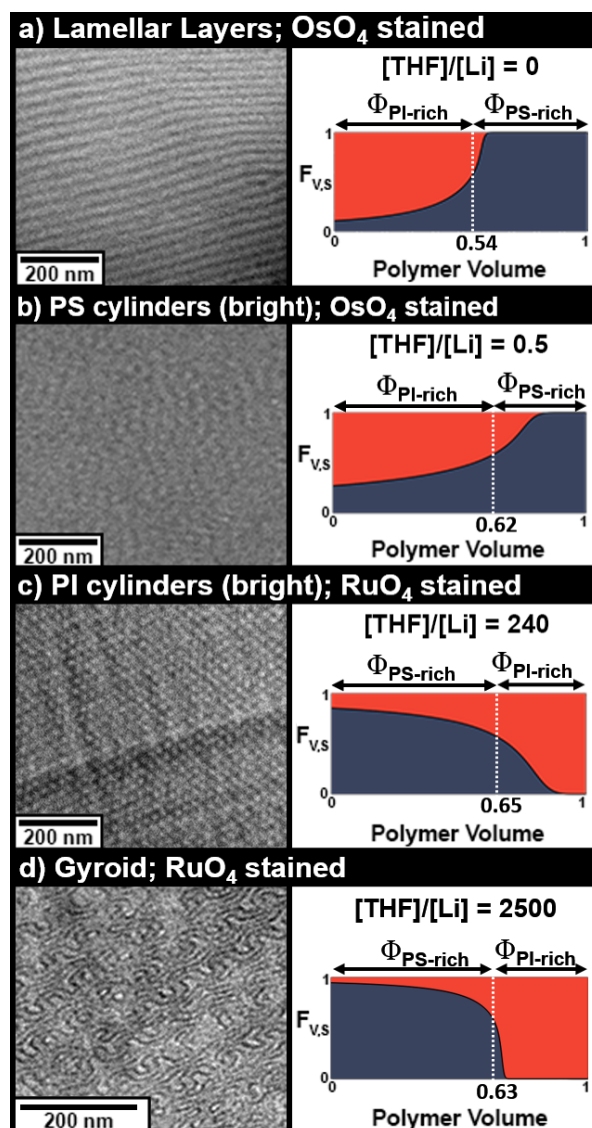


FIGURE 8 TEM images of P(I-co-S) synthesized at [THF]/[Li] ratios as indicated next to the respective polymer volume composition profiles on the right side. For OsO₄-stained (RuO₄-stained) samples PI-rich (PS-rich) phases appear electron opaque (*i.e.* dark). For additional TEM images including further [THF]/[Li] ratios and their discussion, see Supporting Information, section 9.2.

In case of PI-*b*-PS "non-tapered" block copolymers (made by consecutive monomer additions), the applied monomer feed ($f_s = f_l = 50\%_{\text{mol}}$) corresponds to a block volume fraction of $\Phi_{\text{PI}} = 43\%_{\text{vol}}$, which corresponds to a LAM morphology (based on the well-known phase diagram published by Bates *et al.*¹²⁶). However, as shown in our previous work for P(I-co-S) tapered block copolymers, the shape of the gradient can affect the microdomain morphology.⁶⁸ In this

work, we use the same constant monomer feed ($f = 50\%_{\text{mol}}$) but, due to increased amount of THF, the gradient profile changes much more dramatically. This better allows for a correlation of the comonomer sequence with the observed morphologies. Here, the quantification of a block volume fraction, Φ , is not straightforward. Although the gradient profile ($F_{V,S}$ as a function of the polymer volume; Figures 4 and 8) can be determined precisely, the lack of an abrupt, significant change in the comonomer sequence hampers the determination of PI or PS related polymer volumes. A detailed discussion of this problem is given in the Supporting Information, section 9.3. In short, we define PI- and PS-rich parts of the polymer based on a deviation from the random incorporation, which occurs when the instantaneous comonomer incorporation, F , is equal to the monomer feed, f . In this work, due to different monomer volumes, this corresponds to an instantaneous styrene volume incorporation of $F_{V,S} = 57\%_{\text{vol}}$.

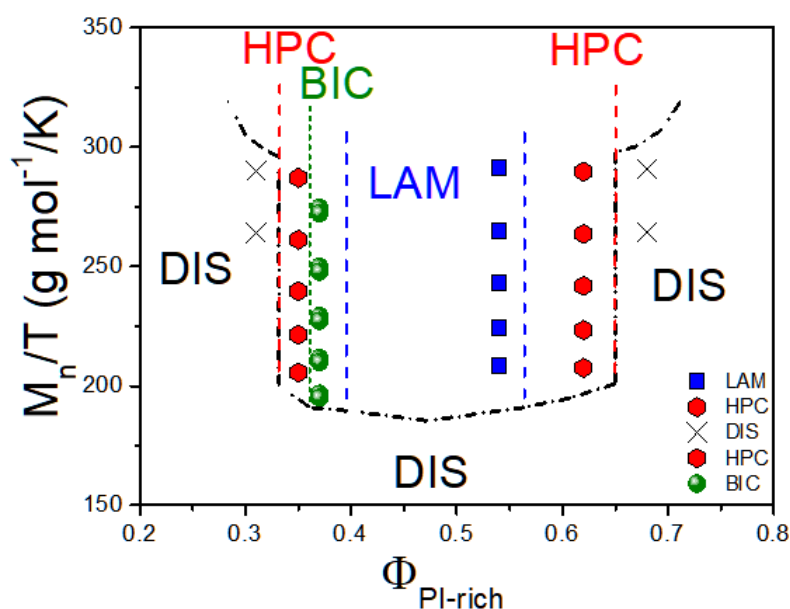


FIGURE 9 Phase diagram for the P(I-co-S) copolymers synthesized in the presence of different [THF]/[Li] ratios indicating lamellae (LAM), hexagonally packed cylinders (HPC), bicontinuous (BIC) and disordered (DIS) morphologies. Vertical lines give the boundaries between the ordered morphologies. The black dash-dotted line gives the hypothetical boundaries to the disordered state.

Our findings on the morphologies can be discussed with respect to the phase diagram of Figure 9. As shown in Table 2 and Figure 5, the content of vinyl-PI (3,4- and 1,2-PI) strongly increases at high [THF]/[Li] ratios. Because of the unknown Flory-Huggins interaction parameter of vinyl-PI with PS we have chosen the M_n/T representation instead of the usual $\chi_{\text{eff}}N$. A different approach – not free of assumptions – is explored in the Supporting Information, Section 9.4. There, the

reduction of the interaction parameter by the gradient structure as well as by the increasing vinyl-PI content is considered for estimating an effective interaction parameter (χ_{eff}) for the P(I-co-S) copolymers. Returning to the phase diagram of Figure 9 we note that the succession of phases, when examined at a fixed M_n/T , is very similar to the PS-*b*-PI case.¹²⁶ At $M_n/T \sim 250 \text{ g mol}^{-1}/\text{K}$, we find DIS-HPC-BIC-LAM phases, e.g. similar to the PS-*b*-PI phases under $\chi N \sim 20$. All phases examined are at equilibrium since the same morphologies were obtained on heating and subsequent cooling (Figure S23). In addition, no order-to-order or order-to-disorder transitions were found, despite the large temperature range investigated (120 K).

Moreover, the phase diagram appears symmetric. We discuss this feature in terms of two parameters, the effective interaction parameter and the conformational asymmetry. The reported solubility parameters for PS and 1,4-PI amount to $18.3 \text{ MPa}^{1/2}$ and $16.7 \text{ MPa}^{1/2}$, respectively. 3,4-PI is reported to have a somewhat lower solubility parameter than 1,4-PI but the precise value is undefined.¹²⁸ Based on this argument (e.g. $\delta_{\text{PS}} > \delta_{1,4\text{-PI}} > \delta_{3,4\text{-PI}}$) the expectation is that a higher [THF]/[Li] ratio will increase the vinyl-PI content (Figure 5) and concomitantly the incompatibility with PS. This should result in an asymmetric phase diagram especially when increasing the PI content. Yet, there is another feature that affects the phase diagram, namely, the asymmetry in the conformational parameters,¹²⁹ ϵ , defined as $\epsilon = \beta_1^2/\beta_2^2$ where $\beta = b^2/6v_0$ is the polymer conformational parameter (b and v_0 are, respectively, the statistical segment length and volume). Given the statistical segment lengths of PS (1.48 nm),¹³⁰ 3,4-PI (1.35 nm)¹³¹ and 1,4-PI (0.89 nm),¹³¹ a more symmetric phase diagram is expected with increasing 3,4-content. Evidently, the two factors give rise to an overall symmetric phase diagram.

Mechanical Properties

As shown by numerous works, the viscoelastic properties of block copolymers are directly governed by the (i) microdomain morphology, (ii) the degree of segregation and (iii) the proximity of glass transition temperatures (see previous sections). These parameters are essential for understanding the mechanical properties of the materials obtained with different THF contents.

Figure 10 provides the results of representative tensile stress-strain (σ - ϵ) curves for different copolymer microstructures. In Figure 11, the remarkably different properties are summarized by plotting the maximum stress, σ_{max} , as well as the strain at break, ϵ_{break} , as a function of the [THF]/[Li] ratio and the morphology. Tapered diblock copolymers synthesized in the absence of THF (0 eq.), show a linear regime of elastic response (stretching of PI domains) as well as a yield point typically ascribed to the break of glassy PS domains.¹³² As already shown in a previous work,¹⁶ break of these lamellar ordered architectures occurs at rather low strains

($\varepsilon_{\text{yield}} \approx \varepsilon_{\text{break}} \approx 10\%$).

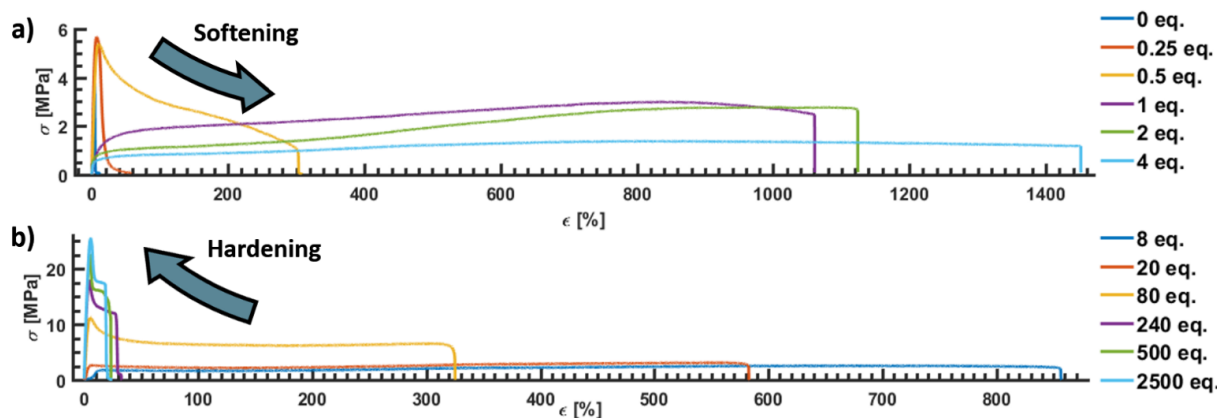


FIGURE 10 Representative tensile testing data obtained for P(I-co-S) copolymers synthesized in the presence of different [THF]/[Li] ratios. a) Increasing the [THF]/[Li] ratio from 0 to 4, leads to soft and stretchable samples (*i.e.* low stress, high strain). b) A further increase of the [THF]/[Li] ratio from 8 to 2500 leads to hard but brittle samples (*i.e.* high stress, low strain).

In contrast, the copolymer obtained for 0.5 eq. THF shows a considerable regime of visco-elastic flow, beyond the yield point until rupture finally occurs ($\varepsilon_{\text{yield}} \approx 5.3\% < \varepsilon_{\text{viscoelastic flow}} < \varepsilon_{\text{break}} \approx 290\%$). This is explained by the switch of the morphology from lamellar (LAM) to PS-rich cylinders embedded in a PI-rich matrix (HPC_{PS}). The isolated nature of the PS-rich domains can suppress crack propagation, enabling a subsequent irreversible flow beyond the yield point. This is further supported by the comparably low Young's modulus ($E(0 \text{ eq.}) \approx 130 \text{ MPa} < E(0.5 \text{ eq.}) \approx 94 \text{ MPa}$; Figure S30, Table S9). The presence of a continuous PI matrix facilitates elastic deformation, less affected by the vitrified, isolated PS-rich domains.

As evident from Figure 10, no yield point is observed for 1-20 THF eq. samples. Hence, stretching results in visco-elastic flow (ductile behavior) even at low strain. This clearly demonstrates the lack of phase separated morphologies, as evidenced in the structural investigations. Although these samples are all in the disordered state, their mechanical properties display exceptional elongation at break. The maximum change of both values is observed at 4 and 8 eq. THF ($\varepsilon_{\text{break}} \approx 1300\%$; $\sigma_{\text{max}} \approx 1.4 \text{ MPa}$), which reflects the random monomer sequence observed for these copolymers.

Further increase to 80 eq. THF, leads to the reappearance of the yield point (*i.e.* recovery of elastic properties for ($\varepsilon < \varepsilon_{\text{yield}}$)). This is explained by the presence of phase separated PS-rich domains, as indicated by the SAXS and TEM studies (Figures 7 and S25B). For 240 eq. THF, PI-rich cylinders embedded in a PS-rich matrix were obtained (Figure 7, 8c and S25B). This is also

supported by the mechanical data. The presence of a continuous PS-rich matrix leads to rather hard and brittle materials ($\sigma_{\max}(\text{HPC}_{\text{PI}}) \approx 17 \text{ MPa} > \sigma_{\max}(\text{HPC}_{\text{PS}}) \approx 5.3 \text{ MPa}$, but $\epsilon_{\text{break}}(\text{HPC}_{\text{PI}}) \approx 32\% < \epsilon_{\text{break}}(\text{HPC}_{\text{PS}}) \approx 290\%$). This “hardening” is further enhanced for the bicontinuous morphologies found for 500 and 2500 THF eq (Figures 7 and 8d). Also in these morphologies, the continuous PS matrix leads to a comparably high yield stress ($\sigma_{\max}(500 \text{ eq.}) \approx 23 \text{ MPa}$; $\sigma_{\max}(2500 \text{ eq.}) \approx 26 \text{ MPa}$).¹³³ The higher value observed for 2500 eq. THF can presumably be ascribed to the higher purity of the PS-rich phase, caused by the lower incorporation of isoprene units in the PS-rich part of the polymer chains. This is further supported by the thermal data, showing an increase of $\Delta T_{\text{g,PSrich}} = 13 \text{ K}$, respectively (Table 2, Figure 5). The yield point, as well as the toughness are also a function of the $[\text{THF}]/[\text{Li}]$ ratio, *i.e.* the morphology (see Figures S31, 32 and Table S8 for detailed discussion).

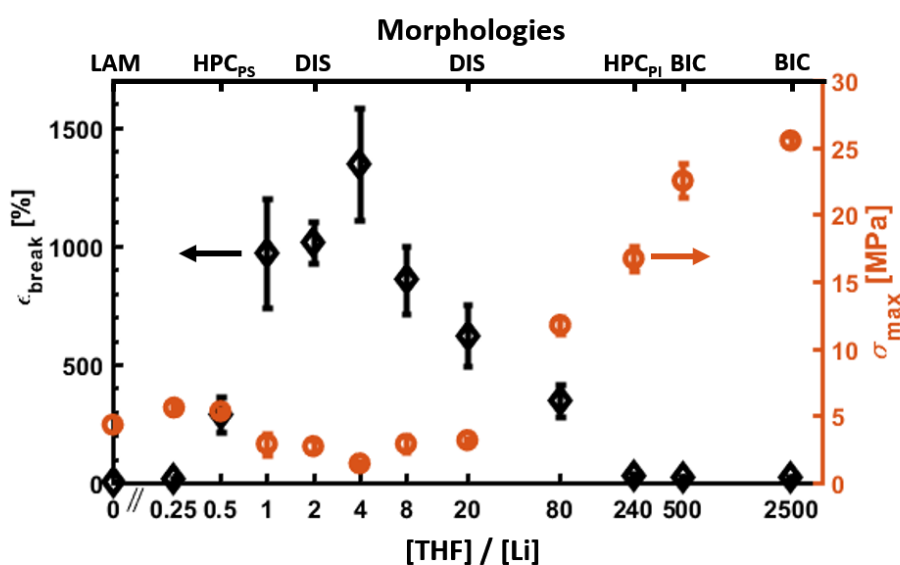


FIGURE 11 Overview of the tensile properties determined by uniaxial drawing experiments as shown in Figure 10. Values are determined as the average of 5 to 9 independent measurements. Errors are given in the 1σ interval. The remarkably different properties obtained are dictated by the respective morphology in the bulk state, indicated at the top.

To summarize the results, the mechanical data show excellent agreement with the morphologies and thermal behavior. To our surprise, even the disordered samples show a good correlation of mechanics (elongation at break, toughness) with the comonomer sequences obtained by NIR probing. The results underline the sensitivity of mechanical properties with respect to subtle changes in the comonomer sequence and the importance of their precise determination.

Outlook: THF-modified I/S Copolymers as Building Blocks for TPEs

As pointed out in the introduction one major problem in TPEs based on styrene-diene triblock copolymers is shifting the T_{ODT} into the temperature range suitable for processing. A number of possible solutions based on tapered structures was already proposed as shown in Figures 1a-c. These studies revealed the compositional gradient as a reasonable parameter to decouple the phase segregation strength ($\chi_{eff}N < \chi N$) from the molecular weight ($M_n \sim N$).^{5,6,16,32,38,51,134} As a consequence, high molecular weight polymers can be synthesized, which provide good mechanical properties (due to entanglements), and possess a T_{ODT} shifted to lower values. The latter is desired, as the disorder state provides lower viscosities and facilitates high-speed melt processing.¹¹ However, the disparate reactivity ratios in the hydrocarbon solvents typically lead to steep gradient profiles (i.e. block-like structures; Figure 1a).^{67,68} The comonomer gradient can be controlled by a number of parameters. Increase of the polymerization temperature can lead to a certain flattening of the gradient, which, however may not be large enough.⁶⁸ In contrast, changes for the variation of the comonomer structure are larger (e.g. alkyl styrene derivatives, other 1,3-dienes),^{20,27,52,135-138} albeit also a result of the monomer combination (χ_{AB}).^{51,86} affect other parameters considerably (e.g. χ_{AB} , entanglement molecular weights, thermal stabilities).

In this publication we presented the full control of comonomer profiles leading to remarkably different morphological and mechanical properties. Unfortunately, their direct use as TPE materials is not possible for two reasons: (i) increased phase miscibility and the high vinyl-PI microstructure result in T_{gs} close to room temperature (Table 2 and Figure 6). As expected, (ii) IS diblock architectures show comparably low elastic moduli and toughness compared to SIS tri- or (IS)_n multiblock structures. Here SIS block sequences effectively connect vitrified PS domains beyond entanglements.^{4,139-142} As shown here, both issues can be solved performing a multi-step polymerization in the presence of THF as randomizer in one reaction vessel ("one-pot") without intermediate work-up.

Here we present the synthesis (on ≈ 80 g scale) of a representative tapered triblock copolymer (Figure 12) with adjusted gradient profile (P(I-co-S) with $[THF]/[Li]=2$), that can solve the problems of multi-step polymerizations in the presence of (homogenous dissolved) polar modifiers, by tracking the monomer consumption during multiple steps by the absorption in the NIR region (Supporting Information section 1.3 and Figure S32). According to Figure 12, first of all a sequential polymerization of styrene and then isoprene was performed in hydrocarbon solution, to afford a desired high content 1,4-PI regioisomers ($\approx 95\%_{mol}$ as $[THF]/[Li]=0$). Then a "randomized" ($\approx 75\%_{mol}$ 1,4PI for $[THF]/[Li]=2$) statistical P(I-co-S) copolymer block was attached (for the gradient profile, see Figure S15e), followed by a final addition of styrene to the living

polymer, respectively also in the presence of THF added for the previous tapered sequence. A homogenous, quantitative re-initiation in each of the multiple steps was proven by SEC, validating the targeted molecular weight with a narrow distribution ($M_{n,target} = 120 \text{ kg}\cdot\text{mol}^{-1}$; $\bar{D} = 1.04$; Figure S33). Following this synthetic strategy, ^1H NMR spectroscopy confirmed the desired, high fraction of 1,4PI in total ($\approx 87\%$; Figure S34). The combination of the latter with comparably large homopolymer segments (Figure 12) enables their use as TPE materials.^{32,35}

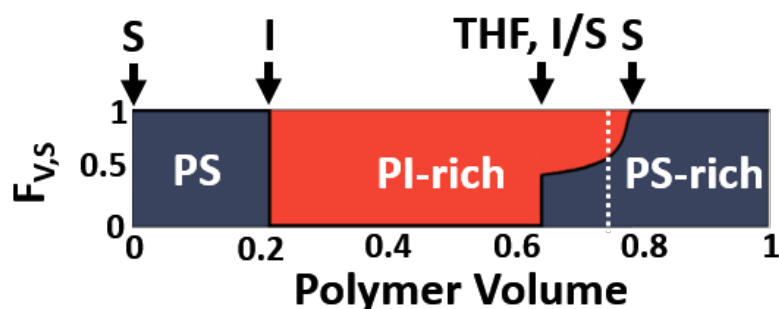


FIGURE 12 Volume composition profile of the PS-*b*-PI-*b*-P(I-co-S)-*b*-PS tapered block copolymer synthesized in a fourstep procedure. Monomer addition steps are indicated by arrows. The white dotted line separates PI- and PS-rich volumes of the taper (see morphology section and Table S7), leading to an SIS-type composition.

In the case of selective hydrogenated polyisoprene blocks, tapering (*i.e.* lowering of χ_{eff}) is especially important, as the hydrogenation remarkably increases the interaction parameter. This leads to inaccessible T_{ODT} s for already comparably low molecular weights.¹⁴³ Such structures, advantageous in terms of their thermal stability of the low T_g block,^{1,3} are also shown accessible by selective, quantitative ($\geq 99\%$) hydrogenation of the PI units using the diimide hydrogenation method (see Supporting Information section 1.5; Figures S33 and S34). Both the hydrogenated and the non-hydrogenated tapered triblock copolymer architectures open a vast field, permitting to vary multiple parameters, e.g. the composition and the fraction of the gradient block, in a versatile manner, which is the focus of our current studies.

CONCLUSIONS

We investigated the effect of THF on the alkyllithium initiated copolymerization of styrene and isoprene in cyclohexane by systematically increasing the $[\text{THF}]/[\text{Li}]$ ratio from 0 to 2500 (29%_{vol}). An in-depth kinetic study using *in situ* near-infrared (NIR) spectroscopy revealed a highly accelerated consumption of the individual comonomers, in particular of styrene. A dramatic effect of THF on the determined reactivity ratios is observed. This explained by the individual rate

constants of homo- and cross-propagation being dependent on the aggregation and complexation equilibria in the system. With increasing [THF]/[Li] ratio the reactivity ratios change from $r_I \gg r_S$ over $r_I \approx r_S$ to $r_I \ll r_S$, leading to an inversion of the copolymer gradient. Hence, adding rather small amounts THF (0.1 %_{vol}) allows for a stepwise flattening of the gradient, leading from tapered PS block copolymers (PI-rich gradient attached to a PS block), to gradient and random copolymers. Increasing [THF]/[Li] further affords tapered PI block copolymers (inverted PS-rich gradient attached to a PI block). The concurrent shift in the PI regioisomer composition with added THF was observed by NMR spectroscopy. Both the isomer composition and the comonomer sequence correlate with thermal properties as well as morphologies.

Although a constant comonomer composition of 50%_{mol} isoprene was chosen, the shape of the gradient remarkably affects the microdomain structure. SAXS and TEM measurements confirmed the phase inversion giving rise to an overall symmetric phase diagram. The succession of phases, when examined at a fixed M_n/T , was very similar to the PS-*b*-PI case. At $M_n/T \sim 250 \text{ g mol}^{-1}/\text{K}$ we found DIS-HPC-BIC-LAM phases including a gyroid phase, e.g. similar to the PS-*b*-PI phases under $\chi N \sim 20$. This is discussed in terms of the increasing incompatibility of PS with 3,4-PI and the more symmetric polymer conformational parameter.

A dramatic change in mechanical properties is observed, in particular in relation to the phase state. This leads to highly stretchable, but soft materials for the random composition (disordered phase). The potential use of those structures as phase compatibilizing block in TPEs was finally demonstrated by the synthesis of a PI-selective hydrogenated "tapered triblock" with the well-established SIS triblock architecture and the use of THF as microstructural modifier.

ACKNOWLEDGEMENTS

The authors thank Jürgen Ludwig for specialty glassware and Monika Schmelzer for valuable support with SEC measurements. Andreas Hanewald and Kaloian Koynov are acknowledged for help with the mechanical characterization. Marcel Fickenscher is thanked for helpful discussions. MG thanks for partial support of this work by the DFG project GA2169/7-1.

REFERENCES

- (1) Hadjichristidis, N.; Pispas, S.; Floudas, G. *Block Copolymers*; John Wiley & Sons, Inc: Hoboken, USA, 2002.
- (2) Hsieh, H. L.; Quirk, R. P. *Anionic Polymerization: Principles and Practical Applications*; *Plastics Engineering* 34; Dekker: New York, 1996.
- (3) Noshay, A.; McGrath, J. E. *Block copolymers: Overview and critical survey*, 2. print; Acad. Pr: Orlando u.a., 1987.
- (4) Morton, M. In *Multicomponent polymer systems: A symposium co-sponsored by the Division of Industrial and Engineering Chemistry, the Division of Polymer Chemistry at the 159th meeting of the American Chemical Society*, Houston, Tex., Feb. 23 - 26, 1970; Platzner, N. A. J., Ed.; *Advances in chemistry series 99*; American Chemical Society: Washington, DC, 1971; pp 490–509.
- (5) Geoffrey, H.; Milkovich, R. Block polymers of monovinyl aromatic hydrocarbons and conjugated dienes. *3,265,765*, Jan 29, 1962.
- (6) Cunningham, R. E.; Treiber, M. R. *J. Appl. Polym. Sci.* **1968**, 12 (1), 23–34. DOI: 10.1002/app.1968.070120104.
- (7) Bishop, E. T.; Davison, S. J. *Polym. Sci. C Polym. Symp.* **1969**, 26 (1), 59–79. DOI: 10.1002/polc.5070260105.
- (8) Morton, M.; McGrath, J. E.; Juliano, P. C. *J. Polym. Sci. C Polym. Symp.* **1969**, 26 (1), 99–115. DOI: 10.1002/polc.5070260107.
- (9) Lin, C. C.; Jonnalagadda, S. V.; Kesani, P. K.; Dai, H. J.; Balsara, N. P. *Macromolecules* **1994**, 27 (26), 7769–7780. DOI: 10.1021/ma00104a035.
- (10) Mark, J. E. *Physical Properties of Polymer Handbook*, 2nd ed; Springer: New York, 2006.
- (11) Knoll, K.; Nießner, N. *Macromol. Symp.* **1998**, 132 (1), 231–243. DOI: 10.1002/masy.19981320122.
- (12) Gouinlock, E. V.; Porter, R. S. *Polym. Eng. Sci.* **1977**, 17 (8), 535–543. DOI: 10.1002/pen.760170809.
- (13) Sinturel, C.; Bates, F. S.; Hillmyer, M. A. *ACS Macro Lett.* **2015**, 4 (9), 1044–1050. DOI: 10.1021/acsmacrolett.5b00472.
- (14) Leibler, L. *Macromolecules* **1980**, 13 (6), 1602–1617. DOI: 10.1021/ma60078a047.
- (15) Hashimoto, T.; Tsukahara, Y.; Kawai, H. *Polym. J.* **1983**, 15 (10), 699–711. DOI: 10.1295/polymj.15.699.
- (16) Steube, M.; Johann, T.; Galanos, E.; Appold, M.; Rüttiger, C.; Mezger, M.; Gallei, M.; Müller, A. H. E.; Floudas, G.; Frey, H. *Macromolecules* **2018**, 51 (24), 10246–10258. DOI: 10.1021/acs.macromol.8b01961.
- (17) Worsfold, D. J. *J. Polym. Sci. A* **1967**, 5 (11), 2783–2789. DOI: 10.1002/pol.1967.150051106.
- (18) Patterson, A. L.; Yu, B.; Danielsen, S. P. O.; Davidson, E. C.; Fredrickson, G. H.; Segalman, R. A. *Macromolecules* **2020**. DOI: 10.1021/acs.macromol.9b02426.
- (19) Handlin, D. L.; Williamson, D. T.; Willis, C. L. Block copolymer. 6,699,941, Nov 7, 2002.
- (20) Johnson, A. F.; Worsfold, D. J. *Makromol. Chem.* **1965**, 85 (1), 273–279. DOI: 10.1002/macp.1965.020850122.
- (21) O'Driscoll, K. F.; Kuntz, I. J. *J. Polym. Sci.* **1962**, 61 (171), 19–24. DOI: 10.1002/pol.1962.1206117104.
- (22) Quirk, R. P. In *Encyclopedia of Polymer Science and Technology*; Wiley Interscience: Hoboken, NJ, 2004; pp 197–235.
- (23) *Anionic polymerization: Principles, practice, strength, consequences and applications*; Hadjichristidis, N., Hirao, A., Eds.; Springer: Tokyo, 2015.
- (24) Szwarc, M. In *Living Polymers and Mechanisms of Anionic Polymerization; Advances in Polymer Science*; Springer Berlin Heidelberg: Berlin, Heidelberg, 1983; pp 1–177.
- (25) Corbin, N.; Prud'homme, J. J. *Polym. Sci. Polym. Chem. Ed.* **1976**, 14 (7), 1645–1659. DOI: 10.1002/pol.1976.170140708.

- (26) Corbin, N.; Prud'homme, J. J. *Polym. Sci. Polym. Phys. Ed.* **1977**, *15* (11), 1937–1951. DOI: 10.1002/pol.1977.180151106.
- (27) Grune, E.; Johann, T.; Appold, M.; Wahlen, C.; Blankenburg, J.; Leibig, D.; Müller, A. H. E.; Gallei, M.; Frey, H. *Macromolecules* **2018**, *51* (9), 3527–3537. DOI: 10.1021/acs.macromol.8b00404.
- (28) Tsukahara, Y.; Nakamura, N.; Hashimoto, T.; Kawai, H.; Nagaya, T.; Sugimura, Y.; Tsuge, S. *Polym. J.* **1980**, *12* (7), 455–466. DOI: 10.1295/polymj.12.455.
- (29) Zhao, Y.; Miyamoto, N.; Koizumi, S.; Hashimoto, T. *Macromolecules* **2010**, *43* (6), 2948–2959. DOI: 10.1021/ma902542e.
- (30) Hutchings, L. R.; Brooks, P. P.; Shaw, P.; Ross-Gardner, P. *J. Polym. Sci. A* **2019**, *57* (3), 382–394. DOI: 10.1002/pola.29208.
- (31) Zelinski, R.; Childers, C. W. *Rubber Chem. Technol.* **1968**, *41* (1), 161–181. DOI: 10.5254/1.3539168.
- (32) Hodrokoukes, P.; Floudas, G.; Pispas, S.; Hadjichristidis, N. *Macromolecules* **2001**, *34* (3), 650–657. DOI: 10.1021/ma001479i.
- (33) Brown, J. R.; Sides, S. W.; Hall, L. M. *ACS Macro Lett.* **2013**, *2* (12), 1105–1109. DOI: 10.1021/mz400546h.
- (34) Kelsey, J.; Pickering, N.; Clough, A.; Zhou, J.; White, J. L. *Macromolecules* **2017**, *50* (18), 7233–7240. DOI: 10.1021/acs.macromol.7b01476.
- (35) Annighöfer, F.; Gronski, W. *Colloid Polym. Sci.* **1983**, *261* (1), 15–25. DOI: 10.1007/BF01411513.
- (36) Gronski, W.; Annighöfer, F.; Stadler, R. *Makromol. Chem.* **1984**, *6* (S19841), 141–161. DOI: 10.1002/macp.1984.020061984111.
- (37) Henderson, J. F.; Szwarc, M. *J. Polym. Sci. Macromol. Rev.* **1968**, *3* (1), 317–401. DOI: 10.1002/pol.1968.230030105.
- (38) Singh, N.; Tureau, M. S.; Epps, I. T. H. *Soft Matter* **2009**, *5* (23), 4757. DOI: 10.1039/b908739g.
- (39) Roy, R.; Park, J. K.; Young, W.-S.; Mastroianni, S. E.; Tureau, M. S.; Epps, T. H. *Macromolecules* **2011**, *44* (10), 3910–3915. DOI: 10.1021/ma1025847.
- (40) Luo, M.; Brown, J. R.; Remy, R. A.; Scott, D. M.; Mackay, M. E.; Hall, L. M.; Epps, T. H. *Macromolecules* **2016**, *49* (14), 5213–5222. DOI: 10.1021/acs.macromol.6b00946.
- (41) Annighöfer, F.; Gronski, W. *Makromol. Chem.* **1984**, *185* (10), 2213–2231. DOI: 10.1002/macp.1984.021851016.
- (42) Ashraf, A. R.; Ryan, J. J.; Satkowski, M. M.; Lee, B.; Smith, S. D.; Spontak, R. J. *Macromol. Rapid Commun.* **2017**, *38* (17). DOI: 10.1002/marc.201700207.
- (43) Kelley, D. J.; Tobolsky, A. V. *J. Am. Chem. Soc.* **1959**, *81* (7), 1597–1600. DOI: 10.1021/ja01516a021.
- (44) Kuntz, I. *J. Polym. Sci.* **1961**, *54* (160), 569–586. DOI: 10.1002/pol.1961.1205416020.
- (45) Zelinski, R. Preparation of Copolymers in the Presence of an Organo-Lithium Catalyst and a Solvent Mixture Comprising a Hydrocarbon and an Ether, Thioether or Amine. 2,975,160, Apr 23, 1958.
- (46) Antkowiak, T. A.; Oberster, A. E.; Halasa, A. F.; Tate, D. P. *J. Polym. Sci. A* **1972**, *10* (5), 1319–1334. DOI: 10.1002/pol.1972.150100504.
- (47) Wofford, C. F. Production of Random Copolymers in Organolithium Polymerization Systems. 3,498,960, Mar 3, 1970.
- (48) Kraus, G.; Childers, C. W.; Gruver, J. T. *J. Appl. Polym. Sci.* **1967**, *11* (8), 1581–1591. DOI: 10.1002/app.1967.070110819.
- (49) Kraus, G.; Rollmann, K. W. *Angew. Makromol. Chemie* **1971**, *16* (1), 271–296. DOI: 10.1002/apmc.1971.050160115.
- (50) Adhikari, R.; Huy, T. A.; Buschnakowski, M.; Michler, G. H.; Knoll, K. *New J. Phys.* **2004**, *6*, 28. DOI: 10.1088/1367-2630/6/1/028.

- (51) Galanos, E.; Grune, E.; Wahlen, C.; Müller, A. H. E.; Appold, M.; Gallei, M.; Frey, H.; Floudas, G. *Macromolecules* **2019**, *52* (4), 1577–1588. DOI: 10.1021/acs.macromol.8b02669.
- (52) Grune, E.; Bareuther, J.; Blankenburg, J.; Appold, M.; Shaw, L.; Müller, A. H. E.; Floudas, G.; Hutchings, L. R.; Gallei, M.; Frey, H. *Polym. Chem.* **2019**, *50* (1), 3. DOI: 10.1039/C8PY01711E.
- (53) Johnson, A. F.; Worsfold, D. J. *J. Polym. Sci. A: Gen. Pap.* **1965**, *3* (2), 449–455. DOI: 10.1002/pol.1965.100030204.
- (54) Worsfold, D. J.; Bywater, S. *Can. J. Chem.* **1960**, *38* (10), 1891–1900. DOI: 10.1139/v60-254.
- (55) Morton, M.; Fetters, L. J.; Bostick, E. E. *J. Polym. Sci. C Polym. Symp.* **1963**, *1* (1), 311–323. DOI: 10.1002/polc.5070010121.
- (56) Cubbon, R.C.P.; Margerison, D. *Proc. R. Soc. Lond. A* **1962**, *268* (1333), 260–275. DOI: 10.1098/rspa.1962.0138.
- (57) Cubbon, R.C.P.; Margerison, D. *Polymer* **1965**, *6* (2), 102–106. DOI: 10.1016/0032-3861(65)90022-4.
- (58) Hsieh, H. L. *J. Polym. Sci. A: Gen. Pap.* **1965**, *3* (1), 173–180. DOI: 10.1002/pol.1965.100030119.
- (59) Fetters, L. J.; Balsara, N. P.; Huang, J. S.; Jeon, H. S.; Almdal, K.; Lin, M. Y. *Macromolecules* **1995**, *28* (14), 4996–5005. DOI: 10.1021/ma00118a031.
- (60) Worsfold, D. J.; Bywater, S. *Macromolecules* **1972**, *5* (4), 393–397. DOI: 10.1021/ma60028a012.
- (61) Fetters, L. J.; Morton, M. *Macromolecules* **1974**, *7* (5), 552–559. DOI: 10.1021/ma60041a004.
- (62) Watanabe, H.; Oishi, Y.; Kanaya, T.; Kaji, H.; Horii, F. *Macromolecules* **2003**, *36* (1), 220–228. DOI: 10.1021/ma0213697.
- (63) Niu, A. Z.; Stellbrink, J.; Allgaier, J.; Willner, L.; Radulescu, A.; Richter, D.; Koenig, B. W.; May, R. P.; Fetters, L. J. *J. Chem. Phys.* **2005**, *122* (13), 134906. DOI: 10.1063/1.1866092.
- (64) Margl, P. *Can. J. Chem.* **2009**, *87* (7), 891–903. DOI: 10.1139/V09-032.
- (65) Bywater, S. *Macromolecules* **1998**, *31* (18), 6010–6013. DOI: 10.1021/ma970963r.
- (66) Müller, A. H.E. In *Comprehensive polymer science: The synthesis, characterization, reactions et applications of polymers*; Allen, G., J.C. Bevington, Eds.; Pergamon Press: Oxford, 1989; pp 387–423.
- (67) Quinebèche, S.; Navarro, C.; Gnanou, Y.; Fontanille, M. *Polymer* **2009**, *50* (6), 1351–1357. DOI: 10.1016/j.polymer.2009.01.041.
- (68) Steube, M.; Johann, T.; Plank, M.; Tjaberings, S.; Gröschel, A. H.; Gallei, M.; Frey, H.; Müller, A. H. E. *Macromolecules* **2019**, *52* (23), 9299–9310. DOI: 10.1021/acs.macromol.9b01790.
- (69) Morton, M.; Ells, F. R. *J. Polym. Sci.* **1962**, *61* (171), 25–29. DOI: 10.1002/pol.1962.1206117105.
- (70) Spirin, Y. L.; Arest-Yakubovich, A. A.; Polyakov, D. K.; Gantmakher, A. R.; Medvedev, S. S. *J. Polym. Sci.* **1962**, *58* (166), 1181–1189. DOI: 10.1002/pol.1962.1205816674.
- (71) Morton, M.; Fetters, L. J. *J. Polym. Sci. A: Gen. Pap.* **1964**, *2* (7), 3311–3326. DOI: 10.1002/pol.1964.100020726.
- (72) Morton, M.; Bostick, E. E.; Livigni, R. A.; Fetters, L. J. *J. Polym. Sci. A: Gen. Pap.* **1963**, *1* (5), 1735–1747. DOI: 10.1002/pol.1963.100010525.
- (73) Bywater, S.; Johnson, A. F.; Worsfold, D. J. *Can. J. Chem.* **1964**, *42* (6), 1255–1260. DOI: 10.1139/v64-197.
- (74) Hsieh, H.; Tobolsky, A. V. *J. Polym. Sci.* **1957**, *25* (109), 245–247. DOI: 10.1002/pol.1957.1202510918.
- (75) Foster, F. C.; Binder, J. L. In *Homogeneous transition metal catalyzed reactions: Developed from a symposium*; Moser, W. R., Slocum, D. W., Eds.; Advances in chemistry series 230; The Society: Washington, DC, 1992; pp 26–33.
- (76) Morita, H.; Tobolsky, A. V. *J. Am. Chem. Soc.* **1957**, *79* (22), 5853–5855. DOI: 10.1021/ja01579a004.
- (77) Szwarc, M. *J. Polym. Sci.* **1959**, *40* (137), 583–586. DOI: 10.1002/pol.1959.1204013734.
- (78) Bywater, S.; Worsfold, D. J. *J. Organomet. Chem.* **1978**, *159* (3), 229–235. DOI: 10.1016/S0022-328X(00)93801-4.

- (79) Zelinski, R. Preparation of Polymers of Conjugated Dienes Using Organolithium/Polar Compound Catalyst Systems. 3,301,840, Jan 31, 1967.
- (80) Bywater, S.; Firat, Y.; Black, P. E. *J. Polym. Sci. Polym. Chem. Ed.* **1984**, 22 (3), 669–672. DOI: 10.1002/pol.1984.170220316.
- (81) Garton, A.; Bywater, S. *Macromolecules* **1975**, 8 (6), 694–697. DOI: 10.1021/ma60048a002.
- (82) Worsfold, D. J.; Bywater, S. *Macromolecules* **1978**, 11 (3), 582–586. DOI: 10.1021/ma60063a030.
- (83) McDonald, R. T.; Bywater, S. *Organometallics* **1986**, 5 (8), 1529–1532. DOI: 10.1021/om00139a003.
- (84) McDonald, R. T.; Bywater, S.; Black, P. *Macromolecules* **1987**, 20 (6), 1196–1199. DOI: 10.1021/ma00172a005.
- (85) Garton, A.; Chaplin, R. P.; Bywater, S. *Eur. Polym. J.* **1976**, 12 (10), 697–700. DOI: 10.1016/0014-3057(76)90078-1.
- (86) Zhao, J.; Ediger, M. D.; Sun, Y.; Yu, L. *Macromolecules* **2009**, 42 (17), 6777–6783. DOI: 10.1021/ma9008516.
- (87) Widmaier, J. M.; Meyer, G. C. *Macromolecules* **1981**, 14 (2), 450–452. DOI: 10.1021/ma50003a041.
- (88) Pinazzi, C. P.; Soutif, J. C.; Brosse, J. C. *Eur. Polym. J.* **1975**, 11 (7), 523–525. DOI: 10.1016/0014-3057(75)90104-4.
- (89) Gabor, A. H.; Lehner, E. A.; Mao, G.; Schneggenburger, L. A.; Ober, C. K. *Chem. Mater.* **1994**, 6 (7), 927–934. DOI: 10.1021/cm00043a011.
- (90) Ameduri, B.; Boutevin, B.; Nouiri, M. *J. Polym. Sci. A* **1993**, 31 (8), 2069–2080. DOI: 10.1002/pola.1993.080310813.
- (91) Rüttiger, C.; Appold, M.; Didzoleit, H.; Eils, A.; Dietz, C.; Stark, R. W.; Stühn, B.; Gallei, M. *Macromolecules* **2016**, 49 (9), 3415–3426. DOI: 10.1021/acs.macromol.6b00577.
- (92) *Rubber compounding: Chemistry and applications*; Rodgers, B., Ed., Second edition; CRC Press an imprint of Taylor & Francis Group an informa business: Boca Raton, 2016.
- (93) *Anionic polymerization*; Fetters, L. J., Ed.; Advances in Polymer Science 56; Springer-Verlag: Berlin, 1984.
- (94) Baskaran, D.; Müller, A. H. E. In *Controlled and living polymerizations: Methods and materials*; Müller, A. H. E., Matyjaszewski, K., Eds.; Wiley-VCH: Weinheim, 2009; pp 1–56.
- (95) Zhao, Z.; Shen, H.; Sui, K.; Wang, G. *Polymer* **2018**, 137, 364–369. DOI: 10.1016/j.polymer.2017.12.070.
- (96) Liao, M.; Wang, Q.; Wang, N.; Xu, L.; Li, C.; Liang, A. *Polym. Sci. Ser. B* **2014**, 56 (6), 753–761. DOI: 10.1134/S1560090415010108.
- (97) Moczygomba, G. A.; Trepka, W. J. Tapered Block Styrene/Butadiene Copolymers. 5,227,419, Dec 20, 1990.
- (98) Moczygomba, G. A.; Knight, N. R.; Trepka, W. J.; Stacy, N. E. Block Copolymers of Monovinylarenes and Conjugated Dienes Containing Two Interior Tapered Blocks. 5,399,628, Dec 2, 1993.
- (99) Moczygomba, G. A.; Nash, L. L.; Trepka, W. J.; DePorter, C. D.; Stacy, N. E.; Farrar, R. C.; Selman, C. M. Block Copolymers of Monovinylarenes and Conjugated Dienes and Preparatin Thereof. 5,426,298, Sep 19, 1994.
- (100) Welch, F. J. *J. Am. Chem. Soc.* **1960**, 82 (23), 6000–6005. DOI: 10.1021/ja01508a009.
- (101) O'Driscoll, K. F.; Tobolsky, A. V. *J. Polym. Sci.* **1959**, 35 (128), 259–265. DOI: 10.1002/pol.1959.1203512821.
- (102) Bywater, S.; Worsfold, D. J. *Can. J. Chem.* **1962**, 40 (8), 1564–1570. DOI: 10.1139/v62-236.
- (103) Bywater, S. In *Non-radical polymerisation*; Bamford, C. H., Tipper, C. F. H., Eds.; Comprehensive Chemical Kinetics v. 15; Elsevier Scientific Pub. Co: Amsterdam, New York, 1976; pp 1–65.
- (104) Long, T. E.; Liu, H. Y.; Schell, B. A.; Teegarden, D. M.; Uerz, D. S. *Macromolecules* **1993**, 26 (23), 6237–6242. DOI: 10.1021/ma00075a018.
- (105) Meyer, V. E.; Lowry, G. G. *J. Polym. Sci. A: Gen. Pap.* **1965**, 3 (8), 2843–2851. DOI: 10.1002/pol.1965.100030811.

- (106) Kolling, O. W. *Transactions of the Kansas Academy of Science* **1991**, 94 (3/4), 107. DOI: 10.2307/3627858.
- (107) Morton, M.; Rembaum, A. A.; Hall, J. L. *J. Polym. Sci. A: Gen. Pap.* **1963**, 1 (1), 461–474. DOI: 10.1002/pol.1963.100010140.
- (108) Morton, M.; Bostick, E. E.; Clarke, R. G. *J. Polym. Sci. A: Gen. Pap.* **1963**, 1 (1), 475–482. DOI: 10.1002/pol.1963.100010141.
- (109) Bovey, F. A.; v. d. Tiers, G.; Filipovich, G. *J. Polym. Sci.* **1959**, 38 (133), 73–90. DOI: 10.1002/pol.1959.1203813308.
- (110) Mochel, V. D. *Macromolecules* **1969**, 2 (5), 537–540. DOI: 10.1021/ma60011a017.
- (111) Forens, A.; Roos, K.; Dire, C.; Gadenne, B.; Carlotti, S. *Polymer* **2018**. DOI: 10.1016/j.polymer.2018.07.071.
- (112) Tobolsky, A. V.; Rogers, C. E. *J. Polym. Sci.* **1959**, 40 (136), 73–89. DOI: 10.1002/pol.1959.1204013605.
- (113) Tobolsky, A. V.; Rogers, C. E. *J. Polym. Sci.* **1959**, 38 (133), 205–207. DOI: 10.1002/pol.1959.1203813317.
- (114) Gebert, W.; Hinz, J.; Sinn, H. *Makromol. Chem.* **1971**, 144 (1), 97–115. DOI: 10.1002/macp.1971.021440109.
- (115) Morton, M.; Rupert, J. R. In *Initiation of polymerization: ACS Polymer Symposia*; Bailey, F. E., Ed.; ACS Symposium Series 212; American Chemical Society: Washington, DC, 1983; pp 283–289.
- (116) Hsieh, H.; Kelley, D. J.; Tobolsky, A. V. *J. Polym. Sci.* **1957**, 26 (113), 240–242. DOI: 10.1002/pol.1957.1202611315.
- (117) Ura-neck, C. A. *J. Polym. Sci. A* **1971**, 9 (8), 2273–2281. DOI: 10.1002/pol.1971.150090814.
- (118) Morton, M.; Calderon, N.; Fetters, L. J.; Meier, J. F. *Polym. Eng. Sci.* **1962**, 2 (2), 106–107. DOI: 10.1002/pen.760020210.
- (119) Worsfold, D. J.; Bywater, S. *Can. J. Chem.* **1964**, 42 (12), 2884–2892. DOI: 10.1139/v64-426.
- (120) *Polymer handbook*; Brandrup, J., Ed., 4. ed.; Wiley: Hoboken, N. J., 1999.
- (121) Odian, G. *Principles of Polymerization*, 4th ed.; Wiley-Interscience: S.I., 2004.
- (122) Zhang, L.; Luo, Y.; Hou, Z. *J. Am. Chem. Soc.* **2005**, 127 (42), 14562–14563. DOI: 10.1021/ja055397r.
- (123) Jia, X.; Zhang, X.; Gong, D. *J. Polym. Sci. A* **2018**, 56 (20), 2286–2293. DOI: 10.1002/pola.29201.
- (124) Lodge, T. P.; McLeish, T. C. B. *Macromolecules* **2000**, 33 (14), 5278–5284. DOI: 10.1021/ma9921706.
- (125) Gennes, P.-G. de. *Scaling concepts in polymer physics*; Cornell Univ. Press: Ithaca, NY, 1979.
- (126) Khandpur, A. K.; Förster, S.; Bates, F. S.; Hamley, I. W.; Ryan, A. J.; Bras, W.; Almdal, K.; Mortensen, K. *Macromolecules* **1995**, 28 (26), 8796–8806. DOI: 10.1021/ma00130a012.
- (127) Hajduk, D. A.; Harper, P. E.; Gruner, S. M.; Honeker, C. C.; Kim, G.; Thomas, E. L.; Fetters, L. J. *Macromolecules* **1994**, 27 (15), 4063–4075. DOI: 10.1021/ma00093a006.
- (128) Avgeropoulos, A.; Paraskeva, S.; Hadjichristidis, N.; Thomas, E. L. *Macromolecules* **2002**, 35 (10), 4030–4035. DOI: 10.1021/ma010824g.
- (129) Bates, F. S.; Schulz, M. F.; Khandpur, A. K.; Förster, S.; Rosedale, J. H.; Almdal, K.; Mortensen, K. *Faraday Discuss.* **1994**, 98, 7–18. DOI: 10.1039/FD9949800007.
- (130) Fetters, L. J.; Lohse, D. J.; Richter, D.; Witten, T. A.; Zirkel, A. *Macromolecules* **1994**, 27 (17), 4639–4647. DOI: 10.1021/ma00095a001.
- (131) Thudium, R. N.; Han, C. C. *Macromolecules* **1996**, 29 (6), 2143–2149. DOI: 10.1021/ma9512465.
- (132) Long, D.; Sotta, P. *Rheol Acta* **2007**, 46 (8), 1029–1044. DOI: 10.1007/s00397-007-0187-6.
- (133) Dair, B. J.; Honeker, C. C.; Alward, D. B.; Avgeropoulos, A.; Hadjichristidis, N.; Fetters, L. J.; Capel, M.; Thomas, E. L. *Macromolecules* **1999**, 32 (24), 8145–8152. DOI: 10.1021/ma990666h.

- (134) Jouenne, S.; González-Léon, J. A.; Ruzette, A.-V.; Lodéfier, P.; Leibler, L. *Macromolecules* **2008**, *41* (24), 9823–9830. DOI: 10.1021/ma801327x.
- (135) Johann, T.; Leibig, D.; Grune, E.; Müller, A. H.E.; Frey, H. *Macromolecules* **2019**, *52* (12), 4545–4554. DOI: 10.1021/acs.macromol.9b00747.
- (136) Leibig, D.; Messerle, M.; Johann, T.; Moers, C.; Kaveh, F.; Butt, H.-J.; Vollmer, D.; Müller, A. H. E.; Frey, H. *J. Polym. Sci.* **2020**, *58* (1), 181–192. DOI: 10.1002/pola.29515.
- (137) Natalello, A.; Alkan, A.; Tiedemann, P. von; Wurm, F. R.; Frey, H. *ACS Macro Lett.* **2014**, *3* (6), 560–564. DOI: 10.1021/mz500255h.
- (138) Tiedemann, P. von; Blankenburg, J.; Maciol, K.; Johann, T.; Müller, A. H. E.; Frey, H. *Macromolecules* **2019**. DOI: 10.1021/acs.macromol.8b02280.
- (139) Georgopoulos, P.; Handge, U. A.; Abetz, C.; Abetz, V. *Polymer* **2016**, *104*, 279–295. DOI: 10.1016/j.polymer.2016.02.039.
- (140) Qiao, L.; Leibig, C.; Hahn, S. F.; Winey, K. I. *Ind. Eng. Chem. Res.* **2006**, *45* (16), 5598–5602. DOI: 10.1021/ie0511940.
- (141) Drolet, F.; Fredrickson, G. H. *Macromolecules* **2001**, *34* (15), 5317–5324. DOI: 10.1021/ma0100753.
- (142) Spontak, R. J.; Smith, S. D. *J. Polym. Sci. B* **2001**, *39* (9), 947–955. DOI: 10.1002/polb.1070.
- (143) Adams, J. L.; Quiram, D. J.; Graessley, W. W.; Register, R. A.; Marchand, G. R. *Macromolecules* **1998**, *31* (1), 201–204. DOI: 10.1021/ma9710500.

SUPPORTING INFORMATION

1 Materials and Experimental Procedures

All chemicals and solvents were purchased from Acros Organics Co., Carl Roth GmbH and Sigma-Aldrich Co.

1.1 Purification of the Materials

Prior use, all glass ware was flame-dried under vacuum and flushed with argon at least twice. Prior to the use of isoprene and styrene, the monomers were filtered through a column containing basic aluminum oxide to remove stabilizer. Subsequently, the targeted monomer volumes of isoprene and styrene were transferred into a flask, dried for one day at room temperature over finely ground CaH_2 , degassed by three cycles of freeze-pump-thaw and distilled ($1 \cdot 10^{-3}$ mbar) into a flask containing trioctylaluminum obtained by evaporation of solvent from a trioctylaluminum solution under reduced pressure. After stirring at room temperature overnight, the monomers were degassed by one cycle of freeze-pump-thaw and distilled into a graduated ampoule. The combined monomer volume was determined by the graduation and typically showed a loss 1.5%_{vol} in respect to the targeted value. This can be explained by the loss of monomer during distillation (autopolymerization of the monomers) as well as volume contraction caused by the miscibility.

Cyclohexane was dried over sodium with benzophenone as an indicator under reflux in an argon atmosphere. The dried cyclohexane was distilled into a Morton flask glass reactor, equipped with a neodymium magnetic stir bar under normal pressure. The NIR probe was introduced via an additional glass joint (Figure S1b), as also described in a previous work.¹

THF was dried over diphenylethylenyllithium. For this purpose, a molar ratio of *sec*-BuLi to diphenylethylene of 1:1.2 was used to prevent the presence of *sec*-BuLi, which is not stable in the presence of THF at ambient temperature.² An excess of dry THF was distilled under reduced pressure.

1.2 Synthesis of Copolymers with THF addition

Removal of the stabilizer from the monomer was carried out in separate flasks (see Purification of the Materials). Drying of the monomers was carried out in one flask to reduce the number of distillation steps. As the first step, the required amount of dry cyclohexane was distilled under normal pressure into the reaction flask, containing the neodymium magnetic stir bar and the NIR probe. THF was added to the cyclohexane containing reactor via a graduated ampoule or syringe depending on the amount of THF. The NIR background spectrum was measured. Subsequently

the monomer mixture was added via a graduated ampoule, followed by initiation via *sec*-BuLi solution.

The temperature of the reaction flask was controlled by an external, stirred water bath containing an electronic temperature sensor with a stirring plate as a heating source, a copper-made cooling coil attached to a cryostat as a cooling source, as well as a calibrated temperature data logger.

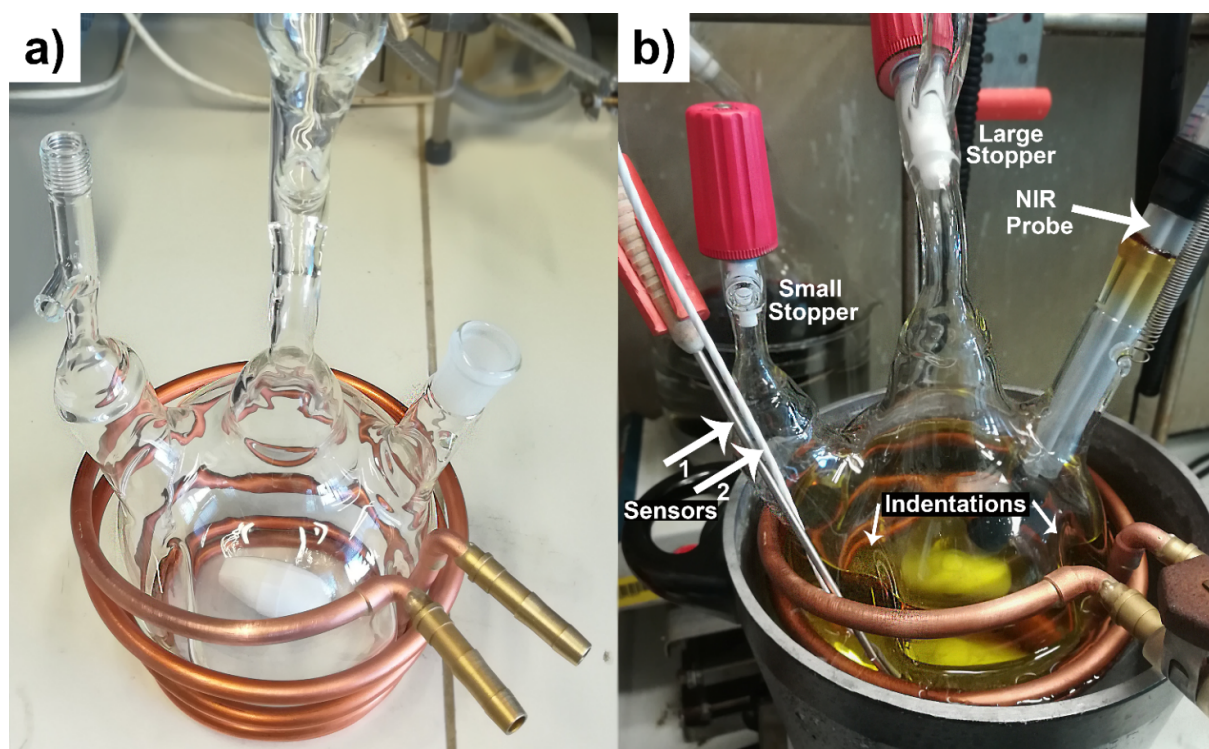


FIGURE S1 a) The reaction flask with the copper-made cooling coil. The radius of the cooling coil was adjusted to the reaction flask. b) A copolymerization of isoprene and styrene in the glass reactor that was used for NIR probing. The yellow color of the solution indicates the presence of living polystyryllithium chain ends. The NIR probe (right) was introduced via a glass joint. The small Teflon stopper (left) was used to add initiator (or THF) via syringe while flushing the reaction system with Argon 5.0. The large Teflon stopper (middle) was used for monomer (or THF) addition via ampoule and serves as a connection to the Schlenk line. Temperature Sensor 1 was attached to the heating plate. Temperature Sensor 2 was attached to the glass surface and served as a temperature data logger (see Figure S3 for temperature profiles).

1.3 Synthesis of a Tapered SIS Triblock Copolymer

Removal of the stabilizer from the monomer, was carried out in separate flasks (see Purification of the Materials). Drying of the monomers was carried out in three flasks for styrene, isoprene as well as the styrene/isoprene mixture. As the first step, the required amount of dry cyclohexane was distilled under normal pressure into the reaction flask, containing the neodymium magnetic stir bar and the NIR probe. The NIR background spectrum was measured and *in situ* monitoring

started.

Subsequently the required proportion of styrene (19.5 mL, 0.17 mol, 262.0 eq.; see Figure S2 for applied temperature program and time dependent NIR absorption) was added via a graduated ampoule, followed by initiation via *sec*-BuLi solution (0.5 mL, 1.3 mol/L, 0.65 mmol, 1.0 eq.).

After a certain time, the tracked absorption in the NIR region reached a plateau value. Hence, full monomer conversion was concluded, and isoprene (43 mL, 0.43 mol, 660.0 eq.) was added via a graduated ampoule. Based on the absorption, full conversion of *isoprene* was observed and THF was added. As THF also shows absorption in the measured NIR range, the time was noted, and later used for baseline corrections for subsequent addition steps.

Subsequently, the *equimolar I/S monomer mixture* (14.2 mL) was added via a third graduated ampoule, and left for polymerization overnight.

After full conversion, the remaining styrene (19.5 mL, 0.17 mol, 262.0 eq.) was added dropwise over a timeperiod of ≈ 4 min, by continuously cooling the reaction during the monomer addition. Full monomer conversion was achieved at elevated temperatures (Figure S2).

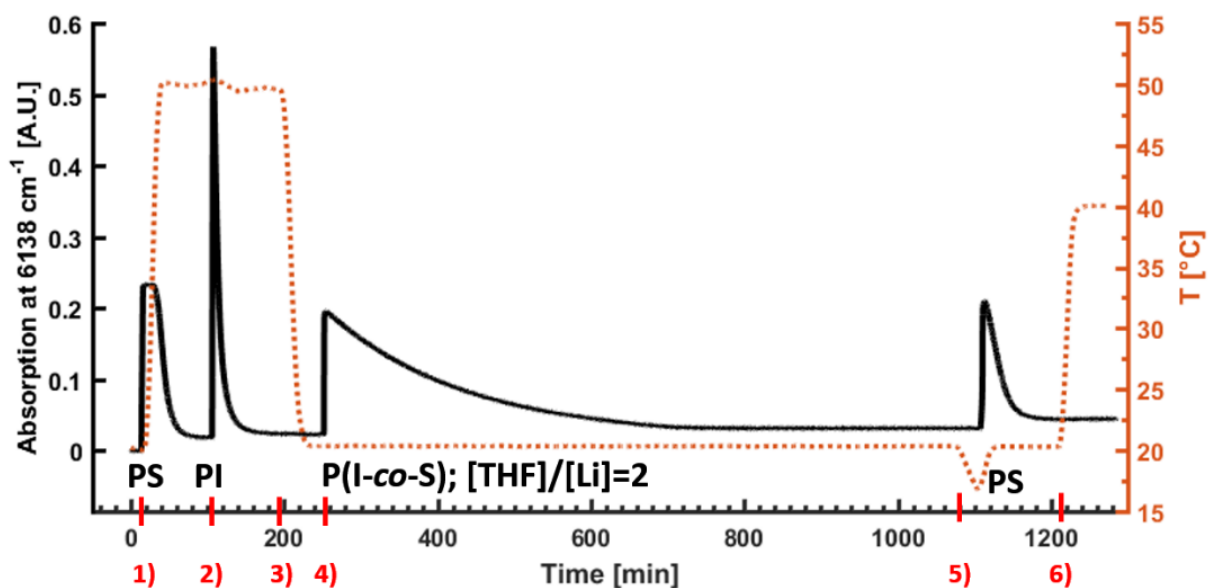


FIGURE S2 Applied temperature (dotted line) and measured NIR absorption at 8138 cm^{-1} for the synthesis of the "tapered triblock" copolymer. (see Figure S33 for other wavelengths). 1) Addition of styrene, followed by initiation at $T=20$ °C with subsequent heating to $T=50$ °C. 2) Addition and full conversion of isoprene at $T=50$ °C. 3) Cooling to $T=20$ °C 4) Copolymerisation of styrene and isoprene in the presence of THF ($[\text{THF}]/[\text{Li}]=2$). 5) As styrene consumption was found to be strongly accelerated in the presence of THF, the cryostat (Figure S1) was used for active cooling and styrene was added carefully ($T \approx 16$ °C). As a moderate heat tone was observed, the reaction was allowed to warm up and polymerize at $T=20$ °C. 6) Finally, the reaction solution was heated to 40 °C to secure full monomer conversion.

1.4 Termination and work-up

Isopropyl alcohol was degassed by three cycles of freeze-pump-thaw prior to use. The living chain ends were terminated by adding degassed methanol via syringe. To precipitate the polymer, the mixture was poured into an 8-fold volume excess of 50%_{vol} mixture of isopropyl alcohol and methanol, dried at reduced pressure and stored at -20 °C in the absence of light. The pure, colorless polymer was obtained in a quantitative yield.

1.5 Hydrogenation Reaction

The reaction was carried out in a 250 mL Schlenk flask, equipped with a neodymium magnetic stir bar, a reflux condenser and a septum. The apparatus was flushed with dry argon, then the unsaturated tapered triblock (1.80 g; 0.015 mmol, 0.0013 eq; 44%_{mol} PS and 56%_{mol} PI), and toluene (119.0 mL) added. After dissolution of the polymer *p*-toluenesulfonyl hydrazide (TSH, 16.66 g, 89 mmol, 7.5 eq referred to the PI units) was added and the solution degassed by the freeze-pump-thaw technique (1 cycle). The pressure equilibrated solution was heated to 90 °C for 4 days under argon atmosphere, accompanied by a color change (colorless to yellow). The progress of the reaction was tracked by ¹H NMR and SEC measurements.

Upon quantitative, selective hydrogenation of the PI-units ($\geq 99\%$), the mixture was allowed to cool to room temperature, followed by precipitation and removal of excessive TSH and the byproduct *p*-toluenesulfonyl acid (TSA) by filtration. Subsequently, toluene was removed under reduced pressure and the obtained solid (*i.e.* the contaminated hydrogenated copolymer) dissolved in cyclohexane. For purification purposes, the polymer solution was cooled overnight, centrifuged (4500 rpm, 15 min, 0 °C) and decanted until no further precipitation (*i.e.* TSH and TSA) was observed (5 times). The hydrogenated copolymer was obtained by precipitation as described in the previous section (0.92 g, 0.0076 mmol, 51% yield).

2 Instrumentation

2.1 Reaction Monitoring via NIR Spectroscopy

Near infrared spectra were recorded on a *Nicolet Magna 560 FT-IR* spectrometer using the *Omnic 7.4 Thermo Scientific* software suite on a PbS detector and a CaF₂ beam splitter. An IR laser source was employed as IR light source, with an aperture of 88, mirror speed of 0.6329 and internal ADC amplification of 8. The data interval was set to 1.928 cm⁻¹ with an internal resolution of 4. Typically, 12,000 spectra were recorded with up to 32 scans per spectrum, depending on the measurement time. The NIR probe was connected via glass fibers. All spectra were recorded in the range of 5900 to 6250 cm⁻¹. A background spectrum was measured at the same conditions with at least 64 scans before every experiment series. After the experiment, each individual spectrum was exported to the corresponding binary file, imported to MATLAB and processed, as described in a previous work.³ To consider changes in the PI microstructure, in dependence of the THF concentration, the following procedure was applied: From the final polymer spectrum the concentration weighted PS spectrum was leading to the experimental PI spectrum. This experimental PI spectrum was then used for the deconvolution process. Due to the absorption of THF in the range of 5900-5950 cm⁻¹, the signal to noise ratio for PI_{THF} is decreased. Hence deconvolution for samples with high amount of THF was only performed in the range from 5950-6250 cm⁻¹.

Temperature Profiles

Temperature profiles were recorded by a LOG200-E temperature logger attached to an external PT100 temperature sensor, enabling measurements in the range from -200 °C to 250 °C. The calibration was certified by DOSTMANN electronic GmbH, Germany ($T=23\text{ °C}$; Deviation = $\pm 0.5\text{ K}$; Uncertainty = $\pm 0.5\text{ K}$). All temperature profiles were recorded with a measurement rate of 6 s^{-1} .

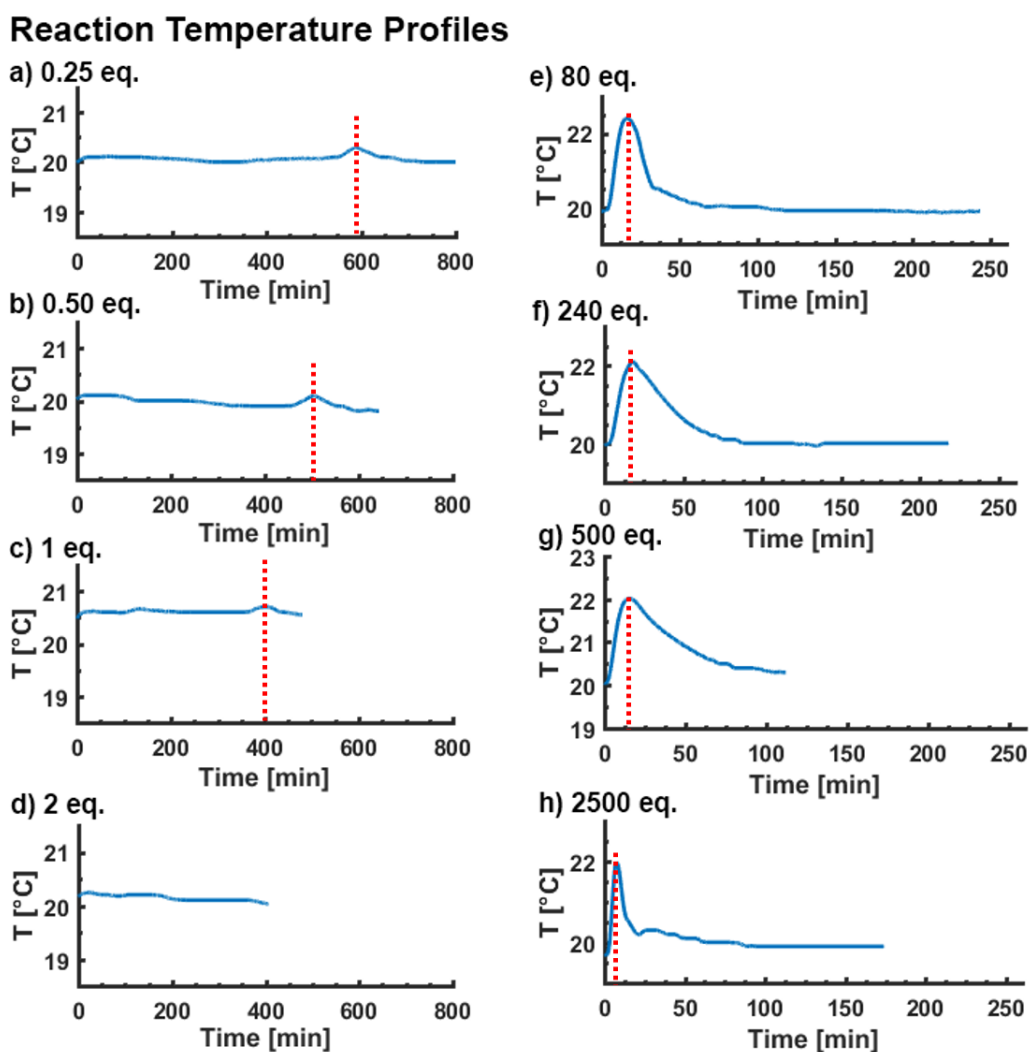


FIGURE S3 Temperature profiles during the S/I copolymerizations at various [THF]/[Li] ratios. Temperature spikes are indicated by a red dotted line.

An explanation can be given, by comparing these data with the time-dependent individual monomer concentrations obtained by NIR probing (compare with Figure S5):

a)-c): The temperature spikes at 630 min, 540 min and 420 min, respectively, indicate an increase of the polymerization rate, caused by the formation of the PS block.

d): No temperature spike is observed, as the size of the PS block is comparatively small, and the increase of the polymerization rate can be neglected.

e)-h): The styrene consumption dominates at the beginning of the polymerization. An increasing amount of THF further increases the styrene incorporation rate at very early stages of the polymerizations, as visualized by a shift of the temperature spike from 30 min (80 eq.) to 10 min (2500 eq.).

2.3 NMR Spectroscopy

NMR spectra were recorded on a Bruker Avance III 600 spectrometer at 600 MHz (^1H NMR) or 151 MHz (^{13}C NMR) using a 5 mm TCI-cryo probe with z-gradient and ATM. For the tapered triblock copolymers, NMR spectra were recorded on a Bruker Avance II 400 spectrometer with 400 MHz (^1H NMR) or 101 MHz (^{13}C NMR). The signals are referenced internally to residual proton signals of the deuterated solvent.

Peaks of residual solvents are assigned with the respective chemical sum formula and crossed out with a diagonal line.⁴ Proton Peaks are assigned to the structure pictured in the respective spectrum, and the assignment is given in small letters. Capital Letters are used for the respective carbon atoms. Consequently, the ^1H - ^{13}C coupling signals are assigned by using a small letter for the proton and a capital letter for the carbon atom. For example, the coupling between the proton a and the carbon B is expressed as a/B.

2.4 Size Exclusion Chromatography (SEC)

SEC measurements were performed with THF as the mobile phase (flow rate 1 mL min^{-1}) on an SDV column set from PSS (SDV 10^3 , SDV 10^5 , SDV 10^6) at $30 \text{ }^\circ\text{C}$. Polymer concentrations with a maximum of 1 mg/mL turned out to be suitable to prevent concentration effects.

As indicated, calibration was carried out using polystyrene standards from PSS Polymer Standard Service, Mainz.

2.5 Differential Scanning Calorimeter (DSC)

Films were prepared with a thickness of approximately 0.2 mm , obtained by slow evaporation from a chloroform solution, followed by full removal of the solvent under reduced pressure. The thermal properties of the tapered diblock copolymer films were studied with a PerkinElmer DSC 8500 differential scanning calorimeter (DSC) calibrated using *n*-decane and indium standards. The scans were corrected using a multi-point baseline to remove drifting of the heat flow and

normalized by the sample mass. Two heating and one cooling cycle were performed at a rate of 20 K/min in a temperature range between -80 and 130 °C and the glass transition temperatures were extracted from the second heating cycle.

2.6 X-Ray Scattering

Small-angle X-ray scattering (SAXS) measurements were made using $\text{CuK}\alpha$ radiation (Rigaku MicroMax 007 X-ray generator, Osmic Confocal Max-Flux curved multilayer optics). 2D diffraction patterns were recorded on an Mar345 image plate detector at a sample-detector distance of 2097 mm calibrated with a silver behenate standard. Intensity distributions as a function of the modulus of the total scattering vector, $q = (4\pi/\lambda) \sin(2\theta/2)$, where 2θ is the scattering angle, were obtained by radial averaging of the 2D datasets. Samples in the form of thick films (~ 1 mm) were prepared by slow solvent casting. Temperature-dependent measurements of 1 hour long were made by heating the films from 30 °C to 150 °C in 30 °C steps and by subsequent cooling to 30 °C aiming at identifying the different equilibrium morphologies

2.7 TEM Measurements

For characterization of the tapered block copolymer morphology in the bulk state, the prepared films were temperature annealed (120 °C; 16 h) and afterwards microtomed from surface to surface at -80 °C into thin slices of 50-70 nm thickness. The collected ultrathin sections were subsequently stained with osmium tetroxide (OsO_4) for selective staining of the PI domains or with ruthenium tetroxide (RuO_4) for a predominant staining of the PS domains, followed by investigation by TEM measurements.

Transmission electron microscopy (TEM) experiments were carried out using a JEOL JEM-2100 electron microscope (200 kV; 0.14 nm resolution) and a Gatan Orius SC1000 camera (Binning 2; 1024x1024 pixels) in bright field mode. Camera was computer-aided using the Digital Micrograph software from Gatan.

2.8 Tensile Tests

Tensile tests were performed using a materials testing machine Z005 (Zwick/Roell, Germany). Tensile tests were carried out by exposing the stamped polymer dogbones to a uniaxial tension. Bone shape samples with thicknesses from 0.2 mm to 0.5 mm were drawn with a rate of 10 mm/min at ≈ 22 °C. A Pre-Load of 0.025 N was applied with a Pre-Load speed of 5 mm/min. Dependencies of stress vs. draw ratio were recorded. Elastic modulus, elongation at break and stress at break were determined as averages of 5–9 independent drawing experiments per-

formed at the same conditions. All films were prepared with a thickness around 0.3 mm, obtained by slow evaporation from a chloroform solution followed a full removal of the solvent under reduced pressure (10 mbar at 22 °C for ≥ 3 weeks) and used for tensile tests without prior thermal annealing.

3 Copolymerization Kinetics and Determination of Reactivity Ratios

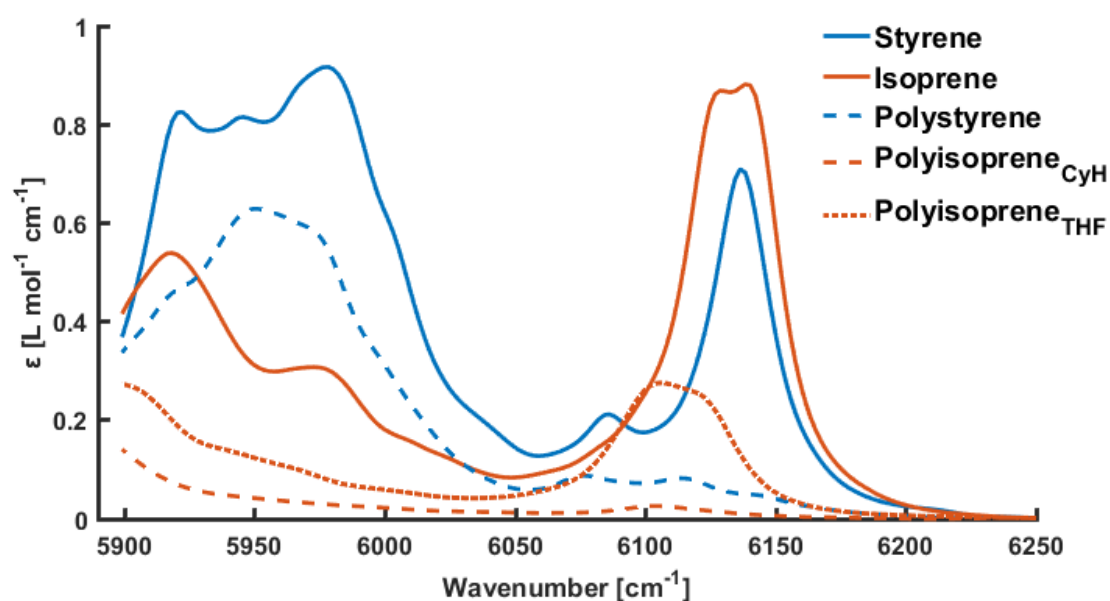


FIGURE S4 Molar attenuation coefficients of all reagents (S, I) and reaction products (PS, PI) during polymerization. The molar attenuation coefficient of PI_{CyH} represents the typical isomer mixture obtained in cyclohexane (95% 1,4; 5% 3,4). The molar attenuation coefficient of PI_{THF} represents the typical isomer mixture obtained in pure THF (1,4: 18% ; 3,4: 57% ; 1,2: 25%) as determined via NMR spectroscopy (see section 7).

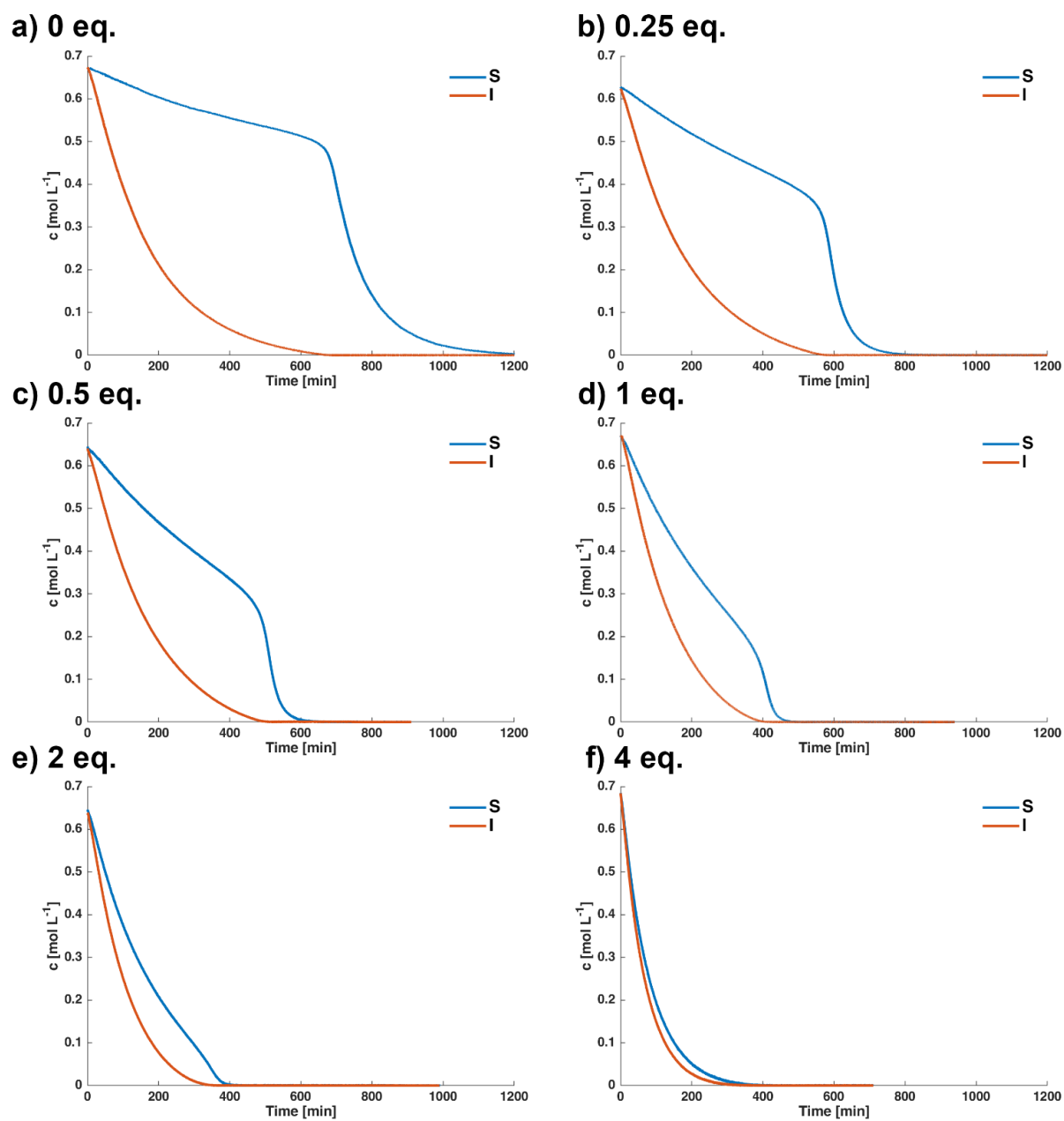


FIGURE S5A Individual time-conversion plots at various [THF]/[Li] ratios.

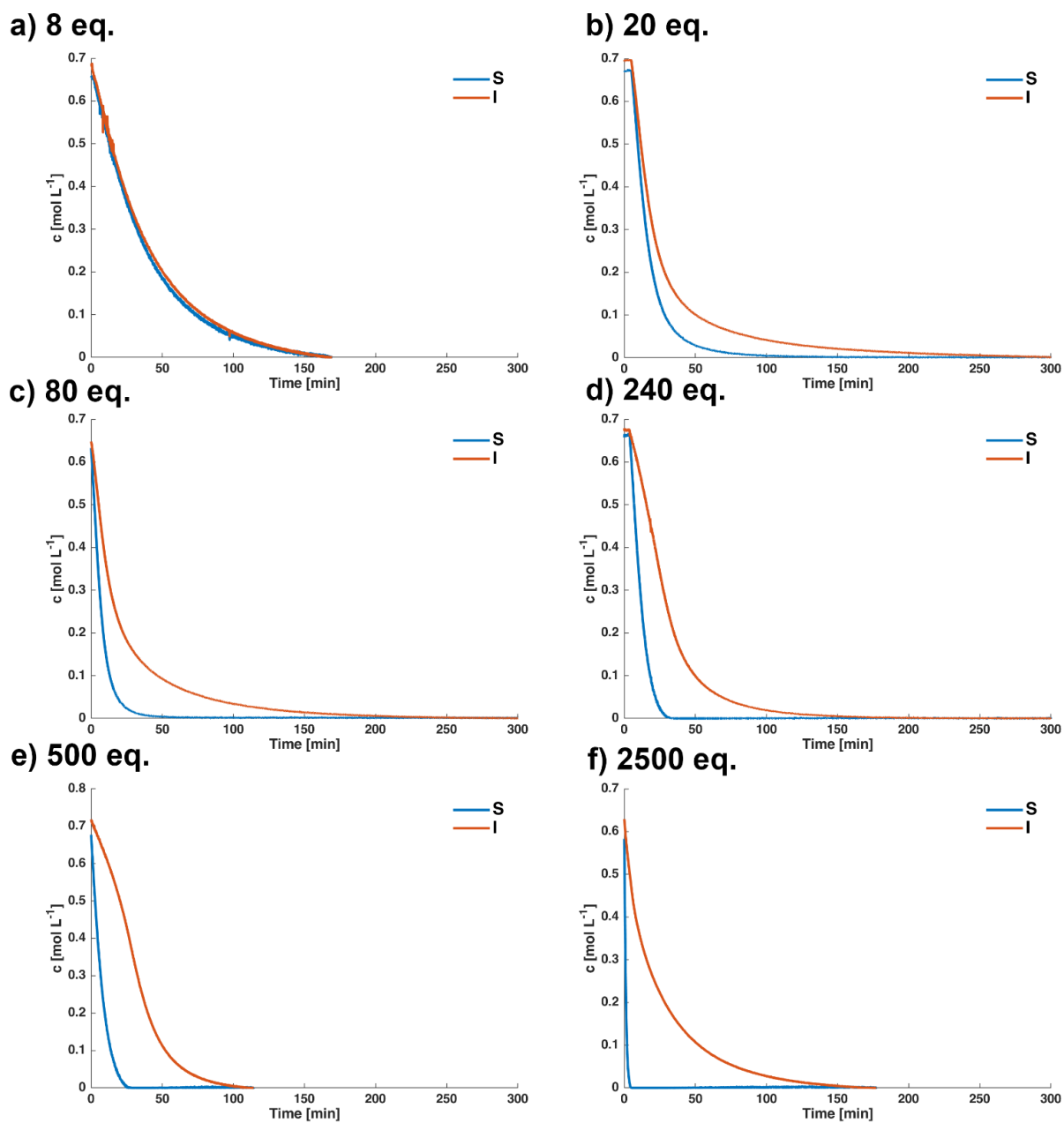


FIGURE S5B Individual time-conversion plots at various [THF]/[Li] ratios.

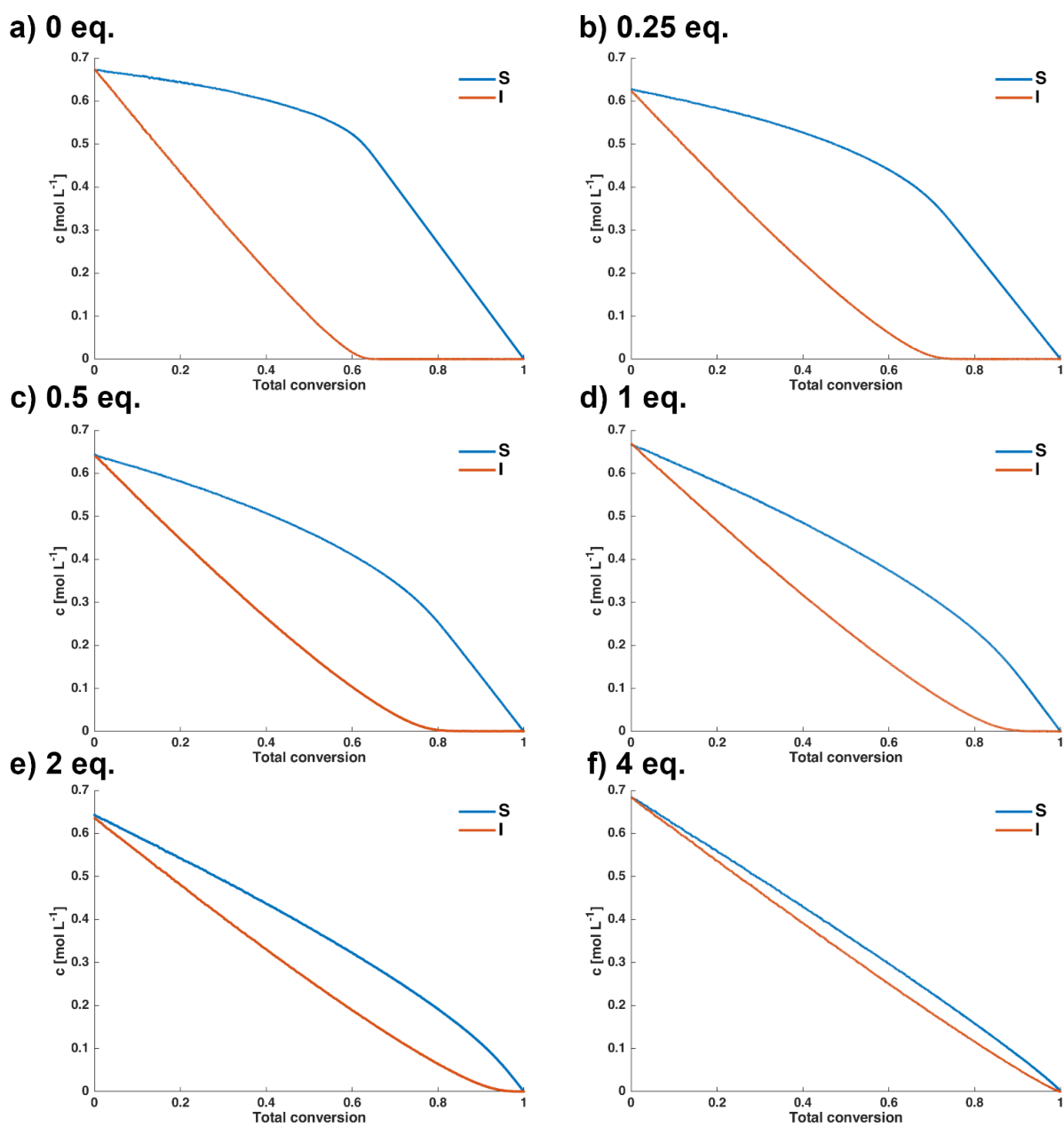


FIGURE S6A Individual monomer concentrations as a function of the total monomer at various [THF]/[Li] ratios.

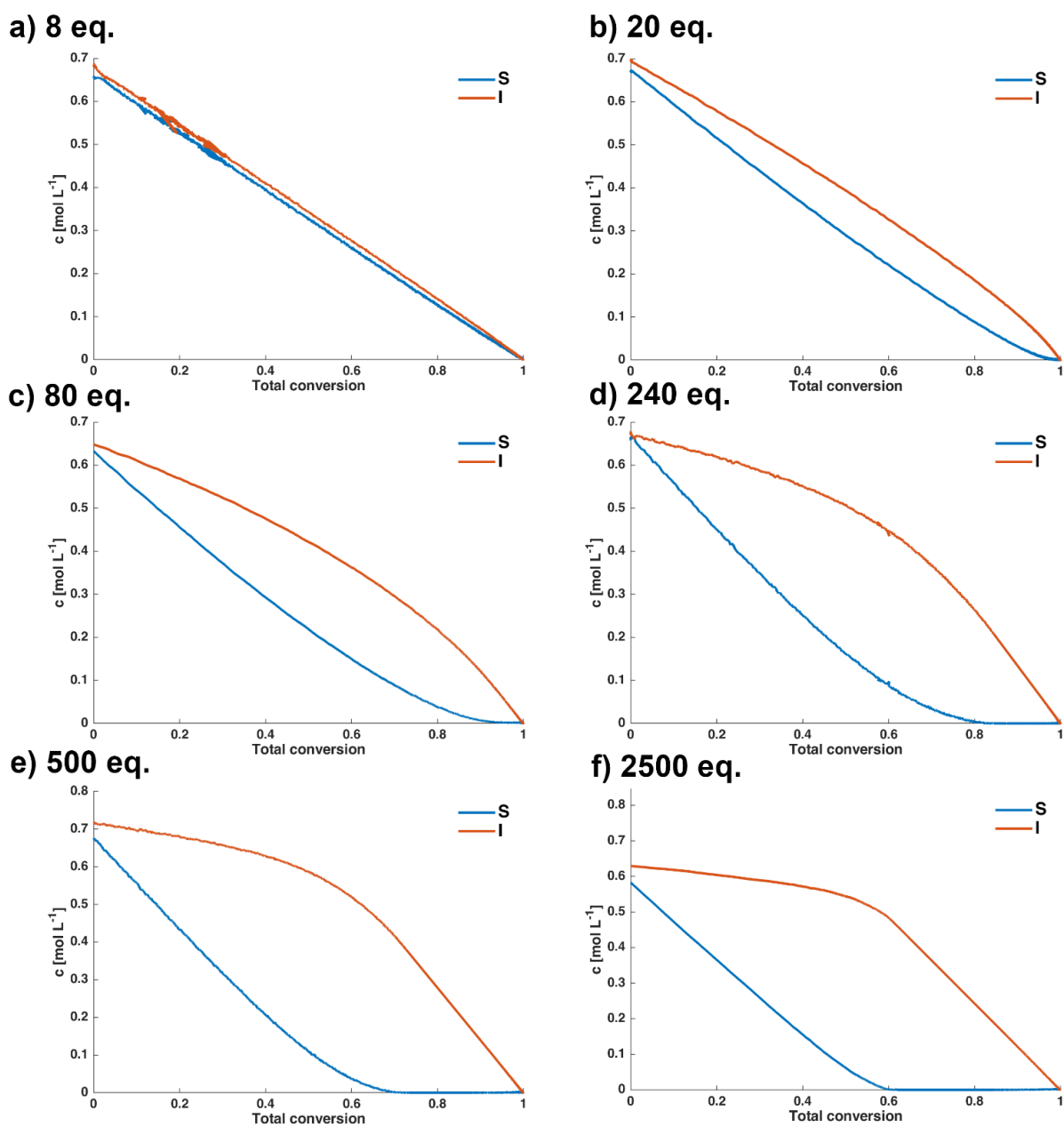


FIGURE S6B Individual monomer concentrations as a function of the total monomer at various [THF]/[Li] ratios.

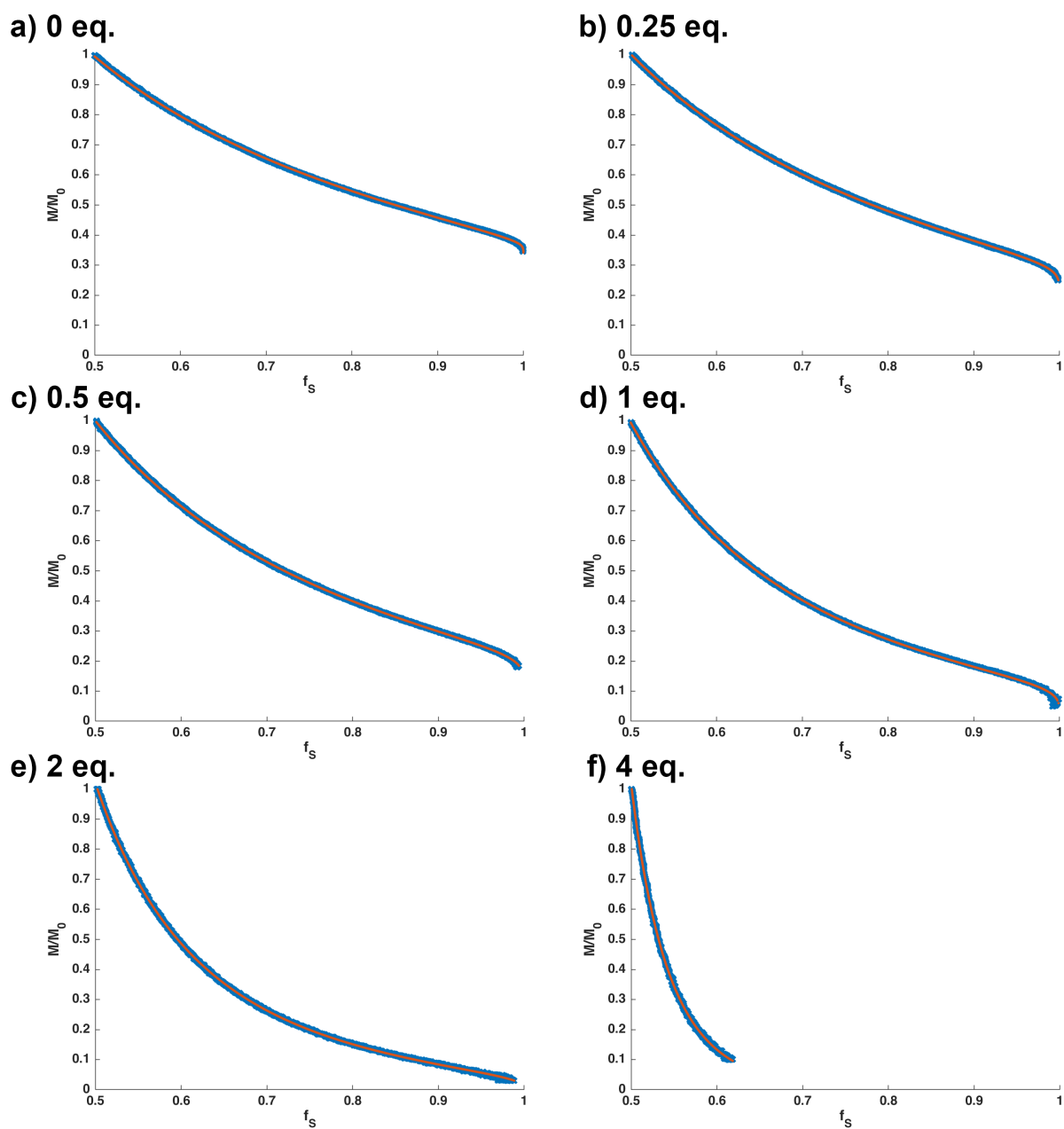


FIGURE S7A Meyer-Lowry fits (red line) for copolymerizations at various [THF]/[Li] ratios. The monomer conversion ($[M]/[M]_0$) versus the actual fraction of styrene in the feed (f_S), was used for the evaluation of the reactivity ratios. In all cases excellent correlation was obtained. Due to this excellent correlation the data points (blue dots) are fully overlaid by the Meyer-Lowry fit.

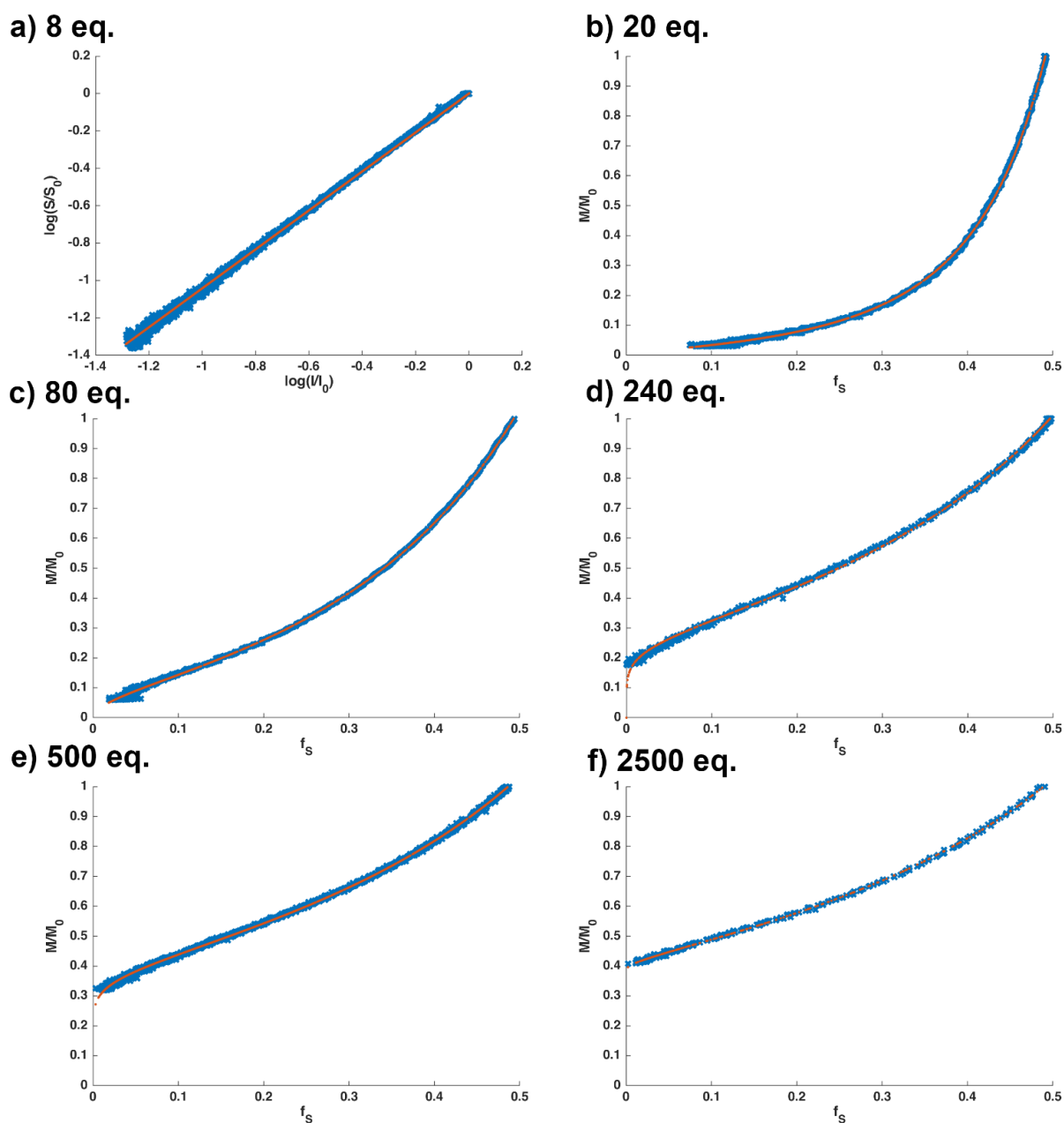


FIGURE S7B Meyer-Lowry fits (red line) for copolymerizations at various [THF]/[Li] ratios. The monomer conversion ($[M]/[M]_0$) versus the actual fraction of styrene in the feed (f_S), was used for the evaluation of the reactivity ratios. In all cases excellent correlation was obtained. Due to this excellent correlation the data points (blue dots) are completely overlaid by the Meyer-Lowry fit.

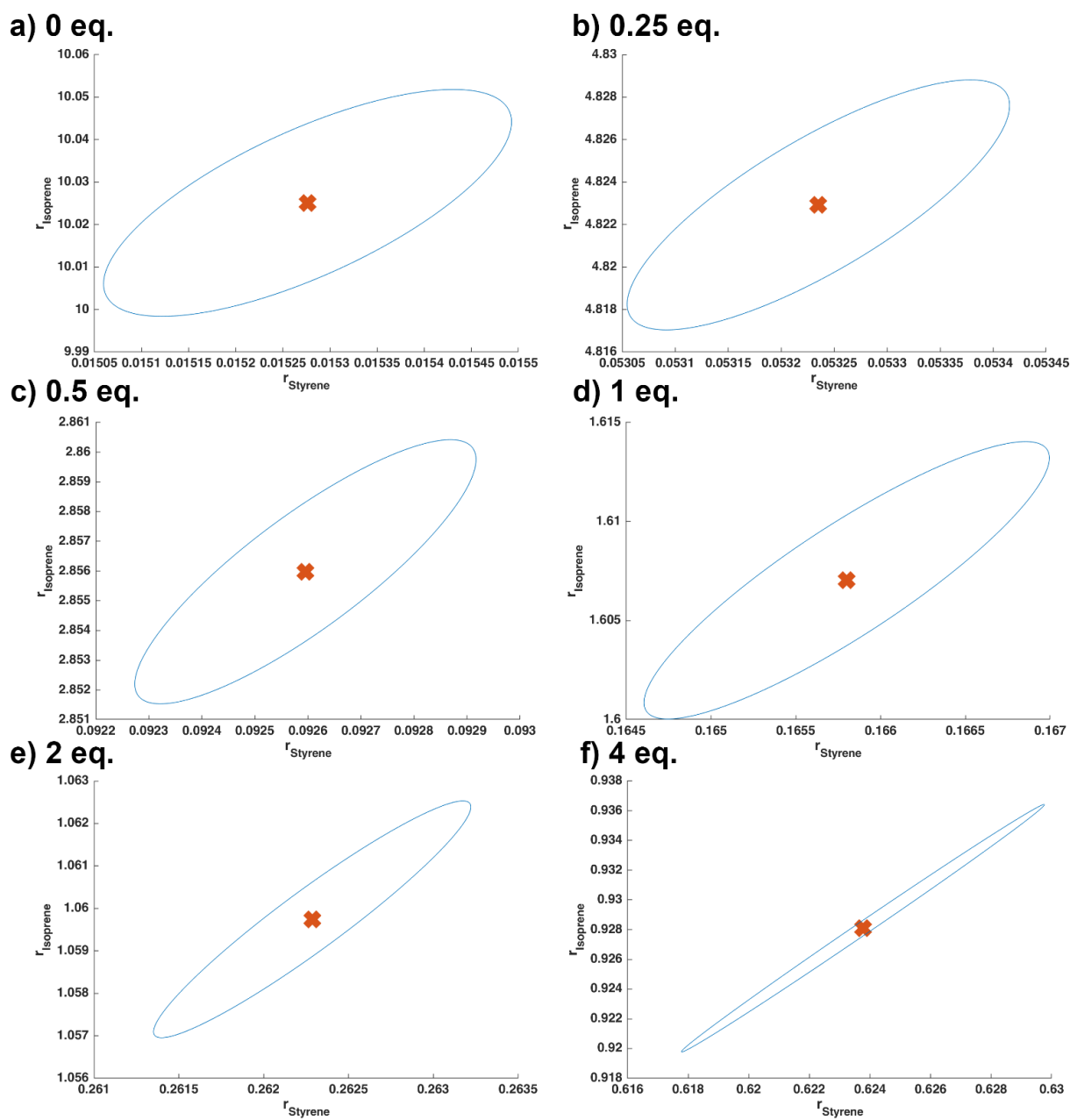
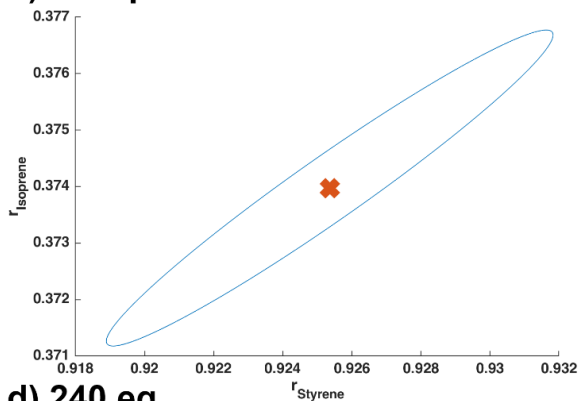


FIGURE S8A Joint confidence regions of Meyer-Lowry fits for copolymerizations at various [THF]/[Li] ratios.

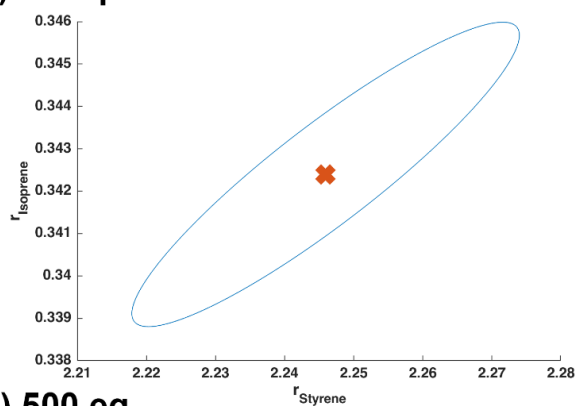
a) 8 eq.

not determined

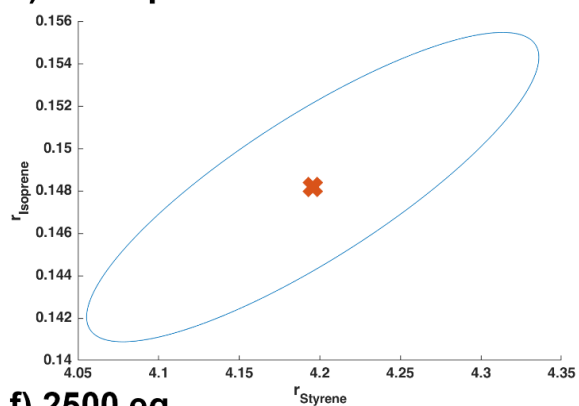
b) 20 eq.



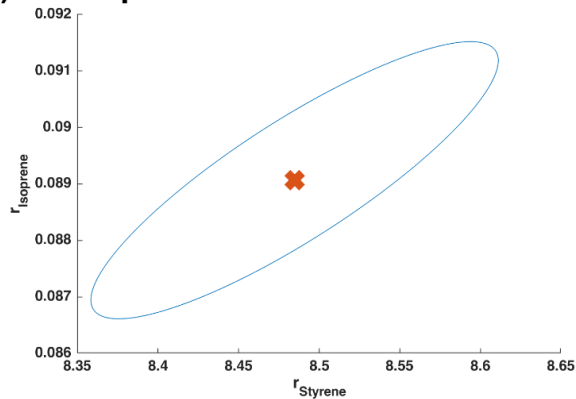
c) 80 eq.



d) 240 eq.



e) 500 eq.



f) 2500 eq.

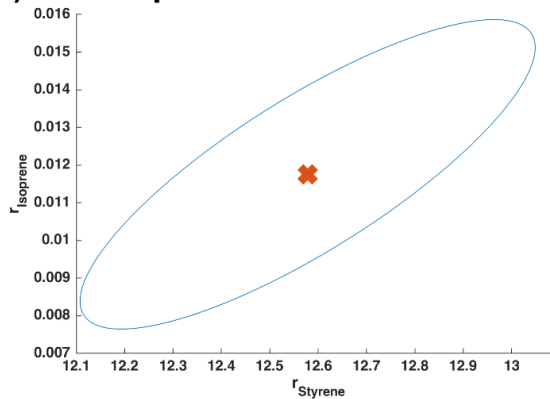


FIGURE S8B Joint confidence regions of Meyer-Lowry fits for copolymerizations at various [THF]/[Li] ratios.

All function evaluations were performed by non-linear least square fitting. The resulting Jacobian matrix (J) and residuals (R) was then used to calculate the covariance matrix via $\text{inv}(J' \cdot J) \cdot (R' \cdot R) / (\text{number of data elements} - \text{number of parameters})$. The covariance matrix was then used to calculate the joint confidence regions by drawing the corresponding error ellipse.

$[\text{THF}]/[\text{Li}] = 8$; Isoprene Fraction = 70%_{mol}

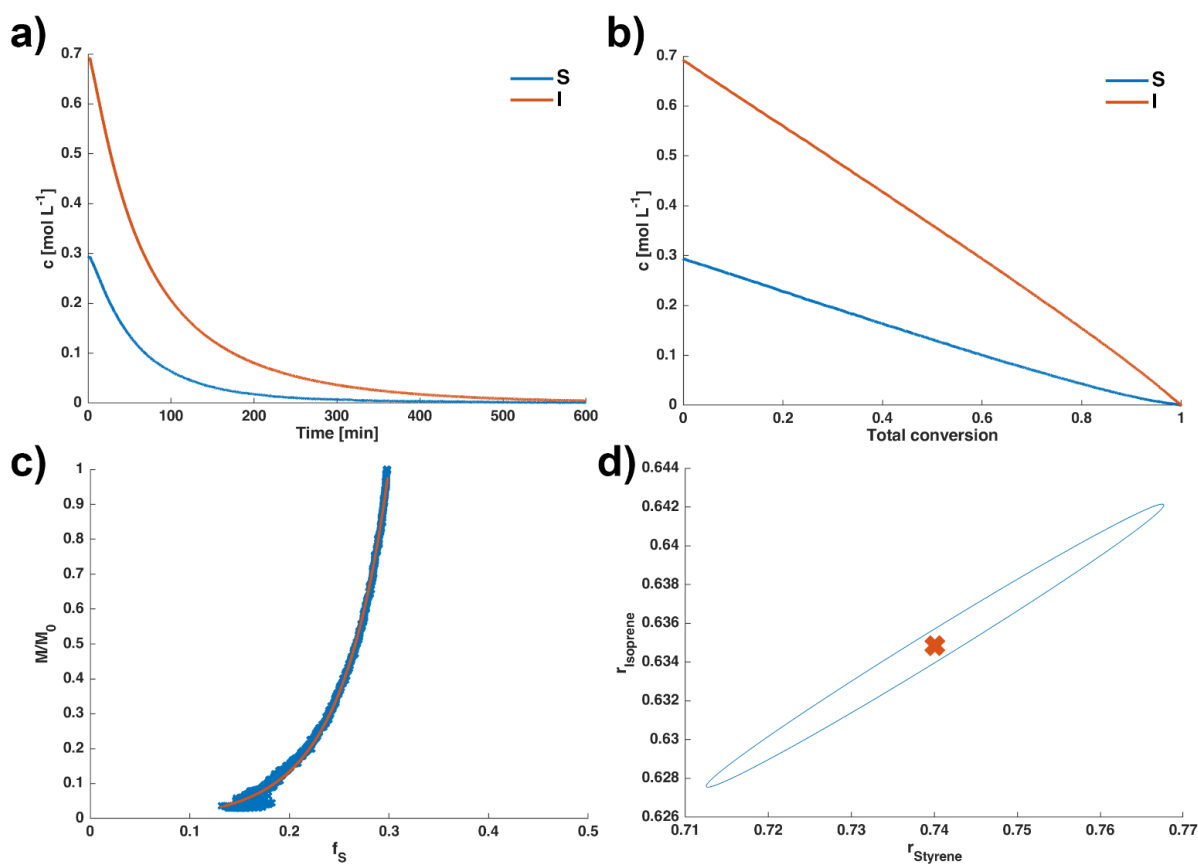


FIGURE S9 Kinetic Data of the P(I-co-S) copolymer synthesized at an isoprene mole fraction $f_I = 70\%$ _{mol}. a) Individual time-conversion plots; b) Individual monomer conversions as a function of the total conversion; c) Meyer-Lowry fit; d) Joint confidence region.

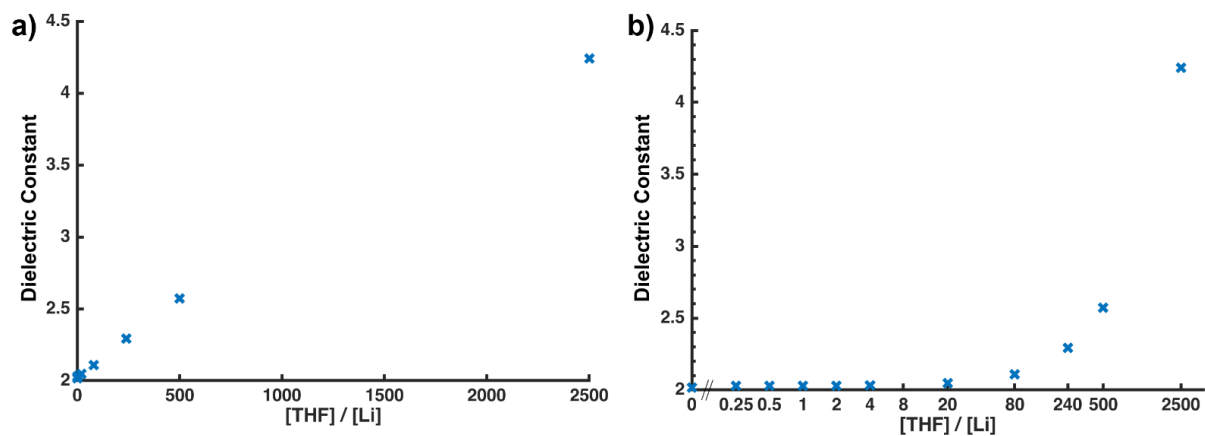


FIGURE S10 Dielectric constant (ϵ) as a function of the THF content. $[\text{THF}]/[\text{BuLi}] = 0$ represents the value of pure cyclohexane: $\epsilon(\text{CyH}) = 2.018$.⁵

Dielectric constants were calculated by extrapolating the values reported by Kolling for cyclohexane/THF mixtures.⁵ For this purpose a linear fit was used to determine ϵ as a function of the molar THF content. The molar THF fraction of the experiments performed in this work was calculated by the $[\text{THF}]/[\text{BuLi}]$ ratio using the known initiator concentrations.

4 Estimation of Propagation Rate Constants

4.1 Fitting Procedure

In copolymerization the individual monomer consumption is a function of the homo- and cross-propagation constants. Therefore, the determination of the individual propagation rates is not straightforward. Nevertheless, we were able to obtain the individual rate constants for all samples.

To estimate the individual rate constants from the copolymerization measurements the differential equation system describing the copolymerization was fitted to the experimental data via non-linear least square fitting. This differential equation system is based on the fundamental equations proposed by Mayo and Lewis.

In case of tapered copolymers, the homopolymerization region was used to determine either $k_{\text{II}}^{\text{app}}$ or $k_{\text{SS}}^{\text{app}}$ first (Method A and B). To further tighten the boundaries of the fitting algorithm the via Meyer-Lowry determined reactivity ratios were used to build dependencies between $k_{\text{II}}^{\text{app}}$ and $k_{\text{IS}}^{\text{app}}$ as well as $k_{\text{SS}}^{\text{app}}$ and $k_{\text{SI}}^{\text{app}}$. Via this approach only one unknown parameter in case of tapered polymers and two parameters for the gradient and random copolymer samples were estimated, leading to the high precision of this method.

We did not calculate so-called effective rate constants (in $(\text{L/mol})^x \text{s}^{-1}$; $1/4 \leq x \leq 1$; x = degree of association) since the degree of association changes in an unknown manner with increasing THF content; see Scheme 1.

Depending on the $[\text{THF}]/[\text{Li}]$ ratio (corresponding to a certain comonomer sequence), different methods were used for data evaluation:

Method A) $[\text{THF}]/[\text{Li}] = 0\text{-}2$: Tapered PS block copolymers

A pure PS block is formed in the late stage of the polymerization. In this period, only styrene is consumed. Hence, we were able to determine $k_{\text{SS}}^{\text{app}}$ by linear fitting of the first-order time-conversion plot for styrene (Figure S11A). This was used to calculate: $k_{\text{SI}}^{\text{app}} = k_{\text{SS}}^{\text{app}}/r_{\text{S}}$

Using these constants, k_{II}^{app} was obtained by numerically integrating the ordinary differential equations of copolymerization and fitting to the time-conversion data (Figure S12A). This was used to calculate: $k_{IS}^{app} = k_{II}^{app} / r_1$.

Method B) [THF]/[Li] = 240-2500: Tapered PI copolymers

A pure PI block is formed in the late stage of the polymerization. At this time, only isoprene is consumed. Hence, we were able to determine k_{II}^{app} by linear fit of the first-order time-conversion plot for isoprene (Figure S11B). This was used to calculate: $k_{IS}^{app} = k_{II}^{app} / r_1$. Using these constants, k_{SS}^{app} was obtained by fitting and numerically solving the ordinary differential equations and fitting to the time-conversion data (Figure S12B). This was used to calculate: $k_{SI}^{app} = k_{SS}^{app} / r_S$.

Method C) [THF]/[Li] = 4-80: Copolymers with flat gradient

No block is formed at any stage of the polymerization. Hence k_{SS}^{app} and k_{II}^{app} were obtained by numerically solving the ordinary differential equations and fitting to the time-conversion data (Figure S12). The cross-propagation constants were calculated with the determined reactivity ratios $k_{SI}^{app} = k_{SS}^{app} / r_S$; $k_{IS}^{app} = k_{II}^{app} / r_1$.

All results are summarized in Table S1 and discussed subsequently.

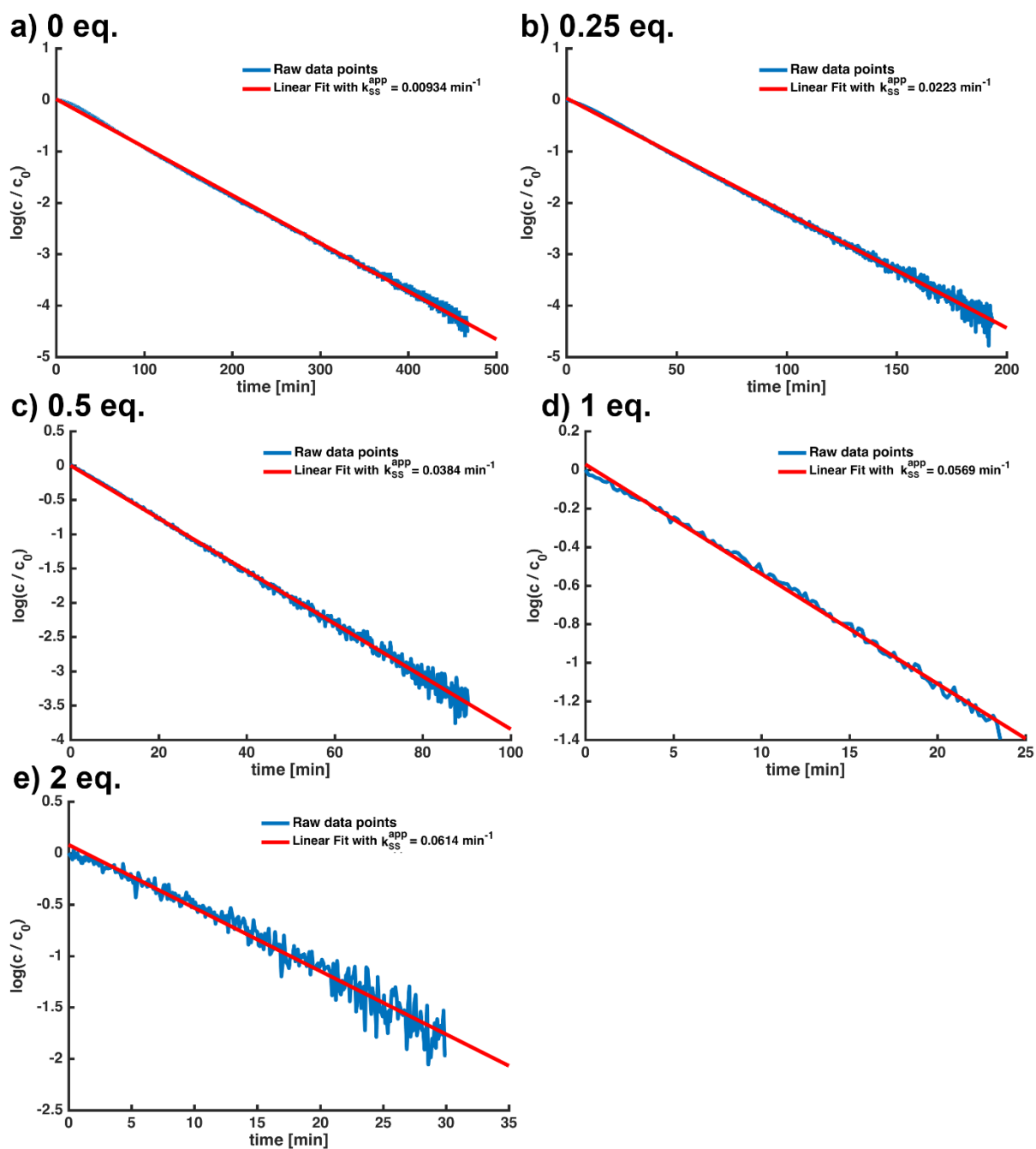


FIGURE S11A Linear fits of the first-order time-conversion curve of styrene for k_{SS}^{app} at low THF content.

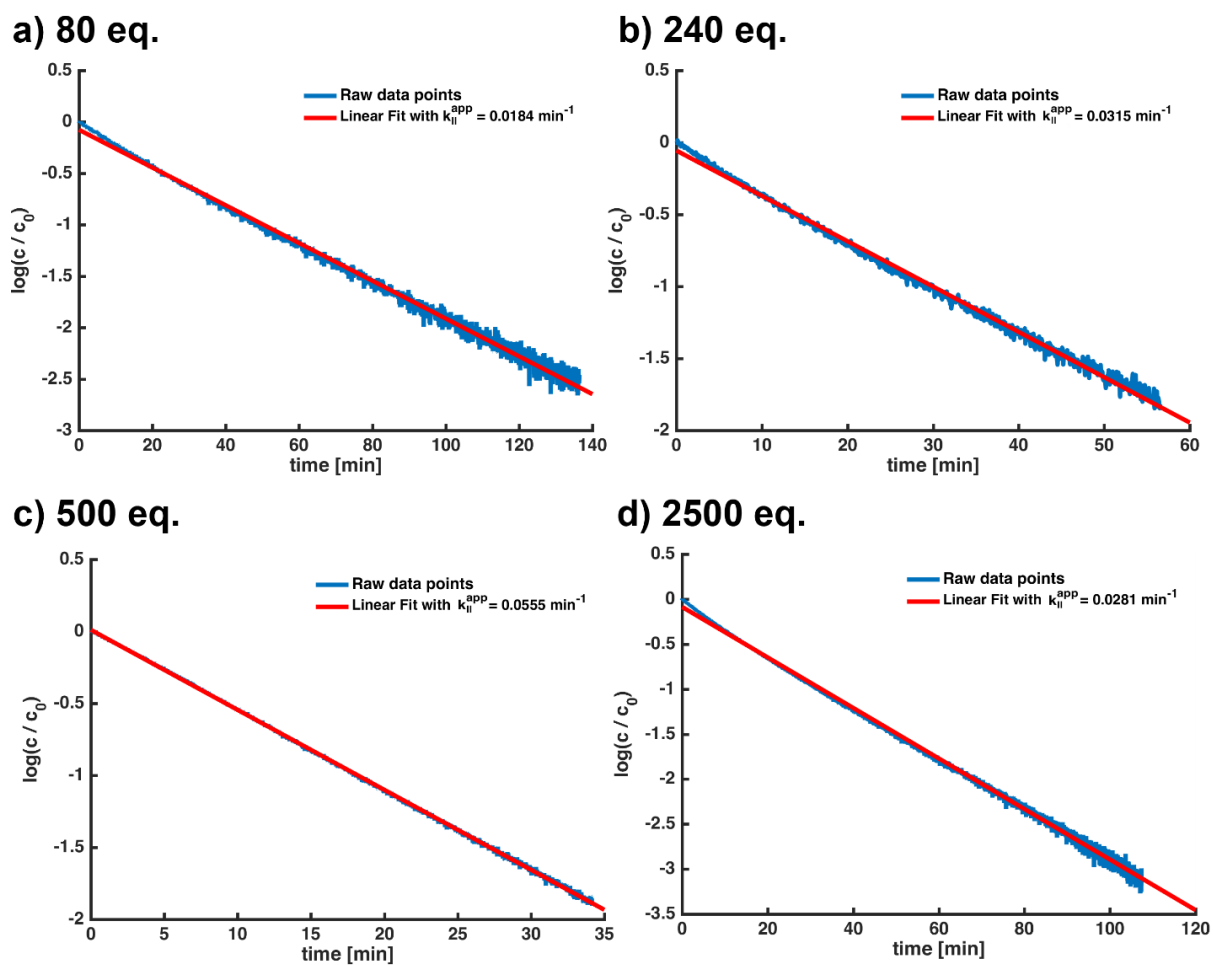


FIGURE S11B Linear fits of the first-order time-conversion curve of isoprene for k_{II}^{app} at high THF content.

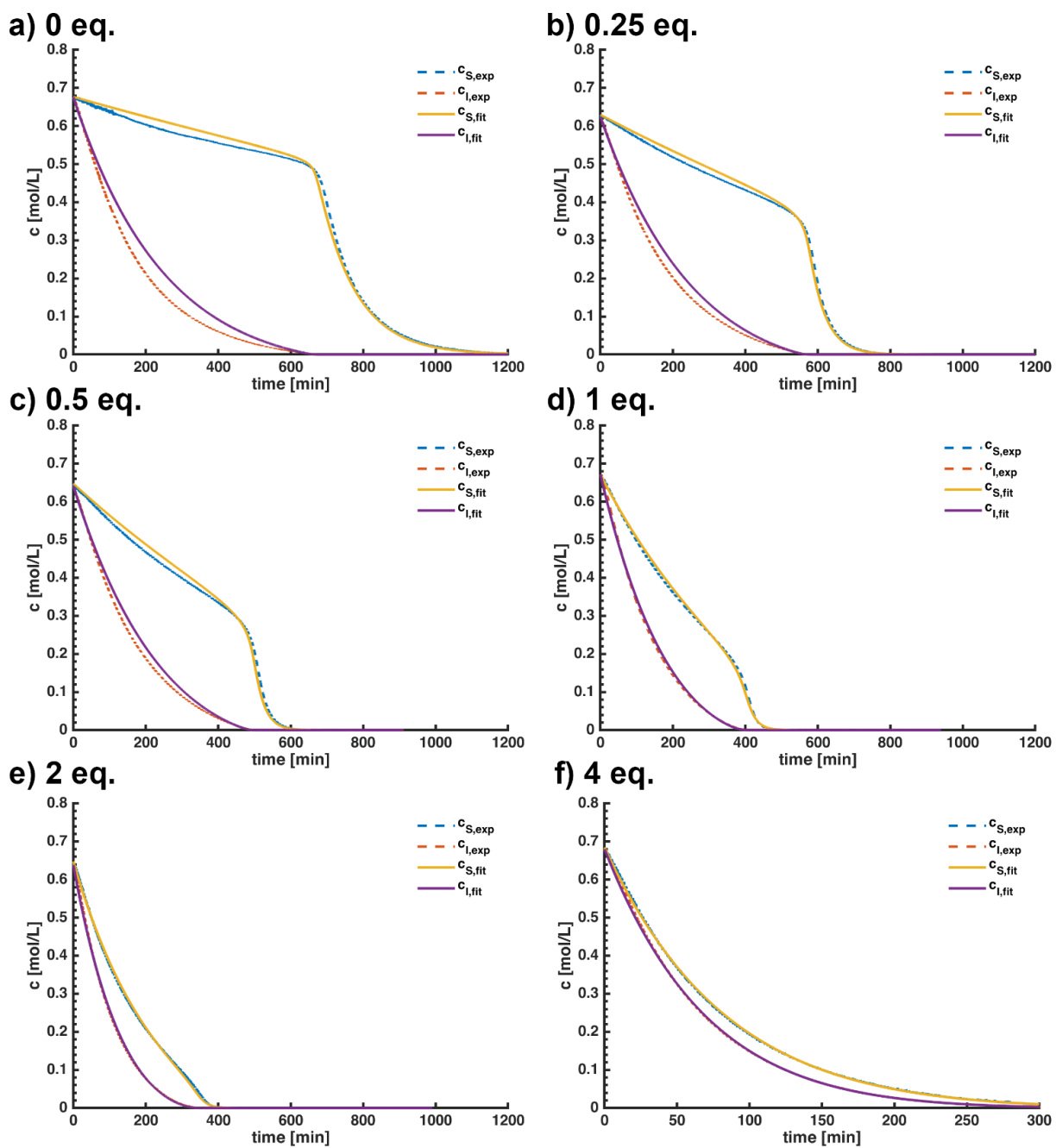


FIGURE S12A Fitting of the time-conversion curves by numerically solving the ordinary differential equations of copolymerization.

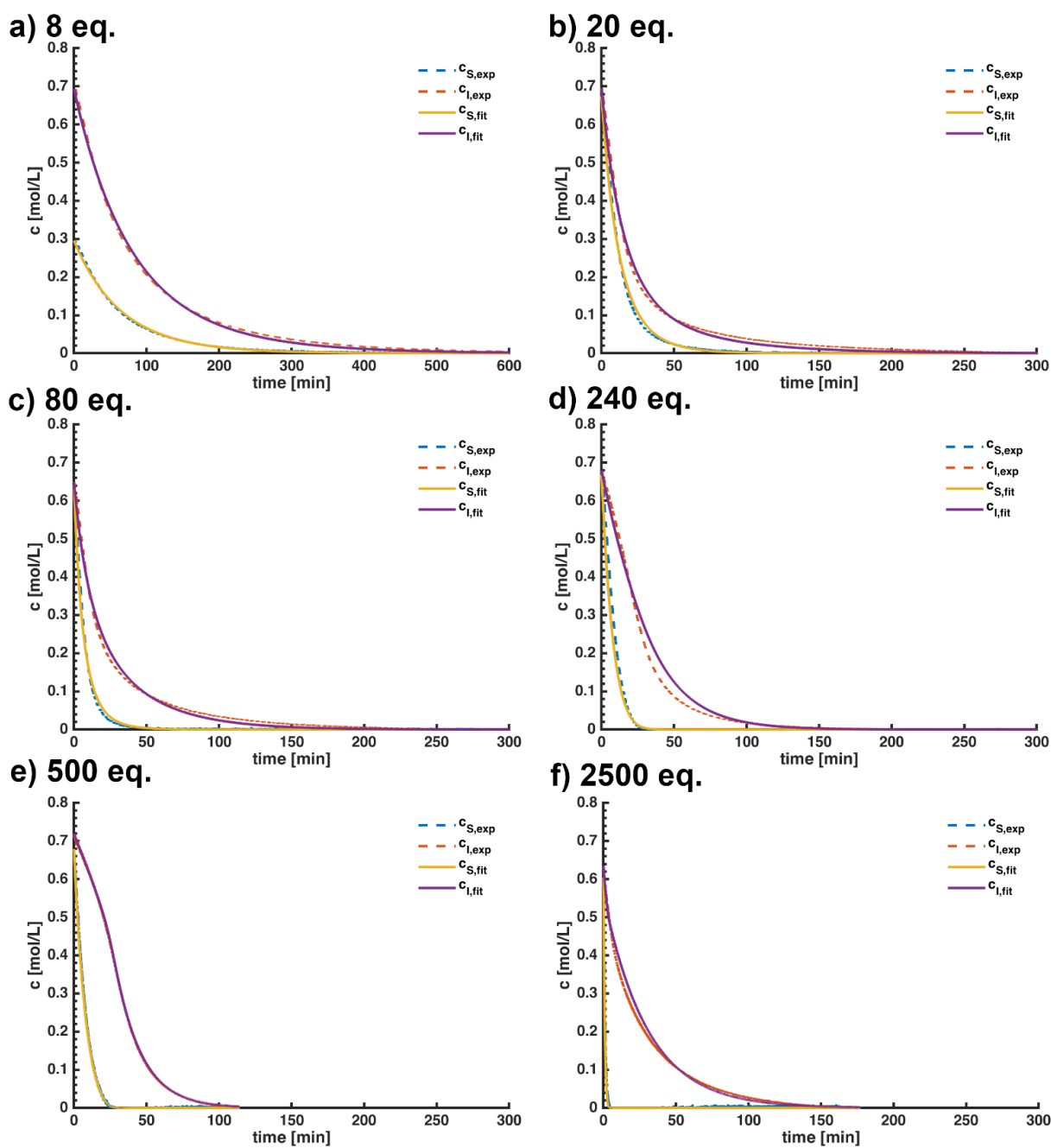


FIGURE S12B Fitting of the time-conversion curves by numerically solving the ordinary differential equations of copolymerization.

TABLE S1 Apparent rate constants of homo- and cross-propagation. For visualization, see Figures S13.

Method	[THF] / [Li]	$10^5 \cdot k_{II}^{app} [s^{-1}]$	$10^5 \cdot k_{SS}^{app} [s^{-1}]$	$10^5 \cdot k_{IS}^{app} [s^{-1}]$	$10^5 \cdot k_{SI}^{app} [s^{-1}]$
A	0	6.6 ^d	16 ^a	0.65 ^d	1100 ^b
A	0.25	6.1 ^d	39 ^a	1.3 ^d	730 ^b
A	0.5	5.9 ^d	66 ^a	2.1 ^d	720 ^b
A	1	6.4 ^d	83 ^a	4.0 ^d	500 ^b
A	2	7.2 ^d	98 ^a	6.8 ^d	370 ^b
C	4	13 ^d	74 ^d	14 ^d	120 ^d
C	8	13 ^d	530 ^d	20 ^d	720 ^d
C	20	28 ^d	2300 ^d	75 ^d	2500 ^d
B	80	43 ^d	490 ^d	130 ^d	220 ^d
B	240	63 ^a	190 ^d	430 ^c	45 ^d
B	500	91 ^a	190 ^d	1000 ^c	22 ^d
B	2500	55 ^a	1700 ^d	4700 ^c	130 ^d

a) Linear fit of the first-order time-conversion plot during formation of PS end block. b) Calculated by $k_{SI} = k_{SS} / r_S$. c) Calculated by $k_{IS} = k_{II} / r_I$. d) Linear fit of the first-order time-conversion plot during formation of PI end block.

4.2 Discussion of Apparent Rate Constants.

Unfortunately, a direct comparison of the apparent rate constants with the work of Fetters⁶ and Bywater⁷ is not possible, as the investigations were performed under different reaction conditions (initiator concentration, solvent, and temperature). However, we assume a similar effect of the [THF]/[Li] ratio on the propagation rate constants, independent of the respective initial reaction conditions. Consequently, a comparison of the data is possible by dividing the determined propagations rate constants in the presence of THF by the values obtained in pure hydrocarbon solvent $k_{THF}^{app} / k_{hydrocarbon}^{app}$; see Figure S13).

Homopolymerization of isoprene (Figure S13A a)

A direct comparison of $k_{II,THF}^{app} / k_{II,hydrocarbon}^{app}$ with the results of Fetters *et al.* (provided in Table IX of the respective work)⁶, shows a reasonable agreement. Indeed, we also found a comparable maximum acceleration in the magnitude of the factor 10 at [THF]/[Li] \approx 600. Such a maximum was explained by both Fetters and Bywater by the gradual shift in the equilibria in Scheme 1 to the right-hand side and the relatively high reactivity of the mono-etherate ($k_{THF, Mono} > k_{THF, Di} \approx k_{II}$).

Homo-propagation of styrene (Figure S13A b)

As the results of Bywater *et al.*, are not tabulated, we refer to the original work.⁷ In accordance with Bywater *et al.*, we also found a maximum acceleration at [THF]/[Li] \approx 20. However, we observe a considerably higher acceleration in the magnitude of \approx 100 whereas Bywater *et al.*

found a relative acceleration by only ≈ 10 . This might be due to Bywater using benzene as an aromatic hydrocarbon. A reasonable difference was also discussed in a previous work, which focused on the polymerization in pure cyclohexane.³

In addition, we found another increase at $[\text{THF}]/[\text{Li}] = 2500$. Bywater did not extend his experiments into this region. Since we have only one data point, we do not want to overstate this phenomenon. Such a second increase is also not observed for k_{SI} (see below). Unfortunately, kinetic measurements at higher THF contents were not possible due to the strong acceleration of styrene polymerization and the accompanying exothermicity.

Cross-propagation (Figure S13A c-d)

The trends of the k_{IS} and k_{SI} cross-propagation constants follow the trends of the respective chain ends in the homo-propagation (maximum at a certain THF content) with one difference: In contrast to the homo-propagation of isoprene ($k_{\text{II}}^{\text{app}}$), the cross-propagation of polyisoprenyllithium ($k_{\text{IS}}^{\text{app}}$) with styrene shows an increasing acceleration up to $[\text{THF}]/[\text{Li}] = 2500$, but no maximum (Figure S12c). It is open whether such a maximum is just shifted to 2500 or more equivalents.

Similar to the homo-propagation of styrene ($k_{\text{SS}}^{\text{app}}$), the cross-propagation of polystyryllithium ($k_{\text{SI}}^{\text{app}}$) with isoprene shows a maximum at $[\text{THF}]/[\text{Li}] = 20$, however, no increase at $[\text{THF}]/[\text{Li}] = 2500$ (Figure S12d). In contrast, there is a surprising trend of decreasing rates with increasing THF content. This is even more clearly observed in the double-logarithmic plot in Figure S13b.

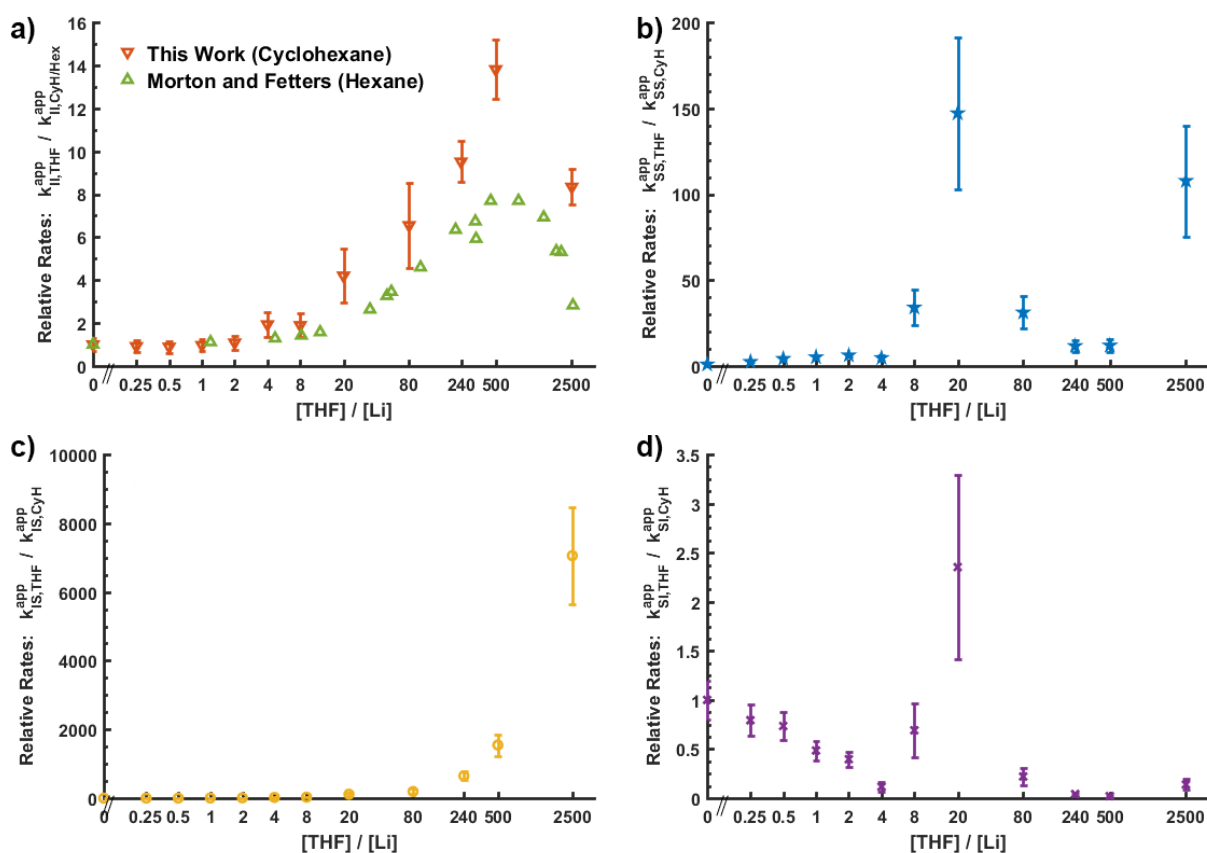


FIGURE S13A Relative apparent propagation rate constants of the polymerization in the presence of THF ($k_{\text{THF}}^{\text{app}}$) relative to the respective rate constants in hydrocarbon solvents as indicated ($k_{\text{hydrocarbon}}^{\text{app}}$). Relative rates for a) II, b) SS, c) IS, d) SI are given.

As indicated by the results, the complex behavior of THF in the copolymerization of styrene and isoprene cannot be fully described by the [THF]/[Li] ratio, as well as by the type of active chain end. This is further supported by the different magnitudes of the relative acceleration ($k_{\text{THF}}^{\text{app}}/k_{\text{hydrocarbon}}^{\text{app}}$) for the same type of active chain ends (II«IS and SS»SI, see Figure S13B).

As already evident by comparing the individual monomer conversions as a function of the time (Figure 1 and Figure S4), the increase of [THF]/[Li] leads to an increased incorporation of styrene at an early stage of the polymerization. Quantitative visualization is made by dividing the individual half-lives of styrene and isoprene in presence of THF (*i.e.*, the time to reach 50% conversion) by those in pure cyclohexane. As evident in Figure S13a), the half-life of styrene decreases much faster with increasing THF content. This is in accordance with the relative acceleration of the individual rate constants ($k_{\text{THF}}^{\text{app}}/k_{\text{hydrocarbon}}^{\text{app}}$), which is approximately found to increase in the order (IS>SS>II>SI; Figure S13b). Both trends, the comparably fast styrene consumption as well

as the comparably strong acceleration of propagation steps leading to the addition of styrene are in accordance. These results underline the quality of the fits.

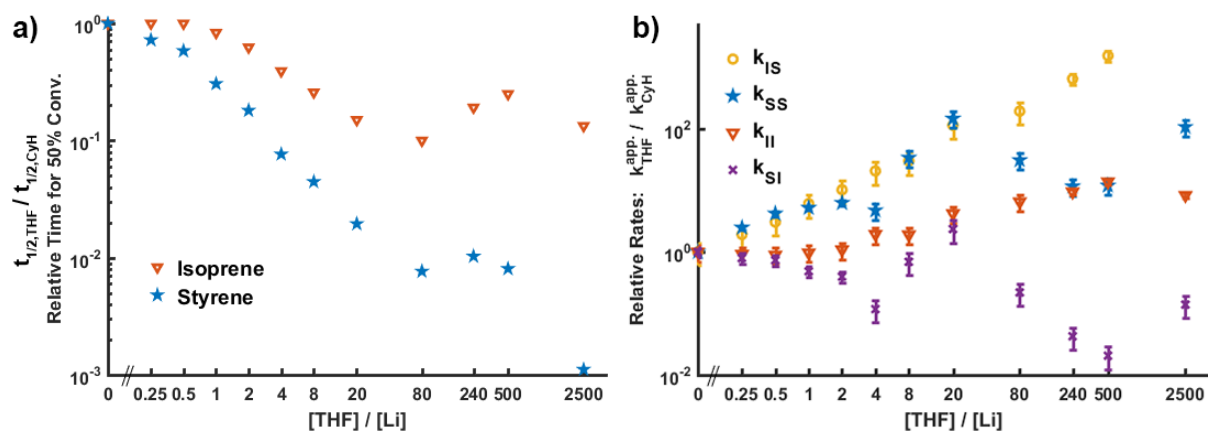


FIGURE S13B a) Half-lives of styrene and isoprene conversion in presence of THF ($t_{1/2,THF}$) relative to those in cyclohexane ($t_{1/2,CyH}$) calculated by Table 1. b) Apparent propagation rate constants in presence of THF (k_{THF}^{app}) relative to the apparent propagation rate in cyclohexane (k_{CyH}^{app}).

5 Copolymer Composition

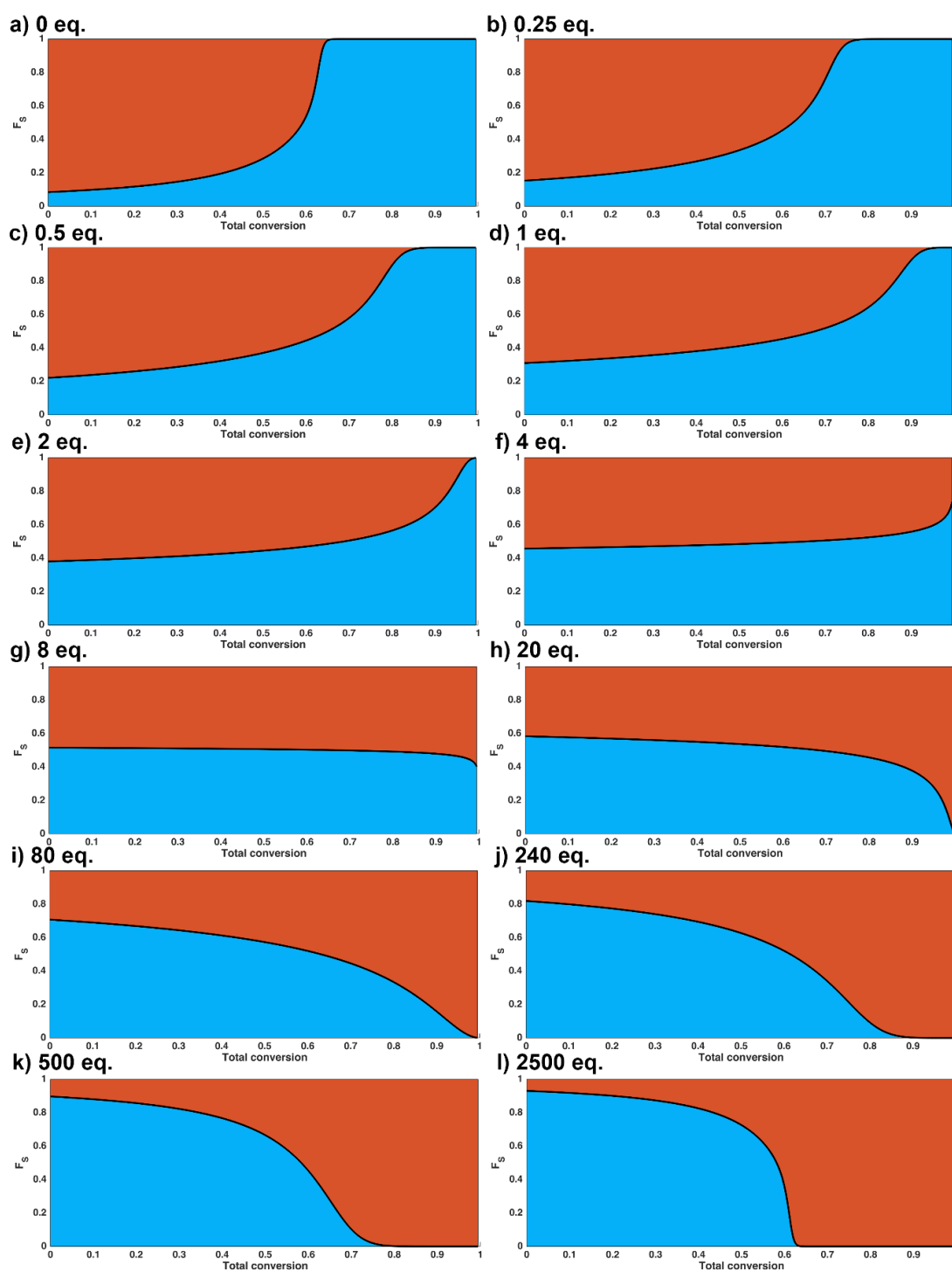


FIGURE S14 Polymer composition profiles visualized by the instantaneous styrene incorporation (F_S) as a function of the total conversion. The equivalents of THF with respect to the active chain ends, were increased in the following order. a-l): [THF] / [Li] = 0; 0.25; 0.50; 1; 2; 4; 8; 20; 80; 240; 500; 2500.

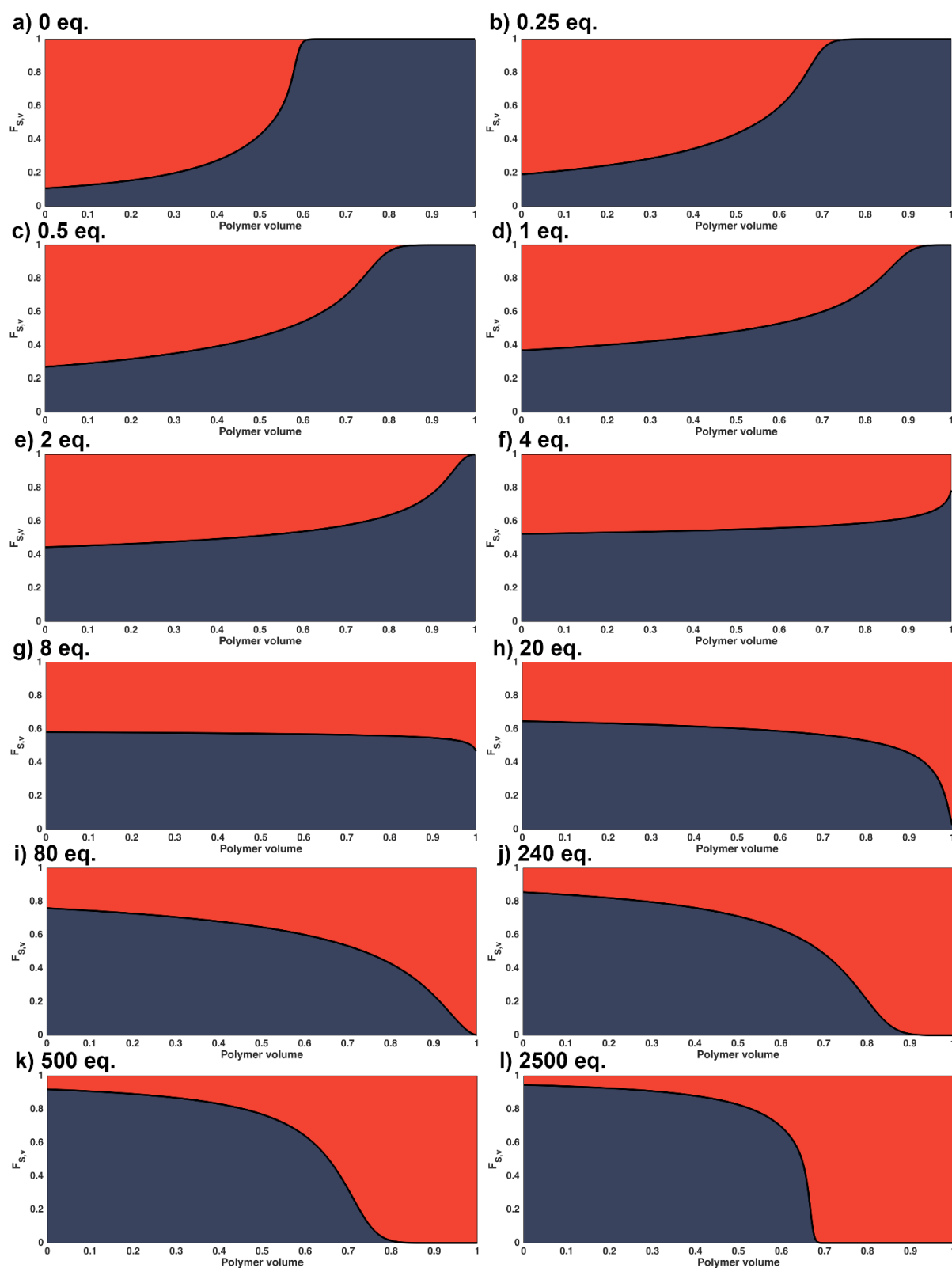


FIGURE S15 Polymer volume composition profiles visualized by the instantaneous styrene volume incorporation ($F_{S,V}$) as a function of the polymer volume. The equivalents of THF with respect to the active chain ends, were increased in the following order. a-l): $[THF] / [Li] = 0; 0.25; 0.50; 1; 2; 4; 8; 20; 80; 240; 500; 2500$. 50%_{mol} fraction, reactivity ratios according to Table 1.

While the evaluation of kinetic and spectroscopic data is usually attributed to the respective repeating units (molar fraction), bulk morphologies depend on the volume fraction of each block.

The conversion diagram (Figure S14) depicts the instantaneous styrene incorporation (F_S) versus the total conversion during the polymerization. To yield the volumerelated diagram (volume of instantaneous styrene incorporation ($F_{v,S}$) vs. polymer volume fraction) both axes need to be weighted by the molecular weight and the density of the repeating unit, which is described in detail in the Supporting Information of our previous work.¹ The volume fractions of the repeating units are based on the published homopolymer densities at 140 °C ($\rho_{PI} = 0.83 \text{ g/cm}^3$, $\rho_{PS} = 0.97 \text{ g/cm}^3$).⁸ In general a higher molar fraction of polyisoprene units is necessary for a comparable volume of polystyrene repeating units.

6 SEC Traces

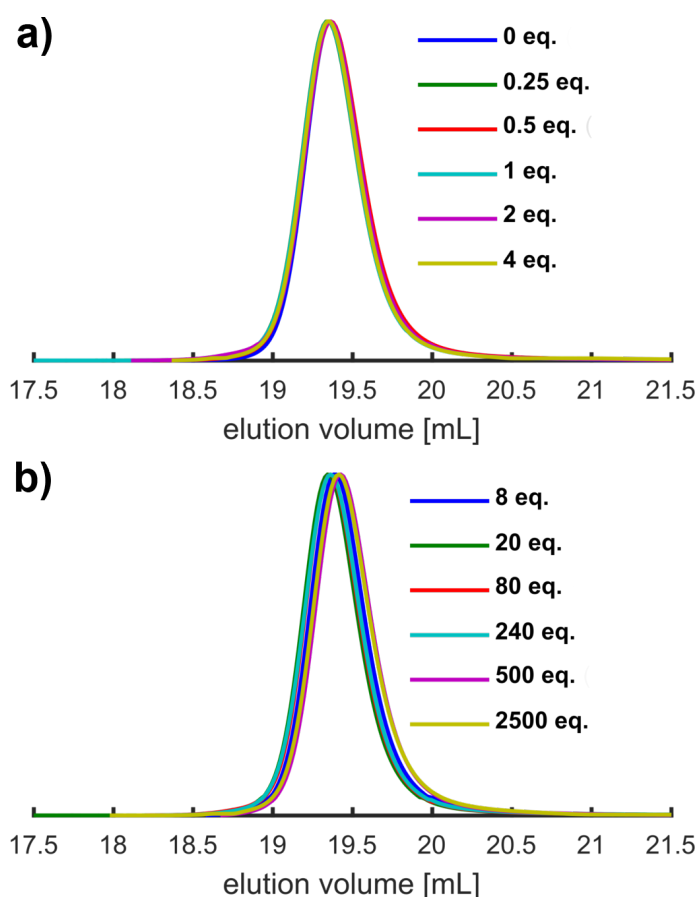


FIGURE S16 SEC traces of P(I-co-S) copolymers synthesized with different equivalents of THF relative to the active chain ends (all data of the samples are given in Table 1, main manuscript).

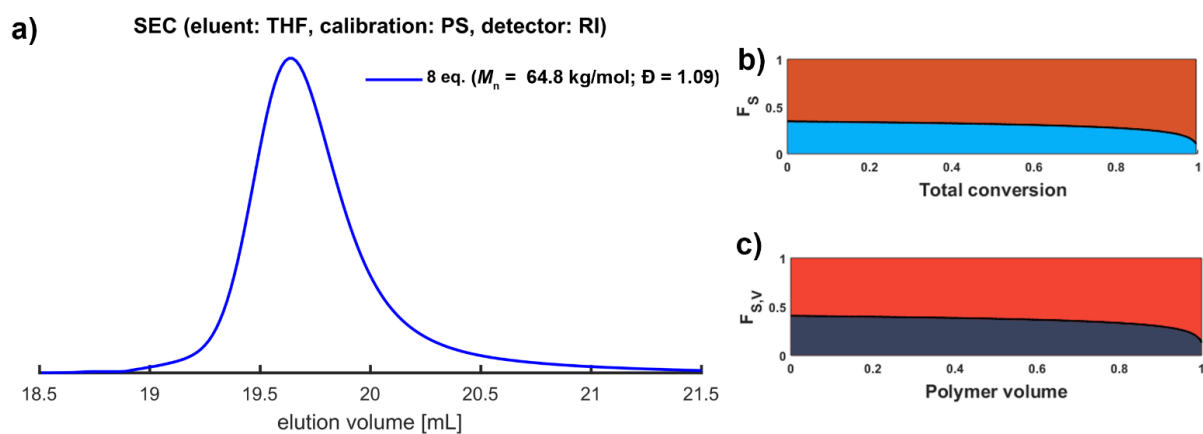


FIGURE S17 SEC traces of P(I-co-S) copolymers with an isoprene fraction of 70%_{mol} synthesized with 8 eq. of THF relative to the active chain end. The value of M_n is larger than the targeted molecular weight ($M_{n,target} = 53$ kg/mol) due to the comparably larger isoprene fraction in the copolymer and the use of PS standards.³

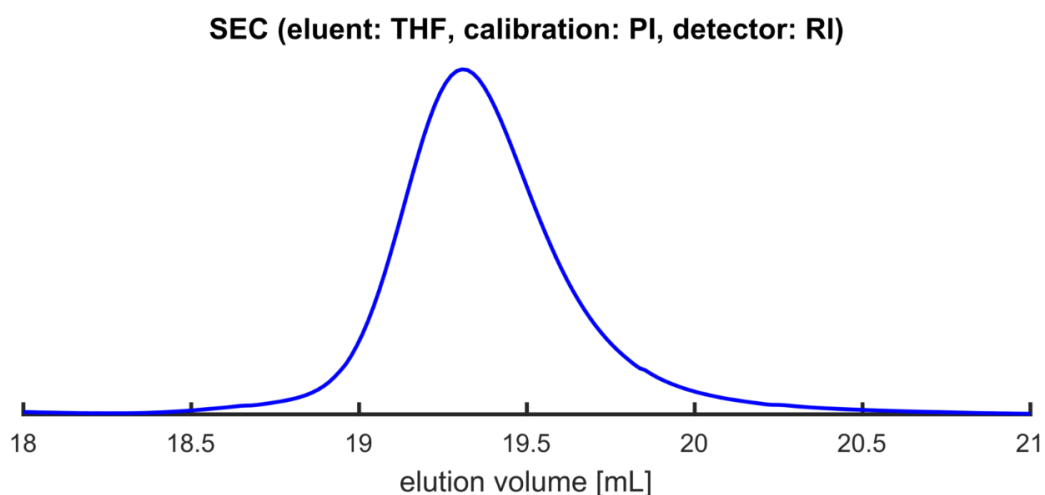
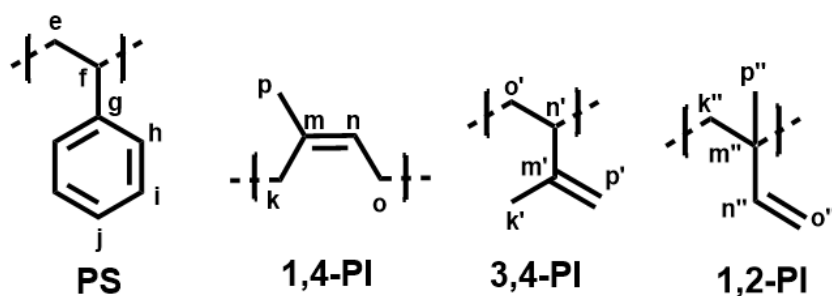


FIGURE S18 SEC trace of PI synthesized in THF (PI_{THF}) at 30 °C. The molecular weight is slightly underestimated ($M_{n,target} = 80$ kg/mol; $M_{n,exp.} = 72.3$ kg/mol; $\mathcal{D} = 1.06$). The used 1,4-PI calibration (3,4: 5%) tends to underestimate the molecular weight, since the sample contains a larger vinyl content as side groups (3,4: 57% ; 1,2: 25%; see Section 7).

7 Microstructural Investigations

In this work, the traditional quantification of PI isomers via *mid*-IR spectroscopy has been replaced by the NMR spectroscopic method introduced by Chen,⁹ leading to more reliable and reproducible results.^{10,11}

SCHEME S1 Repeating units present in the synthesized P(I-co-S) copolymers. As indicated, letters were used to assign the NMR signals. Lowercase letters are used for ¹H resonance signals. Uppercase letters are used for ¹³C resonance signals.



Assignment of the peaks in the ¹H and ¹³C NMR spectrum of the polyisoprene,^{3,9,12-19} polybutadiene^{9,12,20} as well as polystyrene²¹⁻²³ homopolymers is not trivial and has been discussed in several works. The precise data evaluation is even more challenging by the copolymerization with styrene, as the chemical shift of the individual repeating units is also a function of the adjacent units (*i.e.* triad composition), as well as different configurations (head-to-head, tail-to-tail, head-to-tail and the respective inverse configurations) lead to a spectrum that is very rich in signals.

Signals have been assigned with respect to the existing literature for polyisoprene^{3,9,12-19} as well as polystyrene.²¹⁻²³ Additionally, we supported the data by two-dimensional NMR methods, which was crucial due to the highly diverging monomer sequences (*i.e.* triads) existing in this work. Assignment of the signals was studied in depth in a previous work for PS, PI and P(I-co-S) homo- and copolymers synthesized in cyclohexane.³ In this work, we focus on the quantification of the different PI regioisomers. For this purpose, the assignment of aromatic and olefinic signals, is a straightforward method, as these regions possess less signal overlay. Further on, these signals possess a comparably large difference in their chemical shifts, as seen in the HSQC NMR spectrum. As already mentioned, the assignment of the peaks in the aliphatic region was discussed in other works.

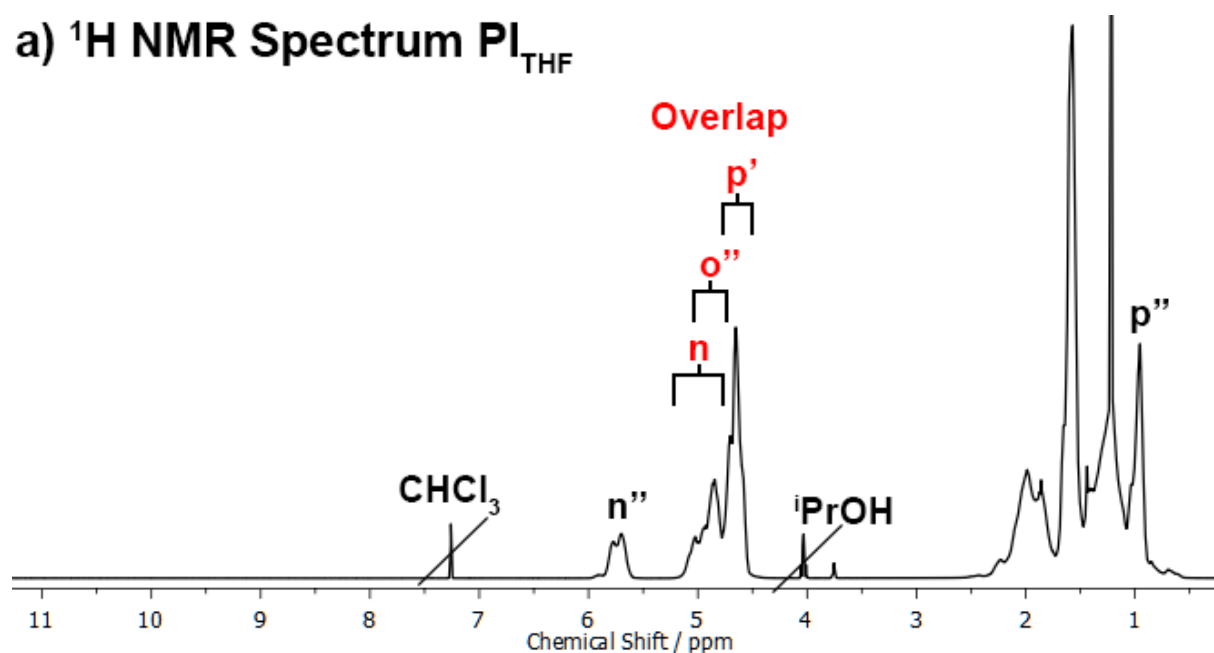
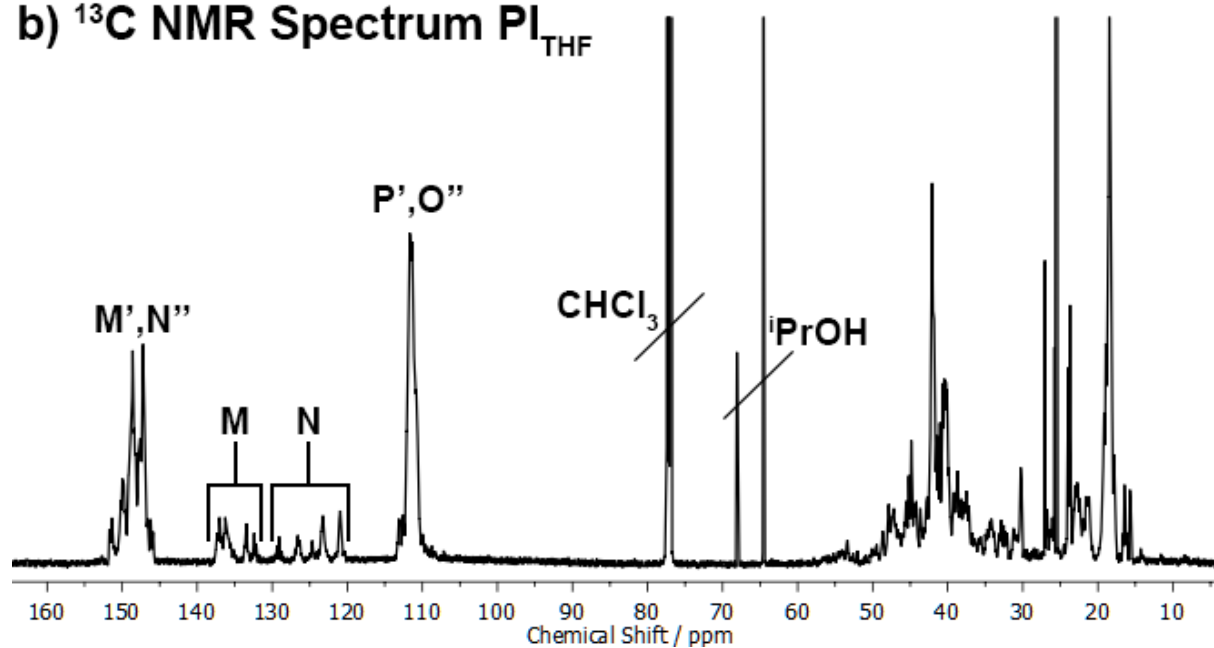
7.1 NMR Evaluation of Polyisoprene synthesized in THF (PI_{THF})a) ¹H NMR Spectrum PI_{THF}b) ¹³C NMR Spectrum PI_{THF}

FIGURE S19A Assigned NMR signals of polyisoprene synthesized in THF. Signals were assigned by ¹H-¹³C HSQC NMR spectroscopy (Figure S19B). a) ¹H NMR spectrum (600 MHz; CDCl₃), b) Inverse Gated ¹³C NMR spectrum (150 MHz, CDCl₃). The PI microstructure was determined as 1,4: 18% ; 3,4: 57% ; 1,2: 25%

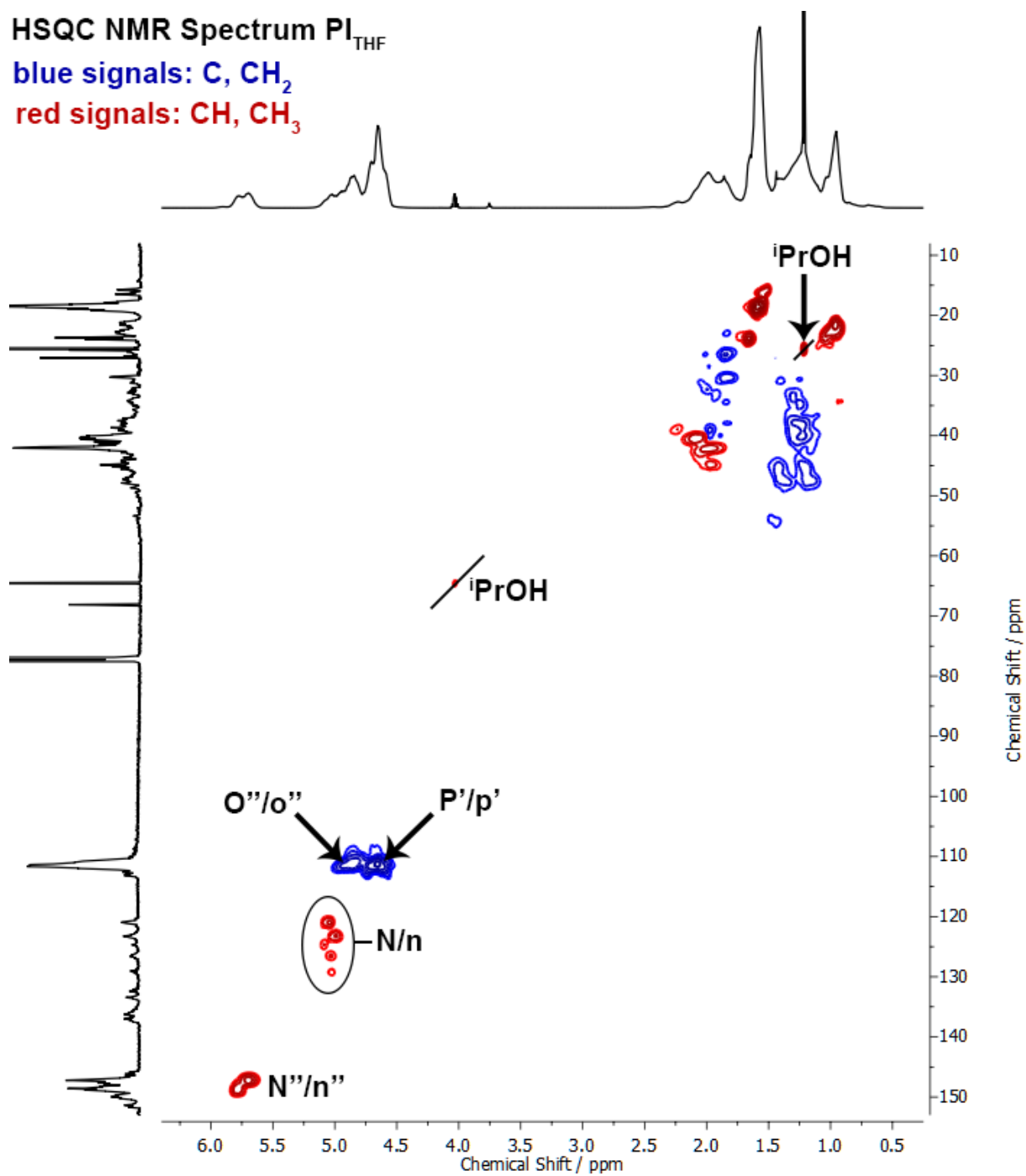


FIGURE S19B ^1H - ^{13}C HSQC NMR spectrum (CDCl_3) of polyisoprene synthesized in THF.

7.2 NMR evaluation of P(I-co-S) Copolymers synthesized with various amounts of THF

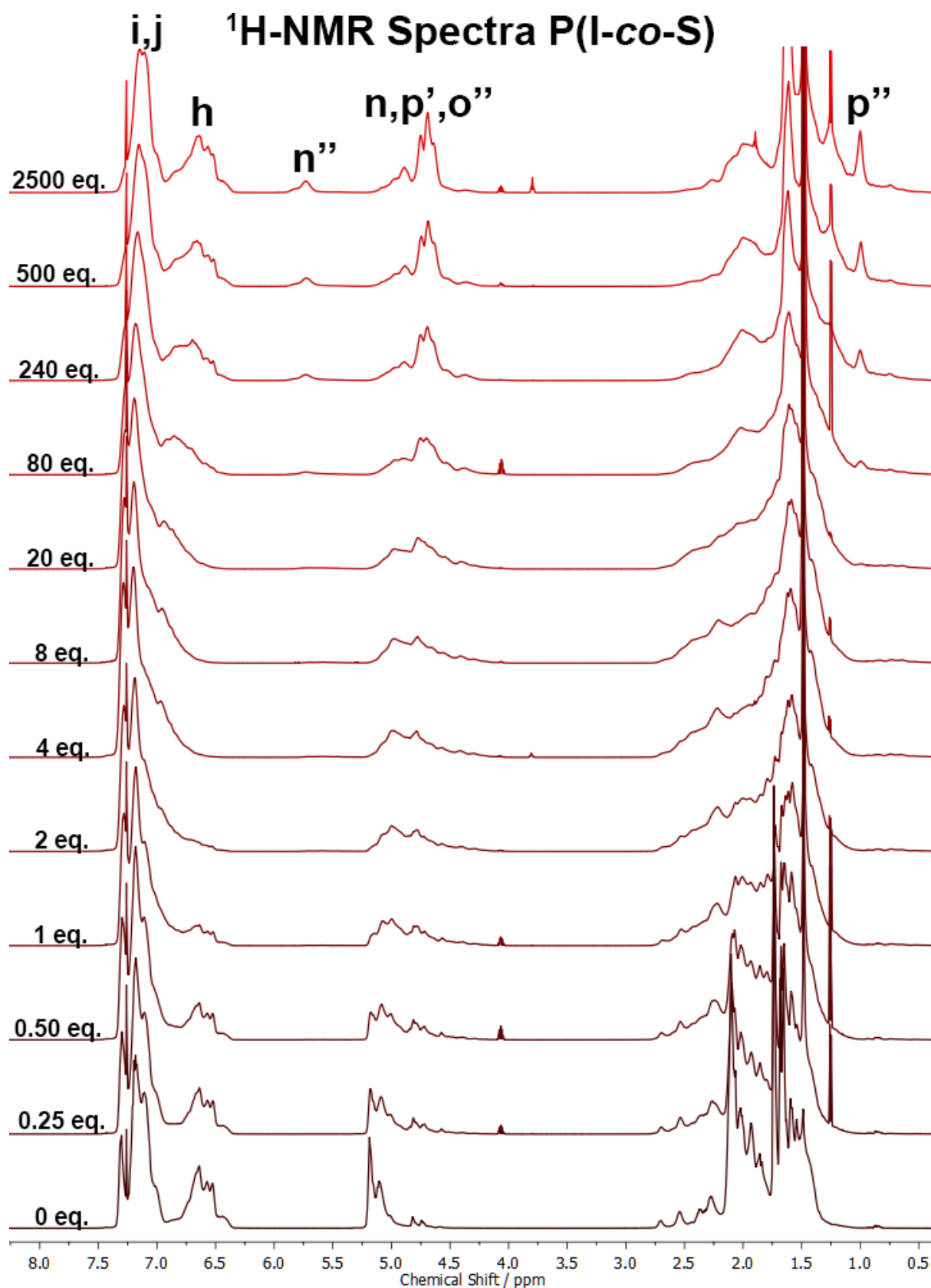


FIGURE S20A Stacked ¹H NMR spectra (600 MHz; CDCl₃) of the 50%_{mol} P(I-co-S) copolymers synthesized in this work. The equivalents of THF in respect to the active chain ends were increased as indicated at the spectra.

Strategy for PI Microstructure Determination

As visible in Figure 19A and 20A, the ^1H NMR signals of the P(I-co-S) copolymers are not sufficient for the precise determination of the PI microstructure. In pure cyclohexane, the 1,4- and 3,4-PI content is typically determined by the signal n (1,4: $\delta = 5.23\text{-}4.84$ ppm) and p' (3,4: $\delta = 4.84\text{-}4.56$ ppm). For increasing THF contents, both signals are broadened and show significant overlap. Additionally, the signal o" (1,2: $\delta = 5.05\text{-}4.76$ ppm) of the 1,2-PI rises, also overlapping with both, 1,4 and 3,4-PI. However, the 1,2-PI unit also gives rise to a well-separated signal n" (1,2: $\delta = 5.90\text{-}5.22$ ppm).

Hence, the ^1H (Figure 20A) and ^{13}C NMR shifts (Figure 20C) of the olefinic signals were assigned via HSQC NMR spectroscopy for each sample (Figure S20D and S20E and Table S2). Subsequently, the 1,4 and the vinyl content (3,4 and 1,2) were quantified via Inverse Gated ^{13}C NMR spectroscopy (Figure 20F, Table S3), followed by determination of the 1,2 and 3,4 content via ^1H NMR spectroscopy (Table S4).

Evaluation of the "Blockiness"

Aromatic signals of the PS units show an interesting phenomenon already described by Bovey and Mochel.^{21,22} The well separated signal of the ortho-protons h continuously shifts downfield from 6.7 to 7 ppm by increasing the [THF]/[Li] ratio from 0 to 8. A further increase reverses the effect. The upfield signal of the ortho proton resonance is explained by the "ring current" effect and an overlapping of the phenyl rings of neighboring styrene units.²² As a consequence, these so-called SSS triads can be quantified, leading to a quick estimate of a parameter called "blockiness",²⁴ corresponding to the molar fraction of block-like PS repeating units, which in turn is defined as PS sequences exceeding 3 uninterrupted PS repeating units, *i.e.* at least SSS triads.

However, the signals used for data evaluation using this method show significant overlap, leading to less precise results. Additionally, it is not clear, how the integral is affected for different triad compositions, e.g. ISS triads, as well as different repeating units, e.g. 1,4- vs. 3,4-PI. Nevertheless, this straightforward method can be used for a rough estimate of the styrene triads, enabling the differentiation of tapered, gradient and block copolymer sequences by offline ^1H NMR spectroscopy.

As visible in Figure S20B and Table S2, the values decrease from $\approx 70\%$ to $\approx 10\%$. This trend is in good agreement with the observed copolymer compositions determined by *in situ* NIR spectroscopy. A further increase of the THF equivalents leads to an increased "blockiness" again. This trend is also in line with the copolymer composition determined by *in situ* NIR spectroscopy. The values for the tapered PI copolymers generally exceed the values of the tapered PS, although

the latter exhibits a pure PS block. However, due to the reasons discussed earlier, these results regarding the blockiness should not be overrated and can only be used for a quick estimate of the experimental results.

TABLE S2 Determination of the "Blockiness" of P(I-co-S) copolymers via inverse-gated ^{13}C NMR spectroscopy.

[THF] / [Li]	Relative Integrals Signals $i+j+h$ ^{a)} : Signal h ^{b)}	n_{PS} ^{c)} : n_{SSS} ^{d)}	Blockiness ^{e)} [% _{mol}]	Copolymer Compositon
0	100 : 29	20 : 14.4	72	Tapered PS
0.25	100 : 23	20 : 11.6	58	Tapered PS
0.5	100 : 18	20 : 9.3	46	Tapered PS
1	100 : 13	20 : 6.6	33	Tapered PS
2	100 : 8.6	20 : 4.3	21	Gradient
4	100 : 5.3	20 : 2.6	13	Random
8	100 : 6.1	20 : 3.1	15	Random
20	100 : 9.7	20 : 4.9	24	Gradient
80	100 : 18	20 : 8.8	44	Gradient
240	100 : 26	20 : 13.1	66	Tapered PI
500	100 : 31	20 : 15.5	77	Tapered PI
2500	100 : 34	20 : 16.9	85	Tapered PI

a) The following area has been used for integration: $\delta = 7.4\text{-}6.24$ ppm. b) The following area has been used for integration: $\delta = 6.85\text{-}6.24$ ppm. c) The relative number of styrene units (n_{PS}) was calculated by dividing the integral of the signals $i+j+h$ by the 5 aromatic PS protons. d) The relative number of block-like PS repeating units (n_{SSS}) was calculated by dividing the integral of the signals h by the 2 aromatic *ortho* protons. e) The blockiness was calculated by $n_{\text{SSS}} / n_{\text{PS}} = ((\text{integral}_{\text{signal } h}) / 2) / (\text{integral}_{\text{signal } i+j+h}) / 5$

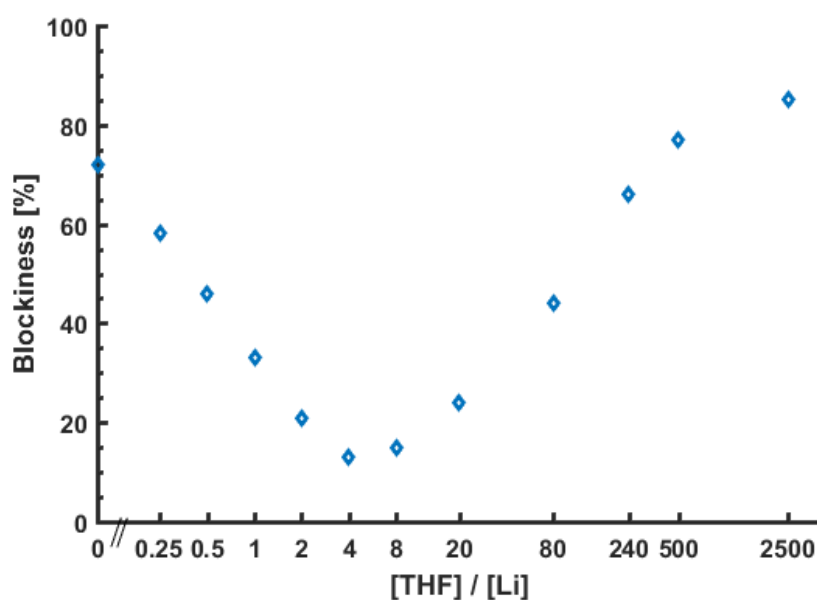


FIGURE S20B Blockiness as a function of the [THF]/[Li] ratio. A minimum is observed for [THF]/[Li], validating the random sequence observed by *in situ* NIR spectroscopy (Figure 4, Table 1).

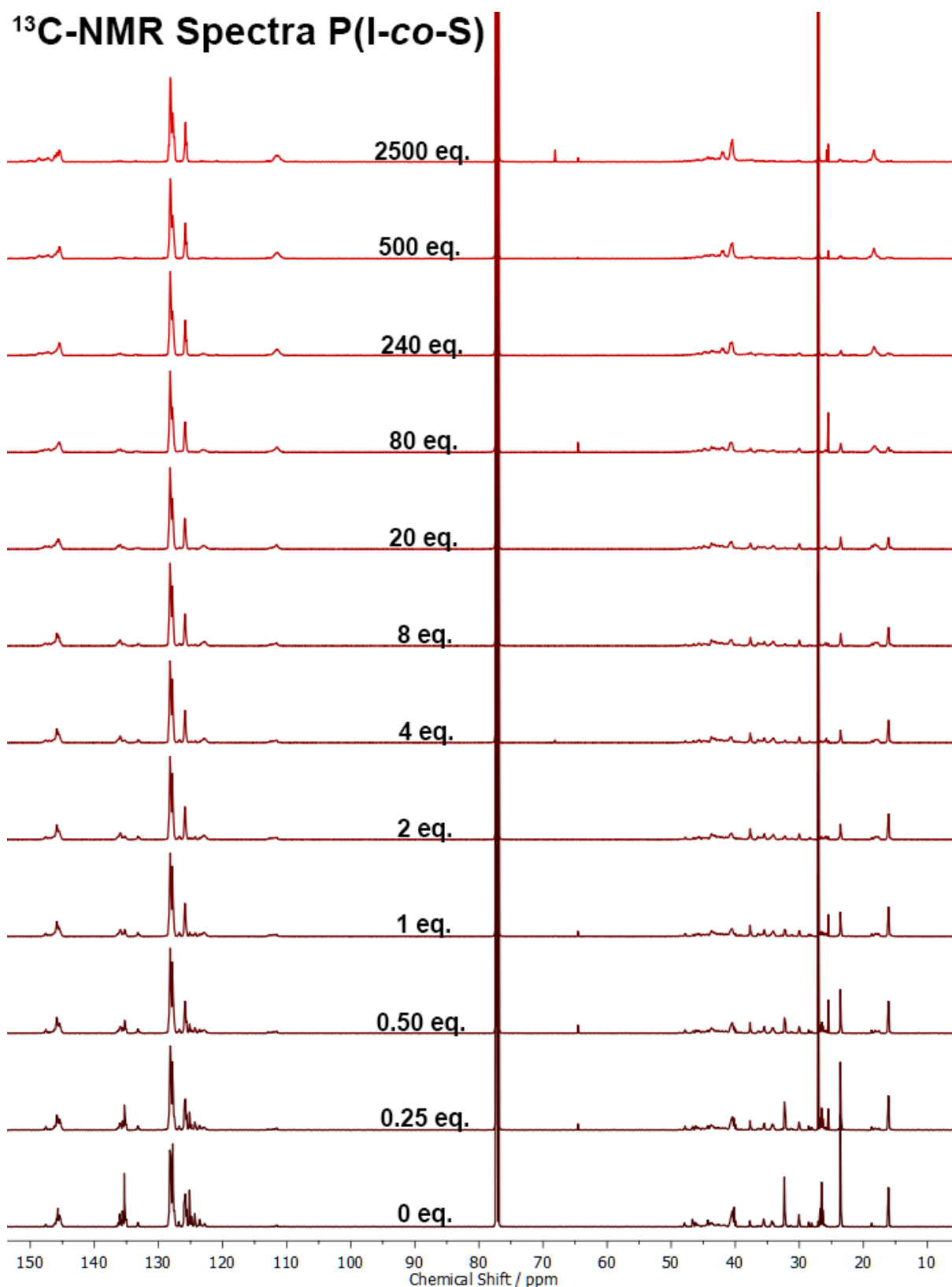
Evaluation of the PI Microstructure with Inverse Gated ^{13}C NMR ^{13}C -NMR Spectra P(I-co-S)

FIGURE S20C Stacked Inverse-Gated ^{13}C NMR spectra (150 MHz, CDCl_3) of the 50% $_{\text{mol}}$ P(I-co-S) copolymers synthesized in this work. The equivalents of THF in respect to the active chain ends were increased as indicated at the spectra.

blue signals: CH, CH₃, red signals: C, CH₂

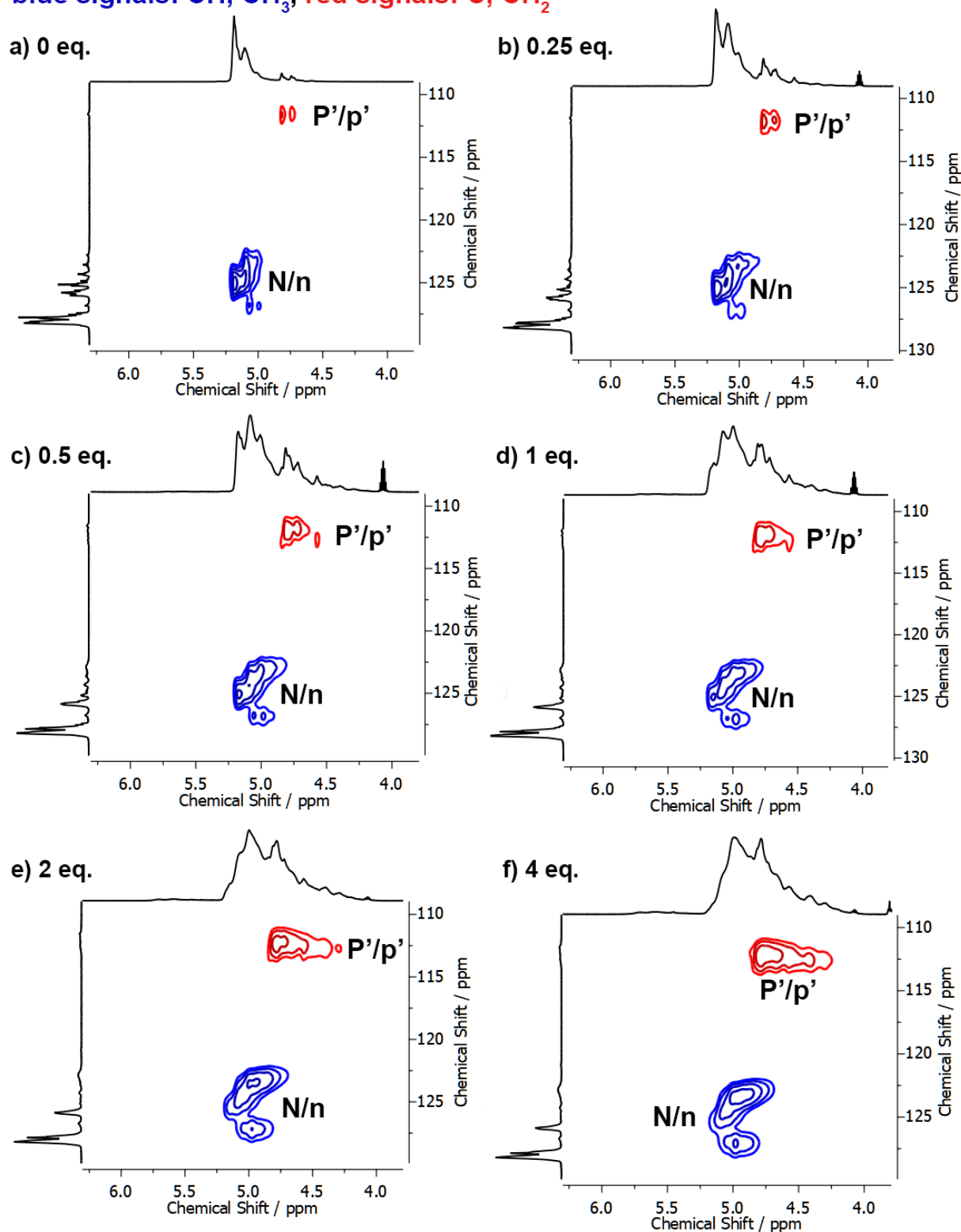


FIGURE S20D ¹H-¹³C HSQC NMR spectra (CDCl₃) of the 50%_{mol} P(I-co-S) copolymers synthesized in this work. The equivalents of THF in respect to the active chain ends were increased as indicated at the spectra.

blue signals: CH, CH₃, red signals: C, CH₂

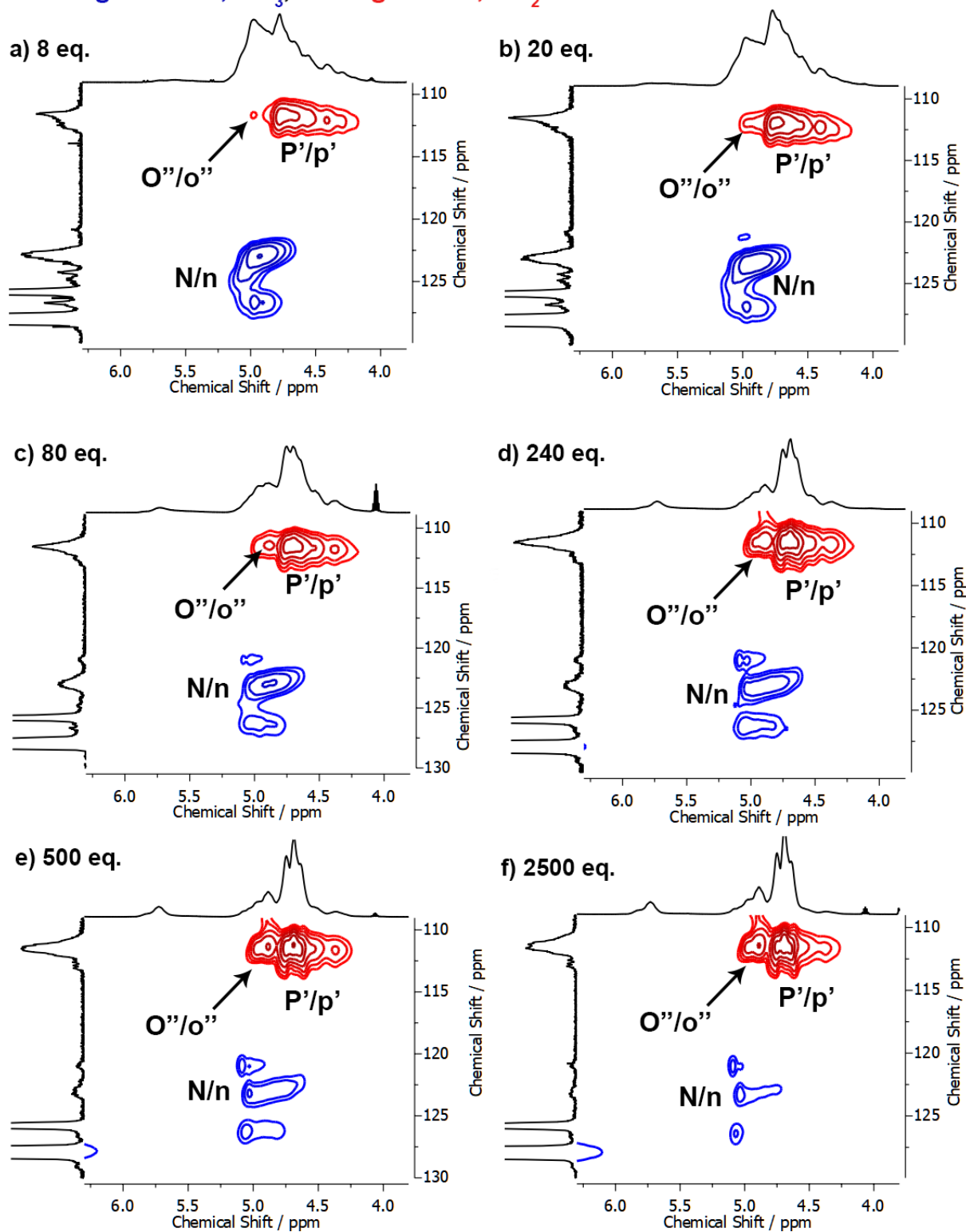
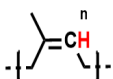
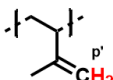
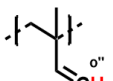
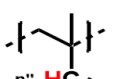
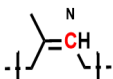
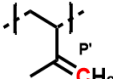
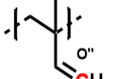
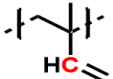


FIGURE S20E ¹H-¹³C HSQC NMR spectra (CDCl₃) of the 50%_{mol} P(I-co-S) copolymers synthesized in this work. The equivalents of THF in respect to the active chain ends were increased as indicated at the spectra.



FIGURE S20F Zoom of the olefinic and aromatic region: Stacked Inverse Gated ^{13}C NMR spectra (150 MHz, CDCl_3) of the 50% $_{\text{mol}}$ P(I-co-S) copolymers. The equivalents of THF in respect to the active chain ends, was increased as indicated at the spectra. Black font: separated signals used for data evaluation, red font: overlaid signals.

TABLE S3 Overview of PI isomers of occurring in P(I-co-S) copolymers randomized with THF, as well as the assigned chemical shift (δ) in ^1H and ^{13}C NMR spectra.

PI Unit	Structural Formula	Nucleus	Assigned Letter	Nucleus per repeating unit	δ [ppm]	Comment for Data Evaluation
1,4		^1H	n	1	5.23 - 4.84	Broadening of the signal for increasing [THF]/[BuLi] leads to overlap with Signal p' and o''
3,4		^1H	p'	2	4.84 - 4.56	Overlap with o''; overlap with n for increasing [THF]/[BuLi]
1,2		^1H	o''	2	5.05 - 4.76	Overlap with p'; overlap with n for increasing [THF]/[BuLi]
		^1H	n''	1	5.90 - 5.30	Well Separated Signal
1,4		^{13}C	N	1	130.3 - 128.5 127.2 - 126.2 125.4 - 122 122 - 119	Splitting caused by S/I Triads
3,4		^{13}C	P'	1	110 - 113.5	Overlap with O''
1,2		^{13}C	O''	1	110 - 113.5	Overlap with P'
		^{13}C	N''	1	150 - 148 148 - 146	Splitting caused by S/I Triads; both signals overlap with signals of polystyrene

The ^1H NMR spectroscopic signals, used for the quantification of the 1,2-PI Microstructure in P(I-co-S) copolymers are visualized in the stacked ^1H NMR spectrum in Figure 20A.

The ^{13}C signals, used for the quantification of the Vinyl-PI Microstructure in P(I-co-S) copolymers are visualized in the zoom of the stacked ^{13}C NMR spectra in Figure 20F.

TABLE S4 Determination of the 1,4-PI Content of P(l-co-S) copolymers via Inverse-Gated ^{13}C NMR spectroscopy.

[THF] / [Li]	Relative Integrals 1,4-PI ^{a)} : 1,2-PI + 3,4-PI ^{b)}	Calculated Content _{1,4 PI}	Calculated Content _{1,2 PI+3,4 PI}
0	100 : 4.69	96%	4%
0.25	100 : 11.8	89%	11%
0.5	100 : 17.6	85%	15%
1	100 : 26.1	79%	21%
2	100 : 33.4	75%	25%
4	100 : 39.2	72%	28%
8	100 : 46.7	68%	32%
20	100 : 69.0	59%	41%
80	100 : 105	49%	51%
240	100 : 183	35%	65%
500	100 : 273	27%	73%
2500	100 : 322	24%	76%

a) The following signals have been used for integration: $\delta = 130.3\text{-}128.5$; $127.2\text{-}126.2$ ppm; $125.4\text{-}122$ ppm; and $122\text{-}119$ ppm. b) The following signal has been used for integration: $\delta = 113\text{-}110.5$ ppm.

The molar content of the 1,4-PI units is given by:

$$\text{Content}_{1,4\text{-PI}} = \frac{\text{Integral}_{1,4\text{-PI}}}{\text{Integral}_{1,4\text{-PI}} + \text{Integral}_{1,2\text{-PI}+3,4\text{-PI}}}$$

The Vinyl-PI units correspond to the sum of the 1,2-PI and 3,4-PI units. Their molar content is given by:

$$\text{Content}_{1,2\text{-PI}+3,4\text{-PI}} = 1 - \text{Content}_{1,4\text{-PI}} = \frac{\text{Integral}_{1,2\text{-PI}+3,4\text{-PI}}}{\text{Integral}_{1,4\text{-PI}} + \text{Integral}_{1,2\text{-PI}+3,4\text{-PI}}}$$

TABLE S5 Determination of the 1,2- and 3,4-PI content via ^1H NMR spectroscopy.

[THF]/ [Li]	Relative Integrals: 1,4 + 1,2 + 3,4-PI ^{a)} : 1,2-PI ^{b)}	Average Olefinic Protons per PI Repeating Unit ($H_{\text{olefinic,average}}$)	Calculated Content _{3,4 PI}	Calculated Content _{1,2 PI}
0	100 : 0.621	1.04	3.8%	0.6%
0.25	100 : 0.376	1.11	10%	0.4%
0.5	100 : 0.820	1.15	14%	0.9%
1	100 : 1.17	1.21	19%	1.4%
2	100 : 1.83	1.25	23%	2.3%
4	100 : 2.14	1.28	25%	2.7%
8	100 : 2.83	1.32	28%	3.7%
20	100 : 3.25	1.41	36%	4.6%
80	100 : 4.91	1.51	44%	7.4%
240	100 : 7.27	1.65	53%	12%
500	100 : 8.71	1.73	58%	15%
2500	100 : 8.62	1.76	61%	15%

a) The following signals have been used for integration: $\delta = 5.23\text{-}4.56$ ppm. b) The following signal has been used for integration: $\delta = 5.90\text{-}5.30$ ppm.

The molar content of the 1,2-PI units is given by:

$$\text{Content}_{1,2\text{-PI}} = \frac{\text{Integral}_{1,2\text{-PI}}}{\frac{\text{Integral}_{\text{PI,total}}}{H_{\text{olefinic,average}}}} = \frac{\text{Integral}_{1,2\text{-PI}} \cdot H_{\text{olefinic,average}}}{\text{Integral}_{\text{PI,total}}} = \frac{DP_{1,2\text{-PI}}}{DP_{\text{PI,total}}}$$

As the molar content of 1,4-PI units and 1,2-PI units is known, the molar content of 3,4-PI units is given by:

$$\text{Content}_{3,4\text{-PI}} = 1 - \text{Content}_{1,4\text{-PI}} - \text{Content}_{1,2\text{-PI}}$$

7.5 Comparison of NIR and NMR for the Determination of the Vinyl Content

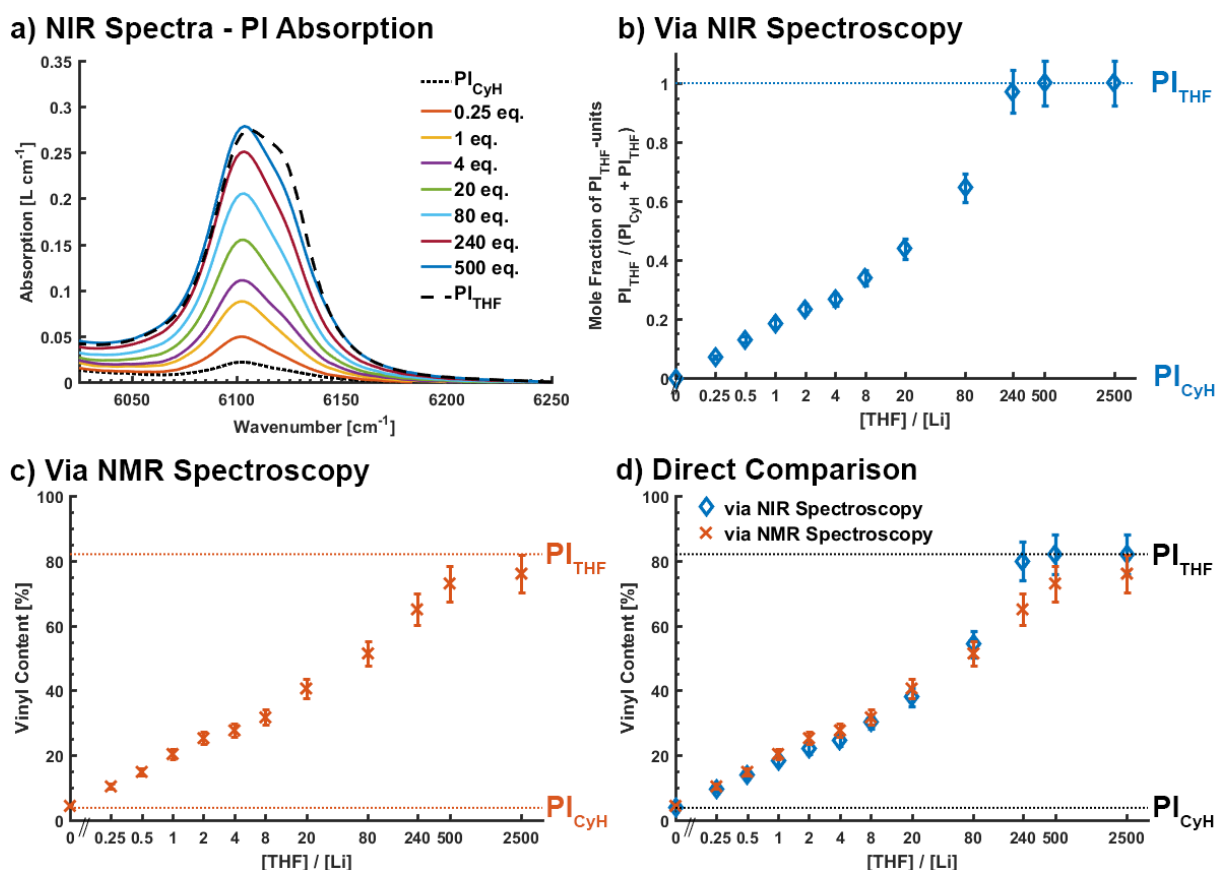


FIGURE S21 a) NIR spectra of isoprene units in P(I-co-S) obtained at various [THF]/[Li] ratios; b-d) determined PI vinyl content of the P(I-co-S) copolymers by NIR (b) and NMR (c) as well as comparison (d).

a-b) Estimation of the Vinyl Content via NIR Spectroscopy:

The values of the P(I-co-S)) vinyl content determined by NIR spectroscopy are based on the deconvolution of the absorption spectra with the known extinction coefficients, ϵ (see Figure S3).

To obtain an absorption spectrum solely ascribed to the absorption of PI units ($[PI_{CyH}] \cdot \epsilon_{PI,CyH} + [PI_{THF}] \cdot \epsilon_{PI,THF}$); Figure S21a), by deconvolution we subtracted the PS units related absorption ($[PS] \cdot \epsilon_{PS}$) from the spectra taken at full monomer conversion. A strong absorption of the PI units at $\approx 6100 \text{ cm}^{-1}$ is observed, increasing with the [THF]/[Li] ratio. This trend can be ascribed to an increasing mole fraction of repeating units with a regioisomeric composition corresponding to that of PI synthesized in THF, PI_{THF} (18% 1,4, 82% vinyl, determined by NMR) (Figure S21b). This isomeric composition shows a comparably larger extinction coefficient, ϵ , in this range (see Figure S3), ascribed to the larger content of vinyl-side chain units compared to PI synthesized in

cyclohexane, PI_{CyH} (96% 1,4, 4% vinyl, determined by NMR).

Consequently, a value of 0, is attributed to the typical microstructure of PI_{CyH}. A value of 1, represents the typical microstructure obtained for PI_{THF}, see Section 7). As visualized in Figure S21 a,b the fraction of PI_{THF} units determined for [THF]/[Li] = 500 approaches unity. A similar vinyl content of these copolymers compared to the homopolymer PI_{THF} is concluded.

c) Determination of the Vinyl Content via NMR Spectroscopy

As described in detail in Section 7, the vinyl content was also determined via NMR spectroscopy. The vinyl content of the PI_{THF} and the PI_{CyH} homopolymer used for the determination of the extinction coefficients (Figure S3), is indicated by red dotted lines.

d) Direct comparison of both methods

The values of both methods, NIR and NMR spectroscopy, are compared in Figure S21c). For this purpose, the vinyl content of the molar fraction x of PI_{THF} as determined by NIR spectroscopy, was calculated by the following equation:

$$\text{Vinyl Content(NIR)} = x(\text{PI}_{\text{THF}}) \cdot \text{Content}_{\text{PI,Vinyl,THF}} + ((1 - x(\text{PI}_{\text{THF}})) \cdot \text{Content}_{\text{PI,Vinyl,CyH}})$$

with $\text{Content}_{\text{PI,Vinyl,THF}} = 0.82$ and $\text{Content}_{\text{PI,Vinyl,CyH}} = 0.04$.

8 Thermal Properties

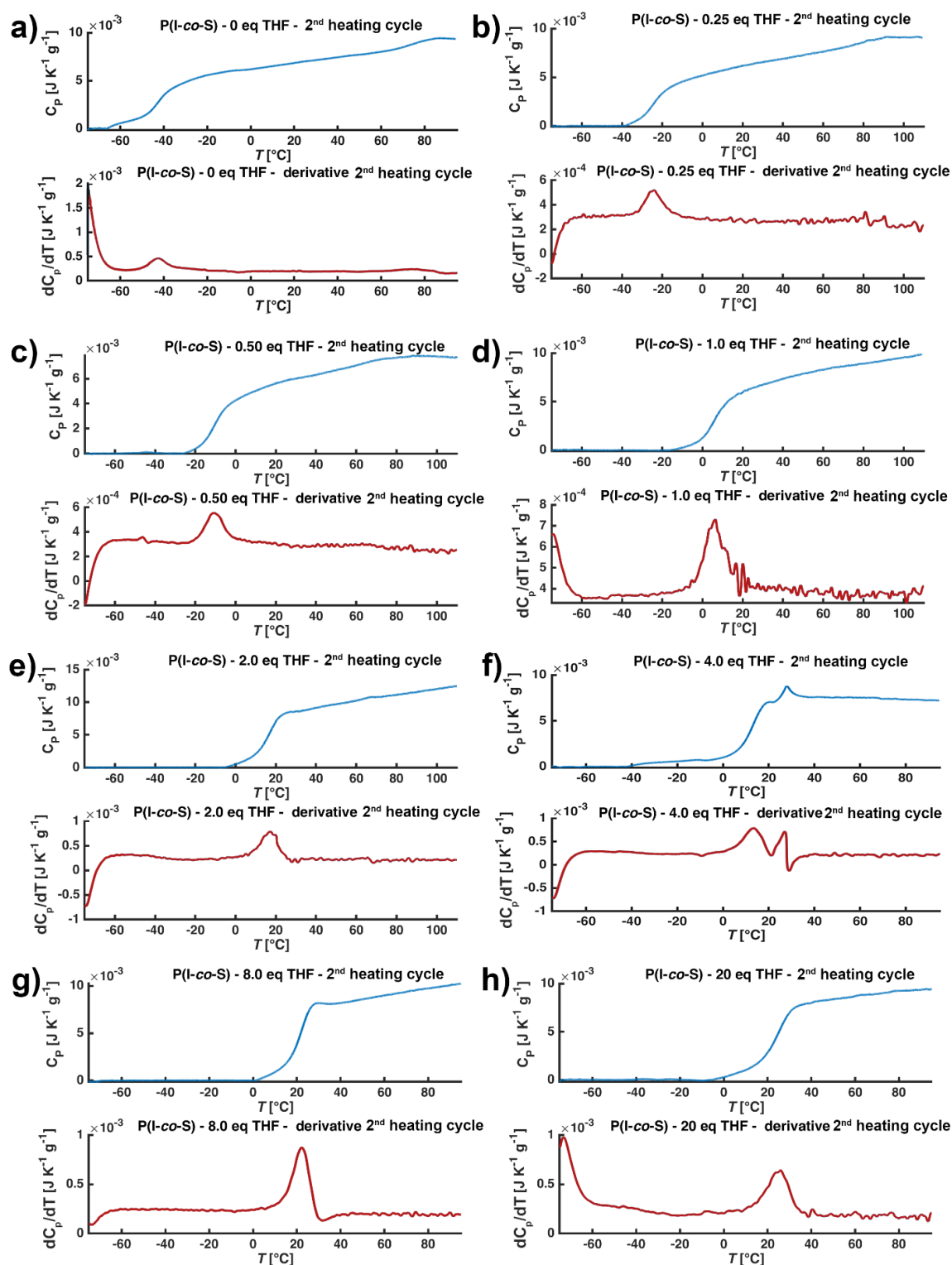


FIGURE S22A DSC data (blue: measurements and red: first derivative) for P(l-co-S) copolymers synthesized with [THF]/[Li] ratios from 0 to 20 eq.

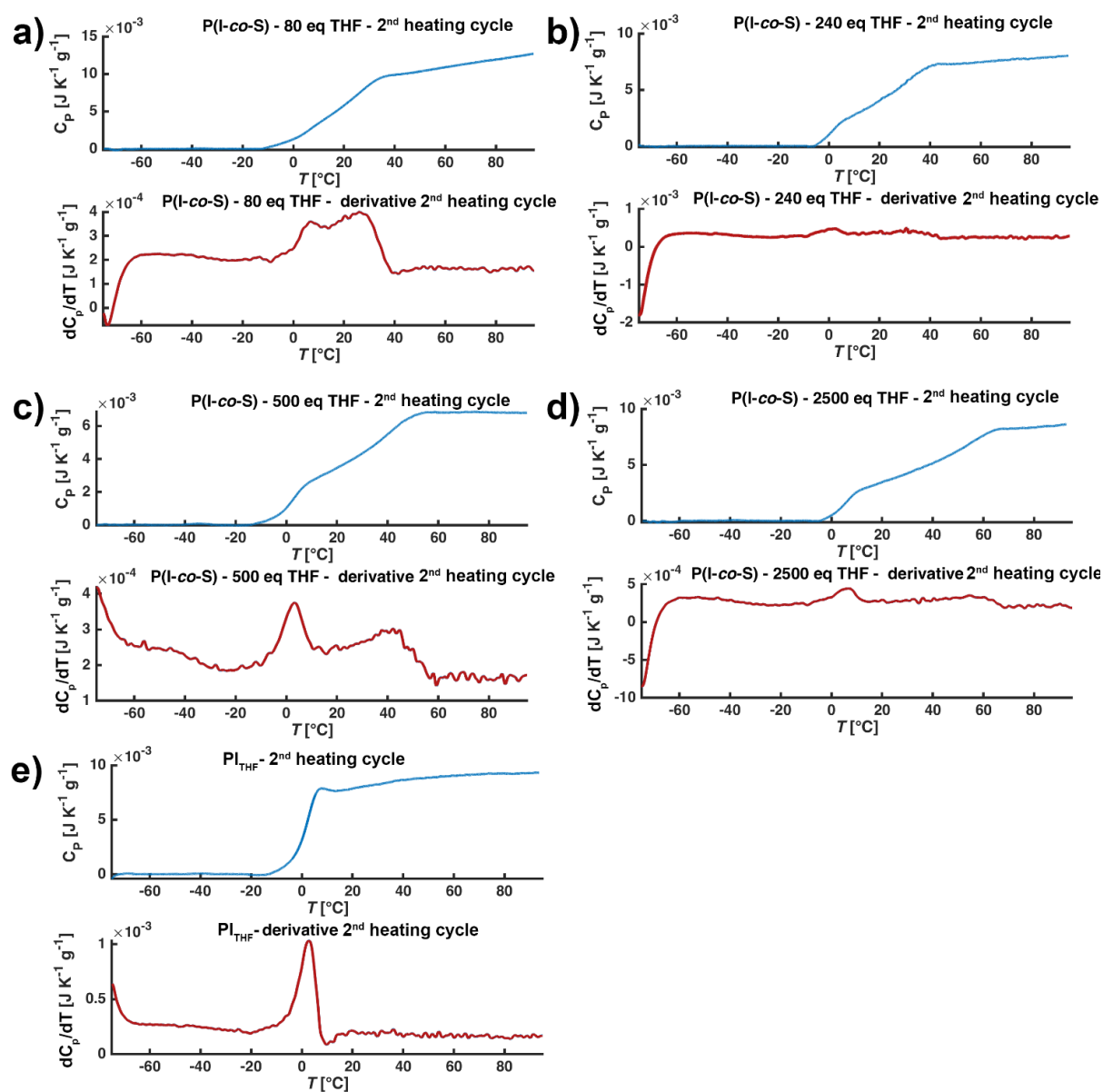


FIGURE S22B DSC data (blue: measurements and red: first derivative) for P(l-co-S) copolymers synthesized with [THF]/[Li] ratios from 80 to 2500 eq. e) PI synthesized in pure THF.

9 Copolymer Morphologies

9.1 Small-Angle X-Ray Diffractograms

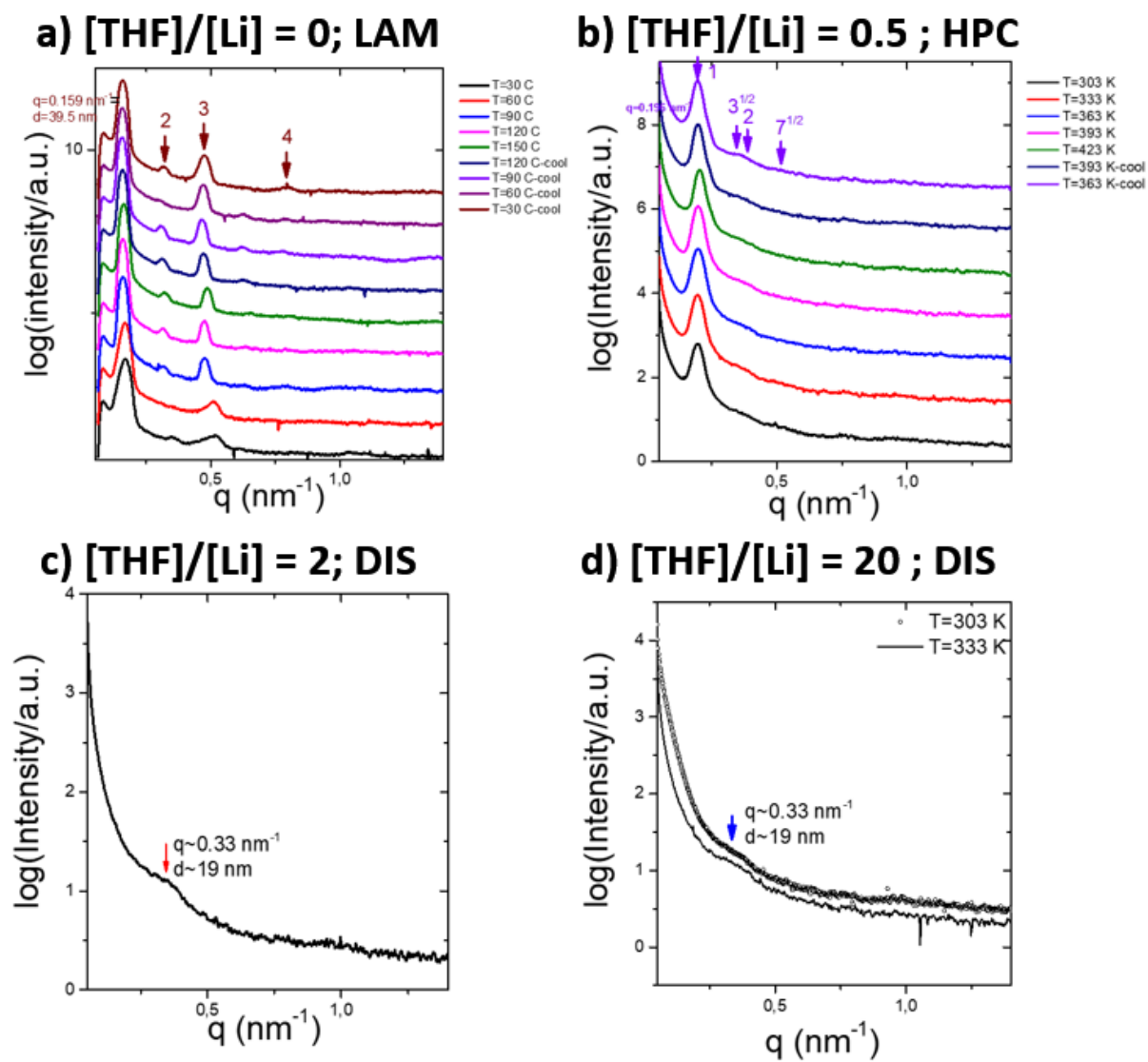
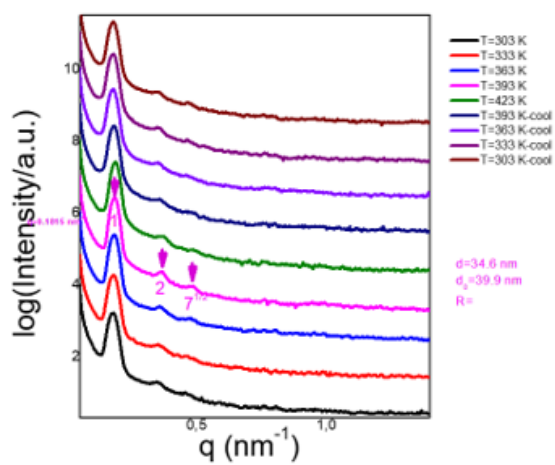
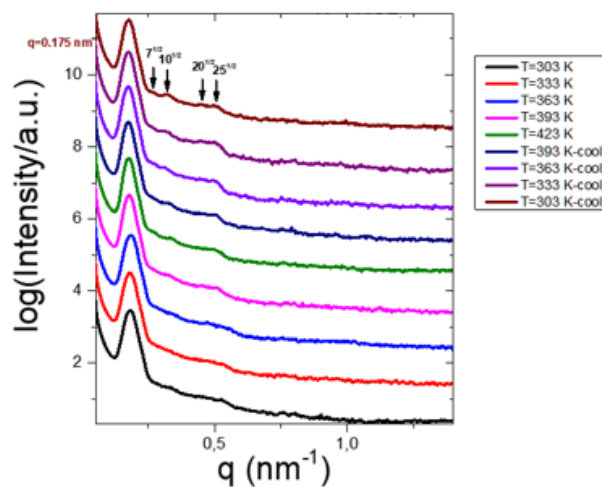
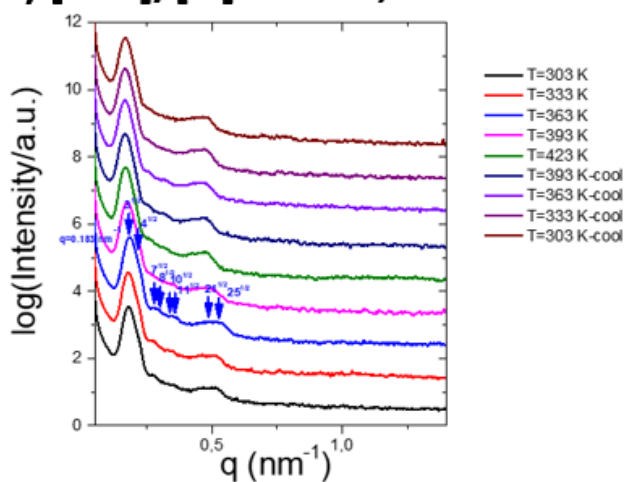


FIGURE S23A Temperature dependent SAXS measurements on P(I-co-S) samples.

a) [THF]/[Li] = 240; HPC**b) [THF]/[Li] = 500 ; BIC****c) [THF]/[Li] = 2500; BIC****FIGURE S23B** Temperature dependent SAXS measurements on P(I-co-S) samples.

9.2 Transmission Electron Microscopy

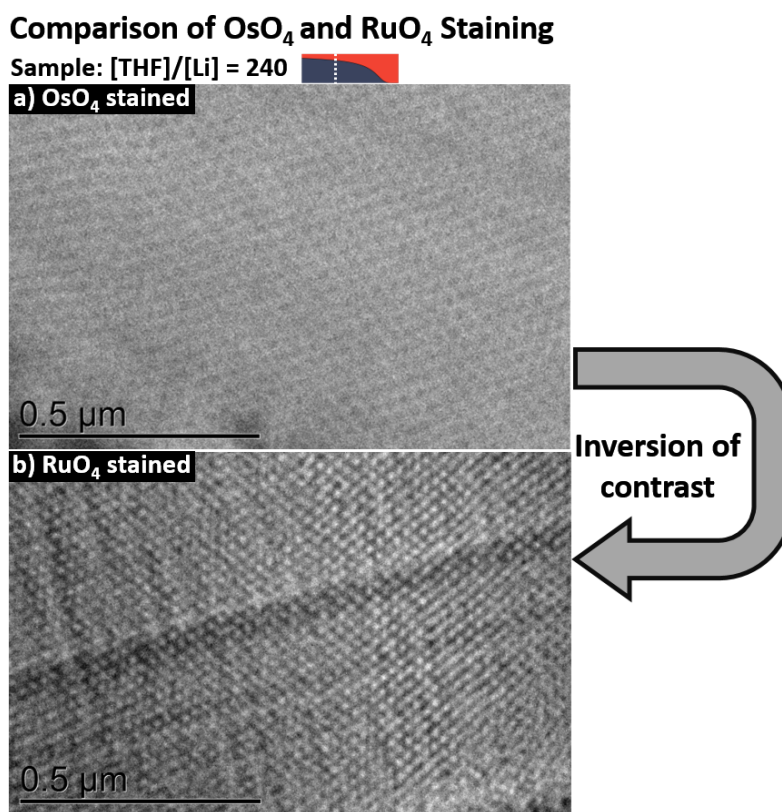


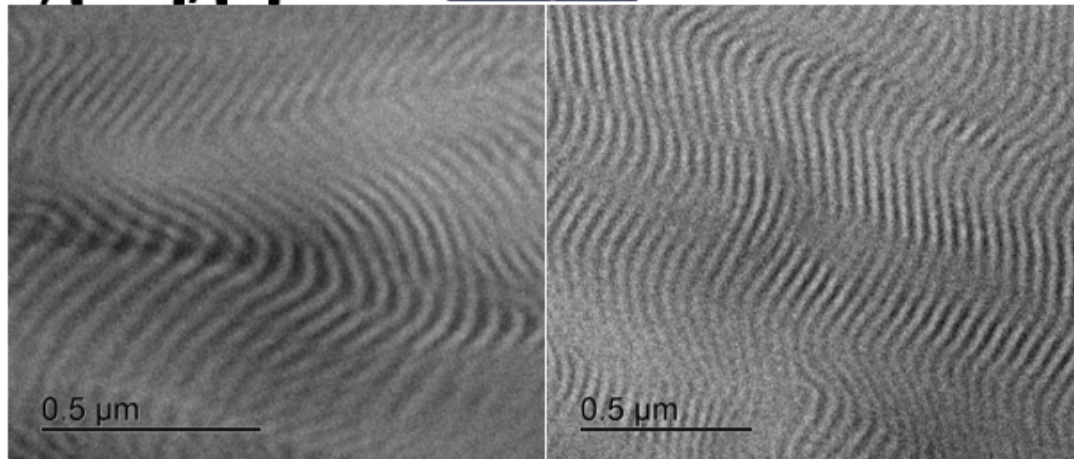
FIGURE S24 TEM images of RuO₄ and OsO₄-stained P(l-co-S) samples (annealed for 16 h at 120 °C). Polymer volume composition profiles are indicated next to the image (PS = grey; PI = red). A more detailed visualization, including the axes is given in Figure S15. The white dotted lines separate the PI-rich and PS-rich polymer volumes (see Supporting Information Section 9.3).

Osmium tetroxide (OsO₄) can selectively stain olefinic double bonds (e.g. PI-units) in the presence of aromatic groups (e.g. PS-units). In accordance with previous works on tapered PS block copolymers,^{1,3,25} OsO₄ was found suitable to produce a contrast ([THF]/[Li] = 0-0.5; see Figure S24B; PI-rich phases appear electron opaque, *i.e.* dark). In contrast, inverted tapered PI block copolymers were comparably poor in contrast (*cf.* images in Figure S24A).

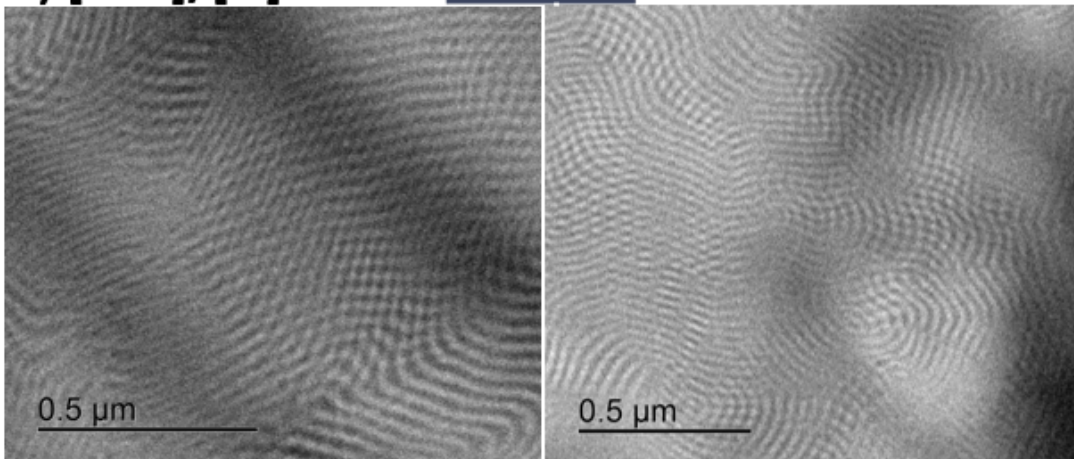
However, ruthenium tetroxide (RuO₄) can react with the aromatic double bonds of PS, which is known to result in a phase contrast for segregated PI/PS based block copolymers. Here, the PS-units appear electron-opaque (dark). This staining-reagent was found suitable for imaging of the phase contrast in inverse tapered PI block copolymers ([THF]/[Li] = 80-2500; Figure S24C and D). The expected inversion of the phase contrast, caused by the change from OsO₄ to RuO₄ was validated for P(l-co-S) block copolymers investigated in this work (*cf.* images in Figure S24A).^{26,27}

TEM Images - OsO₄ stained

a) [THF]/[Li] = 0



b) [THF]/[Li] = 0.25



c) [THF]/[Li] = 0.5

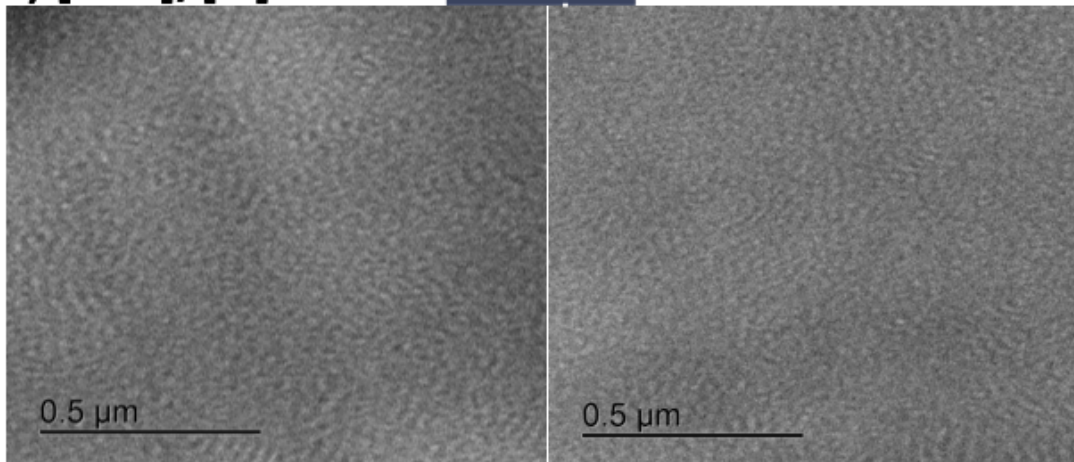
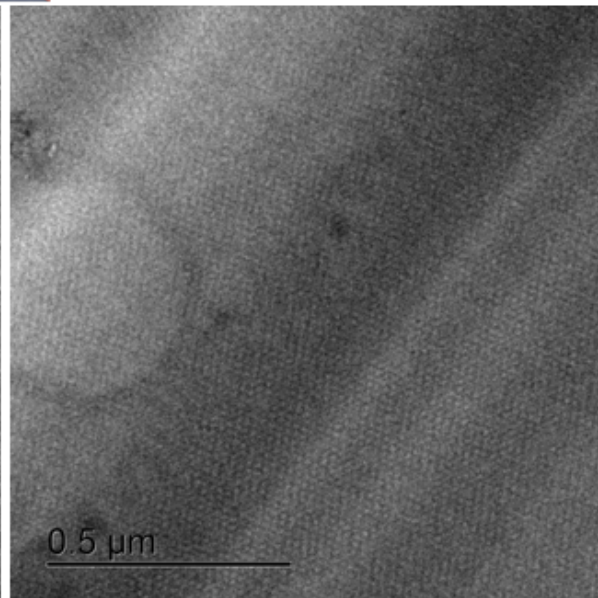
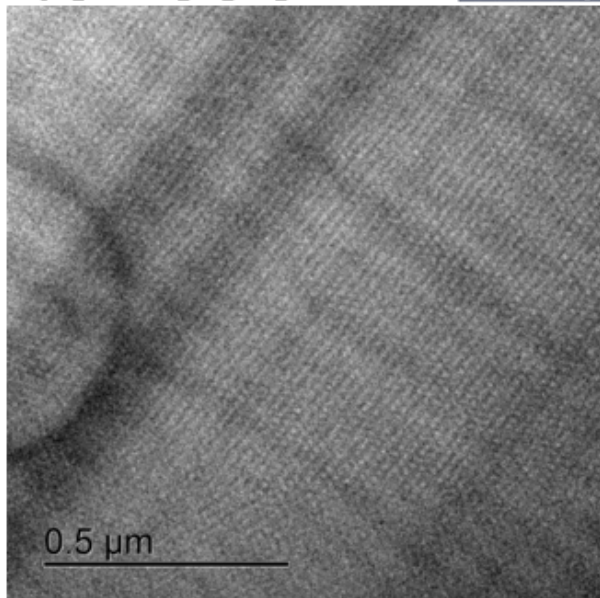


FIGURE S25A TEM images of OsO₄-stained P(I-co-S) samples (annealed for 16 h at 120 °C). PI-rich domains appear electron-opaque (dark). Polymer volume composition profiles are indicated next to the images (PS = grey; PI = red). A more detailed visualization, including the axes, is given in Figure S15. The white dotted lines separate the PI-rich and PS-rich polymer volumes (see Supporting Information Section 9.3).

TEM Images - RuO₄ stained

a) [THF]/[Li] = 80



c) [THF]/[Li] = 240

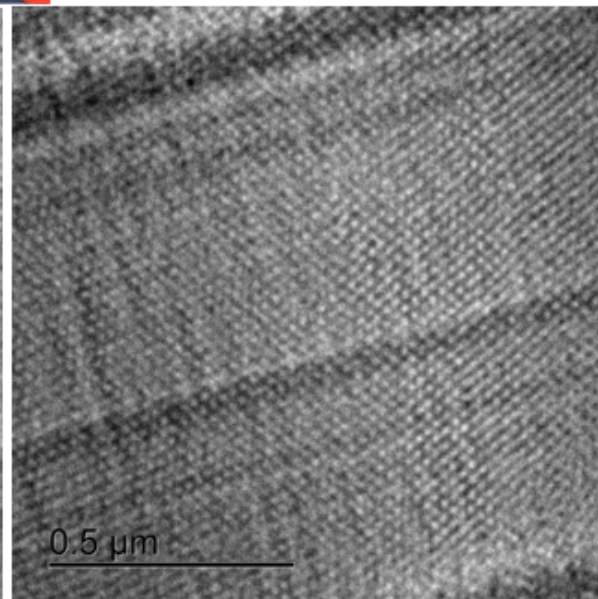
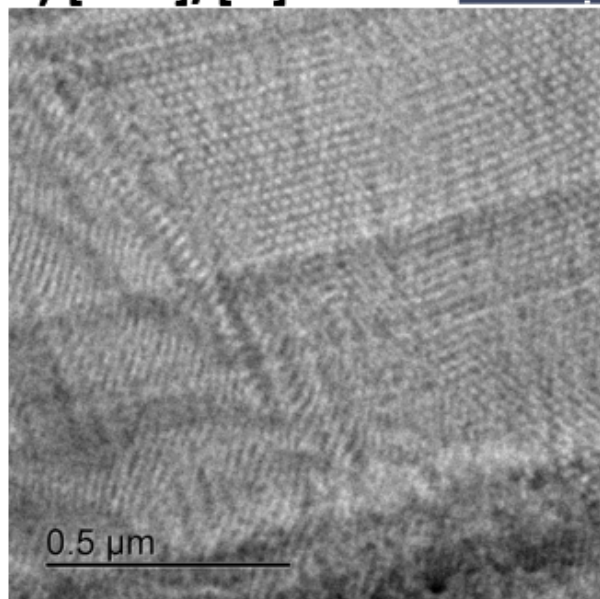
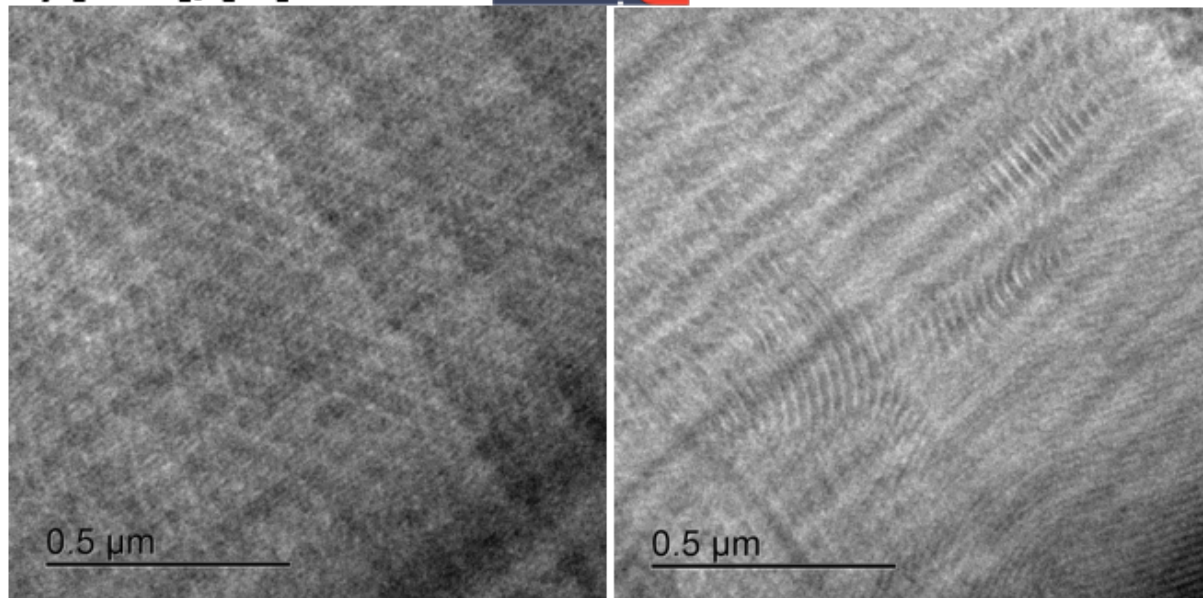


FIGURE S25B TEM images of RuO₄stained P(I-co-S) samples (annealed for 16 h at 120 °C). PS-rich domains appear electron-opaque (dark). Polymer volume composition profiles are indicated next to the images (PS = grey; PI = red). A more detailed visualization, including the axes, is given in Figure S15. The white dotted lines separate the PI-rich and PS-rich polymer volumes (see Supporting Information Section 9.3).

TEM Images - RuO₄ stained

a) [THF]/[Li] = 500



b) [THF]/[Li] = 2500

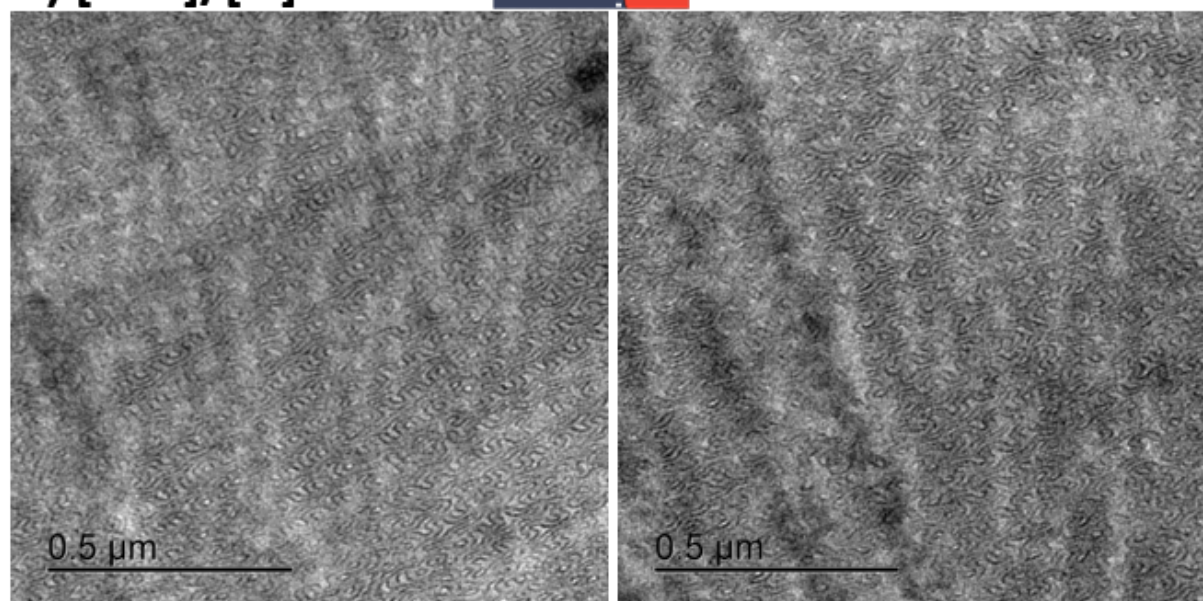


FIGURE S25C TEM images of RuO₄stained P(I-co-S) samples (annealed for 16 h at 120 °C). PS-rich domains appear electron-opaque (dark). Polymer volume composition profiles are indicated next to the images (PS = grey; PI = red). A more detailed visualization, including the axes, is given in Figure S15. The white dotted lines separate the PI-rich and PS-rich polymer volumes (see Supporting Information Section 9.3).

Discussion of TEM Images

1) OsO₄ Stained Samples (PI-rich phases appear dark)

[THF]/[Li] = 0 (Figure 25A a)

The lamellar morphology observed for the sample synthesized in the absence of THF is in accordance with the SAXS studies in this work (Figure S23A), as well as with results for a polymerization temperature of $T = 40\text{ }^{\circ}\text{C}$ reported in previous works (this work $T = 20\text{ }^{\circ}\text{C}$).^{1,3}

[THF]/[Li] = 0.25 (Figure 25A b)

A similar pattern was observed in TEM studies in our previous work for a sample synthesized in absence of THF at a polymerization temperature of $T = 80\text{ }^{\circ}\text{C}$ (this work $T = 20\text{ }^{\circ}\text{C}$), which also leads to a flattening of the gradient and an increase of the PI-rich polymer volume (Table S7).³ In comparison to the sample shown here, the increase of the PI-rich polymer volume was less remarkable. As shown by TEM tomography, the change in morphology only occurred partially, leading to a mixture of lamellae with tetragonally packed cylinders (TPC) and tetragonally perforated lamellae (TPL).³

Here we expect a similar tetragonal morphology. The larger shift in the PI-rich volume fraction is suspected to facilitate the formation of the tetragonally ordered morphology, leading to large areas showing the tetragonal pattern. Further studies are currently in progress to explain the formation of this rather rarely described microdomain morphology.

[THF]/[Li] = 0.5 (Figure 25A c)

The TEM measurements show cylinders consisting of PS-rich (bright appearance) domains in a PI-rich matrix (electron opaque; *i.e.* dark appearance). The results are in accordance with our SAXS studies, revealing hexagonally packed cylinders (Figure S23A).

2) RuO₄ Stained (PI-rich phases appear bright)

[THF]/[Li] = 80 (Figure 25B a)

The contrast in these images is rather weak, which is explained by the substantial mixing of the PS- and PI-rich phases and expected by the rather smooth gradient profile. Although some areas of the samples show parallel lines, others show a weakly ordered, hexagonal alignment of white dots. This morphology can be tentatively ascribed to hexagonally packed cylinders of polyisoprene (bright appearance). In this case, the lines refer to cylinders that are aligned parallel

to the plane, and the dots to a perpendicular orientation, respectively. However, care should be taken as the contrast in these images is weak and does not allow a clear assignment of the morphology.

[THF]/[Li] = 240 (Figure 25B b)

These observations can be explained by the parallel (bright appearing lines) and perpendicular orientation (bright appearing dots) of hexagonally packed cylinders, consisting of PI-rich (bright appearance) polymer segments. This result is in accordance with our SAXS studies (Figure S23B).

[THF]/[Li] = 500 (Figure 25C a)

In accordance to the previous sample, local areas of the sample (in particular in the right-hand image) are represented by straight lines. With respect to the gradient profile this would suggest a cylindrical order. Although the gradient is steeper (*cf.* [THF]/[Li]=240), the observed contrast is rather weak. Our SAXS data indicate a bicontinuous morphology. These results are possibly explained by the proximity of the phase state to an order-order transition (hexagonally packed cylinders and the gyroid bicontinuous morphology; see [THF]/[Li] = 240 and [THF]/[Li] = 2500), leading to the formation of a metastable, non-equilibrium morphology (spinodal decomposition).

[THF]/[Li] = 2500 (Figure 25C b)

The pattern observed for this sample can be assigned to the gyroid morphology (space group: $Im\bar{3}d$).

TABLE S6 Spacings determined via SAXS and TEM measurements for P(I-co-S) tapered block copolymers. All values in nm.

[THF]/[Li]	$d^{a,b)}$	$d_{PI\ rich}^{a,c)}$	$d_{PS\ rich}^{a,c)}$	$d^{b,d)}$	$d_{PI\ rich}^{c,d)}$	$d_{PS\ rich}^{c,d)}$	Preferred staining reagent	Assigned morphology by SAXS (TEM)
0	n.d.	21.3	18.2	n.d.	16.8 ± 3.4	15.9 ± 2.5	OsO ₄	LAM (LAM)
0.5	37.0	n.d.	n.d.	30.3 ± 4.0	n.d.	14.2 ± 2.8	OsO ₄	HPC _{PS} (HPC _{PS})
80	n.d.	n.d.	n.d.	16.7 ± 2.1	9.9 ± 1.4	n.d.	RuO ₄	n.d. (HPC _{PI})
240	39.9	n.d.	n.d.	21.3 ± 2.3	13.4 ± 1.6	n.d.	RuO ₄	HPC _{PI} (HPC _{PI})
500	n.d.	n.d.	n.d.	n.d.	n.d.	n.d.	RuO ₄	BIC (see discussion)
2500	n.d.	n.d.	n.d.	n.d.	n.d.	n.d.	RuO ₄	BIC (gyroid)

a) Determined via SAXS; b) d : inter-cylinder distance in HPC morphology. c) Lamellar width or cylinder diameter. d) Determined via TEM.

9.3 Volume Considerations for P(I-co-S) Tapered Block Copolymers

As stated in the manuscript, the trend of the changes in the size of the pure terminal blocks (PS block: $F_{V,S} \geq 99.5\%$; PI block: $F_{V,S} \leq 0.5\%$, where $F_{V,S}$ is the instantaneous volume incorporation of styrene) is in qualitative agreement with the observed changes in morphologies based on the phase diagram known for PI-*b*-PS block copolymers.²⁸ However, the absolute volume fraction of the pure PS (or PI) block is not representative for the volume fraction of the PS (or PI) phase in the bulk state. As discussed in our previous works,^{1,3} not only the pure PS block, but also part of the gradient contributes to the observed PS-rich phase in the bulk state. In analogy, for the tapered PI block copolymers also a part of the gradient contributes to the observed PI-rich phase in the bulk state. Hence, taking the volume fraction of the pure PS (PI) block leads to an underestimate of the volume fractions of PS (PI) phases.

Estimation of the PI- and PS-rich Polymer Volumes

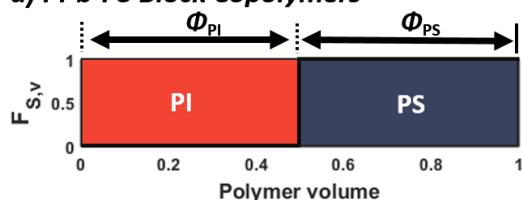
To estimate the PS- or PI-rich polymer volumes, $\Phi_{\text{PS-rich}}$ or $\Phi_{\text{PI-rich}}$, we locate the point in the polymer chain with a random incorporation of comonomers, because a random copolymer cannot show phase separation ($\chi_{\text{eff}} = 0$). For random copolymers the instantaneous monomer incorporation, F , corresponds to the monomer feed, f , independent of the total monomer conversion ($f = F$). Obviously, a deviation from the random incorporation (*i.e.* least repulsive interaction as $\chi_{\text{eff}} = 0$) leads to a PS-rich and PI-rich part ($\chi_{\text{eff}} > 0$). As a consequence, we define the transition from the PI-rich to the PS-rich part of the copolymer by the instantaneous monomer incorporation, achieved in a random copolymer for the given monomer feed f ($F = f$; this work: $f_S = f_I = 0.5$).

Considering the different molar volumes of the comonomer units, the block transition is defined as the polymer volume where $F_{V,S} \approx 0.57$ (Figure S25). As described in detail in the Supporting Information of our previous work, the domain sizes determined by TEM are suspected to underestimate the volume fraction of the PI-rich phase compared to values expected by polymer volume composition profile. This is explained by hampered OsO_4 staining, larger PS-contents in the PI-rich phase (successful staining estimated for $F_{V,S} \approx 0. \dots 0.43$).³

As seen in Figure S27 and Table S8 the size of the PI-rich part starts to increase with increasing $[\text{THF}]/[\text{Li}]$ ratio. This is explained by a flattening of the gradient, which shifts the point where $F_{V,S} = 57\%$ to larger polymer volumes (Figure S15). For $[\text{THF}]/[\text{Li}] = 20$ the value instantaneously decreases to $\approx 31\%$ caused by the inversion of the gradient (*i.e.* inversion of the PI- and PS-rich part in the polymer volume). For $[\text{THF}]/[\text{Li}] \geq 20$ the size PI-rich polymer volume increases again. This is explained by the gradient becoming steeper. Hence $F_{V,S} = 57\%$ shifts to smaller polymer volumes and increases $\Phi_{\text{PI-rich}}$. No values are given for $[\text{THF}]/[\text{Li}] = 4$ and 8, as one observes

a random incorporation of the monomer units. In this context we also want to note, that the gradient in $[\text{THF}]/[\text{Li}] = 2$ and 20 is rather weak, and no phase separation was evident in SAXS measurements for the molecular weight (80 kg/mol) investigated in this work. Nevertheless, these values are given for a better visualization.

a) PI-*b*-PS Block Copolymers



b) P(I-co-S) Tapered Block Copolymers: Block Transition defined at $F_{V,S} = f_v$

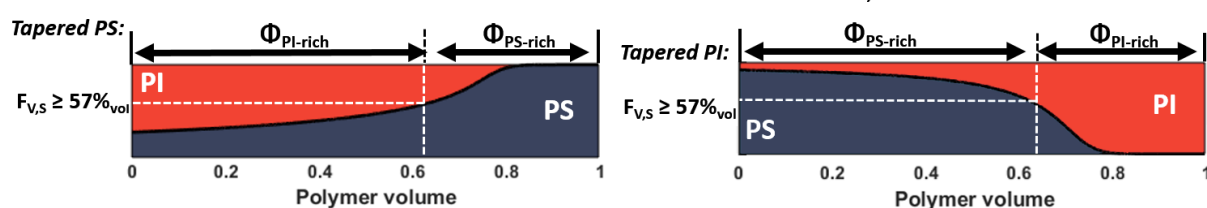


FIGURE S26 Evaluation of the volume fraction ($\Phi_{PI\text{-rich}}$) of the PI-rich part, by considering The $F_{V,S} = 0.57$ as block transition, which is the volume based value of $F_S = 0.5$. Examples based on Figure S15 (0.5 eq. and 500 eq. THF, respectively).

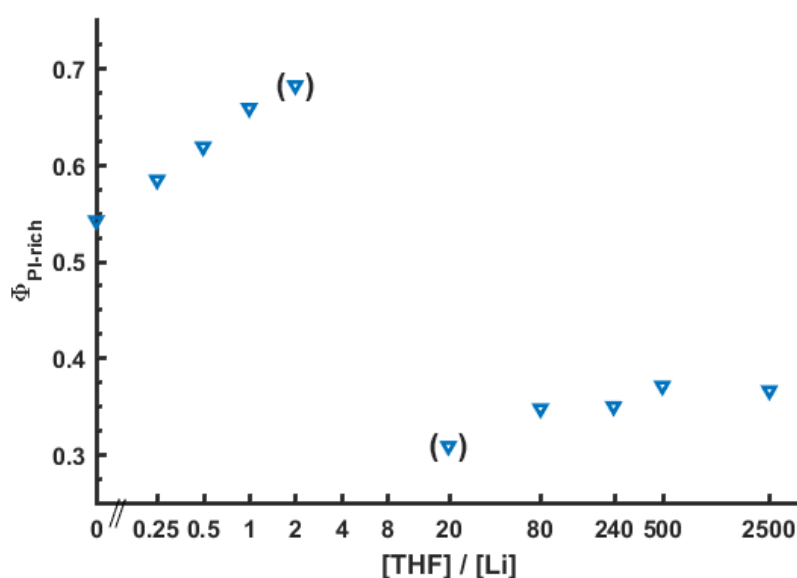


FIGURE S27 Volume fractions of the PI-rich parts in the P(I-co-S) samples.

9.4 Estimation of the Effective Flory-Huggins Parameter, χ_{eff} .

To estimate the effective Flory-Huggins Parameter of the P(I-co-S) copolymers, the reduction by the gradient structure as well as the influence of the increased vinyl-PI content was considered.

9.4.1 Effect of the Gradient Shape.

1) Determination of the PS content in the PI- and PS-rich volumes

To estimate χ_{eff} , the volume fractions of PS in the PI- or PS-rich parts of the polymer ($\Phi_{\text{PS in PI-rich}}$ and $\Phi_{\text{PS in PS-rich}}$, respectively) were calculated on the basis of the polymer volume composition (i.e. $F_{V,S}$ as a function of the polymer volume; see above discussion) as well as the volume fractions of the PI-rich phase ($\Phi_{\text{PI-rich}}$; Figure S26 and S27; Table S8).

For this purpose, the $F_{V,S}$ values were numerically integrated as given in Equations S9.1-S9.4.

PS tapered block copolymers:

$$\Phi_{\text{PS in PI-rich}} = \frac{\int_0^{\Phi_{\text{PI-rich}}} F_{V,S} dV_{\text{Polymer}}}{\Phi_{\text{PI-rich}}} \quad (\text{Equation S9.1})$$

$$\Phi_{\text{PS in PS-rich}} = \frac{\int_{\Phi_{\text{PI-rich}}}^1 F_{V,S} dV_{\text{Polymer}}}{1 - \Phi_{\text{PI-rich}}} \quad (\text{Equation S9.2})$$

PI tapered block copolymers:

$$\Phi_{\text{PS in PI-rich}} = \frac{\int_{\Phi_{\text{PI-rich}}}^1 F_{V,S} dV_{\text{Polymer}}}{1 - \Phi_{\text{PI-rich}}} \quad (\text{Equation S9.3})$$

$$\Phi_{\text{PS in PS-rich}} = \frac{\int_0^{\Phi_{\text{PI-rich}}} F_{V,S} dV_{\text{Polymer}}}{\Phi_{\text{PI-rich}}} \quad (\text{Equation S9.4})$$

Data are visualized in Figure S28 and given in Table S7.

2) Calculation of χ_{eff}

According to binary interaction theory,²⁹⁻³² Φ_{PS} of the PI- and PS-rich block (Figure S27) were used to calculate the relative reduction of the effective Flory Huggins-Parameter caused by the gradient structure ($\chi_{\text{eff,Gradient}}/\chi_{\text{IS}}$; Equation S9.5; Figure S29a; Table S8).

$$\frac{\chi_{\text{eff,Gradient}}}{\chi_{\text{IS}}} = (\Phi_{\text{PS in PS-rich}} - \Phi_{\text{PS in PI-rich}})^2 \quad (\text{Equation S9.5})$$

By increasing $[\text{THF}]/[\text{Li}]$ from 0 to 2, Φ_{PS} decreases for the PS-rich block and increases for the PI-rich block. This is attributed to the observed flattening of the gradient profile and the affiliated less block-like structure. This trend is inverted by a further increase of the $[\text{THF}]/[\text{Li}]$ ratio, explained by more block-like structures for increasing $[\text{THF}]/[\text{Li}]$ (compare to Figure S15). No values are given for $[\text{THF}]/[\text{Li}] = 4$ and 8 (random structures, discussed for Figure S27).

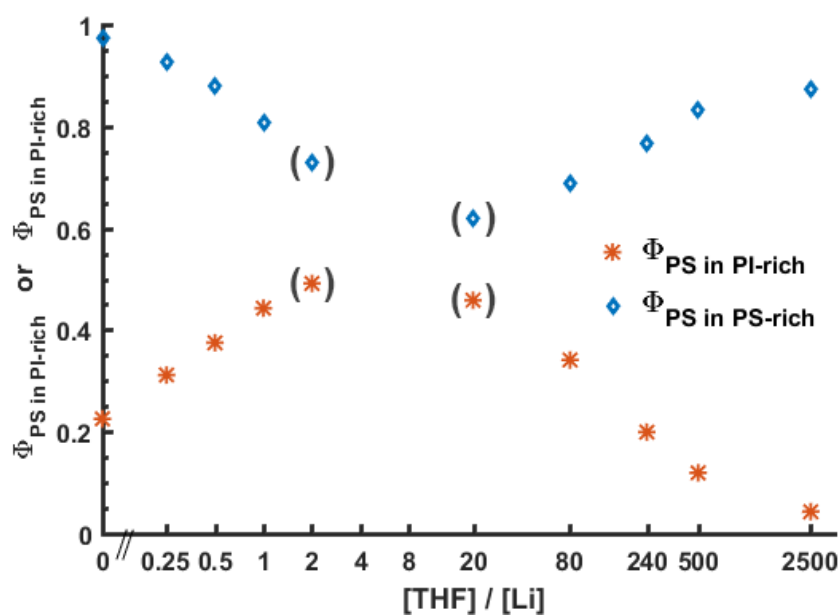


FIGURE S28 Volume fractions of PS (Φ_{PS}) in $\Phi_{\text{PI-rich}}$ and $\Phi_{\text{PS-rich}}$ parts, the latter determined as shown in Figure S26.

9.4.2 Influence of the Vinyl-PI Content.

To estimate differences in the Flory-Huggins parameters of the vinyl-PI units and styrene, the solubility parameters of 1,4, 3,4, and 1,2-PI and PS were calculated (Equation 9.6, Table S7) which enabled to estimate changes in the Flory-Huggins parameters (Equations 9.7-9.9).

TABLE S7 Calculation of Solubility Parameters by using the molar attraction constants of the increments (G).³³ Densities are based on data from Fetters *et al.*⁸

Parameter	PS	1,4-PI	3,4-PI	1,2-PI
G_1 [(cal·cm ³) ^{1/2} /mol]	735	133	214	133
G_2 [(cal·cm ³) ^{1/2} /mol]	111	19	19	-93
G_3 [(cal·cm ³) ^{1/2} /mol]	190	111	28	111
G_4 [(cal·cm ³) ^{1/2} /mol]	-	133	133	190
G_5 [(cal·cm ³) ^{1/2} /mol]	-	214	190	214
$\sum G$ [(cal·cm ³) ^{1/2} /mol]	1036	610	584	555
ρ [g/mL]	0.97	0.83	0.83	0.83
M [g/mol]	104.15	68.12	68.12	68.12

$$\delta = \frac{\rho}{M} \cdot \sum G \quad (\text{Equation S9.6})$$

$$\chi_{AB} = \frac{V_0}{RT} (\delta_A - \delta_B)^2 \quad (\text{Equation S9.7})$$

$$\frac{\chi_{3,4\text{-PI,PS}}}{\chi_{IS}} = 1.13 \quad (\text{Equation S9.8})$$

$$\frac{\chi_{1,2\text{-PI,PS}}}{\chi_{IS}} = 1.27 \quad (\text{Equation S9.9})$$

$$\frac{\chi_{\text{eff,Vinyl}}}{\chi_{IS}} = \frac{((n_{1,4\text{-PI}} + 0.05) \cdot \chi_{IS} + (n_{3,4\text{-PI}} - 0.05) \cdot \chi_{3,4\text{-PI,PS}} + n_{1,2\text{-PI}} \cdot \chi_{1,2\text{-PI,PS}})}{\chi_{IS}} \quad (\text{Equation S9.10})$$

where χ_{1S} refers to polyisoprene with 95%_{mol} 1,4 content²⁸ and V_0 is the geometric mean of the polymer segment molar volumes.³⁴

Hence, an increase of the effective Flory Huggins Parameter is estimated by the increasing proportion of the vinyl-PI content. Equations S9.8-S9.10 allow to estimate the values by weighting the respective Flory-Huggins Parameter to χ_{1S} . For this purpose, the molar fractions (n) of the PI isomers were used, as determined by NMR spectroscopy ($n_{1,4}$, $n_{3,4}$ and $n_{1,2}$ given in Table 3). A correction of 0.05 is applied, as χ_{1S} already exhibits a 3,4-PI content of 5%, as stated by Bates *et al.*²⁸ The result of both effects, the gradient (Section 9.4.1) as well as the vinyl content (this section), is visualized in Figure S29a.

9.4.3 Comparison with the Phase Diagram for PI-*b*-PS Block Copolymers

The Flory-Huggins parameter for 1,4-PI and PS, χ_{1S} , for $T=T_{g,PS-rich}$ was calculated according to Bates *et al.* (Equation S9.11) for $T=T_{g,PS-rich}$ ($T_{g,PS-rich}$ values are given in Table 2).²⁸ To estimate the effective Flory-Huggins parameter, Equation S9.12 was used to account for the reduction of the Flory-Huggins parameter by the gradient structure (Equation S9.5) and the increase by the vinyl-PI content (Equation S9.10).

$$\chi_{1S} = \frac{71.4}{T} - 0.0857 \quad (\text{Equation S9.11})$$

$$\chi_{eff} = \chi_{1S} \frac{\chi_{eff,Vinyl}}{\chi_{1S}} \cdot \frac{\chi_{eff,Gradient}}{\chi_{1S}} \quad (\text{Equation S9.12})$$

The total degree of polymerization ($N = 928$) was used to estimate $\chi_{eff} \cdot N$ (Table S8) and compare the $\Phi_{PI-rich}$ and $\chi_{eff} \cdot N$ with the phase diagram of Bates *et al.* found for PI-*b*-PS block copolymers (Figure S29b).

An interesting comparison can be made, by comparing $\chi_{eff} \cdot N$ (Table S8) and $\Phi_{PI-rich}$ (Figure S27 and Table S8) of the experimentally found morphologies (Table S8), with respect to the phase diagram found for PI-*b*-PS block copolymers (Figure S29b).²⁸ In theoretical works, Hall *et al.* systematically studied the effect of tapering on the phase diagram. For example, tapering was found to widen the bicontinuous gyroid region (Ia $\bar{3}d$ space group) of the phase diagram.³⁵ As discussed in the manuscript, the increased vinyl-PI content and the presence of PS in the PI-rich phase (*vide versa*), should also lead to a more symmetric phase diagram.

TABLE S8 Determined volume fractions and effective Flory-Huggins parameters (relative to PI-*b*-PS) for P(I-co-S) block copolymers.

[THF]/[Li]	$\Phi_{PI\ rich}^a$ [%]	$\Phi_{PS\ in\ PI\ rich}^b$ [%]	$\Phi_{PS\ in\ PS\ rich}^b$ [%]	$\chi_{eff,Gradient}/\chi_{IS}^c$	$\chi_{eff,Vinyl}/\chi_{IS}^c$	$\chi_{eff} \cdot N^c$ at $T=T_{g,PS\ rich}$	Morphology ^{d)}
0	54	23	97	0.56	1.00	60	LAM (LAM)
0.25	58	31	93	0.38	1.00	41	n.d. (TPC or TPL)
0.5	62	37	88	0.26	1.01	30	HPC _{PS} (HPC _{PS})
(1)	66	44	81	0.13	1.02	21	n.d. (n.d.)
(2)	68	49	73	0.06	1.03	8.6	(DIS) (n.d.)
(20)	31	46	62	0.03	1.05	3.8	(DIS) (n.d.)
80	35	34	69	0.12	1.07	19	n.d. (HPC _{PI})
240	35	20	76	0.32	1.09	47	HPC (HPC _{PI})
500	37	12	83	0.51	1.11	73	BIC (see discussion)
2500	37	4.3	87	0.69	1.11	93	BIC (gyroid)

a) Determined as illustrated in Figure S26 and visualized in Figure S27. b) Obtained according to Eq. S9.1-S9.4. Visualized in Figure S28. c) Obtained according to Equations S9.5-S9.8. Visualized in Figure S28b and S29. d) Morphologies determined via SAXS (TEM) experiments for the P(I-co-S) copolymers synthesized in this work.

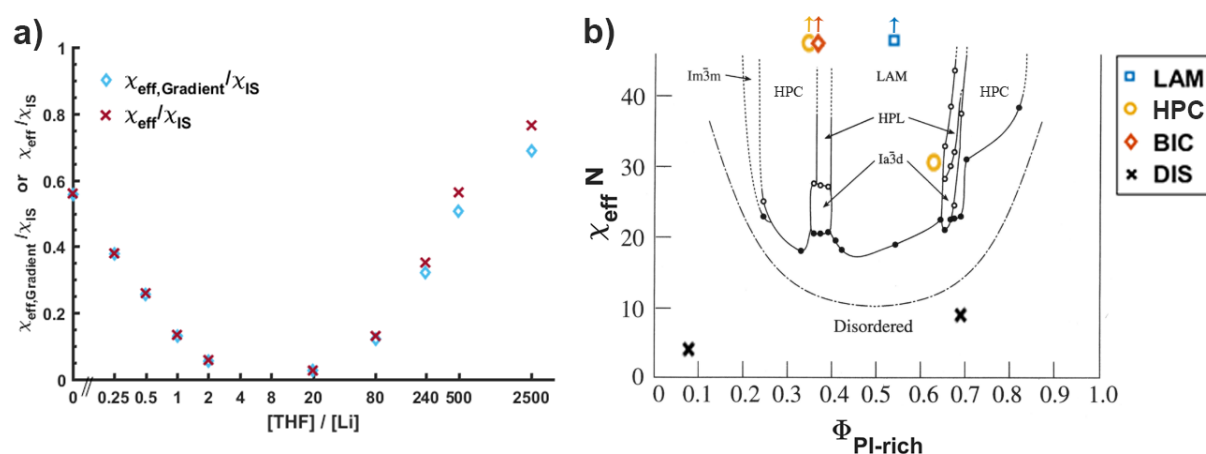


FIGURE S29 a) Relative reduction of the Flory-Huggins Parameter by the gradient structure as well as both by the gradient structure and the vinyl-PI content (Equation S9.12). b) Comparison of morphologies found for P(I-co-S) copolymers, with the phase diagram for PI-*b*-PS block copolymers published by Bates *et al.*²⁸ Reprinted (adapted) with the permission from Khandpur, A. K.; Förster, S.; Bates, F. S.; Hamley, I. W.; Ryan, A. J.; Bras, W.; Almdal, K.; Mortensen, K. *Macromolecules* **1995**, 28 (26), 8796–8806. DOI: 10.1021/ma00130a012. Copyright (2020) American Chemical Society.

Considering these differences, a reasonable agreement is found in respect to $\Phi_{PI-rich}$. However, the HPC-phase located at $\Phi_{PI-rich} \approx 62\%$ is found in the LAM state. As mentioned, this is possibly explained by a more symmetric phase diagram expected for P(I-co-S) copolymers. This would result in a shift of the HPC phase at $\Phi_{PI} \approx 0.70-0.85$ to lower values and a better agreement with the value found for respective HPC phase.

Based on the reduction of χ_{eff} by the gradient profile (section 9.4.1) and the increase of χ_{eff} estimated for an increasing vinyl-PI content (section 9.4.2), the absolute values of $\chi_{\text{eff}}N$ are widely spread (Table S7). In contrast to the phase diagram for PI-*b*-PS, we observe two BIC phases estimated at comparably high values of $\chi_{\text{eff}}N$ ($\chi_{\text{eff}}N$ (500 eq.) = 73; $\chi_{\text{eff}}N$ (500 eq.) = 93). This is tentatively explained by the widening of the BIC region, as reported by Hall.³⁵ Nevertheless, the estimate of $\chi_{\text{eff}}N$ can explain the disordered phase state found for [THF]/[Li]=2 and 20 ($\chi_{\text{eff}}N$ (2 eq.) = 8.6; $\chi_{\text{eff}}N$ (20 eq.) = 3.8).

Consequently, the concept of defining a block transition at ($F=f$) for the gradient structures is a reasonable strategy and can be used to roughly estimate the expected morphology and its dependence on the shape of the gradient. Care must be taken, as this concept has not yet proven to be sufficient for other monomer composition deviating from $f=0.5$ = equimolar feed, as investigated in this work. In addition, the comonomer sequence as well as the PI microstructure, are known to affect the phase diagram. Hence deviations from the classical PI-*b*-PS phase diagram are found.^{3,28,35,36}

10 MECHANICAL PROPERTIES

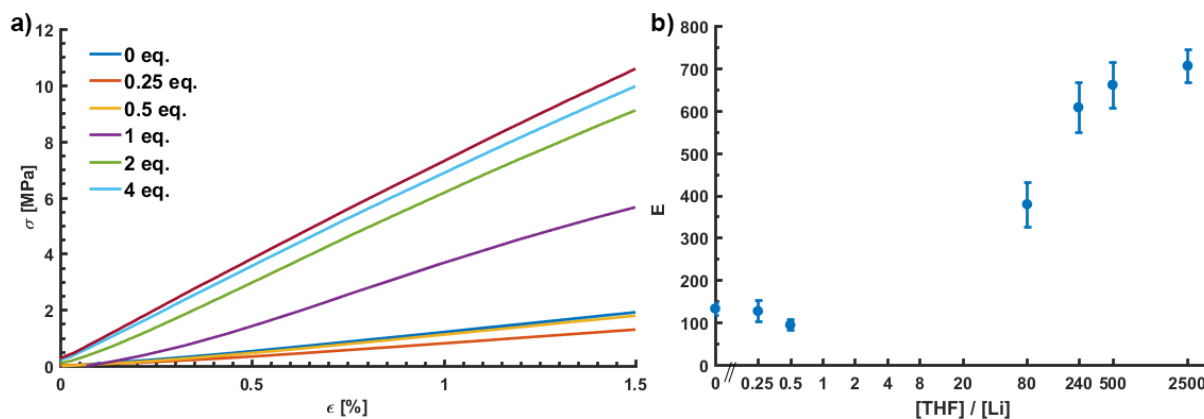


FIGURE S30 a) Linear regime of the σ - ϵ strain curves ($\epsilon < 1.5\%$), which was used to determine the Young's modulus, E , via linear fitting. b) Young's moduli as a function of the [THF]/[Li] ratio.

Increasing the [THF]/[Li] ratio from 0 to 0.5 leads to a decrease of the Young's modulus (E , Figure S30 and Table S9), explained by the formation of a continuous PI phase. No Young's moduli were determined for [THF]/[Li] = 1-20, as the samples are disordered, and the T_g approaches room temperature. Young's moduli determined for [THF]/[Li] = 80-2500, show much higher values compared to the [THF]/[Li] = 0-0.5 region. This is explained by the presence of a continuous high T_g PS phase for these samples. Hence, deformation indispensably leads to the deformation

of PS segments, possibly also affecting the reversibility of this deformation process at even low strains $\varepsilon \leq 1.5\%$.

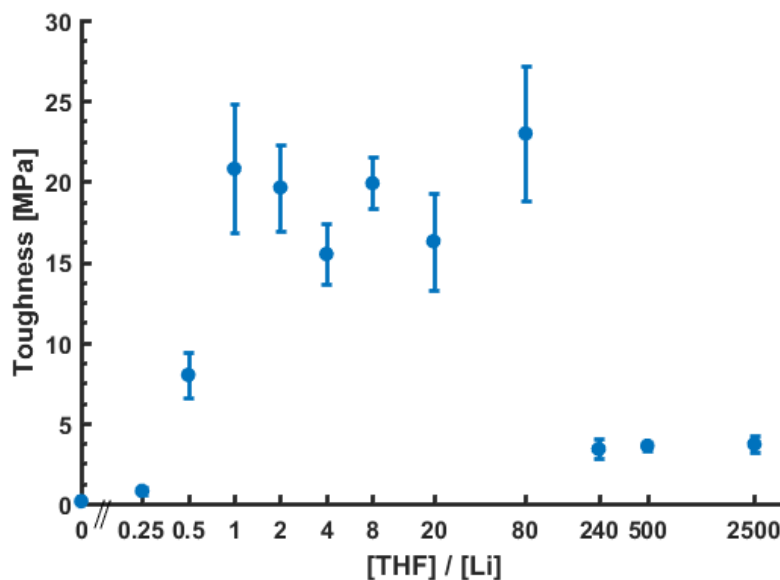


FIGURE S31 Toughness as a function of the [THF]/[Li] ratio. The toughness was obtained by numerical integration of the σ - ε curves.

The toughness (Figure S31) shows comparatively high values for $[\text{THF}]/[\text{Li}] \approx 1$ -80. These large values are explained by the relatively large region of viscoelastic flow, exceeding the yield-strain point, $\varepsilon_{\text{yield}}$, by far (Figure 9), leading to a dissipation of the induced strain by irreversible flow.

The strong increase of $\varepsilon_{\text{yield}}$ (Figure 32) by increasing $[\text{THF}]/[\text{Li}]$ from 0 to 0.5 is tentatively explained by a change of the morphology from lamellar to a continuous PI phase (PS cylinders). This is expected to enable further stretching of the material without breaking the glassy domains (*i.e.* yield point). Hence, rather low values of $\varepsilon_{\text{yield}}$ for $[\text{THF}]/[\text{Li}] = 80$ -2500 are caused by the formation of a vitrified continuous PS phase.

The yield stress (σ_{yield}) shows an inverted trend compared to the yield strain: For $[\text{THF}]/[\text{Li}] = 0$ -0.5 low values for σ_{yield} were obtained. This corresponds to a low force necessary to break the PS phase (minor fraction). For $[\text{THF}]/[\text{Li}] = 80$ -2500 the forces continuously increase, as the continuity of the PS phase is increased (Cylinder = 2D phase, BIC = 3D phase), as well as the volume fraction of the PS-rich phase (major fraction).

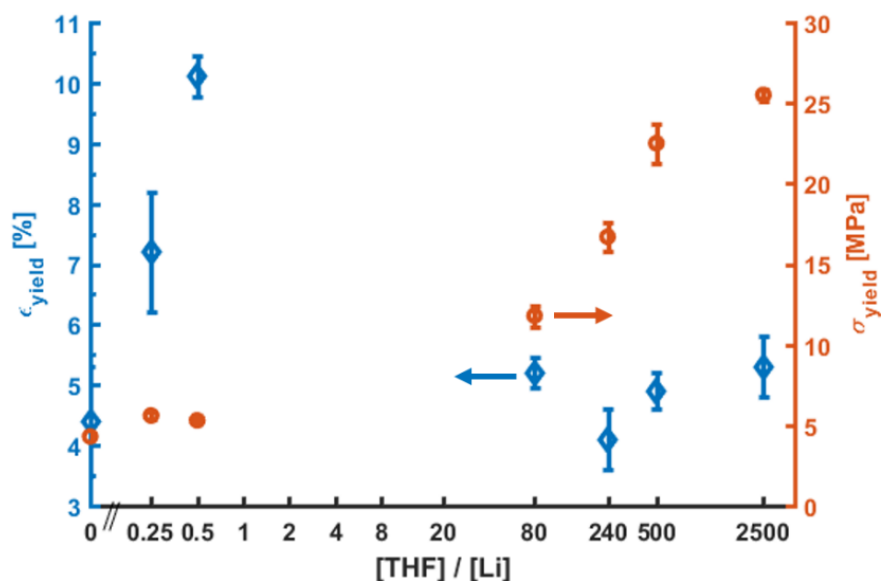


FIGURE S32 Yield Strain, ϵ_{yield} , and yield stress, σ_{yield} , as a function of the [THF]/[Li] ratio.

TABLE S9 Mechanical Properties determined by uniaxial drawing experiments.

[THF]/[Li]	E [MPa] ^{a)}	Toughness [MPa] ^{b)}	ϵ_{yield} [%] ^{c)}	σ_{yield} [MPa] ^{c)}
0	130 ± 16	0.16 ± 0.01	4.4 ± 0.9	4.3 ± 0.1
0.25	130 ± 25	0.80 ± 0.20	7.2 ± 1.0	5.6 ± 0.2
0.5	94 ± 12	8.0 ± 1.4	10 ± 0.3	5.3 ± 0.1
1	n.d. ^{d)}	21 ± 4.0	n.d. ^{e)}	n.d. ^{e)}
2	n.d. ^{d)}	20 ± 2.7	n.d. ^{e)}	n.d. ^{e)}
4	n.d. ^{d)}	16 ± 1.9	n.d. ^{e)}	n.d. ^{e)}
8	n.d. ^{d)}	20 ± 1.6	n.d. ^{e)}	n.d. ^{e)}
20	n.d. ^{d)}	16 ± 3.0	n.d. ^{e)}	n.d. ^{e)}
80	380 ± 53 ^{f)}	23 ± 4.2	5.2 ± 0.3	12 ± 0.7
240	610 ± 59 ^{f)}	3.4 ± 0.60	4.1 ± 0.5	17 ± 0.9
500	660 ± 53 ^{f)}	3.6 ± 0.30	4.9 ± 0.3	23 ± 1.2
2500	710 ± 40 ^{f)}	3.7 ± 0.40	5.3 ± 0.5	16 ± 0.4

a) Determined by linear fitting of the σ - ϵ curves at $\epsilon \leq 1.5\%$ (Figure S_{Tensile}1). b) Determined by numerical integration of the σ - ϵ curves. c) The yield point ($\epsilon_{\text{yield}}/\sigma_{\text{yield}}$) was determined as the maximum in σ for $\epsilon \leq 10\%$. d) No Young's moduli were determined, as these samples are in the disordered state, as well as they exhibit a T_g in proximity to room temperature. Therefore, no full reversibility for drawing the sample in the region $\epsilon \leq 1.5\%$ was observed. This is supported by the non-linearity observed in the σ - ϵ curves. e) Samples are disordered and do not exhibit glassy domains. Therefore, no yield point is observed. f) As these samples exhibit a continuous, glassy, high T_g phase, drawing in this region is expected to be accompanied by irreversible viscous flow.

11 Outlook: THF modified I/S Copolymers as Building Blocks for TPEs

Although "randomizing agents" have proven efficient in the modification of copolymerization kinetics (*i.e.* the resulting copolymer composition, decreasing χ_{eff}), multi-step polymerization in the presence of polar additives is not straightforward and only rarely described. Adding monomer to the living polymer solution (*i.e.* multi-step synthesis) can be regarded as a re-initiation process which requires good mixing (*i.e.* homogenous initiation; see Figure S1) depending on the rate of polymerization.^{37,38} However, the synthetic challenge is evident with respect to the accelerated polymerization rates in the presence of THF (in particular for styrene; Figures S12 and S13): the resulting evolution of reaction heat (self-acceleration) and the comparably high viscosity of concentrated, high molecular weight polymer solutions.⁷ In addition, the lack of aggregation constants of the anionic chain-ends (Supporting Information, section 4) hampers the calculation of reaction times.^{1,3} These are crucial, as the desired block sequence can only be obtained by postponing the monomer addition until the majority of the previous addition step has been completed (see Figure S32).¹

NIR Tracking of Consecutive Addition Steps

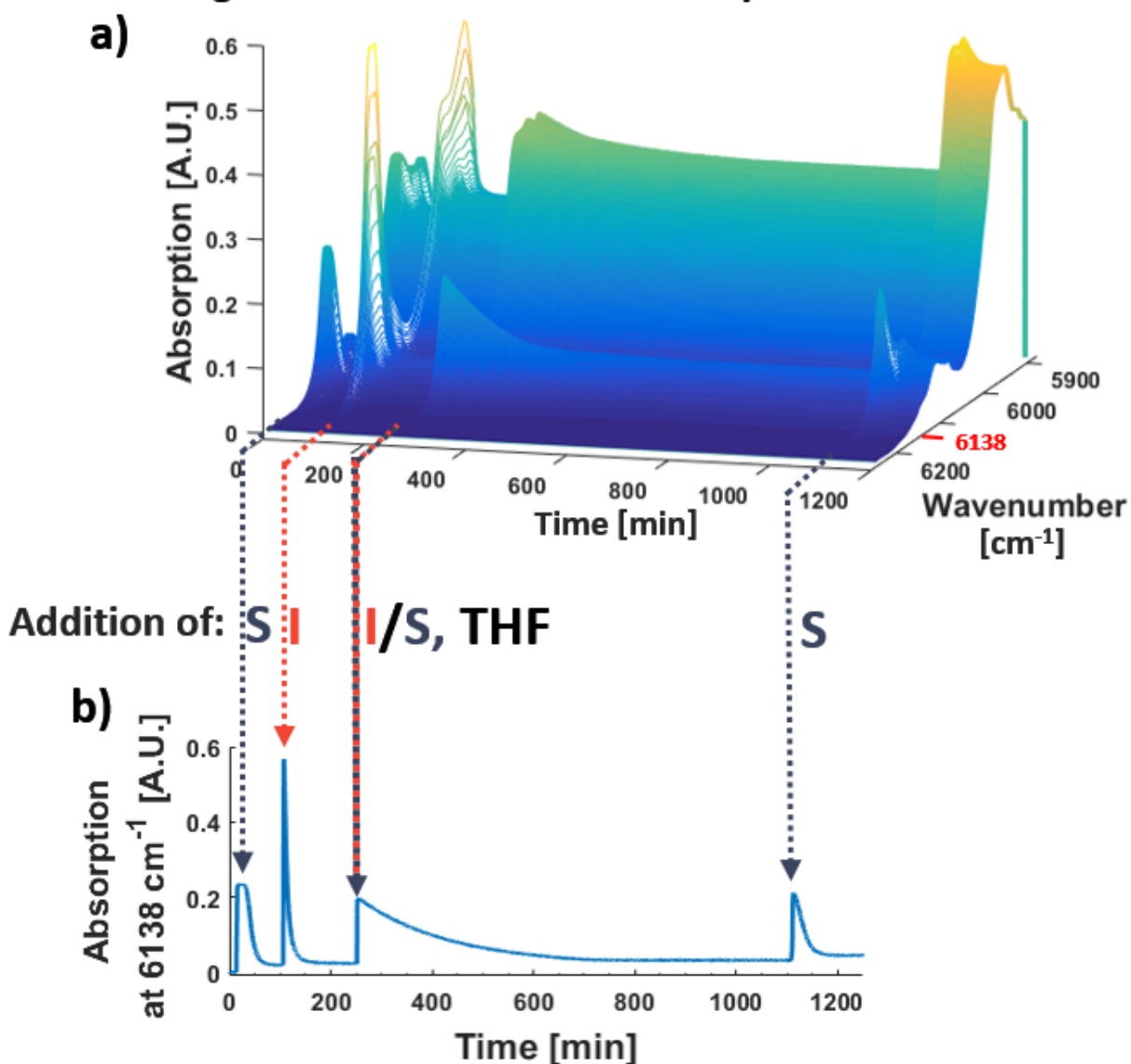


FIGURE S33 Tracking of the NIR absorbance during the synthesis of the tapered triblock copolymer. a) Time dependent absorption in the NIR range, typically used for data evaluation (compare to Figure S4). The consecutive addition monomer addition steps are listed below. b) For better visualization the absorption at a single wavelength (6138 cm⁻¹) is given as function of the time. The applied temperature program as well as a detailed description of the synthetic procedure and the measurement is given in sections 1.3 and 2.1.

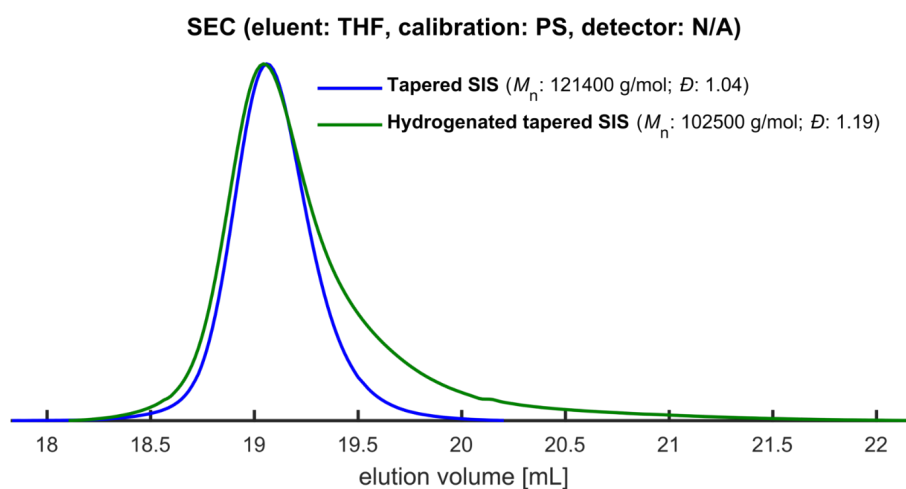


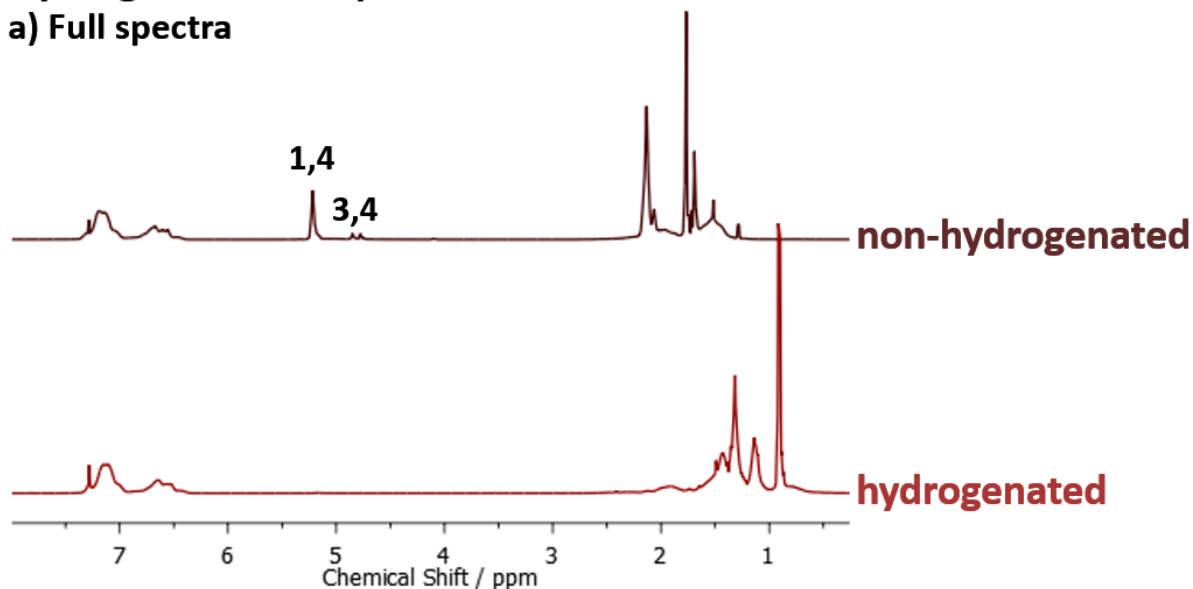
FIGURE S34 SEC measurements and determined molecular weights (RI detector, PS standard) of the tapered SIS triblock copolymer as well as its hydrogenated product. The results are discussed below.

Hydrogenated tapered SIS triblock Copolymer

A slight shift of the maximum in the elugram towards lower values (*i.e.* higher molecular weights) is observed (Figure S33). This is explained by the increase of the molecular weight by the hydrogenation of the PI units and is in accordance with literature.³⁹ Furthermore, the SEC trace exhibits a slight tailing towards higher elution volume (*i.e.* small molecular weight). This is explained by a certain extend of chain degradation, also described in literature.⁴⁰ This leads to the minor decrease in M_n and increase in dispersity (\mathcal{D}).

Hydrogenation – tapered SIS triblock

a) Full spectra



b) Zoom: Olefinic Signals

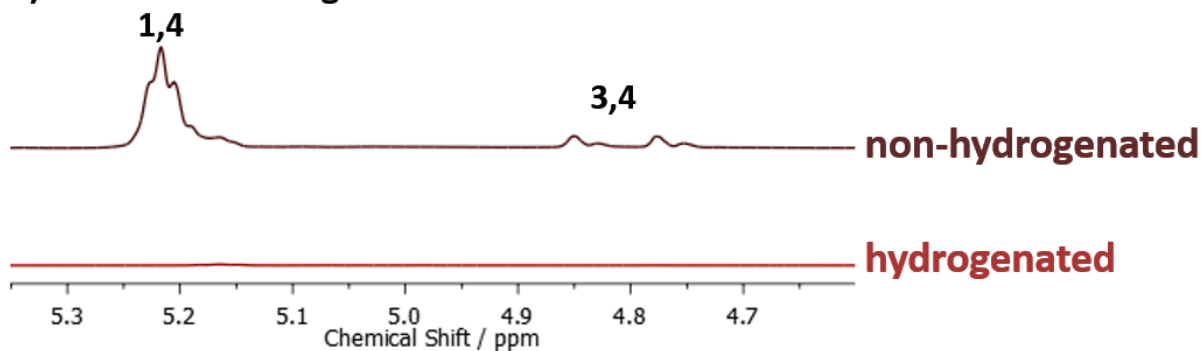


FIGURE S35 ^1H NMR (CDCl_3 , 400 MHz) spectra of the tapered SIS block copolymer as well as the hydrogenation product. The results are discussed below. The 1,4-PI content was determined via ^1H NMR spectroscopy, integrating the well-separated signals of 1,4 and 3,4-PI (Table 2). The degree of hydrogenation was determined to be $\geq 99\%$ by evaluating the relative depletion of the olefinic signals referred to the *ortho* proton signal of PS (Table S2).

11 REFERENCES

- (1) Steube, M.; Johann, T.; Galanos, E.; Appold, M.; Rüttiger, C.; Mezger, M.; Gallei, M.; Müller, A. H. E.; Floudas, G.; Frey, H. *Macromolecules* **2018**, 51 (24), 10246–10258. DOI: 10.1021/acs.macromol.8b01961.
- (2) Elschenbroich, C. *Organometallchemie*, 6., überarb. Aufl.; Teubner-Studienbücher Chemie; Vieweg+Teubner Verlag/GWV Fachverlage GmbH Wiesbaden: Wiesbaden, 2008.
- (3) Steube, M.; Johann, T.; Plank, M.; Tjaberings, S.; Gröschel, A. H.; Gallei, M.; Frey, H.; Müller, A. H. E. *Macromolecules* **2019**, 52 (23), 9299–9310. DOI: 10.1021/acs.macromol.9b01790.
- (4) Fulmer, G. R.; Miller, A. J. M.; Sherden, N. H.; Gottlieb, H. E.; Nudelman, A.; Stoltz, B. M.; Bercaw, J. E.; Goldberg, K. I. *Organometallics* **2010**, 29 (9), 2176–2179. DOI: 10.1021/om100106e.
- (5) Kolling, O. W. *Transactions of the Kansas Academy of Science* **1991**, 94 (3/4), 107. DOI: 10.2307/3627858.
- (6) Morton, M.; Fetters, L. J. *J. Polym. Sci. A: Gen. Pap.* **1964**, 2 (7), 3311–3326. DOI: 10.1002/pol.1964.100020726.
- (7) Bywater, S.; Worsfold, D. J. *Can. J. Chem.* **1962**, 40 (8), 1564–1570. DOI: 10.1139/v62-236.
- (8) Fetters, L. J.; Lohse, D. J.; Richter, D.; Witten, T. A.; Zirkel, A. *Macromolecules* **1994**, 27 (17), 4639–4647. DOI: 10.1021/ma00095a001.
- (9) Chen, H. Y. *Anal. Chem.* **1962**, 34 (9), 1134–1136. DOI: 10.1021/ac60189a032.
- (10) Worsfold, D. J.; Bywater, S. *Can. J. Chem.* **1964**, 42 (12), 2884–2892. DOI: 10.1139/v64-426.
- (11) Hsieh, H. L.; Quirk, R. P. *Anionic Polymerization: Principles and Practical Applications*; Plastics Engineering 34; Dekker: New York, 1996.
- (12) Tanaka, Y.; Takeuchi, Y.; Kobayashi, M.; Tadokoro, H. *J. Polym. Sci. B* **1971**, 9 (1), 43–57. DOI: 10.1002/pol.1971.160090104.
- (13) Tanaka, Y.; Sato, H.; Seimiya, T. *Polym. J.* **1975**, 7 (2), 264–266. DOI: 10.1295/polymj.7.264.
- (14) Gronski, W.; Murayama, N.; Cantow, H.-J.; Miyamoto, T. *Polymer* **1976**, 17 (4), 358–360. DOI: 10.1016/0032-3861(76)90199-3.
- (15) Tanaka, Y. *Polymer* **1976**, 17 (2), 113–116. DOI: 10.1016/0032-3861(76)90078-1.
- (16) Tanaka, Y.; Sato, H.; Ogura, A.; Nagoya, I. *J. Polym. Sci. Polym. Chem. Ed.* **1976**, 14 (1), 73–81. DOI: 10.1002/pol.1976.170140107.
- (17) Beebe, D. H. *Polymer* **1978**, 19 (2), 231–233. DOI: 10.1016/0032-3861(78)90049-6.
- (18) Sato, H.; Tanaka, Y. *Rubber Chem. Technol.* **1980**, 53 (2), 305–312. DOI: 10.5254/1.3535042.
- (19) Rozentsvet, V. A.; Khachaturov, A. S.; Ivanova, V. P. *Polym. Sci. Ser. A* **2009**, 51 (8), 870–876. DOI: 10.1134/S0965545X09080045.
- (20) Forens, A.; Roos, K.; Dire, C.; Gadenne, B.; Carlotti, S. *Polymer* **2018**. DOI: 10.1016/j.polymer.2018.07.071.
- (21) Bovey, F. A.; v. d. Tiers, G.; Filipovich, G. *J. Polym. Sci.* **1959**, 38 (133), 73–90. DOI: 10.1002/pol.1959.1203813308.
- (22) Mochel, V. D. *Macromolecules* **1969**, 2 (5), 537–540. DOI: 10.1021/ma60011a017.
- (23) Harwood, H. J.; Chen, T.-K.; Lin, F.-T. In *Initiation of polymerization: ACS Polymer Symposia*; Bailey, F. E., Ed.; ACS Symposium Series 212; American Chemical Society: Washington, DC, 1983; pp 197–222.
- (24) Handlin, D. L.; Williamson, D. T.; Willis, C. L. Block copolymer. 6,699,941, Nov 7, 2002.
- (25) Grune, E.; Johann, T.; Appold, M.; Wahlen, C.; Blankenburg, J.; Leibig, D.; Müller, A. H. E.; Gallei, M.; Frey, H. *Macromolecules* **2018**, 51 (9), 3527–3537. DOI: 10.1021/acs.macromol.8b00404.

- (26) Schmalz, H.; Böker, A.; Lange, R.; Krausch, G.; Abetz, V. *Macromolecules* **2001**, *34* (25), 8720–8729. DOI: 10.1021/ma010875d.
- (27) Hadjichristidis, N.; Pispas, S. In *Ordered Polymeric Nanostructures at Surfaces*; Vancso, G. J., Ed.; Advances in Polymer Science; Springer Berlin Heidelberg: Berlin, Heidelberg, 2006; pp 37–55.
- (28) Khandpur, A. K.; Förster, S.; Bates, F. S.; Hamley, I. W.; Ryan, A. J.; Bras, W.; Almdal, K.; Mortensen, K. *Macromolecules* **1995**, *28* (26), 8796–8806. DOI: 10.1021/ma00130a012.
- (29) Watanabe, H.; Matsumiya, Y.; Sawada, T.; Iwamoto, T. *Macromolecules* **2007**, *40* (19), 6885–6897. DOI: 10.1021/ma0712495.
- (30) Roe, R.-J.; Zin, W.-C. *Macromolecules* **1980**, *13* (5), 1221–1228. DOI: 10.1021/ma60077a037.
- (31) Brinke, G. ten; Karasz, F. E.; MacKnight, W. J. *Macromolecules* **1983**, *16* (12), 1827–1832. DOI: 10.1021/ma00246a006.
- (32) Paul, D. R.; Barlow, J. W. *Polymer* **1984**, *25* (4), 487–494. DOI: 10.1016/0032-3861(84)90207-6.
- (33) Small, P. A. *J. Appl. Chem.* **1953**, *3* (2), 71–80. DOI: 10.1002/jctb.5010030205.
- (34) Mark, J. E. *Physical Properties of Polymer Handbook*, 2nd ed.; Springer: New York, 2006.
- (35) Brown, J. R.; Sides, S. W.; Hall, L. M. *ACS Macro Lett.* **2013**, *2* (12), 1105–1109. DOI: 10.1021/mz400546h.
- (36) Förster, S.; Khandpur, A. K.; Zhao, J.; Bates, F. S.; Hamley, I. W.; Ryan, A. J.; Bras, W. *Macromolecules* **1994**, *27* (23), 6922–6935. DOI: 10.1021/ma00101a033.
- (37) Gold, L. *J. Chem. Phys.* **1958**, *28* (1), 91–99. DOI: 10.1063/1.1744088.
- (38) *Anionic polymerization: Principles, practice, strength, consequences and applications*; Hadjichristidis, N., Hirao, A., Eds.; Springer: Tokyo, 2015.
- (39) Ashraf, A. R.; Ryan, J. J.; Satkowski, M. M.; Smith, S. D.; Spontak, R. J. *ACS Appl. Mater. Interfaces* **2018**, *10* (4), 3186–3190. DOI: 10.1021/acsami.7b19433.
- (40) Hahn, S. F. *J. Polym. Sci. A* **1992**, *30* (3), 397–408. DOI: 10.1002/pola.1992.080300307.

APPENDIX

CHAIN RELAXATIONS IN TAPERED MULTIBLOCK COPOLYMERS

APPENDIX

Published in *Macromolecules* 2020, 53, 3042-3051

DOI: 10.1021/acs.macromol.0c00445

Local and Subchain Relaxation of Polyisoprene in Multiblock Copolymers with a Tapered Interface

Chrysoula Livitsanou¹, Marvin Steube², Tobias Johann², Holger Frey^{2*} and George Floudas^{1,3,4*}

¹Department of Physics, University of Ioannina, 451 10 Ioannina, Greece

²Department of Chemistry, Johannes Gutenberg-University, 55128 Mainz, Germany

³Institute of Materials Science and Computing, 451 10 Ioannina, Greece

⁴Max Planck Institute for Polymer Research, 55128 Mainz, Germany

This work is closely connected to the investigations in chapter 1, which deals with the multi-step copolymerization of styrene and isoprene as well as the material properties of the resulting tapered multiblock copolymers. The author of this thesis contributed to this work by theoretical investigations, such as performing kMC simulations to predict the experimental outcome of the multiblock synthesis by evaluating the segment length distributions.

Local and Subchain Relaxation of Polyisoprene in Multiblock Copolymers with a Tapered Interface

Chrysoula Livitsanou, Marvin Steube, Tobias Johann, Holger Frey,* and George Floudas*

Cite This: *Macromolecules* 2020, 53, 3042–3051

Read Online

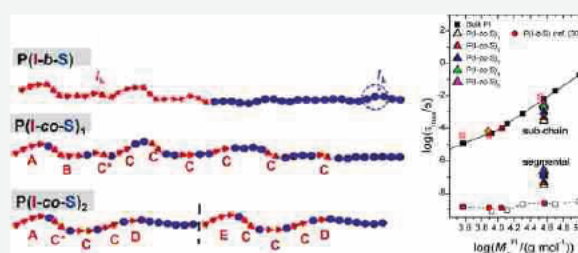
ACCESS |

Metrics & More

Article Recommendations

Supporting Information

ABSTRACT: We report on the local and (sub) chain dynamics in a new class of tapered multiblock copolymers synthesized by the repeated statistical living anionic copolymerization of a mixture of isoprene and styrene $P(I\text{ co }S)_n$ as well as a mixture of isoprene with 4-methylstyrene $P(I\text{ co }4MS)_n$ with up to 10 blocks ($1 \leq n \leq 5$). Unlike ordinary diblock copolymers, these multiblock copolymers have a broad interface but at the same time exhibit superior mechanical properties because of the multiblock structure. We employ dielectric spectroscopy aiming at the local and chain dynamics of polyisoprene (PI). To this end, we compare and contrast tapered multiblock copolymers to homopolymers and sequential diblock copolymers, exploiting the distinctive dynamic behavior of PI. Dielectric spectroscopy probes mainly the Rouse dynamics of the PI subchain with the free end and provides an “effective” PI chain length, participating in the dynamics. The estimated PI chain lengths in the tapered di- and multiblock architectures are in qualitative agreement with the lengths obtained by oxidative degradation experiments and by independent Monte Carlo simulations. A quantitative comparison revealed considerably longer chain lengths by dielectric spectroscopy (by nearly a factor of 6). The consistently smaller molecular weight in the simulation could result from an overestimation (underestimation) of the reactivity ratios of S (I) units.



1. INTRODUCTION

Block copolymers are known to exist in a disordered or in an ordered, nanophase separated state. The latter is the most prominent feature of block copolymers composed of immiscible segments that inspired several studies as a function of the interaction parameter, chain length, composition, segment length asymmetry, and polymer topology.^{1–5} The transition from the ordered to the disordered state, known as order to disorder transition (ODT), is characterized as a fluctuation driven first order, even in the case of diblock copolymers with symmetric composition.⁶ The resulting nanodomain structures as well as their effect on the physical and the mechanical properties have been extensively studied before, especially in the case of the polyisoprene *b* polystyrene (PI *b* PS) diblock copolymers.^{7–9} In recent years, there is motivation to develop new thermoplastic elastomers¹⁰ based on flexible/glassy blocks that combine a controlled phase state—spanning from weakly segregated to strongly segregated—with high toughness. The latter can be accomplished by the synthesis of tapered or gradient copolymers. Of particular interest have been tapered multiblock copolymers where the number of blocks affects the chain conformations and concomitantly the thermomechanical properties.^{11–20} There, the repeated statistical living anionic copolymerization afforded tapered block copolymers based on the extremely slow crossover from isoprene to the styrenic monomer.^{20–22} Subsequent structural studies revealed that tapered multiblock

copolymers of isoprene and styrene as well as of isoprene and 4-methylstyrene exhibit some differences in domain spacings when compared to the sequential ones. The molecular weight dependence of the domain spacing ($d \approx N^\delta$) scales as $\delta \approx 0.62$ for $P(I\text{ co }S)_n$ and as $\delta \approx 0.55 \pm 0.02$ for $P(I\text{ co }4MS)_n$, suggesting stretched chains with nonideal (Gaussian) configurations ($\delta \approx 1/2$), as with sequential diblock copolymers.^{21,22} However, tapered multiblock copolymers of $P(I\text{ co }S)_n$ showed different domain spacings when compared at a fixed overall molecular weight with increasing number of blocks, n , scaling as $d \approx n^{-0.83 \pm 0.02}$. On the other hand, the domain spacing at a fixed block length was found to scale as $d \approx n^{-0.75}$. The reduction in domain spacing by increasing the number of blocks, both at a fixed overall molecular weight and at a fixed block length, is anticipated by the conformational properties of the middle blocks, that is, the loop formation.^{21–23}

The type A dipoles of $PI^{24–29}$ —that provide simultaneous access to the local and global dynamics of PI—have been utilized to investigate the PI dynamics in PI *b* PS diblock

Received: February 25, 2020

Revised: March 29, 2020

Published: April 9, 2020



Table 1. Molecular Characteristics of the Tapered Multiblock Copolymers P(I-co-S)

sample	target M_n [kg mol ⁻¹]	# of blocks	target M_n (AB-unit) [kg mol ⁻¹]	M_n (SEC) ^a [kg mol ⁻¹]	$\bar{D} = M_w/M_n^a$
P(I-co-S) ₁	80	2	80	92	1.07
P(I-co-S) ₂	80	4	40	86	1.08
P(I-co-S) ₃	80	6	27	87	1.06
P(I-co-S) ₄	80	8	20	82	1.06
P(I-co-S) ₅	80	10	16	83	1.09
P(I-co-S) ₃	240	6	80	268	1.13
P(I-co-S) ₅	400	10	80	515	1.28

^aDetermined by size exclusion chromatography (SEC) at 25 °C in tetrahydrofuran. Values are based on PS calibration.

copolymers by dielectric spectroscopy (DS).^{30–45} A number of experiments in ordered block copolymer morphologies reported shifts in either or both the normal and segmental processes relative to their homopolymer counterparts depending on the type of confinement (soft vs hard).^{30,31,46–50} In the case of hard confinement where the soft PI blocks are constrained by the glassy PS domains, three temperature regimes could be distinguished. At temperatures below the glass temperature of the PS domains ($T < T_g^{PS}$), one PI chain end is spatially fixed at the interface with the glassy PS segments. As a result, the dynamics of the PI chains are somewhat slower and much broader than in the homopolymer. The latter feature was discussed in terms of the *spatial confinement* by the glassy PS domain and the *thermodynamic constraints* on PI to maintain a uniform density.³⁰ At temperatures in the vicinity of the T_{ODT} ($T \leq T_{ODT}$), the relaxation spectrum was affected by the composition fluctuations of the blocks.³¹ Finally, at $T > T_{ODT}$, local mixing of segments is expected to affect both the time scale and broadening of the chain dynamics.

Herein, we explore the effect of the tapered interface on the segmental and chain dynamics of PI in the disordered as well as in the ordered states. The local and, more importantly, the global chain dynamics in multiblock copolymers with a tapered interface are essential in understanding their unique thermomechanical properties including their use as thermo plastic elastomers. In these copolymers, the length and the configuration of subchains formed during copolymerization dictate the elastomeric properties. Despite this, there is not even a single investigation on the dynamics of such copolymers. In addition, predicting the local and global chain dynamics in copolymers with complex topologies—as in multiblock copolymers with a tapered interface—constitutes a challenge for every experimental polymer physicist. DS allows the selective probing of the PI dynamics using the weak PI dipole moment ($\mu = 0.29$ debye²⁵) as an intrinsic label. Two cases of tapered multiblock copolymers are considered: (a) with a fixed overall molecular weight by increasing the number of blocks and (b) with a constant block length by increasing the number of blocks. The results on the phase state and dynamics are compared with PI *b* PS, prepared sequentially. In both cases, because of the special tapered interface, I segments are interrupted by S segments. In this topology, although all I segments are capable of performing local segmental motion as evidenced by the segmental process, only a fraction of I segments can participate in the longer Rouse type chain dynamics. We found that in copolymers with a tapered interface, DS probes the sub Rouse dynamics of the longer PI segments with a free end. By comparison of the PI *b* PS block copolymer and PI homopolymer relaxation times, we obtain the *effective* length of PI chains participating in the sub Rouse

dynamics. The extracted lengths are compared to the PI lengths obtained chemically (by oxidative degradation) and by independent Monte Carlo simulations. Although both experiment and simulation suggest a shorter sub Rouse chain participating in the dynamics, the effective length of PI chains was considerably longer in the experiment (by nearly a factor of 6). The smaller molecular weight in the simulation could result from an overestimation (underestimation) of the reactivity ratios of S (I) units.

2. EXPERIMENTAL SECTION

2.1. Samples. In this work, we focus on the study of symmetric tapered multiblock copolymers consisting of equimolar amounts of both monomers, translating to 43% volume PI and 57% volume PS as well as 40% volume PI and 60% volume poly(4-methylstyrene), respectively. The synthesis and characterization of the tapered copolymers were recently reported.^{21,22} Because of the incorporation of styrene units during the formation of the isoprene-rich block, this first block expands in volume, while the second pure PS [poly(4-methylstyrene)] block shrinks. Three constant molecular weight series of tapered I/S multiblock copolymers with approximate molecular weights of 80, 240, and 400 kg mol⁻¹ and with narrow molecular weight distribution were prepared, covering a broad range of segment architectures, ranging from diblock to decablock copolymers for each series. The molecular characteristics for the P(I-co-S)_{*n*} system are provided in Table 1. The respective data for the P(I-co-4MS)_{*n*} systems are provided in Table S1 (Supporting Information).

2.2. Differential Scanning Calorimetry. The thermal properties of the sequential diblock copolymer and tapered multiblock copolymers were studied with a Q2000 (TA Instruments) differential scanning calorimeter. The instrument was calibrated for the baseline using a sapphire standard, for the enthalpy and temperature using indium as a standard, and for the heat capacity using sapphire as a standard. Two cooling and heating cycles were performed at a rate of 10 K min⁻¹ in a temperature range between 173 and 433 K, and the glass temperatures were extracted from the second cycle. In addition, two cooling and heating cycles were performed at rates of 20, 10, and 5 K min⁻¹ in order to determine the T_{ODT} and the corresponding enthalpy change, ΔH_{ODT} .

2.3. Temperature-Modulated Differential Scanning Calorimetry. Temperature-modulated differential scanning calorimetry (TM-DSC) measurements were made with a Q2000 (TA Instruments) using cooling/heating rates in the range of 10⁻¹ K min⁻¹ and oscillation periods from 20 to 200 s. A specific rate/period pair was employed for each measurement according to

$$\beta = \frac{\Delta T_g}{cP} 60 \text{ s/min} \quad (1)$$

Here, β is the cooling/heating rate, ΔT_g is the full width at half-height of T_g , c is the number of cycles across the T_g width, and P is the oscillation period. The rate/period pairs used in this study were as follows: 20 s, 10 K min⁻¹; 40 s, 5 K min⁻¹; 60 s, 3.3 K min⁻¹; 80 s, 2.4 K min⁻¹; 100 s, 2 K min⁻¹; 150 s, 1.3 K min⁻¹; and 200 s, 1 K min⁻¹. TM-DSC measurements were made within the temperature range from 173 to 433 K.

2.4. Dielectric Measurements. The sample cell consisted of two gold electrodes, 20 mm in diameter and 50 μm in thickness, maintained by Teflon spacers. Samples were prepared as melts under vacuum by pressing the electrodes to the spacer thickness. DS measurements were performed with a Novocontrol Alpha frequency analyzer as a function of temperature within the range from 190 to 415 K in a step of 5 K for frequencies in the range from 10^{-2} to 10^7 Hz. The complex dielectric permittivity $\epsilon^* = \epsilon' - i\epsilon''$, where ϵ' is the real and ϵ'' is the imaginary part, was obtained as a function of frequency ω and temperature T , that is, $\epsilon^*(T, \omega)$.^{51–53} The analysis of the DS curves was based on the empirical equation of Havriliak and Negami (HN)

$$\frac{\epsilon^*(\omega, T) - \epsilon_\infty(T)}{\Delta\epsilon(T)} = \frac{1}{(1 + (i\omega\tau_{\text{HN}})^m)^n} + \frac{\sigma_0(T)}{i\epsilon_f\omega} \quad (2)$$

Here, $\Delta\epsilon(T)$ is the relaxation strength, which in general depends on temperature (T), τ_{HN} is the relaxation time of the equation, m, n ($0 < m, n \leq 1$) describes the symmetrical and asymmetrical broadening of the distribution of relaxation times, and ϵ_∞ is the dielectric permittivity at the limit of high frequencies. The relaxation times at maximum loss (τ_{max}) for the process under investigation, k_i , are presented herein and have been analytically obtained from the HN equation as follows

$$\tau_{\text{max}} = \tau_{\text{HN}} \sin^{-1/m} \left(\frac{\pi n k_i}{2(1 + n k_i)} \right) \sin^{-1/n} \left(\frac{\pi m k_i n_k}{2(1 + n k_i)} \right) \quad (3)$$

These relaxation times correspond to the global chain relaxation in the bulk or to the relaxation of the most intense chain mode in the copolymers, as well as the relaxation times of the segmental process. At lower frequencies, ϵ'' rises because of the conductivity ($\epsilon'' = \sigma/(\omega \cdot \epsilon_f)$, where σ is the dc conductivity and ϵ_f is the permittivity of free space). The conductivity contribution has also been taken into account during the fitting process. In addition to the measured ϵ'' , the derivative of the real part of the dielectric permittivity ϵ' ($d\epsilon'/d\ln \omega \approx (2/\pi)\epsilon''$) was used in the dynamic behavior analysis.

3. RESULTS AND DISCUSSION

3.1. Dynamics in the Sequential Diblock Copolymer PI-*b*-PS. The dynamics of PI *b* PS diblock copolymers prepared sequentially have been studied earlier as a function of molecular weight, temperature, and phase state.^{30–45,48} DSC thermograms showed distinct thermal features with onset temperatures corresponding to T_{ODT} .^{54,55} Herein, in order to facilitate the comparison with the tapered multiblock copolymers, we first report on the thermodynamics and dynamics of a symmetric diblock copolymer, PI *b* PS, made sequentially with a total molecular weight M_w of 18.8 kg mol⁻¹. The derivative of the heat flow obtained during the second DSC heating run is shown in Figure 1. Two distinct glass temperatures, corresponding to PI and PS rich domains, at lower and higher temperatures, respectively, are clearly seen.³⁷ Besides, a weak but distinct feature is observed in the DSC trace at $T = 376$ K, with a magnitude that depends on the heating rate. Based on rheology (Figure S3) of the same diblock copolymer, this feature is assigned to the ODT temperature ($T_{\text{ODT}} = 376$ K). In the case of the tapered multiblock copolymer, the derivative of the heat flow is featureless (Figures S1 and S2), signifying a weak first order transition.

The segmental and chain dynamics of PI and the segmental dynamics of PS in the diblock copolymer can be discussed with respect to Figure 2. All processes conform to the Vogel–Fulcher–Tammann (VFT) equation

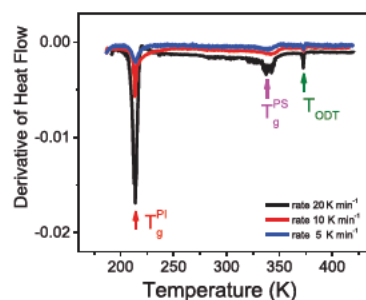


Figure 1. Derivative of heat flow obtained during the second heating runs of the sequential diblock copolymer with an approximate molecular weight of 18.8 kg mol⁻¹ with rates of 20 (black line), 10 (red line), and 5 K min⁻¹ (blue line). Vertical arrows indicate the transition temperatures.

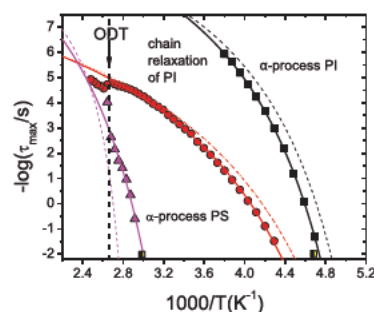


Figure 2. Relaxation map for the sequential diblock copolymer of PI-*b*-PS with a total molecular weight M_w of 18.8 kg mol⁻¹. The different processes correspond to the segmental process of PI (black squares), the chain relaxation of the PI block (red spheres), and the segmental process of PS (magenta up triangles), all obtained via DS. Solid lines represent fits to the VFT equation. Dashed lines depict simulations of the VFT equations for the homopolymers PI (black; segmental; red: chain relaxation) and PS (magenta: segmental). Half-filled symbols at $\tau \approx 100$ s correspond to the glass temperatures obtained from DSC.

$$\tau = \tau_0 \exp \left(\frac{B}{T - T_0} \right) \quad (4)$$

Here, τ_0 is the relaxation time in the limit of very high temperatures, B is the activation parameter, and T_0 is the “ideal” glass temperature. The figure depicts one segmental process corresponding to PI and a much weaker process assigned to PS that are only slightly slower (faster) than the corresponding homopolymers. This is a clear indication that PI *b* PS is located in the ordered (lamellar) phase where the domains are well separated. The same information is extracted from the PI most intense normal mode being only slightly longer than in the PI homopolymer. On approaching the ODT temperature, the most intense normal mode changes discontinuously to longer relaxation times as a result of local mixing of S and I segments. Despite the fact that the segmental (α) process of PI is located outside of the experimental window in the temperature range of interest ($T \geq T_{\text{ODT}}$), the chain relaxation of PI is well resolved and can be used as a probe to the changes in the local environment upon mixing. At $T < T_{\text{ODT}}$, the proximity of the segmental relaxations to the corresponding homopolymers demonstrates the effect of nanophase segregation on the local segmental dynamics. Moreover, at $T \geq T_{\text{ODT}}$, changes in the PI chain relaxation

are driven by the bimodal segmental process but with time scales in closer proximity. Within this temperature range, the same arguments apply as for miscible polymer blends.⁵⁶

3.2. Dynamics in Tapered Multiblock Copolymers P(I-co-S)_n. Because of the highly disparate reactivity ratios of isoprene and styrene ($r_1 = 12.8$ and $r_2 = 0.051$), the statistical copolymerization of I and S leads to tapered diblock copolymers of the (AB)_n type with up to 10 blocks ($1 \leq n \leq 5$).^{21,22} Figure 3 illustrates the PI (in red) and the PS (in blue)

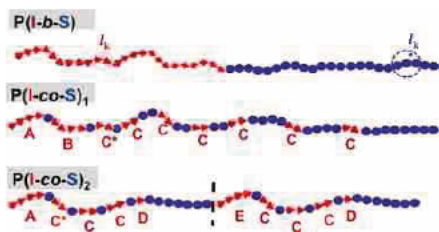


Figure 3. Schematic representation of a single chain in (top) the sequential diblock copolymer PI-*b*-PS, (middle) the tapered diblock P(I-co-S)₁, and (bottom) the tetrablock copolymer P(I-co-S)₂. The PI and PS Kuhn lengths ($l_K(\text{PI}) = 0.93$ nm and $l_K(\text{PS}) = 1.48$ nm, respectively⁵⁷) are also shown. Arrows indicate the component of dipole moment along the PI chain. PI subchains are labeled with different capital letters (see text).

subchains in the tapered diblock copolymer P(I-co-S)₁ and in the tapered tetrablock copolymer P(I-co-S)₂. The PI subchains are labeled in capital letters and arrows indicate the component of PI dipoles along the chain. Herein, the dielectric behavior of tapered multiblock copolymers is investigated for the first time and compared to a diblock copolymer prepared sequentially. In the case of tapered multiblock copolymers, the component of PI's dipole moment, aligned along the backbone, is interrupted by various S segments, unlike for the case of sequential diblock copolymers (also depicted in Figure 3 as PI *b* PS). This study of the local and chain PI dynamics in the presence of a tapered interface is divided into two parts. In the first part, we report the dynamics at a fixed total molecular weight by increasing the number of blocks. The PI dynamics is compared with a sequential diblock copolymer. Subsequently, we report the local and chain dynamics of PI in tapered multiblock copolymers at a fixed block length as a function of the number of blocks and the total molecular weight.

3.2.1. Case I: Comparison under a Constant Molecular Weight. In this part, we employ a series of tapered multiblock copolymers with an approximate total molecular weight of 80 kg mol⁻¹ (Table 1) and investigate the dynamics as a function of increasing number of blocks. Increasing number of blocks at a fixed total molecular weight results in a broad interfacial mixing. A schematic representation of the tapered multiblock copolymers is shown in Figure 3.

From the series of tapered multiblock copolymers with an approximate molecular weight of 80 kg mol⁻¹, only P(I-co-S)₂ exhibits an ODT at an accessible temperature according to X-ray scattering and rheology measurements.²¹ On the other hand, the absence of an endothermic peak in the DSC heating trace suggests that the ODT in the tapered multiblock copolymer is weakly first order (Figure S3). This is in agreement with rheological studies on the same copolymer.²¹ On the other hand, all copolymers with $n \geq 3$ are in the disordered phase at temperatures above ambient conditions.

The distinguishing feature of tapered multiblock copolymers compared to that of the sequential copolymer is the discontinuity in PI dipoles along the chain by the incorporation of S segments. This results in an interesting situation, where a PI subchain with one free end (A in Figure 3) is followed by a sequence of shorter PI subchains having both ends fixed to PS segments (shown as B, C*, and C for $n = 1$). The PI subchains in P(I-co-S)₂ are labeled as A, C*, C, D, and E for reasons that will become clearer below. By increasing the number of blocks at a fixed overall molecular weight, the number of the shorter PI subchains is reduced (see the discussion below).

The particular chain topology of PI dipoles interrupted by PS segments is expected to alter the PI local and chain dynamics and to create a broad distribution of relaxation times. Indeed, the dielectric spectra of tapered multiblock copolymers shown in Figures S5 and S6 exhibit low and high frequency slopes that are different from a PI homopolymer as well as from a PI *b* PS diblock copolymer. The results for the distribution of relaxation times, the dielectric strength, and the actual relaxation times are discussed with respect to Figures 4–6, respectively. With increasing number of blocks, the values for the low and high frequency slope, m and mn for the segmental and most intense PI Rouse mode, respectively, revealed considerable broadening of the relaxation processes (Figure 4, left). The parameter m of the HN function (see eq 2) of the most intense chain mode differs significantly from 1 (applicable to homopolymer PI) and 0.5 (sequential diblock

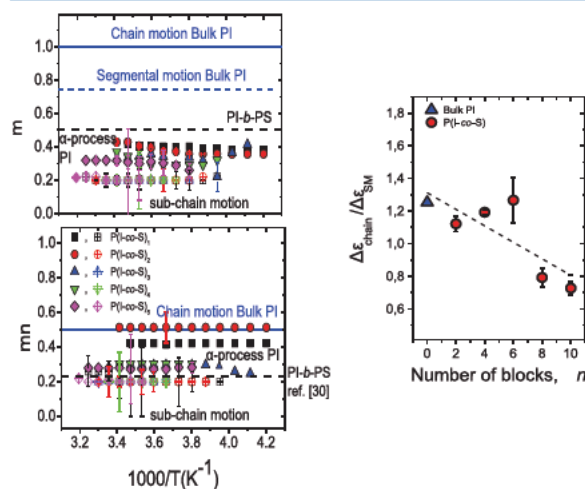


Figure 4. (Left) Comparison of low- (top) and high- (bottom)-frequency slopes, m and mn , respectively, for tapered multiblock copolymers of P(I-co-S) with a total molecular weight M_w of 80 kg mol⁻¹, with a different number of blocks: P(I-co-S)₁ (black squares), P(I-co-S)₂ (red spheres), P(I-co-S)₃ (blue up triangles), P(I-co-S)₄ (green down triangles), P(I-co-S)₅ (magenta rhombi), with the segmental process of PI (filled squares) and the respective subchain motion (crossed center symbols). Blue solid and dashed lines represent the parameters for the global and segmental motion of bulk PI, respectively. Black dashed line represents the parameters of the most intense Rouse mode in sequential PI-*b*-PS from ref 30. (Right) Ratio of the dielectric strength of the longest subchain mode of PI and the corresponding dielectric strength of the segmental motion as a function of the number of blocks for the tapered multiblock copolymers of P(I-co-S) (red spheres) compared to the bulk PI (blue triangle).

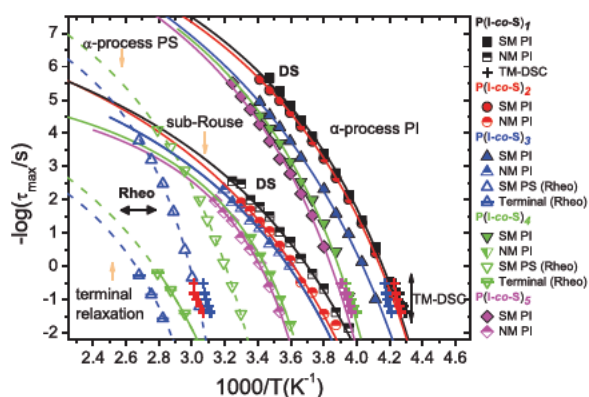


Figure 5. Relaxation map for the tapered multiblock copolymers of $P(I-co-S)_n$ with an approximate total molecular weight M_w of 80 kg mol^{-1} and different numbers of blocks: $P(I-co-S)_1$ (black squares), $P(I-co-S)_2$ (red spheres), $P(I-co-S)_3$ (blue up triangles), $P(I-co-S)_4$ (green down triangles), and $P(I-co-S)_5$ (magenta rhombi). The different symbols correspond to the segmental process of PI (filled symbols) and PI subchain relaxation (crossed center symbols) obtained via DS, while the segmental process of PS (hollow symbols) and terminal relaxation (equatorial crossed symbols) are obtained from rheology. Crosses indicate TM-DSC results. Solid lines represent fits to the VFT equation.

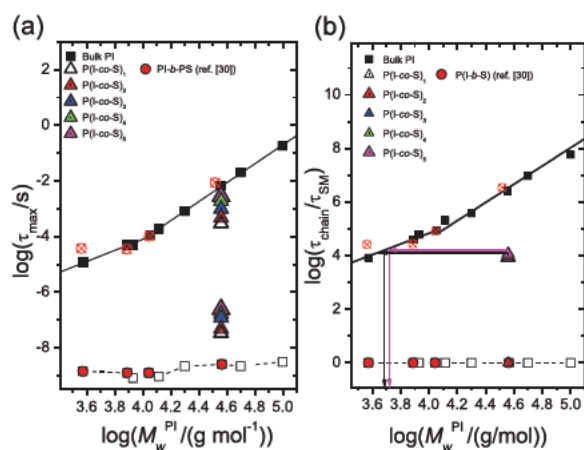


Figure 6. (a) Log log plot of the terminal (bulk PI: black filled squares), subchain (tapered $P(I-co-S)$), most intense Rouse mode (PI-*b*-PS) from ref 30 (red crossed circles) with the corresponding segmental dynamics (bulk PI: black open squares, PI-*b*-PS: red filled circles) as a function of PI molecular weight at the same temperature $T = 333 \text{ K}$. (b) Same data normalized to the corresponding segmental dynamics. Arrows indicate the effective molecular weight of PI participating in the subchain dynamics. The latter is used to estimate the length of the PI subchain with the free end (labeled as A in Figure 3).

copolymers) and amounts to 0.25 ± 0.04 in the ordered state and 0.2 ± 0.1 in the disordered state. Such a broadening is anticipated by the distribution in subchains predominantly of the kind A (Figures 3 and 7).

In addition to broadening, the dielectric strength of the most intense PI Rouse submode is also affected with increasing number of blocks. Under a fixed total molecular weight, the increasing number of blocks results in a reduced number of shorter PI subchains at the end (labeled A in Figure 3). Based

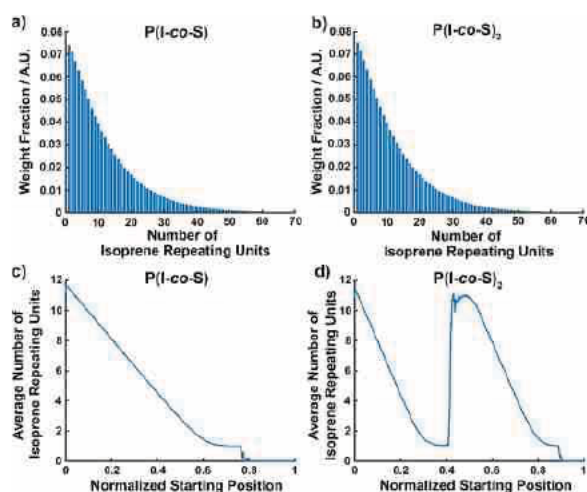


Figure 7. Visualization of the copolymer composition for the tapered diblock $P(I-co-S)$ and tetrablock $P(I-co-S)_2$ copolymers both with $M_n = 80 \text{ kg mol}^{-1}$, obtained by kinetic Monte Carlo simulations under equimolar composition. The number of isoprene repeating units is limited by the concurrent incorporation of styrene units during the copolymerization. (a,b) Weight distributions of PI segments. (c,d) Average number of isoprene units as a function of the normalized starting position along the polymer chain (0: initiator, 1 represents the PS chain end).

on this expectation, the normalized dielectric strength, $\Delta\epsilon_{\text{chain}}/\Delta\epsilon_{\text{SM}}$, decreases, indicating the smaller number of Rouse subchains of A type (Figure 4, right).

The relaxation times in the tapered multiblock copolymers are depicted in the Arrhenius representation of Figure 5. Four relaxation processes are depicted: two are obtained from DS and two from rheology. The characteristic relaxation times, τ_{max} for all processes were obtained during heating and correspond to temperatures above the glass temperature of PI. The faster and slower DS processes are assigned, respectively, to the segmental and longest subchain modes. Both processes depend strongly on the number of blocks and display retardation in dynamics as a result of mixing at the broad interface. On the other hand, rheology could identify the segmental relaxation of PS and the terminal relaxation of the disordered copolymers $P(I-co-S)_3$ and $P(I-co-S)_4$. The PS segmental process could not be detected in DS because of the broadening in the relaxation mode distribution and the proximity to the PI subchain modes. By analogy to the slowing down of the segmental mode of PI, the segmental (α) process of PS is accelerated with increasing number of blocks. As a result, the segmental processes of PS and PI approach each other with increasing number of blocks, indicating that segmental mobilities are in proximity, in agreement with the DSC and TM DSC measurements.²¹

To get more insights into the effect of the tapered interface on the PI chain dynamics, we plot in Figure 6a the subchain and segmental dynamics in the tapered multiblock copolymers together with the segmental and terminal dynamics of PI homopolymers (filled squares) as a function of PI molecular weight at a given temperature ($T = 333 \text{ K}$). In the same figure, we include the most intense Rouse mode from the sequential diblock copolymers (PI *b* PS) of ref 30. The segmental times of PI in PI *b* PS are slightly longer than in the respective homopolymers. This difference is attributed to some mixing at

the interface, as discussed with respect to Figure 2. On the other hand, the relaxation times corresponding to the most intense Rouse mode are longer by a factor of 3–4 in the case of $M_{PI} > 10^4$ g mol⁻¹ and by a factor of 15 in the unentangled regime, relative to the bulk PI. Yao et al.³⁰ proposed that the longest relaxation time for a tethered chain is 4 times longer than that of a free Gaussian chain with the same length because of the difference in the wavelength of the slow normal modes for end grafted and free Gaussian chains.

Hereafter, we focus our attention on the sub Rouse modes of the tapered multiblock copolymers. As shown in Figure 6a, the segmental dynamics of PI are always slower, while the PI chain dynamics are always faster than the respective PI homopolymers and the PI block in the PI *b* PS sequential copolymers. This result for the segmental process originates from the mixing of PI segments by PS at the broad interface. The effect of the tapered interface on the local (and the chain) dynamics of PI becomes more pronounced with increasing number of blocks. Because both processes are affected by the tapered interface, any comparison of the chain dynamics should be made under reduced times. As seen in Figure 6b, the normalized (to the corresponding segmental mode) relaxation times of chain modes are much shorter than in the PI homopolymers showing, unambiguously, that shorter PI chains, for example, subchains, participate in the Rouse dynamics. An estimate of the effective molecular weight of PI subchains that participate in the Rouse dynamics can be provided by projecting the relaxation times to the bulk PI line. This procedure results in an effective M_w for PI in the range from 4800 g mol⁻¹ (P(I *co* S)₁) to 5300 g mol⁻¹ (P(I *co* S)₅).

These results can be discussed in view of the PI subchains shown in Figure 3. Four PI subchains are indicated for P(I *co* S)₁ in Figure 3 (A, B, C*, and C), but not all are dielectrically active. Subchain A has a free end, and the end to end vector can fluctuate and hence become dielectrically active. In subchain B, both ends are connected to PS segments, and, in principle, the end to end vector cannot fluctuate. However, because of extensive segmental mixing, the first S segment is actually plasticized, and at the reference temperature of 333 K, it can still fluctuate. Hence, although the main contribution toward the subchain modes is expected through segments labeled as A, a small contribution from segments labeled as B (and perhaps C*) cannot be excluded. The pronounced broadening of the relaxation spectrum (Figure S6) suggests the participation of A subchains with a variety of lengths because of the statistical nature of the copolymerization and possibly some minor participation from other (shorter) modes than A. On the other hand, moving toward the PS block, the subchain labeled as C has both ends tethered by the stiff (glassy) PS segments, the subchains cannot fluctuate, and any normal mode is deactivated. The situation with P(I *co* S)₂ is somewhat different. First, the terminal free PI subchain is of the same length (A) (see simulation results below), but their number is reduced. This is in line with the reduced dielectric strength shown in Figure 4. Second, the internal modes are not equivalent; for example, the subchain E, although of the same length as A, can only partially fluctuate—both ends are fixed to PS, but because of plasticization one end is still possible to relax (the other end is fixed by the long PS block). All this gives rise to a very broad spectrum of modes obtained experimentally.

To get further insights into the polymer composition along the chain, copolymerizations were performed in silico via

kinetic Monte Carlo simulations. An overview of the weight distribution and actual positions of I (Figure 7) and S (Figure S9) repeating units along the chain are given for the tapered diblock P(I *co* S) and tetrablock copolymer P(I *co* S)₂ of similar molecular weight ($M_n = 80$ kg mol⁻¹). At first glance, the similar fractions of I repeating units in the two copolymers (Figure 7a,b) could be surprising in view of the different block lengths. As visualized in Figure 7c,d, the copolymer architectures differ in their arrangement of the I repeating units. In both cases, there exist a few long PI subchains at the PI free end composed of ~50–60 repeat units. However, because of the statistical nature of incorporation of I and S units, there is a distribution of PI subchains near the free end with an average of about 12 repeat units (Figure 7c). As expected, in P(I *co* S)₂, the average number of I repeating units decreases faster compared to that of the P(I *co* S) diblock copolymer. More importantly, although the fraction of PI subchains at the chain end is unaltered, their number is reduced in P(I *co* S)₂. This finding is in excellent agreement with the identical PI subchain dynamics observed experimentally with increasing n (Figure 6).

To sum up the results of this part, the effect of the tapered interface in P(I *co* S) is first to change both the PI and PS segmental dynamics. These results are in agreement with previous studies using DSC and rheology techniques.²¹ Second, the relaxation time spectra for both segmental and subchain dynamics were broadened in comparison to the sequential diblock copolymers and PI homopolymers. Furthermore, it was shown that the dielectric strength of the PI subchains is reduced with increasing number of blocks, revealing a reduced length of PI segments participating in the subchain dynamics. The relaxation times of the latter modes are employed to estimate the effective molecular weight of PI subchains participating in the relaxation. An effective M_w of about 4800 g mol⁻¹ was obtained, corresponding mainly to the PI subchain with one free end (indicated as A in Figure 3). This molecular weight is closer to the longest PI subchains found in the simulations but different from the average molecular weight (~820 g mol⁻¹) found therein.

3.2.2. Case II. Comparison at Constant Block Length. In this part, we investigate the dynamics of PI under a fixed block length as a function of the number of blocks for P(I *co* S)_{*n*}. Data for the P(I *co* 4MS)_{*n*} copolymers are presented in the Supporting Information. From the samples of Table 1 (and Table S1), there exist three copolymers that fulfill this requirement; tapered diblock (P(I *co* S)) with a total molecular weight M_w of ~80 kg mol⁻¹, tapered hexablock (P(I *co* S)₃) with a total molecular weight M_w of ~240 kg mol⁻¹, and tapered decablock (P(I *co* S)₅) with a total molecular weight M_w of ~400 kg mol⁻¹. The exact molecular weights for P(I *co* S)_{*n*} and P(I *co* 4MS)_{*n*} are shown in Tables 1 and S1, respectively. A schematic representation of the tapered multiblock copolymers with constant block length is shown in Figure 8. All three copolymers are in the ordered (or weakly ordered) state, forming a lamellar morphology with respective domain spacings of 39.5, 29.6, and 29.8 nm.^{21,22}

The dielectric loss curves for the three P(I *co* S)_{*n*} copolymers (in comparison to a PI homopolymer of 50 kg mol⁻¹) are compared at the same reduced temperature $T_g/T = 0.82$ in Figure 9. The curves indicate the segmental mode and a broad spectrum of normal modes to be discussed below.

The broadening and dielectric strengths of the modes are discussed with respect to Figure 10. As in the previous study,

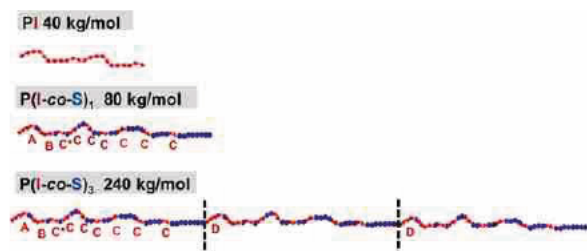


Figure 8. Schematic representation of the chains for tapered diblock $P(I-co-S)_1$ with a molecular weight M_w of $\approx 80 \text{ kg mol}^{-1}$ and hexablock copolymer $P(I-co-S)_3$ with a molecular weight M_w of $\approx 240 \text{ kg mol}^{-1}$. For comparison, a homopolymer PI chain with $M_w \approx 40 \text{ kg mol}^{-1}$ is shown. Arrows indicate the component of dipole moment along the PI chain. Circles indicate the Kuhn lengths of the homopolymers PI and PS.

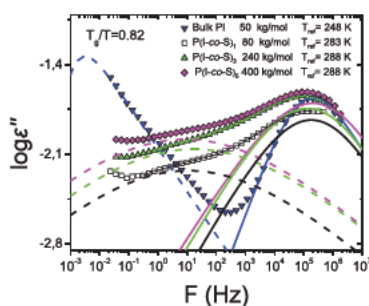


Figure 9. Dielectric loss spectra of tapered multiblock copolymers $P(I-co-S)$ with constant block length: $P(I-co-S)_1$ with $M_w \approx 80 \text{ kg mol}^{-1}$ (black squares), $P(I-co-S)_3$ with $M_w \approx 240 \text{ kg mol}^{-1}$ (green up triangles), $P(I-co-S)_5$ with $M_w \approx 400 \text{ kg mol}^{-1}$ (magenta rhombi), and bulk PI with $M_w \approx 50 \text{ kg mol}^{-1}$ (blue down triangles), compared at $T_g/T = 0.82$. Solid and dashed lines give the contributions of the segmental and subchain modes, respectively. Notice the broadening of all modes and the speedup of the subchain dynamics in the tapered copolymers relative to bulk PI.

the mode distribution is much broader, especially in the case of the subchain process. In particular, the low frequency side of the subchain motion has $m \approx 0.25 \pm 0.13$, which differs substantially from the case of the homopolymer PI ($m \approx 1$). This result reveals the dominant effect of the tapered interface and the (local) composition fluctuations. For the segmental process, the high frequency slope is similar to that of the homopolymer. However, the low frequency slope reveals a pronounced asymmetry, which reflects the intramolecular (due to the covalent attachment to the glassy styrene blocks) effects hindering the motions of the PI chains. The corresponding parameters for the segmental motion of bulk PI are shown by the solid and dashed lines (low and high frequency slopes of $m \approx 0.7$ and $mn \approx 0.34$, respectively).

The dielectric strength of both processes is also depicted in Figure 10 as a function of the number of blocks. The reduced dielectric intensity, $\Delta\epsilon_{\text{chain}}/\Delta\epsilon_{\text{SM}}$, is highly affected by the tapered interface and by the incorporated S segments. The chain dynamics of the PI blocks include mainly the free PI chain end, illustrated as A in Figure 8. As before, some minor contribution from parts B and C* cannot be excluded, as the attached PS segments are plasticized by mixing with the PI segments at the interface. Notice that subchain D is not identical to A despite the same length, as in D there is no free

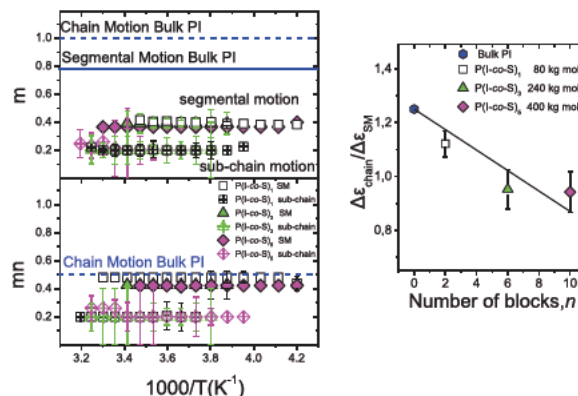


Figure 10. (Left) Comparison of low- (up) and high- (down)-frequency slopes, m and mn , respectively, for tapered multiblock copolymers of $P(I-co-S)$ with constant block length: $P(I-co-S)_1$ with $M_w \approx 80 \text{ kg mol}^{-1}$ (black squares), $P(I-co-S)_3$ with $M_w \approx 240 \text{ kg mol}^{-1}$ (green up triangles), and $P(I-co-S)_5$ with $M_w \approx 400 \text{ kg mol}^{-1}$ (magenta rhombi). Blue dashed and solid lines represent the parameters for the terminal and the segmental motion of bulk PI, respectively. (Right) Ratio of the dielectric strength of the longest normal mode in bulk PI (blue sphere) and the subchain mode in tapered multiblock copolymers to the corresponding strength of the segmental mode plotted as a function of the numbers of blocks for tapered multiblock copolymers of $P(I-co-S)$: diblock with $M_w \approx 80 \text{ kg mol}^{-1}$ (black squares), $P(I-co-S)_3$ with $M_w \approx 240 \text{ kg mol}^{-1}$ (green up triangles), and $P(I-co-S)_5$ with $M_w \approx 400 \text{ kg mol}^{-1}$ (magenta rhombi). The solid line is a guide for the eye.

end. Overall, the PI segments capable of subchain relaxation are reduced with the increasing number of blocks, as shown in Figure 10.

The temperature dependence of the relaxation times corresponding to tapered multiblock copolymers $P(I-co-S)$ is shown in the Arrhenius plots of Figure 11 in a T_g scaled representation. The PI segmental dynamics in the tapered multiblock copolymers are slower as compared to the bulk PI because of mixing with the slower PS segments, in agreement with the glass temperatures obtained from DSC and TM-DSC.

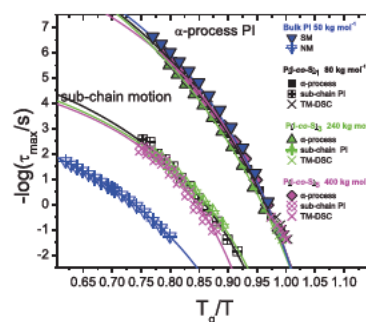


Figure 11. Relaxation map for the tapered multiblock copolymers of $P(I-co-S)$ with constant block length: tapered diblock with $M_w \approx 80 \text{ kg mol}^{-1}$ (black squares), tapered hexablock with $M_w \approx 240 \text{ kg mol}^{-1}$ (green up triangles), and tapered decablock with $M_w \approx 400 \text{ kg mol}^{-1}$ (magenta rhombi) compared to the bulk PI (blue up triangles). The segmental and longest Rouse modes of a PI homopolymer ($M_w \approx 50 \text{ kg mol}^{-1}$) are shown with filled down triangles and open triangles, respectively. Solid lines represent fits to the VFT equation. Results from TM-DSC are shown with crosses.

However, in the T_g scaled representation of Figure 11, all segmental processes overlap.

The subchain motion of tapered multiblock copolymers is faster compared to that of the homopolymer as a result of the shorter I subchains participating in the Rouse dynamics. The temperature dependence of the Rouse relaxation times in the tapered copolymers is very similar, as expected based on the similar length of the A subchains. More informative is the comparison of the segmental and subchain relaxation times in the tapered multiblock copolymers with the segmental and Rouse modes of PI homopolymers as a function of molecular weight at a single temperature ($T = 333$ K), as shown in Figure 12. From the scaled relaxation times in Figure 12b, the

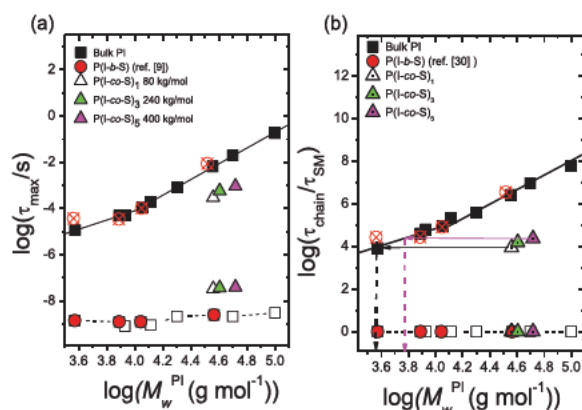


Figure 12. (a) Log log plot of the terminal (bulk PI: black filled squares), subchain (tapered P(I-co-S)), most intense Rouse mode (PI-b-PS) from ref 30 (red crossed circles) with the corresponding segmental dynamics (bulk PI: black open squares, PI-b-PS: red filled circles) as a function of PI molecular weight at the same temperature $T = 333$ K; (b) same data, albeit normalized to the corresponding segmental dynamics. Arrows indicate the PI effective molecular weight participating in the subchain dynamics.

effective molecular weight of PI subchains participating in the chain motion can be estimated by projecting the reduced relaxation time of the normal mode to the Rouse regime. It was shown that the effective M_w of PI is in the range of 3.7 kg mol⁻¹ (P(I co S)₁ with $M_w \approx 80$ kg mol⁻¹) to 5.8 kg mol⁻¹ (P(I co S)₅ with $M_w \approx 400$ kg mol⁻¹).

In addition to P(I co S), the effect of the tapered interface on the dynamic behavior of PI at a fixed block length as a function of the number of blocks and the total molecular weight was investigated for the case of copolymers based on isoprene and 4 methylstyrene, P(I co 4MS)_n. The latter system exhibits a steeper gradient²² than that of the IS system because of the very different reactivity ratios for isoprene and 4 methylstyrene, resulting in a more bulklike dynamic behavior of the components. By following the same procedure, as with P(I co S), the PI chains participating in the sub Rouse motion were estimated. It was shown (Figure S8) that the effective M_w of PI is in the range of 7.4 kg mol⁻¹. By comparing the two systems, longer PI subchains are capable of Rouse relaxation in the P(I co 4MS) copolymers because of the narrower interface. These results are in accord with simulations on the P(I co 4MS) copolymers (see the Supporting Information). There, striking differences are observed for the copolymer composition of isoprene and 4 methylstyrene as compared to isoprene

and styrene (Figures S10 and S11). The disparity in reactivity ratios (I/S: $r_{4\text{MS}} = 0.007$ and $r_{\text{I}(4\text{MS})} = 25.4$;²⁰ I/4MS: $r_{\text{S}} = 0.029$ and $r_{\text{I}(\text{S})} = 10.9$ ⁵⁸) approximately doubles the average number of PI repeat units in the P(I co 4MS) case.

A pertinent structural feature in the tapered multiblock copolymers is the reduction in domain spacing by increasing the number of blocks both at a fixed overall molecular weight and at a fixed block length. This reflects the conformational properties of the middle blocks and the formation of loops that are increasingly favored with increasing n . Despite the increased fraction of loops as compared to bridges, the dielectric relaxation of the copolymers is unaffected. Instead, any differences in the subchain dynamics as evidenced by DS (A subchains in Figures 3 and 8) can be attributed to the differences at the total molecular weight and to the statistical nature of copolymerization (e.g., A subchains have a distribution).

4. CONCLUSIONS

The local segmental and subchain dynamics were investigated in tapered di and multiblock copolymers of PI with PS or P4MS with respect to the number of blocks and the total molecular weight. Because of the tapered interface, I segments carrying a dipole moment along the chain are interrupted by shorter dielectrically inactive S segments. Unsurprisingly, the segmental dynamics of the soft and rigid phases, PI and PS/P4MS, respectively, approach each other because of mixing of segments within the respective Kuhn volumes. This results in changes of the PI glass temperature by as much as 45 K in the case of the decablock P(I co S)₅ with the lower molecular weight (80 kg mol⁻¹). However, more drastic is the effect of the tapered interface on the PI chain relaxation. Based on the reduced relaxation strength and much faster dynamics, DS proved that the longer scale motion of I segments in tapered multiblock copolymers originates mainly from the PI subchain with one free end. Some minor contribution from internal subchains that fluctuate cooperatively with a few plasticized PS segments cannot be excluded. DS afforded the estimation of the effective molecular weight of PI subchains participating in the relaxation. Interestingly, the subchain length obtained from DS is longer than the average length obtained by Monte Carlo simulations in the same tapered multiblock copolymers, being comparable to the longer lengths of the distribution obtained in simulations. The smaller molecular weight in the simulation could result from an overestimation (underestimation) of the reactivity ratios of S (I) units. This is an important issue as simulated reactivity ratios are currently employed at the industrial scale. Motivated by the success in predicting the effective molecular weight of PI subchains, we went one step further by comparing two tapered multiblock copolymers of P(I co S)_n and P(I co 4MS)_n where the vastly different reactivity ratios of I and 4MS give rise to a narrower interphase in the latter. As a consequence of the shorter taper in this system, a longer subchain was found to participate in the PI dynamics of P(I co 4MS)_n, in agreement with the simulation results for the same system. Overall, DS has shown to be a valuable tool in determining the subchain dynamics in a tapered chain topology where PI dipoles are interrupted by S units.

■ ASSOCIATED CONTENT

● Supporting Information

The Supporting Information is available free of charge at <https://pubs.acs.org/doi/10.1021/acs.macromol.0c00445>.

DSC data on the glass temperatures of the PI *b* PS and P(I *co* S)₂ copolymers; DS data on the P(I *co* S)_n and P(I *co* 4MS)_n systems including the effective molecular weight of subchain PI modes in the latter; and details on the copolymerization via kinetic Monte Carlo simulations (PDF)

■ AUTHOR INFORMATION

Corresponding Authors

Holger Frey – Department of Chemistry, Johannes Gutenberg—University of Mainz, 55128 Mainz, Germany; orcid.org/0000-0002-9916-3103; Email: hfrey@uni-mainz.de

George Floudas – Department of Physics, University of Ioannina, 451 10 Ioannina, Greece; University Research Center of Ioannina (URCI), Institute of Materials Science and Computing, 451 10 Ioannina, Greece; Max Planck Institute for Polymer Research, 55128 Mainz, Germany; orcid.org/0000-0003-4629-3817; Email: gfloudas@uoi.gr

Authors

Chrysoula Livitsanou – Department of Physics, University of Ioannina, 451 10 Ioannina, Greece

Marvin Steube – Department of Chemistry, Johannes Gutenberg—University of Mainz, 55128 Mainz, Germany

Tobias Johann – Department of Chemistry, Johannes Gutenberg—University of Mainz, 55128 Mainz, Germany

Complete contact information is available at:

<https://pubs.acs.org/doi/10.1021/acs.macromol.0c00445>

Notes

The authors declare no competing financial interest.

■ ACKNOWLEDGMENTS

This work was supported by the Hellenic Foundation for Research and Innovation (H.F.R.I.) under the “First Call for H.F.R.I. Research Projects to support Faculty members and Researchers and the procurement of high cost research equipment grant” (project number: 183). We thank Eftyx Galanos for the rheology measurements and Eduard Grune and Christian Wahlen for the synthesis of P4MS based copolymers.

■ REFERENCES

- (1) Bates, F. S.; Fredrickson, G. H. Block Copolymers Designer Soft Materials. *Macromolecules* **1999**, *32*, 32–38.
- (2) Bates, C. M.; Bates, F. S. 50th Anniversary Perspective: Block Polymers Pure Potential. *Macromolecules* **2017**, *50*, 3–22.
- (3) Polymeropoulos, G.; Zapsas, G.; Ntetsikas, K.; Bilalis, P.; Gnanou, Y.; Hadjichristidis, N. 50th Anniversary Perspective: Polymers with Complex Architectures. *Macromolecules* **2017**, *50*, 1253–1290.
- (4) Hadjichristidis, N.; Floudas, G.; Pispas, S. *Block Copolymers: Synthetic Strategies, Physical Properties, and Applications*; Wiley-Interscience: Hoboken, N.J., 2003.
- (5) Hamley, I. *The Physics of Block Copolymers*; Oxford University Press, 1999.
- (6) Fredrickson, G. H.; Helfand, E. Fluctuation Effects in the Theory of Microphase Separation in Block Copolymers. *J. Chem. Phys.* **1987**, *87*, 697–705.

(7) Foerster, S.; Khandpur, A. K.; Zhao, J.; Bates, F. S.; Hamley, I. W.; Ryan, A. J.; Bras, W. Complex Phase Behavior of Polyisoprene-Polystyrene Diblock Copolymers Near the Order-Disorder Transition. *Macromolecules* **1994**, *27*, 6922–6935.

(8) Khandpur, A. K.; Foerster, S.; Bates, F. S.; Hamley, I. W.; Ryan, A. J.; Bras, W.; Almdal, K.; Mortensen, K. Polyisoprene-polystyrene Diblock Copolymer Phase Diagram near the Order-Disorder Transition. *Macromolecules* **1995**, *28*, 8796–8806.

(9) Watanabe, H. “Rheology of Multiphase Polymeric Systems”. In *Structure and Properties of Multiphase Polymeric Materials*; Araki, T., Tran-Cong, Q., Shibayama, M., Eds.; Marcel Dekker: New York, 1998; Chapter 9.

(10) Zelinski, R.; Childers, C. W. Linear Elastomeric Block Polymers. *Rubber Chem. Technol.* **1968**, *41*, 161–181.

(11) Kraus, G.; Childers, C. W.; Gruver, J. T. Properties of Random and Block Copolymers of Butadiene and Styrene. I. Dynamic Properties and Glassy Transition Temperatures. *J. Appl. Polym. Sci.* **1967**, *11*, 1581–1591.

(12) Knoll, K.; Nießner, N. Styrolux+ and Styroflex+ - From Transparent High Impact Polystyrene to New Thermoplastic Elastomers: Syntheses, Applications and Blends with Other Styrene Based Polymers. *Macromol. Symp.* **1998**, *132*, 231–243.

(13) Hodrokoukes, P.; Floudas, G.; Pispas, S.; Hadjichristidis, N. Microphase Separation in Normal and Inverse Tapered Block Copolymers of Polystyrene and Polyisoprene. I. Phase State. *Macromolecules* **2001**, *34*, 650–657.

(14) Morris, M. A.; Gartner, T. E.; Epps, T. H. Tuning Block Polymer Structure, Properties, and Processability for the Design of Efficient Nanostructured Materials Systems. *Macromol. Chem. Phys.* **2017**, *218*, 1600513.

(15) Roy, R.; Park, J. K.; Young, W.-S.; Mastroianni, S. E.; Tureau, M. S.; Epps, T. H. Double-Gyroid Network Morphology in Tapered Diblock Copolymers. *Macromolecules* **2011**, *44*, 3910–3915.

(16) Luo, M.; Brown, J. R.; Remy, R. A.; Scott, D. M.; Mackay, M. E.; Hall, L. M.; Epps, T. H. Determination of Interfacial Mixing in Tapered Block Polymer Thin Films: Experimental and Theoretical Investigations. *Macromolecules* **2016**, *49*, 5213–5222.

(17) Singh, N.; Tureau, M. S.; Epps, T. H., III Manipulating Ordering Transitions in Interfacially Modified Block Copolymers. *Soft Matter* **2009**, *5*, 4757.

(18) Brown, J. R.; Sides, S. W.; Hall, L. M. Phase Behavior of Tapered Diblock Copolymers from Self-Consistent Field Theory. *ACS Macro Lett.* **2013**, *2*, 1105–1109.

(19) Adhikari, R.; Godehardt, R.; Lebek, W.; Weidisch, R.; Michler, G. H.; Knoll, K. Correlation between Morphology and Mechanical Properties of Different Styrene/butadiene Triblock Copolymers: A Scanning Force Microscopy Study. *J. Macromol. Sci., Part B: Phys.* **2001**, *40*, 833–847.

(20) Grune, E.; Johann, T.; Appold, M.; Wahlen, C.; Blankenburg, J.; Leibig, D.; Müller, A. H. E.; Gallei, M.; Frey, H. One-Step Block Copolymer Synthesis versus Sequential Monomer Addition: A Fundamental Study Reveals That One Methyl Group Makes a Difference. *Macromolecules* **2018**, *51*, 3527–3537.

(21) Steube, M.; Johann, T.; Galanos, E.; Appold, M.; Rüttiger, C.; Mezger, M.; Gallei, M.; Müller, A. H. E.; Floudas, G.; Frey, H. Isoprene/Styrene Tapered Multiblock Copolymers with up to Ten Blocks: Synthesis, Phase Behavior, Order, and Mechanical Properties. *Macromolecules* **2018**, *51*, 10246–10258.

(22) Galanos, E.; Grune, E.; Wahlen, C.; Müller, A. H. E.; Appold, M.; Gallei, M.; Frey, H.; Floudas, G. Tapered Multiblock Copolymers Based on Isoprene and 4-Methylstyrene: Influence of the Tapered Interface on the Self-Assembly and Thermomechanical Properties. *Macromolecules* **2019**, *52*, 1577–1588.

(23) Spontak, R. J.; Zielinski, J. M.; Lipscomb, G. G. Effect of Looping on the Microstructure of Linear Multiblock Copolymers. *Macromolecules* **1992**, *25*, 6270–6276.

(24) Adachi, K.; Kotaka, T. Dielectric Normal Mode Relaxation. *Prog. Polym. Sci.* **1993**, *18*, 585–622.

- (25) Adachi, K.; Kotaka, T. Dielectric Normal Mode Process in Undiluted cis-Polyisoprene. *Macromolecules* **1985**, *18*, 466–472.
- (26) Boese, D.; Kremer, F.; Fetters, L. J. Molecular Dynamics in Linear and Multiarmed Star Polymers of cis-Polyisoprene as Studied by Dielectric Spectroscopy. *Macromolecules* **1990**, *23*, 1826.
- (27) Boese, D.; Kremer, F. Molecular Dynamics in Bulk cis-polyisoprene as Studied by Dielectric Spectroscopy. *Macromolecules* **1990**, *23*, 829.
- (28) Schönhals, A. Relation Between Main and Normal Mode Relaxations for Polyisoprene Studied by Dielectric Spectroscopy. *Macromolecules* **1993**, *26*, 1309.
- (29) Floudas, G.; Gravalides, C.; Reisinger, T.; Wegner, G. Effect of Pressure on the Segmental and Chain Dynamics of Polyisoprene. Molecular Weight Dependence. *J. Chem. Phys.* **1999**, *111*, 9847.
- (30) Yao, M. L.; Watanabe, H.; Adachi, K.; Kotaka, T. Dielectric Relaxation Behavior of Styrene-Isoprene Diblock Copolymers: Bulk Systems. *Macromolecules* **1991**, *24*, 2955–2962.
- (31) Stühn, B.; Stickel, F. Dielectric Normal Mode Spectroscopy in the Ordered and Disordered States of Diblock Copolymers. *Macromolecules* **1992**, *25*, 5306–5312.
- (32) Yao, M. L.; Watanabe, H.; Adachi, K.; Kotaka, T. Dielectric Relaxation of Styrene-Isoprene Diblock Copolymer Solutions: a Selective Solvent System. *Macromolecules* **1991**, *24*, 6175.
- (33) Yao, M. L.; Watanabe, H.; Adachi, K.; Kotaka, T. Dielectric Relaxation of Styrene-Isoprene Diblock Copolymer Solutions: a Common Solvent System. *Macromolecules* **1992**, *25*, 1699–1704.
- (34) Watanabe, H. Slow Dielectric Relaxation of a Styrene-Isoprene-Styrene Triblock Copolymer with Dipole Inversion in the Middle Block: a Challenge to a Loop/Bridge Problem. *Macromolecules* **1995**, *28*, 5006.
- (35) Sato, T.; Watanabe, H.; Osaki, K.; Yao, M.-L. Relaxation of Spherical Micellar Systems of Styrene-Isoprene Diblock Copolymers. 1. Linear Viscoelastic and Dielectric Behavior. *Macromolecules* **1996**, *29*, 3881.
- (36) Sato, T.; Watanabe, H.; Osaki, K. Rheological and Dielectric Behavior of a Styrene-Isoprene-Styrene Triblock Copolymer in n-Tetradecane. 1. Rubbery-Plastic Viscous Transition. *Macromolecules* **1996**, *29*, 6231.
- (37) Watanabe, H.; Sato, T.; Osaki, K.; Yao, M.-L.; Yamagishi, A. Rheological and Dielectric Behavior of a Styrene-Isoprene-Styrene Triblock Copolymer in Selective Solvents. 2. Contribution of Loop-Type Middle Blocks to Elasticity and Plasticity. *Macromolecules* **1997**, *30*, 5877.
- (38) Watanabe, H.; Sato, T.; Osaki, K.; Matsumiya, Y.; Anastasiadis, S. H. Effects of Spatial Confinement on Dielectric Relaxation of Block Copolymers having Tail, Loop, and Bridge Conformations. *J. Soc. Rheol., Jpn.* **1999**, *27*, 173–182.
- (39) Karatasos, K.; Anastasiadis, S. H.; Pakula, T.; Watanabe, H. On the Loops-to-Bridges Ratio in Ordered Triblock Copolymers: An Investigation by Dielectric Relaxation Spectroscopy and Computer Simulations. *Macromolecules* **2000**, *33*, 523.
- (40) Karatasos, K.; Anastasiadis, S. H.; Semenov, A. N.; Fytas, G.; Pitsikalis, M.; Hadjichristidis, N. Composition Fluctuation Effects on Dielectric Normal-Mode Relaxation in Diblock Copolymers. 1. Weak Segregation Regime. *Macromolecules* **1994**, *27*, 3543.
- (41) Karatasos, K.; Anastasiadis, S. H.; Floudas, G.; Fytas, G.; Pispas, S.; Hadjichristidis, N.; Pakula, T. Composition Fluctuation Effects on Dielectric Normal-Mode Relaxation in Diblock Copolymers. 2. Disordered State in Proximity to the ODT and Ordered State. *Macromolecules* **1996**, *29*, 1326.
- (42) Alig, I.; Floudas, G.; Avgeropoulos, A.; Hadjichristidis, N. Junction Point Fluctuations in Microphase Separated Polystyrene-Polyisoprene Polystyrene Triblock Copolymer Melts. A Dielectric and Rheological Investigation. *Macromolecules* **1997**, *30*, 5004.
- (43) Floudas, G.; Paraskeva, S.; Hadjichristidis, N.; Fytas, G.; Chu, B.; Semenov, A. N. Dynamics of Polyisoprene in Star Block Copolymers Confined in Microstructures: A Dielectric Spectroscopy Study. *J. Chem. Phys.* **1997**, *107*, 5502.
- (44) Floudas, G.; Hadjichristidis, N.; Iatrou, H.; Pakula, T. Microphase Separation in Model 3-Miktoarm Star Co- and Terpolymers. 2. Dynamics. *Macromolecules* **1996**, *29*, 3139.
- (45) Floudas, G.; Meramveliotaki, K.; Hadjichristidis, N. Segmental and Chain Dynamics of Polyisoprene in Block Copolymer/Homopolymer Blends. A Dielectric Spectroscopy Study. *Macromolecules* **1999**, *32*, 7496–7503.
- (46) Lorthioir, C.; Alegría, A.; Colmenero, J.; Deloche, B. Heterogeneity of the Segmental Dynamics of Poly(dimethylsiloxane) in a Diblock Lamellar Mesophase: Dielectric Relaxation Investigations. *Macromolecules* **2004**, *37*, 7808–7817.
- (47) del Valle-Carrandi, L.; Alegría, A.; Colmenero, J. PDMS Behaviour Under Confinement in Strongly Segregated Mesophases of PS-PDMS Diblock Copolymers. *Eur. Phys. J.: Spec. Top.* **2010**, *189*, 257–261.
- (48) Jencyk, J.; Dobies, M.; Makrocka-Rydzky, M.; Wypych, A.; Jurga, S. The Segmental and Global Dynamics in Lamellar Microphase-Separated Poly(styrene-*b*-isoprene) Diblock Copolymer Studied by ¹H NMR and Dielectric Spectroscopy. *Eur. Polym. J.* **2013**, *49*, 3986–3997.
- (49) Mok, M. M.; Masser, K. A.; Runt, J.; Torkelson, J. M. Dielectric Relaxation Spectroscopy of Gradient Copolymers and Block Copolymers: Comparison of Breadths in Relaxation Time for Systems with Increasing Interphase. *Macromolecules* **2010**, *43*, 5740–5748.
- (50) Lund, R.; Barroso-Bujans, F.; Slimani, M. Z.; Moreno, A. J.; Willner, L.; Richter, D.; Alegría, A.; Colmenero, J. End-to-end Vector Dynamics of Nonentangled Polymers in Lamellar Block Copolymer Melts: the Role of Junction Point Motion. *Macromolecules* **2013**, *46*, 7477–7487.
- (51) Kremer, F.; Schönhals, A. *Broadband Dielectric Spectroscopy*; Springer: Berlin, 2002.
- (52) Floudas, G.; Paluch, M.; Grzybowski, A.; Ngai, K. L. *Molecular Dynamics of Glass-Forming Systems: Effects of Pressure*; Springer, 2011.
- (53) Floudas, G. Dielectric Spectroscopy. In *Polymer Science: A Comprehensive Reference*; Matyjaszewski, K., Möller, M., Eds.; Elsevier BV: Amsterdam, 2012; Vol. 2.32, pp 825–845.
- (54) Stühn, B. The relation between the microphase separation transition and the glass transition in diblock copolymers. *J. Polym. Sci., Part B: Polym. Phys.* **1992**, *30*, 1013–1019.
- (55) Voronov, V. P.; Buleiko, V. M.; Podneks, V. E.; Hamley, I. W.; Fairclough, J. P. A.; Ryan, A. J.; Mai, S.-M.; Kiao, B.-X.; Booth, C. A. High-Resolution Calorimetry Study of the Order-Disorder Transition in a Diblock Copolymer Melt. *Macromolecules* **1997**, *30*, 6674.
- (56) Lodge, T. P.; McLeish, T. C. B. Self-concentrations and Effective Glass Transition Temperatures in Polymer Blends. *Macromolecules* **2000**, *33*, 5278–5284.
- (57) Fetters, L. J.; Lohse, D. J.; Richter, D.; Witten, T. A.; Zirkel, A. Connection between Polymer Molecular Weight, Density, Chain Dimensions, and Melt Viscoelastic Properties. *Macromolecules* **1994**, *27*, 4639.
- (58) Steube, M.; Johann, T.; Plank, M.; Tjabering, S.; Gröschel, A. H.; Gallei, M.; Frey, H.; Müller, A. H. E. Kinetics of Anionic Living Copolymerization of Isoprene and Styrene Using in Situ NIR Spectroscopy: Temperature Effects on Monomer Sequence and Morphology. *Macromolecules* **2019**, *52*, 9299–9310.

Supporting information

Local and Sub-chain Relaxation of Polyisoprene in Multiblock Copolymers with a Tapered Interface

Chrysoula Livitsanou,¹ Marvin Steube,² Tobias Johann,² Holger Frey,^{2*} and George Floudas^{1,3,4*}

¹ Department of Physics, University of Ioannina, P.O. Box 1186, 451 10 Ioannina, Greece

² Department of Chemistry, Johannes Gutenberg – University, Duesbergweg 10-14, 55128 Mainz (Germany)

³ University Research Center of Ioannina (URCI) - Institute of Materials Science and Computing

⁴ Max Planck Institute for Polymer Research, 55128 Mainz, Germany

(A) Synthesis of the diblock copolymer

(B) Differential scanning calorimetry

(C) Rheology

(D) Dielectric Spectroscopy (tapered P(I-co-S), P(I-co-4MS))

(E) Monte Carlo Simulations

(A) Copolymer Synthesis

Block¹ and Tapered Block Copolymers² were synthesized as described elsewhere. Reaction times were calculated as described elsewhere² and prolonged by $\approx 15\%$ in respect to the calculated values. If necessary, homo and cross propagation rate constants, were extrapolated to the reaction temperature by the respective activation energies.¹

Standard Size Exclusion Chromatography (SEC)

SEC measurement was performed with THF as the mobile phase (flow rate 1 mL min⁻¹) on an SDV column set from PSS (SDV 10³, SDV 10⁵, SDV 10⁶) at 30 °C. Polymer concentrations with a maximum of 1 mg/mL were used. Calibration was carried out using Polystyrene standards (from Polymer Standard Service, Mainz).

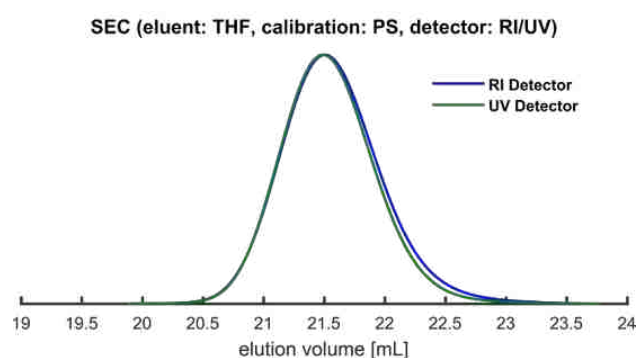


Figure S1. SEC trace of a PI-*b*-PS block copolymer ($f_{PI} = 57\%_{mol} = 50\%_{vol}$), synthesized in cyclohexane ($T_{reaction} = 24^{\circ}C$). The eluogram shows a narrow, monomodal distribution, with a reasonable overlap of both detectors. The molecular weight obtained by PS calibration ($M_{n,PS\ calibr.} = 17.6\ kg/mol$; $D = 1.07$) exceeds the target molecular weight by $\Delta M_n \approx 17\%$. This result is in accordance with previous works ($\Delta M_n \approx 10\%$ for $f_{PI} = 50\%_{mol}$).^{1,2} Hence the block copolymer synthesis was successful.

Table S1. Molecular characteristics of the tapered multiblock copolymers P(I-co-4MS).

Sample	target M_n [kg mol ⁻¹]	# of blocks	target M_n (AB-unit) [kg mol ⁻¹]	M_n (SEC) ^a [kg mol ⁻¹]	$\mathcal{D} = M_w / M_n$ ^a
P(I-co-4MS) ₁	80	2	80	94.7	1.07
P(I-co-4MS) ₂	80	4	40	82.4	1.08
P(I-co-4MS) ₃	80	6	27	81.1	1.06
P(I-co-4MS) ₄	80	8	20	78.7	1.06
P(I-co-4MS) ₅	80	10	16	77.5	1.09
P(I-co-4MS) ₃	240	6	80	240.1	1.15
P(I-co-4MS) ₅	400	10	80	335.3	1.21

^a Determined by SEC at 25°C in THF, values are based on PS calibration.

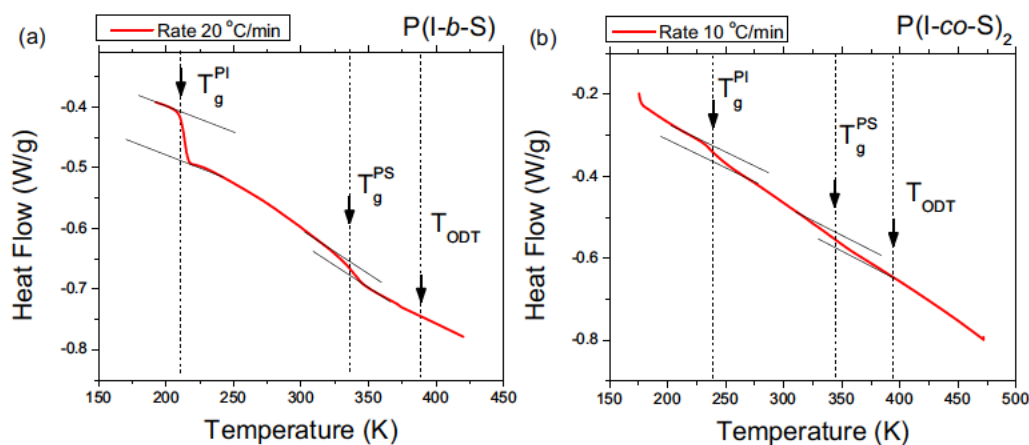
(B) Differential scanning calorimetry

Figure S2. Heat flow obtained during the second heating runs of (a) PI-*b*-PS with $M_n = 17.6$ kg/mol and a rate of 20 K min⁻¹ and (b) P(I-*co*-S)₂ with approximate molecular weight of 80 kg mol⁻¹ with a rate of 10 K min⁻¹. Vertical arrows indicate the glass and ODT temperatures.

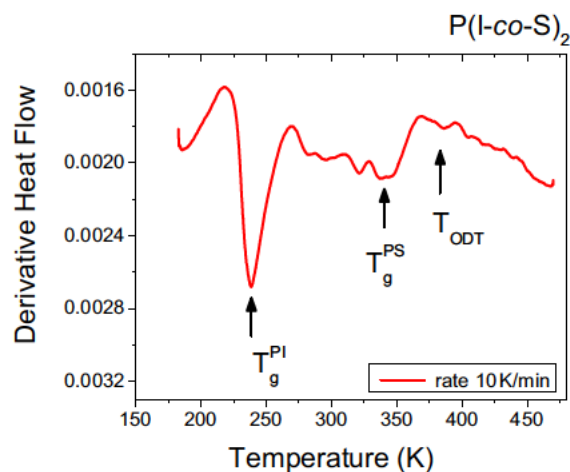


Figure S3. Derivative of heat flow obtained during the second heating runs of P(I-*co*-S)₂ with approximate molecular weight of 80 kg mol⁻¹ with a rate of 10 K min⁻¹. Vertical arrows indicate the glass and ODT temperatures. Notice the absence of any feature at the T_{ODT} for the P(I-*co*-S)₂.

(C) Rheology

A TA Instruments, AR-G2, with a magnetic bearing that allows for nanotorque control was used for recording the viscoelastic properties of the tapered multiblock copolymers. Measurements were made with the environmental test chamber (ETC) as a function of temperature. Samples were prepared on the lower rheometer plate (8 mm and 25 mm), the upper plate was brought into contact, and the gap thickness was adjusted. The linear and nonlinear viscoelastic regions were determined by the strain amplitude dependence of the complex shear modulus $|G^*|$ at $\omega = 10$ rad/s. A low strain amplitude (typically below 1 %) was used to avoid non-linearities in the multiblock copolymers. Subsequent measurements involved (i) isothermal frequency scans within the range $10^{-1} < \omega < 10^2$ rad/s at several temperatures and (ii) isochronal temperature ramps with $\omega = 0.5$ rad/s and a heating rate of 1 K min^{-1} between 298 K and 473 K. The result of an isochronal temperature ramp for the P(I-co-S)_2 used to identify the order-to-disorder transition is shown in **Figure S4**.

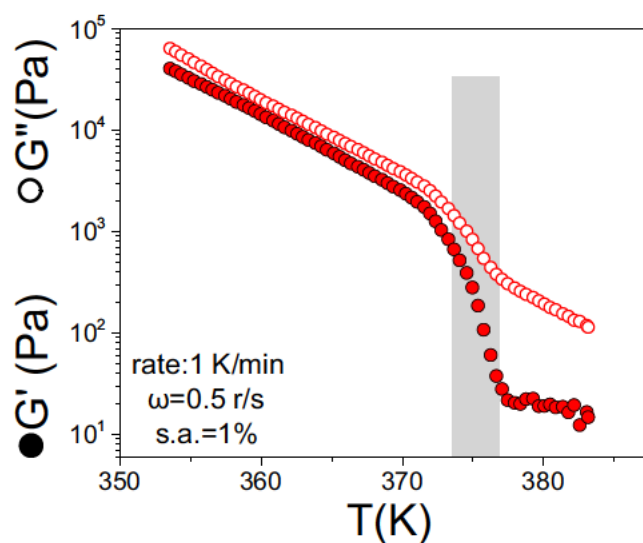


Figure S4. Storage (filled symbols) and loss (open symbols) shear moduli for the tapered multiblock copolymer P(I-co-S)_2 with approximate molecular weight of 80 kg mol^{-1} . The shaded area indicates the order-to-disorder transition temperature ($T_{\text{ODT}} = 376 \text{ K}$).

(D) Dielectric Spectroscopy

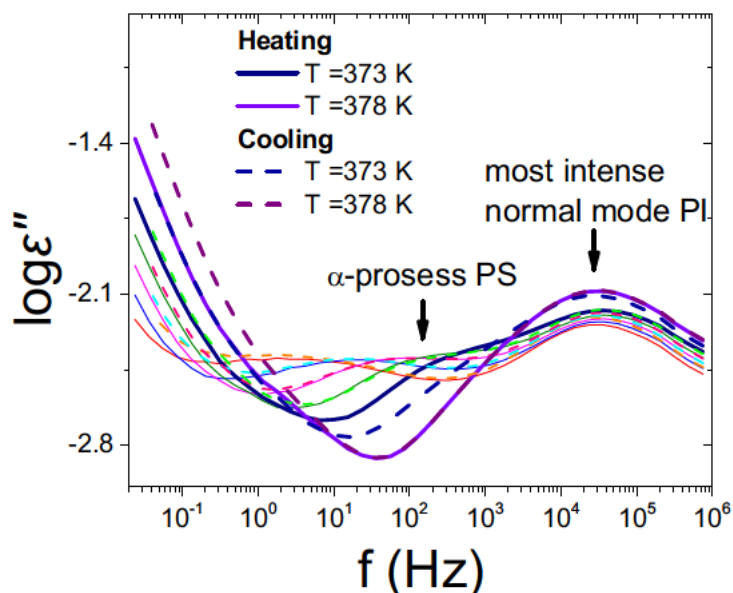


Figure S5. Dielectric loss curves over frequency for the sequential diblock copolymer with $M_n = 17.6$ kg/mol. Data are obtained on heating (solid lines) and subsequent cooling (dashed lines). Arrows indicate the segmental (α) process of PS and the most intense normal mode of PI.

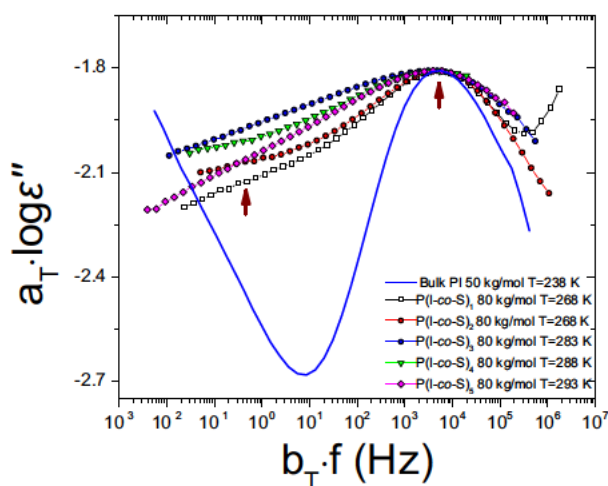


Figure S6. Comparison of the dielectric loss curves over frequency for the P(I-co-S) tapered multiblock copolymers with approximate molecular weight of 80 kg mol⁻¹ at a similar $T_g/T=0.86$; (black line) P(I-co-S)₁ $T=268$ K, (red line) P(I-co-S)₂ $T=268$ K, (blue line) P(I-co-S)₃ $T=283$ K, (olive line) P(I-co-S)₄ $T=288$ K,

(magenta line) P(I-co-S)₅ $T=293$ K. Blue line indicated homopolymer PI with approximate molecular weight of 50 kg mol⁻¹, at $T=238$ K. Arrows indicate the position of the segmental and most intense Rouse mode in the P(I-co-S)₁.

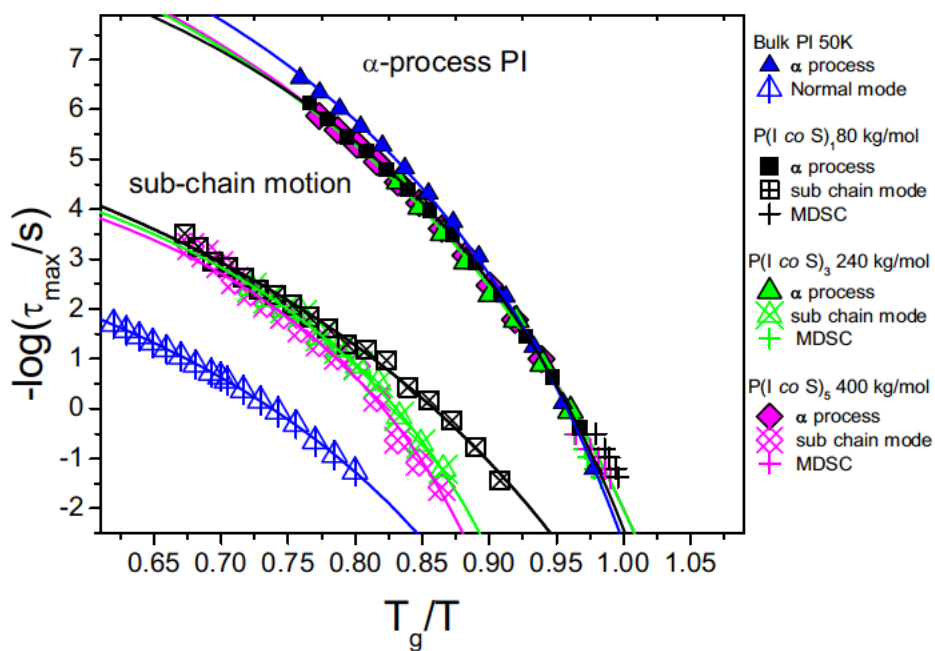


Figure S7. Relaxation map for the tapered multiblock copolymers of P(I-co-4MS) all with a constant block length: tapered diblock with $M_w \sim 80$ kg mol⁻¹ (black squares), tapered hexablock with $M_w \sim 240$ kg mol⁻¹ (green up triangles), tapered decablock with $M_w \sim 400$ kg mol⁻¹ (magenta rhombi) compared to the bulk PI (blue up triangles). Solid lines represent fits to the VFT equation. Blue triangles give the data for a homopolymer PI ($M_w \sim 50$ kg mol⁻¹).

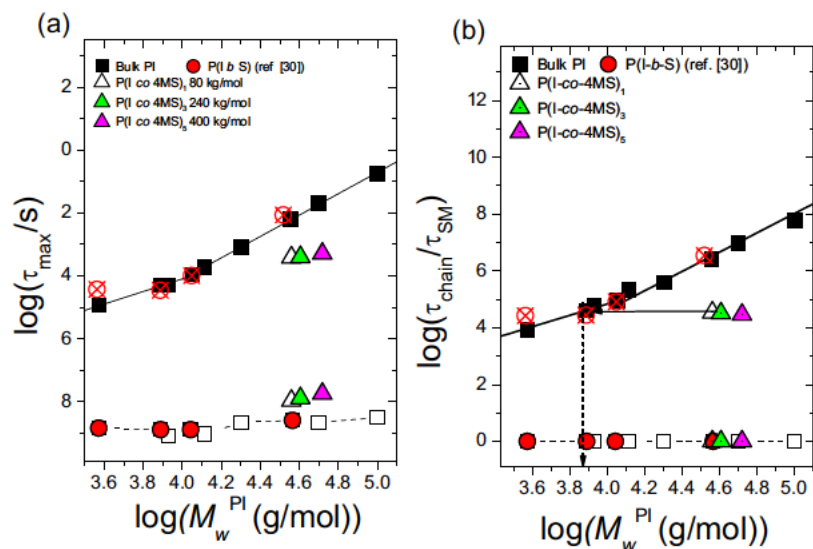


Figure S8. (a) Log-log plot of the terminal (bulk PI), sub-chain of tapered P(I-co-4MS), most intense Rouse mode (P(I-b-S)) from literature ref. [30] and the corresponding segmental dynamics as a function of PI molecular weight. (b) The same data now normalized to the corresponding segmental dynamics. Arrows indicate the PI effective molecular weight participating in the sub-chain dynamics.

Table S2. VFT parameters for the segmental and sub-chain modes of PI in tapered multiblock copolymers under fixed block length.

Sample	$-\log(\tau_0/s)$	B (K)	T_0 (K)
P(I-co-S) ₁ 80 kg mol ⁻¹	-12.9 ± 0.5	1900 ± 110	177 ± 3
P(I-co-S) ₃ 240 kg mol ⁻¹	-12.9 ± 0.4	2000 ± 160	177 ± 4
P(I-co-S) ₅ 400 kg mol ⁻¹	-12.6 ± 0.3	1800 ± 110	179 ± 2
P(I-co-4MS) ₁ 80 kg mol ⁻¹	-12.3 ± 0.4	1700 ± 180	168 ± 5
P(I-co-4MS) ₃ 240 kg mol ⁻¹	-12.8 ± 0.9	1950 ± 700	160 ± 14
P(I-co-4MS) ₅ 400 kg mol ⁻¹	-12.9 ± 0.4	1940 ± 160	163 ± 3

(E) Kinetic Monte Carlo calculations (KMC)

The model was developed based on the stochastic simulation algorithm by Gillespie.^{3,4} Continuum-based reaction rates were converted to number-based probabilities using the following equations:

$$kMC_{II} = \frac{k_{II}}{(NV)^{1/4}} \quad (S1)$$

$$kMC_{SS} = \frac{k_{SS}}{(NV)^{1/2}} \quad (S2)$$

$$kMC_{IS} = \frac{k_{IS}}{(NV)^{1/4}} \quad (S3)$$

$$kMC_{SI} = \frac{k_{SI}}{(NV)^{1/2}} \quad (S4)$$

Concentrations have been converted by multiplying with Avogadro's number N and simulation volume V . The typical simulation volume was in range of $8E-16$ L to $8E-19$ L. For each simulation, 10^6 chains were used. All simulations were performed up to 99 % conversion. Each reaction probability was calculated based on the fraction of the total reaction rate:

$$P_v = \frac{R_v}{\sum_{M=1}^{\mu} R_M} \quad (S5)$$

The corresponding reaction was chosen using a uniform distributed random number r_1 [0..1] based on the reaction probabilities:

$$\sum_{v=1}^{\mu-1} P_v < r_1 < \sum_{v=1}^{\mu} P_v \quad (S6)$$

The time interval corresponding to the chosen reaction step was calculated using another uniformly distributed random number r_2 [0..1]:

$$\tau = \frac{1}{\sum_{v=1}^M R_v} \ln\left(\frac{1}{r_2}\right) \quad (S7)$$

After a reaction was stochastically selected, one randomly corresponding chain was chosen and used to proceed the reaction step. The monomer composition of all chains was tracked. For performance improvement the main stochastic model was implemented in C code, compiled using MinGW GCC compiler 5.1.0, while evaluation of the computed data was performed using custom written MATLAB scripts.^{5,6}

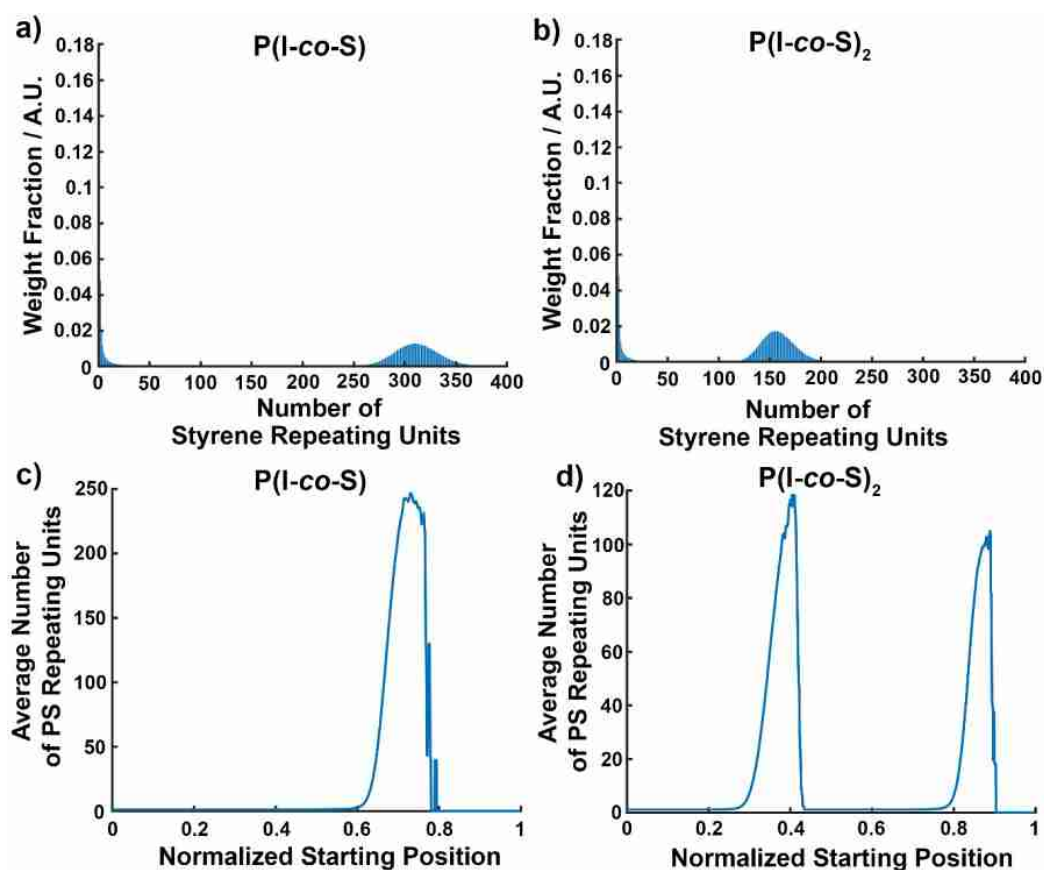


Figure S9. Visualization of the copolymer composition for a tapered diblock P(I-co-S) and tetrablock P(I-co-S)₂ copolymer with $M_{n,chain} = 80 \text{ kg mol}^{-1}$ obtained by kinetic Monte Carlo Simulation at equimolar composition. The number of styrene repeating units is limited by the concurrent incorporation of isoprene units during the copolymerization. (a) and (b): Weight distributions of PS homopolymer segments. (c) and

(d): Average number of styrene units in PS repeat units as a function of the normalized starting position in the polymer chain (0: initiator, 1 represents the chain end).

For both P(I-co-S) and P(I-co-S)₂, the weight distribution of the styrene repeating units (**Figure S9**) is split in two maxima. A few styrene repeating units are incorporated during the early stage of the polymerization, where isoprene is preferentially polymerized. Hence, rather long isoprene segments (sub-chains) are interrupted occasionally by a few styrene units. The corresponding weight distributions are similar, as they are solely dictated by the reactivity ratios and the monomer feed, which are the same for both tapered block architectures of P(I-co-S) and the P(I-co-S)₂.⁵ As the copolymerization proceeds, the progressive depletion of isoprene leads to an increase in the number of styrene repeating units and finally to the formation of a pure PS end-block.⁶ In contrast to the distribution for the small number of styrene repeating units, the larger ones differ by a factor of two when comparing the P(I-co-S) and the P(I-co-S)₂. When isoprene is fully consumed, only homopolymerization of styrene occurs. At this point (Normalized Starting Position ≈ 0.8), no “new” PS segments are generated, leading to a drop of the average number of PS repeating units to 0. Hence, after 0.8 only the already existing PS segments grow. This leads to a segment length, which is equal to the degree of polymerization ($P_n \sim [S]/[Ini]$). [S] is half this value for P(I-co-S)₂ as this polymer architecture is based on two subsequent polymerization steps.⁷

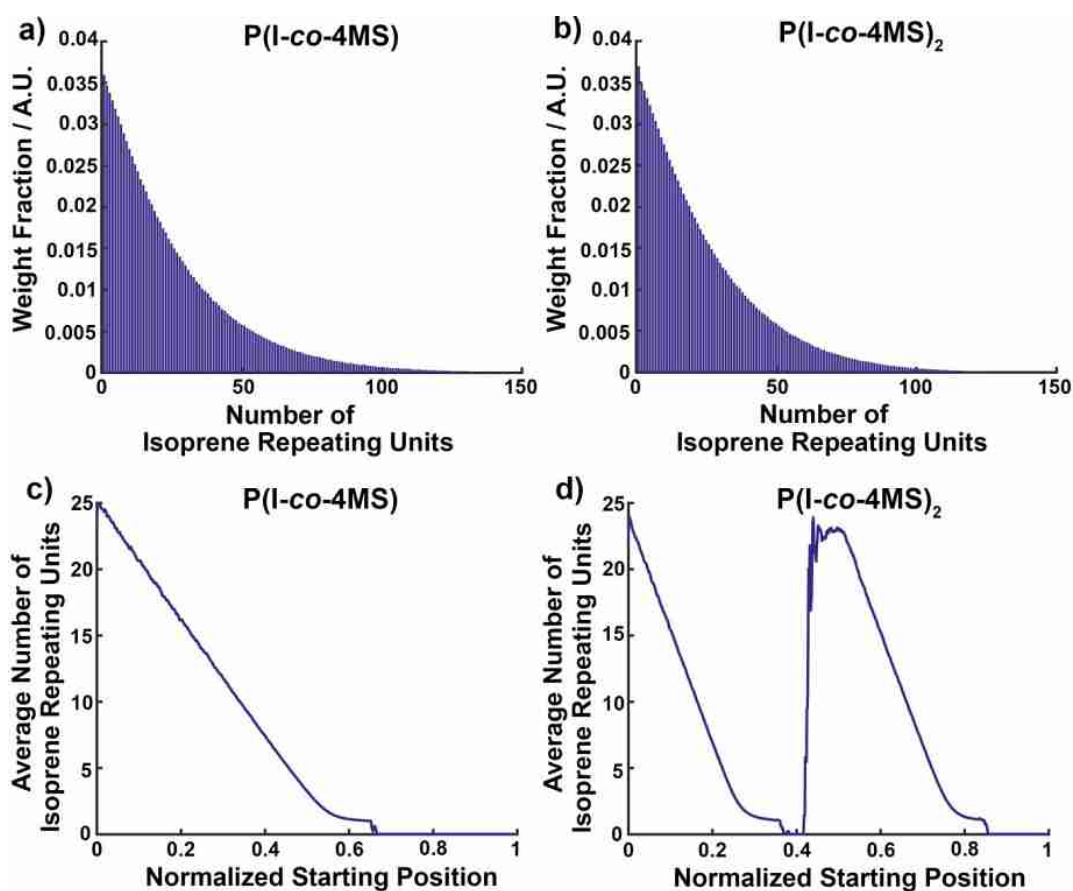


Figure S10. Visualization of the copolymer composition for a tapered diblock $P(I-co-4MS)$ and tetrablock $P(I-co-S)_2$ copolymer with $M_{n,chain} = 80 \text{ kg mol}^{-1}$ obtained by kinetic Monte Carlo Simulation at equimolar composition. The number of isoprene repeating units is limited by the concurrent incorporation of styrene units during the copolymerization. (a) and (b): Weight distributions of PI segments. (c) and (d): Average number of isoprene units as a function of the normalized starting position in the polymer chain (0: initiator, 1 represents the chain end).

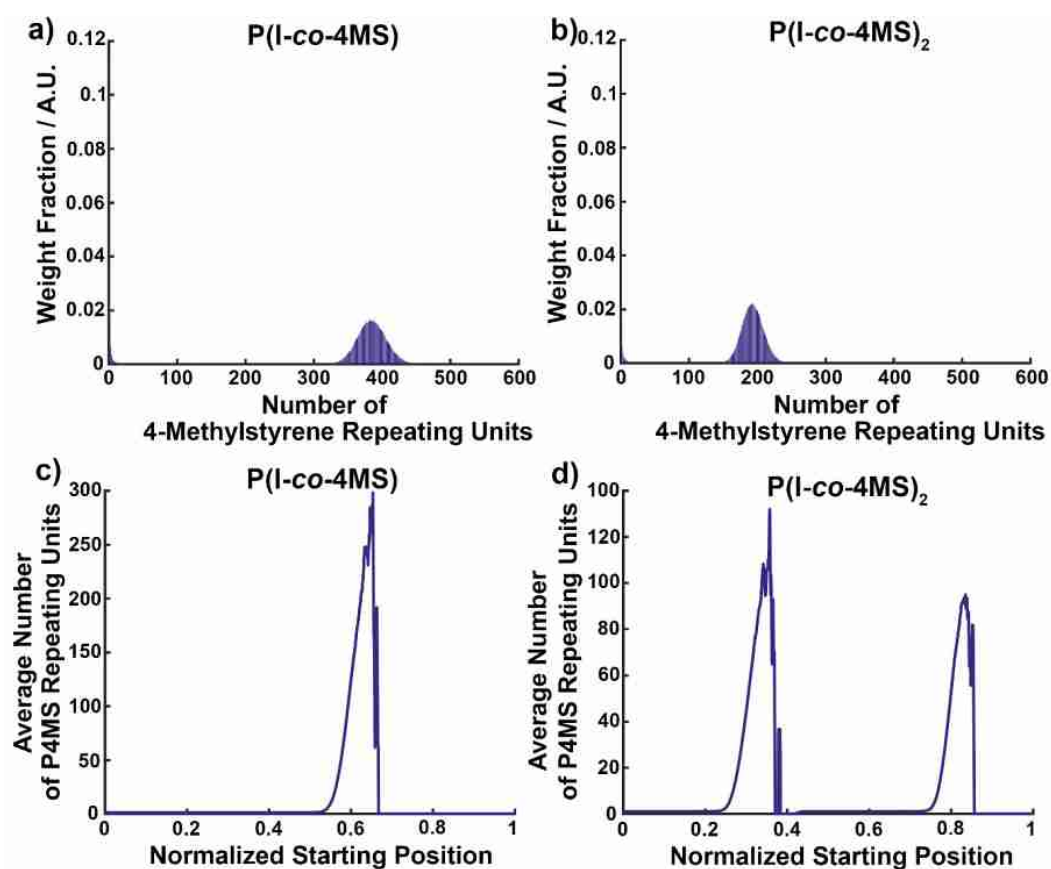


Figure S11. Visualization of the copolymer composition for a tapered diblock P(I-co-4MS) and tetrablock P(I-co-S)₂ copolymer with $M_{n,chain} = 80 \text{ kg mol}^{-1}$ obtained by kinetic Monte Carlo Simulation at equimolar composition. The number of 4-methylstyrene repeating units is limited by the concurrent incorporation of isoprene-units during the copolymerization. (a) and (b): Weight distributions of P4MS segments. (c) and (d): Average number of 4-methylstyrene repeat units as a function of the normalized starting position in the polymer chain (0: initiator, 1 represents the chain end).

Differences of P(I-co-4MS) and P(I-co-4MS)₂ can be discussed in the same manner as done for tapered copolymers based on styrene and isoprene (Figure 8 and Figure S9). Compared to the PS copolymers, the weight distribution of 4-methylstyrene repeating units is shifted to larger values, which is attributed to the highly disparate reactivity ratios causing a more block-like structure. This is also visualized by the comparable step increase of the average number of the 4MS repeating units following isoprene depletion.

References

- (1) Steube, M.; Johann, T.; Plank, M.; Tjaberings, S.; Gröschel, A. H.; Gallei, M.; Frey, H.; Müller, A. H. E. *Macromolecules* 2019, 52 (23), 9299–9310. DOI: 10.1021/acs.macromol.9b01790.
- (2) Steube, M.; Johann, T.; Galanos, E.; Appold, M.; Rüttiger, C.; Mezger, M.; Gallei, M.; Müller, A. H. E.; Floudas, G.; Frey, H. *Macromolecules* 2018, 51 (24), 10246–10258. DOI: 10.1021/acs.macromol.8b01961.
- (3) Gillespie, D. T. A general method for numerically simulating the stochastic time evolution of coupled chemical reactions. *J. Comput. Phys.* 1976, 22, 403–434.
- (4) Gillespie, D. T. Exact stochastic simulation of coupled chemical reactions. *J. Phys. Chem.* 1977, 81, 2340–2361.
- (5) Meyer, V. E.; Lowry, G. G. Integral and differential binary copolymerization equations. *J. Polym. Sci. A: Gen. Pap.* 1965, 3, 2843–2851.
- (6) Mayo, F. R.; Lewis, F. M. Copolymerization. I. A Basis for Comparing the Behavior of Monomers in Copolymerization; The Copolymerization of Styrene and Methyl Methacrylate. *J. Am. Chem. Soc.* 1944, 66, 1594–1601.
- (7) Grune, E.; Johann, T.; Appold, M.; Wahlen, C.; Blankenburg, J.; Leibig, D.; Müller, A. H. E.; Gallei, M.; Frey, H. *Macromolecules* 2018, 51 (9), 3527–3537. DOI: 10.1021/acs.macromol.8b00404.

Marvin Steube



Address Untere Zahlbacher Str. 94
55131 Mainz

Phone 0178 1104660

E-Mail marvin.steube@web.de

Date and place of birth 17/03/1992 / Heppenheim

Education and Work Experience

03/2017 – now

PhD candidate

Johannes Gutenberg University (JGU), Mainz

Research group of Prof. Dr. Holger Frey

Main topics:

- Polymer chemistry and organic synthesis
- Reaction kinetics and spectroscopy
- Block copolymer synthesis, thermoplastic elastomers (TPE) based on dienes and styrene
- Correlation of monomer sequences with morphological, thermal und mechanical properties

Collaborations:

- 1 Industrial collaboration project
- Collaboration partners at 8 more universities and institutes

Supervision of:

- 1 Bachelor student, 4 master students
- Supervision of students in 4 lab courses

10/2014 – 03/2017

Master of Science (1.6) in chemistry, JGU Mainz

Topic: "Phase separation of siloxane modified block copolymers" (1.0)

Focus:

- Synthesis of block-like structures via carbanionic polymerization
- Post-polymerization modification
- Consequences of the functionalization reaction for microphase separation

08/2015 – 02/2016

Semester abroad University of Toronto, Canada

Scholarship: DAAD, ISAP-program

Focus: Synthesis of Poly(3-alkyltellurophene)s

10/2011 – 08/2014

Bachelor of Science (2.2) in chemistry, JGU Mainz

Topic: "Controlled synthesis of hyperbranched polyglycerol with adjustable degree of polymerization" (1.0)

Focus: Polymer synthesis

Specialized Skills

Polymer Synthesis	Carb- and oxyanionic polymerization, Grignard metathesis polymerization
Post Polymerization Modification	Selective hydrogenation, Alder-Ene reaction, hydrosilylation and Thiol-Ene-Click reaction of polyisoprene/polystyrene block copolymers with organic synthesis of related compounds
Experimental Design and Scale-Up	Design of reactors for multi-step synthesis and in situ monitoring, polymerization of butadiene (dismantling and documentation of butadiene installation), design and construction of an polymer extruder
Reaction kinetics and -monitoring	Homo- and copolymerization kinetics of styrene and isoprene, real-time monitoring by near-IR probing and further sensors (temperature, color)
Spectroscopic Methods	<i>in situ</i> near-IR, IR, NMR (1D- und 2D techniques).
Further Methods	TLC, MALDI-ToF, DSC, SAXS, TEM, tensile-tests, rheology, HPLC, ultracentrifugation

Scientific Contributions

Conferences	5 International conferences with oral or poster presentations <i>Best Poster Award, Meeting GDCh-Division, Karlsruhe 2018</i>
Publications	5 Publications in peer-reviewed journals See detailed list at: https://www.ak-frey.chemie.uni-mainz.de/marvin-steube/

Languages and Skills

Languages	German (first language), English (fluent), French (basic knowledge)
IT	Scientific Computing Software <i>MATLAB, LaTeX, Origin, Office-Software, ChemDraw, MestreNova, WinGPC Unichrom</i> Working knowledge in graphical design <i>Photoshop, Illustrator, Indesign, Office-Software</i>
Courses	Project management, good scientific practice

Interests

Hobbies	Fitness, playing football, graphical design, cooking
----------------	--

List of Publications

2020

[1] C. Livitsanou, M. Steube, T. Johann, H. Frey, G. Floudas, Local and Subchain Relaxation of Polyisoprene in Multiblock Copolymers with a Tapered Interface. *Macromolecules* **2020**, 53 (8), 3042–3051.

Submitted

[2] M. Steube, T. Johann, H. Hübner, M. Koch, T. Dinh, M. Gallei, G. Floudas, H. Frey, A. H.E. Müller, THF- More than a „Randomizer“ in the Living Anionic Copolymerization of Styrene and Isoprene: Kinetics , Microstructures, Morphologies, and Mechanical Properties. *Macromolecules*, **submitted**.

To be submitted

[3] [REDACTED]

[4] [REDACTED]

[5] [REDACTED]

[6] [REDACTED]

2019

[7] M. Steube, T. Johann, M. Plank, M. Gallei, H. Frey, A. H. E. Müller, Kinetics of Anionic Living Copolymerization of Isoprene and Styrene Using in Situ NIR Spectroscopy: Temperature Effects on Monomer Sequence and Morphology, *Macromolecules*, **2020**, 52, 23, 9299-9310.

2018

[8] M. Steube, T. Johann, E. Galanos, M. Appold, C. Rüttiger, M. Mezger, M. Gallei, A. H. E. Müller, G. Floudas, H. Frey, Isoprene / Styrene Tapered Multiblock Copolymers with up to Ten Blocks: Synthesis, Phase Behavior, Order, and Mechanical Properties, *Macromolecules*, **2018**, 51, 24, 10246-10258.

[9] C. Schubert, M. Schömer, M. Steube, S. Decker, Systematic Variation of the Degree of Branching (DB) of Polyglycerol via Oxyanionic Copolymerization of Glycidol with a Protected Glycidyl Ether and Its Impact on Rheological Properties, *Macromol. Chem. Phys.*, **2018**, 219, 1700376.

2016

[10] [REDACTED]

Conferences

- 01/2020 **Macromolecular Colloquium, Freiburg, Germany**
Talk: „Building Bridges by Blending: How to Transform AB Block-Copolymers into Tough Nanostructured Materials“ presented by Prof. Dr. H. Frey.
- 09/2019 **International Symposium on Ionic Polymerization, Beijing, China**
Talk „Tapered Multiblock Copolymers Based on Styrene and Isoprene“.
- 09/2018 **Meeting of the GDCh-Division, Karlsruhe, Germany**
Wiley Poster Awards; Poster: „(AB)_n Multiblock Copolymers: Tapered Systems up to 10 Blocks Based on Styrene and Isoprene“.
- 05/2018 **Bordeaux Polymer Conference, Bordeaux, France**
Poster „(AB)_n Multiblock Copolymers: Tapered Systems up to 10 Blocks Based on Styrene and Isoprene“.
- 09/2017 **International Symposium on Ionic Polymerization, Durham, Great Britain**
Poster „Siloxane Modified Alkenylfunctional Block Copolymers: A Strategy for Strongly Segregated Morphologies“.